Light Curves of Type Ia Supernovae and Preliminary Cosmological Constraints from the ESSENCE Survey

Light Curves of Type Ia Supernovae and Preliminary Cosmological Constraints from the ESSENCE Survey

A DISSERTATION PRESENTED
BY
GAUTHAM SIDDHARTH NARAYAN
TO
THE DEPARTMENT OF PHYSICS

IN PARTIAL FULFILLMENT OF THE REQUIREMENTS
FOR THE DEGREE OF
DOCTOR OF PHILOSOPHY
IN THE SUBJECT OF
PHYSICS

HARVARD UNIVERSITY
CAMBRIDGE, MASSACHUSETTS
MAY 2013

Thesis advisor: Christopher William Stubbs Gautham Siddharth Narayan

Light Curves of Type Ia Supernovae and Preliminary Cosmological Constraints from the ESSENCE Survey

Abstract

The ESSENCE survey discovered 213 type Ia supernovae at redshifts $0.10 < z < 0.81$ between 2002 and 2008. We present their *R* and *I* band light curve measurements, obtained using the MOSAIC II imager at the CTIO 4 m, along with rapid response spectroscopy for each object from a range of large aperture ground based telescopes. We detail our program to obtain quantitative classifications and precise redshifts from our spectroscopic follow-up of each object. We describe our efforts to improve the precision of the calibration of the CTIO 4 m natural photometric system. We use several empirical metrics to measure our internal photometric consistency and our absolute calibration of the survey. We assess the effect of various sources of systematic error on our measured fluxes, and estimate that the total systematic error budget from the photometric calibration is $\sim$1%. We combine 108 ESSENCE SN Ia that pass stringent quality cuts with a compilation of 441 SN Ia from 3 year results presented by the Supernova Legacy Survey and Baryon Acoustic Oscillation measurements from the Sloan Digital Sky Survey to produce preliminary cosmological constraints employing the SN Ia . This constitutes the largest sample of well-calibrated, spectroscopically confirmed SN Ia to date. Assuming a flat Universe, we obtain a joint constraint of $\Omega_M = 0.266^{+0.026}_{-0.016}$ (stat 1σ), and $w = -1.112^{+0.069}_{-0.072}$ (stat 1σ). These measurements are consistent with a cosmological constant.

Contents

Listing of figures

For Amali.

Acknowledgments

The advantage to spending a long time in graduate school is that you get to work with a lot of amazing people.

In particular, it has been an absolute privilege to learn from, and work closely with, Armin Rest, Ryan Foley and Michael Wood-Vasey. I owe more to them than I can find the words for here, not merely for improving my research, but for making me a better researcher. While none of them play cricket, they are all incredible people who have willingly run up against the wind while bowling in the death.

Pete Challis, Brian Stalder, Ryan Chornock, Mark Huber and Tony Stark have bought me more than my fair share of beer. I value their friendship, and will endeavor to cause Brad Tucker to lose more poker hands in order to pay them back.

I would be remiss not to thank the entire ESSENCE collaboration for their contributions to, insights into, and comments on the work summarized in the following chapters. I would especially like to acknowledge Saurabh Jha, Peter Garnavich, Alejandro Clocchiatti, Jesper Sollerman, Kevin Krisciunas, and Stéphane Blondin for their time and effort, and Brian Schmidt, Bruno Leibundgut, and Tamara Davis for their kinds words of encouragement.

The entire ESSENCE survey team is very grateful to the scientific and technical staff at the observatories we have been privileged to use:

Facilities: Blanco (MOSAIC II), CTIO:0.9m (CFCCD), Gemini:South (GMOS), Gemini:North (GMOS), Keck:I (LRIS), Keck:II (DEIMOS, ESI), VLT (FORS1), Magellan:Baade (IMACS), Magellan:Clay (LDSS2).

This thesis made extensive use of the Odyssey Cluster administered by the FAS-IT Research Computing Group at Harvard, and I am thankful to the staff (both current

and former) there, particularly John Brunelle, Chris Walker, Paul Edmon, Michael Ethier, Matt Nicholson, and Suvendra Dutta. I'm also indebted to the Computation Facility at the CfA, and Physics IT.

Lisa Cacciabaudo, Sheila Ferguson, Dayle Maynard, Kelly Coulburn, Carol Davis, Jan Ragusa, Maggie McFee, Bill Walker, and the other staff at Harvard Physics helped with numerous pieces of paperwork, supplied printer codes and numerous adapter dongles, were instrumental in me successfully getting away with rarely filing CHD reports on time, and provided most excellent candy. Getting to dog-sit Issac (who may have been allowed to preoccupy himself rummaging through trash cans, despite Jan's explicit instructions) for a few hours was one of the highest honors the Department could bestow.

I am deeply thankful for having made numerous friends at Harvard and elsewhere, including (in no particular order), Kaisey Mandel, Jina Suh, Rob MacRae, Adam Pivonka, Jason Forster, Beezer DeMartelly, Prakrit Jena, Robin Johnson, Brad Tucker, Jonathan Ruel, Verena Martinez-Outschoorn, Tongyan Lin, Kushal Mehta, Hayley Finley, Meredith Hughes, Douglas MacLean, Stephanie Bush, Daniyar Nurgaliev, Anahita Tafvizi, Srivas Prasad, Lisa Krebs, Will High, Malcolm Hicken, Mallika Sen, Arti Garg, David Woolf, Dave Kaz, Erin Boyd, Shannon Fogwell, Amy Buenning, Kevin Sturm, Michelle Megan, Ryan Forster, Joe Jasinski, Mariano Lizano and several others. Some of my best memories are of times with them.

I'm very grateful to Doug Finkbeiner for agreeing to be on my thesis committee on relatively short notice, and for useful conversations on dust and extinction in the early days of Pan-STARRS.

I'm still amazed that I've gotten to work with advisors like Bob Kirshner and Chris Stubbs. Both emphasized the big picture, when it's easy to get caught up in the little details.

Bob was very kind to include me in the CfA Supernova Group, and that early experience as a observer was invaluable. It taught me the difference between textbook descriptions and real conditions. He has been the source of numerous insightful questions (including the only ones that had me completely stumped during my oral examination). Bob has always found a way to significantly improve any text I've run by him. Getting to observe with him was the frosting on the Oreo.

Chris' advice has helped me grow not just as a scientist, but as a person. He has not only given me the guidance to carry out my research, but he's kept faith in me, when at

times I had no faith in myself. His concern and support to both Amali and I during our hardest times provided us with comfort and peace of mind. I cannot thank Chris enough for the time and resources he has invested in me.

Finally, this dissertation would not have been written without the loving support of my fiancée (and editor-in-chief) Amali, and my parents.

From our home on the Earth, we look out into the distances and strive to imagine the sort of world into which we are born... But with increasing distance our knowledge fades, and fades rapidly, until at the last dim horizon we search among ghostly errors of observations for landmarks that are scarcely more substantial. The search will continue. The urge is older than history. It is not satisfied and it will not be suppressed.

Edwin P. Hubble, The George Darwin Lecture [60]

1

The State of SN Ia Cosmology

This thesis presents the calibrated photometry of 213 Type Ia supernovae (SN Ia) measured by the ESSENCE Survey between 2002 and 2008. Our report more than doubles the sample presented in Miknaitis et al. [87] and Wood-Vasey et al. [149]. We have made a significant effort to improve the photometric calibration of the survey. As ESSENCE only observed in two passbands, our measurements of luminosity distance are strongly correlated with extinction in the host galaxy of the SN Ia and very sensitive to the systematic error budget from photometry. In particular, the light curves in this work are computed only using data taken with the 4 m Blanco Telescope at the Cerro-Tololo Inter-American Observatory, eliminating cross-telescope systematics present in the calibration of Miknaitis et al. [87]. Companion works [86, 142, in prep.] will report on the spectroscopy and properties of the host galaxies of our SN Ia sample respectively. In future work, we will use this sample along with low-redshift SN Ia from the literature to perform a full cosmological analysis and improve constraints on the nature of the dark energy.

Shortly after Sandage [121] proposed the deviation of the redshift-magnitude diagram from linearity as a test to discriminate between different cosmological models,

type I supernovae [88] emerged as a strong candidate standard candle to constrain the deceleration parameter, q_o [19, 120, 144]. Kowal [71] used measurements of type I supernovae to measure H_o, but the combination of non-linear photographic detectors and the inability to distinguish between different types of supernovae led to a $\sim$30% scatter in distance about the Hubble Law. Careful spectroscopic follow-up [16, 143, 147] led to type I supernovae being subdivided into two distinct categories: SN Ia events, arising from thermonuclear explosions of a white dwarf near the Chandrashekar limit, and SN Ib/c, arising from the core-collapse of massive stars that have lost their hydrogen envelopes.

The advent of large CCD detectors enabled the current era of precision supernova cosmology, producing accurate multi-color light curves of SN Ia outside the linear Hubble flow. However, these SN Ia light curves appeared to span a factor of $\sim$3 in intrinsic luminosity, ranging from the very bright SN 1991T [34, 104] to the unusually faint SN 1991bg [33, 80] – much wider than desirable for standard candles. Building on early work by Pskovskii [109], Phillips [103] employed new precise CCD light curves to conclusively demonstrate that the intrinsic luminosity of SN Ia was strongly correlated with their light curve shapes, providing a method to correct for the large range in intrinsic luminosity. Early well-sampled multi-color CCD light curves published by the Calán-Tololo Supernova Search [50] were used to derive empirical relations between SN Ia shape, color and intrinsic luminosity [45, 105, 115].

Two groups, the High-Z Supernova Search Team [125] and the Supernova Cosmology Project (SCP, Perlmutter et al. [100]), used the 16 Mega pixel Big Throughput Camera [BTC, 148] at CTIO with a high cadence observing schedule, near real-time difference imaging search pipeline, and rapid spectroscopic follow-up to produce several multi-color SN Ia light curves at high redshift. The distance moduli derived for these SN Ia indicated that the Universe was *accelerating* [101, 116]. SN Ia observations have remained our most sensitive cosmological probe of the expansion history. The accelerating expansion has been modeled by introducing a fluid with negative pressure, called the dark energy, into the Friedmann equation:

$$h(a)^2 = h_o^2 \left(\frac{\Omega_M}{a^3} + \frac{\Omega_v}{a^4} + \frac{\Omega_k}{a^2} + \Omega_{\rm DE} \exp[3(1+w)] \right) \tag{1.1}$$

where h is the Hubble parameter, $h_o = H_o/100$ km s^{-1} Mpc^{-1}, a is the scale factor, and

Ω is the total energy density of matter (M), photons (v), curvature (k) and the dark energy (DE), respectively. Several groups have focused on measuring the ratio of pressure to density – the equation of state of this fluid, $w = P/(\rho c^2)$ – to distinguish between different models of the dark energy.

High-redshift SN Ia surveys [47, 119, 149] have independently reported measurements of w consistent with -1, in good agreement with a classical cosmological constant. However, despite the rapidly growing number of SN Ia, the precision of the measurement of w has stubbornly remained at the 10% level, dominated by various sources of systematic uncertainty. Several groups have attempted to reduce the effect of systematic errors in SN Ia measurements on the dark energy figure of merit [FoM, 2], by either incorporating new sources of data, or improving the calibration of existing data.

Early work by Krisciunas et al. [72] demonstrated uniformity in the evolution of near-IR colors of SN Ia, and the potential of NIR measurements for cosmology [73]. Using increasingly large and better calibrated samples of nearby-SN Ia with JHK_s measurements, Wood-Vasey et al. [150], Mandel et al. [83] and Barone-Nugent et al. [7] have shown that the near-IR light curves of SN Ia span a smaller range in luminosity than in the optical. Because distance moduli derived from NIR measurements are less susceptible to host-galaxy dust absorption, the residual scatter in a Hubble diagram generated from infra-red light curves alone is comparable to the scatter derived from *light curve shape-corrected* optical data. Consequently, high-z surveys have increasingly attempted to probe further into the rest-frame infrared. Freedman et al. [40] presented the first IR Hubble diagram to $z\sim0.7$, but were limited by a relatively small sample size, systematic uncertainties in their photometric calibration, and the difficulty of obtaining IR data at high-z, where it is redshifted to even longer wavelengths. Future high-redshift surveys, such as RAISIN (R. P. Kirshner – HST Proposal 13046), will provide valuable high-redshift SN Ia measurements that probe the rest frame NIR.

Kelly et al. [67] illustrated that in addition to demographic differences between SN Ia from passive and star-forming hosts, the Hubble diagram residuals are correlated with derived host-galaxy size and stellar mass. This correlation indicates that the empirical luminosity-shape relations employed by SN Ia light curve fitters do not fully account for the spread in intrinsic luminosity. In an effort to reduce this dispersion, Lampeitl et al. [75] employed a simple linear correction based on host-galaxy stellar mass and found an improvement in statistical fit to the SN Ia measurements. Sullivan

et al. [137] used different SN Ia absolute magnitudes for high and low mass hosts in their cosmological fits and found a significant improvement in χ^2 over using a relation based on host-galaxy mass. However, although metallicity, extinction properties and specific star formation rate correlate with host-galaxy mass, the fundamental relation underlying this correlation with SN Ia luminosity is not well understood. In addition, there are challenges in deriving host galaxy properties from broadband optical photometry at high redshift in a manner that does not introduce additional systematic uncertainty into SN Ia measurements. ESSENCE has undertaken a significant effort to determine host-galaxy morphology and properties for our sample, to appear in Tucker et al. [142, in prep.].

Several authors [15, 37, 93, 129, 145, 146] have found that measurements from spectra of SN Ia correlate with the residual intrinsic color dispersion after light curve shape correction. They further find that these measurements, typically derived from pseudo equivalent widths of Ca or Si, can be used to improve the precision of distance moduli, although Blondin et al. [15] find that the improvement is not statistically significant ($< 2\sigma$). While promising, this approach is limited by the need for high S/N spectra of SN Ia. Additionally, the dependence on measuring the Si II 6355 Å feature limits its use at high-z, where the redshifted Si features are often not covered by the high-throughput low-dispersion spectrographs used by SN Ia surveys.

While obtaining additional data holds great promise for improving distance precision for future SN Ia surveys, existing high-redshift surveys have focused efforts on improving their overall photometric calibration. The detailed and thorough re-calibration effort undertaken by the Supernova Legacy Survey [11, 111, hereafter SNLS] in particular has set an extremely high standard that current and future SN Ia surveys must strive to meet. As SN Ia surveys constrain w by comparing the luminosity distances of distant supernovae derived from optical observations with their nearby counterparts, the precision of their photometric calibration contributes significantly to their systematic error budget. Wood-Vasey et al. [149] found that systematic uncertainties from the photometry alone could lead to an $\sim$4% change in w.

Kessler et al. [68] demonstrated that measurements of w are extremely sensitive to the calibration of the U band at low-redshift: inclusion of rest frame U-band data at all redshifts causes a 0.12 mag shift in distance moduli, corresponding to an enormous 0.3 change in the equation of state parameter, w. The U-band anomaly might arise from differences between the spectral energy distribution (SED) of SN Ia that correlate with

host-galaxy properties or between objects at low and high redshift [39, 82]. This ultra-violet catastrophe led the SDSS to eliminate all rest frame *U*-band measurements, while the SNLS eliminated measurements of nearby objects observed in *U* or *u*.

Additionally, *U*-band measurements of the same nearby SN Ia from different telescopes often exhibited differences that were inconsistent with the stated photometric uncertainties. These differences are likely the result of systematic errors in estimating the total *U*-band throughput, either from uncertainty in estimating the extinction correction, or from incomplete knowledge of the *U*-band filter and atmospheric transmission for the various nearby samples. Krisciunas et al. [74] have demonstrated that careful modelling of the *U*-band transmission with appropriate *S*-corrections can resolve the differences between SN Ia measurements.

Larger, more accurately calibrated nearby samples [42, 55, 89, 96], along with better calibration of high-z SN Ia surveys, offer the most direct path to reducing the systematic uncertainty on the equation of state parameter of the dark energy. Wide-field deep surveys such as Pan-STARRS will obtain SN Ia measurements over $0 < z < 0.8$ [113, in prep.], further reducing systematic uncertainties from photometry by avoiding any errors associated with cross-telescope calibration and weakening the sensitivity of w to the overall photometric calibration of the survey [127, in prep.]. Recognizing the need for precision calibration to reduce systematics [134, 141], and following the example set by the Sloan Digital Sky Survey [SDSS, 62, 99], current surveys have undertaken ambitious calibration programs. These efforts combine high resolution measurements of system throughput calibrated to laboratory standards, with atmospheric data, and repeated observations of stellar standards to obtain $< 1\%$ photometry over much of the sky [123, 136, 140]. This work details the calibration of the ESSENCE survey, with a focus on minimizing the systematic error budget from photometry.

We provide a brief overview of the ESSENCE survey in §2, followed by our photometric data reduction and calibration in §3. We discuss our spectroscopic follow-up and classification is §4. We illustrate our SN Ia light curves, compare and contrast our methodologies for light curve fitting, and detail the properties of the full ESSENCE 6 year sample in §5. Additionally, we impose stringent light curve quality cuts on our sample and combine 108 spectroscopically confirmed ESSENCE SN Ia with a compilation of 441 SN Ia from the 3 year results presented by the SNLS, and provide preliminary cosmological constraints of Ω_M and w. Our photometric error

budget from various sources with systematic uncertainty is detailed in §6. We conclude in §7. The appendices contain further information on the computation of illumination corrections, the properties of the CTIO 4 m natural magnitude system employed in this work, tables containing the photometry of ESSENCE SN Ia and "Ia?" objects during the year of discovery, and light curve fit parameters using the two most common methodologies.

2

The ESSENCE Survey Operations

Previous ESSENCE publications have described the survey strategy, fields, data processing [87, hereafter M07], spectroscopic selection criteria and follow-up [38, 85], as well as performed a preliminary cosmological analysis [149, hereafter WV07], and scrutinized exotic cosmological models [26]. The WV07 analysis of 60 ESSENCE SN Ia, together with 45 low-z SN Ia from the literature, found $w = -1.05 \pm 0.13(\text{stat}) \pm 0.13$ (sys). Here we provide a brief summary of the ESSENCE operations for context.

The SN Ia search was carried out on the CTIO 4 m Blanco telescope (hereafter, 4m) over 197 half-nights in dark and grey time between September and January from 2002 to 2008. Science images were obtained using the 64 Mega pixel MOSAIC II camera with an Atmospheric Dispersion Corrector (ADC) through two primary filters (denoted R and I) similar to Cousins R_C and I_C. The field of view of the system is 0.36 deg^2 on the sky at the $f/2.87$ prime focus.

The imager consists of eight 2kx4k CCDs arranged in two rows of four. Each CCD is bisected along its length, and each section is read out in parallel, resulting in 16 amplifier images for every science exposure. Readout times are approximately

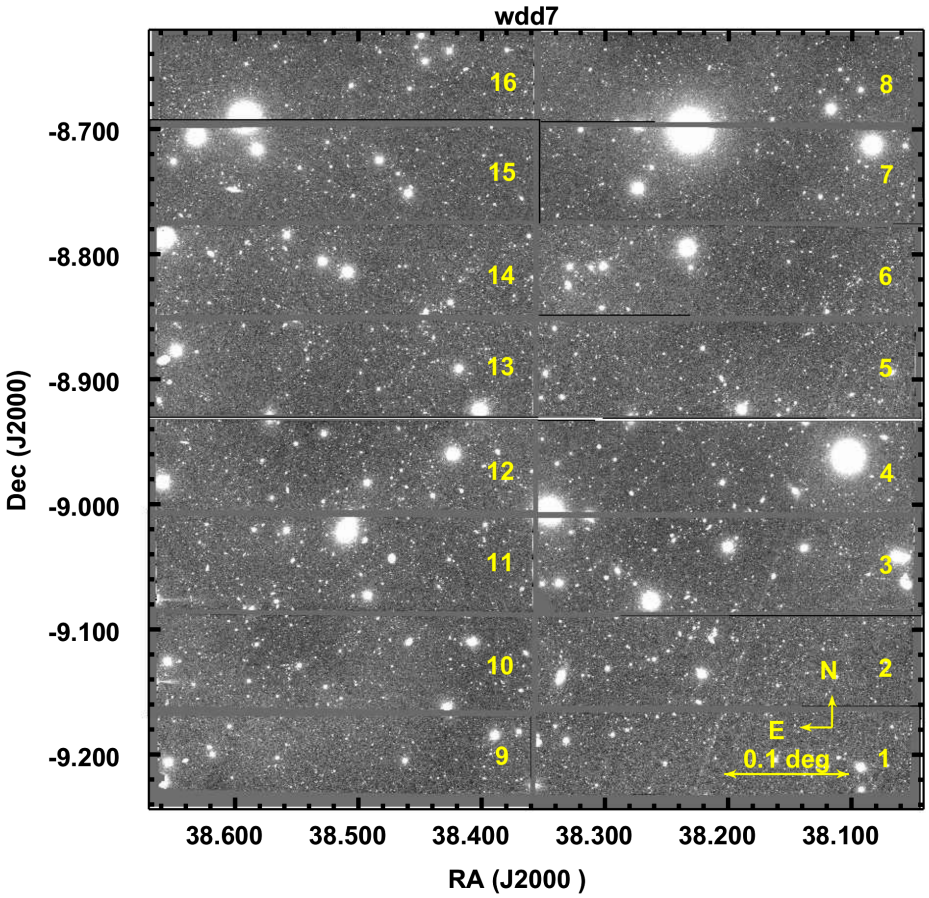

Figure 2.1: A representative *R*-band image of the wdd7 field from MOSAIC II. Amplifiers are indicated by the yellow numerals. The image has been flattened, illumination corrected and warped onto a common astrometric grid. Some compression artifacts are introduced when exporting the original FITS image for publication.

100 seconds. Each pixel subtends 0.27″ at the center of the field. Optical distortions cause a radial variance of ∼8% in the plate scale. The gaps between CCDs correspond to 50 pixels between rows and 35 pixels between columns. The imager is shuttered using two pneumatically driven opposing sliding blades with independently controlled slots for the TV guide camera that are closed during image de-trending frame acquisition. A representative CCD image is shown in Figure 2.1.

Table 2.1: Primary ESSENCE fields

Field	RA (J2000) Dec		NImages
	h m s	° ′ ″	
waa	23:27:27	−09:51:00	172
wbb	01:12:00	−00:20:17	275
wcc	02:07:41	−04:55:00	289
wdd	02:28:36	−08:24:17	293

Following preliminary operations, the survey covered a set of 4 primary fields (listed in Table 2.1), each consisting of 8 sub-fields, clustered spatially. Fields were selected to be equatorial but outside the Galactic and ecliptic planes, in regions with low Milky Way extinction and minimal IR cirrus, and with coverage from existing surveys (including SDSS, the NOAO Deep Wide-Field Survey, and the Deep Lens Survey) where possible. The fields were spaced to ensure that science images could be taken at low airmass. Fields were divided into two sets and each set was imaged in both filters every other observing night resulting in a typical cadence of 4 days. Science frames are exposed for 200 seconds in *R* and 400 seconds in *I*, while exposure times for calibration frames ranged from 5 – 200 seconds. M07 described the optimization of the survey strategy to find SN Ia at $z\sim0.4$, and achieve the strongest constraint on a *constant* dark energy equation-of-state parameter, w, per unit telescope time.

The El Niño-Southern Oscillation was in effect during our inaugural observing season, and led to thick cloud cover, resulting in lost observing time or shallow and unphotometric imaging data. The original *I* filter (NOAO code c6005) sustained significant damage on 10 Nov 2002, severely degrading the image quality of *I*-band data in CCDs 1 and 2 (amplifiers 1–4). The filter was replaced on 2003 May 25. In addition, a catastrophic failure of the newly installed computing cluster at CTIO shortly after the

2002 observing season began led to significant delays in the processing of MOSAIC images. Taken together, these set-backs caused a ∼33% loss in efficiency in 2002, compared to 2004–7. CCD 3 failed shortly before the start of the 2003 observing season, resulting in a 12.5% loss in efficiency until it was replaced in 2004.

Survey images were reduced at CTIO using the "photpipe" pipeline developed for use on the CTIO 4 m by the SuperMACHO survey [43, 87, 112] that operated contemporaneously with the ESSENCE survey. Each science image was calibrated and aligned with a fixed astrometric grid. We subtracted a reference template for each field, constructed using deep images from previous observations. PSF photometry from the resulting difference image was combined to identify sources that had varied over multiple epochs, while eliminating sources of contamination such as difference image artifacts and diffraction spikes from saturated stars. However, not all sources exhibiting variability over multiple epochs were SN Ia. ESSENCE is spectroscopy limited: several objects that have light curves photometrically classifiable as SN Ia lack follow-up spectroscopy. With limited time for spectroscopic follow-up, we were forced to employ various cuts and selection criteria in order to determine the most promising candidates for follow-up.

Potential candidates were checked for variability in previous survey years where possible, and against lists of known variable stars and active galactic nuclei (AGN). We further required that the candidate had the same PSF as stars in the unsubtracted image and vetoed objects with significant amounts of pixels with negative flux to reject spurious detections caused by subtraction artifacts. We selected against targets within 1 pixel of the centroid of objects in the reference image, as these are frequently AGN, and spectroscopic follow-up of such targets is affected by strong galaxy contamination. Preliminary light curves allowed us to reject objects with the wrong light curve shape and color.

We generated webpages that provided the light curve, colors, difference image "postage stamps", PSF and host-galaxy properties, finding charts, and other information for each candidate. All candidate webpages were visually inspected to select targets for spectroscopic follow-up to classify them and obtain redshifts. We produced a preliminary reduction of all spectra in real-time, using standard IRAF[1] routines and some custom IDL routines to facilitate data-processing for the various

[1]IRAF is distributed by the National Optical Astronomy Observatory, which is operated by AURA under cooperative agreement with the NSF.

instruments. Estimates of the redshift and classification were obtained on-site using SuperNova Identification code [12, SNID,]. When preliminary classifications were unclear, we relied on the experience of the observers to determine if additional spectroscopic follow-up was warranted. Fields containing candidates with a clear classification as SN Ia were followed for the remainder of the observing season. Following survey operations, all data were transferred, initially to the Hydra Computing Cluster maintained by the Smithsonian Institution, and later to the Odyssey Compute Cluster, hosted by the Research Computing Group at Harvard University, for the analysis presented in this thesis. All data are also available through the NOAO archive[2].

[2] http://archive.noao.edu/nsa/

3

Data Reduction

3.1 Image De-trending

The eight CCDs of MOSAIC II were read out in pairs, through two amplifiers per chip, by four Arcon controllers. This resulted in the introduction of "ghosts" of bright objects on one CCD appearing on its pair during read out. This cross-talk is a completely deterministic $< 0.1\%$ effect, and was subtracted using the *xtalk* task from the *mscred* package for IRAF using recent values of the cross talk coefficients measured by CTIO staff. All CCD images are de-biased and trimmed and masking was applied to bad pixels and columns. The mask is propagated through all subsequent reduction stages.

Counts across science images were normalized in a two stage process. First, a screen inside the 4m dome was illuminated and observed multiple times through each filter by the imager to construct an average dome flat-field image for each filter, every night. These flats accurately corrected for pixel-to-pixel variations but large-scale variations were introduced as a result of uneven illumination of the dome screen and stray light paths in the optical system. While the precision obtained from dome flat images alone is suitable for many projects, we required higher precision for SN Ia cosmology and

strived to minimize potential systematic errors in our photometry. We therefore accounted for large-scale illumination variation by constructing an illumination correction from the science images.

We applied the nightly dome flat image to all science images to construct a temporary preliminary flattened image. The resulting images were masked to remove contamination from all astrophysical sources, aligned to common astrometric grid, normalized to have the same sky value, and then averaged. The derived calibration image was inverted, smoothed with a large kernel and scaled to have a mean of unity. This illumination correction was applied to the dome flat images to take out residual large scale gradients. The science images were reprocessed with this final flat field image.

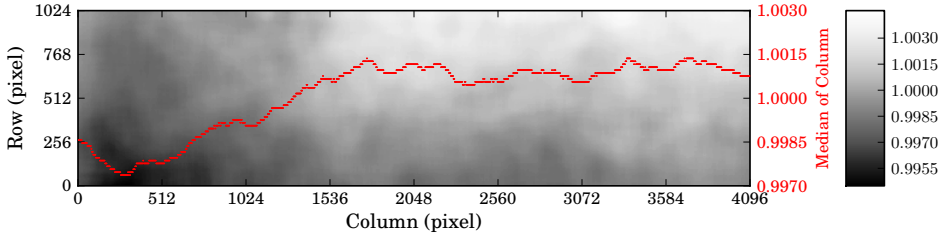

Figure 3.1: A representative *R*-band illumination correction for amplifier 6 of the MOSAIC II. The primary structure in the illumination correction is a ∼0.5% gradient from left to right and top to bottom. The median value of each column is indicated in red. The bar at right indicates the grey scale values.

To estimate the night-to-night stability of the illumination correction, we took the ratio of the correction image between different nights of a single run – a period of time during which MOSAIC II was permanently mounted on the telescope, typically one lunation. We found that the gradient pattern (a representative example is shown in Fig. 3.1) was very stable within a lunar cycle. The standard deviation of the ratio without sigma-clipping was typically less that 0.1%, and the absolute value of the maximum difference between the ratio and the average of the ratio image was < 0.003. Therefore, on nights with few science images of sparse fields or with excess stray light – either from insufficient baffling or around full moon – we exploited the stability of the gradient pattern to estimate the illumination correction from nearby nights. This estimation and temporal stability of the illumination corrections is examined in further detail in Appendix A.

Surveys that use master flats constructed per run are susceptible to systematic trends, such as long period variations in amplifier gain. By contrast, our procedure avoids such effects: science frames were normalized with nightly flat frames and primarily used illumination corrections determined from the same, or at the least extrapolated only from nearby, nights.

3.2 Astrometric Calibration

In order to construct difference images to search for and measure the flux of variable and transient objects, we first imposed a consistent astrometric solution and warped all the science images to a consistent pixel coordinate system. The transformation between the local image pixel coordinate system and the FK5 World Coordinate System is dominated by optical distortions that are well described by a low-order polynomial in radius from the field center. We determined the polynomial terms of the distortion function from images of dense LMC fields using the IRAF task, *msctpeak*. The distortion terms were used in combination with the IRAF task *msccmatch* to derive a WCS solution for each field. The distortion terms were re-computed monthly as they vary over time scales of 6 months. If left uncorrected, this variation would introduce systematic offsets at the $\sim 0.01''$ level.

With the distortion modeled, the astrometric solution for any image with the equatorially mounted 4m reduces to determining the linear rotation matrix with respect to the center. We used the IRAF task *mscmatch* from the *mscred* package to match pixel coordinates for objects in the image to an existing catalog of the field with precise astrometry. We generated an initial astrometric solution for the survey using reference catalogs derived from the Sloan Digital Sky Survey DR7 [1] wherever possible, and defaulting to astrometry from the USNO CCD Astrograph catalog 2 [UCAC, 151] where SDSS coverage was unavailable. As the SDSS is itself tied to the UCAC, and as we only require precise *relative* astrometric calibration to precisely position the PSF and measure flux, errors caused by the differences of the astrometric solution between the two different reference catalogs are negligible. We used this initial solution to generate secondary astrometric catalogs using our multiple observations of each field.

Finally, we used the astrometric solution and the SWarp [9] package to re-sample each image to a common pixel coordinate system using a flux-conserving Lanczos

windowed sinc kernel. We generated weight maps for each image to account for the change in the noise properties produced by re-sampling. Some covariance between pixels is introduced as a result of the re-sampling process and we accounted for it during difference imaging.

3.3 Flux Measurement

We used the DoPHOT photometry package [122] to identify and measure sources within the warped images. Pixel clusters that are significantly above the background were detected, and sorted by brightness. Objects appearing to be stellar were fit with the DoPHOT "Waussian" PSF model:

$$I(z^2) = I_0 \left[1 + z^2 + \frac{1}{4}\beta_4 (z^2)^2 + \frac{1}{6}\beta_6 (z^2)^3\right]^{-1} + I_s \tag{3.1}$$

with

$$z^2 = \frac{1}{2}\left[\frac{(x-x_0)^2}{\sigma_x^2} + 2\sigma_{xy}(x-x_0)(y-y_0) + \frac{(y-y_0)^2}{\sigma_y^2}\right]$$

where (x_0, y_0) are the object centroids, (I_0, I_s) are the peak intensity and sky background, and $\sigma_{(x,y,xy)}$ are the shape parameters determined per image. β_4 and β_6 were set to unity, such that the model is a truncated "wingy" Gaussian power series. DoPHOT is appropriate for point source photometry. Tucker et al. [142, in prep.] will report on photometry of extended sources. The total measured flux reported is the integral of the analytic PSF, φ.

3.4 Photometric Calibration

High-redshift SN Ia surveys typically report observations in their natural photometric system, relating magnitudes to measured flux via:

$$m_{T,i} = -2.5 \log_{10}(\varphi_{ADU,T,i}) + \mathrm{ZP}_{T,i} \tag{3.2}$$

where m is the natural magnitude, φ the measured flux and $ZP_{T,i}$ is the instrumental zero point of the image, i, observed through passband T.

Natural magnitudes have several advantages: they allow surveys to schedule observations in different passbands independently, as the SN Ia colors at every epoch are not needed, and they avoid the additional photometric errors that arise from converting the observed supernova flux to a standard system. These transformations are non-trivial, as the simple linear transformations derived for stars are not directly applicable to SN Ia with their more complex SED. However, as these measurements are reported in a non-standard magnitude system, surveys must establish a network of stellar calibrators in the natural system of the telescope to derive accurate and precise zero points. In addition, an accurate model of the survey throughput in each passband is required so measurements in the natural system can be compared to synthetic fluxes generated from models derived from SN Ia measurements at low-redshift in the standard system.

3.4.1 Improvements in the Photometric Calibration of the CTIO 4 m

The 4-year dataset presented in M07 was calibrated by an auxiliary program to observe Landolt standard fields [denoted with a subscript L 77] and ESSENCE science field stars with the CTIO 0.9 m (hereafter, 0.9m) over 16 photometric nights. The 0.9m measurements were transferred to the natural system of the 4m to establish a set of standard stars in each science field that could be used to derive zero points. Unfortunately, this process introduced several sources of systematic error.

First, the transmission function – mirror reflectivity, passband and quantum efficiency as a function of wavelength – of the 0.9m does not match that on the 4m exactly. This chromatic term is typically described by a simple linear term in color. As the 4m images are considerably deeper than those of the 0.9m, several stars imaged by the 0.9m were saturated in the 4m data. The reduced overlap in magnitudes resulted in several sub-fields having a relatively small number of usable calibration stars in the Landolt $0.3 < (R-I)_L < 0.8$ color range. To compensate for the small number of usable calibration stars, faint red stars (with $(R-I)_L > 0.8$) were included in the calibration. However, over such an extended range in color, the typical and simple linear term in color is insufficient to describe the transformation between the Landolt network and the 4m natural system. M07 also employed synthetic photometry of

spectrophotometric standards in the process of color term determination. The resulting color terms are dependent on the model for the passbands for both the 0.9m and the 4m, and their related uncertainties.

In addition, because the field of view of the 0.9m with the Tek2k camera only covers $\sim$2 amplifiers of MOSAIC II, the photometric calibration had to be transferred between the different amplifiers of the imager, rather than determined independently for each amplifier. The photometric calibration therefore depended on the aperture correction differences between amplifiers and their uncertainties. A custom code to determine the aperture corrections for images was created for M07, but inadequacies in the algorithm used resulted in erroneous values for the aperture correction in several images. This introduced an effectively pseudo-random error into the 3σ-clipped magnitudes for stars.

We detail the improvements to the photometric calibration for the survey in the next sub-sections. We have eliminated any dependence on the 0.9 m data, have developed various metrics to quantify our internal photometric consistency, and verified our zero point consistency using the SDSS.

3.4.2 Aperture Corrections

We have significantly refined the algorithm used to generate aperture corrections for images. For each sub-field, we identified several isolated objects (typically 10–25 per amplifier) with S/N$>$20 that are consistent with a point-source PSF in multiple images. We took care to eliminate instances where we found flux measurements from isolated, but non-stellar objects in the growth curves computed for M07. We measured the flux of each star using aperture radii from 5–40 pixels, accounting for the weight map and any flux lost to masked pixels. We constructed differential growth curves for each image (a representative example is provided in Fig. 3.2). The growth curves of individual stars that indicate contamination by a secondary source (cosmic rays, stray reflections, streaks) were removed. If more than 25% of the stars were clipped, the aperture correction for the image was flagged "bad". We checked that the growth curves asymptotically approached a constant value for all apertures larger than 22 pixels, and flagged those that did not. We measured the total aperture correction to an aperture radius of 25 pixels, or $\sim$13.5″ in diameter, chosen to effectively enclose the total flux for all ESSENCE images, which have a typical FWHM of the PSF of $\sim$1.2″ in

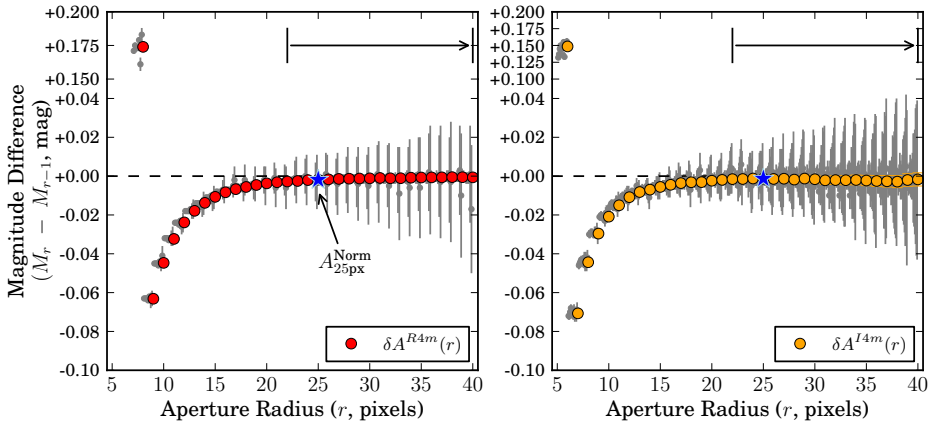

Figure 3.2: Typical differential curves of growth for R (left, red) and I (right, orange) on 20071103, for amplifier 4 (both randomly selected). The smallest point is the difference between the DoPHOT magnitude of the object and magnitude with an aperture radius of 5 pixels. We have used a piecewise y-axis scale to show the full range of the data without compressing local variations. We have plotted the individual isolated stars in grey. We offset each individual star slightly from the aperture through which the flux is measured along the $-x$ direction for clarity. We checked that the growth curve is consistent with a constant for apertures larger than 22 pixels, indicated by vertical lines with an arrow in between. Errors in the average measurement at each aperture, δA, are typically smaller than the plot symbols. We propagated the covariance matrix between apertures to determine the final aperture correction at a radius of 25 pixels (indicated with a blue star, and labeled in the left panel).

both passbands (see Fig. 3.3).

3.4.3 Choice of Standard Star Network and a Fundamental Spectrophotometric Standard

While several standard stellar catalogs exist, and report broadband magnitudes in different photometric systems through a range of passbands [62, 76, 78, 131], the standard star network of Landolt [77] extended by Stetson [132], remains the most obvious choice to tie to the Johnson-Morgan-Cousins photometric system. The R_C and I_C Cousins filters are broadly similar to those used on the 4m (see Fig. 3.4), and the magnitudes reported by low-redshift SN Ia surveys are converted into the Johnson system using observations of the Landolt network stars. This allows us to minimize

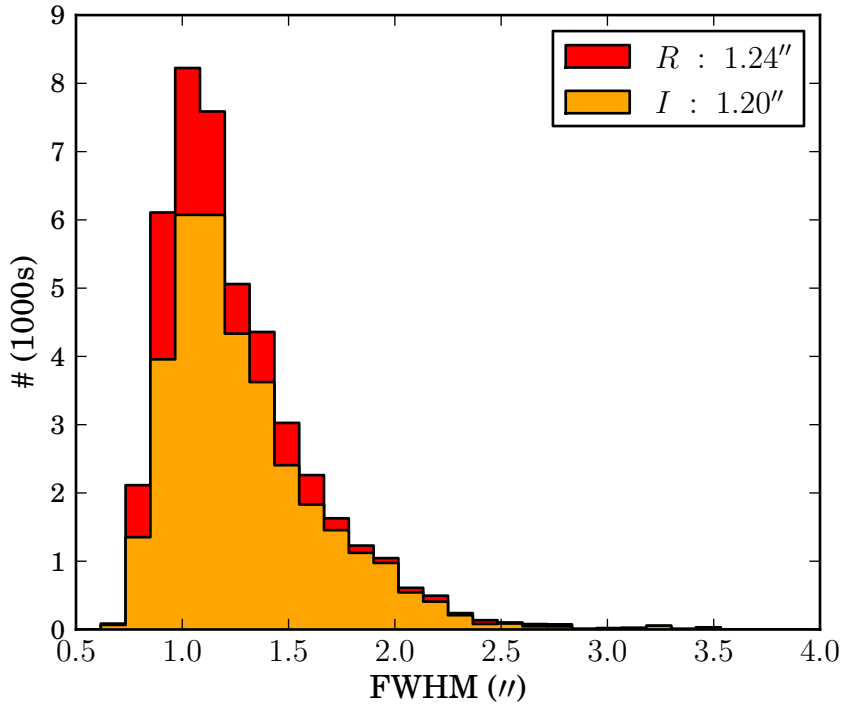

Figure 3.3: FWHM Distribution of R and I science images from the survey. The mean FWHM is 1.24″for the R band and 1.2″for I.

systematic uncertainties when comparing our data to the nearby sample.

The choice of standard star network and the transformation equations derived between the natural and standard system also play a critical role in determining the absolute throughput of each passband. This calibration enables SED models of SN Ia generated from low-redshift observations to be converted into the 4m natural magnitude system via:

$$m_T = -2.5 \log_{10} \left(\int F(\lambda) T(\lambda) \frac{\lambda}{hc} \, \mathrm{d}\lambda \right) + \mathrm{ZP}_T \tag{3.3}$$

This equation is inverted to determine the zero point, ZP_T, for the full optical system (detector, optics, filter, and atmosphere) with dimensionless total photon efficiency, $T(\lambda)$, using a star with a well-measured SED, $F(\lambda)$[1], whose magnitudes, m_T, are known in the natural system – a "fundamental spectrophotometric standard".

Unfortunately, most well measured spectrophotometric standards are too bright to be measured directly by the 4m. We must therefore infer the 4m natural magnitudes of the fundamental standard using the star's standard magnitudes. The most direct way of achieving this is to define the transformation equations such that the Landolt and natural system magnitudes agree at some color.

Historically, the choice for the fundamental standard for SN Ia surveys has been α-Lyr (Vega), either implicitly when the rest-frame SN Ia model is constructed from low-z data, or explicitly, when defining the passband zero points for high-redshift surveys [6, 24, 53, 55, 87]. Vega was one of six A0V stars used to establish the color zero point on the photometric system of Johnson and Morgan [65] by defining the mean $U - B$ and $B - V$ color of the six to be zero, and this definition was further extended to Cousins $R_C - I_C$. Vega's SED was tied to tungsten-ribbon filament lamps and laboratory blackbody sources employed as fundamental standards [97]. With the widespread adoption of the Landolt standard star network to tie instrumental photometry to the Johnson system, the use of Vega as fundamental spectrophotometric

[1]The formalism employed throughout this thesis represents SEDs as power per unit wavelength as a function of wavelength, while the system throughput is represented as a dimensionless photon efficiency. The former is typically provided in ergs s^{-1} cm^{-2} Å^{-1}. If the system throughput is provided in ergs Å^{-1}, then the extra factor of the inverse energy, $\frac{\lambda}{hc}$, must be dropped to removed to account for the Jacobian of the transformation.

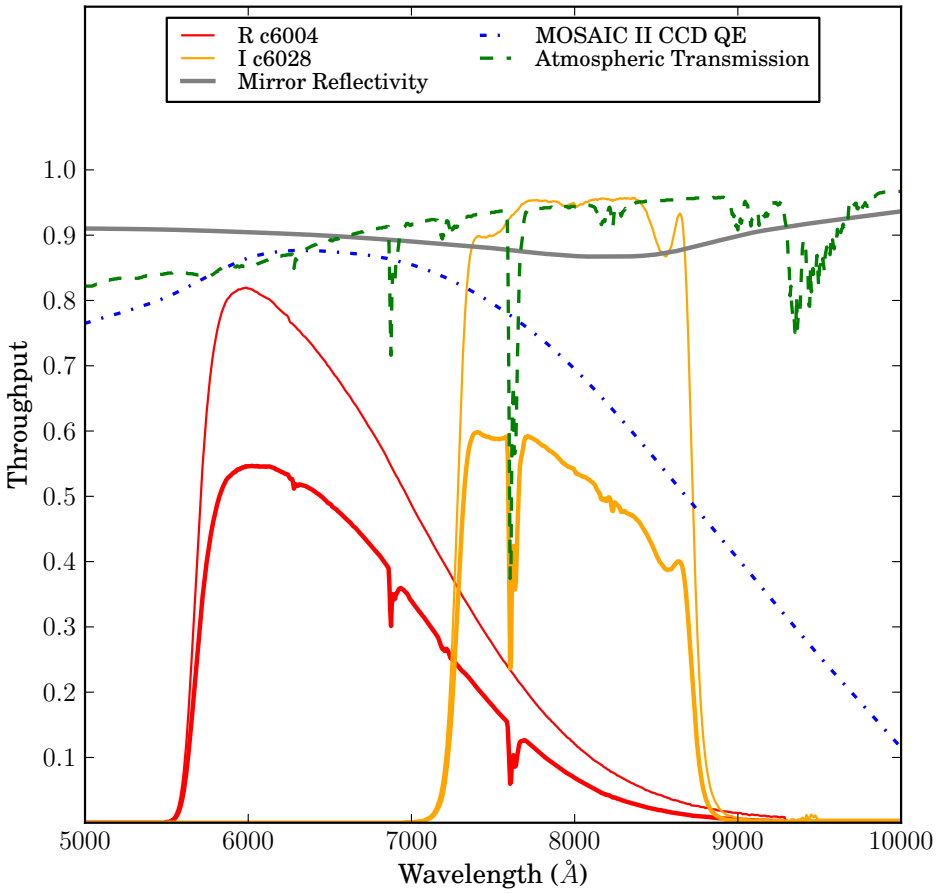

Figure 3.4: Throughput curves for CTIO 4 m R and I passbands (thick red and orange respectively), representing full system throughput including wavelength dependence of CCD quantum efficiency (dot-dashed blue), aluminium reflectance of the mirrors (solid grey) in the 4m telescope, the optical filters (thin red and orange) and a model of the atmosphere (dashed green) generated using the MODTRAN4 code at an airmass of 1 with 2 mm PMW of water vapor at an altitude of 2 km, and a contribution from aerosols, appropriate for the CTIO 4 m site. The measurement of the various components of the system throughput is discussed in §B.1, and the response curves are listed in Table B.2.

standard became ubiquitous.

However, as discussed in Regnault et al. [111], Vega is far from an ideal choice for the fundamental standard. Taylor [138] found that in order for several sources of synthetic and observed Cousins $R_C - I_C$ measurements to agree, the I_C transmission curve had to be shifted to the red by 50 – 100Å. With this shift, the synthetic color of Vega was found to be 0.006 mag. Fukugita et al. [41] report a similar value. Further, the Landolt $(R-I)_L$ color of Vega is significantly more blue than the average for the Landolt standard star network (with $(R-I)_L \sim 0.47$ mag) and consequently, any systematic error in the color term or the Landolt $(R-I)_L$ color of Vega has a much larger systematic effect on the *RI* natural magnitudes than would a standard with a color closer to the average Landolt standard. Vega may exhibit some photometric variability [31]. In addition, its SED is rife with several unusually shaped absorption lines and an excess of NIR emission, as a result of its rapid rotation [102], that may introduce systematic errors when models are used to extend the observed SED of Vega into the UV and IR.

Following several groups including the SDSS [62] and the SNLS [111], we instead select BD+17°4708 as our fundamental spectrophotometric standard. At $(R-I)_L = 0.32$ mag, the color of BD+17°4708 is considerably closer to the average Landolt network star than Vega. The HST CALSPEC program has measured the SED of BD+17°4708 covering 0.17 – 1 μm with an uncertainty of $< 0.5\%$ in the flux calibration derived from the three primary HST WD standards and $\sim 2\%$ in the relative flux calibration over the entire wavelength range.

3.4.4 Transformation Between Landolt Network and the CTIO 4 m Natural System

In order to calibrate the natural system of the 4m, we obtained several images of three Landolt standard fields (L92, L95, Ru149) directly with the 4m/MOSAIC II over 63 nights in 2006 and 2007. The images covered a wide range of airmass and exposure time and the calibration fields were dithered across the entire field of view. With this large dataset, we robustly determined extinction and color terms between the 4m and the Landolt network using the relations

$$
\begin{aligned}
R^{\rm Ins}_{4m} + A_i =& R_L + k_{R_{4m}}(X_i - 1) \\
&+ c^{R_{4m}}_{(R-I)_L}((R-I)_L - 0.32) - Z_i \\
I^{\rm Ins}_{4m} + A_i =& I_L + k_{I_{4m}}(X_i - 1) \\
&+ c^{I_{4m}}_{(R-I)_L}((R-I)_L - 0.32) - Z_i
\end{aligned}
\tag{3.4}
$$

where R and I denote the R and I band magnitudes in the Landolt (L) and CTIO 4 m instrumental $(4m)$ systems, and A, X and Z denote the aperture correction, airmass and zero point of an image, i respectively. These relations are defined such that at the color of BD+17°4708, the calibrated magnitudes of the 4m system match those of Landolt.

We expect differences in the aperture corrections between science and calibration field frames. Images of the calibration fields were generally short exposures ($<$60 s) and often un-guided, while science images are 200 s in R and 400 s in I. We found typical systematic differences of 1–3% between the aperture corrections measured in the calibration fields and the mean aperture correction of all science fields observed on the same nights. The aperture correction differences are correlated with the PSF size and ellipticity measured in the calibration fields. We accounted for these aperture correction differences while extrapolating zero points between images to construct the tertiary photometric catalogs in §3.5.

The average offset between Landolt magnitudes for catalog stars and measured instrumental magnitudes was calculated for each field, fitting for a single linear term in Landolt $0.3 < (R-I)_L < 0.8$ color. As there were insufficient stars covering the full color range in any single image, the weighted mean color term for all calibration field images with at least 20 stars in I and 50 stars in R was computed. Computing the color term image by image allowed us to look for trends in the color-term with time and airmass. While this procedure leads to slightly higher statistical uncertainties than if a single-color term was determined simultaneously for all images, it produces a robust estimate of the color-term, and as shown in §6, the systematic uncertainties in the photometric calibration are dominated by the uncertainty in determining the absolute zero-points.

We found color terms of $c^R_{R-I} = -0.030 \pm 0.001$ and $c^I_{R-I} = 0.022 \pm 0.001$. These

values are in good agreement with measurements by observatory staff[2] for the 4m. The dispersion about the fitted value is ∼2.5% in R and ∼1.5% in I. The value in R is the same as that used in M07, while we find c^I_{R-I} to be slightly lower than that work. We attribute this difference to the different methodology used and the redder color range of stars selected for photometric calibration in the M07 analysis. We found that the color term did not have a very strong dependence on the particular CCD of the MOSAIC camera, and consequently elected to use a single color term for the entire imager, as in M07.

[2] http://www.ctio.noao.edu/mosaic/ZeroPoints.html

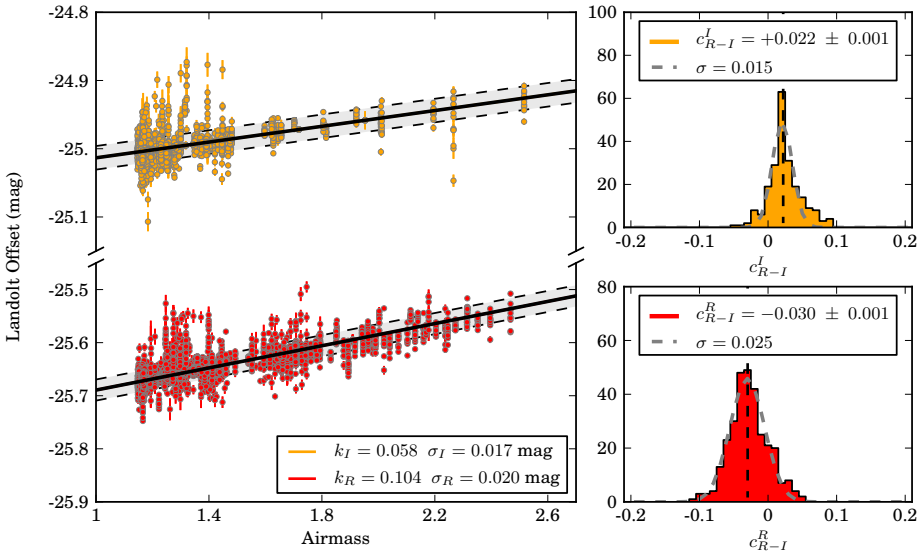

Figure 3.5: (Left) Extinction relation for CTIO 4 m system in R and I using calibration data for three Landolt fields (L92, L95 and Ru149) imaged during the 2006 and 2007 observing seasons. The vertical axis is the difference between instrumental aperture magnitudes, and Landolt catalog magnitudes, corrected for exposure time and variation with Landolt $R-I$ color. We find extinction law slopes of 0.104 mag/airmass and 0.058 mag/airmass in R and I respectively.(Right) Distribution of color terms, determined per-image, to Landolt $R-I$ for the CTIO 4 m system in I (above) and R (below), using calibration data from 2006 – 7. Only images with at least 50 stars in R and at least 20 stars in I were used in the analysis. As there are typically insufficient stars spanning the full color range in any single image, the weighted mean color term for all the images is computed (indicated by dashed vertical lines) and used for all further analysis. We find color terms of $c^{R_{4m}}_{(R-I)_L} = -0.030 \pm 0.001$ and $c^{I_{4m}}_{(R-I)_L} = 0.022 \pm 0.001$.

The offset was re-fit with the color term fixed to this value and the aperture correction was added. Thus, the offset represents the average difference between the Landolt catalog magnitudes and our instrumental magnitudes through a consistent 25 pixel aperture. These aperture-corrected zero points were then regressed against the airmass to determine the slope of the extinction law and intercept.

We found no improvement in allowing the extinction term to vary between survey years. Rather, we found that we could sufficiently account for year-to-year changes in the overall transparency at the CTIO site by decomposing the survey zero point into a dominant constant term with a small night-to-night variation. We measured extinction

law slopes of 0.104 mag/airmass and 0.058 mag/airmass in R and I respectively, with dispersions of $\sim$0.02 mag about the fitted linear relation. The airmass relation and color terms determined are shown in Fig. 3.5.

On extremely non-photometric nights, we found that the non-linear component of the extinction law was non-negligible at even moderate airmass. Such nights are therefore completely excluded from any further analysis. The residual outliers scatter preferentially above the relation, because unidentified thin or intermittent cloud cover on photometric nights increases the effective slope of the extinction law.

3.5 Tertiary Catalogs and Zero Points

Having calibrated the amplifiers within the footprint of the Landolt standard field, we derived an extended standard catalog covering the entire field of view of MOSAIC II. As this catalog was generated by extrapolating the zero point to other amplifiers of the same image, we accounted for the differences in the aperture correction between amplifiers. This procedure prevented any systematic errors arising from either a mis-estimation of the extinction coefficient or short time-scale variations in transparency from affecting the extended standard catalog.

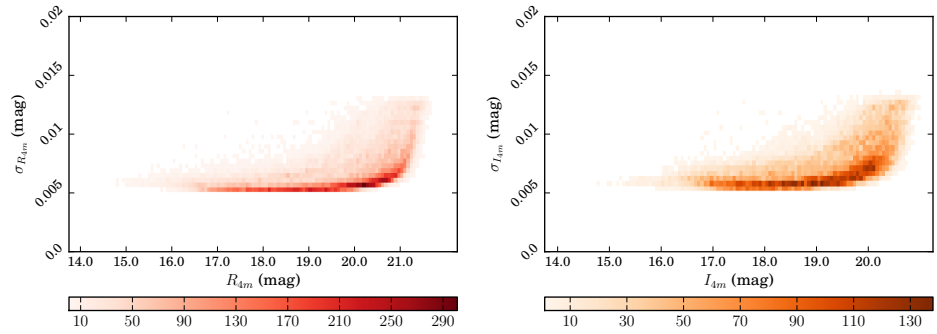

Figure 3.6: Total Uncertainty (statistical + systematic) in the 4 m photometry of ESSENCE reference catalog stars as a function of magnitude for R and I The color of each bin indicates the number of stars in that bin. Individual stars require at least 3 measurements in each filter.

The zero points were then re-determined using the extended catalog, without any additional color correction applied. We extrapolated these zero points to science images on the same nights as the calibration images, adjusting for differences in

exposure time, aperture correction, and airmass. For each star in the science fields, we determined the 3σ-clipped weighted magnitudes to generate our final photometric reference catalog for each field. Stars with a high RMS scatter relative to their mean magnitude were rejected as variable. The resulting catalogs typically have $\sim$30 stars per amplifier, with at least 3 observations in both filters, and a median of 8 observations each in R and 5 in I. A flat 0.4% uncertainty was added in quadrature to all stars, in order to make the average reduced χ^2 unity. The error-magnitude distribution of the reference catalog stars is shown in Fig. 3.6.

These reference catalogs were used to determine zero points for all science images. To examine the temporal stability of the zero points, we adjusted them for differences in aperture correction, airmass and exposure time, but not nightly variations in transparency or variation between different amplifiers. The adjusted zero points of all available amplifiers were averaged together to construct the average adjusted zero point for a given image. In Fig. 3.7, we plot this quantity vs the time since the start of the each year's observing season: the conditions at the 4m remained very stable over the entire duration of the survey. We also constructed the nightly average zero point, and the histogram of residuals to the nightly average zero point is plotted in Fig. 3.8. The residual scatter is $<$ 2% in both R and I.

3.6 Image subtraction

Having established zero points for each science image, we used image subtraction to remove the background light of the host-galaxies. Prior to subtraction, the PSF of each image was first determined from field stars. We used the "High Order Transform Of PSF And Template Subtraction" (HOTPANTS)[3] package to determine the convolution kernel between each image and template pair. For each pair, the image with the narrower PSF was convolved to match the image with the broader PSF. All $N(N-1)/2$ possible pairs of image and reference templates from at least three observing seasons were used to create difference images for each object, following the algorithm of Barris et al. [8]. We used a version of DoPHOT [122], modified to use

[3] http://www.astro.washington.edu/users/becker/hotpants.html

Figure 3.7: Average zero points for images, adjusted for differences in exposure time, aperture correction, and airmass over the full duration of the ESSENCE survey in R (top) and I. In 2002, the I filter (NOAO code c6005) was damaged and replaced. The zero point evolution is correlated in both R and I, and the small time-scale variations correspond to changes in weather conditions at CTIO, whereas the gradual drift in zero points is likely due to the increasing accumulation of dust in the optical system.

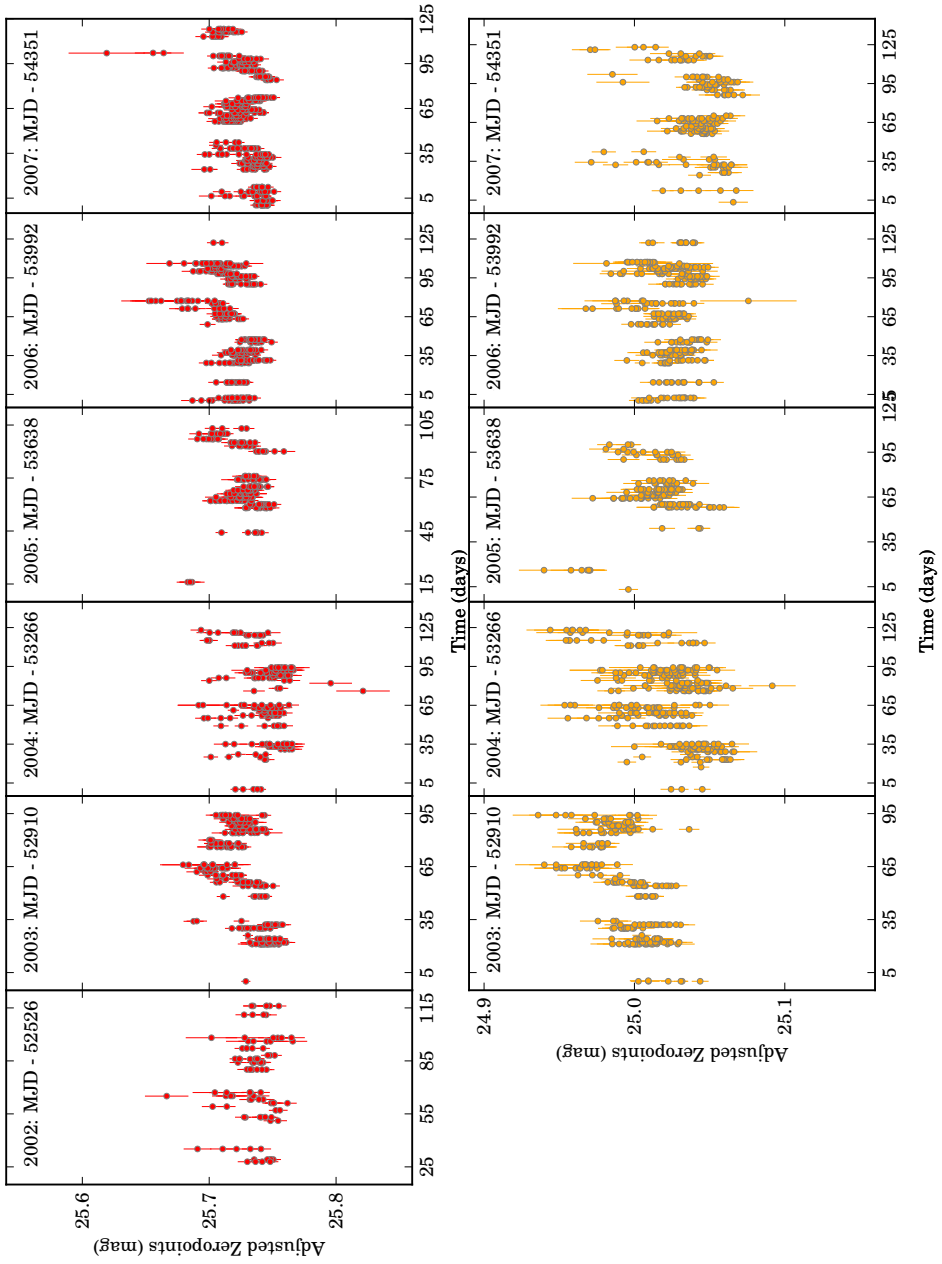

Figure 3.7: (Continued)

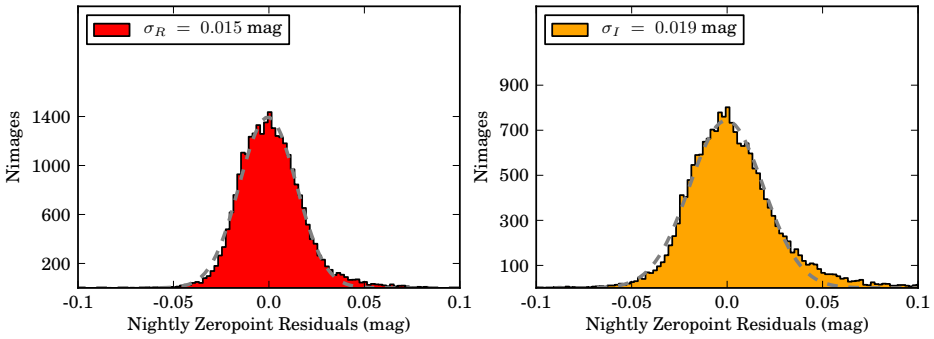

Figure 3.8: Histograms of the residuals of R (Left) and I (Right) zero points to the average nightly zero point, adjusted for differences in exposure time, airmass and the aperture correction. The scatter is $< 2\%$ in both passbands, and very comparable to the values found in M07, illustrating that zero points are very consistent from field to field. The dashed grey lines are Gaussian fits to the data.

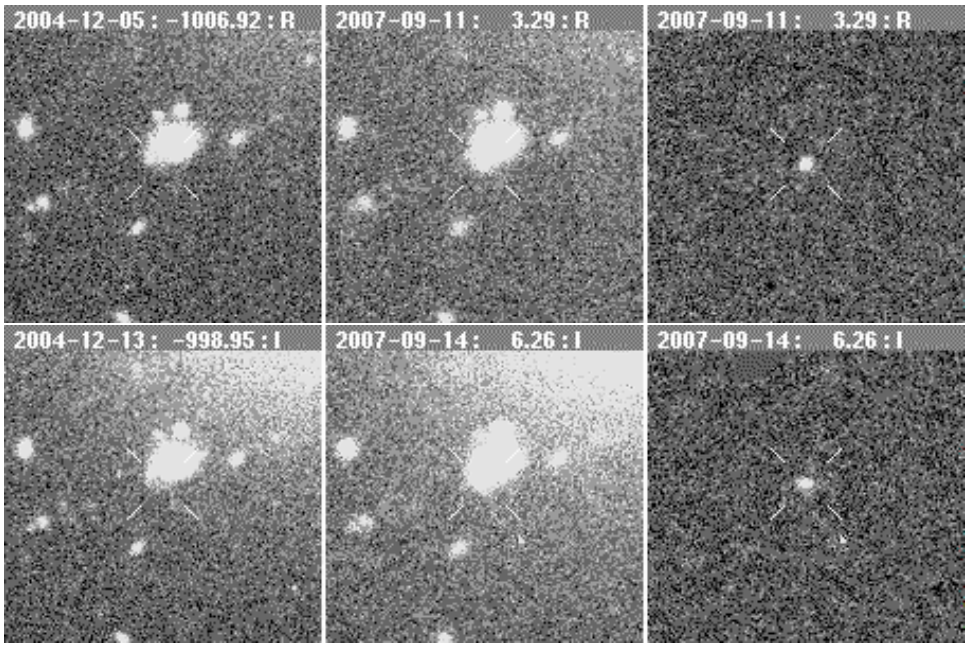

Figure 3.9: Representative difference imaging "postage stamps" in R (Top) and I (Bottom) for *x025*, a SN Ia at $z = 0.35$ near the median redshift of the survey. HOTPANTS convolves the reference (Left) and image (Middle) to produce the difference image (Right). Despite the complex gradient in the background, and clear differences in PSF and depth between the reference and image, the difference image background is extremely uniform, and free of false residuals.

the PSF and flux calibration of the image with the broader PSF, to measure flux in the difference image. The flux calibration of the difference image was adjusted by the normalization of the convolution kernel. The position of the supernova was measured by taking the weighted mean of all detections with a S/N>5. The derived positions are accurate to 0.02″. The flux in each difference image was measured with the PSF centroid fixed to the position of the supernova. A representative example of our image subtractions is provided in Figure 3.9.

As described in M07, the uncertainties in flux in our difference image are underestimated due to pixel-pixel covariance introduced during the re-sampling process. Rather than scale the noise in each image up by a constant factor of 1.2, as in M07, we determined a correction for each individual difference image using flux measurements across the frame. We convolved the PSF on a regular grid across the difference image, measured the standard deviation of the distribution of flux/$\sigma_{\rm flux}$, and scaled each noise image by this factor. This process effectively accounts for the small residual pixel-pixel covariance introduced by distorting each image onto a common astrometric grid, and by the PSF convolution.

Additionally, we constructed a light curve for each object using a single deep reference image, observed in photometric conditions with excellent seeing, to identify any potential problems introduced in processing the thousands of difference images produced by the NN2 process. We found excellent agreement between the fluxes measured in the single template and in the NN2 process, with the uncertainty in the flux being lower in the latter, as is expected by the use of multiple images to measure the galaxy template and sky background at each epoch.

4

Spectroscopy

Cosmological studies with SN Ia rely on constraining the evolution of the scale factor, a, over time. The distance modulus derived from the light curve determines the travel time for photons, and constrains the epoch of the measurement. Measurements of the scale factor rely on spectroscopy: the scale factor is directly related to the measured redshift via:

$$a(t) = \frac{1}{1+z} \tag{4.1}$$

Our spectroscopy program is therefore motivated by the need to discriminate between SN Ia and other variables and explosive transients found during the search, as well as obtaining a precise measurement of the redshift. We tried to follow-up of as many promising candidates as possible, while maximizing the S/N obtained for each object within the time constraints of a classically scheduled follow-up program. Wherever possible, slits were aligned to obtain spectra of the host galaxy of the candidates.

The first two years of spectroscopic data from ESSENCE were presented in

Matheson et al. [85], while M07 detailed our selection criteria and classification algorithms. The spectroscopic observations for the objects included in M07 were presented in Foley et al. [38]. The 6 year spectroscopic sample from the ESSENCE survey, including all the objects in this work, will be presented in [86, in prep.]. As this work employs the determined redshifts of SN Ia in §5, we present a brief summary of the spectroscopic observations, data reduction, and the process of candidate classification and redshift determination.

4.1 Selection Criteria for Imaging Candidates

As discussed in §2, over the 6 years of survey operation, ESSENCE detected thousands of objects exhibiting variability over multiple epochs, at a significance of S/N>5. Given the limited spectroscopic resources for follow-up, it was impossible to obtain spectra of all candidates. We employed various selection criteria to narrow the list of candidates from the imaging search to the subset with the most promise of being SN Ia. The first set of these selection criteria was implemented as software cuts in our search pipeline. We required that:

1. candidates detected in differences images have the same PSF as stellar objects in the source image that was convolved by HOTPANTS.

2. candidates exhibit no significant negative flux ($<$ 30% of the total number of pixels within an aperture of radius 1.5$\times$FWHM around the detection) to select against difference image artifacts, such as dipoles resulting from slight image misalignment.

3. candidates did not exhibit significant variability in ESSENCE data from previous years, to reject variable stars and AGN.

4. candidates in the difference image are not within 1 pixel (0.27″) of objects in the template image, as these are frequently AGN and spectroscopic follow-up of such candidates suffer from excessive host galaxy contamination, making classification very uncertain.

5. candidates exhibit at least two coincident detections with S/N >5, in both passbands or within a 5 night window, to reject moving objects within the solar system.

These selection criteria eliminated most false positives, but the resulting candidate list still contained some spurious detections: subtraction artifacts masquerading as astrophysical sources, and variable objects that had not exhibited sufficient variability in previous ESSENCE data to be excluded. We relied on human inspection to detect and eliminate these unwanted detections. For our final two years of operation, we made improvements to the masking around saturated stars, which in turn reduced subtraction artifacts in the difference images, and considerably decreased the fraction of false positives in our candidate list.

In order to select SN Ia from the resulting list of candidates, we fit preliminary light curves using a *BV* template of a normal SN Ia ($\Delta m_{15} = 1.1$ mag) constructed from well-sampled low-z SN Ia. This template is a good match to SN Ia observed in *RI* at $z \sim 0.4$, typical for the ESSENCE survey. Using χ^2 minimization, we determined the time of *B* maximum, the *RI* magnitudes at maximum, and the light curve stretch, s. These factors allowed us to determine an approximate photometric redshift for the object, which, along with the $R - I$ color, and rise-time information where available, was used to select likely SN Ia. The list of likely SN Ia candidates was passed to team members for spectroscopic observations.

An additional level of selection cuts was imposed by the observers on-site. Observers tended to favor candidates thought to be in elliptical or low surface brightness hosts, as the former are reliably SN Ia, while the latter aid in extraction of a clean spectrum. As the various facilities and instruments have different capabilities, and reach different depths, our faintest objects were preferentially followed up at larger aperture facilities (VLT, Keck). Observing time at some facilities was occasionally lost to thick cloud cover. Prevailing wind conditions at the various facilities occasionally restricted the pointing of the telescopes, and therefore the candidates that could be observed. Occasionally, when follow-up time was available at multiple facilities concurrently or on consecutive nights, lower priority candidates were observed, to maximize the total number of candidates with follow-up.

4.2 Spectroscopic Observations and Reduction

We obtained spectroscopic follow-up of targets to confirm SN types and measure redshifts, using a range of facilities including the Blue Channel spectrograph on the

MMT [126]; IMACS on Baade [27] and LDSS2 [3] and LDSS3[1] on Clay at the Las Campanas Observatory; GMOS on Gemini North and South [57]; FORS1 on the 8 m VLT [5]; and LRIS [98] , ESI [128] and DEIMOS [29] at the W. M. Keck Observatory. A single spectrum was obtained with the 1.5 m Tillinghast and FAST spectrograph [30] at the F. L. Whipple Observatory. We used nod-and shuffle techniques [44] with GMOS and some IMACS observations to improve sky subtraction at red wavelengths.

Spectra were processed and extracted using standard IRAF routines. Except for VLT data, all spectra were extracted using the optimal algorithm of Horne [58]. VLT spectra were extracted using a novel two-channel Richardson-Lucy restoration algorithm developed by Blondin et al. [13] to minimize galaxy contamination in the target spectra. Spectra were wavelength calibrated using calibration-lamp spectra (usually HeNeAr) fit with low-order polynomials, and were flux calibrated using a suite of IRAF and IDL procedures, including the removal of telluric lines using the well-exposed continua of spectrophotometric standards.

4.3 Classification and Redshift Determination

The classification of supernovae is derived from the early-time optical spectra [32] and is critical to their use for cosmological inference. Any contamination of the SN Ia cosmological sample can bias the inference of w dramatically. Supernovae have distinctive broad spectral features (6000–10,000 km s^{-1}) that clearly distinguish them from AGN, galaxies, stars and other astrophysical objects. However, it is essential that we differentiate between the different sub-classes of supernovae as well: Type I supernovae are characterized by the lack of the hydrogen features that are apparent in Type II SNe. SN Ia are further differentiated from SN Ib/c by a strong Si II $\lambda 6355$[2] feature and the absence of any He features. The high-velocity ejecta from the SN causes the Si feature to be blue-shifted to $\sim\lambda 6150$. SN Ib exhibit He I lines and a weaker $\lambda 6355$ absorption, while SN Ic are devoid of He I features and display very weak Si II absorption.

Unfortunately, the spectra obtained by high-redshift SN Ia surveys typically have

[1] http://www.lco.cl/telescopes-information/magellan/instruments/ldss-3/

[2] By convention, the wavelength is reported in Å and units are not explicitly listed following the feature.

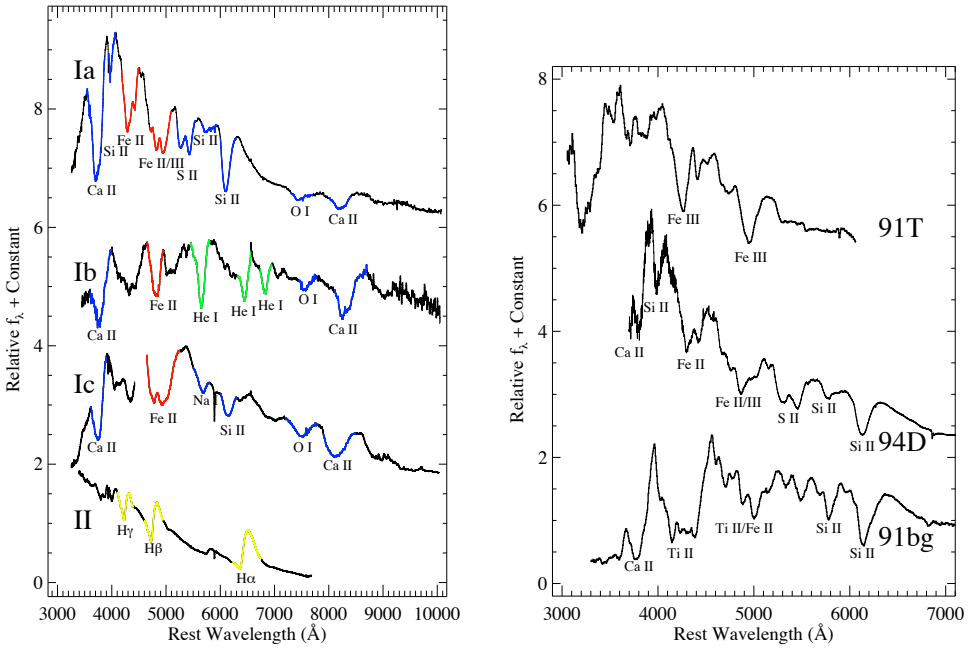

Figure 4.1: (Left) Spectra of different classes of supernovae around *B*-band maximum. The various spectral features that constitute the fingerprint of different classes of supernovae are indicated. (Right) SN Ia spectra exhibit significant diversity, ranging from that of the bright, broad SN 1991T, to the faint SN 1991bg. Various other sub-classes are now known to exist. A Branch-normal SN Ia SN 1994D, is shown for comparison. A version of this figure first appeared in Foley [36]. It has been adapted for use here with the permission of the author.

low S/N, and considerable contamination from the host galaxy. Additionally, above $z\sim$0.4, the distinctive Si II λ6355 feature is redshifted outside the wavelength range accessible by most low-dispersion, high-throughput optical spectrographs. Several other prominent features, such as the Ca II H and K $\lambda\lambda$3934, 3968 doublet, are common to both SN Ia and SN Ib/c. Therefore, the identification of SN Ia depends on various weak blue features shortward of $\sim$5000Å including Si II λ4130, Mg II λ4481, Fe II λ4555, Si III λ4560, Si II λ4816, and Si II λ5051. Several of these features, and the differences between spectra of different classes of supernovae, are illustrated in Figure 4.1. To avoid relying on subjective assessments of noisy data, we employed the SuperNova Identification (SNID) algorithm [12] to determine SN types objectively and reproducibly.

SNID is based on the cross-correlation techniques of Tonry and Davis [139]. The

input spectrum is compared to a large library of template spectra at zero redshift, including nearby SN of all types (Ia, Ib, Ic, II and sub-types such as Ia-pec, 91T, and 91bg), as well as other astrophysical sources such as luminous blue variables (LBVs) and other variable stars, galaxies and AGN. The SNID algorithm has been used to classify, determine the redshift, and constrain the age of all ESSENCE spectra presented in Matheson et al. [85] and Foley et al. [38]. The SNID algorithm fits, and subsequently divides out, a spline to the input spectrum to remove the pseudocontinuum. This process ensures that the correlation is not sensitive to flux scaling, calibration errors and reddening. The input and template library are binned on a common logarithmic wavelength scale, such that a redshift corresponds to a uniform shift in $\log(\lambda)$. The input is then cross-correlated against all the spectra in the template library. The highest peak in the correlation function corresponds to the correlation redshift, $z_{\rm cor}$.

The "goodness" of correlations, $r(\mathrm{lap})$, is measured by the product of the correlation parameter, r, defined as the ratio of the height of the correlation peak to the RMS of the antisymmetric component about z_{cor}, and the overlap in $\log(\lambda)$ ("lap"). Following M07, we only considering correlations with $r(\mathrm{lap}) = r \times \mathrm{lap} \geq 5$ and $\mathrm{lap} = \log(\lambda_1 \,/\, \lambda_0) \geq 0.40$, to ensure that there is sufficient overlap in the wavelength range $[\lambda_0, \lambda_1]$, between input and template, for the correlation parameter to be determined reliably. SNID computes an initial redshift from the $r(\mathrm{lap})$-weighted mean of all correlation redshifts. Wavelength ranges over which the input and template do not overlap at this redshift are masked and the cross-correlation process is repeated. A new $r(\mathrm{lap})$-weighted median redshift, $z_{\rm wmed}$ is computed and templates that do not satisfy the previous criteria, as well as $|z_{\rm wmed} - z_{\rm cor}| < 0.02$ are removed from the cross-correlation. The remaining templates are considered "good". The reported redshift, $z_{\rm SNID}$, and it's uncertainty, σ_z, are the non-weighted median, and standard deviation of all good correlation redshifts respectively.

When the fraction of good correlations that corresponds to a specific class of SNe exceeds 50%, the input is asserted to belong to that class. Where the redshift of the host galaxy is available, we forced SNID to look for correlations at that redshift (± 0.02) to determine SN type. No prior from the host-galaxy redshift is used to derive $z_{\rm SNID}$. Further details on determining subtype and age are provided in Foley et al. [38]. A representative ESSENCE spectrum, and the best-match SNID template from

the classification and redshift-determination process, are illustrated in Figure 4.3.

4.4 Removal of Host-Galaxy Contamination

A small number of objects have spectra that could not be classified by SNID, owing to excessive host galaxy contamination and low S/N. SNID's estimate of the redshift is strongly sensitivity to contamination when input spectra consist of more than 50% galaxy light. Based on the work of Howell et al. [59], we used the *superfit* IDL package to process these spectra, and determine the galaxy fraction and type that best matches the input spectra to low-redshift SN Ia using χ^2 minimization. The output galaxy-subtracted spectrum produced by *superfit* was processed with SNID as above. Foley et al. [38] employed this procedure to classify one additional object with heavily contaminated spectra as SN Ia. We expect that the updates and additions to the SNID spectral library, together with our program to obtain deep GALEX U+$BVRI$ imaging of the host galaxies of ESSENCE objects [142, in prep.] , will allow us to classify a further $\sim$10 objects that are extremely likely to be SN Ia from their well-sampled light curves. We present and fit their light curves in this work, but only use the objects that have been definitively spectroscopically classified as SN Ia as of this writing for further cosmological analysis. While *superfit* does apply an extinction estimate and subtract a template galaxy spectrum from the input spectra, SNID is relatively insensitive to these changes, as it normalizes all spectra to have a flat continuum.

A list of all objects selected for spectroscopic follow-up is provided in Table 4.1. An analysis of the spectroscopic efficiency of the ESSENCE survey was presented in Foley et al. [38]. In Figure 4.2, we demonstrate the correlation between the redshift provided by SNID and the redshift determined from the host galaxy where available. The redshift distribution of all ESSENCE SN Ia is shown in Figure 4.4.

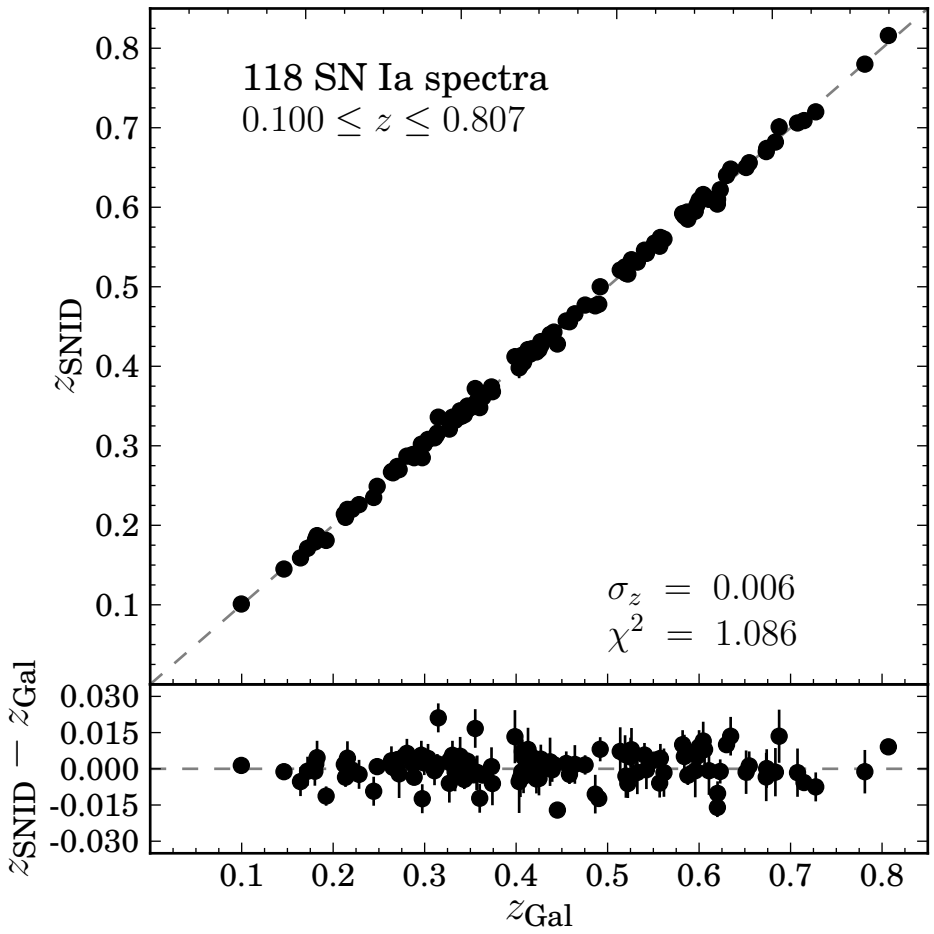

Figure 4.2: Comparison of 118 ESSENCE SN Ia with redshifts determined from cross-correlations with SN Ia spectral templates using SNID ($z_{\rm SNID}$), and from narrow emission and/or absorption features in the host-galaxy spectrum ($z_{\rm Gal}$; upper panel). We show the residuals vs $z_{\rm Gal}$ in the lower panel. The standard deviation σ_z is $\sim$0.006. We have excluded two objects reported in Table 4.1 here: *r317* and *z208*. The galaxy observed together with *r317* has a redshift of $z_{\rm Gal} = 0.3361$, while *r317* has a redshift of $z_{\rm SNID} = 0.736$, and the two are extremely unlikely to be related. Excluding the last object observed by ESSENCE, *z208*, we found a reduced χ^2 of unity. *z208* has a reported host-galaxy redshift of 0.53, while the redshift derived from SNID is only 0.502. The host galaxy was not observed in the unsubtracted images of *z208*, and we have not located a reference for the reported host-galaxy redshift as of this writing.

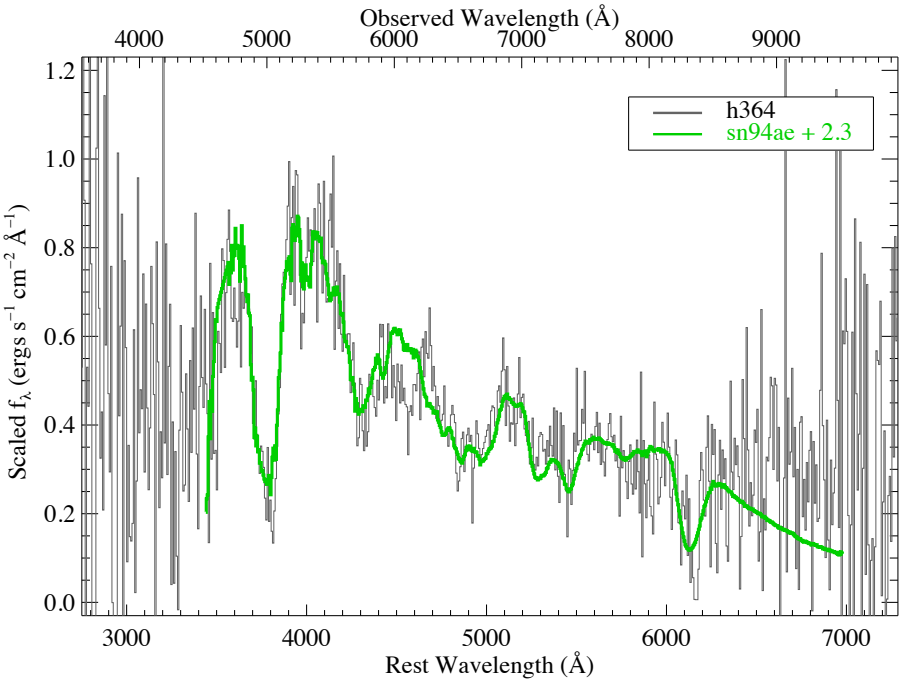

Figure 4.3: The spectrum of ESSENCE object *h364*, with the best-matching SNID template from SN 1994ae overlaid in green. The object is classified as an SN Ia at $z = 0.34$, $\sim$2.3 days past B-band maximum. The difference between the S/N of this object, below the median redshift of the ESSENCE survey, and the high S/N template at low-z, illustrates the challenge in classification and redshift determination for high-z SN Ia surveys. A version of this figure first appeared in Foley [36]. It has been adapted for use here with the permission of the author.

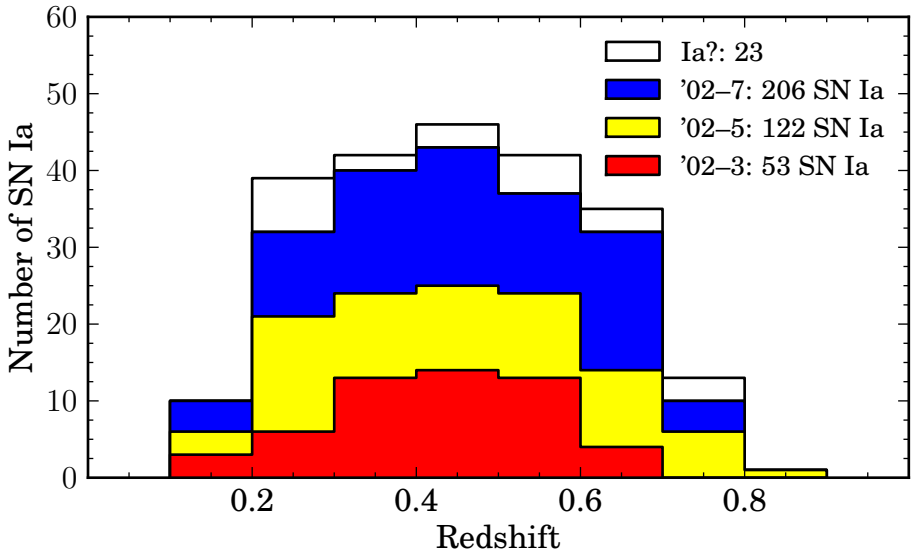

Figure 4.4: The redshift distribution of spectroscopically identified SN Ia from the ESSENCE survey. Candidates which have a high confidence of being of Type Ia (all objects whose SNID correlations with SN Ia templates exceed 50%) are plotted in the shaded region. The histogram is shown for observing seasons spanning 2002–3 (red), 2002–5 (yellow), and 2002–7 (blue), along with *cumulative* totals, to illustrate the evolution of the redshift distribution over the course of the survey. Candidates for which we have less confidence have been classified "Ia?", but have well measured redshifts, typically from a measurement of the host-galaxy spectrum, are shown in the open region.

Table 4.1: Transient Objects considered for follow-up by the ESSENCE survey

ID	IAU	Type[1]	Field	Amp	RA (J2000)	Dec(J2000)	z_{SNID}[2]	$\sigma_{z_{\mathrm{SNID}}}$	z_{GAL}	$\sigma_{z_{\mathrm{GAL}}}$	$MW_{E(B-V)}$[3]
a002	—	Gal	wxc1	4	23:34:48.580	−10:11:02.260	—	—	0.3155	0.0002	0.02469
b001	—	Unk	wxc1	14	23:36:07.860	−10:02:26.660	—	—	—	—	0.02580
b002	—	Star	wxh1	1	00:12:51.140	−10:38:27.050	—	—	−0.0003	0.0002	0.03826
b003	2002iu	Ia	wx06	14	00:13:33.100	−10:13:09.920	0.115	0.005	—	—	0.03980
b004	2002iv	IaT	wx17	6	02:19:16.110	−07:44:06.720	0.226	0.006	0.2283	0.0006	0.02329
b005	2002iw	Gal	wxd1	11	23:43:07.250	−09:48:05.200	—	—	0.2048	0.0003	0.02989
b006	2002ix	II?	waa7	16	23:31:00.863	−09:29:07.205	—	—	—	—	0.02854
b008	2002jq	Ia	wx01	5	23:35:57.960	−10:05:56.880	0.477	0.005	—	—	0.02647
b010	2002iy	Ia	wdd5	7	02:30:40.022	−08:11:40.469	0.594	0.005	0.587	0.0010	0.03252
b013	2002iz	Ia	wdd5	10	02:31:20.745	−08:36:13.414	0.427	0.003	0.4274	0.0005	0.03283
b014	—	Gal	wdd5	15	02:31:11.408	−08:10:53.113	—	—	0.2689	0.0002	0.03390
b015	—	Gal	wcx1	9	23:36:44.070	−10:24:23.300	—	—	0.2070	0.0002	0.02875
b016	2002ja	Ia	waa7	15	23:30:09.685	−09:35:01.809	0.334	0.008	—	—	0.03111
b017	2002jb	Ia	waa7	6	23:29:44.149	−09:36:34.508	0.272	0.006	—	—	0.03442
b019	—	Gal	wxd1	4	23:40:47.490	−09:42:19.340	—	—	0.2129	0.0007	0.03084
b020	2002jr	Ia	wcc9	1	02:04:41.039	−05:09:40.727	0.431	0.004	—	—	0.02485
b022	2002jc	Ia	wcc2	3	02:07:27.285	−03:50:20.744	0.534	0.008	—	—	0.02457
b023	2002js	Ia	wx18	9	02:20:35.390	−09:34:43.900	0.557	0.003	—	—	0.02399
b024	—	Star	wxc1	16	23:36:31.330	−09:55:01.600	—	—	0.0001	0.0002	0.02861
b025	—	Unk	wxa1	5	23:24:11.150	−09:13:20.120	—	—	—	—	0.03153
b027	2002jd	Ia	wx11	16	00:28:38.390	+00:40:29.290	0.316	0.003	—	—	0.02587
c002	—	Unk	wbb6	14	01:10:05.029	+00:16:31.437	—	—	—	—	0.02483
c003	2002jt	Ia	wx06	15	00:13:36.700	−10:08:24.000	0.565	0.006	—	—	0.03682
c005	—	AGN	waa7	10	23:30:54.777	−09:56:47.863	0.248	0.002	—	—	0.02350
c012	2002ju	Ia	wx18	16	02:20:11.000	−09:04:37.500	0.349	0.005	0.3473	0.0001	0.02649
c014	2002jv	Ib	wcc3	3	02:04:34.815	−03:51:57.919	—	—	0.2203	0.0001	0.02400
c015	2002jw	Ia	wdd5	2	02:30:00.539	−08:36:22.561	0.356	0.007	0.3575	0.0006	0.03399
c016	2002jx	Gal	wxm1	4	00:26:54.136	+00:22:49.750	—	—	0.8446	0.0004	0.02350
c020	—	Unk	wxt2	15	02:20:32.124	−07:36:02.690	—	—	—	—	0.02342
c022	—	Ib	wxu2	15	02:21:06.336	−09:06:51.820	—	—	0.2123	0.0003	0.02529
c023	—	Ia	wx11	15	00:28:03.160	+00:37:50.430	0.412	0.011	0.3987	0.0003	0.02295
c024	—	Gal	wdd5	5	02:29:56.521	−08:23:52.283	—	—	0.3174	0.0001	0.03786
c025	—	AGN	waa7	14	23:30:18.309	−09:38:02.438	0.361	0.002	—	—	0.02845

Continued on next page

Table 4.1 (Continued)

ID	IAU	Type	Field	Amp	RA (J2000)	Dec(J2000)	z_{SNID}	$\sigma_{z_{\mathrm{SNID}}}$	z_{GAL}	$\sigma_{z_{\mathrm{GAL}}}$	$MW_{E(B-V)}$
c027	—	Gal	wxm1	4	00:27:56.787	+00:25:19.760	—	—	0.4534	0.0002	0.02240
c028	—	AGN	wxu2	16	02:20:03.304	−09:05:20.990	2.033	0.004	—	—	0.02664
d009	—	Ia	waa6	16	23:25:55.900	−08:56:41.300	0.351	0.002	0.3535	0.0002	0.03752
d010	2003jp	Ic	waa6	16	23:26:03.281	−08:59:22.829	—	—	0.0829	0.0001	0.03668
d029	—	AGN	waa6	13	23:25:11.206	−09:13:38.505	2.584	0.003	—	—	0.03429
d033	2003jo	Ia	waa6	10	23:25:24.047	−09:26:00.659	0.530	0.008	0.5251	0.0003	0.03621
d034	—	AGN	waa7	10	23:30:31.616	−09:56:24.390	2.285	0.007	—	—	0.02421
d051	—	Gal	wcc8	2	02:06:48.703	−05:08:46.023	—	—	0.3817	0.0002	0.02180
d057	2003jk	Unk	wbb6	3	01:08:06.169	+00:02:20.636	—	—	—	—	0.02948
d058	2003jj	Ia	wbb6	3	01:07:58.519	+00:03:01.918	0.589	0.009	0.5839	0.0002	0.02883
d059	—	Gal	wcc5	3	02:06:49.459	−04:26:47.244	—	—	0.2076	0.0002	0.02262
d060	—	Star	wcc7	3	02:09:02.757	−05:03:39.667	0.001	0.003	—	—	0.02159
d062	—	AGN	wcc9	3	02:04:19.323	−05:01:44.661	2.433	0.004	—	—	0.02430
d083	2003jn	IaT	wdd9	12	02:29:21.199	−09:02:15.490	0.330	0.006	—	—	0.02798
d084	2003jm	Ia	wdd9	11	02:28:50.940	−09:09:58.077	0.516	0.006	0.5221	0.0002	0.02516
d085	2003jv	Ia	waa5	16	23:27:58.197	−08:57:11.687	0.401	0.008	0.4047	0.0001	0.03495
d086	2003ju	Ia	waa5	3	23:27:01.704	−09:24:04.573	0.201	0.003	—	—	0.03459
d087	2003jr	Ia	wbb5	4	01:11:06.232	+00:13:44.210	0.337	0.004	0.3400	0.0003	0.02516
d089	2003jl	Ia	wdd6	8	02:28:28.568	−08:08:44.932	0.425	0.005	—	—	0.02997
d091	—	Unk	wcc1	2	02:09:35.211	−03:56:17.327	—	—	—	—	0.02298
d093	2003js	Ia	wdd5	3	02:29:52.152	−08:32:28.155	0.361	0.003	0.3636	0.0001	0.03212
d097	2003jt	Ia	wdd5	10	02:31:54.595	−08:35:48.609	0.430	0.005	—	—	0.03114
d099	2003ji	Ia	wcc2	16	02:07:54.841	−03:28:28.055	0.216	0.003	—	—	0.02456
d100	2003jq	IaP	waa7	16	23:30:51.191	−09:28:34.044	0.158	0.003	—	—	0.02863
d115	—	Unk	wbb6	11	01:09:45.163	+00:02:02.740	—	—	—	—	0.03106
d117	2003jw	Ia	wdd8	16	02:31:06.836	−08:45:36.535	0.301	0.005	0.2968	0.0002	0.02918
d120	—	AGN	wcc1	2	02:09:44.494	−03:57:02.923	1.279	0.005	—	—	0.02299
d123	—	Gal	wcc9	16	02:06:08.565	−04:39:08.710	—	—	0.4995	0.0004	0.02430
d124	—	AGN	wcc9	15	02:06:04.554	−04:41:45.145	0.617	0.023	—	—	0.02348
d149	2003jy	Ia	wcc4	11	02:10:53.987	−04:25:49.436	0.344	0.008	0.3388	0.0002	0.02020
d150	—	Gal	wcc1	12	02:10:12.486	−03:49:09.928	—	—	0.1910	0.0003	0.02450
d156	2003jx	Unk	wcc2	4	02:06:33.398	−03:48:39.117	—	—	—	—	0.02311
e018	—	AGN	wbb7	2	01:13:59.547	+00:32:48.750	0.181	0.001	—	—	0.02879
e020	2003kk	Ia	waa6	9	23:25:36.054	−09:31:44.807	0.159	0.006	0.1643	0.0008	0.03411
e022	2003kj	IIP	wbb7	12	01:14:36.556	+00:23:58.180	—	—	0.0784	0.0001	0.02926

Continued on next page

Table 4.1 (Continued)

ID	IAU	Type	Field	Amp	RA (J2000)	Dec(J2000)	$z_{\rm SNID}$	$\sigma_{z_{\rm SNID}}$	$z_{\rm GAL}$	$\sigma_{z_{\rm GAL}}$	$MW_{E(B-V)}$
e025	—	Gal	wdd3	15	02:29:07.399	−07:36:34.479	—	—	0.1797	0.0002	0.02982
e027	—	Gal	wcc7	16	02:11:09.129	−04:39:19.417	—	—	0.8043	0.0000	0.01969
e029	2003kl	Ia	wbb3	15	01:09:48.798	+01:00:05.496	0.332	0.008	0.3333	0.0009	0.03509
e103	—	Unk	wbb9	2	01:09:32.340	+00:36:43.930	—	—	—	—	0.02437
e106	—	Unk	wbb6	11	01:09:45.163	+00:02:02.740	—	—	0.3219	0.0009	0.03106
e108	2003km	Ia	wdd8	4	02:30:09.001	−09:04:35.621	0.473	0.009	—	—	0.03216
e118	—	AGN	waa5	11	23:27:48.448	−09:22:53.295	0.552	0.007	—	—	0.03665
e119	—	Gal	wbb1	7	01:14:16.912	+01:03:06.427	—	—	0.5584	0.0002	0.03121
e120	—	Gal	waa5	9	23:28:37.492	−09:30:30.569	—	—	0.2974	0.0002	0.03937
e132	2003kn	Ia	wcc1	7	02:09:15.549	−03:35:41.010	0.235	0.006	0.2443	0.0003	0.02585
e133	—	Gal	wcc1	7	02:09:17.662	−03:35:41.255	—	—	0.2450	0.0003	0.02596
e136	2003ko	Ia	wcc1	12	02:11:06.495	−03:47:55.899	0.348	0.006	0.3602	0.0008	0.02329
e138	2003kt	Ia	wdd4	1	02:33:46.992	−08:36:22.141	0.608	0.006	—	—	0.03294
e140	2003kq	IaT	wdd5	15	02:31:04.089	−08:10:56.603	0.614	0.006	0.6060	0.0002	0.03341
e141	—	Ib	wdd7	2	02:32:30.272	−09:05:53.662	—	—	0.0982	0.0001	0.02972
e143	—	Unk	wdd7	3	02:33:11.715	−09:03:32.183	—	—	0.1107	0.0001	0.02632
e147	2003kp	Ia	wdd5	9	02:31:02.652	−08:39:50.909	0.647	0.008	—	—	0.03419
e148	2003kr	Ia	wdd5	10	02:31:20.960	−08:36:14.195	0.431	0.006	0.427	0.0010	0.03281
e149	2003ks	Ia	wdd5	10	02:31:34.528	−08:36:46.462	0.498	0.008	—	—	0.03166
e309	—	Star	waa9	14	23:25:14.230	−09:44:25.810	0.001	0.003	—	—	0.02968
e315	2003ku	Ia	wbb9	3	01:08:36.253	−00:33:20.780	—	—	—	—	0.03573
e418	—	Unk	wcc2	8	02:07:30.851	−03:30:49.497	—	—	—	—	0.02304
e501	—	Unk	waa1	1	23:29:20.159	−08:54:27.836	—	—	—	—	0.03161
e504	—	AGN	waa3	4	23:25:01.338	−08:41:49.753	0.675	0.005	—	—	0.04289
e510	—	Unk	waa1	13	23:30:59.971	−08:37:34.344	—	—	—	—	0.03116
e528	—	Unk	wcc5	3	02:07:37.767	−04:27:06.738	—	—	—	—	0.02129
e529	—	Unk	wcc5	3	02:06:42.954	−04:26:31.293	—	—	—	—	0.02226
e531	2003kv	Ia?	wcc1	4	02:09:42.519	−03:46:48.442	—	—	—	—	0.02288
e604	—	Gal	waa6	8	23:23:51.868	−08:59:17.456	—	—	0.4357	0.0001	0.03519
f001	2003lg	IIP	wbb7	1	01:13:32.675	+00:36:57.310	0.171	0.006	—	—	0.02730
f011	2003lh	Ia	wcc7	12	02:10:19.505	−04:59:32.063	0.544	0.006	—	—	0.02000
f017	—	AGN	wdd9	10	02:28:38.844	−09:11:09.202	0.725	0.004	—	—	0.02542
f041	2003le	Ia	wbb6	8	01:08:08.739	+00:27:09.580	0.560	0.004	—	—	0.02934
f044	—	Ia	wbb8	8	01:11:20.561	+00:04:10.020	—	—	0.4078	0.0003	0.02544
f076	2003lf	Ia	wbb9	1	01:08:49.807	−00:44:13.490	0.408	0.004	—	—	0.03948

Continued on next page

Table 4.1 (Continued)

ID	IAU	Type	Field	Amp	RA (J2000)	Dec(J2000)	$z_{\rm SNID}$	$\sigma_{z_{\rm SNID}}$	$z_{\rm GAL}$	$\sigma_{z_{\rm GAL}}$	$MW_{E(B-V)}$
fo95	—	Gal	wcc2	8	02:06:56.203	−03:31:07.936	—	—	0.3130	0.0008	0.02336
fo96	2003lm	Ia	waa3	3	23:24:25.501	−08:45:50.834	0.413	0.004	0.4080	0.0001	0.04193
f123	—	Ia	wcc1	7	02:09:57.282	−03:32:26.609	0.534	0.009	0.5261	0.0002	0.02410
f213	—	Unk	wbb4	12	01:14:50.770	+00:14:35.919	—	—	—	—	0.03231
f216	2003ll	Ia	wdd4	15	02:35:41.190	−08:06:29.788	0.595	0.011	0.5958	0.0001	0.03288
f221	2003lk	Ia	wcc4	14	02:11:12.817	−04:13:52.110	0.443	0.004	0.4413	0.0003	0.02044
f231	2003ln	Ia	waa1	13	23:30:27.131	−08:35:46.927	0.615	0.003	—	—	0.02860
f235	2003lj	Ia	wbb5	13	01:12:10.034	+00:19:51.267	0.422	0.006	0.4171	0.0006	0.03243
f244	2003li	Ia	wdd3	8	02:27:47.294	−07:33:46.220	0.546	0.005	0.5403	0.0002	0.02690
f247	—	Gal	wbb8	10	01:12:32.219	+00:31:12.730	—	—	0.4306	0.0003	0.03018
f301	—	Ia	wdd6	1	02:27:26.513	−08:42:24.782	0.514	0.011	—	—	0.03007
f304	—	Unk	wdd6	2	02:28:23.108	−08:34:22.780	—	—	—	—	0.03088
f308	—	Ia	wdd6	10	02:29:22.391	−08:37:38.480	0.388	0.010	—	—	0.02955
f401	—	Gal	waa1	1	23:29:40.692	−08:56:37.030	—	—	0.2023	0.0002	0.02929
f441	—	Unk	wbb6	7	01:08:58.453	+00:22:15.570	—	—	—	—	0.02517
g001	2004fi	Ia	waa1	1	23:29:45.348	−08:54:36.347	0.268	0.002	0.2648	0.0002	0.02895
g004	—	Ic	wbb4	14	01:15:06.214	+00:23:38.571	0.143	0.006	—	—	0.02853
g005	2004fh	Ia	waa2	13	23:28:27.197	−08:36:55.071	0.220	0.006	—	—	0.02759
g009	—	Gal	wbb4	13	01:14:28.998	+00:16:56.247	—	—	0.1831	0.0003	0.02991
g014	—	Gal	wbb1	6	01:13:18.202	+00:57:00.728	—	—	0.1949	0.0003	0.02787
g043	2004fj	IIP	wbb6	16	01:09:51.075	+00:27:20.934	0.190	0.002	0.1874	0.0008	0.02529
g046	—	Gal	wcc9	14	02:05:34.300	−04:46:30.968	—	—	0.1833	0.0002	0.02507
g050	2004fn	Ia	waa7	10	23:30:20.114	−09:58:30.698	0.616	0.008	0.6045	0.0003	0.02444
g052	2004fm	Ia	waa8	7	23:26:58.138	−09:37:19.346	0.381	0.007	—	—	0.03110
g053	2004fl	Ia?	waa8	7	23:26:57.910	−09:37:18.984	—	—	0.6329	0.0022	0.03110
g055	2004fk	Ia	wbb7	7	01:13:35.842	−00:09:27.500	0.302	0.006	0.2964	0.0004	0.02823
g097	—	Ia	waa8	16	23:27:37.164	−09:35:21.041	0.339	0.004	0.3434	0.0002	0.03130
g108	2004fp	IIP	wdd8	4	02:29:53.012	−09:01:16.554	0.162	0.004	—	—	0.03378
g120	2004fo	Ia	wbb1	1	01:13:28.975	+00:35:16.179	0.507	0.004	—	—	0.02854
g128	—	II?	waa2	5	23:26:43.669	−08:37:31.458	—	—	0.1642	0.0006	0.02539
g133	—	Ia	wcc4	7	02:09:49.626	−04:10:55.064	0.422	0.003	—	—	0.02434
g142	—	Ia	waa2	11	23:28:37.713	−08:45:03.948	0.398	0.013	0.4033	0.0001	0.02842
g151	2004fq	Ic	waa2	14	23:27:45.638	−08:31:12.785	0.455	0.003	0.1462	0.0004	0.02689
g160	2004fs	Ia	wdd8	15	02:31:19.943	−08:49:21.751	0.507	0.019	—	—	0.02952
g166	2004fr	Gal	wdd9	14	02:28:43.772	−08:54:24.030	—	—	0.2016	0.0007	0.02988

Continued on next page

Table 4.1 (Continued)

ID	IAU	Type	Field	Amp	RA (J2000)	Dec(J2000)	$z_{\rm SNID}$	$\sigma_{z_{\rm SNID}}$	$z_{\rm GAL}$	$\sigma_{z_{\rm GAL}}$	$MW_{E(B-V)}$
g181	—	Unk	wdd9	2	02:28:35.984	−09:13:43.261	—	—	0.5324	0.0002	0.02629
g185	—	II	waa2	1	23:26:56.854	−08:55:12.970	0.345	0.007	—	—	0.03440
g199	2004ft	Gal	wdd4	7	02:33:32.622	−08:09:34.178	—	—	0.7665	0.0002	0.03713
g204	—	Unk	wcc2	13	02:08:26.690	−03:44:44.620	—	—	0.1114	0.0001	0.02356
g213	—	Gal	wbb8	6	01:11:54.176	−00:13:45.690	—	—	0.8423	0.0002	0.02886
g219	—	II?	wbb9	10	01:10:27.165	−00:39:11.615	—	—	—	—	0.03111
g225	—	Ia	waa5	2	23:27:15.685	−09:27:59.728	0.579	0.009	—	—	0.03504
g230	—	Ia	wbb5	3	01:11:56.314	+00:07:27.441	—	—	0.3934	0.0001	0.03077
g240	—	Ia	waa1	14	23:30:41.823	−08:34:10.893	0.696	0.007	—	—	0.02974
g276	—	Gal	wcc1	7	02:09:17.715	−03:35:43.709	—	—	0.2442	0.0002	0.02597
h280	—	II	wbb6	10	01:09:28.330	−00:01:22.880	—	—	0.2633	0.0005	0.03395
h283	2004ha	Ia	wcc9	5	02:04:27.005	−04:52:46.192	0.498	0.008	—	—	0.02678
h293	—	Unk	wcc9	2	02:05:11.580	−05:09:04.692	—	—	0.5462	0.0001	0.02479
h296	—	Gal	wdd6	12	02:28:45.533	−08:27:36.835	—	—	0.0590	0.0003	0.03198
h299	2004hb	Gal	wcc8	15	02:08:09.708	−04:41:51.880	—	—	0.7186	0.0002	0.02098
h300	—	Ia	wdd8	15	02:31:40.680	−08:49:03.377	0.657	0.003	—	—	0.02939
h304	—	Gal	wcc1	2	02:09:10.894	−03:58:00.789	—	—	—	—	0.02352
h311	2004hc	Ia	waa3	4	23:24:32.664	−08:41:03.574	0.752	0.003	—	—	0.04188
h317	—	Gal	wcc8	10	02:08:21.585	−05:05:09.208	—	—	0.6377	0.0001	0.02130
h319	2004hd	Ia	wcc5	11	02:08:48.217	−04:26:10.319	0.478	0.002	0.4903	0.0002	0.02047
h323	2004he	Ia	wdd6	13	02:29:48.797	−08:20:45.875	0.603	0.007	0.5978	0.0003	0.03481
h336	—	Gal	waa3	7	23:24:56.441	−08:28:40.498	—	—	0.3916	0.0005	0.03609
h342	2004hf	Ia	wdd5	9	02:32:00.143	−08:42:23.852	0.421	0.005	—	—	0.02867
h345	2004hg	Unk	wdd4	10	02:34:55.193	−08:30:43.591	—	—	—	—	0.03145
h352	—	Gal	wcc4	13	02:10:48.002	−04:17:54.131	—	—	0.1807	0.0002	0.02172
h353	—	Gal	waa2	15	23:28:14.068	−08:26:54.628	—	—	0.2196	0.0002	0.02513
h359	2004hi	Ia	wcc8	10	02:08:38.835	−05:08:11.825	0.347	0.005	—	—	0.02095
h361	—	Unk	wcc7	13	02:11:14.030	−04:53:40.148	—	—	—	—	0.02149
h363	2004hh	Ia	wcc9	16	02:06:25.028	−04:38:04.035	0.211	0.006	—	—	0.02475
h364	2004hj	Ia	wdd9	16	02:29:41.943	−08:43:49.480	0.344	0.003	—	—	0.03400
k374	—	Gal	wdd9	1	02:27:34.292	−09:17:08.085	—	—	0.1423	0.0004	0.02785
k396	2004hk	Ia?	waa2	5	23:27:04.384	−08:38:45.178	0.271	0.006	—	—	0.02637
k397	—	Unk	wcc1	7	02:09:31.278	−03:34:21.189	—	—	—	—	0.02564
k402	—	Unk	wbb5	12	01:12:54.197	+00:11:25.151	—	—	—	—	0.03139
k411	—	IaP	waa3	10	23:26:11.781	−08:50:17.355	0.562	0.004	—	—	0.03456

Continued on next page

Table 4.1 (Continued)

ID	IAU	Type	Field	Amp	RA (J2000)	Dec(J2000)	z_{SNID}	$\sigma_{z_{\mathrm{SNID}}}$	z_{GAL}	$\sigma_{z_{\mathrm{GAL}}}$	$MW_{E(B-V)}$
k425	2004hl	Ia	wbb7	3	01:13:38.174	−00:27:39.045	0.274	0.003	0.2702	0.0001	0.02922
k426	—	Gal	wdd8	4	02:30:51.203	−09:04:27.406	—	—	0.7572	0.0003	0.02568
k429	2004hm	Ia	wdd3	6	02:28:03.110	−07:42:29.656	0.171	0.006	0.1720	0.0006	0.03060
k430	2004hn	Ia	wbb1	2	01:13:32.382	+00:37:15.455	0.576	0.007	—	—	0.02719
k432	—	Ia	waa2	3	23:26:46.120	−08:45:42.405	0.706	0.010	—	—	0.02786
k437	2004ho	Gal	wcc3	11	02:06:16.041	−03:52:27.803	—	—	0.2878	0.0001	0.02292
k440	—	Unk	wbb4	7	01:14:18.151	+00:29:02.397	—	—	—	—	0.02874
k441	2004hq	Ia	wdd5	5	02:30:18.037	−08:22:25.045	0.669	0.006	—	—	0.04245
k442	—	Unk	wcc3	10	02:06:19.076	−03:58:01.372	—	—	—	—	0.02295
k443	2004hp	Unk	wcc1	4	02:09:35.522	−03:46:23.520	—	—	—	—	0.02244
k444	—	Gal	wdd5	2	02:30:00.763	−08:37:25.930	—	—	0.1921	0.0002	0.03426
k448	2004hr	Ia	wbb6	2	01:08:48.336	+00:00:49.449	0.405	0.007	0.4081	0.0001	0.03243
k453	—	Gal	wdd8	13	02:31:36.957	−08:58:10.962	—	—	0.5418	0.0003	0.02825
k459	—	Unk	wcc7	10	02:10:28.886	−05:07:11.337	—	—	—	—	0.01991
k467	—	Ia?	wdd2	13	02:31:11.801	−07:47:34.124	0.607	0.008	—	—	0.02913
k472	—	Gal	wcc3	15	02:06:29.663	−03:33:08.079	—	—	0.1368	0.0002	0.02320
k485	2004hs	Ia	wcc4	6	02:09:33.689	−04:13:03.931	0.417	0.003	—	—	0.02454
k490	—	Ia	wdd2	4	02:30:24.320	−07:53:20.935	0.709	0.001	0.7147	0.0009	0.03220
k505	—	Gal	wcc3	13	02:06:11.608	−03:44:17.379	—	—	0.2405	0.0001	0.02248
k509	—	Gal	waa5	10	23:28:31.296	−09:25:39.880	—	—	0.2064	0.0001	0.03928
m001	—	Ia	wbb6	1	01:08:22.010	−00:05:46.654	0.290	0.004	—	—	0.03584
m002	—	Gal	waa6	15	23:26:06.272	−09:05:22.919	—	—	0.3545	0.0002	0.03602
m003	—	IIP	wcc9	15	02:05:27.303	−04:42:53.777	—	—	0.2014	0.0003	0.02508
m004	—	Gal	wcc8	8	02:07:12.708	−04:37:27.898	—	—	0.3834	0.0004	0.02205
m006	—	Ib/c?	wdd8	1	02:30:27.266	−09:16:10.189	0.051	0.001	0.0572	0.0002	0.02980
m010	—	Ib	wdd8	9	02:31:46.238	−09:16:25.667	—	—	0.2156	0.0003	0.02735
m011	—	II	wcc5	16	02:08:06.229	−04:03:51.137	—	—	0.2045	0.0003	0.02310
m012	—	Gal	wdd3	16	02:29:13.485	−07:34:07.335	—	—	0.1138	0.0002	0.02954
m014	—	II	wcc5	3	02:07:12.911	−04:26:40.049	—	—	0.1988	0.0001	0.02264
m022	—	Ia	waa1	14	23:30:02.706	−08:33:36.539	0.238	0.004	—	—	0.03070
m025	—	Gal	waa6	11	23:25:11.601	−09:23:41.144	—	—	0.7008	0.0001	0.03662
m026	—	Ia	waa5	12	23:28:39.960	−09:19:49.986	0.656	0.006	0.6548	0.0003	0.03742
m027	—	Ia	wbb6	12	01:09:15.013	+00:08:14.797	0.285	0.003	0.2885	0.0002	0.02834
m028	—	Gal	wcc5	12	02:08:49.544	−04:23:12.189	—	—	0.6075	0.0001	0.02094
m032	—	Ia	waa7	2	23:29:35.343	−09:58:46.304	0.154	0.003	—	—	0.02911

Continued on next page

Table 4.1 (Continued)

ID	IAU	Type	Field	Amp	RA (J2000)	Dec(J2000)	z_{SNID}	$\sigma_{z_{\mathrm{SNID}}}$	z_{GAL}	$\sigma_{z_{\mathrm{GAL}}}$	$MW_{E(B-V)}$
m034	—	Ia	wdd3	2	02:27:50.324	−07:59:11.705	0.562	0.006	0.5577	0.0002	0.03114
m035	—	AGN	waa1	5	23:28:55.967	−08:38:18.364	1.497	0.009	—	—	0.03167
m037	—	Gal	wdd3	10	02:29:03.971	−07:59:43.697	—	—	0.2397	0.0002	0.02607
m038	—	II	wcc9	6	02:05:10.823	−04:47:13.982	—	—	0.0507	0.0004	0.02412
m039	—	Ia	wdd3	6	02:28:04.636	−07:42:44.373	0.249	0.003	0.2481	0.0002	0.03069
m040	—	Ia	wdd3	6	02:27:30.201	−07:41:49.985	0.481	0.003	—	—	0.03237
m041	—	IIP	wcc7	7	02:09:49.784	−04:45:10.513	0.220	0.006	—	—	0.02231
m042	—	Gal	waa6	3	23:24:23.781	−09:22:12.082	—	—	0.1254	0.0001	0.03098
m043	—	Ia	waa1	1	23:29:51.729	−08:56:46.084	0.266	0.003	0.2654	0.0010	0.02926
m057	—	Ia	wcc4	11	02:10:56.774	−04:27:29.962	0.183	0.004	0.1810	0.0002	0.01992
m062	—	Ia	wbb3	10	01:09:52.911	+00:36:19.019	0.316	0.004	0.3139	0.0001	0.02457
m070	—	Ia	wdd4	7	02:33:46.821	−08:08:26.888	0.214	0.003	0.2122	0.0002	0.03753
m075	—	Ia	waa3	7	23:24:42.288	−08:29:08.021	0.101	0.003	0.0996	0.0002	0.03620
m078	—	Gal	wcc2	5	02:07:05.775	−03:41:28.385	—	—	0.3951	0.0005	0.02350
m082	—	Unk	wcc2	4	02:07:13.757	−03:49:12.890	—	—	0.3472	0.0002	0.02425
m087	—	Ia	wdd4	3	02:33:37.004	−08:27:32.462	0.289	0.006	0.2870	0.0003	0.03448
m095	—	AGN	wdd2	3	02:30:26.427	−07:57:27.227	0.992	0.012	—	—	0.03305
m111	—	AGN	wcc7	11	02:10:36.083	−05:00:57.306	1.001	0.004	—	—	0.02014
m135	—	Gal	waa1	2	23:29:32.878	−08:51:20.312	—	—	0.2887	0.0001	0.02885
m138	—	Ia	wbb3	3	01:08:56.340	+00:39:25.350	0.585	0.004	0.5877	0.0001	0.02758
m139	—	IIn	waa3	7	23:23:57.823	−08:27:08.205	—	—	0.2113	0.0001	0.03730
m142	—	Unk	wbb1	12	01:15:17.691	+00:47:17.513	—	—	—	—	0.03129
m158	—	Ia	waa6	3	23:24:03.540	−09:23:18.267	0.461	0.006	—	—	0.03056
m161	—	Gal	wdd9	4	02:28:23.645	−09:03:12.171	—	—	0.2304	0.0001	0.02661
m166	—	AGN	waa1	5	23:29:20.817	−08:36:48.770	0.304	0.002	—	—	0.02623
m193	—	Ia	wdd3	14	02:28:52.199	−07:42:09.763	0.336	0.006	0.3304	0.0002	0.02804
m219	—	Gal	wdd4	5	02:34:28.090	−08:15:19.399	—	—	0.3104	0.0003	0.03676
m226	—	Ia	wcc9	16	02:06:03.688	−04:39:59.080	0.674	0.008	0.6739	0.0013	0.02413
n244	—	Unk	wdd3	7	02:28:11.797	−07:36:29.340	—	—	—	—	0.02938
n246	—	Ia?	wbb7	11	01:14:33.074	−00:26:23.184	0.503	0.005	0.7055	0.0005	0.03047
n255	—	Gal	wcc7	5	02:09:05.303	−04:53:36.615	—	—	0.1369	0.0002	0.02116
n256	—	Ia	wdd3	5	02:28:09.012	−07:47:49.616	0.620	0.007	—	—	0.02975
n258	—	Ia	wcc5	4	02:06:42.346	−04:22:36.982	0.525	0.008	0.5191	0.0002	0.02257
n260	—	AGN	wcc8	2	02:06:36.320	−05:06:45.964	2.013	0.006	—	—	0.02087
n261	—	AGN	wbb7	16	01:14:59.513	−00:05:55.501	3.540	0.040	—	—	0.03026

Continued on next page

Table 4.1 (Continued)

ID	IAU	Type	Field	Amp	RA (J2000)	Dec(J2000)	z_{SNID}	$\sigma_{z_{\mathrm{SNID}}}$	z_{GAL}	$\sigma_{z_{\mathrm{GAL}}}$	$MW_{E(B-V)}$
n263	—	Ia	wcc9	4	02:05:14.946	−04:56:39.087	0.365	0.003	—	—	0.02569
n268	—	Gal	wdd6	15	02:29:19.971	−08:12:02.467	—	—	0.2791	0.0004	0.03090
n271	—	IIP	wbb5	16	01:13:06.506	+00:30:04.835	0.236	0.003	—	—	0.03371
n278	—	Ia	waa5	11	23:28:17.550	−09:23:12.360	0.308	0.006	0.3037	0.0002	0.03983
n284	—	AGN	waa1	8	23:29:38.374	−08:21:32.166	1.990	0.008	—	—	0.02812
n285	—	Ia	waa3	8	23:23:51.357	−08:23:18.503	0.531	0.009	0.5325	0.0001	0.03738
n295	—	AGN	waa3	3	23:24:03.280	−08:44:36.907	1.235	0.007	—	—	0.03854
n312	—	Gal	wdd9	14	02:28:45.104	−08:55:47.232	—	—	0.2860	0.0002	0.02937
n322	—	Ia	wdd9	12	02:29:00.487	−09:02:52.992	0.753	0.006	—	—	0.02713
n326	—	Ia	waa1	10	23:29:58.590	−08:53:12.468	0.267	0.006	0.2637	0.0002	0.02986
n346	—	IIn	waa1	3	23:28:58.301	−08:46:52.839	—	—	0.2661	0.0002	0.02994
n368	—	Ia	waa7	9	23:30:32.013	−10:03:22.140	0.342	0.006	0.3419	0.0002	0.02315
n395	—	Gal	wcc8	7	02:07:32.469	−04:42:10.706	—	—	0.4617	0.0002	0.02208
n400	—	Ia	wbb8	12	01:13:13.258	−00:23:25.853	0.421	0.007	0.4250	0.0001	0.03102
n404	—	Ia	wdd8	14	02:31:31.433	−08:55:11.512	0.211	0.005	—	—	0.02875
n406	—	Ia?	wdd8	16	02:31:19.601	−08:45:09.787	0.7700	0.01	—	—	0.02933
n408	—	Gal	wbb9	16	01:09:49.036	−00:07:42.929	—	—	0.9198	0.0003	0.03468
p415	—	Gal	waa3	16	23:26:02.504	−08:21:10.846	—	—	0.3434	0.0002	0.02900
p425	—	Ia	waa1	14	23:29:56.189	−08:34:24.400	0.456	0.004	0.4583	0.0001	0.03095
p429	—	Ia?	waa3	13	23:26:02.216	−08:35:47.978	—	—	0.5482	0.0002	0.02983
p434	—	Ia	wbb5	12	01:12:40.253	+00:14:56.591	—	—	0.3383	0.0004	0.03441
p444	—	Ia	wcc2	5	02:06:36.165	−03:41:33.614	0.633	0.004	—	—	0.02423
p445	—	Ia	wbb1	4	01:13:14.547	+00:48:47.659	0.816	0.002	0.8069	0.0002	0.02458
p454	—	Ia	wcc2	15	02:08:32.461	−03:33:34.241	0.691	0.008	—	—	0.02282
p455	—	Ia	wcc4	15	02:11:00.014	−04:09:37.601	0.285	0.006	0.2974	0.0002	0.02023
p458	—	Unk	waa3	10	23:25:30.268	−08:52:04.940	—	—	—	—	0.03947
p459	—	Ia	wcc4	10	02:10:20.082	−04:33:13.440	0.702	0.004	—	—	0.02173
p461	—	Gal	waa5	6	23:26:42.317	−09:07:28.646	—	—	0.4075	0.0005	0.03451
p520	—	Ia?	wcc2	12	02:08:09.339	−03:48:04.967	—	—	—	—	0.02298
p521	—	Gal	wcc7	14	02:10:17.525	−04:46:52.214	—	—	0.3053	0.0002	0.02171
p524	—	Ia	wdd8	6	02:30:10.156	−08:52:50.856	0.516	0.004	—	—	0.03528
p527	—	Ia?	wcc2	15	02:08:10.469	−03:32:17.637	—	—	0.4351	0.0002	0.02451
p528	—	Ia	wcc2	8	02:07:04.661	−03:28:04.268	0.780	0.009	0.7812	0.0001	0.02355
p534	—	Ia	wcc3	4	02:04:56.094	−03:49:03.645	0.610	0.005	0.6202	0.0011	0.02438
p535	—	Unk	wcc5	13	02:08:28.123	−04:16:34.893	—	—	—	—	0.02216

Continued on next page

Table 4.1 (Continued)

ID	IAU	Type	Field	Amp	RA (J2000)	Dec(J2000)	z_{SNID}	$\sigma_{z_{\mathrm{SNID}}}$	z_{GAL}	$\sigma_{z_{\mathrm{GAL}}}$	$MW_{E(B-V)}$
q002	—	Ia	wcc3	6	02:05:12.945	−03:39:00.723	0.350	0.003	0.3469	0.0002	0.02326
q006	—	Ia?	wcc1	10	02:10:52.276	−03:57:39.374	0.290	0.010	—	—	0.02208
q007	2006lw	Ia	wcc2	10	02:08:33.670	−03:57:12.888	0.210	0.004	0.2135	0.0002	0.02401
q008	2006ly	Ia?	wdd4	10	02:34:42.381	−08:30:39.885	0.287	0.010	0.2913	0.0002	0.03191
q014	2006lx	Ia	wdd5	8	02:30:10.389	−08:06:54.094	0.270	0.003	0.2693	0.0002	0.03147
q018	—	Ia?	wdd5	14	02:31:39.017	−08:18:05.170	0.270	0.010	—	—	0.03499
q021	—	Ia?	wdd4	7	02:33:43.919	−08:05:50.050	0.360	0.010	—	—	0.03818
q022	—	Ia?	wbb5	9	01:12:03.875	−00:01:29.045	0.226	0.010	—	—	0.03038
q031	—	Gal	wbb6	2	01:08:42.081	−00:00:57.201	—	—	0.2697	0.0002	0.03289
q036	2006lz	II-pec	wdd6	8	02:27:40.742	−08:10:08.182	0.179	0.006	—	—	0.02762
q048	2006ma	Ia	wbb7	11	01:15:11.657	−00:28:03.151	0.440	0.010	0.4371	0.0007	0.03018
q049	2006mc	Ia	wdd8	11	02:32:02.611	−09:07:21.181	0.421	0.005	0.4204	0.0001	0.02963
q054	2006mb	Ia	wdd8	5	02:30:54.298	−08:57:42.078	0.331	0.005	0.3275	0.0003	0.02705
q060	—	IIP	wbb1	11	01:14:48.945	+00:44:47.120	—	—	0.1441	0.0002	0.03191
q061	2006me	Ia	wbb4	11	01:14:47.189	+00:10:13.284	0.302	0.005	0.2996	0.0001	0.03176
q067	2006mf	Ia	wdd2	3	02:30:37.318	−07:57:04.538	0.187	0.007	0.1824	0.0003	0.03380
q069	2006md	Ia?	wbb5	6	01:11:31.492	+00:24:34.163	0.262	0.010	0.2470	0.0004	0.02595
q070	—	Gal	wdd6	6	02:28:04.925	−08:15:40.481	—	—	0.1256	0.0003	0.02960
q075	2006mg	Ia	wdd2	9	02:31:37.750	−08:06:40.098	0.427	0.005	—	—	0.04023
q102	2006mh	Ia?	wbb4	14	01:15:13.398	+00:23:57.312	0.435	0.010	0.4359	0.0008	0.02898
q106	2006mk	Ia	wdd5	1	02:30:16.911	−08:40:47.345	0.477	0.004	0.4754	0.0001	0.03976
q107	2006mj	Ia	wcc1	8	02:09:03.042	−03:28:27.832	0.650	0.009	0.6514	0.0001	0.02406
q108	2006mi	Ia	wcc3	9	02:05:55.040	−04:00:53.216	0.622	0.005	0.6231	0.0001	0.02476
q112	2006ml	Ia	wbb9	3	01:08:43.977	−00:31:36.593	0.637	0.003	—	—	0.03642
q114	2006mm	Ia	wbb6	6	01:08:48.662	+00:17:22.315	0.701	0.011	0.6875	0.0002	0.02730
q125	2006mn	Ia	wbb6	1	01:07:48.392	−00:06:35.454	0.347	0.004	0.3486	0.0004	0.03112
q150	—	Unk	wdd5	16	02:31:18.622	−08:07:11.563	—	—	—	—	0.03639
r184	2006sa	IIP	wcc9	6	02:05:14.944	−04:48:51.685	—	—	0.1609	0.0002	0.02442
r185	—	Ia	wbb8	3	01:11:48.238	−00:29:49.579	0.179	0.006	0.1800	0.0003	0.02423
r186	2006sb	Ia	wcc5	8	02:06:30.312	−04:05:30.553	0.313	0.004	0.3126	0.0001	0.02101
r190	2006sc	Ia	wcc7	15	02:10:10.226	−04:44:12.545	0.355	0.007	0.3568	0.0002	0.02261
r192	—	Gal	wcc9	13	02:05:23.959	−04:52:16.485	—	—	0.6336	0.0001	0.02426
r193	2006sm	Ia	wdd4	2	02:33:29.487	−08:30:11.879	0.609	0.005	—	—	0.03296
r195	2006si	Ia	wcc1	5	02:09:51.320	−03:43:32.520	0.542	0.008	0.5424	0.0001	0.02335
r196	2006sh	IIn	wcc1	5	02:09:11.064	−03:44:42.104	0.260	0.010	0.2639	0.0001	0.02275

Continued on next page

Table 4.1 (Continued)

ID	IAU	Type	Field	Amp	RA (J2000)	Dec(J2000)	z_{SNID}	$\sigma_{z_{\mathrm{SNID}}}$	z_{GAL}	$\sigma_{z_{\mathrm{GAL}}}$	$MW_{E(B-V)}$
r199	2006sl	Ia?	wdd7	6	02:32:15.952	−08:48:34.335	0.410	0.010	0.4180	0.0002	0.02808
r200	2006sd	Ia	wbb1	7	01:14:24.151	+01:02:39.488	0.283	0.007	—	—	0.03124
r204	—	Gal	wcc1	7	02:09:47.393	−03:34:25.676	—	—	0.4212	0.0001	0.02441
r205	—	IIn	wcc1	7	02:09:37.948	−03:31:20.238	—	—	0.0517	0.0004	0.02574
r206	2006se	Ia	wbb4	11	01:14:48.050	+00:06:39.370	0.610	0.010	0.6108	0.0003	0.03126
r207	2006sf	Ia	wcc2	11	02:08:11.658	−03:51:40.230	0.560	0.010	0.5616	0.0006	0.02335
r209	2006sg	Ia	wcc2	12	02:08:13.041	−03:46:21.937	0.428	0.003	0.4451	0.0002	0.02290
r212	2006sj	Ia	wcc1	15	02:10:22.419	−03:33:09.269	—	—	0.6535	0.0004	0.02468
r213	2006sk	Ia	wcc4	16	02:10:33.800	−04:04:03.845	0.321	0.008	0.3270	0.0001	0.02228
r215	—	Unk	wcc7	4	02:08:55.716	−04:59:46.063	—	—	—	—	0.02095
r225	2006sn	Ia	wcc9	13	02:06:18.251	−04:51:33.148	0.415	0.006	0.4149	0.0001	0.02228
r230	2006so	Ia	wdd7	12	02:33:49.152	−08:59:15.768	0.259	0.005	—	—	0.03030
r311	2006sp	Ia	wbb8	3	01:10:55.171	−00:27:52.289	—	—	0.7989	0.0002	0.02510
r314	—	Gal	wcc4	5	02:09:59.003	−04:18:53.926	—	—	0.1092	0.0003	0.02445
r317	—	Ia	wbb1	5	01:13:24.658	+00:51:27.757	0.736	0.005	0.3361	0.0004	0.02550
r318	2006sq	Ia	wcc2	2	02:07:11.267	−03:57:07.942	0.222	0.002	—	—	0.02526
r322	2006tg	Ia	wcc9	8	02:04:14.168	−04:40:18.623	0.521	0.010	0.5138	0.0002	0.02531
r328	2006th	II	waa1	1	23:29:00.954	−08:54:04.953	—	—	0.1463	0.0002	0.03533
r329	—	Gal	wcc2	16	02:07:48.017	−03:29:12.632	—	—	0.6209	0.0001	0.02405
r331	—	Gal	waa1	14	23:30:49.841	−08:32:37.728	—	—	0.4225	0.0003	0.02973
r334	2006ti	II	waa1	3	23:29:13.133	−08:47:57.762	—	—	0.2051	0.0004	0.02897
s340	2006tj	Ia	wbb3	4	01:09:23.284	+00:42:42.313	0.528	0.006	—	—	0.02954
s346	2006tl	Ia	wbb9	1	01:09:17.282	−00:40:27.967	0.270	0.010	0.2721	0.0006	0.03367
s347	2006tk	Ia	wbb6	8	01:07:52.640	+00:27:55.293	0.313	0.003	—	—	0.02954
s349	2006tm	Ia	wbb6	12	01:09:17.297	+00:09:11.389	0.220	0.007	0.2156	0.0002	0.02782
s350	2006to	Ia	wcc2	1	02:07:34.387	−04:00:04.177	0.682	0.010	0.6834	0.0001	0.02453
s351	2006tp	Ia	wcc4	1	02:09:14.040	−04:37:11.970	0.720	0.006	0.7275	0.0002	0.02118
s353	2006tr	Ia?	wdd3	4	02:28:29.532	−07:53:28.493	0.581	0.010	0.5956	0.0002	0.02658
s354	—	Ia?	wcc9	10	02:06:10.482	−05:05:23.000	—	—	0.5588	0.0004	0.02130
s355	2006tn	Ia	wcc9	10	02:05:36.019	−05:08:46.272	0.670	0.010	0.6734	0.0002	0.02461
s362	2006tq	Ib-pec	wcc4	8	02:10:00.697	−04:06:00.903	0.262	0.001	0.2622	0.0001	0.02390
s370	2006tu	Ia	wdd2	2	02:29:56.534	−07:59:50.850	0.439	0.005	0.4394	0.0002	0.03014
s371	—	II?	wbb8	11	01:12:57.431	−00:26:54.525	—	—	0.2499	0.0001	0.02858
s372	—	Ia	wcc2	16	02:08:24.257	−03:27:32.636	0.706	0.010	0.7076	0.0014	0.02480
s373	2006tt	Ia	wcc4	12	02:10:47.935	−04:24:56.952	0.630	0.003	—	—	0.02041

Continued on next page

Table 4.1 (Continued)

ID	IAU	Type	Field	Amp	RA (J2000)	Dec(J2000)	z_{SNID}	$\sigma_{z_{\mathrm{SNID}}}$	z_{GAL}	$\sigma_{z_{\mathrm{GAL}}}$	$MW_{E(B-V)}$
s374	2006tv	Ia?	wdd4	9	02:35:34.225	−08:34:22.069	0.757	0.010	0.7581	0.0002	0.02855
s375	2006ts	IaT	wcc1	15	02:10:18.687	−03:32:26.335	0.551	0.006	0.5569	0.0003	0.02473
s377	2006tw	IaT	wbb6	6	01:08:54.227	+00:17:56.510	—	—	0.3987	0.0005	0.02658
s378	2006tx	SN?	wbb9	11	01:10:26.793	−00:34:07.640	—	—	0.5005	0.0002	0.02851
s379	2006ty	Ia	wbb3	10	01:10:45.361	+00:34:04.408	0.181	0.004	0.1923	0.0001	0.02689
s380	—	Ia	wcc7	2	02:09:00.048	−05:07:41.787	—	—	0.6355	0.0002	0.02096
s383	2006tz	SN?	wcc4	13	02:10:27.034	−04:17:08.159	—	—	0.3920	0.0001	0.02371
x005	2007sz	IIP	wcc8	2	02:07:00.230	−05:06:08.212	0.046	0.005	—	—	0.02235
x016	2007td	IIn	wcc3	5	02:04:26.895	−03:44:18.859	—	—	0.3442	0.0002	0.02666
x017	2007ta	Ia	wbb4	1	01:13:15.801	−00:01:31.428	0.418	0.006	0.4222	0.0004	0.02770
x020	2007te	Ia	wcc1	7	02:09:29.402	−03:35:35.054	0.686	0.008	—	—	0.02540
x022	2007sx	IIP	wbb9	9	01:10:09.249	−00:42:08.035	0.12	0.01	0.1171	0.0004	0.03418
x024	2007sy	II?	wbb1	12	01:15:25.989	+00:49:06.597	0.19	0.01	0.1936	0.0002	0.03165
x025	2007tb	Ia	wbb1	12	01:14:41.252	+00:46:51.824	0.372	0.008	0.3553	0.0001	0.03295
x027	—	Unk	wcc2	12	02:08:15.486	−03:49:35.804	—	—	—	—	0.02259
x028	2007tc	Ia	wbb4	13	01:14:46.894	+00:17:06.778	0.609	0.007	0.600	0.0010	0.03209
x033	2007tf	Ia	wbb6	10	01:09:59.349	−00:01:06.947	0.405	0.007	0.4062	0.0012	0.03114
x034	2007th	Ia	wcc7	11	02:10:57.582	−05:00:24.789	0.508	0.003	—	—	0.02021
x035	—	Gal	wcc9	11	02:05:24.988	−05:03:33.228	—	—	0.4029	0.0002	0.02415
x038	2007tg	Ia	wcc9	15	02:06:10.505	−04:42:23.286	0.512	0.008	—	—	0.02367
x039	—	Ia	wdd3	15	02:29:18.063	−07:39:01.433	0.771	0.004	—	—	0.02975
x055	2007tk	Ia?	wdd5	6	02:30:24.609	−08:17:54.401	—	—	0.3495	0.0002	0.03726
x066	2007tj	Ia	wcc4	14	02:11:04.611	−04:11:50.056	0.331	0.003	0.3286	0.0002	0.02047
x068	—	Gal	wdd5	14	02:31:12.905	−08:18:18.552	—	—	0.4350	0.0002	0.03451
x071	2007ti	Ia	wcc7	16	02:10:09.836	−04:39:49.342	0.476	0.008	0.4865	0.0002	0.02324
x072	—	Gal	wcc8	16	02:08:37.294	−04:37:35.354	—	—	0.1919	0.0001	0.02107
x076	2007tn	II	wdd6	2	02:28:14.790	−08:36:32.198	—	—	—	—	0.03026
x077	2007tp	Ia	wdd8	2	02:30:23.940	−09:13:39.846	0.517	0.009	0.520	0.0010	0.03026
x080	2007tl	Ia	wbb8	6	01:11:04.912	−00:15:43.364	0.374	0.008	0.3731	0.0002	0.02838
x084	—	Gal?	wdd3	12	02:29:20.643	−07:51:00.932	—	—	—	—	0.02666
x085	2007to	Ia	wdd9	12	02:29:42.061	−09:02:05.252	0.648	0.008	0.6345	0.0001	0.03208
x089	2007tm	IaT	wcc3	15	02:06:04.748	−03:32:29.261	0.5	0.05	0.4919	0.0001	0.02307
x093	—	Ia	wdd9	11	02:29:43.134	−09:06:54.931	—	—	0.5004	0.0001	0.03314
x103	—	Ia?	wbb5	4	01:10:48.009	+00:13:36.806	—	—	—	—	0.02585
x107	2007tq	Ia	wdd3	12	02:29:23.345	−07:52:27.686	0.145	0.002	0.1462	0.0009	0.02682

Continued on next page

Table 4.1 (Continued)

ID	IAU	Type	Field	Amp	RA (J2000)	Dec(J2000)	z_{SNID}	$\sigma_{z_{\mathrm{SNID}}}$	z_{GAL}	$\sigma_{z_{\mathrm{GAL}}}$	$MW_{E(B-V)}$
x113	—	II?	wdd4	16	02:34:36.128	−08:01:11.116	—	—	—	—	0.03962
y117	—	Unk	wcc5	16	02:08:14.332	−04:05:09.772	—	—	—	—	0.02299
y118	2007tu	IIP	wbb7	1	01:14:05.219	−00:36:25.629	0.222	0.007	—	—	0.02995
y122	2007tx	Ic	wdd6	2	02:28:33.314	−08:35:25.690	0.674	0.006	0.6764	0.0001	0.03035
y123	—	Gal	wdd7	2	02:32:56.953	−09:08:21.287	—	—	0.1939	0.0007	0.02755
y125	2007tv	Ia	wcc9	3	02:05:13.326	−05:01:42.415	0.310	0.006	0.3108	0.0003	0.02459
y126	—	Gal	wcc9	3	02:04:27.408	−05:01:59.892	—	—	0.7944	0.0002	0.02355
y127	2007ty	Ia	wdd6	5	02:28:34.381	−08:23:49.491	0.518	0.003	—	—	0.03131
y131	2007tw	SN?	wcc9	11	02:05:32.964	−05:02:46.626	—	—	0.6654	0.0001	0.02404
y134	2007ts	Ia	wbb6	8	01:07:58.159	+00:27:48.972	0.336	0.006	0.3149	0.0002	0.02953
y136	2007tz	Ia?	wdd8	8	02:30:07.153	−08:43:09.354	—	0.001	0.5200	0.0010	0.03795
y137	2007tt	Ia	wbb8	6	01:11:20.516	−00:12:19.423	0.368	0.009	0.3741	0.0004	0.02732
y142	2007ud	Ia	wdd8	1	02:30:13.145	−09:15:39.519	0.592	0.006	0.5820	0.0010	0.02938
y143	2007ub	Ia	wcc2	3	02:07:24.132	−03:51:55.226	0.466	0.008	0.4642	0.0003	0.02487
y145	2007ua	Ia	wbb3	10	01:10:31.955	+00:35:49.434	0.555	0.001	0.5514	0.0003	0.02788
y146	—	Unk	wdd6	12	02:29:26.184	−08:27:52.797	—	—	—	—	0.03430
y151	2007uc	Ia?	wcc4	16	02:10:15.529	−04:04:06.465	—	—	0.5837	0.0006	0.02255
y154	2007ug	Ia?	wcc7	5	02:09:36.845	−04:51:52.280	—	—	0.6540	0.0001	0.02246
y155	—	PISN?	wbb6	6	01:07:56.085	+00:17:41.484	—	—	0.7973	0.0000	0.03096
y156	2007ue	Ia	wbb9	7	01:09:09.843	−00:14:01.124	—	—	0.6614	0.0004	0.03364
y158	2007uf	Ia	wcc5	7	02:06:30.881	−04:09:55.047	—	—	0.4856	0.0001	0.02182
y163	2007uh	Ia	wcc3	9	02:06:05.200	−04:01:37.458	0.640	0.003	0.630	0.0010	0.02411
y173	—	Ic?	wdd4	13	02:35:34.821	−08:19:07.016	—	—	0.4078	0.0002	0.03593
y175	2007ui	Ia	wdd4	16	02:34:57.445	−08:03:57.919	0.421	0.009	0.4130	0.0002	0.03688
y177	2007uj	Ia	wdd4	2	02:33:19.036	−08:32:30.217	0.303	0.004	—	—	0.03212
z179	—	Gal	wbb8	4	01:11:21.637	−00:22:45.114	—	—	0.4462	0.0007	0.02664
z180	2007uk	Ia	wbb8	4	01:10:55.006	−00:22:53.197	0.447	0.004	—	—	0.02561
z181	2007ul	Ia	wcc8	7	02:07:16.534	−04:42:23.201	0.604	0.004	0.620	0.0010	0.02248
z183	2007un	Ia	wbb1	8	01:14:22.736	+01:07:45.632	0.287	0.006	0.2806	0.0001	0.03050
z184	2007up	Gal	wcc4	3	02:09:56.068	−04:28:57.352	—	—	0.6116	0.0002	0.02245
z185	2007uv	Ia	wbb4	9	01:15:11.994	−00:02:08.387	0.414	0.005	0.4068	0.0001	0.02924
z187	2007um	Ia	wbb5	13	01:12:29.210	+00:17:01.211	0.293	0.004	—	—	0.03491
z195	—	Unk	wdd9	12	02:29:47.674	−09:01:08.431	—	—	—	—	0.03279
z200	2007uo	Ia	wbb1	13	01:14:43.186	+00:54:27.657	0.457	0.005	0.4548	0.0002	0.03175
z202	2007uq	Ia	wcc3	3	02:04:21.320	−03:54:10.960	0.220	0.005	0.2205	0.0002	0.02510

Continued on next page

Table 4.1 (Continued)

ID	IAU	Type	Field	Amp	RA (J2000)	Dec(J2000)	z_{SNID}	$\sigma_{z_{\mathrm{SNID}}}$	z_{GAL}	$\sigma_{z_{\mathrm{GAL}}}$	$MW_{E(B-V)}$
z203	2007ur	Ia?	wcc2	15	02:08:41.591	−03:34:10.527	—	0.001	0.2500	0.0010	0.02317
z204	2007us	Ia	wdd3	2	02:27:54.863	−08:00:55.479	—	—	0.6201	0.0002	0.03008
z205	2007ut	Ia	wdd8	2	02:30:23.642	−09:12:20.022	0.416	0.020	—	—	0.03042
z208	2007uu	Ia	wbb1	5	01:14:01.011	+00:53:47.598	0.502	0.008	0.5300	0.0010	0.03017

[1]

- Ia = type Ia supernova, no sub-type reported
- IaT = similar to the overluminous type Ia supernovav SN 1991T or SN 1999aa
- IaP = similar to peculiar type Ia supernovae SN 2000cx or SN 2002cx
- Ib = type Ib supernova, no sub-type reported
- Ib-pec = type Ib supernova with peculiar spectral features
- Ic = type Ic supernova, no sub-type reported
- II = type II supernova, no sub-type reported
- IIn = type II supernova with narrow emission lines
- IIP = type II supernova with a "plateau" in the light curve
- II-pec = type II supernova with peculiar spectral features
- Classifications followed by a "?" are not definitively spectroscopically typed
- PISN? = Possible pair-instability supernova (P. Garnavich, private communication)
- Gal = Galaxy, sub-types are reported in Tucker et al. [142]
- AGN = Active Galactic Nucleus
- Unk = Not observed or could not be classified based on spectra.

[2] z_{SNID} and z_{GAL} are reported in the heliocentric frame, and must be converted into the cosmic microwave background (CMB) frame, while accounting for local peculiar velocities at low-z.

[3] For this thesis, we have employed the Milky-Way reddening values from Schlegel et al. [124], rather than the updated values provided by Schlafly et al. [123], to facilitate the combination of our objects with literature samples.

5

SN Ia Light Curves from the ESSENCE Six-Year Sample

Of the 422 objects listed in Table 4.1, 233 are typed SN Ia or "Ia?". We have extracted complete light curves of 213 of these targets. Spectra were obtained for 229 of those 233 objects. 206 objects have been definitively classified as SN Ia. Despite being classified as a SN Ia (IAUC 8251[1]), a redshift from SNID has not been reported for *e315* at the time of this writing, and we do not include it in this total. Of the 20 objects for which photometry was not extracted:

- 8 objects (*b003*, *b004*, *b008*, *b023*, *b027*, *c003*, *c012*, and *c023*) were observed in 2002, in non-standard fields (prefixed with "wx"). These fields do not overlap with the final science fields, and were not observed at the same time as calibration fields. It was not possible to produce a tertiary photometric catalog for these fields using the procedure in §3.5. It may be possible to calibrate these fields using transfer standards from science fields. However, the poor weather

[1] http://www.cbat.eps.harvard.edu/iauc/08200/08251.html

conditions in 2002 caused several gaps in the photometric record of these objects, and they are unlikely to be useful for SN Ia cosmology.

- We were unable to consistently measure the flux of 6 objects. Of those six, 4 objects (*d087*, *f076*, *f221*, and *n368*) are affected by masking of nearby saturated stars, while 2 (*d009* and *h342*) are extremely close to the edges of their respective amplifiers. We expect to be able to recover the photometry of the 4 objects affected by masking by reducing the masking radius for the saturated star near these objects. We have been able to extract some photometry for *h342*. M07 used a custom astrometric projection to extract photometry from difference images of *h342*. As a custom set of procedures has to be employed for these 5 objects, we do not include their photometry in this thesis. We will include their photometry in Narayan et al. [91, in prep.]. Unfortunately, following an inspection of the unwarped science images, we do not expect to be able to extract a light curve for *d009*.

- 2 objects (*e029* and *y156*) were affected by numerous *I*-band difference image failures in the NN2 process, likely due to the fields being observed in poor conditions. Stronger cuts on the images included in the NN2 process should allow us to recover these objects. We have been able to extract an *R*-band light curve for both objects.

- 3 objects (*f044*, *q018* and *q021*) were not initially identified as "Ia?" based on their light curves, and were not included in the database from which our light curves were generated. Nevertheless, these objects were followed up spectroscopically due to a paucity of high-likelihood "Ia?" candidates during the allotted spectroscopic follow-up time. *f044* has been classified as SN Ia. Neither *q018* nor *q021* has been definitively classified as a SN Ia. The author was unaware of these spectroscopic observations until very recently, and was not able to include these objects at the time of this writing. We do not expect any difficulties in extracting photometry for these objects for inclusion in Narayan et al. [91, in prep.].

- As discussed previously, *e315* was reported as an SN Ia in IAUC 8251 (SN 2003ku). We have not located a redshift for this object, and elected not to include it in a photometric sample until its status is clarified.

The final *RI* photometry of the 213 SN Ia and "Ia?" objects presented in this thesis is listed in Table C.1. Only measurements from the year of the event are presented here. Full light curves, including non-SN Ia objects, and measurements of the baseline flux will be made available as machine-readable tables[2] along with Narayan et al. [91, in prep.]. Photometry is presented in linear flux units, φ, in the 4m natural system for each passband, T. Fluxes can be converted to calibrated magnitudes via:

$$m_T = -2.5 \log_{10}(\varphi_T) + 25. \tag{5.1}$$

The system throughput curves and zero points required to derive magnitudes in our passbands from SED models using Equation 3.3 are provided in Appendix B. The ESSENCE SN Ia and "Ia?" light curves are illustrated in Figure 5.7.

Not all of the presented light curves are useful for cosmological studies. Some objects are detected past maximum near the beginning of an observing season, while others do not reach maximum before the end of the observing season. Two objects, *e531* and *p520*, were selected for spectroscopic followup and observed with LDSS3 on Magellan. No significant traces were found in these spectra despite long (3×1800 sec and 3×1200 & 4×1200 sec respectively) integrations. *e531* has a well-sampled light curve consistent with a SN Ia at $z \sim 0.75$. The light curve of *p520* appears to reach maximum before the end of the 2005 observing season, and appears to be consistent with a SN Ia at $z \sim 0.65$. One object, *x103*, has an extremely well-sampled light curve, consistent with a SN Ia at $z \sim 0.28$, but was never observed spectroscopically.

5.1 Extracting Luminosity Distances from Light Curves

The goal of high-z supernova surveys is to derive accurate and precise luminosity distances from SN Ia light curves. SN Ia light curves span a factor of ~ 3 in intrinsic luminosity. However, strong correlations exist between luminosity, light curve shape [103], and rest-frame color (illustrated with the SN Ia light curve templates in Figure 5.1). Light curve fitters exploit these correlations to reduce the dispersion in absolute maximum luminosity to ~ 0.15 mag, enabling the use of SN Ia as standard

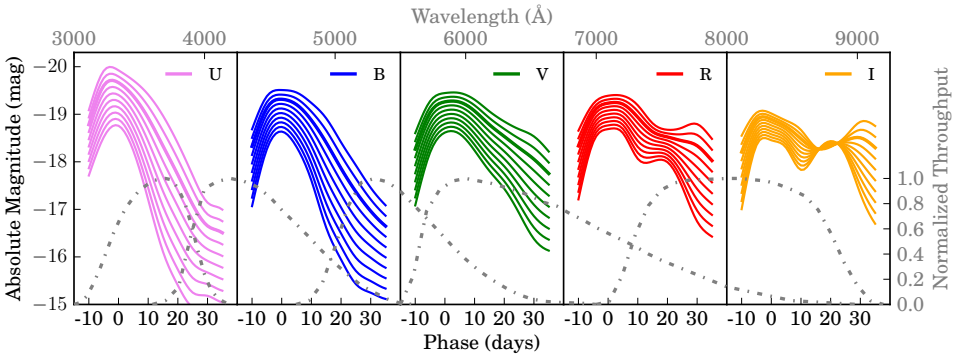

Figure 5.1: Updated *UBVRI* templates for MLCS on nearby SN Ia from LOSS, CfA3, and CSP developed for Narayan and Mandel [90, in prep.]. The thickest colored line corresponds to $\Delta m_{15}(B) = 1.1$ mag. The initial estimates of light curve shape and extinction are critical to successful training. We used all nebular phase data ($B >$ 35 days) to estimate the distribution of intrinsic color and extinction. The models magnitudes are reported through the Bessell passbands (shown as dotted gray lines). Various light curve properties including shape, phase and strength of the secondary *I*-band maximum correlate with peak luminosity.

candles.

Several different algorithms to fit SN Ia optical photometry exist, including *MLCS2k2* [64], *BayeSN* [84], *SALT2* [46, 47], *SiFTO* [22], and *Dm15* [108]. Each of these corrects for the shape and color relations, but they diverge when making two choices: the proper way to train their spectral models and the proper way to account for intrinsic and extrinsic color variation. This divergence results in a dichotomy between a physical model, where color variation is decomposed into an intrinsic variance and a reddening, attributed to extinction due to dust (*MLCS2k2* and *BayeSN*), vs. an empirical model, where all color variation is directly correlated with luminosity (*SALT2* and *SiFTO*). In this thesis, we will focus on *MLCS2k2* and *SALT2* to facilitate a direct comparison with the results presented in WV07. We will include an analysis employing *BayeSN* in the publication based on this thesis [91, in prep.]. *SALT2* and *SiFTO* yield very similar cosmological results when their SED models are trained using the same high-z data, and we do not believe we need to include both here.

We discuss the methodology of both methods, their merits and shortcomings, and the systematics that result from their differences in the following sections.

[2]Available through FAS Research Computing at Harvard - http://telescopes.rc.fas.harvard.edu/index_w.html

5.2 The *MLCS2k2* Methodology

MLCS2k2 is trained exclusively on well-sampled low-z SN Ia *UBVRI* photometry. The model characterizes SN Ia light curve shape variations (intrinsic color variation, rate of decline, and peak brightness) as a quadratic in the shape parameter, Δ - roughly equivalent to the variation in peak visual luminosity. Any other estimate of the light curve shape, for instance the B-band decline rate over 15 days post-maximum, $\Delta m_{15}(B)$, can be used as an initial guess for the shape parameter, and the model is fairly insensitive to this choice.

Color variations are attributed to two factors: an intrinsic Gaussian variance that is not correlated with luminosity, and a strictly positive reddening, attributed to dust in the host galaxy of the supernova. Underluminous SN Ia, similar to SN 1991bg, are included in the *MLCS2k2* training sample make a significant impact on the model colors. The quadratic term in Δ is needed to model the underluminous SN Ia. The impact of this choice is examined further in §5.5. The training procedure exploits the observed linear evolution of rest-frame $B-V$ color $\sim$35 days past B-band maximum [81] to constrain the color excess, $E(B-V)$, in the host galaxy of the supernova. The host-galaxy dust is *assumed* to follow the Milky Way reddening law with $R_V = 3.1$. The templates - the quadratic coefficients of Δ - M_T, P_T, and Q_T are iteratively determined.

The resulting rest-frame model is K-corrected [49, 70, 79, 94] into the observer frame. χ^2 minimization is used to determine the distance modulus, μ, extinction, A_V, and light curve shape, Δ, that best match the observations, m_T, of a SN Ia at heliocentric redshift, z, via:

$$m_T = M_S + P_S\Delta + Q_S\Delta^2 + \mu + \left(a_S + \frac{b_S}{R_V}\right) A_V\tau_S + \mathrm{KC}_{S,T} + \mathrm{GX}_T \qquad (5.2)$$

where τ relates the host-extinction at any phase to the host-extinction at B-band maximum, and the coefficients a_S and b_S relate the host-extinction between the rest-frame passband, S, and the V-band. Note that we have suppressed the explicit time dependence for notational brevity. The K-correction from the rest-frame to the

observer-frame passband, T, $\mathrm{KC}_{S,T}$ is given by:

$$\begin{aligned}\mathrm{KC}_{S,T} =& 2.5\log_{10}(1+z) - 2.5\log_{10}\left(\frac{\int F_S(\lambda)S(\lambda)\lambda\,\mathrm{d}\lambda}{\int F_T(\lambda)T(\lambda)\lambda\,\mathrm{d}\lambda}\right)\\ &+2.5\log_{10}\left(\frac{\int I(\lambda)S(\lambda)\lambda\,\mathrm{d}\lambda}{\int I(\frac{\lambda}{1+z})T(\lambda)\lambda\,\mathrm{d}\lambda}\right)\end{aligned} \tag{5.3}$$

where $F(\lambda)$ is the SED of the fundamental spectrophotometric standard, and $I(\lambda)$ is the SN Ia SED. The Galactic extinction, GX_T, is computed by warping the SN Ia SED with the reddening law of O'Donnell [95] and the Milky-Way $E(B-V)$ from the dust maps of Schlegel et al. [124], and computing the difference in synthetic photometry between the reddened and un-extincted SED.

MLCS2k2 is therefore properly thought of as a distance estimator, rather than a light curve fitter. This forward-modeling approach does not require extremely well-sampled data (in color, or time), as compared to light curve fitters that attempt to correct observations into the supernova rest-frame. The shape of the observer-frame model is much more tightly constrained than models that warp spectral sequences to match observed photometry, as the warping function (typically a smooth polynomial) often cannot match the complex and rapid variation in light curve shape, particularly in the rest-frame I-band post-maximum. *MLCS2k2* allows physically motivated priors on parameters to be incorporated naturally. Attributing color variations to extinction due to dust is well-justified by observations, as there are numerous examples of SN Ia being clearly extincted by dust, from photometric observations, spectroscopy and studies of SN Ia remnants.

Nevertheless, as the explosion mechanisms of SN Ia certainly involve more than a single parameter (composition of the progenitor, ignition conditions, flame properties etc.), it is possible that some properties of the SN Ia impact the colors, beyond the simple Gaussian variation that is addressed by Δ. Further, if the color variation is not entirely due to dust, the application of a strictly positive prior on the extinction can introduce a systematic error with redshift, and a bias in cosmological inference. As the model is based on photometric observations in discrete passbands, rather than a continuous spectral sequence, the observer frame model exhibits discontinuities at specific redshifts, where the mapping between the observer-frame and rest-frame passbands changes.

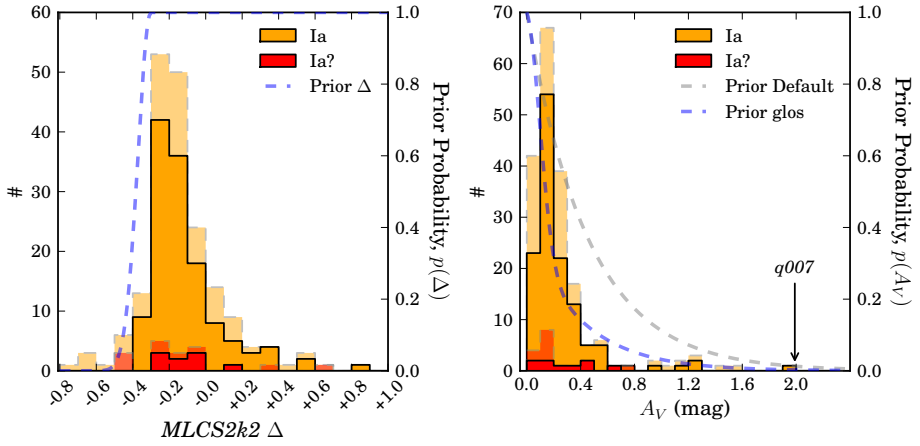

Figure 5.2: The light curve shape, Δ (left panel), and extinction, A_V (right panel), distributions estimated by *MLCS2k2* for ESSENCE SN Ia (orange) and "Ia?" (red) objects.

Objects that pass the selection cuts (excepting the cuts on the parameter being plotted itself) imposed in WV07 are indicated in the solid regions, while objects that fail are shown in the light regions bounded by dashed lines. The *MLCS2k2* priors employed in the light curve fitting are shown as dashed blue lines. The "default" prior is the extinction distribution derived from low-z SN Ia during the training procedure. Objects with $\Delta > 1.0$ are underluminous relative to normal-SN Ia, and are more rare. Consequently, we are extremely unlikely to find any at the redshifts probed by the ESSENCE survey. Objects that appear to be extremely overluminous (very negative values of Δ) relative to the training sample of Jha et al. [64] typically have little or no high-significance flux measurements pre-maximum, but have well measured declines post-maximum. Without a good constraint on the peak and time of maximum, light curve fitters typically explore unphysical regions of parameter space. The χ^2/DoF of these light curve fits is often relatively high (> 3) and all fail the quality cuts of WV07, either due to a high χ^2/DoF or because of insufficient observations pre-maximum.

The A_V distribution for ESSENCE SN Ia is consistent with the "glos" model discussed in §5.5. The distribution is significantly narrower than the *MLCS2k2* "default" distribution, derived from nearby-SN Ia, as we are unlikely to find highly extincted and therefore faint objects, at high-z. As *MLCS2k2* is a magnitude based fitter, it rejects measurements with S/N <5. Most of the objects that fail the selection cuts in the right panel are extremely faint or at high-z.

We employ "v007" of *MLCS2k2* with the "tweaked-slowz" vectors. These vectors, and the corresponding matrix of model uncertainties (denoted S), are trained using the low-z Hubble-flow sample in Jha et al. [64] (hence "slowz") and "tweaked" with small magnitude offsets (typically < 0.005 mag) to match the color-extinction distribution zero point, and extended to -20 days prior to B-band maximum. We follow WV07 in using the "glosz" prior on extinction, and assume $R_V = 3.1$. The choice of prior is discussed further in §5.5. This implementation of *MLCS2k2* fits light curves provided in magnitudes, and rejects all data with S/N< 5. Unfortunately, this does not make use of the information in the baseline flux measurements, which help constrain the epoch of maximum and decline rate. Additionally, while all the light curves are fit, not all the fits are reliable, as several objects lack high significance measurements of flux pre or post-maximum, and these typically exhibit high χ^2/DoF. Further, objects in Table 4.1 without determined redshifts are not fit.

The *MLCS2k2* light curve shape, Δ, and extinction, A_V, distributions for ESSENCE SN Ia and "Ia?" objects are shown in Figure 5.2. The *MLCS2k2* light curve fit parameters for the ESSENCE sample are provided in Table C.2. Additionally, we have indicated if the objects pass the light curve quality cuts used by WV07 for the 4 year sample. 126 of our spectroscopically confirmed SN Ia pass these cuts and are useful for cosmological inference. This doubles the 4 year sample of 60 SN Ia.

With the recovery of $\sim$11 additional objects discussed at the beginning of this chapter, whose light curves have not been reported in this work, we expect that our final sample will consist of $\sim$140 spectroscopically confirmed SN Ia, as additionally, it is very likely that a few "Ia?" objects will be definitively classified as SN Ia by the ongoing work by Matheson et al. [86, in prep.]. The quality cuts we have imposed are preliminary, and are conservative compared to those imposed by C11.

Note that Figure 5.2 shows the distribution for all recovered fits, and several of these objects do not have light curve fits that meet the quality cuts of WV07. Quality cuts are imposed to select spectroscopically confirmed SN Ia, with several high S/N measurements over rest-frame phase $-5 \leq \Phi \leq 20$ days, to ensure that the derived distance moduli are unbiased, whereas derived light curve shape and extinction are generally less susceptible to poor phase coverage.

Unfortunately, *MLCS2k2* has not been updated to make use of the latest re-calibration of the SNLS 3 year and SDSS Supernova Survey data. In particular, the transmission of the 3.6 m Canada-France-Hawai'i Telescope (CFHT) and Megacam

imager used by the SNLS is a strong function of focal plane position, while our implementation of *MLCS2k2* generates *K*-correction lookup tables using the overall transmission properties of the survey. While it was possible to modify the light curve fitter to employ SN-by-SN system response curves, the resulting output was not compatible with various codes we had developed to process the results, and we leave the further development of *MLCS2k2* to independent parallel efforts elsewhere.

5.3 The *SALT2* Methodology

The *SALT2* methodology differs significantly from that of *MLCS2k2*. The model is developed from a combination of SN Ia photometry as well as hundreds of SN Ia spectra, including objects at high-z, to constrain the color evolution with time. The model is characterized by three parameters: x_0, x_1, and c. The x_0 parameter is directly related to the B-band magnitude at maximum; x_1 can be considered the numerical factor by which the time-scale of a fiducial B-band light curve needs to be "stretched" to match the observations; and the color variations are quantified by c. Two-dimensional surfaces in time and wavelength are constructed from the training sample. The spectral surfaces describe the evolution of the rest-frame SN Ia SED with a temporal and spectral resolution of 1 day and 10 Å respectively. The rest-frame flux is given by:

$$F_{\mathrm{Rest}}(t,\lambda) = \int x_0 \left(M_0(t,\lambda) + x_1 \times M_1(t,\lambda)\right) \exp[c \times \mathrm{CL}(\lambda)]\, \mathrm{d}\lambda \qquad (5.4)$$

The spectral surfaces, M_0 and M_1, contain information about the standard template at various phases, and the variability in the correlation of luminosity with stretch and color. The color law, CL, describes the variation in intrinsic color. If the color variation was entirely modeled by dust, as with *MLCS2k2*, this would be well approximated by a CCM89 law. The observer-frame model is constructed by redshifting the rest-frame spectral sequence, applying Galactic extinction, and determining the synthetic flux in the observer frame passbands.

SALT2 does not directly produce estimates of the distance modulus; these are determined simultaneously for all SN Ia via:

$$\mu_B = m_B - \mathcal{M} + \alpha x_1 - \beta c \qquad (5.5)$$

with

$$m_B = -2.5 \log_{10} \int x_0 M_0(t, \lambda) T_B(\lambda)\, d\lambda \tag{5.6}$$

We define $\mathcal{M}$ as:

$$\mathcal{M} = M + 5log_{10}\left(\frac{c_\gamma}{h_0}\right) + 15 \tag{5.7}$$

where c_γ is the speed of light. $\mathcal{M}$ can be treated as a nuisance parameter when deriving cosmological constraints.

The advantage of the *SALT2* approach is that the model does not require explicit computation of cross-passband *K*-corrections, and is continuous with redshift. The model naturally keeps track of the correlations between light curve shape, colors and spectral properties in the fitting process, although the *SALT2* model covariance matrix does not incorporate correlations between different epochs and wavelengths at present. The model's formulation is general enough to treat the color parameter, *c*, as *either* extinction due to dust (where the color law, CL, is interpreted as a CCM89 relation, and β is identified as R_B), or as an intrinsic variation in SN Ia color. If the color is treated as intrinsic variation, and β is determined together with the cosmology, then values ranging from 2 to 3 are found, systematically lower than $R_B = 4.1$. Additionally, the color variation law can be derived directly from the SN Ia data, and differs from the CCM89 relation in the NUV and *U*-band, even for extreme values of R_B [46].

However, it is not possible for surveys to add additional information through priors, as all the distances to SN Ia are determined simultaneously in the *SALT2* methodology. The color relation, parameterized by β, is expected to be constant with redshift if it describes intrinsic color variation. However, Kessler et al. [68, hereafter K09] and Scolnic et al. [127, in prep.], have found significant non-monotonic evolution with redshift, as well as variation based on the choice of SN Ia samples included or excluded in the cosmological fit. This indicates that the value of β is not entirely determined by SN Ia color variation, and is subject to various non-astrophysical considerations. The inclusion of high-z data in the training can potentially bias the distance determination at low-z by incorporating subtle SN Ia evolutionary effects, and makes *SALT2* an inappropriate tool with which to study such effects using SN Ia photometry.

We employ version 2.2.0b of *SALT2* released together with Guy et al. [47, hereafter

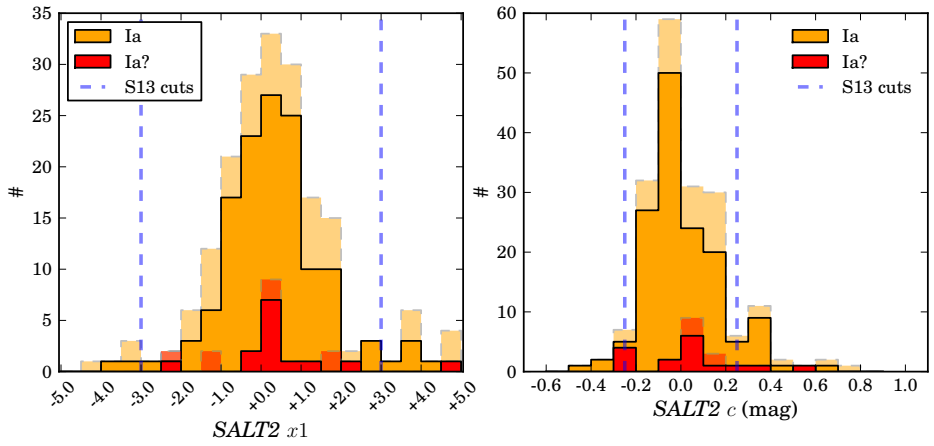

Figure 5.3: The light curve shape, x_1 (left panel), and color, c (right panel), distributions estimated by *SALT2* for ESSENCE SN Ia (orange) and "Ia?" (red) objects. Objects that pass the original *SALT* selection cuts (excepting the cuts on the parameter being plotted itself) imposed in WV07 are indicated in the solid regions, while objects that fail are shown in the light regions bounded by dashed lines. Only the WV07 cuts relating to the sampling and χ^2/DoF of the fit are used here. Based on a visual inspection of all the light curve fits, we required that the fits used at least 8 epochs, rather than the weaker cut of at least 5 epochs employed for *SALT* in WV07. We employ the same cuts as Conley et al. [23] and Scolnic et al. [127, in prep.] on c and x_1 respectively.
Objects with $x_1 < -3.0$ and $x_1 > 3.0$ are poorly represented in the *SALT2* training sample. Fits with these values often have unconstrained rises or peaks, and provide unreliable distance estimates.
Conley et al. [23] required that $-0.25 < c < 0.25$ mag to eliminate blue objects that were not adequately represented in the training sample, as well as objects with very red colors, which they believe are the result of a combination of different effects. It is possible that extinction in the host-galaxy in the SN Ia is one of these effects. Three objects *m040*, *m070* and *m075*, are catastrophic outliers and are not displayed here. All three were discovered near the start of the 2005 observing season, and none have any pre-maximum photometry.

G10][3]. *SALT2* is a flux-based fitter and employs measurements of the baseline flux to restrict the search range for fitted parameters. However, only data within the rest-frame phase range $-15 < \Phi < 45$ days is used in the χ^2 minimization. Measurements in observer-frame filters that map to to the rest-frame wavelength range $3000 < \lambda < 7000$ Å are used in the fit. Model and *K*-correction uncertainties are propagated into the error matrix, and an additional *U*-band calibration uncertainty of 0.1 mag is added in quadrature for low-z NUV data.

An alternate implementation is provided in v10.27b of the SNANA package [69][4]. While the two versions provide the same results to within machine precision, the SNANA version is more easily modified to output the full *SALT2* weight matrix for each fit, and allows detailed Monte-Carlo tests using simulated *SALT2* light curves. We are in the process of modifying our codes to use the SNANA implementation.

The *SALT2* light curve shape, x_1, and color, c, distributions for ESSENCE SN Ia and "Ia?" objects are shown in Figure 5.3. The *SALT2* light curve fit parameters for the ESSENCE sample are provided in Table C.3. Additionally, we have indicated if the objects pass a combination of the light curve quality cuts used by WV07 for the 4 year sample, as well as shape and color cuts employed by Conley et al. [23] and Scolnic et al. [127, in prep.].

133 objects, including 121 of our spectroscopically confirmed SN Ia pass these cuts and are useful for cosmological inference. As *SALT2* is a flux-based fitter, it uses more measurements of the decline, as well as more observations for faint and high-z supernovae. Consequently, only three *SALT2* light curve fits fail for want of observations post-maximum. Despite this, fits for objects discovered towards the end of an observing season are likely suspect. We believe that this result reflects the inadequacy of simple automated cuts to evaluate the light curve fits for a large and diverse SN Ia sample such as ESSENCE. Consequently, we inspect each fit visually to assess if the various selection cuts are well-motivated. We examine the various light curve quality cuts further in the following section.

[3] http://supernovae.in2p3.fr/ guy/salt/
[4] http://sdssdp62.fnal.gov/sdsssn/SNANA-PUBLIC/

5.4 Light Curve Quality Cuts

In order to ensure that the distance estimates derived by light curve fitters are unbiased, it is necessary to impose various cuts, and select a sub-sample of SN Ia with good phase coverage that is well represented by the training samples. However, as a consequence of the diversity of observing strategies employed by various supernova searches, operating at different redshifts, there is no single set of cuts that is universally applicable to all SN Ia surveys. The selection cuts we apply to the ESSENCE sample are combinations of those used in WV07 and Conley et al. [23] (which in turn is informed by the results presented in G10) and are appropriate for high-z SN Ia surveys such as ESSENCE and SNLS. WV07 used an earlier version of the *SALT2* fitter (appropriately called *SALT*) for their analysis. However, the cuts employed are broadly applicable to the new version of the code, modulo a redefinition of the light curve shape parameter. Rest et al. [113, in prep.] and Scolnic et al. [127, in prep.] employ a similar set of cuts for the Pan-STARRS survey (private communication) derived from K09 and the results in G10.

Some selection cuts are common to all SN Ia surveys, and are required to ensure that the light curve fit is well constrained. These cuts are typically expressed in terms of the rest-frame phase $\Phi = (T_{\rm Obs} - T_{\rm Max})/(1+z)$. K09 required at least one measurement with $\Phi < 0.0$. G10 employed a more flexible cut, only requiring a single measurement in the range of $-8 < \Phi < +5$ days, and found that this provided a similar constraint to the K09 cut. Similarly, WV07 required at least one observation with $\Phi \leq +5$ days for both *MLCS2k2* and *SALT*, but also demanded that the observation had S/N > 5, while requiring that the uncertainty on the fit time of maximum, $\sigma_{T_{Max}}$, be < 2 days. The WV07 cut is effective at ensuring that the location and the peak flux is well constrained, and we adopt it here for ESSENCE SN Ia. The compilation of 441 SN Ia presented in C11 uses the weaker G10 cut on observations near-maximum. In addition, G10 does not impose any cut on S/N. However, these objects have observations in more passbands than ESSENCE, and we feel the more conservative cut is appropriate.

When the cut on pre-maximum measurements is not applied, both Δ and x_1 show a significantly increased scatter as a result of light curve fits being ill-constrained with only the post-maximum decline. Scolnic et al. [127, in prep.] also reports that x_1 shows a trend toward bigger values for $z > 0.4$ if the pre-maximum data is excluded. G10 did not find such a trend with high S/N SN Ia at $z < 0.4$, illustrating how the effect of light

curve quality cuts varies with median redshift, and therefore with survey.

WV07 and K09 also required that the fit statistic, χ^2/DoF, be < 3 for both light curve fitters. C11 did not impose any quality-of-fit cut, as they felt that the reported uncertainties for low-z photometry are frequently inaccurate, rendering such a cut misleading. They also suggested that several light curves contain the occasional outlying photometric observation that drives χ^2/DoF to artificially high values, despite having little to no effect on the derived light curve shape and color parameters. C11 also argues that any χ^2-based cut has an asymmetric effect with SN Ia sample, and therefore can potentially a introduce bias with redshift. This in turn could lead to systematic bias on w. While there is merit in this argument, upon visual inspection of our light curve fits, we concluded that the χ^2/DoF statistic did accurately represent the quality of the fit, and that this cut was well motivated. In future work, we will use Monte-Carlo simulations to assess any bias in cosmological inference that result from this cut.

Another common cut is on the minimum number of degrees-of-freedom. Both WV07 and K09 require $N^{\rm min}$ DoF ≥ 5. C11 do not explicitly state such a requirement, but the compilation they presented nevertheless satisfy that requirement. We adopt $N^{\rm min}$ DoF ≥ 5 for *MLCS2k2*. However, we found that this cut had unforeseen consequences. WV07 also required one observation with $\Phi \geq +9$ days for *MLCS2k2*. This cut was intended to ensure that the decline post-maximum is well sampled. As *MLCS2k2* also imposes it own cut by requiring observations with S/N > 5, this cut is considerably more stringent than was intended. This requirement causes a total of 44 SN Ia and "Ia?" objects to fail the selection cuts - by far the single largest cut on our *MLCS2k2* fits. In addition to eliminating observations of faint sources, or sources at high-z with extremely well-sampled declines, the S/N cut imposed by *MLCS2k2* causes several light curves fits to fail the selection cuts as a result of an insufficient observations, given the requirement of $N^{\rm min}$ DoF ≥ 5 in the *MLCS2k2* fit.

By contrast, WV07 only required one observation post B-band maximum for *SALT*, and only three objects in our sample does not meet this cut. We believe that this demonstrates that *MLCS2k2* is being needlessly conservative by requiring that all observations have S/N > 5. However, the intent of the cut on the number of observations post-maximum is to ensure that the light-curve extinction or color is well constrained, and the location of the peak is bounded. We are wary of the relatively weak effect of the post-maximum cut on our *SALT2* light curve fits, and require a

stricter $N^{\min}$ DoF ≥ 8 for that fitter. With the ESSENCE 4 day cadence, this effectively ensures that there are at least four measurements of the observer-frame $R - I$ color. As a result, the number of objects that fail the $N^{\min}$ DoF cut for *MLCS2k2* and *SALT2* are similar, and some of the most egregious outliers in x_1 and c are eliminated.

Based on the results in G10, C11 adopted a requirement of $-0.25 < c < 0.25$ mag. WV07 did not explicitly impose an equivalent cut on A_V for *MLCS2k2*. Several groups have used multi-color photometry of highly-extincted low-z SN Ia to demonstrate that the extinction law in the host-galaxies of these objects appear to follow a CCM law with a significantly lower R_V than the Milky-Way [35, 54, 84]. We discuss this issue further in §5.5, and it is likely that we will impose a cut on the *MLCS2k2* A_V estimate for our final cosmological sample.

Additionally, [127, in prep.] employs a requirement that $-3 < x_1 < 3$ for the upcoming Pan-STARRS SN Ia sample. Both these cuts are well motivated as there are few SN Ia in the *SALT2* training sample outside these ranges, and the fits are likely to be ill-conditioned there. WV07 adopted a requirement of $-0.4 \leq \Delta \leq 1.7$. All objects in our ESSENCE SN Ia sample that fail this requirement, also fail other selection cuts.

A summary of the number of light curves that fail each cut for both *MLCS2k2* and *SALT2* is provided in Table 5.1.

Table 5.1: Effect of Light Curve Quality Cuts on the ESSENCE Sample

Fit	Failed	$\chi^2 > 3$	$N^{\min}$DoF[5]	$\Phi_{\text{First S/N}>5}$[6]	$\sigma_{T_{\text{Max}}}$	Φ_{Last}	$x_1\vert\Delta$ cut	c cut[7]
MLCS2k2	7	10	18	9	5	44	14	NA
SALT2	—	20	20	17	3	3	18	33

Note: The number of SN Ia and "Ia?" objects that are removed by each selection criterion. Many objects fail multiple cuts.

Further cuts are frequently imposed prior to cosmological inference for

[5] We require $N^{\min}$DoF$\geq$ 8 for *SALT2*, rather than the weaker cut of 5 for *MLCS2k2*, as the last phase cut is very ineffective with *SALT2* when our well-sampled NN2 light curves are fit in flux space.

[6] While at first glance it appears that more objects fail the cut on pre-maximum imaging with *SALT2* than with *MLCS2k2*, this is not the case on closer inspection. *MLCS2k2* merely fails catastrophically for objects without pre-maximum imaging, and consequently does not report T_{Max} at all.

[7] WV07 did not employ an extinction cut. It is likely that we will employ a reasonable cut on this value to remove any highly extincted objects at low-z from the ESSENCE sample, as there is considerable uncertainty about the nature of the dust in the host-galaxies of heavily extincted SN Ia.

astrophysical reasons. Most analysis use a cut on the minimum redshift, $z_{\rm min}$, typically 0.015–0.025. This reduces the impact of local correlated flows on the luminosity distance estimates for low-z SN Ia [25, 61]. C11 make a peculiar velocity correction and employ a significantly lower cut at $z_{\rm min} = 0.01$.

There has been much controversy related to the existence of a local-void, and if the Earth occupies a privileged location near its center. Zehavi et al. [152] introduced a toy model with a discontinuous step in the local expansion rate to examine this effect - a so-called "Hubble bubble." [21, 53, 64, 92]. Jha et al. [64] also demonstrated the appearance of a bubble using the CfA2 light curve sample. Conley et al. [21] argues that the bubble is an artifact of the treatment of SN Ia color, combined with the selection effects of the nearby sample. Hicken et al. [54, hereafter H09] presented results that support this argument, demonstrating that the bubble was most significant when using *MLCS2k2* with $R_V = 3.1$. When employing a version of *MLCS2k2* trained with $R_V = 1.9$ and fit with $R_V = 1.7$, the bubble was considerably less significant. Additionally, H09 found that the sign and position of the bubble shifted with the addition of nearby SN Ia. Neill et al. [92] do not find any evidence for a Hubble bubble in the IRAS PSCz density field, and demonstrated that the bubble persisted even on subtraction of a local flow model. This indicates that the structure is not astrophysical in origin, unless the bubble is the result of a structure that is not traced by the IRAS density field. We will examine the significance of the Hubble bubble together with retraining *MLCS2k2* with new low-z samples [90, in prep.].

WV07 imposed a maximum redshift cut on the ESSENCE sample, limiting objects to $z \leq 0.67$ to avoid the use of rest-frame U-band SN Ia models. As *SALT2* inflates the rest-frame U-band uncertainty, objects above this redshift have poorly constrained estimates of the color parameter, c. We will examine the impact of this cut, and assess if it is still warranted given the larger training samples of low-z SN Ia in Narayan et al. [91, in prep.].

Lastly, most surveys impose a restriction on the line-of-sight Milky-Way reddening, $MW_{E(B-V)}$ <0.2–0.5 mag. The dust extinction spectrum is reasonably well defined for $MW_{E(B-V)} < 0.5$ mag, and objects can be dereddened using a CCM89 law to an accuracy of a few percent within that limit.

5.5 Systematic Differences between Light Curve Fitters

Light curve quality cuts are designed to select a high-quality sub-sample of SN Ia, for which distances may be reliably determined, independent of the light curve fitting methodology used. Unfortunately, K09 found that the choice of light curve fitter led to a difference in the equation of state parameter of the dark energy, w, of 0.2, when applied to a large sample consisting of SN Ia from the CfA2 release, SDSS-II, the 4 year ESSENCE sample of M07, the first release of SNLS data, and the HST Higher-Z program. This code-dependent difference was the largest single source of uncertainty in w. The authors thoroughly analyzed both light curve fitters to determine the source of the discrepancy (see §11 in Kessler et al. [68] for a detailed discussion, and Hicken et al. [54] for several detailed comparisons of the two light curve fitters).

K09 found that the discrepancy originated in the difference in training methodology, particularly when applied to the rest-frame U-band, and the treatment of color. The U-band discrepancy was the largest single source of discrepancy between the two light curve fitters, and led to abrupt features in the Hubble diagram. The SDSS-II SN Ia sample was particularly sensitive to this effect as the largest U-band "shift" occurs at the median redshift of the sample. Excluding the U-band data led to shifts in the estimated distance moduli of $+0.12$ mag for *MLCS2k2*, and $+0.008$ mag for *SALT2*, relative to distance moduli determined with the U-band data included.

Guy et al. [47] argued that the *SALT2* methodology is less susceptible to errors in the effective U-band response function that afflict low-z measurements. They attribute these errors to poor knowledge of the detector quantum efficiency and variations in the atmospheric transmission for $\lambda < 3500$ Å. Despite this claimed lower susceptibility to systematics, *SALT2* defaults to inflating the U-band uncertainties by 0.1 mag, to account for calibration errors. However, Krisciunas et al. [74] demonstrated that careful S-corrections can bring U-band measurements using different facilities at different sites into good agreement, indicating that knowledge of the response function is not the cause of the U-band discrepancy.

The difference may originate in the use of high-z spectroscopy in the *SALT2* training methodology. Early spectroscopic studies found no significant evolution in SN Ia properties to $z = 0.4$ [14, 17]. Foley et al. [39] found that low-redshift SN Ia spectra showed ∼20% less flux blueward of 3400 Å than a sample of intermediate redshift SDSS SN Ia observed with Keck. However, the difference was not seen using the full

SDSS-II sample of K09, and may originate from a combination of several small systematic effects.

Foley et al. [39] also found a difference between the UV spectra from low-mass and high-mass host galaxies, but at low statistical significance. Maguire et al. [82] found similar results using HST STIS spectra of 32 low-redshift SN Ia that also exhibit depressed near-ultraviolet flux compared to intermediate-z SN Ia significant at the 3σ level. They also found that brighter SN Ia exhibit broader spectral features, in particular the Ca II H and K doublet. The small sample sizes, various systematic effects affecting the reduction and relative flux calibration of the spectra, and the low significance of the detected difference in NUV flux do not allow a definite answer on the question of evolution of SN Ia or whether such evolution drives the systematic differences between the light curve fitting methodologies.

H09 demonstrated that the inclusion of underluminous SN Ia, similar to SN 1991bg ($MLCS2k2$ $\Delta > 1.2$), introduced a bias in the Hubble residuals even for moderately underluminous objects ($0.7 < \Delta < 1.2$). Excluding these objects from the training sample effectively removes the need for the quadratic term in Δ, and eliminates this bias. While these underluminous SN Ia are not found in high-z surveys such as ESSENCE and SNLS, they have been discovered at the intermediate redshifts probed by the SDSS-II Supernova Survey.

The SDSS-II analysis employed a different extinction prior from the "glosz" model employed by WV07. The "glosz" model is based on a galactic line-of-sight prior (glos), modified to account for selection effects as a function of redshift. The "glos" prior on A_V is given by:

$$p(A_V) \propto \frac{A}{\tau} \exp\left(\frac{-A_V}{\tau}\right) + \frac{2B}{\sqrt{2\pi}\sigma} \exp\left(\frac{-A_V^2}{2\sigma^2}\right) \tag{5.8}$$

where $A = 1$, $B = 0.5$, $\tau = 0.4$, $\sigma = 0.1$, and $p(A_V < 0) = 0$. The form of the prior is based on the studies of the distribution of SN Ia properties in their host galaxies by Hatano et al. [51], Commins [20] and Riello and Patat [114]. The simple exponential plus one-sided narrow Gaussian is convolved with a window function given by:

$$W(A_V, A_{1/2}(z), \sigma_A(z)) = 1 - \int_{-\infty}^{(A_V - A_{1/2}(z))/\sigma_A(z)} e^{-x^2}\, dx \tag{5.9}$$

where $A_{1/2}$ describes where the function drops to half its peak value, and σ_A models the width of that transition. The values for both parameters are determined by simulating SN Ia with realistic noise properties and a flat A_V distribution, and measuring the recovered distance moduli as high-extinction and faint events are lost from the sample.

To compensate for the spectroscopic selection bias favoring SN Ia with low extinction, K09 measured R_V and A_V from a large photometric sample of extincted SDSS SN Ia with measured host-galaxy redshifts, while modeling the spectroscopic efficiency of different surveys using Monte-Carlo simulations, in contrast to the WV07 approach of assuming $R_V = 3.1$ and a spectroscopic targeting efficiency of unity. Using this approach, K09 found a value of $R_V = 2.18$. Further, recent low-z results from the CfA SN group [54, 55] support lower values of R_V, typically closer to 1.7, to minimize the Hubble residuals.

Folatelli et al. [35] and Mandel et al. [84] found that the most heavily extincted objects appear to drive the reddening law to these low values of R_V relative to our Galaxy. If these objects are excluded, the recovered R_V is very close to that of the Milky Way. Folatelli et al. [35] further demonstrated that a power-law model, valid for LMC-type dust, provided a significantly better fit to the observed color excess for highly reddened objects, compared to the canonical Cardelli et al. [18, hereafter, CCM89] relation.

If these findings are supported by further observations, then neither the WV07 or K09 approach is correct, as there is no single extinction distribution for SN Ia events. While these observations also suggest an explanation for the evolution of β with redshift when using *SALT2*, that evolution is not monotonic, with β first increasing towards 4.1, and then decreasing. H09 also found that the light curve shape/luminosity coefficient, α, varied when fit for samples at high and low redshift. This perhaps indicates systematics in the *SALT2* model that are sensitive to host-galaxy properties, and vary with the demographic evolution of the host galaxy sample with redshift.

Further, given the preponderance of observational evidence for dust in the environments of SN Ia, the *SALT2* approach of combining intrinsic color differences with extinction due to dust in a single parameter is unsatisfactory, as these variations originate from completely different physical processes. K09 also constructed "SALTy" *MLCS2k2* vectors to match the *SALT2* models, and found that if *SALTy-MLCS2k2* is employed without any priors on the extinction, A_V, then both light curve fitters agree extremely well, implying that the *U*-band model, and the treatment of extinction and

color, are the dominant causes of the discrepancy between the two methodologies. Disentangling these systematics further is not possible with the single-color information provided by the ESSENCE sample, and is beyond the scope of this thesis. Examining these effects with multi-color samples, such as SN Ia from the Pan-STARRS Medium Deep Survey [113, 127, in prep.], may shed light on the issues of host-galaxy extinction, and help further understand the NUV discrepancies in the models.

5.6 Preliminary Cosmological Constraints Using ESSENCE and literature SN Ia

The primary focus of this thesis is the calibrated photometry of ESSENCE SN Ia. Nevertheless, the principal utility of such a sample is to study the expansion history of the Universe and derive cosmological constraints, in particular on the equation-of-state of the dark energy, w. To that end, we have combined a sub-sample of our spectroscopically confirmed SN Ia, with the literature sample of C11 to produce preliminary cosmological constraints using the largest sample of well-calibrated SN Ia to date. This analysis is intended as a minimal demonstration of the cosmological utility of our SN Ia, and lacks the sophistication of the commendably thorough analyses presented in K09 and C11. We are in the process of developing on the cosmological studies presented in K09 and C11 for Narayan et al. [91, in prep.].

The C11 sample consists of low-z SN Ia from the Calán-Tololo Supernova Search [50], CfA1 [117], CfA2 [63], CfA3 [53], and the CSP [24], intermediate redshift SN Ia from the SDSS-II Supernova Survey [56], the high-z SN Ia presented in R09, and the HST sample of Riess et al. [118], as well as a few other well-calibrated literature SN Ia. Despite being one of the largest cosmological samples of SN Ia, there are very few objects in the overlap between the SDSS-II survey and SNLS roughly spanning $0.20 < z < 0.35$. The ESSENCE SN Ia presented in this thesis more than doubles the number of objects in this range, and can potentially reduce the impact of a relative zero point offset between the SDSS and SNLS on w.

Beginning with the 121 measurements presented in Table C.3, we eliminated any "Ia?" and "IaP" objects, as the former are not spectroscopically confirmed SN Ia, while the latter exhibit spectral features that are not well modeled by *SALT2*. Following WV07, we also eliminated any objects above $z_{\rm Hel} > 0.67$, since these objects map to the rest-frame U-band and are subject to considerably higher uncertainties. This cut

removed 12 SN Ia - a significantly larger fraction than the 3 objects eliminated in WV07. The resulting sample consists of 108 spectroscopically confirmed SN Ia.

5.6.1 Deriving Cosmological Parameters

SN Ia surveys are subject to several sources of systematic uncertainty and the full-error model for cosmological studies is complex and exhibits redshift- and sample-dependent structure (see Fig. 12 of C11). For this simplified treatment, we elected to reduce the covariance matrix of the measurements to a diagonal matrix, such that:

$$\chi^2 = \sum_{n=1}^{N} \frac{[\mu_{\text{Cosmology}} - \mu_B]^2}{\sigma_n^2 + \sigma_{\text{int}}^2} \tag{5.10}$$

where $\mu_{\text{Cosmology}}$ is the distance given a set of cosmological parameters, and μ_B is estimated from the SN Ia light curve fit parameters via Eq 5.5. Intrinsic dispersion, σ_{int}, is added to the sample to mitigate unmodeled astrophysical effects and is determined such that the χ^2/DoF of the fit is unity. The distance modulus, $\mu_{\text{Cosmology}}$ reduces to $5log_{10}\mathcal{D}_L$ with:

$$\mathcal{D}_L(z; w, \Omega_M, \Omega_{DE}, \alpha, \beta, \mathcal{M}) = \frac{1 + z_{\text{Hel}}}{\sqrt{|\Omega_k|}} \mathcal{S}_k \left[\sqrt{|\Omega_k|} \int_0^{z_{\text{CMB}}} \frac{dz'}{h(z')} \right] \tag{5.11}$$

where we have absorbed factors of the speed of light and Hubble's constant into the definition of $\mathcal{M}$ in Eq 5.7. h is the Hubble parameter described by the Friedmann equation (Eq 1.1 where $h_0 = 1$ with our $\mathcal{M}$ convention). The curvature is described by its sign, k, and $\Omega_k \equiv 1 - \Omega_M - \Omega_{\text{DE}}$ and $\mathcal{S}_k$ is defined as:

$$\mathcal{S}_k = \begin{cases} \sin(\chi) & (k = -1) \\ \sinh(\chi) & (k = +1) \\ \chi & (k = \ 0) \end{cases} \tag{5.12}$$

and χ is the radial coordinate of the metric on the three-surface Σ.

In this analysis, we have determined constraints on w and Ω_M in a flat ($k = 0$)

Universe. We used the "simple_cosfitter" package [8] (v1.6.9) released by the SNLS team. We constructed a 101×201 grid in the Ω_w–w plane spanning $0 < \Omega_M < 1$ and $-2 < w < 0$. We used a 21 step grid in $0 < a < 0.2$ and a 71 step grid in $1 < \beta < 4$ to marginalize over the light curve shape and color parameters. These ranges span the most extreme values reported by other SN Ia surveys. As we have not employed any correction for the Malmquist bias, we use the WV07 value for $\sigma_{\rm int} = 0.12$ mag to compensate for the expected increase in scatter. Other surveys have reported values that are 1–2% lower when incorporating a correction for the Malmquist bias.

5.6.2 Results

SN Ia measurements can be thought of as constraining the difference between $\Omega_{\rm DE}$ and Ω_M. To constrain Ω_M itself, we elected to incorporate constraints from Baryon Acoustic Oscillation (hereafter BAO) studies. Following WV07, and several other cosmological studies employing SN Ia data, we use the BAO constraints given by Eisenstein et al. [28]. The BAO places strong constraints on Ω_M, yielding $\Omega_M = 0.29 \pm 0.08$. The SN Ia measurements provide orthogonal constraints to the BAO data in the Ω_M–w plane.

The cosmological constraints from SN Ia alone are relatively weak: we find (Ω_M, w, SN Ia only) = $(0.258^{+0.065}_{-0.100}, -1.134^{+0.224}_{-0.262})$, where the quoted uncertainties are the statistical 1σ values throughout. The combined constraints from the SN Ia and BAO measurements are (Ω_M, w, SN Ia+BAO) = $(0.266^{+0.026}_{-0.016}, -1.112^{+0.069}_{-0.072})$. This is very comparable to the WV07 analysis of nearby+ESSENCE+SNLS1 SN Ia, which reported $w = -1.069^{+0.091}_{-0.093}$ and $\Omega_M = 0.267^{+0.028}_{-0.019}$ using the *MLCS2k2* method. Unlike the results presented in WV07, we do not find strong tension between the SN Ia data and the BAO constraints. We present our cosmological contours in the Ω_M–w plane in Fig. 5.4.

We find the *SALT2* luminosity and color coefficients, α and β, to be $0.1333^{+0.009}_{-0.008}$, and $3.167^{+0.110}_{-0.108}$ respectively. These are in good agreement with values reported by other surveys. If β is identified with extinction in the host-galaxy of the SN Ia then $R_V = \beta - 1 \approx 2.17$. This is in good agreement with the value of $R_V = 2.18$ reported in Ko09 using *MLCS2k2*. While we have not been able to use *MLCS2k2* to complete a

[8] http://qold.astro.utoronto.ca/conley/simple_cosfitter/

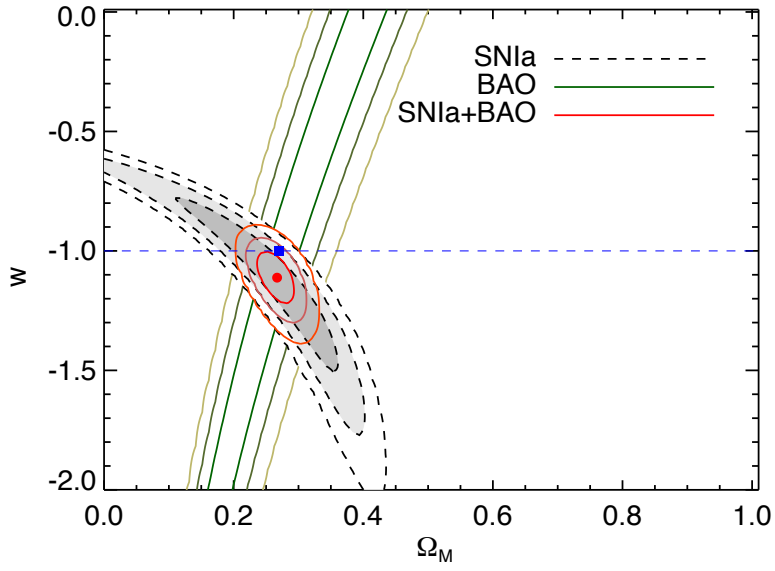

Figure 5.4: 1, 2 and 3σ contours (arranged from darker to lighter colors or shaded regions) in Ω_M–w for our compilation of 108 ESSENCE spectroscopically confirmed SN Ia, together with 441 literature SN Ia presented in C11 (shaded grey). The blue line indicates the equation-of-state for a cosmological constant, $w = -1$, and a canonical (Ω_M, w)=(0.27,-1) cosmology is indicated by a blue point. Our joint constraint from the SN Ia and BAO measurements is (Ω_M, w, SN Ia+BAO) = ($0.266^{+0.026}_{-0.016}$, $-1.112^{+0.069}_{-0.072}$) and is indicated by the red point. The BAO constraints (green) are from Eisenstein et al. [28].

cosmological analysis at the time of this writing, this result suggests that the discrepancies between the two light curve fitting techniques that originate in their treatment of extinction and color are likely to persist.

The combined sample is dominated at high-redshift by the contribution from the SNLS3 SN Ia. We have therefore taken the additional step of eliminating the SNLS3 sample in order to determine cosmological constraints when the high-redshift sample is dominated by the contribution of the ESSENCE SN Ia presented in this thesis. Excluding the SNLS3 data removes 241 objects. Additionally, the ESSENCE sample has been restricted to $z \leq 0.67$. Consequently, the SN Ia only constraints are significantly weakened, and we find (Ω_M, w, Nearby+SDSS+ESSENCE+HST) = ($0.309^{+0.095}_{-0.174}$,$-1.298^{+0.369}_{-0.420}$). These are consistent within 1σ with the constraints from the full sample. There is some tension with both the SN Ia-only constraints and the results from the BAO measurements in this reduced sample, but this is not unanticipated, as this reduced sample has significantly fewer objects above $z = 0.67$, and the leverage on w is significantly reduced. The combined constraints from SN Ia and BAO measurements are (Ω_M, w, Nearby+SDSS+ESSENCE+HST SN Ia+BAO) = ($0.268^{+0.028}_{-0.018}$, $-1.102^{+0.091}_{-0.091}$). Unsurprisingly, these constraints with a larger ESSENCE sample but no SNLS3 SN Ia are very comparable to the WV07 constraints with the 4-year ESSENCE sample but including the SNLS1 data. The results of this analysis are shown in Figure 5.5.

We present a Hubble diagram of the SN Ia employed in this sample in Fig 5.6. Our largest outliers in the Hubble diagram, *s373* and *s380*, are both faint SN Ia at $z\sim0.63$, with relatively poor sampling of their declines. Additionally, we find a few significant outliers in the SNLS3 sample, and 1 each from the nearby (SN 1992ag) and HST samples("Patuxent"), despite their inclusion in the C11 sample. The C11 analysis combined the results from *SALT2* and *SiFTO*, and used cuts derived from both. This is likely the source of the discrepancy for these objects. We treat these outliers as an indication of the need to improve our light curve quality cuts further, but have elected not to exclude them, given the limitations of this analysis.

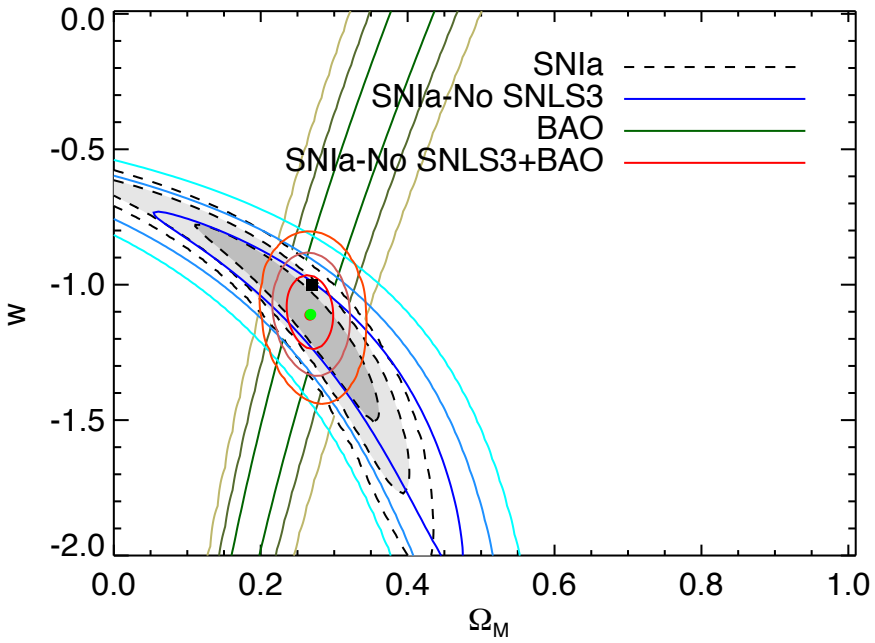

Figure 5.5: 1, 2 and 3σ contours (arranged from darker to lighter colors or shaded regions) in Ω_M–w for our compilation of 108 ESSENCE spectroscopically confirmed SN Ia, together with 234 literature SN Ia from the CfA, CSP, LOSS, SDSS, and the HST. This reduced sample excludes all SNLS3 data. As in Fig. 5.4, the BAO constraints (green) are from Eisenstein et al. [28], and the shaded contours are from the full sample including SNLS3 SN Ia. The blue contours indicate the SN Ia constraints without any SNLS3 SN Ia. As the reduced sample contains 241 fewer SN Ia and the ESSENCE sample used in this thesis is restricted to $z \leq 0.67$, the leverage on w is significantly reduced. Nevertheless, the constraints from the reduced sample encompass the 1σ region of the full sample. The canonical (Ω_M, w)=(0.27,−1) cosmology is indicated by a blue point. Our joint constraint from the reduced SN Ia sample and BAO measurements is (Ω_M, w, SN Ia+BAO) = $(0.268^{+0.028}_{-0.018}, -1.102^{+0.091}_{-0.091})$ and is indicated by the green point. This is in excellent agreement with the constraints from the full sample including SNLS3 SN Ia which provide (Ω_M, w, SN Ia+BAO) = $(0.266^{+0.026}_{-0.016}, -1.112^{+0.069}_{-0.072})$, and is indicated by the red point.

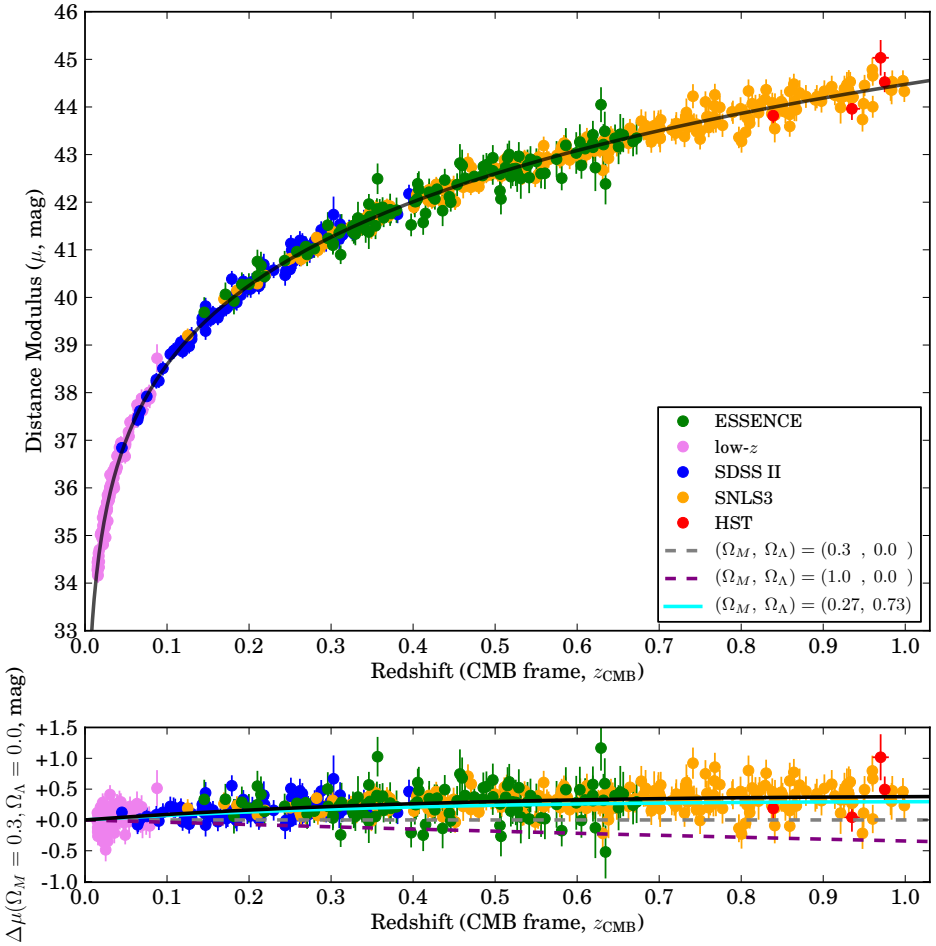

Figure 5.6: The *SALT2* Hubble diagram using a total of 549 ESSENCE and literature SN Ia (Top) and the residuals with respect to a fiducial open (Ω_M, $Omega_\Lambda$) = (0.3, 0.0) Universe (Bottom). We adopted $\sigma_{\rm int} = 0.12$ mag from WV07, higher than contemporary results. The RMS around the best fit is 0.189 mag. This is slightly higher than the 0.15 mag that is typical for distance estimates derived from rest-frame optical light curves of SN Ia, and is likely being driven by two ESSENCE outliers as well as one outlying HST object. The SN Ia data alone rule out a purely matter dominated Universe at high confidence. The χ^2/DoF of the fit is 0.9 on 549 SN Ia.

5.6.3 Limitations of our Cosmological Analysis

This analysis does not include the effect of any systematic biases on the cosmological constraints. We explore the systematics affecting the ESSENCE SN Ia photometry in §6. However, we have not yet analyzed the effect of relative zero point offsets between ESSENCE and other SN Ia surveys, in particular the low-redshift sample. However, there are several other sources of systematic uncertainty afflicting luminosity distances determined from SN Ia light curves, including what fitting methodology is employed as discussed in §5.5. We believe that future studies must incorporate a more detailed analysis of the *U*-band anomaly, and the treatment of host-galaxy extinction and color to address the issues raised in K09. To that end, we are updating the *MLCS2k2* model using new samples of nearby SN Ia, and adapting the *BayeSN* methodology to fit in the observer-frame for the ESSENCE, Pan-STARRS [113, 127, in prep.], and HST WFPC3 F125W and F160W observations from the RAISIN program.

The light curve quality cuts employed in this analysis are preliminary, and we have erred on the side of caution by imposing extremely conservative selection cuts. We have not modeled the selection effects of these cuts, and our final cosmological sample is likely to be significantly larger as a result of recovering the photometry of ∼20 objects not presented in this thesis, the ongoing effort to classify "Ia?" objects, and a more informed assessment of what constitutes a reliable SN Ia light curve fit.

Matheson et al. [86, in prep.] will detail our spectroscopic efficiency, and we are updating our Monte-Carlo simulations to model the Malmquist bias for our SN Ia. We are in the process of studying the impact of several sources of systematic uncertainty on w, and will include the full covariance matrix for all SN Ia measurements in Narayan et al. [91, in prep.]. We discuss various possibilities to improve and extend our cosmological analysis in §7.1. Despite these limitations, we believe that the analysis

presented here demonstrates the utility of the ESSENCE SN Ia sample.

Figure 5.7: ESSENCE R (red) and I (orange) light curves, in units of linear flux, scaled such that a flux of unity corresponds to magnitude 25. Gaps between observing seasons have been removed, and the reported MJD is discontinuous at the locations of the vertical black lines.

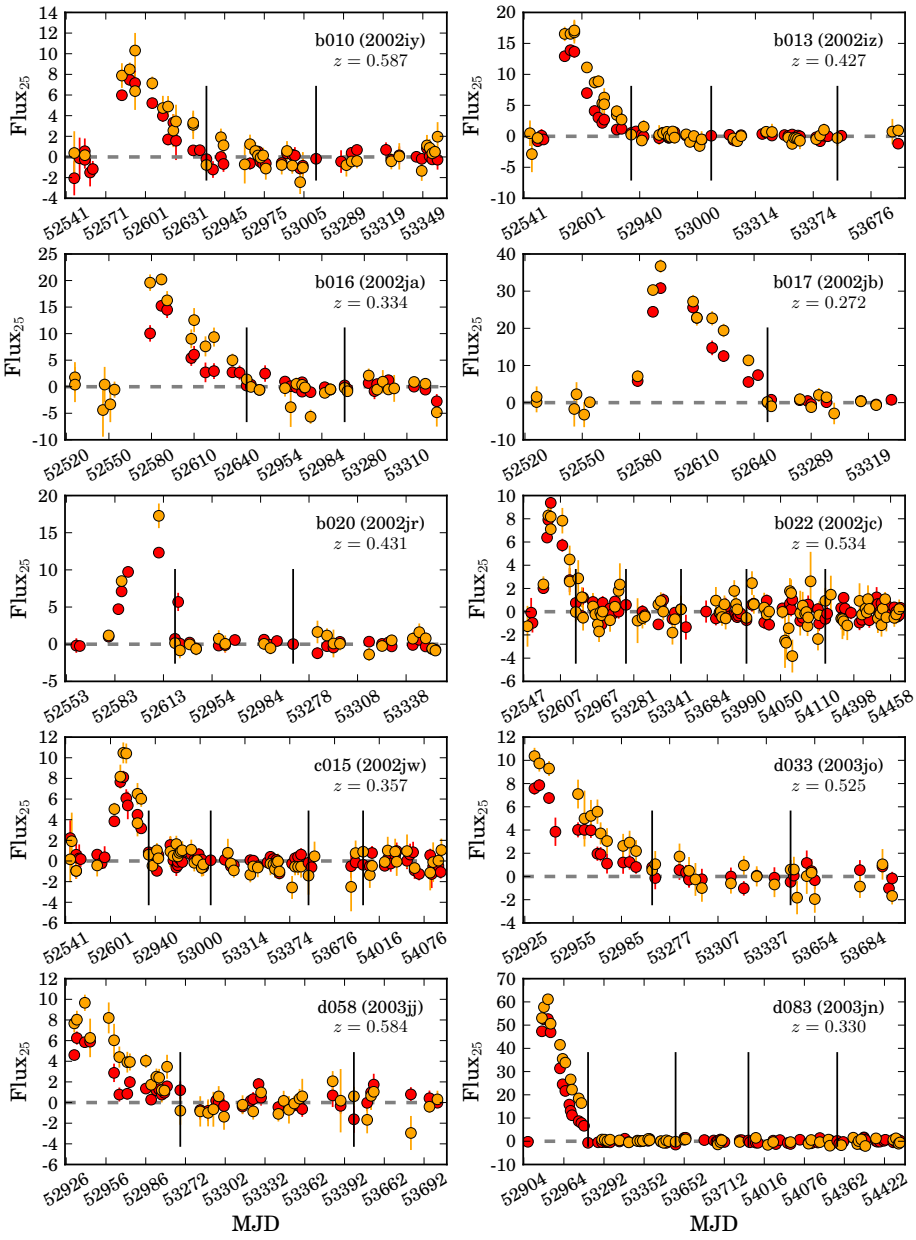

Figure 5.7: (Continued)

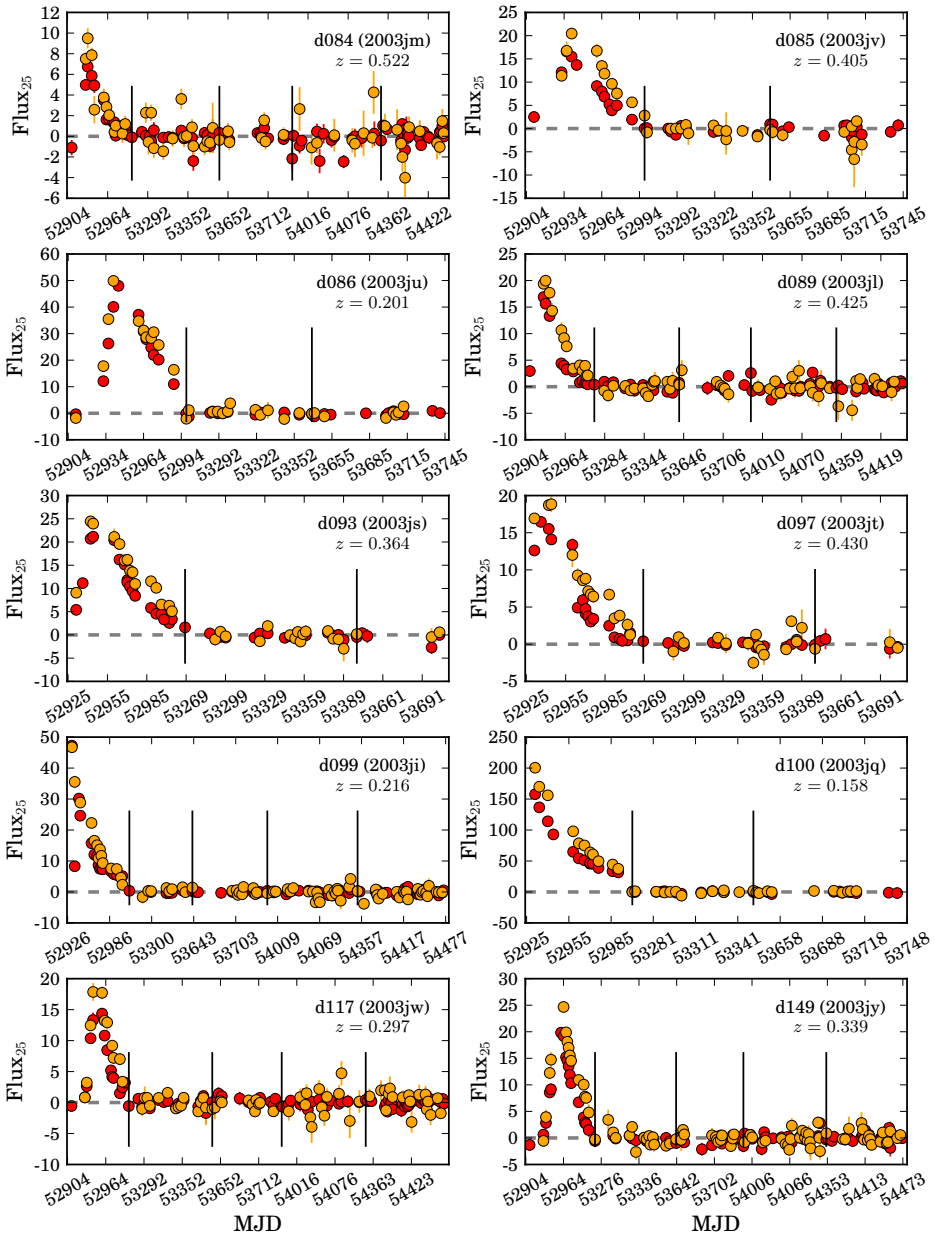

Figure 5.7: (Continued)

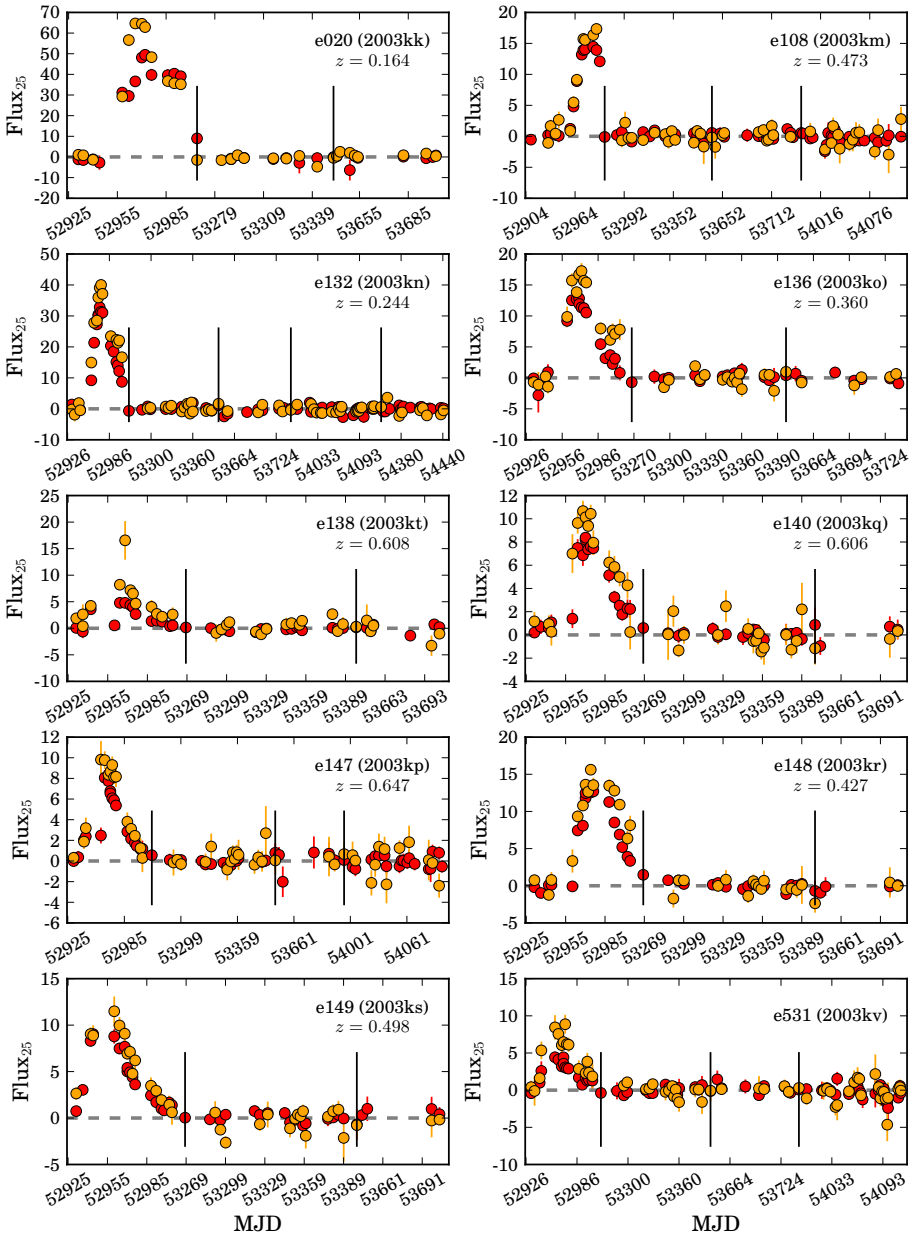

Figure 5.7: (Continued)

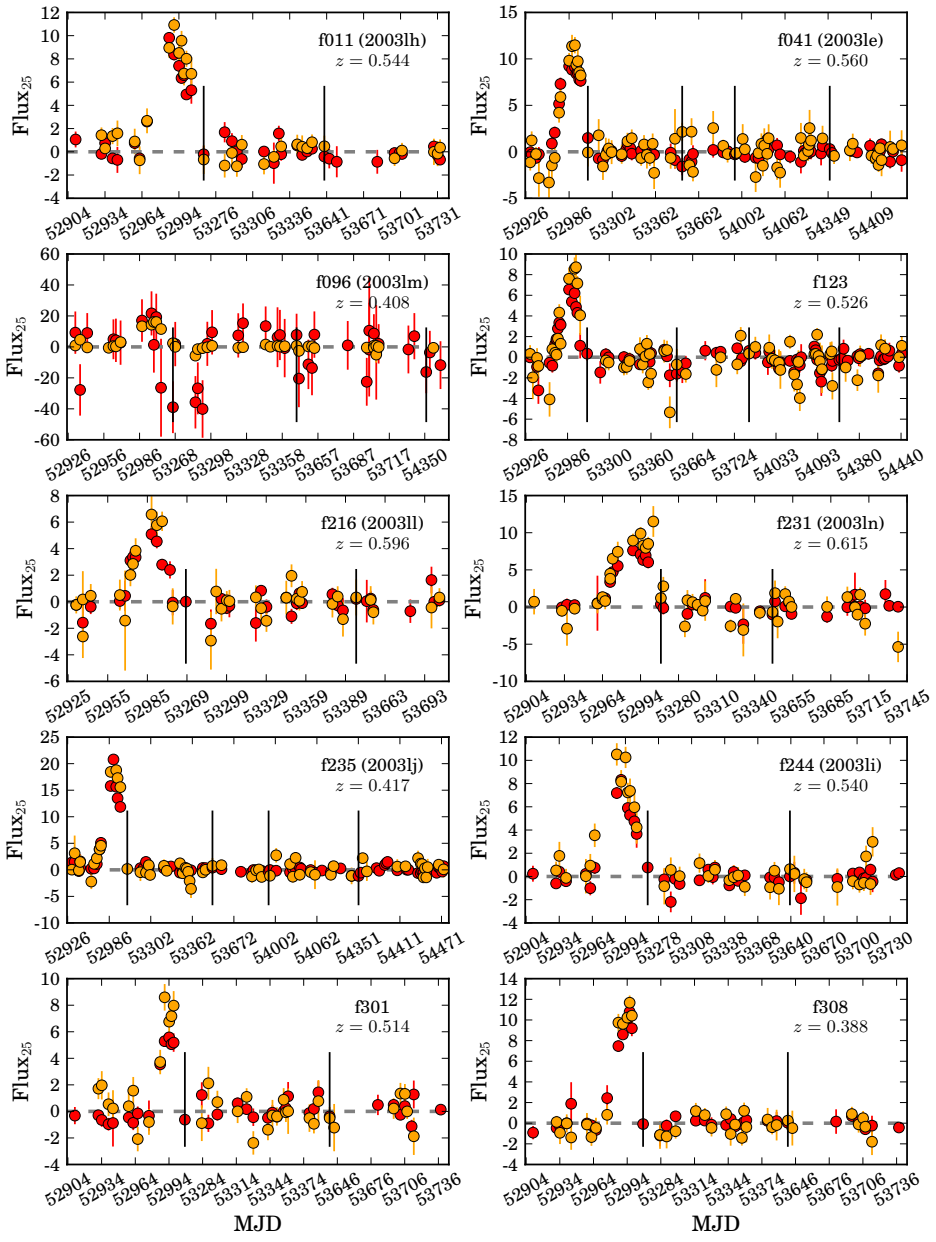

Figure 5.7: (Continued)

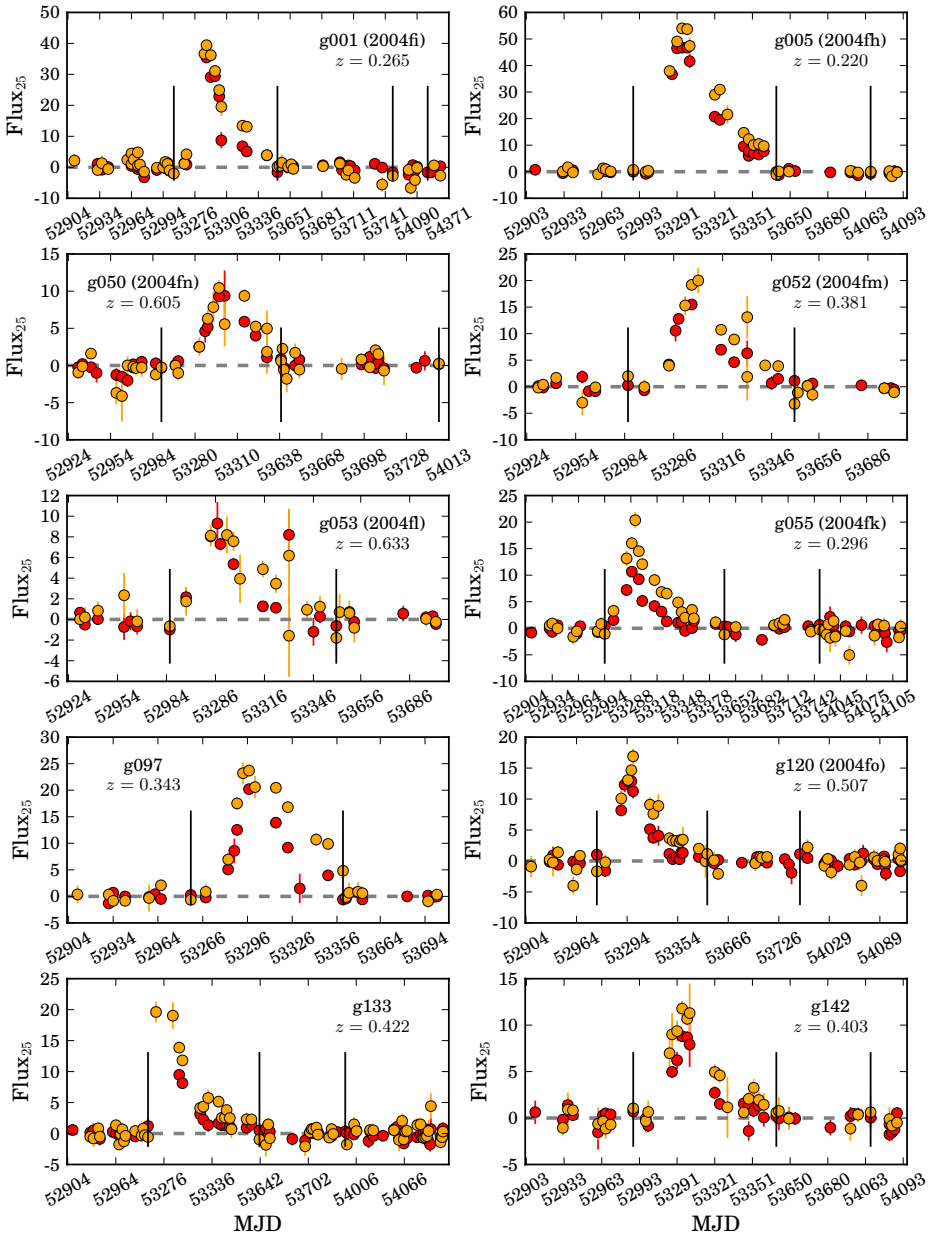

Figure 5.7: (Continued)

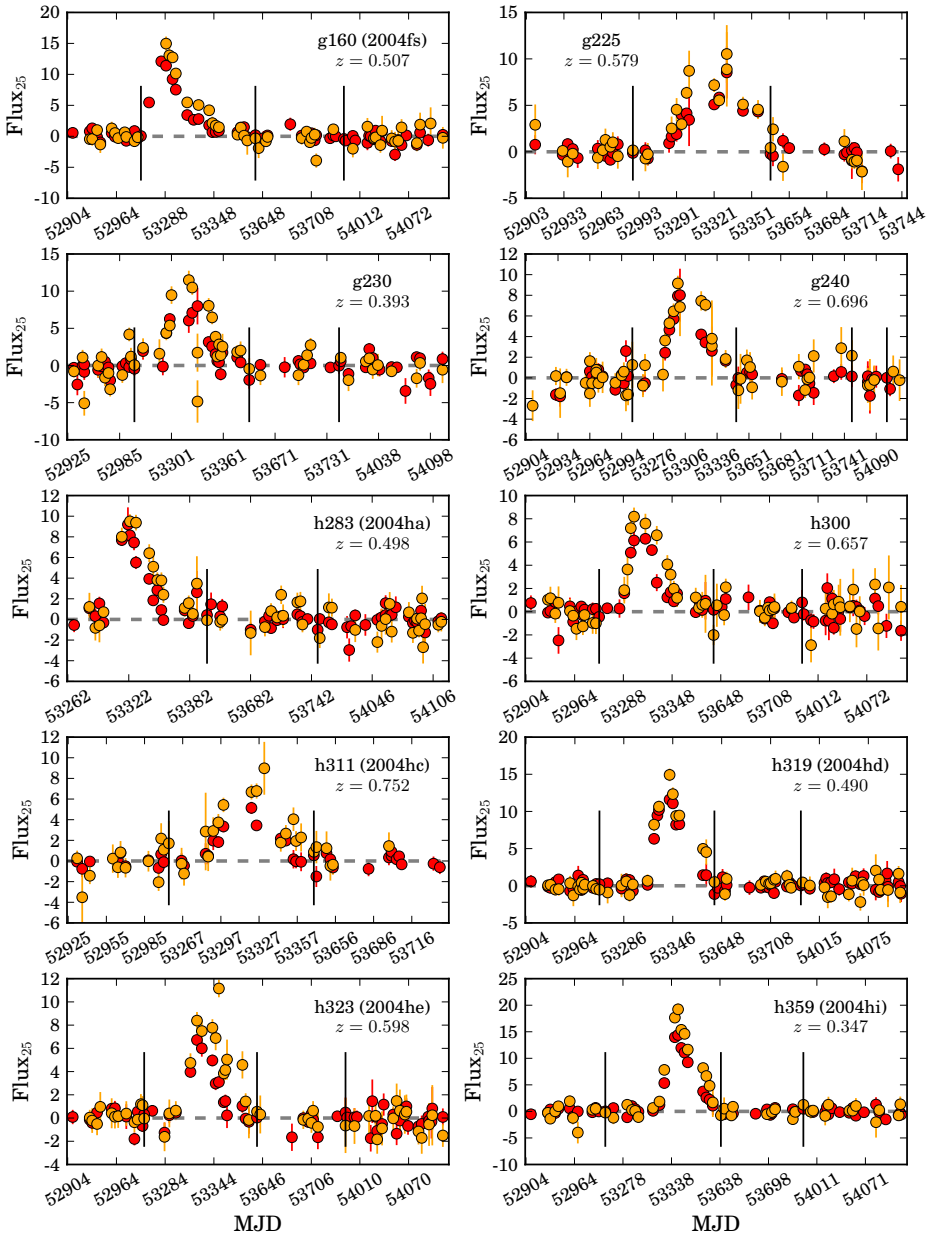

Figure 5.7: (Continued)

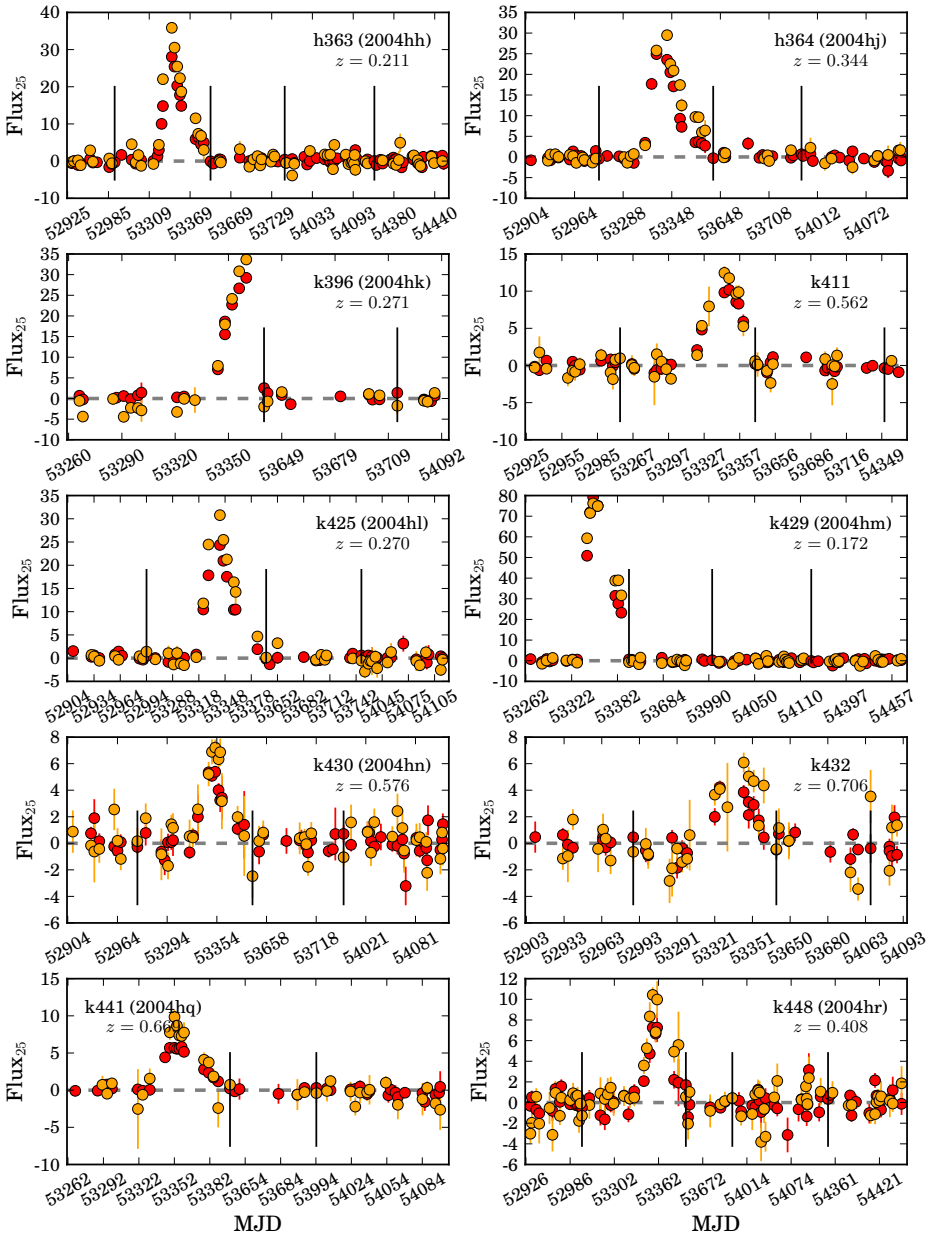

Figure 5.7: (Continued)

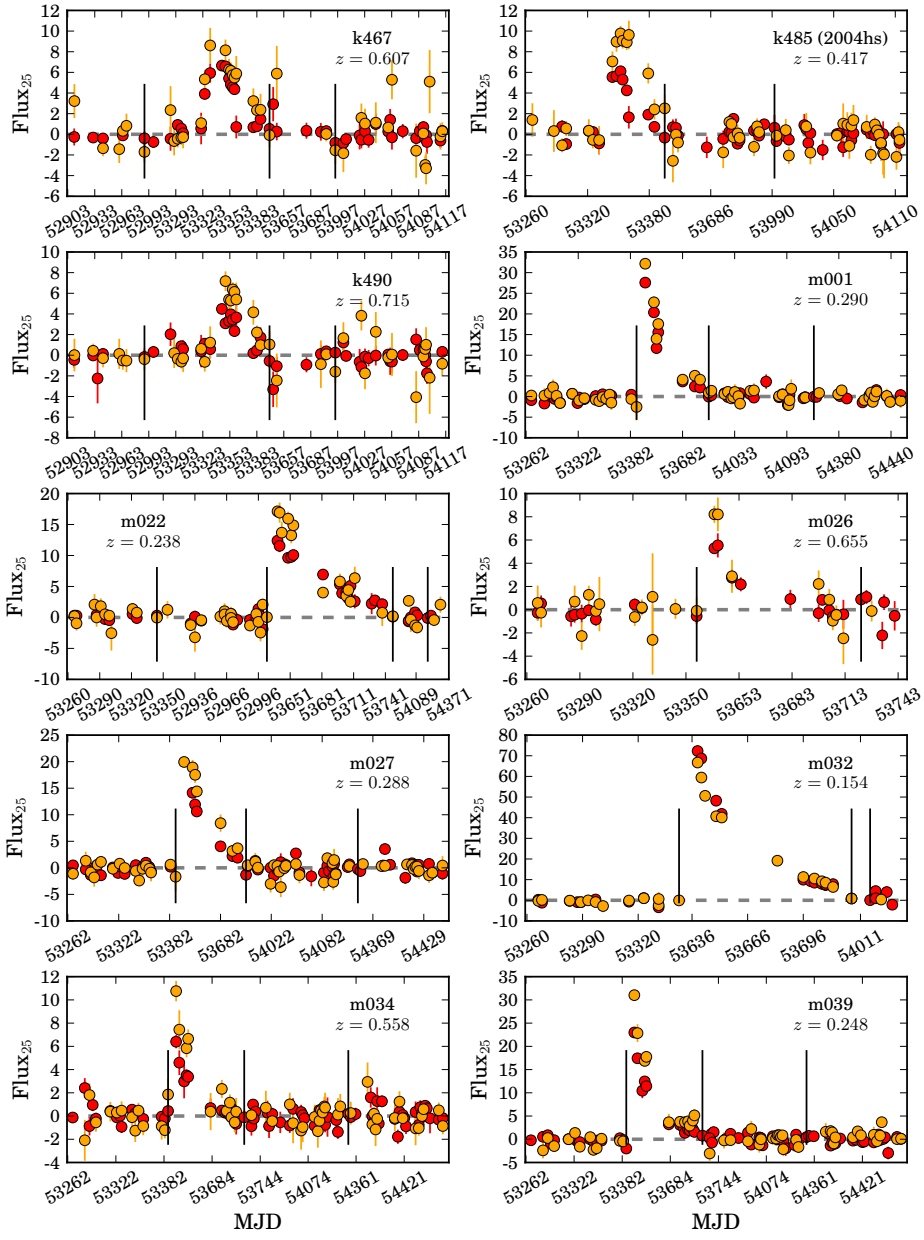

Figure 5.7: (Continued)

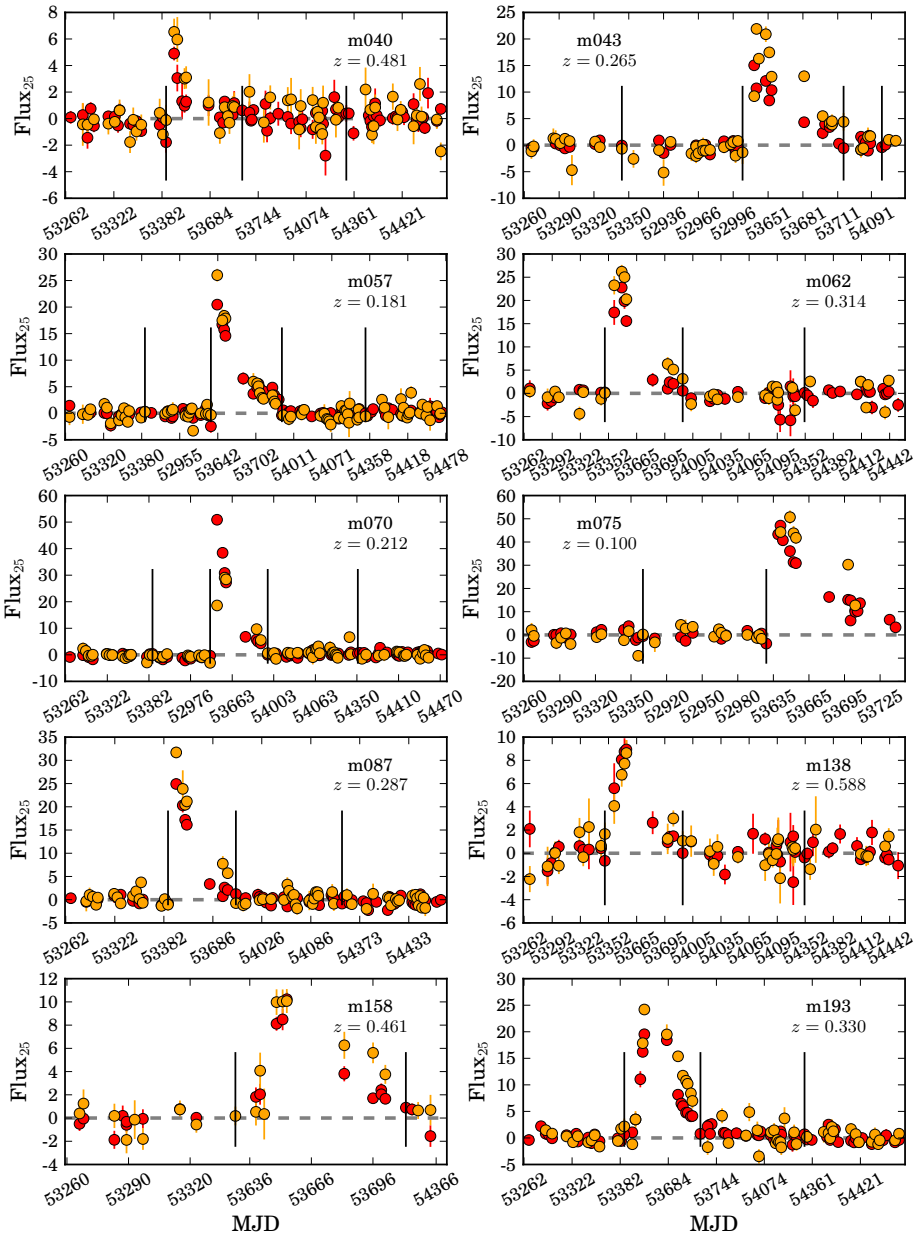

Figure 5.7: (Continued)

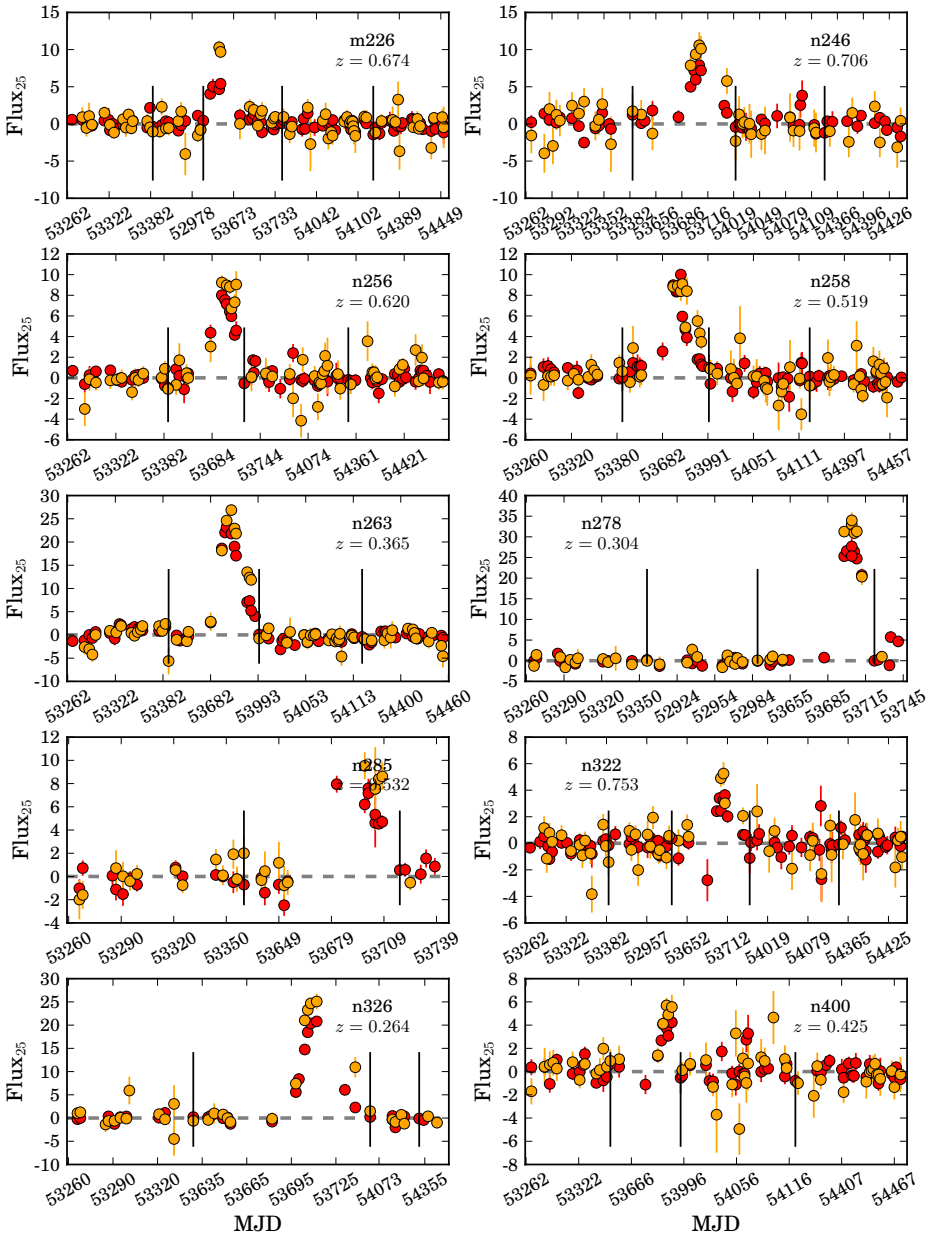

Figure 5.7: (Continued)

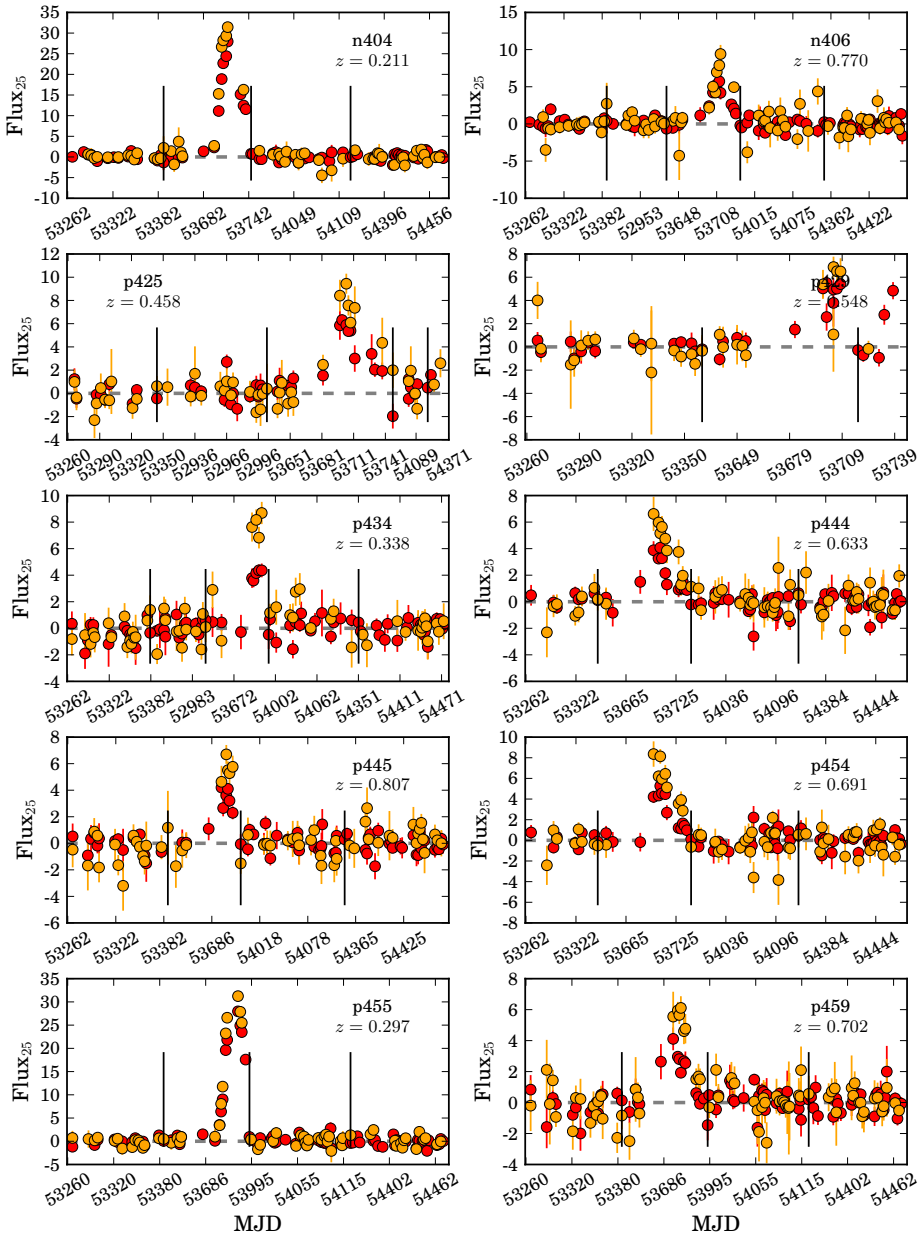

Figure 5.7: (Continued)

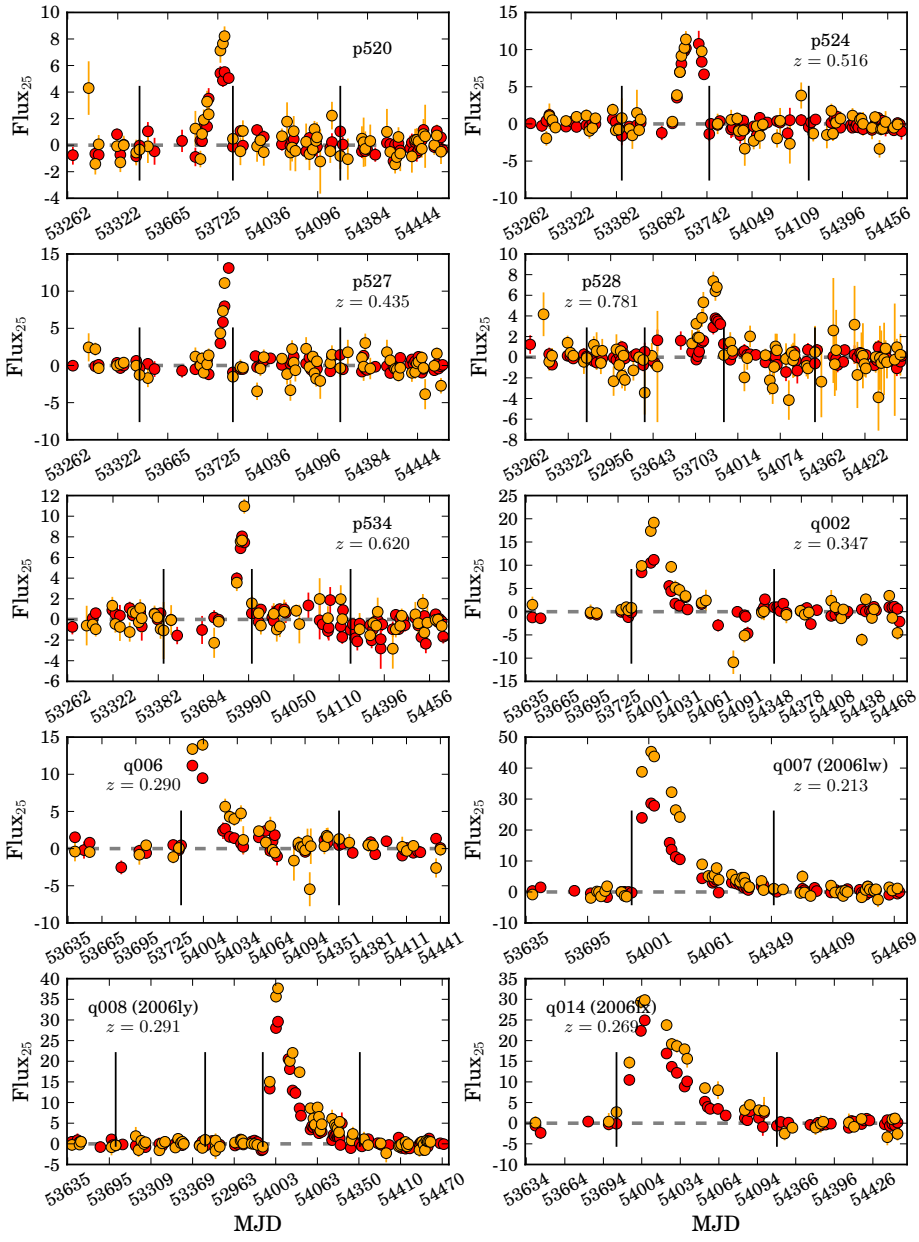

Figure 5.7: (Continued)

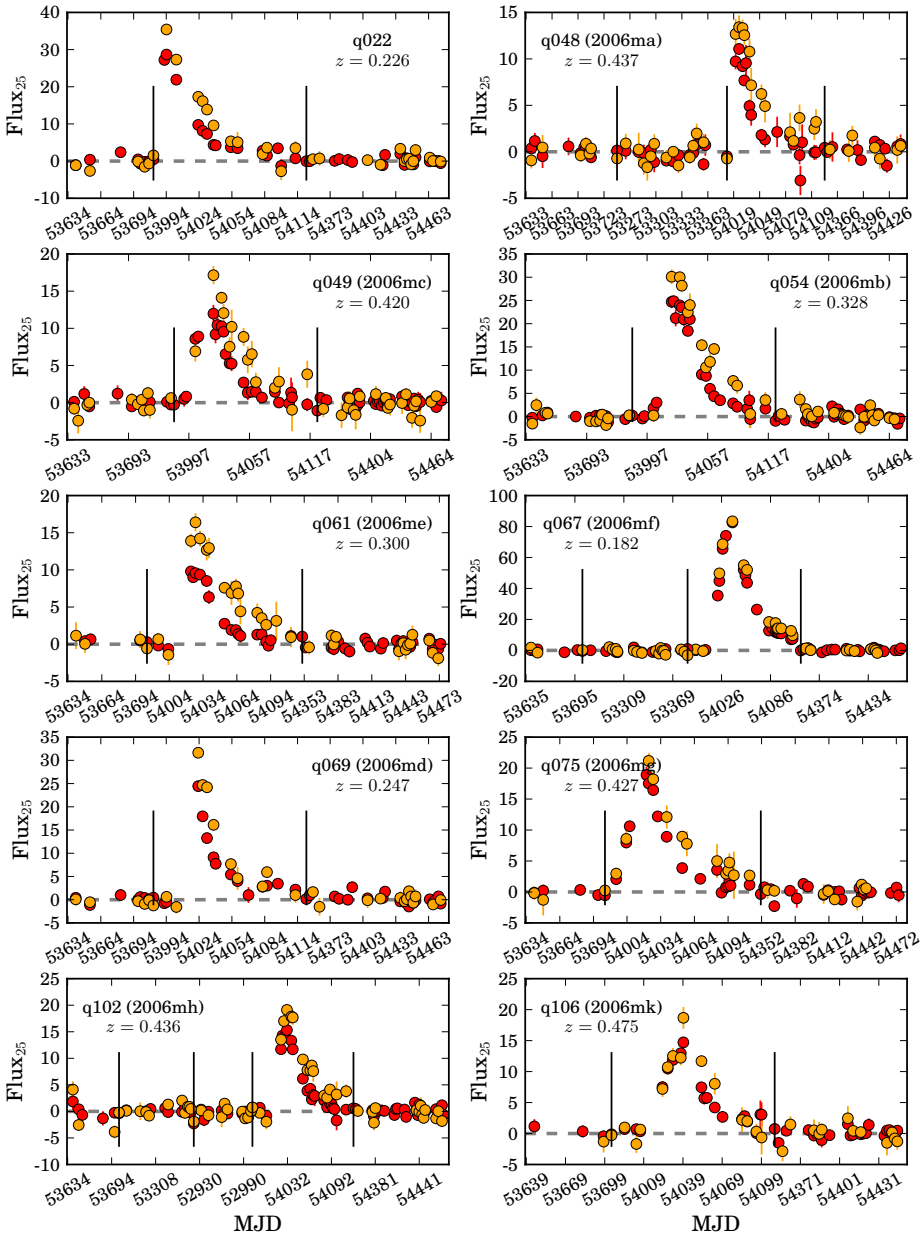

Figure 5.7: (Continued)

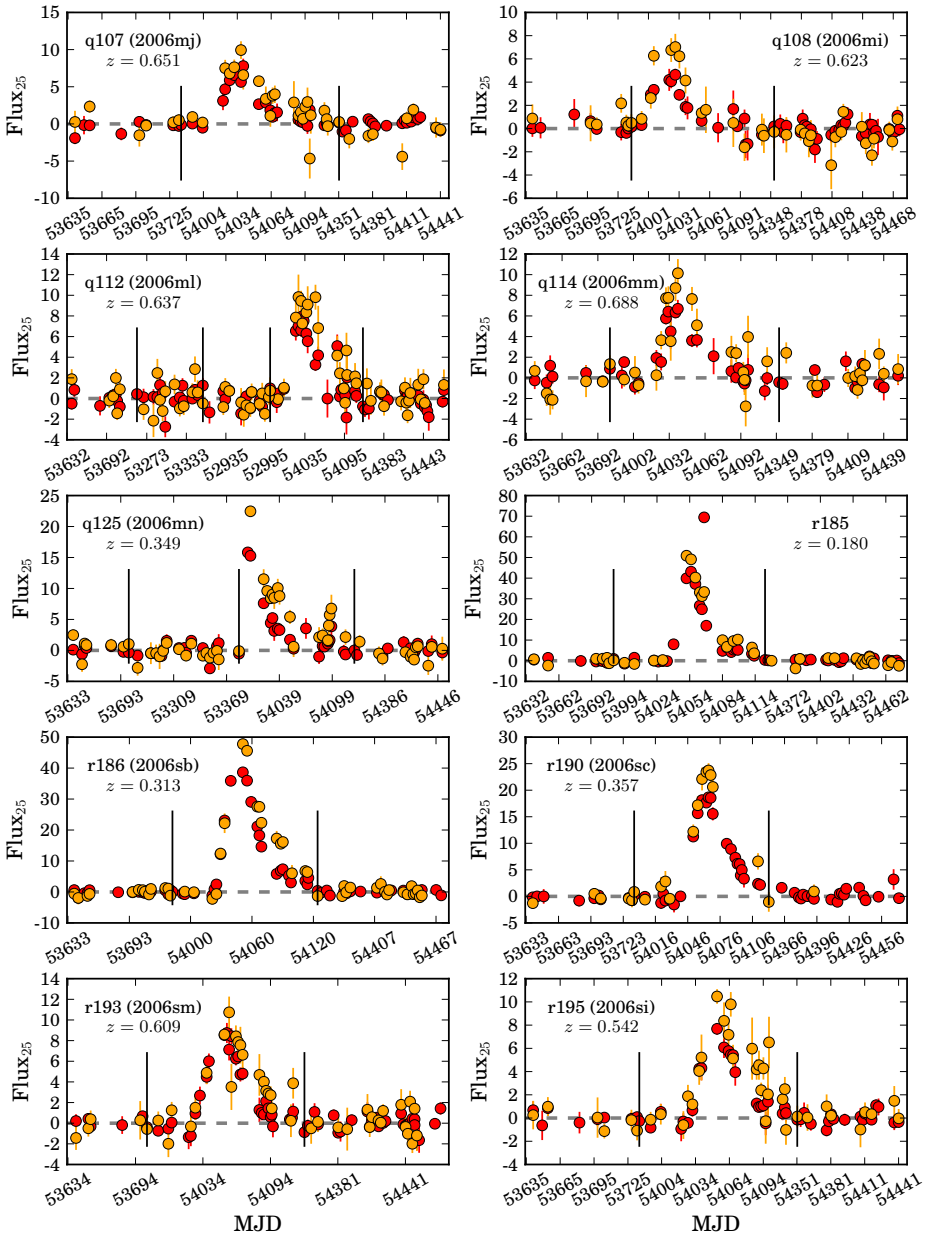

Figure 5.7: (Continued)

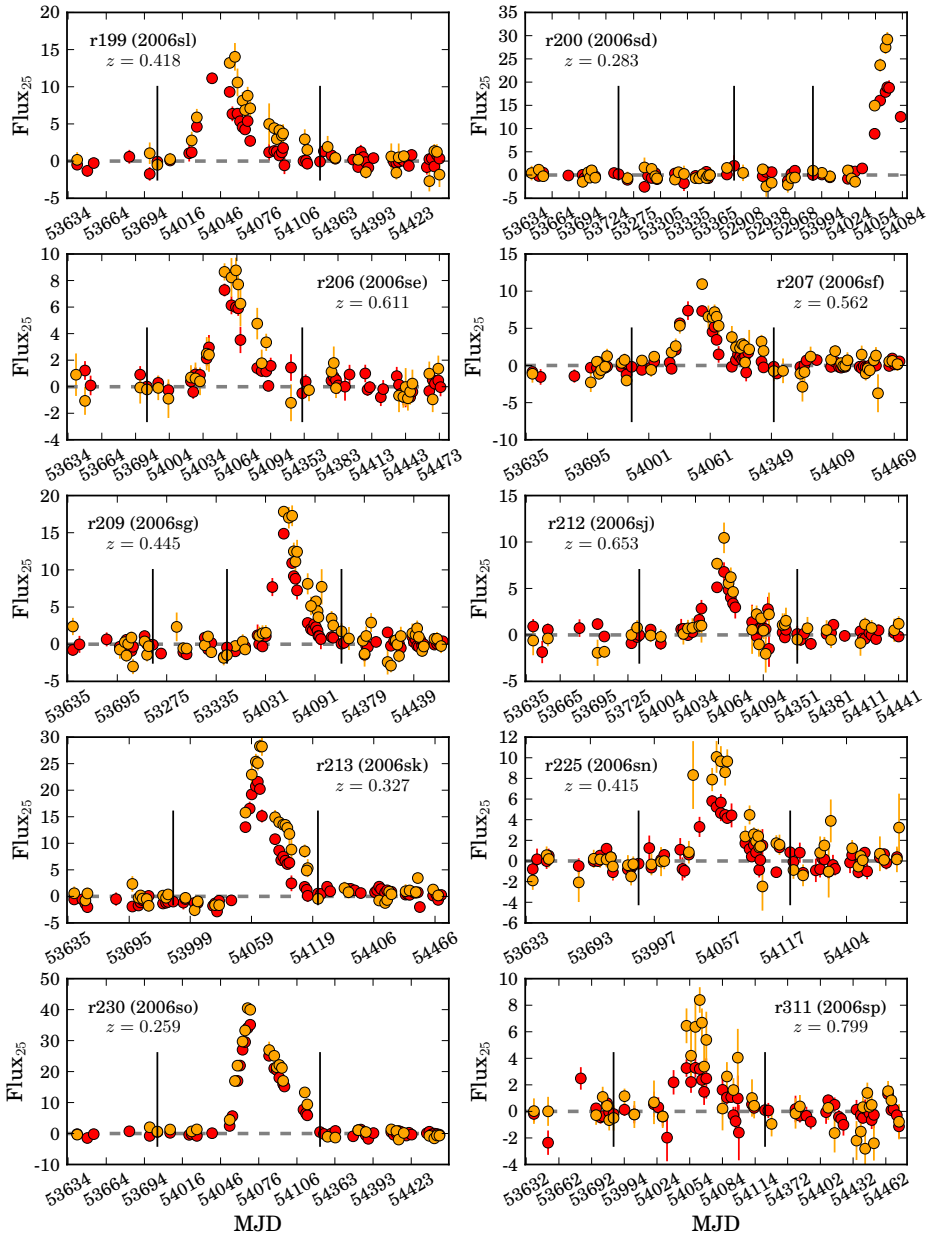

Figure 5.7: (Continued)

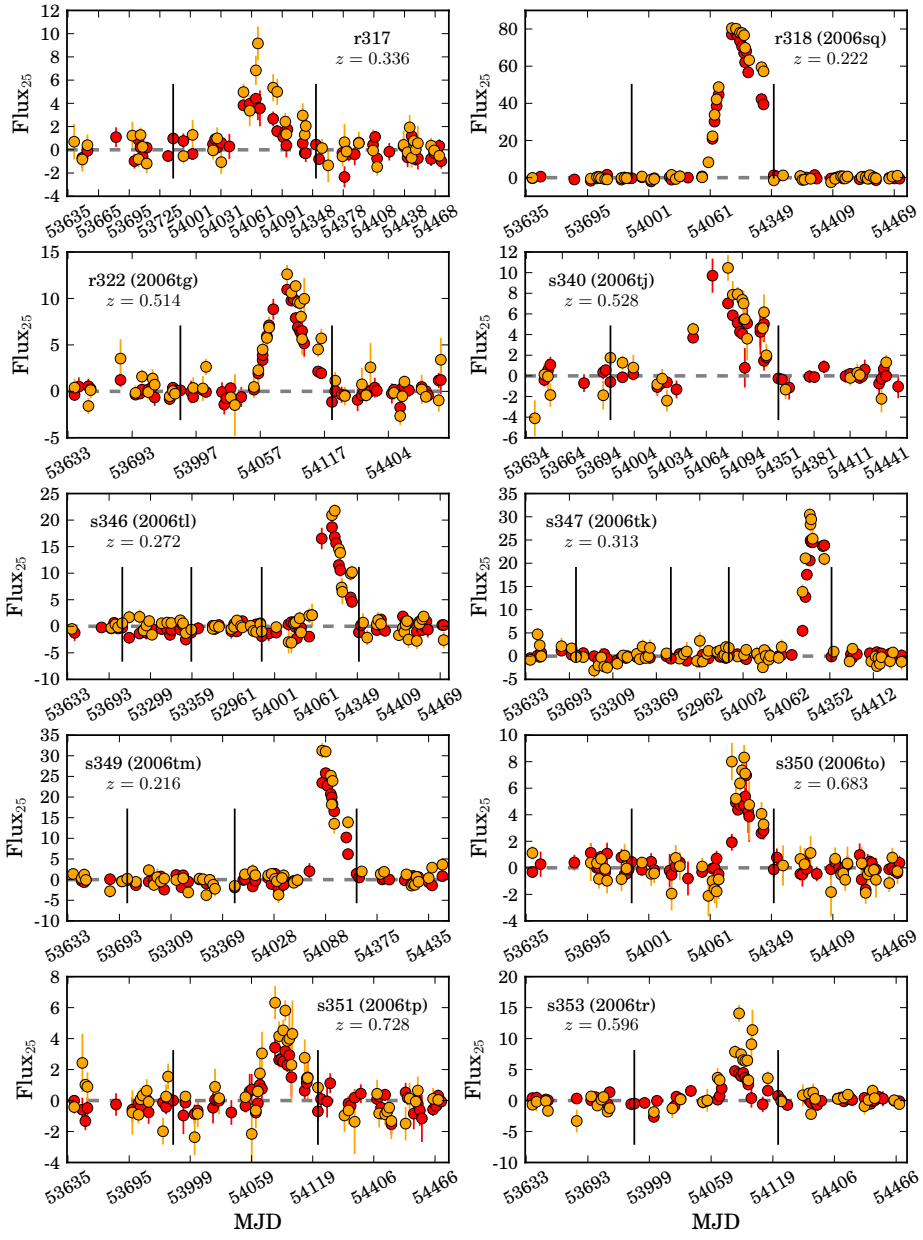

Figure 5.7: (Continued)

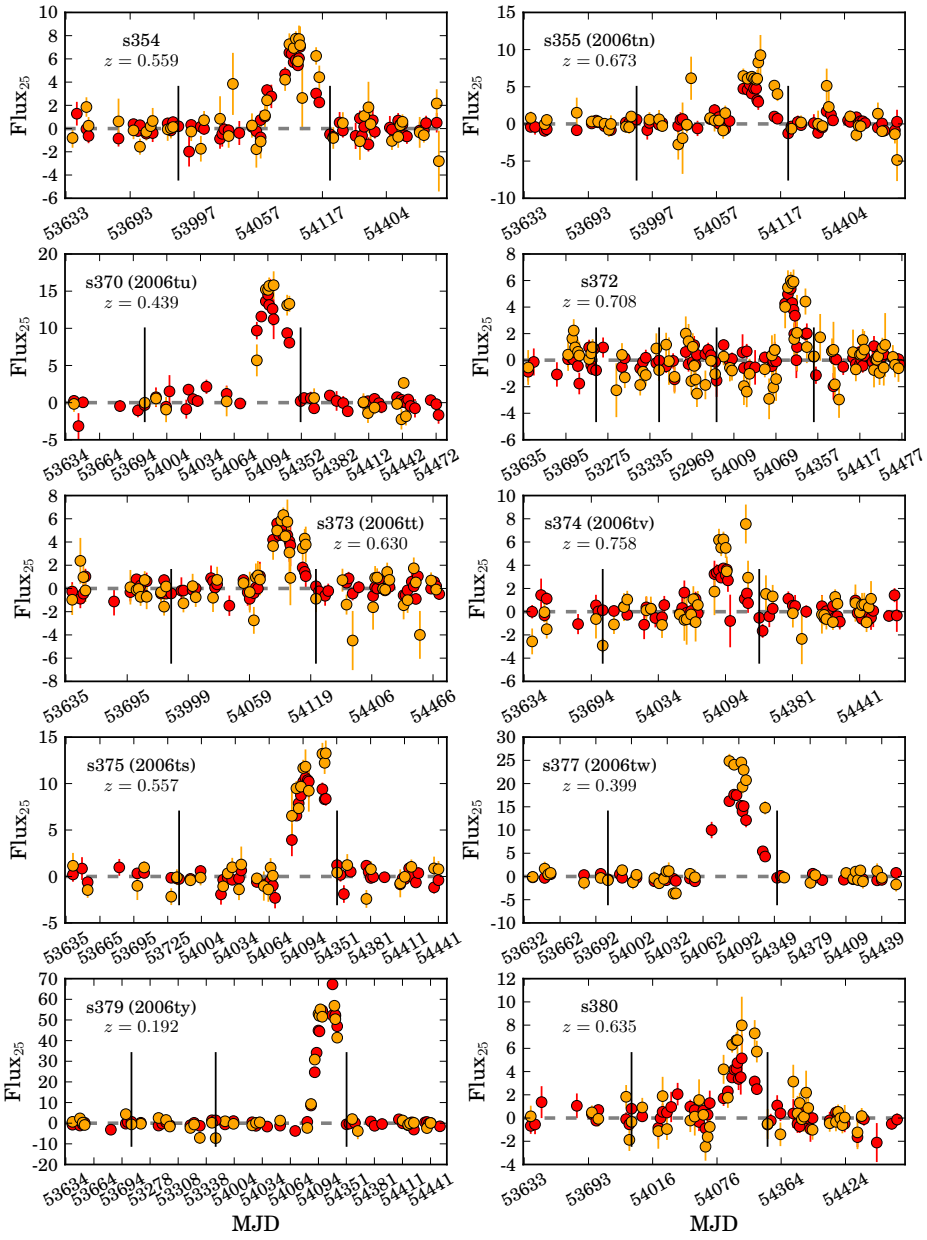

Figure 5.7: (Continued)

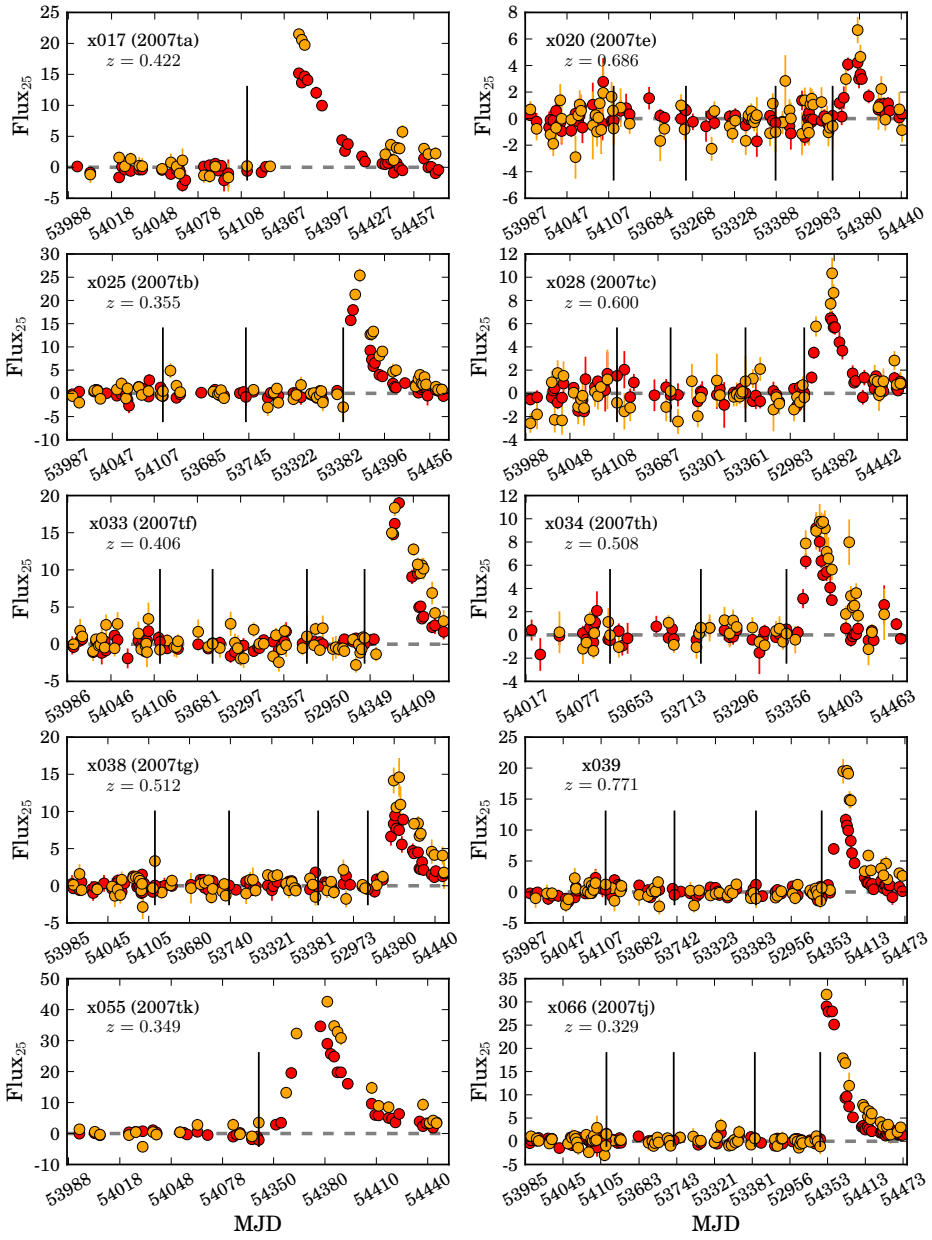

Figure 5.7: (Continued)

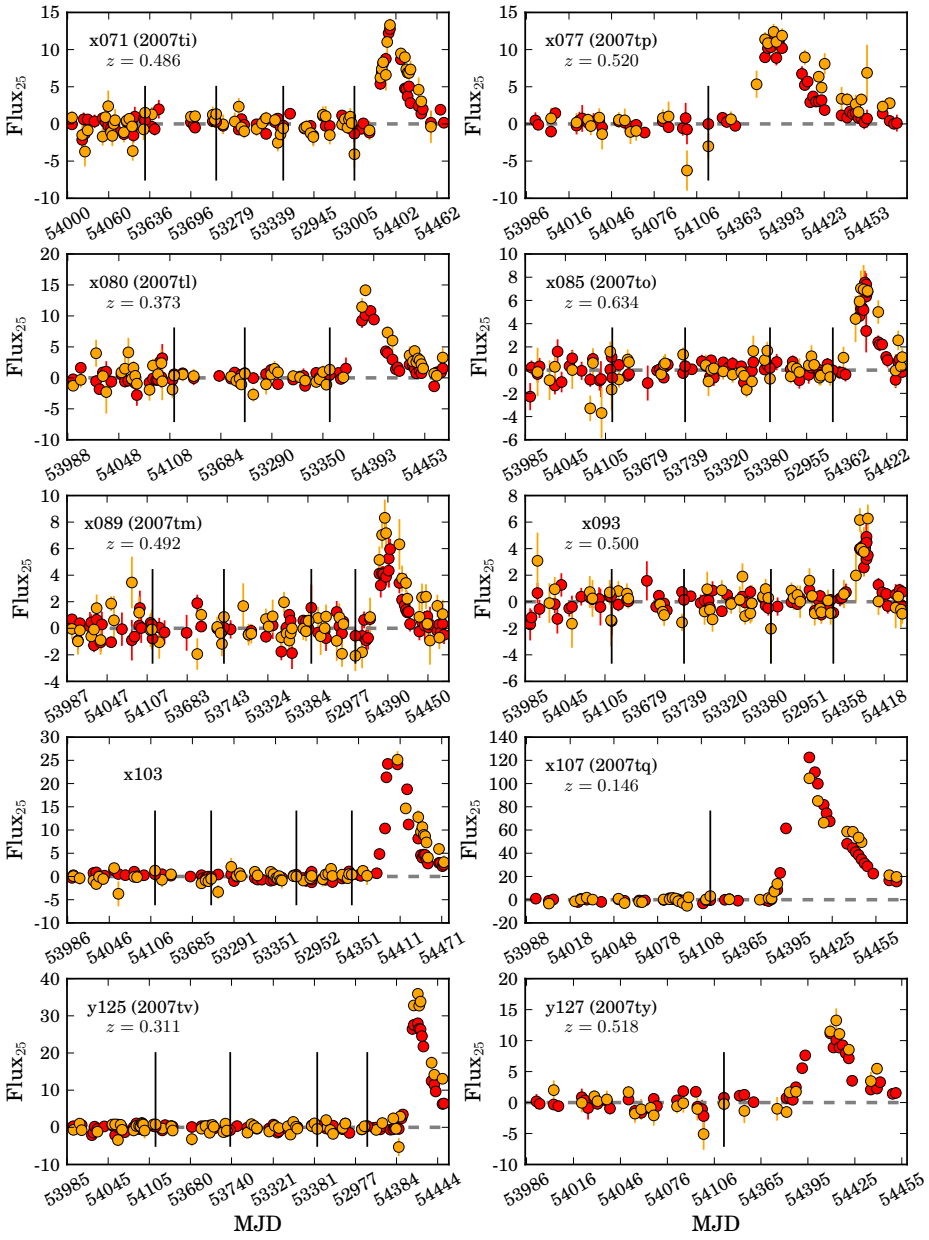

Figure 5.7: (Continued)

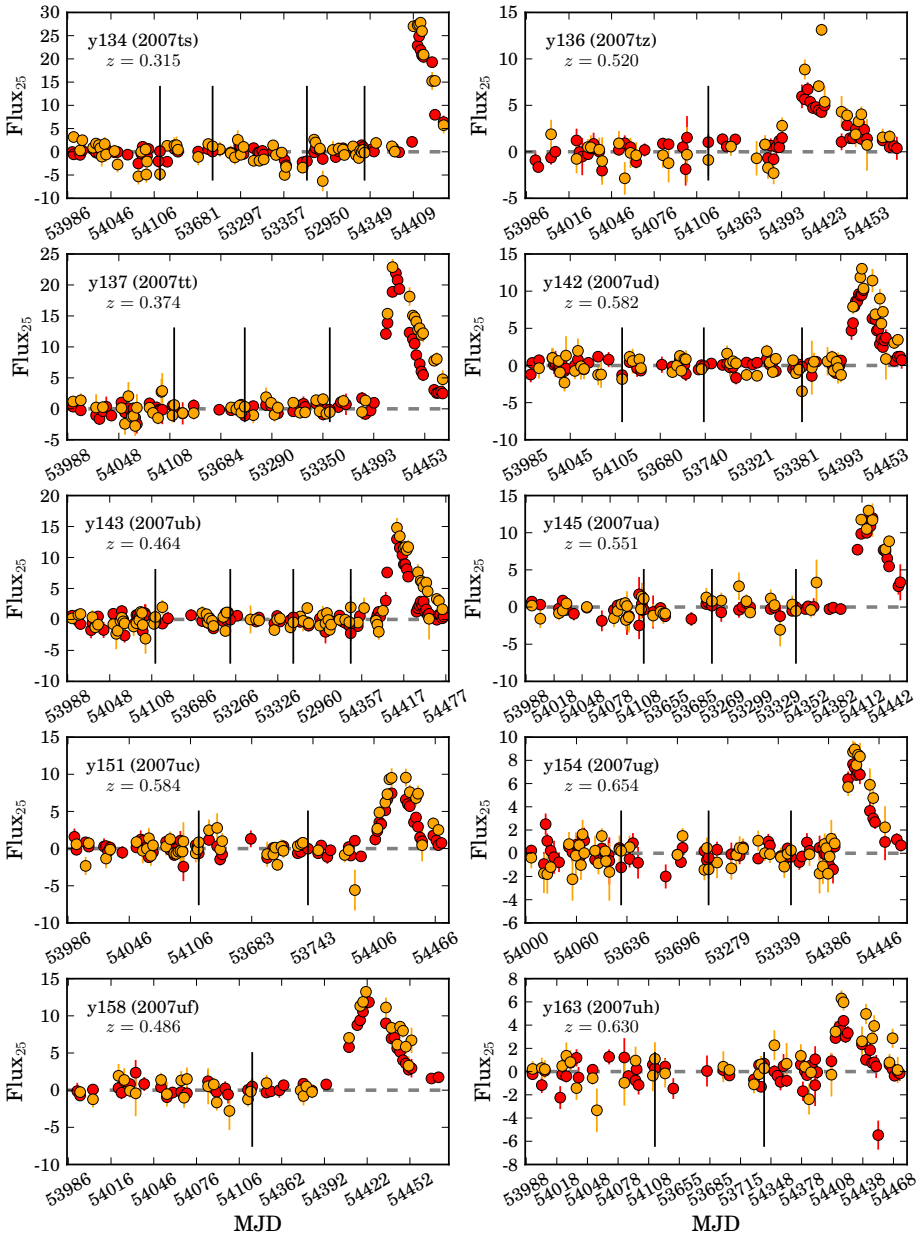

Figure 5.7: (Continued)

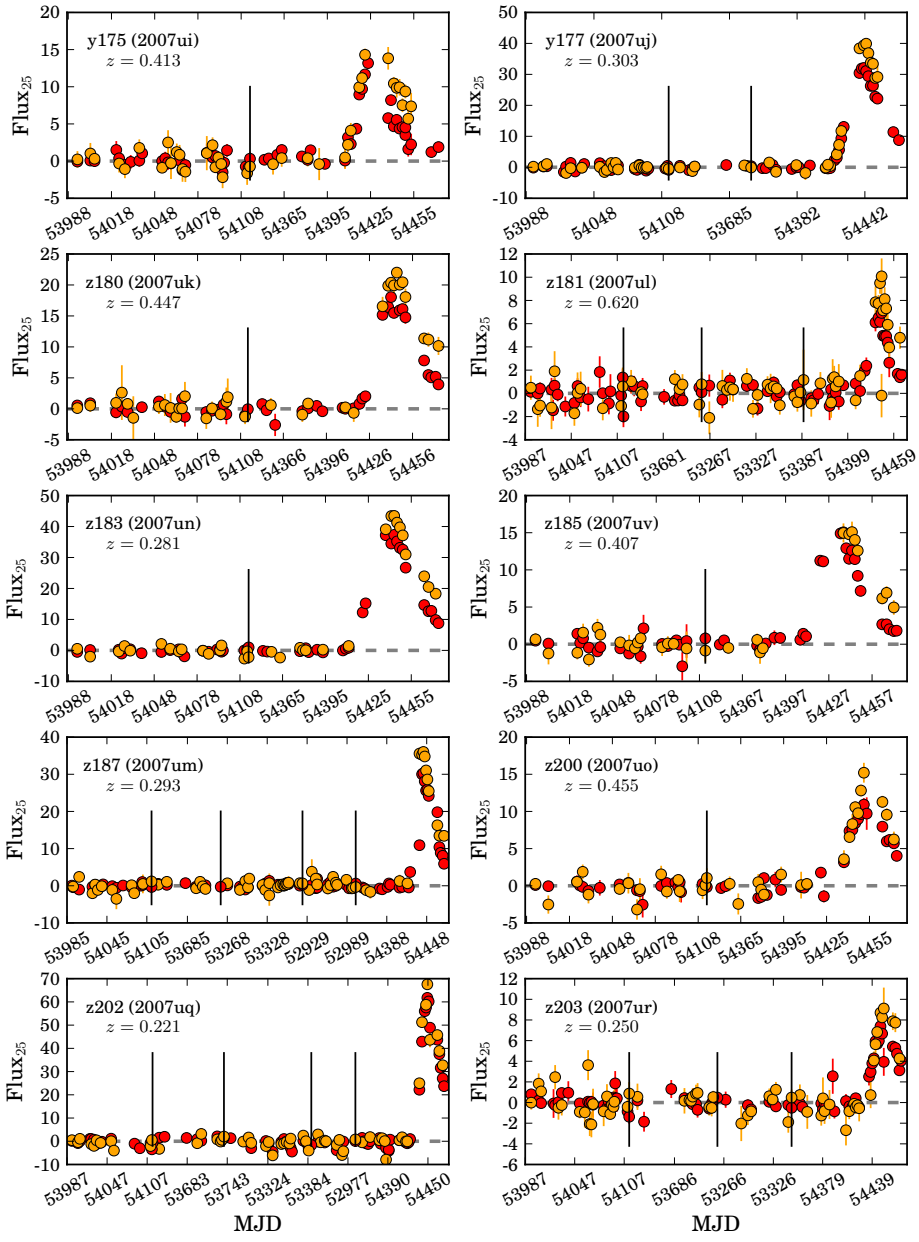

Figure 5.7: (Continued)

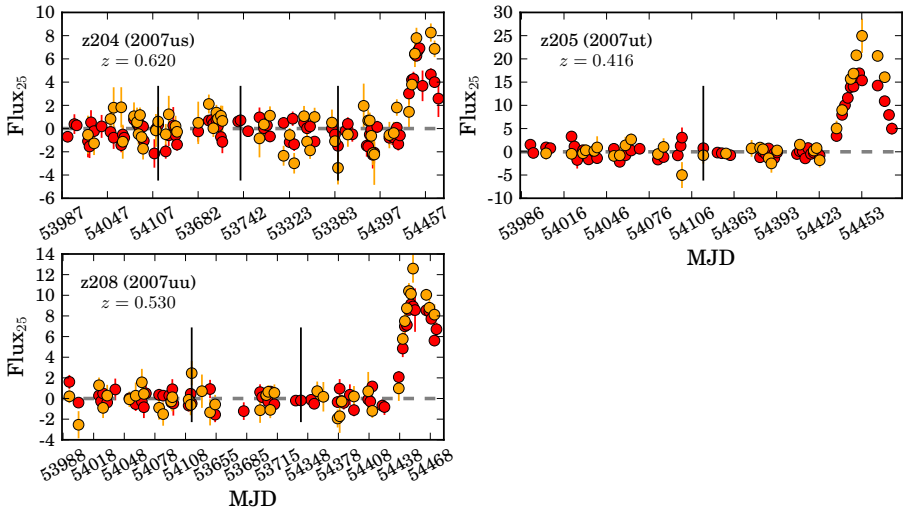

Figure 5.7: (Continued)

The major difference between a thing that might go wrong and a thing that cannot possibly go wrong is that when a thing that cannot possibly go wrong goes wrong it usually turns out to be impossible to get at or repair.

Douglas Adams, Mostly Harmless

6

Systematics Affecting the ESSENCE Survey Photometry

There are various sources of systematic uncertainty that affect our calibrated natural magnitudes. Here we identify and assess the size of each effect using empirical tests of internal and absolute photometric calibration. Wherever possible, we quantify systematics by directly introducing a bias at either the image or catalog level and propagating the bias through our pipeline to measure the effect on output photometry. We also compare our photometry to SDSS photometry converted to the Landolt system, to set an upper limit on our systematic error budget and evaluate our absolute photometric calibration in the different ESSENCE fields.

The systematic effects can be divided into two categories:

1. effects that cause errors in individual photometric measurements, *and correlate with distance, leading to a bias* in cosmological inference.

2. effects that cause errors in individual photometric measurements, but are not correlated with distance, and therefore do not bias the cosmological result, but

nevertheless lead to *increased dispersion* in Hubble residuals.

We list the various sources of photometric error in Table 6.1, and detail and estimate the effect of each in the sections that follow.

Table 6.1: Summary of the systematic uncertainties on calibrated CTIO 4 m natural magnitudes from ESSENCE

Effect	Δ_R (mag)	Δ_I (mag)
Errors in the Measurement of Flux		
Shutter precision	< 0.001	< 0.001
Detector linearity	0.005	0.005
Bias and Flat-field corrections	± 0.005	± 0.005
Astrometric errors	0.005	0.005
Errors in the Photometric Calibration		
$\pm 10\%$ error in extinction slope	∓ 0.001	∓ 0.002
Errors in color term	± 0.005	± 0.005
Errors in the zero point	0.003	0.001
Errors in extrapolating zero points	< 0.001	< 0.001
Magnitudes of BD+17°4708	± 0.002	± 0.002
Total	± 0.011	± 0.010
SED of BD+17°4708	± 0.002	± 0.003
Total	± 0.012	± 0.011

Note: Italicized entries are sources of increased dispersion on distance moduli, but not bias.

6.1 Shutter Precision

The MOSAIC II shutter is described in §2. The shutter blades take 23 msec to cover the entire field, leading to a $\pm 0.5\%$ non-uniformity for a one second exposure. This is a negligible correction for the exposure times of all ESSENCE science (200 s in R and 400 s in I) and calibration frames (>10 s in both filters).

6.2 Detector Linearity

We imaged the Ru149 field in R and I varying the exposure times from 2^1 – 400 seconds. Fluxes are measured for isolated stars using a fixed 20 pixel aperture radius and corrected for extinction. We compute residuals to the average magnitude for

[1] Exposures under 10 seconds are not used outside this analysis of detector linearity.

each star and computed the 3σ clipped average residuals for all stars. We find that these average residuals are < 0.005 mag over the entire range of exposure times for both filters or that the detector is linear to $\sim$0.5%.

6.3 Systematic Errors with Image De-Trending

We avoid most long-period systematic errors with image pre-processing by using biases and flat fields obtained nightly, rather than a global bias or flat field for a full observing season. Any systematic errors caused by a mis-estimation of the bias or the flat field will only exist intra-night. While photometric measurements of objects observed on those nights will be systematically biased, this error does not affect photometric measurements of the same objects from other nights. Consequently, the effect is very unlikely to correlate with distance modulus, and will not lead to a bias in cosmological measurements.

The systematic uncertainties associated with the illumination correction are estimated in Appendix A and found to be $< 0.3\%$. We typically obtain $\sim$10 bias and dome flat images in each filter each observing night. Comparing the combined bias and flat-field images of consecutive nights, we find differences of $\sim$0.1%. We therefore adopt a 0.5% error as the systematic error associated with our image de-trending.

6.4 Astrometric Error

The astrometric uncertainty of a single detection is composed of a systematic floor and a term that is inversely proportional to the S/N ratio and directly proportional to the FWHM of the detection:

$$\sigma_a^2 = \sigma_{sys}^2 + \sigma_d^2 \left(\frac{FWHM}{SNR} \right)^2 \tag{6.1}$$

The uncertainty on a difference in position ΔX along one axis, $\sigma_{\Delta X}$, is $\sqrt{2}\sigma_a$. We can estimate the systematic floor of the astrometric uncertainty by comparing positions measured for a typical image with the average of the positions measured from several images.

$$\sigma_{\Delta X}^2 = 2\sigma_{sys}^2 + \sigma_d^2 \left(\frac{FWHM}{SNR} \right)^2 \tag{6.2}$$

where here the FWHM and SNR are appropriate for the typical image and the second term is negligible in the high-SNR stacked image.

We find that positions for supernovae are accurate to within 0.02″. M07 measured the impact of such an offset by identifying sources of known flux with FWHM typical for the survey, and measuring their flux through a PSF offset by 1″. As our cadence provides S/N>10 for even our highest redshift objects, we find that PSF mis-alignment has only a sub-percent impact on our photometry. As the uncertainty is related to the SNR, we expect increased dispersion at high-z, however, we do find any net bias in the recovered astrometry of known sources with magnitude.

6.5 Errors in Determining the Airmass Relation

An error in the slope of the airmass relation would lead to an error in extrapolating the zero points to and between the ESSENCE fields. This is mitigated by extrapolating the zero point for any given image from other images with a photometric calibration only within an airmass of ± 0.5. We introduce a 10% error in the airmass relation and propagate the error to our photometric catalogs. Such a large error is extremely unlikely, and would be visually apparent, as we obtained images of standard fields over an extended range in airmass, but allows us to place an upper limit on the resulting systematic error in magnitudes.

We find that a $\pm 10\%$ error in the airmass term causes a ∓ 0.001 mag error in R and a ∓ 0.002 mag error in I (see Fig. 6.1). The slightly larger effect in I, despite the weaker extinction coefficient, is a result of the lower number of I images overall, and the larger fraction of I calibration images that were observed at high airmass, relative to R.

We also compute the mean difference in appropriate magnitude bins to evaluate if there is any residual trend as a function of magnitude. This is critical for SN Ia measurements which span a wide range in magnitude as a function of redshift, light curve shape and host-extinction. We find weak $< 0.1\%$ trends as a function of magnitude.

6.6 Errors in Determining the Photometric Transformation to the Landolt System

Extinction due to dust in the host-galaxies of the supernovae makes them appear fainter than predicted for their redshift, mimicking the effect of the dark energy. Accurate measurements of SN Ia color are critical in constraining the reddening, and allow us to disentangle the effect of dust from the dark energy signal.

High-redshift SN Ia surveys are inefficient at finding large numbers of nearby SN and therefore use several literature low-z SN Ia [24, 42, 48, 53, 55, 63, 117] ,as an anchor for cosmological measurements. Thus any *absolute* zero point offsets, even if arising from inaccuracies in the nearby sample, are a common source of systematic error for high-redshift surveys. As most nearby SN Ia surveys are tied to the Landolt network, we can quantify the size of such an offset in part by examining our own calibration to the Landolt network.

In addition, any errors in our R and I flux scaling *relative* to each other would distort the observed color of the entire sample. At the typical redshifts probed by ESSENCE, our RI photometry covers the rest-frame BV, and our inferred host-galaxy extinction is related to the measured rest-frame color excess, $E(B-V)$. If we assume that the slope of the reddening law, R_V, in the host-galaxies of our SN Ia is similar to our own Galaxy ($R_V \approx 3.1$), then any error in our measured color would lead to an error $\sim$3 times larger in the extinction, A_V, and the distance modulus, μ.

SN Ia surveys like ESSENCE are therefore particularly sensitive to systematics affecting measured colors. An error in the photometric transformation can take the form of an error in determining the slope of the color law, or a residual difference in magnitudes around the intercept. The effect of an error in the slope of the color relation is small, as the error is on the order of the product of the error in the color term and the difference between the mean color of our field stars and the color of BD+17°4708. We measure the effect of an error in the color term using synthetic photometry, as described in Appendix B.2, and find that a $\pm$0.02 error in the slope of the color relation would lead to a $\sim\pm$0.003 mag systematic error in the magnitudes of field stars, and derived zero points. We conservatively adopt an error of 0.005 mag as the systematic error resulting from an error in the estimate of the color term.

We measure the residual difference in magnitudes, $M_{4m} - M_{\mathrm{Landolt}}$, for our

calibration fields around $R - I = 0.32$ mag in our standard fields and find these to be -0.003 mag and -0.001 mag in R and I respectively, with an uncertainty of ~ 0.001 mag in both bands (see Fig. 6.2). The dispersions about the mean residual are $\sim 1\%$ in both R and I. The residual is consistent with zero in I, and of low significance in R. We adopt these values as systematic uncertainties in the absolute zero point.

6.6.1 Comparison to the Sloan Digital Sky Survey

While we cannot directly compare our magnitudes to Landolt magnitudes in our science fields, we use stars selected from SDSS DR7 and converted onto the Landolt network using transformation equations. This procedure has some limitations: the SDSS imaging is not as deep as MOSAIC II images of the ESSENCE fields, and SDSS magnitudes converted onto the Landolt network have large statistical uncertainties associated with the transformation between two dissimilar photometric systems. In addition, the wcc field is outside the SDSS footprint, and is not included in the analysis. However, as the SDSS photometry was not used in determining our photometric calibration, it provides a useful, independent test on our photometric accuracy.

We cross-match stars from Stetson [132] in SDSS, and extract Übercal [99] corrected magnitudes. Only objects with clean photometry, point-source PSFs, *gri* uncertainties < 0.1 mag and $\sigma_z < 0.15$ mag without a corresponding entry in the DR7 QSOBest catalog, satisfying

$$\begin{aligned} 0.95 &< u - g < 2.75 \\ -0.01 &< g - r < 1.78 \\ -0.12 &< r - i < 2.74 \\ -0.13 &< i - z < 1.58 \end{aligned}$$

and close proximity to the stellar locus are selected from SDSS (see Fig. 6.3).

We use simple linear transformations for stars with $r - i < 0.8$, determined using the "LINMIX_ERR" routine [66] available in the IDL Astronomy Library[2]. We derive the following transformations (see Fig. 6.4) using > 1300 measured stars:

[2] http://idlastro.gsfc.nasa.gov/

$$
\begin{aligned}
R_L &= r - (0.303 \pm 0.006)(r - i) - (0.133 \pm 0.002) \\
I_L &= i - (0.213 \pm 0.007)(r - i) - (0.388 \pm 0.002)
\end{aligned}
\tag{6.3}
$$

We find large intrinsic dispersions of $\sim$0.025 mag in the relations between the SDSS and Landolt photometry for both R_L and I_L. This dispersion is inherent in the transformation between two photometric systems with very dissimilar transmissions, and significantly different dynamic ranges, and further justifies our choice to base the calibration of the 4m natural system on the Landolt standard network. We do not find any significant trend in the residuals of transformed R_L with $g - r$, or I_L with $i - z$. We apply these transformations to SDSS stars in our science fields, selected using the same criteria, to derive their Landolt magnitudes.

We compared our tertiary photometric catalogs for the science fields to SDSS stars, selected using the same criteria as above, converted to Landolt using our derived transformations. We found no significant field-to-field differences. We measured the offset between the CTIO 4 m natural system and these transformed stars around $R - I = 0.32$ mag as in the standard fields, and found offsets (in the sense of 4m magnitude *minus* transformed SDSS magnitude) of 0.009 ± 0.03 mag in R, and 0.013 ± 0.03 mag in I, consistent with zero. The large uncertainties arise from the intrinsic dispersion in the transformation to R and I, and the r and i uncertainties that are propagated into the uncertainty on the $R - I$.

6.7 Errors in Extrapolating Photometric Zero Points

We evaluate the error in determining the photometric zero point for a single amplifier by extrapolating the zero point of the image using the average of all other amplifiers of the same image, and the average of all other images that are within $\pm$0.5 in airmass and $\pm$100 seconds in exposure time, adjusted for both the difference in airmass and the difference in exposure time. We find the difference between the zero point and the extrapolated zero point to be < 0.001 mag. We also construct this statistic field by field and amplifier by amplifier and find no significant difference in these sub-samples. The histogram of differences between the extrapolated and directly fitted zero points are

shown in Fig. 6.5.

Additionally, we find that the images with the largest differences between fitted and extrapolated zero points are typically taken in non-photometric conditions and fail quality tests for difference imaging. We find no significant trends in the difference between direct and extrapolated zero points with airmass, aperture correction error, exposure time, FWHM or sky background. The standard deviations of the un-clipped data are $\sim$0.01 mag in both *R* and *I*. Either 3σ clipping extreme outliers or using a Gaussian to model the data reduces the estimate of the standard deviation to $<$ 0.01 mag. This is a strong indication that our internal photometric calibration is good to at least 1%.

6.8 Errors in Determining the Natural System Magnitudes of BD+17°4708

The CTIO 4 m natural magnitude system adopted in this work utilizes BD+17°4708 as the fundamental spectrophotometric standard and consequently, the magnitudes of BD+17°4708 in the natural system are close to its Landolt magnitudes by construction. However, there are several astrophysical differences between BD+17°4708 and the "typical" Landolt standard star. We determine the corrections to the first order magnitudes of BD+17°4708 in Appendix B.3. Systematic errors in the magnitudes of BD+17°4708 would lead to an error in the synthetic zero points and *k*-corrections, and the uncertainty budget is dominated by the impact of a potential unresolved binary companion.

6.9 Errors in the SED of BD+17°4708

While the derivation of the magnitudes of BD+17°4708 in the appendix relies on the PHOENIX synthetic spectral library [52, 130, and references therein], the derivation of synthetic zero points requires its true SED. We use the CALSPEC determination of the SED of the BD+17°4708 and adopt a 0.5% uncertainty over 3000-10000Å. These translate into 0.002 mag and 0.003 mag differences in the synthetic *R* and *I* 4m magnitudes.

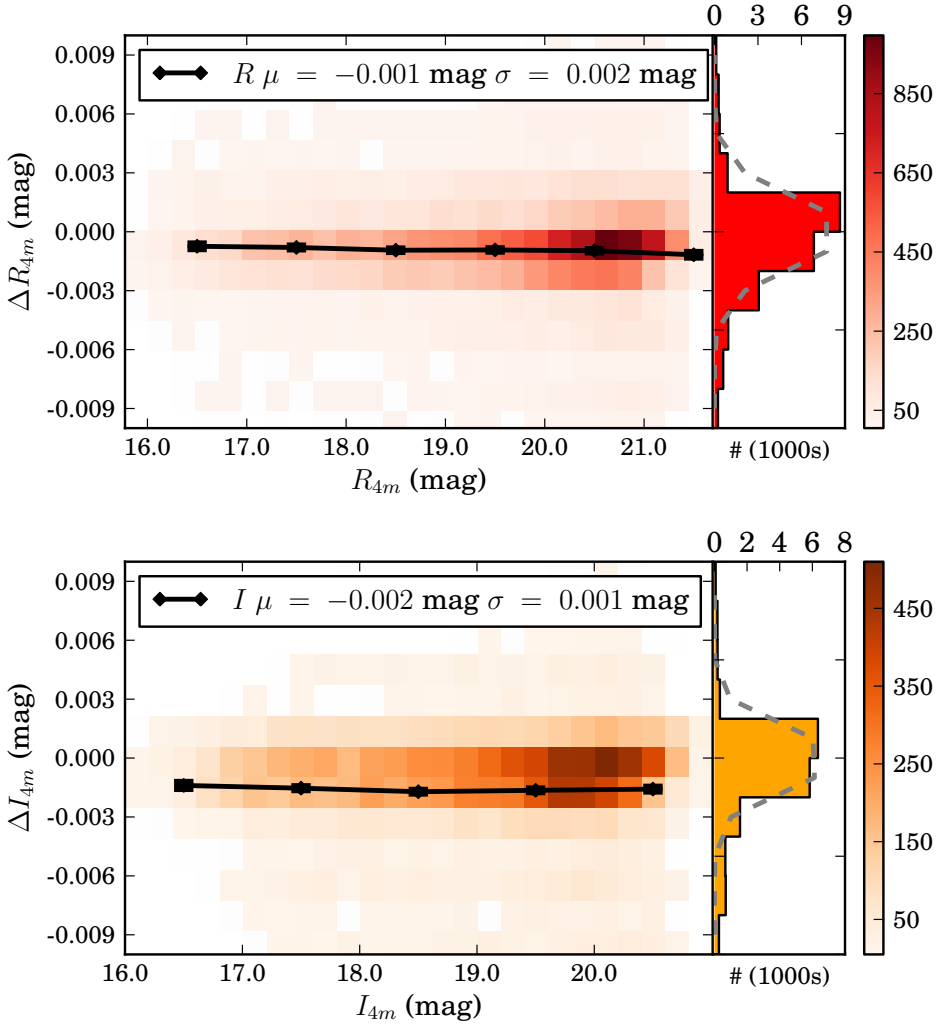

Figure 6.1: Differences in *R*- (Top) and *I*- (Bottom) band photometry with a 10% error in the slope of the airmass relation (in the sense of with offset *minus* no offset), binned as a function of magnitude (Left panel) and for all amplifier images (Right panel). The color bars indicate the number of amplifier images in each bin. The means in bins with 1 mag widths are over plotted (black diamonds). We find a resulting -0.001 mag difference in the R band, and a -0.002 mag difference in the I band. Dispersions are computed using a Gaussian fit to the histogram shown at right.

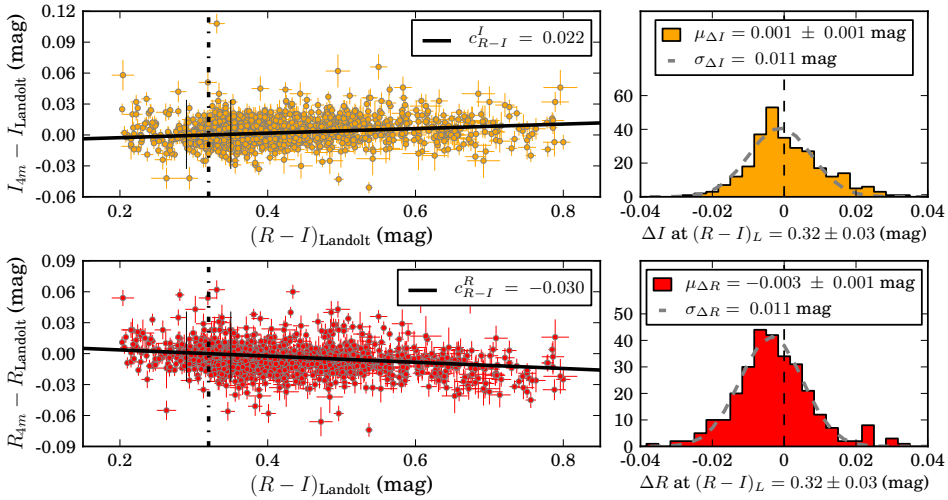

Figure 6.2: Differences in the I- (Upper Left) and R- (Lower Left) band magnitude between the CTIO 4 m and the Landolt network in the standard fields. The solid line indicates the slope of the color relation. The slopes are determined at an intercept of $R - I = 0.32$ mag. We examine the residuals in a range of ± 0.03 mag (this range is indicated by short vertical lines in the left panels) around the color intercept. We find the differences in both R (Lower Right) and I (Upper Right) are consistent with zero, indicating that there is no significant residual offset after the color transformation is determined.

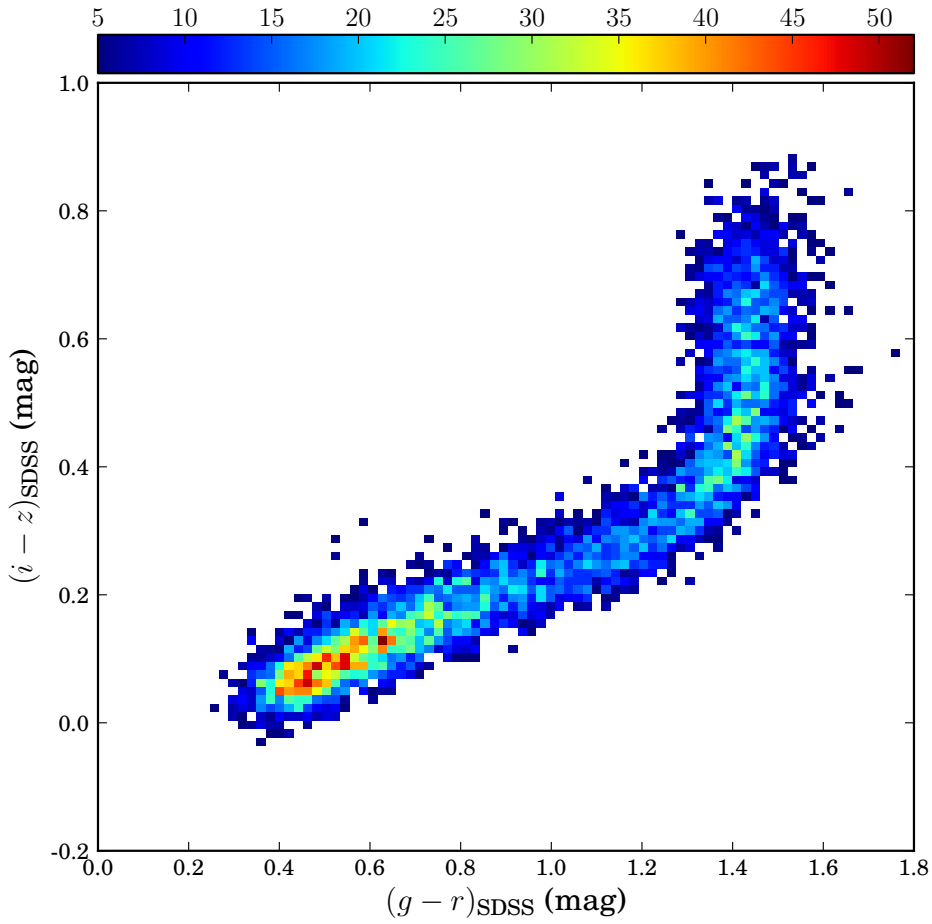

Figure 6.3: Color-color diagram of SDSS stars in ESSENCE fields. Only stars with $r - i < 0.8$ are used to derive transformations to Landolt and assess our absolute photometric consistency.

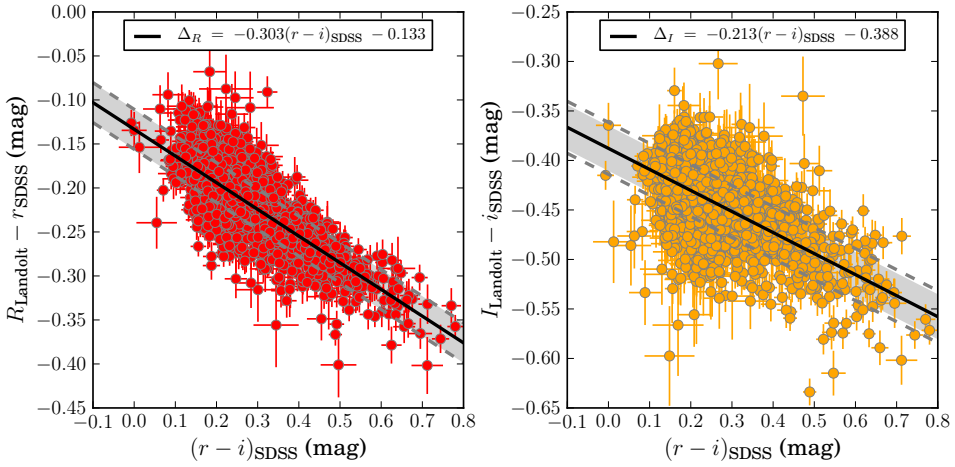

Figure 6.4: Transformations between the Landolt and SDSS photometric system using stars observed by Stetson for R (Left) and I (Right). The shaded gray region enclosed between dashed gray lines indicates the intrinsic dispersion in the fit and is $\sim$0.025 mag for both transformations.

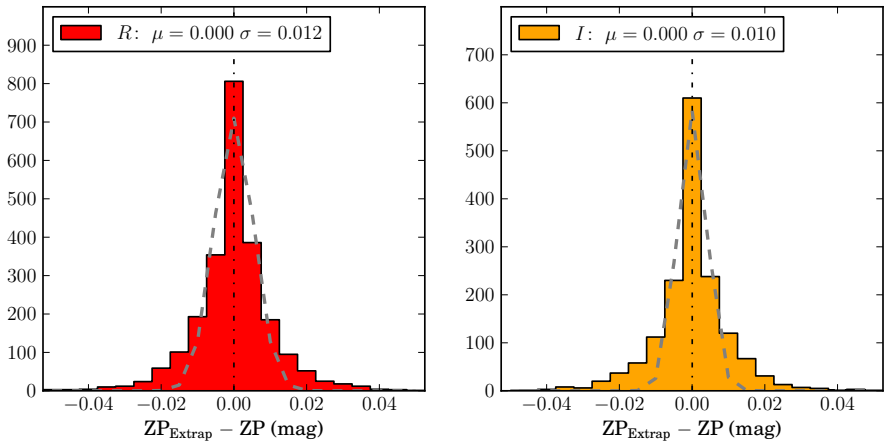

Figure 6.5: Differences between the fitted zero point of an amplifier image and the zero point extrapolated from the average of the other amplifiers of the same image, in R (Left) and I (Right). We find no net offset between the directly fitted and extrapolated zero points. In addition, the standard deviation of the residuals normalized by the uncertainties is close to 1, indicating that the uncertainties are well modeled.

7

Conclusions

We have re-calibrated the CTIO 4 m and MOSAIC II system, with a focus on minimizing the systematic errors that originate from photometry and affect the high-redshift SN Ia measurements from ESSENCE. This calibration supersedes that presented in Miknaitis et al. [87]. We have derived photometric transformations between the Landolt network and the 4m natural system without employing any observations from the CTIO 0.9 m, avoiding cross-telescope systematics.

Additionally, we have selected BD+17°4708 as the fundamental spectrophotometric standard in this work. The $R - I$ color of this standard is considerably closer to the average color of Landolt network stars, as well as SN Ia around the median redshift of ESSENCE. This choice minimizes systematic errors arising from errors in determining the photometric transformation between the Landolt and 4m natural system.

We have employed these transformations to derive secondary photometric catalogs for our Landolt calibration fields that span the MOSAIC II field-of-view. We have demonstrated that we can accurately extrapolate zero points between the different amplifiers of the imager. We have derived tertiary catalogs for ESSENCE fields, and established zero points for our imaging. We have demonstrated that the zero points in

both passbands are stable relative to each other over the entire duration of the survey. We have provided a model of the system response of the *R* and *I* passbands used by ESSENCE, and made a comprehensive estimate of the effect of various systematics on magnitudes in both passbands.

There remain several shortcomings affecting the calibration presented in this thesis. Our imaging of Landolt standard fields was obtained during our 2006–7 observing seasons. Consequently, we only used science images obtained on the same nights to derive our tertiary catalogs, rather than all survey images. While there are clear changes in the zero points over the course of the survey, the lack of standard field imaging covering the same range of time prevents us from deriving the absolute CTIO-to-Landolt photometric transformation as a function of time. As our fundamental spectrophotometric standard, BD+17°4708, was not directly observed using the CTIO 4 m, we derived estimates of its natural system magnitudes using the CTIO-to-Landolt transformations, together with Landolt photometry and the PHOENIX synthetic spectral library [52, 130, and references therein] to characterize the effect of metallicity, surface gravity, and extinction. However, the principal shortcoming of the ESSENCE SN Ia photometry remains its lack of multi-color information. This increases our sensitivity to priors on the colors or extinction of SN Ia. Nevertheless, this work demonstrates that the systematic errors from photometry are ∼1% in both *R* and *I*. This represents a better understanding of the systematic errors arising from photometric calibration, and an overall reduction of its impact on the ESSENCE systematic error budget.

The primary application of this work is the calibration of light curves of SN Ia discovered by ESSENCE, to derive the equation of state parameter of the dark energy, *w*. We have outlined our spectroscopic follow-up and classification program to identify SN Ia within survey data, and presented calibrated light curves in the CTIO 4 m natural system of 213 SN Ia and "Ia?" objects discovered by ESSENCE. We have fit these light curves using two common methodologies: *MLCS2k2* and *SALT2*.

We imposed strict, objective quality cuts, based on WV07 and C11, to identify a sub-sample of our spectroscopically confirmed SN Ia that have reliable light curve fits. We combined a sample of 108 ESSENCE SN Ia with the compilation of 441 SN Ia presented in C11. Our sample adds several additional objects in the overlap between SDSS and the SNLS, and will help mitigate the systematic effects arising from a relative zero point offset between those two samples. This is the largest combined sample of

well-calibrated SN Ia light curves to date.

Using SN Ia data alone, we found $\Omega_M = 0.258^{+0.065}_{-0.100}$ (stat 1σ) and $w = -1.134^{+0.224}_{-0.262}$ (stat 1σ). We have combined our SN Ia measurements with results from the SDSS Baryon Acoustic Oscillations program to derive stronger cosmological constraints, assuming a flat Universe.

The combined constraints from the SN Ia and BAO measurements are $\Omega_M = 0.266^{+0.026}_{-0.016}$ (stat 1σ), and $w = -1.112^{+0.069}_{-0.072}$ (stat 1σ). These results are in good agreement with other studies, and are consistent with a classical cosmological constant. Additionally, we have demonstrated that these constraints are not strongly dependent on the inclusion of the large sample of SN Ia from the SNLS 3-year data release.

We found the *SALT2* luminosity and color coefficients, α and β, to be $0.1333^{+0.009}_{-0.008}$, and $3.167^{+0.110}_{-0.108}$ respectively. While these values are in good agreement with those reported from other surveys, they indicate that the systematic issues related to the treatment of host-galaxy extinction and intrinsic SN Ia color remain unresolved.

While these cosmological constraints are preliminary and limited by the simplifying assumptions made for this thesis, the analysis we have employed is sufficient to demonstrate the cosmological utility of the calibrated ESSENCE SN Ia light curves presented herein. Additionally, these results indicate that we will likely achieve the primary goal of the ESSENCE survey: a reliable measurement of the equation-of-state of the dark energy to 10%.

7.1 The Next Horizon: Scope for Future Work

There remain a small number of SN Ia for which we have not produced light curves. Several of these objects will require some customization of our image processing pipeline. In addition, we will inspect all ESSENCE spectra to obtain as many firm classifications as possible for any remaining "Ia?" objects, as well as rule out any contamination of the SN Ia sample by mis-classification. With the addition of these objects, we will have a sample of $\sim$140 well-calibrated light curves of high-redshift SN Ia capable of passing the stringent quality cuts needed to extract reliable estimates of the distance modulus. This will more than double the 4-year sample presented in M07 and WV07.

While this thesis contains a comprehensive estimate of the systematic error budget afflicting our photometry, there are several other sources of systematics that affect the

measurement of the dark energy equation-of-state, w. We will produce Monte-Carlo simulations of SN Ia light curves to assess the selection effects arising from our spectroscopic efficiency and our light curve quality cuts, and quantify the resulting Malmquist bias.

We are in the process of updating and adapting new light curve fitting codes for use with the ESSENCE data. In particular, we will modify *BayeSN* [84] to fit observer-frame ESSENCE light curves, and re-train *MLCS2k2* using larger, more homogeneously calibrated low-z data sets [90, in prep.]. This will allow us to examine the systematic differences in light curve fitting methodologies related to the model of SN Ia in the rest-frame U-band, and the treatment of intrinsic color and extinction.

We will simulate large samples of SN Ia, consistent with the distributions reported in this thesis, as well as literature samples from various surveys, to make a careful assessment of the effect of various sources of systematic error on cosmological inferences. We will combine our measurements with those from other low and high-redshift SN Ia surveys, as well as the latest constraints from measurements of the cosmic microwave background anisotropy from Planck [106, 107], and baryon acoustic oscillation results from SDSS DR9 and BOSS [4], to place tight constraints on cosmological parameters.

Several groups have incorporated additional data and extra parameters in their cosmological studies. Building on early work by Kelly et al. [67] and Lampeitl et al. [75], the analysis of the C11 sample presented in Sullivan et al. [137] incorporated a linear correction based on host-galaxy stellar mass, and employed different SN Ia absolute magnitudes for low- and high-mass hosts (implemented in simple_cosfitter as two $\mathcal{M}$ parameters). These are significant corrections: initial results from Scolnic et al. [127, in prep.] indicate that magnitudes must be increased by 0.035 mag for host-masses $> 10^{10}\ M_{\odot}$, and downward by the same amount for host-galaxies below that mass limit. Tucker et al. [142, in prep.] will describe the properties of the host-galaxies of ESSENCE SN Ia, and we will combine those measurements together with improved light curve fitters, to extract more precise distance estimates.

Adding additional data from our spectroscopic measurements that will presented in Matheson et al. [86, in prep.], also holds potential for decreasing the scatter in the Hubble residuals further.

Much of the work described in this section will draw on the experience of several members of the ESSENCE survey, spread across four continents. Consequently, it is

rather beyond the scope of this thesis. Beyond the ESSENCE survey, there remains much work to be done to more precisely calibrate ongoing and future wide-field high-redshift surveys such as Pan-STARRS, the Dark Energy Survey (DES), and the Large Synoptic Survey Telescope (LSST).

The non-SN Ia objects discovered by ESSENCE also benefit from the updated photometric calibration presented in this thesis. Some of these objects, in particular *m006* and *y155*, exhibit extremely unusual light curves and spectra, and warrant additional studies. We will also use our non-SN Ia light curves to assess the effect of false-positives in the SN Ia sample on cosmological constraints. This will critical for future wide-field surveys that will have to rely solely on photometry to classify the thousands of transient objects that they will discover.

There remain many interesting and important questions about type Ia supernovae, particularly the nature of their progenitors, the physics of their explosions, explaining several sub-classes of non-standard SN Ia, and of course, improving their precision as standard candles. Further, we must ask what comes after SN Ia as probes of even farther horizons to study the properties of the dark energy, and measure the expansion history of the Universe. We end this report as we began it, with the words of Edwin Hubble [60]: "The search will continue. The urge is older than history. It is not satisfied and it will not be suppressed."

A

Estimation and Properties of the Illumination Correction

Flat-field images obtained with the CTIO 4 m are corrected using an illumination correction derived from science images as described in §3.1. We describe here the estimation of the illumination correction, their time-dependence, and quantify the associated systematic errors with them in further detail below.

A.1 Deriving the Illumination Correction

We create our illumination corrections using the following prescription:

1. Create a master dome flat from the set of dome flats, F_D
2. Calibrate science frames, F_S, with the master dome flats
3. Mask out all stars in the resulting science frames
4. Warp all masked science frames onto a common astrometric grid with a uniform plate scale

5. Normalize the masked science frames to the same average sky value
6. Average the resulting frames to produce one combined image
7. Normalize the combined image to a mean of unity, and take the multiplicative inverse
8. Smooth the normalized combined image with a large kernel to the generate final illumination correction

Mathematically, we can describe our final illumination correction, $I(t)$, as:

$$I = S_K \left(\left\langle \frac{F_S}{\langle F_D \rangle} \right\rangle^{-1} \right) \tag{A.1}$$

where S_K represents the smoothing kernel used in the stage, and angled braces denote the average. We bin each 1024×4096 pixel^2 amplifier image by a factor of 4, and smooth the binned image with a 30×30 pixel^2, before re-expanding the binned image to the original dimensions. This effective 120 pixel scale is larger than the small scale structures of the flat-field, such as out-of-focus dust "donuts", while retaining the large-scale gradients that we seek to correct for. Finally, we construct a master illumination-corrected flat-field image, F_I, via:

$$F_I(t) = F_D(t) \times I(t) \tag{A.2}$$

where I and F_D are normalized to an average value of 1.0, and we introduce t denotes the night of observation. The illumination-corrected flat-field image is used to flatten the science images from the night.

A.2 Temporal Stability of the Illumination Correction

We distinguish two types of changes affecting the optical system:

1. Global changes that affect all images, including new dust grains on the optics, changes in instrument mounting, and mechanical changes in the mirror support.

2. Flat field changes that only affect our dome flat images, including ghosting, non-uniformity of the flat-field screen, as well as instances where a flat-field lamp burnt out.

We examine the temporal stability of the illumination corrected flat-fields when subject to both types of changes. From Equations A.1 and A.2, provided the global changes are small, the product $F_I(t)$ should not be sensitive to changes in the dome flats. We determine the ratios of dome flat, illumination correction, and illumination-corrected flat-fields for all nights within an observing run. This is illustrated in Fig. A.1, where we compare frames between 20030927 and 20031020. The ratio of the illumination-corrected flat-field images is within 0.1% of unity, despite differences at the 0.5% level between the flat-field, and illumination correction frames. We calculate the standard deviation of the ratio images, as well as the maximum difference between the ratio image and the average of the ratio. Nights for which the standard deviation of the ratio is consistently $>$ 0.1%, or the maximum error of the ratio is consistently $>$ 0.3%, are flagged. Comparing our flagged nights to subjective observing logs for the nights, we find that flagged nights have excessive moonlight. We find that the illumination corrections degrade more rapidly towards full moon in R than I, and attribute this to the steeper gradients in the sky brightness in R. We exploit this temporal stability to estimate an illumination correction for flagged nights, using other nights within the observing run. We adopt a 0.3% error as the systematic on the illumination correction frames.

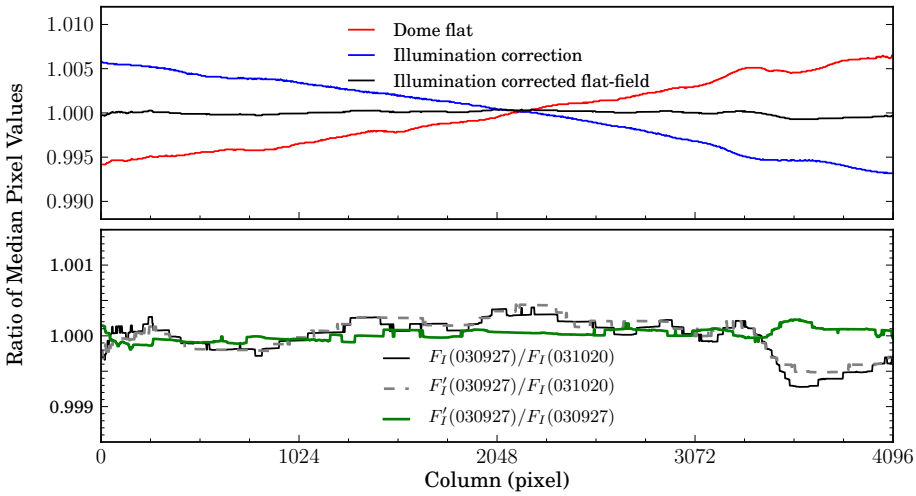

Figure A.1: An illustration of the stability of the illumination corrections from 20030927 (randomly selected) and 20031020 ($\sim$1 month later). (Top) The ratio of the dome flat frames is shown in red, while the ratio of the illumination correction frames is shown in blue. Both ratios indicate that there are differences at the $\sim$0.5% level between these two nights. The ratio of the illumination-corrected flat-field between the two nights, shown in black, is within 0.1% of unity, indicating that the illumination correction is accurately accounting for the variations in the dome flat images, despite them being separated by almost a month. (Bottom) The ratio of the illumination-corrected flat fields between 20030927 and 20031020 is again shown in black on a finer scale to illustrate the structure. We construct an estimated illumination correction for 20030927, F'_I, using the flat and bias images from 20031020, and the science frames from 20030927. The ratio of the flat-field image processed with the estimated illumination correction and the illumination-corrected flat-field for 20031020 is shown as a dashed-grey line. The ratio of the derived and the estimated illumination-corrected flat-fields on 20030927 is shown in green, and illustrates that the illumination-corrected flat-fields are stable to better than 0.1% between the two dates.

B

Properties of the CTIO 4 m Natural System

We describe the properties of the CTIO 4 m natural system in the following sections. We derive the system transmission, and compute synthetic color terms to the Landolt system. We use our determined transmission, along with synthetic photometry of model SEDs, to study the differences between our fundamental spectrophotometric standard, BD+17°4708, and "typical" Landolt stars at similar colors. Finally, we establish synthetic zero points to derive natural system magnitudes from flux-calibrated SEDs.

B.1 Transmission

We model the transmission, T, of the CTIO 4 m system by the product of four components: the atmosphere (Atm), optics (Opt), filter (PB) and the Quantum Efficiency of the MOSAIC II CCDs (QE).

$$T(\lambda) = T_{\mathrm{Atm}}(\lambda) \times T_{\mathrm{Opt}}(\lambda) \times T_{\mathrm{PB}}(\lambda) \times \mathrm{QE}(\lambda) \tag{B.1}$$

B.1.1 Detector Quantum Efficiency

The eight Tek CCDs that comprise the MOSAIC II have slightly different quantum efficiencies (listed in TableB.1). However, we find the differences in synthetic photometry from using different quantum efficiency curves is < 0.001 mag, for both R and I over a wide range of color. Consequently, we elect to use a single average value of the quantum efficiency for all the CCDs.

Table B.1: Quantum Efficiency of the MOSAIC II Imager

Wavelength	Transmission (%)								
(Å)	CCD 1	CCD 2	CCD 3	CCD 4	CCD 5	CCD 6	CCD 7	CCD 8	Average
3000	8.90	9.70	7.60	7.80	9.50	9.40	8.40	9.60	8.86
3200	18.00	18.90	15.80	16.10	18.50	18.50	18.50	19.30	17.95
3340	22.70	27.90	22.40	23.00	26.40	27.10	25.40	27.60	25.31
3650	48.40	52.60	42.10	43.50	53.00	52.70	49.20	54.90	49.55
3800	62.80	56.10	56.20	57.10	62.10	61.90	58.20	65.80	60.02
4050	67.50	68.80	57.90	60.90	63.90	66.90	63.40	72.10	65.17
4500	74.00	74.40	63.60	65.60	70.70	72.50	70.20	78.30	71.16
5000	77.90	79.40	69.90	73.60	76.10	77.80	75.00	81.40	76.39
5500	83.20	83.90	75.30	77.70	81.60	81.40	80.30	86.50	81.24
6000	86.80	87.00	80.30	84.40	88.30	87.70	85.10	89.70	86.16
6500	87.80	88.70	82.70	86.60	89.70	89.20	87.10	90.60	87.80
7000	84.70	86.20	82.80	84.50	88.40	86.30	85.70	88.10	85.84
7500	78.20	78.30	76.40	77.00	81.50	80.50	79.00	80.30	78.90
8000	68.40	68.80	67.00	68.00	71.90	68.10	69.50	70.10	68.97
8500	54.00	54.50	54.70	55.30	57.60	54.00	56.50	56.10	55.34
9000	39.30	40.30	40.20	44.10	41.90	39.20	41.30	40.90	40.90
9500	24.50	25.40	25.40	25.50	26.20	24.50	26.20	26.00	25.46
10000	10.90	11.60	11.80	12.20	12.00	10.60	11.80	11.70	11.57

B.1.2 R and I Optical Filters

The MOSAIC II uses filters that are 146×146 mm and $\sim$12 mm thick. The transmission of the R (NOAO code c6004) and I filter (c6028) were measured by CTIO staff[1] using an OceanOptics S2000 spectrometer. The S2000 is a crossed Czerny-Turner spectrometer, configured with a 600 ln/mm grating, blazed at 750 nm, for measurements over 600–1200 nm. Measurements were obtained through a 10 μm

[1] http://www.ctio.noao.edu/noao/content/mosaic-filters

wide slit coupled to a fiber optic with 400 μm core diameter. The resulting optical resolution is $\sim$10 nm FWHM. The filters are illuminated with a General Electric 787 halogen lamp with quartz bulb, identical to those used to illuminate the 4 m flat-field screen, through a ground glass diffuser. The spectrum is projected onto a 1×2048 pixel CCD array and digitized. An OceanOptics HG-1 He-Ar lamp produces reference spectral features to determine the pixel-to-wavelength transformation. The transformation is modeled as a simple cubic polynomial. The central wavelength of the filters is shifted $\sim$15Å to the blue when mounted in the prime focus of the $f/2.87$ beam with ADC, relative to measurements at normal incidence. The shift is included in the provided transmission curve.

B.1.3 Telescope Optics

As the MOSAIC II is mounted at prime focus, the transmission of the optics is dominated by the wavelength dependent reflectivity of the primary mirror, and is well modeled by the reflectivity of aluminium. The transmission of the ADC[2] was measured to above 85% between 3500–8500 Å. The transmission of the ADC does fall significantly in the ultra-violet, but this has no effect on our *RI* photometry. The drop off in the red is very gradual and the transmission at 10,000Å is $\sim$75%.

B.1.4 Atmospheric Transmission

M07 used a model of the atmospheric transmission derived from observations of spectrophotometric standards, with removal of telluric features. The resulting atmospheric model, while reasonably precise, depends on the standard used, and the details of the reduction, particularly on the fit of a smooth psuedocontinuum. We generate an atmospheric model using the MODTRAN4 code. The generated atmosphere is appropriate for an airmass of 1, and consists of 2 mm PMW of water vapor at an altitude of 2 km, convolved with the atmospheric scattering function and the transmission from aerosols. The differences between our atmospheric model and that employed in M07 are primarily in the strength of the absorption features, with the largest differences on the red-wing of the *I* band ($>$ 9500 Å). The differences result in an $<$ 0.001 mag change in synthetic colors over a wide range (note that the M07

[2] http://www.ctio.noao.edu/mosaic/manual/pfadc_paper.ps

transmission is provided in ergs/Å and must be divided by λ for comparison with this work).

The total system throughput at an airmass of unity is listed in Table B.2. Measurements of the system throughput using a tunable laser, calibrated to a NIST photodiode, were consistent with the product of each component [135]. We could not measure the system throughput of the I filter (c6005) used very early in the survey and replaced after significant damage in November 2002.

B.2 Synthetic Color Relations

We derive synthetic color terms between the CTIO natural system and the Landolt network, using a procedure similar to that of Stritzinger et al. [133]. We approximate the Landolt passbands using the Cousins R_C and I_C transmissions published in Bessell [10], convolved with a model atmosphere, and shifted in wavelength by a small amount $\Delta\lambda$. The shifts are determined by comparing the observed Landolt photometry of the non-variable standards in the spectral library of Stritzinger et al. [133], to their synthetic photometry, and shifting the passbands, without shifting the atmospheric features, until the R and I synthetic and observed photometry agreed, with a color term consistent with zero in $V - R$, $V - I$, and $R - I$. We find that the R and I Bessell filters have to be *blueshifted* by 36 Å and 12 Å in R and I respectively. Using our determination of the CTIO system throughput in Table B.2, we compare synthetic photometry of the spectral library to synthetic photometry through the shifted Bessell passbands. We derive synthetic Landolt-to-CTIO color transformations, and find $c^R_{R-I}(\mathrm{Syn}) = -0.033$ and $c^I_{R-I}(\mathrm{Syn}) = 0.047$. The results of this analysis are presented in Figure B.1.

The synthetic color term in R is in excellent agreement with the color term determined from photometric observations, but there is a significant discrepancy in I. A blueshift of $\sim$40 Å to the I Bessell transmission is required to reproduce the observed Landolt-to-CTIO color term in I, but a shift of this size introduces a non-zero $R - I$ color-term between the observed and synthetic Landolt magnitudes. There is no wavelength shift for the Bessell determination of I, such that the synthetic and observed Landolt magnitudes and the synthetic CTIO and synthetic Landolt magnitudes simultaneously agree with non-zero color terms. Fundamentally,

Figure B.1: (Top and Middle) Residuals between observed (Obs) Landolt magnitudes and synthetic (Syn) magnitudes of 99 non-variable stars in the spectral library of Stritzinger et al. [133], as a function of the observed Landolt color indicated for R (Left panels) and I (Right panels). The Landolt passbands are modeled by shifting the Bessell [10] determinations in wavelength by $\Delta\lambda = -36$ Å and -12 Å in R and I respectively. A solid black line at $\Delta M = 0$ is included as a visual guide. (Bottom) Synthetic color transformations between our determination of the CTIO system throughput and the model Landolt system throughput for R (Left) and I (Right) respectively. The observed color relations from photometric measurements is indicated by dashed blue lines, while the best-fit relation to the synthetic photometry is indicated by a solid black line. There is excellent agreement in R. We believe that the disagreement in I is a result of not modelling the roll-off in the detector quantum efficiency for the model Landolt throughput. A blue shift of -40 Å is sufficient to recover the observed Landolt-to-CTIO color term in I, but introduces a small color term between the observed and synthetic Landolt measurements in $R-I$. The observed and synthetic photometry of BD+17°4708, using the CALSPEC SED, is indicated by a blue square in all the plots. There is a $\sim$1% offset between the flux calibration of the CALSPEC BD+17°4708 SED, and the mean flux calibration of the Stritzinger et al. [133] spectral library.

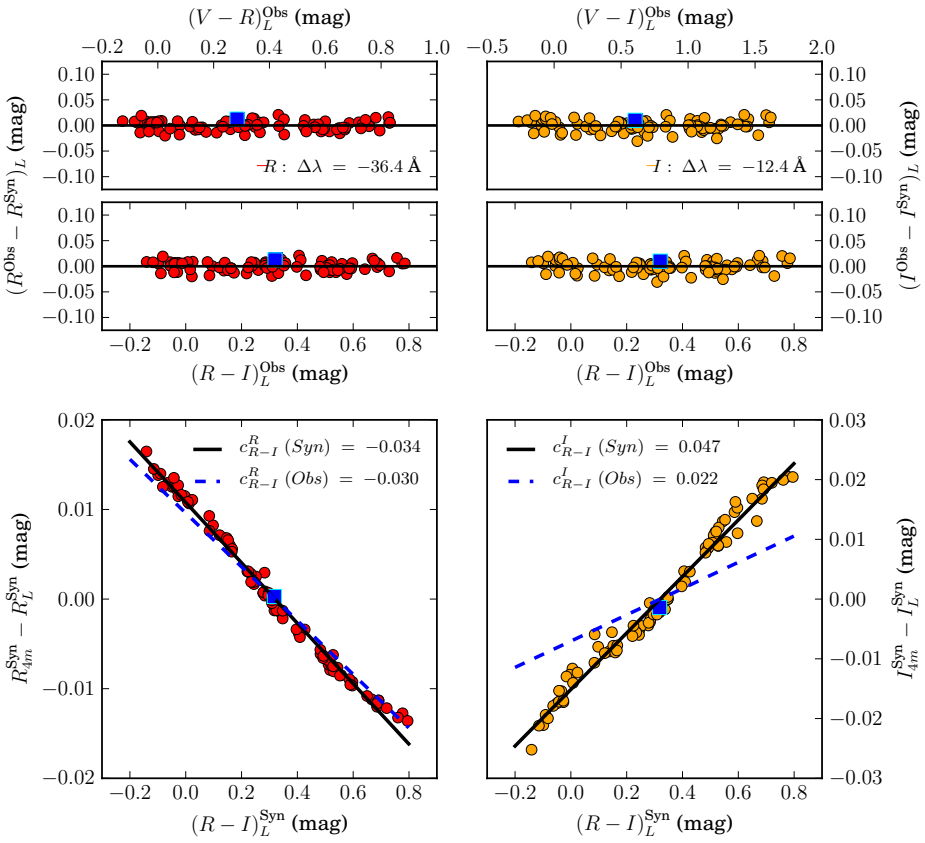

Figure B.1: (Continued)

approximating the Landolt I passband by a shifted Bessell I filter is not accurate, as the shape of these filters differ. Specifically, the transmission in the I band is significantly affected by the roll-off in the detector quantum efficiency, which is not included in the Bessell determination. The detector quantum efficiency is effectively constant over R, and therefore has an insignificant effect on the shape of the transmission. Current and future surveys observing in *griz* will be able to calibrate to photometric systems such as SDSS, Pan-STARRS and SkyMapper, which have well measured system responses.

B.3 The Magnitudes of BD+17°4708 in the CTIO 4 m Natural System

The transformations defined by equation 3.4 are constructed such that, to first order, the natural system magnitudes of BD+17°4708 are equal to its Landolt magnitudes in R and I. However, since we could not observe BD+17°4708 directly, we determine the coefficients of the transformation equations using the Landolt network of stars. In this section, we quantify the difference in natural system magnitudes between BD+17°4708, and Landolt stars with $R - I$ color similar to it by examining the photometric residual:

$$\delta L_T = M_{4m} - M_L - c^{M_{4m}}_{(R-I)_L}((R-I)_L - 0.32) \tag{B.2}$$

By construction, the average residual $\langle \delta L \rangle = 0$ for average Landolt stars. Following Regnault et al. [111], we consider the photometric residual arising from metallicty and surface gravity, extinction differences between BD+17°4708 and the average Landolt star, and consider the systematic effect of a possible faint, unresolved companion. The various effects considered are illustrated in Figure B.2.

B.3.1 Metallicity and Surface Gravity

We determine the difference in synthetic R and I 4m magnitudes residuals between BD+17°4708 and "typical" Landolt stars with metallicity, $[M/H] = -0.5$ and $\log(g) = 4.0$ as a function of the difference in synthetic $R - I$ color, over 5600 K$< T_{\rm eff} <$6500 K. We find the relationship between the mean magnitude

Figure B.2: (Top Left) Synthetic colors of Phoenix SEDs as a function of metallicity, compared to the synthetic color of the CALSPEC SED of BD+17°4708. The best model has $T_{\rm eff} = 6100$ K and $[M/H] = -2.0$ dex. (Top Right) Comparison of the CALSPEC SED and the adopted Phoenix model. The adopted model for the companion of BD+17°4708 has $T_{\rm eff} = 3000$ K and $[M/H] = -2.0$ dex. Normalized CTIO 4 m (solid) and Bessell (dashed) transmissions in R (red) and I (orange) are shown for comparison. (Middle) Difference in photometric residual, δL, (in the sense of BD+17 mag *minus* Landolt mag ($T_{\rm eff}, [M/H]$)) over a range of temperature and metallicity for R (ML) and I (MR) vs the difference in $R - I$ color (in the sense of BD+17 color *minus* Landolt color). The effect of changing metallicity is negligible in I. (Bottom Left) The values of δL at $\Delta(R - I) = 0$ for the different metallicities. The typical metallicity of Landolt stars ($[M/H] = -0.5$ dex) is indicated by the vertical line. (Bottom Right) Deviations from the relation of δL at $[M/H] = -0.5$ dex are shown for changes in surface gravity (dashed), extinction (dot-dashed) and the addition of a companion (dot-dashed grey) for R (red) and I (orange).

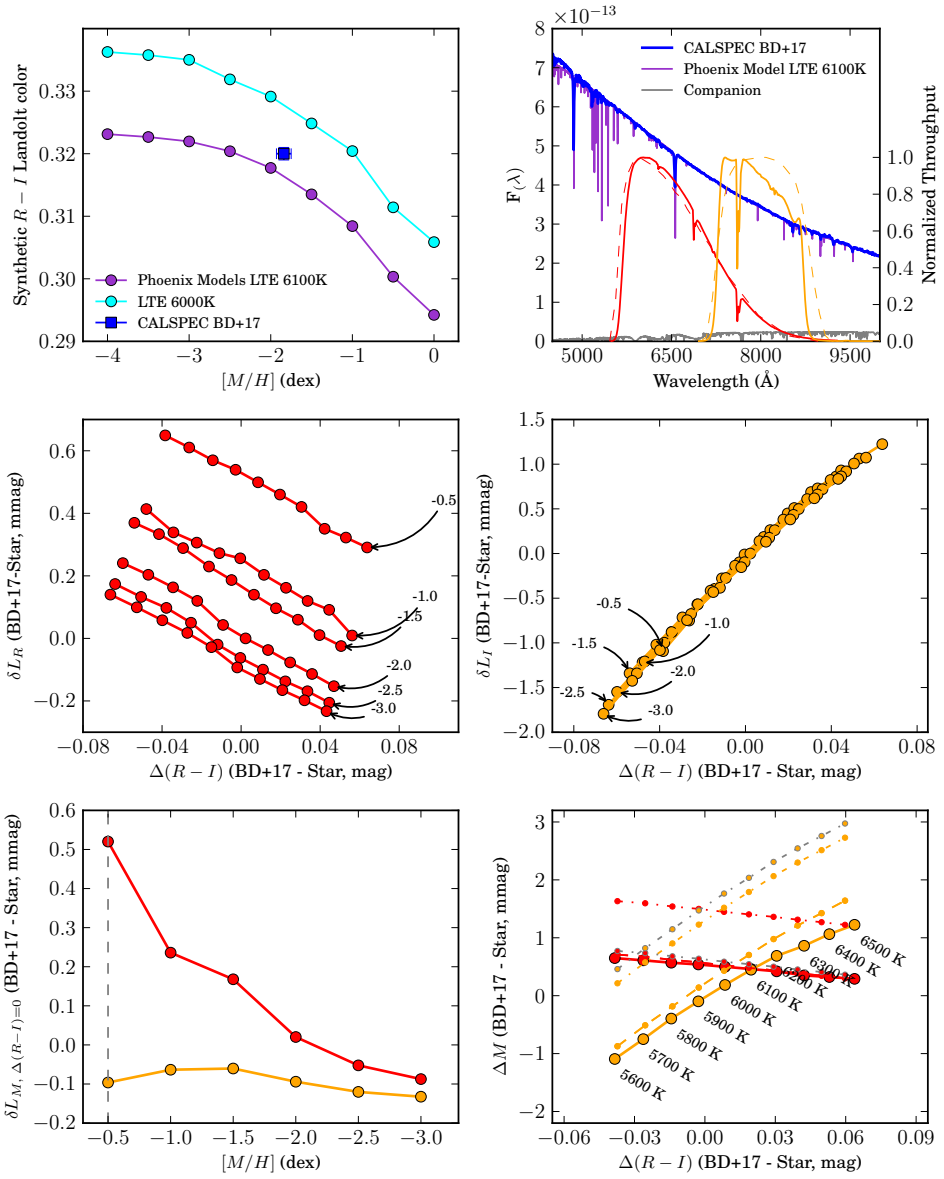

Figure B.2: (Continued)

residual, and difference in $R - I$ color to be linear for both R and I. We determine the intercept at $R - I = 0.32$, and find (in the sense of BD+17°4708 mag *minus* Landolt mag) that $\delta L < 0.001$ mag for both R and I.

To measure the effect of surface gravity alone, we select synthetic SEDs with the same parameters as above, except at $\log(g) = 4.5$. We measure the difference in the residual to normal Landolt stars, δL_M, caused by perturbing the synthetic SEDs from $\log(g) = 4.0$ to $\log(g) = 4.5$. We find the effect of changing surface gravity on the difference in residual (in the sense of residual at $\log(g) = 4.5$ *minus* residual at $\log(g) = 4.0$) is $\delta L_R < 0.001$ mag, while $\delta L_I \approx +0.002$ mag. The combined effect of metallicity and surface gravity leads to a negligible difference in R and a net δL_I of $\sim$0.001 mag.

B.3.2 Extinction

Regnault et al. [111] express the distance of BD+17°4708 from the stellar locus in $V - R, R - I$ in terms of the effect of the difference in extinction and the difference in metallicity (the effect of surface gravity being negligible over the color range in question). Having determined the effect of a difference in metallicity using a procedure similar to that above, they found the difference in the reddening between BD+17°4708 and Landolt stars of similar color to be $\Delta E(B - V)$ $\sim$0.045 mag.

We redden the synthetic SED of BD+17°4708 by this amount, and examine the difference in the residual to normal Landolt stars (in the sense of residual with reddened SED *minus* residual with un-reddened SED) to be less than 0.001 mag in R and $\approx$ 0.001 mag in I.

The combined effect of the difference in metallicity, surface gravity and extinction is found to be $\delta L_R = 0.001$ mag and $\delta L_I = 0.002$ mag. These offsets are added to the first order estimates of the magnitudes of BD+17°4708.

B.3.3 Binarity

Using the estimates from Ramírez et al. [110] for the companion of BD+17°4708 ($T_{\rm eff} = 3000k$, $\log(g) = 4.5$, and $[M/H] = -2$), we compute the difference in photometric residuals and find (in the sense of with companion *minus* without companion) than $\delta L_{R,I} \approx 0.001$ mag. As we do not know the fraction of Landolt stars

that are also in binaries, we treat these offsets as systematic errors.

B.4 Photometric Zero Points

With the Landolt magnitudes of BD+17°4708 (R =9.166 mag and I =8.846 mag) and the photometric residuals caused by the differences in metallicity, surface gravity and extinction to typical Landolt stars computed in the previous section, we invert equation 3.3 to derive synthetic passband zero points for R and I and find:

$$\begin{aligned} \mathrm{ZP}_{R_{4m}} &= -21.649 \pm 0.001 \text{ mag} \\ \mathrm{ZP}_{I_{4m}} &= -22.305 \pm 0.002 \text{ mag} \end{aligned} \tag{B.3}$$

These values differ from the values determined using the Stritzinger et al. [133] SED library by 0.012 mag. This difference is likely the result of a difference in flux calibration between CALSPEC and Stritzinger et al. [133] as illustrated in Figure B.1. We use the CALSPEC SED of BD+17°4708 for the determination of passband zero points, as its flux calibration is not affected by atmospheric transmission, and has been carefully studied by several groups.

B.5 Differences in Natural System Definition to the 4 year Data Release

M07 tied the natural system of the 4m to Landolt using α Lyr as their fundamental standard, with $(R-I)_{Landolt} = 0$. In addition, a slightly steeper c^I_{R-I} color term was employed in that work, and we expect a difference on the order of the product of difference of the color terms, and the average color of Landolt stars, $\langle (R-I)_{Landolt} \rangle$.

To first order, the differences between the photometry of stars in this work and M07 are the result of the differences between the *definition* of the photometric system in Equation 3.4 and the M07 definition:

$$
\begin{aligned}
\Delta R &\approx c^R_{R-I} \times (R-I)_{BD+17} \\
&\approx -0.030 \times 0.32 \\
&\approx -0.01 \text{ mag} \\
\Delta I &\approx c^I_{R-I} \times (R-I)_{BD+17} \\
&\quad + \Delta c^I_{R-I} \times (\langle (R-I)_{Landolt} \rangle - (R-I)_{BD+17}) \\
&\approx (0.030 \times 0.32) - 0.008 \times (0.47 - 0.32) \\
&\approx 0.009 \text{ mag}
\end{aligned}
\tag{B.4}
$$

However, we have taken various measures to improve the calibration of the natural system, with a view to minimizing our overall photometric error budget, as discussed is §3.4.1. Consequently, the methodology used in this thesis differs substantially from that used in M07. In particular, this work uses observations of the ESSENCE fields tied directly to Landolt fields, whereas M07 tied the 4m photometry to 0.9m observations of field stars, that were in turn tied to Landolt. This is a potential source of additional differences above the expected 1% level.

Table B.2: Photon Transmission Function of the ESSENCE Survey

Wavelength	Transmission (%)				
(Å)	QE	Filter	Optics	Atmosphere	Total
		R (c6004)			
5470	0.8018	0.0000	0.9087	0.8400	0.0000
5475	0.8024	0.0000	0.9086	0.8400	0.0000
5480	0.8029	0.0000	0.9086	0.8400	0.0000
5485	0.8034	0.0000	0.9086	0.8410	0.0000
5490	0.8039	0.0009	0.9086	0.8410	0.0006
5495	0.8045	0.0015	0.9085	0.8410	0.0009
5500	0.8050	0.0019	0.9085	0.8410	0.0012
5505	0.8055	0.0020	0.9085	0.8420	0.0012
5510	0.8061	0.0020	0.9084	0.8420	0.0012
5515	0.8067	0.0025	0.9084	0.8420	0.0015
5520	0.8072	0.0030	0.9084	0.8420	0.0019
5525	0.8078	0.0039	0.9084	0.8420	0.0024
5530	0.8084	0.0048	0.9083	0.8420	0.0030
5535	0.8089	0.0056	0.9083	0.8420	0.0035
5540	0.8095	0.0069	0.9083	0.8430	0.0043
5545	0.8101	0.0084	0.9082	0.8430	0.0052
5550	0.8107	0.0100	0.9082	0.8430	0.0062
5555	0.8113	0.0127	0.9082	0.8430	0.0079

Continued on next page

Table B.2 (Continued)

Wavelength	Transmission (%)				
(Å)	QE	Filter	Optics	Atmosphere	Total
5560	0.8119	0.0157	0.9081	0.8430	0.0098
5565	0.8125	0.0188	0.9081	0.8430	0.0117
5570	0.8131	0.0229	0.9081	0.8430	0.0143
5575	0.8138	0.0274	0.9080	0.8430	0.0171
5580	0.8144	0.0333	0.9080	0.8430	0.0208
5585	0.8150	0.0399	0.9080	0.8430	0.0249
5590	0.8156	0.0476	0.9079	0.8430	0.0297
5595	0.8163	0.0565	0.9079	0.8430	0.0353
5600	0.8169	0.0665	0.9079	0.8420	0.0415
5605	0.8175	0.0779	0.9078	0.8420	0.0487
5610	0.8182	0.0908	0.9078	0.8420	0.0568
5615	0.8188	0.1047	0.9078	0.8420	0.0655
5620	0.8195	0.1199	0.9077	0.8420	0.0751
5625	0.8201	0.1365	0.9077	0.8420	0.0856
5630	0.8208	0.1544	0.9077	0.8410	0.0967
5635	0.8214	0.1734	0.9076	0.8410	0.1087
5640	0.8221	0.1934	0.9076	0.8410	0.1214
5645	0.8227	0.2144	0.9076	0.8410	0.1346
5650	0.8234	0.2361	0.9075	0.8410	0.1484
5655	0.8240	0.2581	0.9075	0.8410	0.1623
5660	0.8247	0.2807	0.9075	0.8410	0.1767
5665	0.8254	0.3041	0.9074	0.8400	0.1913
5670	0.8260	0.3276	0.9074	0.8400	0.2063
5675	0.8267	0.3511	0.9073	0.8400	0.2212
5680	0.8274	0.3748	0.9073	0.8400	0.2363
5685	0.8280	0.3981	0.9073	0.8390	0.2509
5690	0.8287	0.4211	0.9072	0.8390	0.2656
5695	0.8294	0.4441	0.9072	0.8390	0.2804
5700	0.8300	0.4661	0.9071	0.8390	0.2944
5705	0.8307	0.4872	0.9071	0.8380	0.3076
5710	0.8314	0.5078	0.9071	0.8380	0.3209
5715	0.8320	0.5275	0.9070	0.8380	0.3336
5720	0.8327	0.5458	0.9070	0.8380	0.3454
5725	0.8334	0.5633	0.9069	0.8370	0.3564
5730	0.8340	0.5811	0.9069	0.8370	0.3679
5735	0.8347	0.5978	0.9069	0.8370	0.3788
5740	0.8354	0.6135	0.9068	0.8370	0.3890
5745	0.8360	0.6283	0.9068	0.8370	0.3987
5750	0.8367	0.6415	0.9067	0.8370	0.4073
5755	0.8373	0.6544	0.9067	0.8380	0.4163
5760	0.8380	0.6669	0.9067	0.8380	0.4246
5765	0.8387	0.6790	0.9066	0.8380	0.4326
5770	0.8393	0.6902	0.9066	0.8380	0.4401
5775	0.8400	0.7001	0.9065	0.8390	0.4473
5780	0.8406	0.7097	0.9065	0.8390	0.4537
5785	0.8413	0.7189	0.9064	0.8400	0.4605
5790	0.8419	0.7265	0.9064	0.8410	0.4662
5795	0.8426	0.7341	0.9064	0.8420	0.4721
5800	0.8432	0.7416	0.9063	0.8430	0.4777
5805	0.8438	0.7482	0.9063	0.8440	0.4829
5810	0.8445	0.7546	0.9062	0.8450	0.4880
5815	0.8451	0.7604	0.9062	0.8460	0.4927
5820	0.8457	0.7653	0.9061	0.8470	0.4967
5825	0.8464	0.7704	0.9061	0.8480	0.5010

Continued on next page

Table B.2 (Continued)

Wavelength	Transmission (%)				
(Å)	QE	Filter	Optics	Atmosphere	Total
5830	0.8470	0.7752	0.9061	0.8480	0.5045
5835	0.8476	0.7796	0.9060	0.8490	0.5083
5840	0.8482	0.7838	0.9060	0.8500	0.5120
5845	0.8488	0.7872	0.9059	0.8500	0.5145
5850	0.8494	0.7899	0.9059	0.8510	0.5172
5855	0.8501	0.7930	0.9058	0.8510	0.5196
5860	0.8507	0.7964	0.9058	0.8520	0.5229
5865	0.8512	0.7992	0.9057	0.8520	0.5249
5870	0.8518	0.8012	0.9057	0.8520	0.5266
5875	0.8524	0.8030	0.9057	0.8520	0.5282
5880	0.8530	0.8040	0.9056	0.8520	0.5292
5885	0.8536	0.8057	0.9056	0.8510	0.5300
5890	0.8541	0.8074	0.9055	0.8510	0.5314
5895	0.8547	0.8087	0.9055	0.8510	0.5326
5900	0.8553	0.8102	0.9054	0.8510	0.5339
5905	0.8558	0.8109	0.9054	0.8520	0.5353
5910	0.8564	0.8112	0.9053	0.8530	0.5365
5915	0.8569	0.8120	0.9053	0.8520	0.5367
5920	0.8574	0.8131	0.9052	0.8520	0.5377
5925	0.8580	0.8140	0.9052	0.8510	0.5380
5930	0.8585	0.8148	0.9052	0.8530	0.5401
5935	0.8590	0.8161	0.9051	0.8530	0.5412
5940	0.8595	0.8170	0.9051	0.8520	0.5415
5945	0.8600	0.8169	0.9050	0.8510	0.5411
5950	0.8605	0.8169	0.9050	0.8520	0.5420
5955	0.8610	0.8175	0.9049	0.8530	0.5433
5960	0.8615	0.8178	0.9049	0.8520	0.5432
5965	0.8619	0.8184	0.9048	0.8530	0.5444
5970	0.8624	0.8187	0.9048	0.8520	0.5443
5975	0.8628	0.8187	0.9047	0.8520	0.5445
5980	0.8633	0.8190	0.9047	0.8520	0.5450
5985	0.8637	0.8196	0.9046	0.8530	0.5462
5990	0.8642	0.8198	0.9046	0.8520	0.5460
5995	0.8646	0.8185	0.9045	0.8530	0.5460
6000	0.8650	0.8182	0.9045	0.8530	0.5461
6005	0.8654	0.8184	0.9045	0.8530	0.5464
6010	0.8658	0.8180	0.9044	0.8530	0.5464
6015	0.8662	0.8172	0.9044	0.8530	0.5461
6020	0.8666	0.8173	0.9043	0.8530	0.5463
6025	0.8669	0.8168	0.9043	0.8540	0.5468
6030	0.8673	0.8159	0.9042	0.8540	0.5464
6035	0.8677	0.8149	0.9042	0.8540	0.5460
6040	0.8680	0.8140	0.9041	0.8550	0.5462
6045	0.8683	0.8134	0.9041	0.8550	0.5460
6050	0.8687	0.8133	0.9040	0.8550	0.5461
6055	0.8690	0.8127	0.9040	0.8560	0.5465
6060	0.8693	0.8112	0.9039	0.8560	0.5456
6065	0.8696	0.8101	0.9039	0.8570	0.5457
6070	0.8699	0.8094	0.9038	0.8570	0.5454
6075	0.8702	0.8088	0.9038	0.8580	0.5458
6080	0.8705	0.8082	0.9037	0.8580	0.5455
6085	0.8708	0.8073	0.9037	0.8590	0.5457
6090	0.8710	0.8069	0.9036	0.8590	0.5455
6095	0.8713	0.8063	0.9036	0.8600	0.5459

Continued on next page

Table B.2 (Continued)

Wavelength	Transmission (%)				
(Å)	QE	Filter	Optics	Atmosphere	Total
6100	0.8715	0.8056	0.9036	0.8600	0.5456
6105	0.8718	0.8047	0.9035	0.8610	0.5457
6110	0.8720	0.8036	0.9035	0.8610	0.5451
6115	0.8723	0.8030	0.9034	0.8620	0.5455
6120	0.8725	0.8028	0.9034	0.8620	0.5455
6125	0.8727	0.8025	0.9033	0.8630	0.5459
6130	0.8729	0.8017	0.9033	0.8630	0.5455
6135	0.8731	0.8005	0.9032	0.8640	0.5454
6140	0.8733	0.7995	0.9032	0.8640	0.5449
6145	0.8735	0.7985	0.9031	0.8640	0.5442
6150	0.8737	0.7970	0.9031	0.8650	0.5440
6155	0.8739	0.7960	0.9030	0.8650	0.5433
6160	0.8741	0.7948	0.9030	0.8660	0.5433
6165	0.8742	0.7929	0.9029	0.8660	0.5420
6170	0.8744	0.7915	0.9029	0.8660	0.5412
6175	0.8745	0.7904	0.9028	0.8670	0.5410
6180	0.8747	0.7894	0.9028	0.8670	0.5405
6185	0.8748	0.7881	0.9027	0.8680	0.5402
6190	0.8750	0.7871	0.9027	0.8680	0.5396
6195	0.8751	0.7861	0.9026	0.8680	0.5390
6200	0.8752	0.7844	0.9026	0.8680	0.5378
6205	0.8753	0.7832	0.9025	0.8680	0.5370
6210	0.8754	0.7821	0.9025	0.8690	0.5370
6215	0.8755	0.7809	0.9024	0.8690	0.5361
6220	0.8756	0.7797	0.9024	0.8690	0.5354
6225	0.8757	0.7788	0.9023	0.8690	0.5348
6230	0.8758	0.7784	0.9023	0.8690	0.5345
6235	0.8759	0.7777	0.9022	0.8700	0.5347
6240	0.8760	0.7764	0.9021	0.8700	0.5338
6245	0.8761	0.7745	0.9021	0.8700	0.5325
6250	0.8761	0.7711	0.9020	0.8700	0.5301
6255	0.8762	0.7674	0.9020	0.8700	0.5277
6260	0.8763	0.7659	0.9019	0.8700	0.5266
6265	0.8763	0.7654	0.9019	0.8700	0.5263
6270	0.8764	0.7645	0.9018	0.8710	0.5263
6275	0.8764	0.7634	0.9018	0.8620	0.5201
6280	0.8765	0.7626	0.9017	0.8490	0.5117
6285	0.8765	0.7615	0.9017	0.8570	0.5158
6290	0.8765	0.7596	0.9016	0.8640	0.5186
6295	0.8766	0.7580	0.9016	0.8620	0.5164
6300	0.8766	0.7563	0.9015	0.8630	0.5158
6305	0.8766	0.7552	0.9014	0.8650	0.5162
6310	0.8766	0.7544	0.9014	0.8690	0.5180
6315	0.8766	0.7533	0.9013	0.8710	0.5184
6320	0.8767	0.7515	0.9013	0.8720	0.5178
6325	0.8767	0.7495	0.9012	0.8740	0.5176
6330	0.8767	0.7479	0.9012	0.8750	0.5170
6335	0.8767	0.7467	0.9011	0.8760	0.5167
6340	0.8767	0.7458	0.9010	0.8760	0.5161
6345	0.8766	0.7448	0.9010	0.8770	0.5159
6350	0.8766	0.7438	0.9009	0.8780	0.5157
6355	0.8766	0.7424	0.9009	0.8790	0.5154
6360	0.8766	0.7410	0.9008	0.8790	0.5143
6365	0.8766	0.7395	0.9007	0.8800	0.5138

Continued on next page

Table B.2 (Continued)

Wavelength	Transmission (%)				
(Å)	QE	Filter	Optics	Atmosphere	Total
6370	0.8765	0.7380	0.9007	0.8810	0.5133
6375	0.8765	0.7366	0.9006	0.8810	0.5123
6380	0.8765	0.7350	0.9006	0.8820	0.5117
6385	0.8764	0.7335	0.9005	0.8830	0.5111
6390	0.8764	0.7323	0.9004	0.8830	0.5103
6395	0.8764	0.7309	0.9004	0.8840	0.5099
6400	0.8763	0.7291	0.9003	0.8840	0.5085
6405	0.8763	0.7274	0.9003	0.8850	0.5079
6410	0.8762	0.7258	0.9002	0.8850	0.5066
6415	0.8762	0.7240	0.9001	0.8860	0.5059
6420	0.8761	0.7223	0.9001	0.8860	0.5047
6425	0.8761	0.7210	0.9000	0.8870	0.5043
6430	0.8760	0.7198	0.8999	0.8870	0.5033
6435	0.8759	0.7184	0.8999	0.8880	0.5028
6440	0.8759	0.7161	0.8998	0.8880	0.5012
6445	0.8758	0.7146	0.8997	0.8880	0.5000
6450	0.8758	0.7134	0.8997	0.8890	0.4997
6455	0.8757	0.7116	0.8996	0.8890	0.4984
6460	0.8756	0.7098	0.8995	0.8890	0.4970
6465	0.8755	0.7082	0.8995	0.8890	0.4958
6470	0.8755	0.7066	0.8994	0.8890	0.4946
6475	0.8754	0.7054	0.8993	0.8890	0.4937
6480	0.8753	0.7031	0.8993	0.8890	0.4920
6485	0.8752	0.7008	0.8992	0.8900	0.4908
6490	0.8752	0.6996	0.8991	0.8890	0.4894
6495	0.8751	0.6984	0.8991	0.8900	0.4891
6500	0.8750	0.6964	0.8990	0.8920	0.4886
6505	0.8749	0.6945	0.8989	0.8930	0.4877
6510	0.8748	0.6928	0.8989	0.8930	0.4865
6515	0.8747	0.6910	0.8988	0.8910	0.4840
6520	0.8747	0.6890	0.8987	0.8920	0.4831
6525	0.8746	0.6871	0.8986	0.8930	0.4822
6530	0.8745	0.6853	0.8986	0.8940	0.4814
6535	0.8744	0.6842	0.8985	0.8940	0.4806
6540	0.8743	0.6829	0.8984	0.8950	0.4801
6545	0.8742	0.6811	0.8984	0.8940	0.4782
6550	0.8741	0.6794	0.8983	0.8940	0.4769
6555	0.8740	0.6776	0.8982	0.8950	0.4761
6560	0.8739	0.6756	0.8981	0.8960	0.4751
6565	0.8738	0.6739	0.8981	0.8960	0.4738
6570	0.8737	0.6724	0.8980	0.8960	0.4727
6575	0.8736	0.6705	0.8979	0.8970	0.4718
6580	0.8735	0.6682	0.8978	0.8970	0.4700
6585	0.8734	0.6660	0.8977	0.8980	0.4689
6590	0.8733	0.6644	0.8977	0.8980	0.4677
6595	0.8732	0.6620	0.8976	0.8990	0.4665
6600	0.8731	0.6604	0.8975	0.8990	0.4652
6605	0.8730	0.6590	0.8974	0.8990	0.4641
6610	0.8729	0.6571	0.8974	0.9000	0.4633
6615	0.8727	0.6554	0.8973	0.9000	0.4619
6620	0.8726	0.6537	0.8972	0.9000	0.4606
6625	0.8725	0.6523	0.8971	0.9010	0.4600
6630	0.8724	0.6499	0.8970	0.9010	0.4582
6635	0.8722	0.6475	0.8970	0.9010	0.4564

Continued on next page

Table B.2 (Continued)

Wavelength	Transmission (%)				
(Å)	QE	Filter	Optics	Atmosphere	Total
6640	0.8721	0.6457	0.8969	0.9010	0.4551
6645	0.8720	0.6437	0.8968	0.9020	0.4540
6650	0.8719	0.6420	0.8967	0.9020	0.4527
6655	0.8717	0.6407	0.8966	0.9020	0.4517
6660	0.8716	0.6390	0.8966	0.9030	0.4509
6665	0.8715	0.6369	0.8965	0.9030	0.4493
6670	0.8713	0.6349	0.8964	0.9030	0.4478
6675	0.8712	0.6328	0.8963	0.9040	0.4467
6680	0.8710	0.6309	0.8962	0.9040	0.4452
6685	0.8709	0.6286	0.8961	0.9040	0.4435
6690	0.8707	0.6265	0.8961	0.9050	0.4424
6695	0.8706	0.6246	0.8960	0.9050	0.4409
6700	0.8704	0.6228	0.8959	0.9050	0.4395
6705	0.8703	0.6208	0.8958	0.9050	0.4380
6710	0.8701	0.6188	0.8957	0.9060	0.4369
6715	0.8699	0.6173	0.8956	0.9060	0.4357
6720	0.8698	0.6152	0.8955	0.9060	0.4341
6725	0.8696	0.6125	0.8955	0.9070	0.4326
6730	0.8694	0.6100	0.8954	0.9070	0.4307
6735	0.8693	0.6080	0.8953	0.9070	0.4292
6740	0.8691	0.6059	0.8952	0.9080	0.4280
6745	0.8689	0.6044	0.8951	0.9080	0.4268
6750	0.8687	0.6026	0.8950	0.9080	0.4254
6755	0.8685	0.6007	0.8949	0.9080	0.4239
6760	0.8683	0.5989	0.8949	0.9090	0.4230
6765	0.8682	0.5966	0.8948	0.9090	0.4213
6770	0.8680	0.5943	0.8947	0.9090	0.4195
6775	0.8678	0.5921	0.8946	0.9090	0.4178
6780	0.8676	0.5904	0.8945	0.9100	0.4170
6785	0.8674	0.5883	0.8944	0.9100	0.4153
6790	0.8671	0.5859	0.8943	0.9100	0.4134
6795	0.8669	0.5840	0.8942	0.9100	0.4120
6800	0.8667	0.5820	0.8941	0.9110	0.4109
6805	0.8665	0.5800	0.8941	0.9110	0.4094
6810	0.8663	0.5779	0.8940	0.9110	0.4077
6815	0.8661	0.5757	0.8939	0.9110	0.4060
6820	0.8658	0.5737	0.8938	0.9110	0.4044
6825	0.8656	0.5715	0.8937	0.9120	0.4032
6830	0.8654	0.5692	0.8936	0.9120	0.4014
6835	0.8651	0.5666	0.8935	0.9120	0.3994
6840	0.8649	0.5644	0.8934	0.9120	0.3977
6845	0.8646	0.5618	0.8933	0.9130	0.3962
6850	0.8644	0.5586	0.8933	0.9130	0.3938
6855	0.8641	0.5562	0.8932	0.9130	0.3919
6860	0.8639	0.5537	0.8931	0.9130	0.3900
6865	0.8636	0.5507	0.8930	0.8560	0.3635
6870	0.8633	0.5483	0.8929	0.7690	0.3250
6875	0.8631	0.5462	0.8928	0.7160	0.3014
6880	0.8628	0.5437	0.8927	0.8020	0.3359
6885	0.8625	0.5414	0.8926	0.8400	0.3501
6890	0.8623	0.5389	0.8925	0.8240	0.3417
6895	0.8620	0.5368	0.8924	0.8300	0.3427
6900	0.8617	0.5344	0.8923	0.8350	0.3431
6905	0.8614	0.5319	0.8923	0.8580	0.3508

Continued on next page

Table B.2 (Continued)

Wavelength	Transmission (%)				
(Å)	QE	Filter	Optics	Atmosphere	Total
6910	0.8611	0.5300	0.8922	0.8620	0.3510
6915	0.8608	0.5283	0.8921	0.8710	0.3534
6920	0.8605	0.5262	0.8920	0.8830	0.3566
6925	0.8602	0.5233	0.8919	0.8930	0.3585
6930	0.8599	0.5206	0.8918	0.8990	0.3589
6935	0.8595	0.5185	0.8917	0.9050	0.3596
6940	0.8592	0.5167	0.8916	0.9060	0.3586
6945	0.8589	0.5143	0.8915	0.9080	0.3576
6950	0.8586	0.5116	0.8914	0.9120	0.3571
6955	0.8582	0.5095	0.8913	0.9120	0.3554
6960	0.8579	0.5073	0.8912	0.9130	0.3541
6965	0.8575	0.5047	0.8911	0.9150	0.3529
6970	0.8572	0.5023	0.8911	0.9180	0.3522
6975	0.8568	0.4998	0.8910	0.9180	0.3503
6980	0.8565	0.4973	0.8909	0.9180	0.3484
6985	0.8561	0.4947	0.8908	0.9160	0.3456
6990	0.8558	0.4919	0.8907	0.9150	0.3431
6995	0.8554	0.4893	0.8906	0.9150	0.3411
7000	0.8550	0.4868	0.8905	0.9170	0.3399
7005	0.8546	0.4846	0.8904	0.9160	0.3378
7010	0.8542	0.4822	0.8903	0.9170	0.3363
7015	0.8538	0.4798	0.8902	0.9170	0.3344
7020	0.8534	0.4777	0.8901	0.9170	0.3327
7025	0.8530	0.4755	0.8900	0.9170	0.3310
7030	0.8526	0.4730	0.8899	0.9180	0.3295
7035	0.8522	0.4708	0.8899	0.9190	0.3281
7040	0.8518	0.4681	0.8898	0.9200	0.3264
7045	0.8514	0.4659	0.8897	0.9190	0.3243
7050	0.8510	0.4640	0.8896	0.9200	0.3232
7055	0.8505	0.4617	0.8895	0.9200	0.3213
7060	0.8501	0.4593	0.8894	0.9200	0.3195
7065	0.8497	0.4571	0.8893	0.9210	0.3181
7070	0.8492	0.4550	0.8892	0.9210	0.3164
7075	0.8488	0.4531	0.8891	0.9220	0.3153
7080	0.8483	0.4506	0.8890	0.9220	0.3133
7085	0.8479	0.4480	0.8889	0.9220	0.3113
7090	0.8474	0.4462	0.8888	0.9220	0.3099
7095	0.8469	0.4441	0.8887	0.9220	0.3082
7100	0.8465	0.4421	0.8886	0.9230	0.3069
7105	0.8460	0.4400	0.8885	0.9230	0.3053
7110	0.8455	0.4374	0.8885	0.9230	0.3033
7115	0.8450	0.4348	0.8884	0.9230	0.3013
7120	0.8445	0.4325	0.8883	0.9240	0.2998
7125	0.8440	0.4300	0.8882	0.9240	0.2978
7130	0.8435	0.4278	0.8881	0.9240	0.2961
7135	0.8430	0.4253	0.8880	0.9240	0.2942
7140	0.8425	0.4230	0.8879	0.9240	0.2924
7145	0.8420	0.4209	0.8878	0.9230	0.2904
7150	0.8415	0.4187	0.8877	0.9230	0.2887
7155	0.8410	0.4162	0.8876	0.9230	0.2868
7160	0.8404	0.4142	0.8875	0.9230	0.2851
7165	0.8399	0.4121	0.8874	0.9200	0.2826
7170	0.8394	0.4099	0.8873	0.9130	0.2787
7175	0.8388	0.4076	0.8872	0.9070	0.2751

Continued on next page

Table B.2 (Continued)

Wavelength	Transmission (%)				
(Å)	QE	Filter	Optics	Atmosphere	Total
7180	0.8383	0.4052	0.8871	0.9010	0.2715
7185	0.8377	0.4031	0.8870	0.8960	0.2684
7190	0.8372	0.4011	0.8869	0.8940	0.2663
7195	0.8366	0.3991	0.8868	0.9010	0.2668
7200	0.8361	0.3971	0.8867	0.8970	0.2641
7205	0.8355	0.3951	0.8866	0.8990	0.2631
7210	0.8349	0.3931	0.8865	0.9120	0.2653
7215	0.8344	0.3908	0.8864	0.9220	0.2665
7220	0.8338	0.3886	0.8863	0.9220	0.2648
7225	0.8332	0.3866	0.8862	0.9210	0.2629
7230	0.8326	0.3844	0.8861	0.9140	0.2592
7235	0.8320	0.3818	0.8860	0.9100	0.2561
7240	0.8314	0.3795	0.8859	0.9010	0.2518
7245	0.8308	0.3774	0.8858	0.9110	0.2530
7250	0.8302	0.3751	0.8857	0.9080	0.2504
7255	0.8296	0.3731	0.8856	0.9120	0.2500
7260	0.8290	0.3708	0.8855	0.9100	0.2477
7265	0.8284	0.3682	0.8854	0.9140	0.2468
7270	0.8278	0.3659	0.8853	0.9130	0.2448
7275	0.8271	0.3633	0.8852	0.9120	0.2426
7280	0.8265	0.3612	0.8851	0.9120	0.2410
7285	0.8259	0.3588	0.8850	0.9170	0.2405
7290	0.8252	0.3564	0.8849	0.9170	0.2386
7295	0.8246	0.3542	0.8848	0.9150	0.2365
7300	0.8240	0.3521	0.8847	0.9170	0.2354
7305	0.8233	0.3499	0.8846	0.9180	0.2339
7310	0.8227	0.3476	0.8845	0.9180	0.2322
7315	0.8220	0.3459	0.8844	0.9200	0.2313
7320	0.8213	0.3442	0.8843	0.9230	0.2307
7325	0.8207	0.3421	0.8841	0.9250	0.2296
7330	0.8200	0.3400	0.8840	0.9270	0.2285
7335	0.8193	0.3379	0.8839	0.9270	0.2268
7340	0.8187	0.3360	0.8838	0.9280	0.2256
7345	0.8180	0.3341	0.8837	0.9290	0.2244
7350	0.8173	0.3321	0.8836	0.9290	0.2228
7355	0.8166	0.3302	0.8835	0.9290	0.2213
7360	0.8159	0.3282	0.8834	0.9290	0.2198
7365	0.8152	0.3262	0.8833	0.9280	0.2180
7370	0.8145	0.3242	0.8831	0.9290	0.2166
7375	0.8138	0.3218	0.8830	0.9300	0.2151
7380	0.8131	0.3196	0.8829	0.9310	0.2136
7385	0.8124	0.3175	0.8828	0.9310	0.2120
7390	0.8117	0.3151	0.8827	0.9310	0.2102
7395	0.8110	0.3132	0.8826	0.9310	0.2087
7400	0.8102	0.3113	0.8825	0.9320	0.2074
7405	0.8095	0.3090	0.8823	0.9320	0.2057
7410	0.8088	0.3069	0.8822	0.9330	0.2043
7415	0.8080	0.3053	0.8821	0.9330	0.2030
7420	0.8073	0.3033	0.8820	0.9330	0.2015
7425	0.8066	0.3009	0.8819	0.9330	0.1997
7430	0.8058	0.2991	0.8817	0.9330	0.1983
7435	0.8051	0.2973	0.8816	0.9330	0.1969
7440	0.8043	0.2952	0.8815	0.9330	0.1953
7445	0.8036	0.2935	0.8814	0.9340	0.1942

Continued on next page

Table B.2 (Continued)

Wavelength	Transmission (%)				
(Å)	QE	Filter	Optics	Atmosphere	Total
7450	0.8028	0.2920	0.8813	0.9340	0.1930
7455	0.8020	0.2896	0.8811	0.9340	0.1911
7460	0.8013	0.2872	0.8810	0.9340	0.1894
7465	0.8005	0.2855	0.8809	0.9340	0.1880
7470	0.7997	0.2838	0.8808	0.9340	0.1867
7475	0.7989	0.2819	0.8806	0.9340	0.1852
7480	0.7982	0.2802	0.8805	0.9340	0.1839
7485	0.7974	0.2783	0.8804	0.9340	0.1825
7490	0.7966	0.2762	0.8803	0.9350	0.1811
7495	0.7958	0.2747	0.8801	0.9350	0.1799
7500	0.7950	0.2727	0.8800	0.9350	0.1784
7505	0.7942	0.2702	0.8799	0.9350	0.1765
7510	0.7934	0.2684	0.8797	0.9350	0.1752
7515	0.7926	0.2665	0.8796	0.9360	0.1739
7520	0.7918	0.2643	0.8795	0.9360	0.1723
7525	0.7910	0.2623	0.8793	0.9360	0.1708
7530	0.7901	0.2603	0.8792	0.9360	0.1692
7535	0.7893	0.2585	0.8791	0.9360	0.1679
7540	0.7885	0.2568	0.8789	0.9370	0.1668
7545	0.7877	0.2550	0.8788	0.9370	0.1654
7550	0.7868	0.2533	0.8787	0.9370	0.1641
7555	0.7860	0.2514	0.8785	0.9370	0.1627
7560	0.7852	0.2493	0.8784	0.9370	0.1611
7565	0.7843	0.2475	0.8783	0.9370	0.1597
7570	0.7835	0.2464	0.8781	0.9370	0.1588
7575	0.7826	0.2449	0.8780	0.9380	0.1578
7580	0.7818	0.2429	0.8778	0.9380	0.1564
7585	0.7809	0.2411	0.8777	0.9370	0.1548
7590	0.7801	0.2394	0.8776	0.8930	0.1464
7595	0.7792	0.2374	0.8774	0.7370	0.1196
7600	0.7783	0.2353	0.8773	0.5260	0.0845
7605	0.7774	0.2338	0.8772	0.3740	0.0596
7610	0.7766	0.2321	0.8770	0.3940	0.0623
7615	0.7757	0.2308	0.8769	0.5680	0.0892
7620	0.7748	0.2294	0.8767	0.6410	0.0999
7625	0.7739	0.2274	0.8766	0.6710	0.1035
7630	0.7730	0.2255	0.8765	0.5650	0.0863
7635	0.7721	0.2240	0.8763	0.5660	0.0858
7640	0.7712	0.2223	0.8762	0.5840	0.0877
7645	0.7703	0.2203	0.8760	0.6420	0.0954
7650	0.7694	0.2183	0.8759	0.7150	0.1052
7655	0.7685	0.2165	0.8758	0.7800	0.1137
7660	0.7676	0.2151	0.8756	0.8280	0.1197
7665	0.7667	0.2135	0.8755	0.8630	0.1237
7670	0.7657	0.2120	0.8753	0.8770	0.1246
7675	0.7648	0.2107	0.8752	0.8860	0.1250
7680	0.7639	0.2092	0.8751	0.8970	0.1254
7685	0.7629	0.2073	0.8749	0.9080	0.1256
7690	0.7620	0.2057	0.8748	0.9230	0.1266
7695	0.7610	0.2042	0.8746	0.9290	0.1263
7700	0.7601	0.2023	0.8745	0.9350	0.1257
7705	0.7591	0.2006	0.8744	0.9350	0.1245
7710	0.7582	0.1991	0.8742	0.9380	0.1238
7715	0.7572	0.1974	0.8741	0.9390	0.1227

Continued on next page

Table B.2 (Continued)

Wavelength	Transmission (%)				
(Å)	QE	Filter	Optics	Atmosphere	Total
7720	0.7563	0.1955	0.8740	0.9390	0.1213
7725	0.7553	0.1941	0.8738	0.9390	0.1203
7730	0.7543	0.1922	0.8737	0.9400	0.1191
7735	0.7533	0.1907	0.8736	0.9400	0.1180
7740	0.7524	0.1893	0.8734	0.9400	0.1169
7745	0.7514	0.1877	0.8733	0.9400	0.1158
7750	0.7504	0.1863	0.8732	0.9400	0.1147
7755	0.7494	0.1849	0.8730	0.9410	0.1138
7760	0.7484	0.1831	0.8729	0.9410	0.1126
7765	0.7474	0.1816	0.8728	0.9410	0.1115
7770	0.7464	0.1802	0.8726	0.9410	0.1104
7775	0.7454	0.1784	0.8725	0.9410	0.1092
7780	0.7443	0.1768	0.8724	0.9410	0.1080
7785	0.7433	0.1755	0.8723	0.9410	0.1071
7790	0.7423	0.1742	0.8721	0.9410	0.1061
7795	0.7413	0.1725	0.8720	0.9410	0.1049
7800	0.7402	0.1712	0.8719	0.9410	0.1040
7805	0.7392	0.1701	0.8718	0.9410	0.1032
7810	0.7381	0.1684	0.8716	0.9420	0.1021
7815	0.7371	0.1669	0.8715	0.9420	0.1010
7820	0.7360	0.1653	0.8714	0.9420	0.0999
7825	0.7350	0.1639	0.8713	0.9420	0.0989
7830	0.7339	0.1629	0.8712	0.9420	0.0981
7835	0.7329	0.1616	0.8710	0.9420	0.0972
7840	0.7318	0.1599	0.8709	0.9420	0.0960
7845	0.7307	0.1589	0.8708	0.9420	0.0952
7850	0.7296	0.1580	0.8707	0.9420	0.0945
7855	0.7285	0.1563	0.8706	0.9430	0.0935
7860	0.7275	0.1548	0.8705	0.9430	0.0924
7865	0.7264	0.1539	0.8704	0.9420	0.0917
7870	0.7253	0.1528	0.8703	0.9420	0.0909
7875	0.7242	0.1515	0.8701	0.9420	0.0899
7880	0.7230	0.1504	0.8700	0.9420	0.0891
7885	0.7219	0.1493	0.8699	0.9420	0.0883
7890	0.7208	0.1480	0.8698	0.9420	0.0874
7895	0.7197	0.1465	0.8697	0.9410	0.0863
7900	0.7186	0.1450	0.8696	0.9410	0.0853
7905	0.7174	0.1436	0.8695	0.9410	0.0843
7910	0.7163	0.1425	0.8694	0.9420	0.0836
7915	0.7152	0.1413	0.8693	0.9420	0.0828
7920	0.7140	0.1395	0.8693	0.9420	0.0816
7925	0.7129	0.1379	0.8692	0.9420	0.0805
7930	0.7117	0.1370	0.8691	0.9420	0.0798
7935	0.7105	0.1359	0.8690	0.9440	0.0792
7940	0.7094	0.1345	0.8689	0.9440	0.0783
7945	0.7082	0.1331	0.8688	0.9440	0.0773
7950	0.7070	0.1317	0.8687	0.9440	0.0764
7955	0.7058	0.1305	0.8686	0.9440	0.0755
7960	0.7047	0.1299	0.8686	0.9420	0.0749
7965	0.7035	0.1291	0.8685	0.9420	0.0743
7970	0.7023	0.1283	0.8684	0.9420	0.0737
7975	0.7011	0.1268	0.8683	0.9440	0.0729
7980	0.6999	0.1253	0.8683	0.9440	0.0719
7985	0.6987	0.1246	0.8682	0.9440	0.0714

Continued on next page

Table B.2 (Continued)

Wavelength	Transmission (%)				
(Å)	QE	Filter	Optics	Atmosphere	Total
7990	0.6974	0.1236	0.8681	0.9440	0.0706
7995	0.6962	0.1221	0.8681	0.9440	0.0697
8000	0.6950	0.1205	0.8680	0.9440	0.0686
8005	0.6938	0.1197	0.8679	0.9430	0.0680
8010	0.6925	0.1186	0.8679	0.9430	0.0672
8015	0.6913	0.1168	0.8678	0.9440	0.0661
8020	0.6900	0.1161	0.8678	0.9440	0.0656
8025	0.6888	0.1155	0.8677	0.9440	0.0652
8030	0.6875	0.1143	0.8677	0.9440	0.0644
8035	0.6863	0.1126	0.8676	0.9440	0.0633
8040	0.6850	0.1114	0.8676	0.9440	0.0625
8045	0.6837	0.1109	0.8675	0.9450	0.0622
8050	0.6825	0.1098	0.8675	0.9450	0.0614
8055	0.6812	0.1088	0.8674	0.9460	0.0608
8060	0.6799	0.1079	0.8674	0.9460	0.0602
8065	0.6786	0.1069	0.8674	0.9460	0.0595
8070	0.6773	0.1059	0.8673	0.9460	0.0588
8075	0.6760	0.1049	0.8673	0.9460	0.0582
8080	0.6747	0.1035	0.8672	0.9460	0.0573
8085	0.6734	0.1026	0.8672	0.9460	0.0567
8090	0.6721	0.1018	0.8672	0.9460	0.0561
8095	0.6708	0.1009	0.8672	0.9450	0.0555
8100	0.6695	0.0998	0.8671	0.9450	0.0547
8105	0.6682	0.0987	0.8671	0.9450	0.0540
8110	0.6668	0.0972	0.8671	0.9440	0.0531
8115	0.6655	0.0964	0.8671	0.9440	0.0525
8120	0.6642	0.0958	0.8670	0.9430	0.0520
8125	0.6628	0.0950	0.8670	0.9420	0.0514
8130	0.6615	0.0939	0.8670	0.9380	0.0505
8135	0.6601	0.0930	0.8670	0.9360	0.0498
8140	0.6588	0.0921	0.8670	0.9340	0.0491
8145	0.6574	0.0913	0.8670	0.9320	0.0485
8150	0.6561	0.0906	0.8670	0.9280	0.0478
8155	0.6547	0.0898	0.8669	0.9300	0.0474
8160	0.6534	0.0888	0.8669	0.9180	0.0462
8165	0.6520	0.0880	0.8669	0.9160	0.0456
8170	0.6506	0.0876	0.8669	0.9210	0.0455
8175	0.6492	0.0863	0.8669	0.9200	0.0447
8180	0.6479	0.0850	0.8669	0.9230	0.0441
8185	0.6465	0.0845	0.8669	0.9210	0.0436
8190	0.6451	0.0841	0.8669	0.9290	0.0437
8195	0.6437	0.0829	0.8669	0.9240	0.0427
8200	0.6423	0.0818	0.8669	0.9310	0.0424
8205	0.6409	0.0812	0.8669	0.9370	0.0423
8210	0.6395	0.0809	0.8669	0.9420	0.0422
8215	0.6381	0.0794	0.8669	0.9430	0.0414
8220	0.6367	0.0781	0.8669	0.9390	0.0405
8225	0.6353	0.0782	0.8669	0.9210	0.0397
8230	0.6339	0.0776	0.8670	0.9130	0.0389
8235	0.6325	0.0768	0.8670	0.9140	0.0385
8240	0.6311	0.0759	0.8670	0.9300	0.0386
8245	0.6297	0.0753	0.8670	0.9420	0.0387
8250	0.6283	0.0748	0.8670	0.9430	0.0384
8255	0.6268	0.0736	0.8670	0.9410	0.0376

Continued on next page

Table B.2 (Continued)

Wavelength	Transmission (%)				
(Å)	QE	Filter	Optics	Atmosphere	Total
8260	0.6254	0.0723	0.8670	0.9400	0.0369
8265	0.6240	0.0723	0.8670	0.9410	0.0368
8270	0.6226	0.0716	0.8671	0.9390	0.0363
8275	0.6211	0.0708	0.8671	0.9380	0.0358
8280	0.6197	0.0703	0.8671	0.9340	0.0353
8285	0.6183	0.0695	0.8671	0.9290	0.0346
8290	0.6168	0.0687	0.8671	0.9320	0.0342
8295	0.6154	0.0679	0.8672	0.9360	0.0339
8300	0.6139	0.0673	0.8672	0.9370	0.0336
8305	0.6125	0.0669	0.8672	0.9380	0.0333
8310	0.6110	0.0664	0.8672	0.9410	0.0331
8315	0.6096	0.0654	0.8673	0.9390	0.0325
8320	0.6081	0.0645	0.8673	0.9400	0.0320
8325	0.6067	0.0641	0.8673	0.9400	0.0317
8330	0.6052	0.0634	0.8674	0.9420	0.0314
8335	0.6038	0.0629	0.8674	0.9450	0.0311
8340	0.6023	0.0622	0.8675	0.9450	0.0307
8345	0.6009	0.0610	0.8675	0.9470	0.0301
8350	0.5994	0.0606	0.8676	0.9470	0.0298
8355	0.5979	0.0605	0.8676	0.9480	0.0298
8360	0.5965	0.0597	0.8677	0.9480	0.0293
8365	0.5950	0.0590	0.8677	0.9480	0.0289
8370	0.5935	0.0585	0.8678	0.9490	0.0286
8375	0.5921	0.0577	0.8678	0.9500	0.0282
8380	0.5906	0.0572	0.8679	0.9500	0.0279
8385	0.5891	0.0566	0.8680	0.9500	0.0275
8390	0.5876	0.0561	0.8680	0.9510	0.0272
8395	0.5862	0.0556	0.8681	0.9510	0.0269
8400	0.5847	0.0552	0.8682	0.9510	0.0266
8405	0.5832	0.0549	0.8683	0.9510	0.0264
8410	0.5817	0.0540	0.8683	0.9510	0.0259
8415	0.5803	0.0534	0.8684	0.9510	0.0256
8420	0.5788	0.0526	0.8685	0.9510	0.0251
8425	0.5773	0.0518	0.8686	0.9510	0.0247
8430	0.5758	0.0510	0.8687	0.9520	0.0243
8435	0.5743	0.0501	0.8688	0.9520	0.0238
8440	0.5728	0.0499	0.8689	0.9520	0.0236
8445	0.5714	0.0494	0.8690	0.9520	0.0234
8450	0.5699	0.0492	0.8691	0.9520	0.0232
8455	0.5684	0.0487	0.8693	0.9520	0.0229
8460	0.5669	0.0478	0.8694	0.9530	0.0225
8465	0.5654	0.0472	0.8695	0.9530	0.0221
8470	0.5639	0.0466	0.8696	0.9530	0.0218
8475	0.5624	0.0462	0.8698	0.9530	0.0215
8480	0.5610	0.0461	0.8699	0.9530	0.0214
8485	0.5595	0.0460	0.8700	0.9530	0.0213
8490	0.5580	0.0456	0.8702	0.9530	0.0211
8495	0.5565	0.0448	0.8703	0.9530	0.0207
8500	0.5550	0.0440	0.8705	0.9530	0.0203
8505	0.5535	0.0434	0.8707	0.9530	0.0199
8510	0.5520	0.0434	0.8708	0.9530	0.0199
8515	0.5505	0.0429	0.8710	0.9530	0.0196
8520	0.5490	0.0422	0.8712	0.9530	0.0192
8525	0.5476	0.0423	0.8714	0.9530	0.0192

Continued on next page

Table B.2 (Continued)

Wavelength	Transmission (%)				
(Å)	QE	Filter	Optics	Atmosphere	Total
8530	0.5461	0.0422	0.8715	0.9530	0.0191
8535	0.5446	0.0415	0.8717	0.9530	0.0188
8540	0.5431	0.0409	0.8719	0.9530	0.0185
8545	0.5416	0.0403	0.8721	0.9530	0.0181
8550	0.5401	0.0400	0.8723	0.9530	0.0180
8555	0.5386	0.0399	0.8725	0.9530	0.0179
8560	0.5371	0.0391	0.8728	0.9540	0.0175
8565	0.5356	0.0384	0.8730	0.9540	0.0171
8570	0.5341	0.0380	0.8732	0.9540	0.0169
8575	0.5326	0.0379	0.8734	0.9540	0.0168
8580	0.5312	0.0376	0.8736	0.9540	0.0166
8585	0.5297	0.0365	0.8739	0.9540	0.0161
8590	0.5282	0.0359	0.8741	0.9540	0.0158
8595	0.5267	0.0356	0.8743	0.9540	0.0156
8600	0.5252	0.0355	0.8746	0.9540	0.0156
8605	0.5237	0.0348	0.8748	0.9540	0.0152
8610	0.5222	0.0343	0.8751	0.9550	0.0150
8615	0.5207	0.0347	0.8753	0.9550	0.0151
8620	0.5192	0.0341	0.8756	0.9550	0.0148
8625	0.5177	0.0338	0.8758	0.9550	0.0146
8630	0.5162	0.0339	0.8761	0.9550	0.0146
8635	0.5147	0.0336	0.8764	0.9550	0.0145
8640	0.5132	0.0328	0.8766	0.9550	0.0141
8645	0.5118	0.0320	0.8769	0.9550	0.0137
8650	0.5103	0.0317	0.8772	0.9550	0.0136
8655	0.5088	0.0316	0.8775	0.9550	0.0135
8660	0.5073	0.0313	0.8777	0.9550	0.0133
8665	0.5058	0.0310	0.8780	0.9550	0.0131
8670	0.5043	0.0306	0.8783	0.9560	0.0130
8675	0.5028	0.0298	0.8786	0.9560	0.0126
8680	0.5013	0.0294	0.8789	0.9560	0.0124
8685	0.4998	0.0294	0.8792	0.9560	0.0124
8690	0.4983	0.0289	0.8795	0.9560	0.0121
8695	0.4968	0.0284	0.8798	0.9560	0.0119
8700	0.4953	0.0286	0.8801	0.9560	0.0119
8705	0.4938	0.0289	0.8804	0.9560	0.0120
8710	0.4923	0.0277	0.8807	0.9560	0.0115
8715	0.4908	0.0265	0.8810	0.9560	0.0110
8720	0.4893	0.0264	0.8813	0.9560	0.0109
8725	0.4878	0.0265	0.8816	0.9560	0.0109
8730	0.4863	0.0259	0.8819	0.9560	0.0106
8735	0.4848	0.0259	0.8822	0.9560	0.0106
8740	0.4833	0.0260	0.8825	0.9570	0.0106
8745	0.4818	0.0256	0.8828	0.9570	0.0104
8750	0.4803	0.0255	0.8831	0.9570	0.0104
8755	0.4788	0.0257	0.8834	0.9570	0.0104
8760	0.4773	0.0256	0.8838	0.9570	0.0103
8765	0.4758	0.0247	0.8841	0.9570	0.0099
8770	0.4743	0.0243	0.8844	0.9570	0.0098
8775	0.4728	0.0241	0.8847	0.9570	0.0096
8780	0.4713	0.0239	0.8850	0.9570	0.0095
8785	0.4698	0.0238	0.8854	0.9570	0.0095
8790	0.4683	0.0238	0.8857	0.9570	0.0094
8795	0.4668	0.0236	0.8860	0.9570	0.0093

Continued on next page

Table B.2 (Continued)

Wavelength	Transmission (%)				
(Å)	QE	Filter	Optics	Atmosphere	Total
8800	0.4653	0.0226	0.8863	0.9570	0.0089
8805	0.4638	0.0225	0.8867	0.9570	0.0089
8810	0.4623	0.0229	0.8870	0.9570	0.0090
8815	0.4608	0.0229	0.8873	0.9570	0.0090
8820	0.4593	0.0224	0.8876	0.9570	0.0087
8825	0.4578	0.0220	0.8880	0.9570	0.0086
8830	0.4563	0.0218	0.8883	0.9570	0.0085
8835	0.4548	0.0214	0.8886	0.9570	0.0083
8840	0.4533	0.0211	0.8889	0.9570	0.0081
8845	0.4518	0.0208	0.8893	0.9570	0.0080
8850	0.4503	0.0207	0.8896	0.9580	0.0079
8855	0.4488	0.0205	0.8899	0.9570	0.0078
8860	0.4473	0.0205	0.8903	0.9570	0.0078
8865	0.4458	0.0202	0.8906	0.9570	0.0077
8870	0.4443	0.0193	0.8909	0.9570	0.0073
8875	0.4428	0.0189	0.8912	0.9570	0.0071
8880	0.4413	0.0189	0.8916	0.9580	0.0071
8885	0.4398	0.0185	0.8919	0.9580	0.0070
8890	0.4382	0.0188	0.8922	0.9570	0.0070
8895	0.4367	0.0184	0.8925	0.9580	0.0069
8900	0.4352	0.0181	0.8928	0.9580	0.0067
8905	0.4337	0.0178	0.8932	0.9580	0.0066
8910	0.4322	0.0173	0.8935	0.9580	0.0064
8915	0.4307	0.0174	0.8938	0.9580	0.0064
8920	0.4292	0.0175	0.8941	0.9570	0.0064
8925	0.4277	0.0172	0.8944	0.9560	0.0063
8930	0.4262	0.0171	0.8948	0.9550	0.0062
8935	0.4247	0.0172	0.8951	0.9550	0.0062
8940	0.4232	0.0169	0.8954	0.9530	0.0061
8945	0.4216	0.0165	0.8957	0.9530	0.0059
8950	0.4201	0.0167	0.8960	0.9480	0.0060
8955	0.4186	0.0162	0.8963	0.9460	0.0057
8960	0.4171	0.0157	0.8966	0.9380	0.0055
8965	0.4156	0.0157	0.8969	0.9320	0.0055
8970	0.4141	0.0156	0.8972	0.9330	0.0054
8975	0.4126	0.0152	0.8975	0.9280	0.0052
8980	0.4111	0.0153	0.8978	0.9320	0.0053
8985	0.4095	0.0155	0.8981	0.9120	0.0052
8990	0.4080	0.0156	0.8984	0.9160	0.0052
8995	0.4065	0.0153	0.8987	0.9120	0.0051
9000	0.4050	0.0147	0.8990	0.9080	0.0049
9005	0.4035	0.0150	0.8993	0.9250	0.0050
9010	0.4020	0.0152	0.8996	0.9160	0.0050
9015	0.4005	0.0150	0.8999	0.9250	0.0050
9020	0.3989	0.0146	0.9001	0.9180	0.0048
9025	0.3974	0.0138	0.9004	0.9220	0.0046
9030	0.3959	0.0130	0.9007	0.9330	0.0043
9035	0.3944	0.0133	0.9010	0.9360	0.0044
9040	0.3929	0.0134	0.9012	0.9500	0.0045
9045	0.3913	0.0135	0.9015	0.9520	0.0045
9050	0.3898	0.0134	0.9018	0.9490	0.0045
9055	0.3883	0.0129	0.9020	0.9470	0.0043
9060	0.3868	0.0124	0.9023	0.9460	0.0041
9065	0.3853	0.0120	0.9026	0.9310	0.0039

Continued on next page

Table B.2 (Continued)

Wavelength	Transmission (%)				
(Å)	QE	Filter	Optics	Atmosphere	Total
9070	0.3838	0.0119	0.9028	0.9310	0.0038
9075	0.3822	0.0116	0.9031	0.9220	0.0037
9080	0.3807	0.0122	0.9033	0.9140	0.0038
9085	0.3792	0.0129	0.9036	0.9230	0.0041
9090	0.3777	0.0124	0.9039	0.9260	0.0039
9095	0.3762	0.0118	0.9041	0.9270	0.0037
9100	0.3746	0.0118	0.9043	0.9270	0.0037
9105	0.3731	0.0119	0.9046	0.9300	0.0037
9110	0.3716	0.0119	0.9048	0.9340	0.0037
9115	0.3701	0.0118	0.9051	0.9340	0.0037
9120	0.3686	0.0118	0.9053	0.9370	0.0037
9125	0.3670	0.0114	0.9056	0.9300	0.0035
9130	0.3655	0.0109	0.9058	0.9150	0.0033
9135	0.3640	0.0107	0.9060	0.9260	0.0033
9140	0.3625	0.0105	0.9063	0.9250	0.0032
9145	0.3610	0.0106	0.9065	0.9310	0.0032
9150	0.3595	0.0108	0.9067	0.9270	0.0033
9155	0.3579	0.0110	0.9070	0.9290	0.0033
9160	0.3564	0.0111	0.9072	0.9290	0.0033
9165	0.3549	0.0109	0.9074	0.9280	0.0033
9170	0.3534	0.0105	0.9076	0.9330	0.0031
9175	0.3519	0.0099	0.9079	0.9340	0.0030
9180	0.3503	0.0095	0.9081	0.9290	0.0028
9185	0.3488	0.0102	0.9083	0.9320	0.0030
9190	0.3473	0.0099	0.9085	0.9400	0.0029
9195	0.3458	0.0094	0.9087	0.9450	0.0028
9200	0.3443	0.0091	0.9089	0.9500	0.0027
9205	0.3428	0.0090	0.9092	0.9490	0.0027
9210	0.3413	0.0093	0.9094	0.9500	0.0027
9215	0.3397	0.0096	0.9096	0.9500	0.0028
9220	0.3382	0.0096	0.9098	0.9490	0.0028
9225	0.3367	0.0097	0.9100	0.9490	0.0028
9230	0.3352	0.0094	0.9102	0.9500	0.0027
9235	0.3337	0.0092	0.9104	0.9500	0.0027
9240	0.3322	0.0097	0.9106	0.9480	0.0028
9245	0.3307	0.0088	0.9108	0.9460	0.0025
9250	0.3292	0.0088	0.9110	0.9480	0.0025
9255	0.3277	0.0085	0.9112	0.9470	0.0024
9260	0.3262	0.0080	0.9114	0.9500	0.0023
9265	0.3246	0.0085	0.9116	0.9520	0.0024
9270	0.3231	0.0093	0.9118	0.9500	0.0026
9275	0.3216	0.0085	0.9120	0.9420	0.0023
9280	0.3201	0.0081	0.9122	0.9350	0.0022
9285	0.3186	0.0090	0.9124	0.9300	0.0024
9290	0.3171	0.0058	0.9126	0.9210	0.0015
9295	0.3156	0.0000	0.9128	0.9150	0.0000
9300	0.3141	0.0000	0.9130	0.9060	0.0000
9305	0.3126	0.0000	0.9132	0.8870	0.0000
9310	0.3111	0.0000	0.9133	0.8530	0.0000
			I (c6028)		
6940	0.8592	0.0000	0.8916	0.9060	0.0000
6945	0.8589	0.0000	0.8915	0.9080	0.0000

Continued on next page

Table B.2 (Continued)

Wavelength	Transmission (%)				
(Å)	QE	Filter	Optics	Atmosphere	Total
6950	0.8586	0.0000	0.8914	0.9120	0.0000
6955	0.8582	0.0000	0.8913	0.9120	0.0000
6960	0.8579	0.0010	0.8912	0.9130	0.0007
6965	0.8575	0.0010	0.8911	0.9150	0.0007
6970	0.8572	0.0010	0.8911	0.9180	0.0007
6975	0.8568	0.0010	0.8910	0.9180	0.0007
6980	0.8565	0.0010	0.8909	0.9180	0.0007
6985	0.8561	0.0010	0.8908	0.9160	0.0007
6990	0.8558	0.0010	0.8907	0.9150	0.0007
6995	0.8554	0.0012	0.8906	0.9150	0.0008
7000	0.8550	0.0012	0.8905	0.9170	0.0008
7005	0.8546	0.0012	0.8904	0.9160	0.0008
7010	0.8542	0.0013	0.8903	0.9170	0.0009
7015	0.8538	0.0017	0.8902	0.9170	0.0012
7020	0.8534	0.0017	0.8901	0.9170	0.0012
7025	0.8530	0.0021	0.8900	0.9170	0.0015
7030	0.8526	0.0022	0.8899	0.9180	0.0015
7035	0.8522	0.0022	0.8899	0.9190	0.0015
7040	0.8518	0.0022	0.8898	0.9200	0.0015
7045	0.8514	0.0028	0.8897	0.9190	0.0019
7050	0.8510	0.0029	0.8896	0.9200	0.0020
7055	0.8505	0.0031	0.8895	0.9200	0.0022
7060	0.8501	0.0032	0.8894	0.9200	0.0022
7065	0.8497	0.0038	0.8893	0.9210	0.0026
7070	0.8492	0.0038	0.8892	0.9210	0.0026
7075	0.8488	0.0041	0.8891	0.9220	0.0029
7080	0.8483	0.0048	0.8890	0.9220	0.0033
7085	0.8479	0.0053	0.8889	0.9220	0.0037
7090	0.8474	0.0060	0.8888	0.9220	0.0042
7095	0.8469	0.0066	0.8887	0.9220	0.0046
7100	0.8465	0.0072	0.8886	0.9230	0.0050
7105	0.8460	0.0081	0.8885	0.9230	0.0056
7110	0.8455	0.0093	0.8885	0.9230	0.0064
7115	0.8450	0.0101	0.8884	0.9230	0.0070
7120	0.8445	0.0114	0.8883	0.9240	0.0079
7125	0.8440	0.0124	0.8882	0.9240	0.0086
7130	0.8435	0.0142	0.8881	0.9240	0.0098
7135	0.8430	0.0163	0.8880	0.9240	0.0113
7140	0.8425	0.0182	0.8879	0.9240	0.0126
7145	0.8420	0.0202	0.8878	0.9230	0.0139
7150	0.8415	0.0230	0.8877	0.9230	0.0159
7155	0.8410	0.0264	0.8876	0.9230	0.0182
7160	0.8404	0.0296	0.8875	0.9230	0.0204
7165	0.8399	0.0337	0.8874	0.9200	0.0231
7170	0.8394	0.0382	0.8873	0.9130	0.0260
7175	0.8388	0.0430	0.8872	0.9070	0.0290
7180	0.8383	0.0487	0.8871	0.9010	0.0326
7185	0.8377	0.0559	0.8870	0.8960	0.0372
7190	0.8372	0.0633	0.8869	0.8940	0.0420
7195	0.8366	0.0721	0.8868	0.9010	0.0482
7200	0.8361	0.0821	0.8867	0.8970	0.0546
7205	0.8355	0.0934	0.8866	0.8990	0.0622
7210	0.8349	0.1060	0.8865	0.9120	0.0716
7215	0.8344	0.1199	0.8864	0.9220	0.0818

Continued on next page

Table B.2 (Continued)

Wavelength	Transmission (%)				
(Å)	QE	Filter	Optics	Atmosphere	Total
7220	0.8338	0.1364	0.8863	0.9220	0.0929
7225	0.8332	0.1541	0.8862	0.9210	0.1048
7230	0.8326	0.1742	0.8861	0.9140	0.1175
7235	0.8320	0.1962	0.8860	0.9100	0.1316
7240	0.8314	0.2201	0.8859	0.9010	0.1461
7245	0.8308	0.2457	0.8858	0.9110	0.1647
7250	0.8302	0.2744	0.8857	0.9080	0.1832
7255	0.8296	0.3045	0.8856	0.9120	0.2040
7260	0.8290	0.3370	0.8855	0.9100	0.2251
7265	0.8284	0.3716	0.8854	0.9140	0.2491
7270	0.8278	0.4066	0.8853	0.9130	0.2721
7275	0.8271	0.4426	0.8852	0.9120	0.2955
7280	0.8265	0.4793	0.8851	0.9120	0.3198
7285	0.8259	0.5159	0.8850	0.9170	0.3458
7290	0.8252	0.5515	0.8849	0.9170	0.3693
7295	0.8246	0.5870	0.8848	0.9150	0.3919
7300	0.8240	0.6225	0.8847	0.9170	0.4161
7305	0.8233	0.6553	0.8846	0.9180	0.4381
7310	0.8227	0.6861	0.8845	0.9180	0.4583
7315	0.8220	0.7149	0.8844	0.9200	0.4781
7320	0.8213	0.7409	0.8843	0.9230	0.4967
7325	0.8207	0.7649	0.8841	0.9250	0.5134
7330	0.8200	0.7865	0.8840	0.9270	0.5285
7335	0.8193	0.8057	0.8839	0.9270	0.5409
7340	0.8187	0.8229	0.8838	0.9280	0.5526
7345	0.8180	0.8370	0.8837	0.9290	0.5621
7350	0.8173	0.8493	0.8836	0.9290	0.5698
7355	0.8166	0.8601	0.8835	0.9290	0.5765
7360	0.8159	0.8689	0.8834	0.9290	0.5818
7365	0.8152	0.8761	0.8833	0.9280	0.5854
7370	0.8145	0.8819	0.8831	0.9290	0.5893
7375	0.8138	0.8863	0.8830	0.9300	0.5923
7380	0.8131	0.8901	0.8829	0.9310	0.5949
7385	0.8124	0.8931	0.8828	0.9310	0.5963
7390	0.8117	0.8948	0.8827	0.9310	0.5969
7395	0.8110	0.8966	0.8826	0.9310	0.5975
7400	0.8102	0.8978	0.8825	0.9320	0.5983
7405	0.8095	0.8983	0.8823	0.9320	0.5980
7410	0.8088	0.8980	0.8822	0.9330	0.5978
7415	0.8080	0.8988	0.8821	0.9330	0.5977
7420	0.8073	0.8980	0.8820	0.9330	0.5966
7425	0.8066	0.8976	0.8819	0.9330	0.5957
7430	0.8058	0.8973	0.8817	0.9330	0.5948
7435	0.8051	0.8970	0.8816	0.9330	0.5940
7440	0.8043	0.8965	0.8815	0.9330	0.5930
7445	0.8036	0.8968	0.8814	0.9340	0.5933
7450	0.8028	0.8967	0.8813	0.9340	0.5926
7455	0.8020	0.8961	0.8811	0.9340	0.5914
7460	0.8013	0.8967	0.8810	0.9340	0.5912
7465	0.8005	0.8976	0.8809	0.9340	0.5912
7470	0.7997	0.8982	0.8808	0.9340	0.5909
7475	0.7989	0.8991	0.8806	0.9340	0.5908
7480	0.7982	0.8997	0.8805	0.9340	0.5906
7485	0.7974	0.8985	0.8804	0.9340	0.5891

Continued on next page

Table B.2 (Continued)

Wavelength	Transmission (%)				
(Å)	QE	Filter	Optics	Atmosphere	Total
7490	0.7966	0.8985	0.8803	0.9350	0.5891
7495	0.7958	0.8991	0.8801	0.9350	0.5888
7500	0.7950	0.8994	0.8800	0.9350	0.5883
7505	0.7942	0.8994	0.8799	0.9350	0.5877
7510	0.7934	0.9004	0.8797	0.9350	0.5876
7515	0.7926	0.9016	0.8796	0.9360	0.5883
7520	0.7918	0.9019	0.8795	0.9360	0.5879
7525	0.7910	0.9032	0.8793	0.9360	0.5880
7530	0.7901	0.9044	0.8792	0.9360	0.5880
7535	0.7893	0.9047	0.8791	0.9360	0.5876
7540	0.7885	0.9049	0.8789	0.9370	0.5876
7545	0.7877	0.9064	0.8788	0.9370	0.5879
7550	0.7868	0.9079	0.8787	0.9370	0.5881
7555	0.7860	0.9089	0.8785	0.9370	0.5881
7560	0.7852	0.9102	0.8784	0.9370	0.5882
7565	0.7843	0.9117	0.8783	0.9370	0.5885
7570	0.7835	0.9141	0.8781	0.9370	0.5893
7575	0.7826	0.9162	0.8780	0.9380	0.5905
7580	0.7818	0.9189	0.8778	0.9380	0.5915
7585	0.7809	0.9211	0.8777	0.9370	0.5915
7590	0.7801	0.9224	0.8776	0.8930	0.5639
7595	0.7792	0.9239	0.8774	0.7370	0.4655
7600	0.7783	0.9255	0.8773	0.5260	0.3324
7605	0.7774	0.9267	0.8772	0.3740	0.2363
7610	0.7766	0.9284	0.8770	0.3940	0.2491
7615	0.7757	0.9304	0.8769	0.5680	0.3595
7620	0.7748	0.9309	0.8767	0.6410	0.4053
7625	0.7739	0.9316	0.8766	0.6710	0.4241
7630	0.7730	0.9328	0.8765	0.5650	0.3571
7635	0.7721	0.9348	0.8763	0.5660	0.3580
7640	0.7712	0.9360	0.8762	0.5840	0.3694
7645	0.7703	0.9377	0.8760	0.6420	0.4062
7650	0.7694	0.9381	0.8759	0.7150	0.4520
7655	0.7685	0.9396	0.8758	0.7800	0.4933
7660	0.7676	0.9417	0.8756	0.8280	0.5241
7665	0.7667	0.9437	0.8755	0.8630	0.5467
7670	0.7657	0.9454	0.8753	0.8770	0.5557
7675	0.7648	0.9472	0.8752	0.8860	0.5617
7680	0.7639	0.9475	0.8751	0.8970	0.5682
7685	0.7629	0.9482	0.8749	0.9080	0.5747
7690	0.7620	0.9489	0.8748	0.9230	0.5838
7695	0.7610	0.9495	0.8746	0.9290	0.5871
7700	0.7601	0.9511	0.8745	0.9350	0.5911
7705	0.7591	0.9509	0.8744	0.9350	0.5901
7710	0.7582	0.9520	0.8742	0.9380	0.5919
7715	0.7572	0.9527	0.8741	0.9390	0.5921
7720	0.7563	0.9532	0.8740	0.9390	0.5916
7725	0.7553	0.9526	0.8738	0.9390	0.5903
7730	0.7543	0.9530	0.8737	0.9400	0.5904
7735	0.7533	0.9533	0.8736	0.9400	0.5897
7740	0.7524	0.9531	0.8734	0.9400	0.5887
7745	0.7514	0.9536	0.8733	0.9400	0.5882
7750	0.7504	0.9535	0.8732	0.9400	0.5873
7755	0.7494	0.9534	0.8730	0.9410	0.5869

Continued on next page

Table B.2 (Continued)

Wavelength	Transmission (%)				
(Å)	QE	Filter	Optics	Atmosphere	Total
7760	0.7484	0.9533	0.8729	0.9410	0.5860
7765	0.7474	0.9536	0.8728	0.9410	0.5854
7770	0.7464	0.9542	0.8726	0.9410	0.5848
7775	0.7454	0.9532	0.8725	0.9410	0.5833
7780	0.7443	0.9525	0.8724	0.9410	0.5820
7785	0.7433	0.9527	0.8723	0.9410	0.5813
7790	0.7423	0.9529	0.8721	0.9410	0.5805
7795	0.7413	0.9527	0.8720	0.9410	0.5795
7800	0.7402	0.9520	0.8719	0.9410	0.5782
7805	0.7392	0.9527	0.8718	0.9410	0.5777
7810	0.7381	0.9527	0.8716	0.9420	0.5774
7815	0.7371	0.9530	0.8715	0.9420	0.5767
7820	0.7360	0.9532	0.8714	0.9420	0.5759
7825	0.7350	0.9528	0.8713	0.9420	0.5748
7830	0.7339	0.9522	0.8712	0.9420	0.5735
7835	0.7329	0.9512	0.8710	0.9420	0.5720
7840	0.7318	0.9509	0.8709	0.9420	0.5709
7845	0.7307	0.9505	0.8708	0.9420	0.5697
7850	0.7296	0.9513	0.8707	0.9420	0.5693
7855	0.7285	0.9509	0.8706	0.9430	0.5687
7860	0.7275	0.9516	0.8705	0.9430	0.5683
7865	0.7264	0.9520	0.8704	0.9420	0.5670
7870	0.7253	0.9519	0.8703	0.9420	0.5660
7875	0.7242	0.9520	0.8701	0.9420	0.5651
7880	0.7230	0.9520	0.8700	0.9420	0.5641
7885	0.7219	0.9518	0.8699	0.9420	0.5630
7890	0.7208	0.9513	0.8698	0.9420	0.5618
7895	0.7197	0.9506	0.8697	0.9410	0.5599
7900	0.7186	0.9509	0.8696	0.9410	0.5592
7905	0.7174	0.9491	0.8695	0.9410	0.5571
7910	0.7163	0.9485	0.8694	0.9420	0.5564
7915	0.7152	0.9477	0.8693	0.9420	0.5550
7920	0.7140	0.9467	0.8693	0.9420	0.5535
7925	0.7129	0.9449	0.8692	0.9420	0.5516
7930	0.7117	0.9449	0.8691	0.9420	0.5506
7935	0.7105	0.9451	0.8690	0.9440	0.5509
7940	0.7094	0.9438	0.8689	0.9440	0.5492
7945	0.7082	0.9435	0.8688	0.9440	0.5480
7950	0.7070	0.9441	0.8687	0.9440	0.5474
7955	0.7058	0.9447	0.8686	0.9440	0.5467
7960	0.7047	0.9456	0.8686	0.9420	0.5452
7965	0.7035	0.9470	0.8685	0.9420	0.5450
7970	0.7023	0.9478	0.8684	0.9420	0.5445
7975	0.7011	0.9472	0.8683	0.9440	0.5443
7980	0.6999	0.9480	0.8683	0.9440	0.5439
7985	0.6987	0.9483	0.8682	0.9440	0.5430
7990	0.6974	0.9495	0.8681	0.9440	0.5426
7995	0.6962	0.9493	0.8681	0.9440	0.5416
8000	0.6950	0.9465	0.8680	0.9440	0.5390
8005	0.6938	0.9440	0.8679	0.9430	0.5360
8010	0.6925	0.9431	0.8679	0.9430	0.5345
8015	0.6913	0.9443	0.8678	0.9440	0.5348
8020	0.6900	0.9450	0.8678	0.9440	0.5342
8025	0.6888	0.9456	0.8677	0.9440	0.5335

Continued on next page

Table B.2 (Continued)

Wavelength	Transmission (%)				
(Å)	QE	Filter	Optics	Atmosphere	Total
8030	0.6875	0.9464	0.8677	0.9440	0.5330
8035	0.6863	0.9474	0.8676	0.9440	0.5325
8040	0.6850	0.9474	0.8676	0.9440	0.5315
8045	0.6837	0.9469	0.8675	0.9450	0.5307
8050	0.6825	0.9472	0.8675	0.9450	0.5300
8055	0.6812	0.9484	0.8674	0.9460	0.5301
8060	0.6799	0.9497	0.8674	0.9460	0.5298
8065	0.6786	0.9506	0.8674	0.9460	0.5293
8070	0.6773	0.9508	0.8673	0.9460	0.5284
8075	0.6760	0.9504	0.8673	0.9460	0.5271
8080	0.6747	0.9507	0.8672	0.9460	0.5262
8085	0.6734	0.9517	0.8672	0.9460	0.5258
8090	0.6721	0.9528	0.8672	0.9460	0.5253
8095	0.6708	0.9535	0.8672	0.9450	0.5242
8100	0.6695	0.9532	0.8671	0.9450	0.5229
8105	0.6682	0.9537	0.8671	0.9450	0.5222
8110	0.6668	0.9546	0.8671	0.9440	0.5210
8115	0.6655	0.9545	0.8671	0.9440	0.5200
8120	0.6642	0.9542	0.8670	0.9430	0.5182
8125	0.6628	0.9550	0.8670	0.9420	0.5170
8130	0.6615	0.9550	0.8670	0.9380	0.5138
8135	0.6601	0.9544	0.8670	0.9360	0.5113
8140	0.6588	0.9537	0.8670	0.9340	0.5088
8145	0.6574	0.9548	0.8670	0.9320	0.5072
8150	0.6561	0.9553	0.8670	0.9280	0.5043
8155	0.6547	0.9555	0.8669	0.9300	0.5043
8160	0.6534	0.9555	0.8669	0.9180	0.4968
8165	0.6520	0.9564	0.8669	0.9160	0.4952
8170	0.6506	0.9563	0.8669	0.9210	0.4967
8175	0.6492	0.9563	0.8669	0.9200	0.4951
8180	0.6479	0.9558	0.8669	0.9230	0.4955
8185	0.6465	0.9563	0.8669	0.9210	0.4936
8190	0.6451	0.9558	0.8669	0.9290	0.4966
8195	0.6437	0.9556	0.8669	0.9240	0.4927
8200	0.6423	0.9547	0.8669	0.9310	0.4949
8205	0.6409	0.9552	0.8669	0.9370	0.4973
8210	0.6395	0.9550	0.8669	0.9420	0.4987
8215	0.6381	0.9542	0.8669	0.9430	0.4977
8220	0.6367	0.9535	0.8669	0.9390	0.4942
8225	0.6353	0.9542	0.8669	0.9210	0.4840
8230	0.6339	0.9529	0.8670	0.9130	0.4781
8235	0.6325	0.9525	0.8670	0.9140	0.4774
8240	0.6311	0.9538	0.8670	0.9300	0.4854
8245	0.6297	0.9541	0.8670	0.9420	0.4907
8250	0.6283	0.9541	0.8670	0.9430	0.4901
8255	0.6268	0.9551	0.8670	0.9410	0.4884
8260	0.6254	0.9552	0.8670	0.9400	0.4869
8265	0.6240	0.9548	0.8670	0.9410	0.4861
8270	0.6226	0.9556	0.8671	0.9390	0.4844
8275	0.6211	0.9565	0.8671	0.9380	0.4832
8280	0.6197	0.9567	0.8671	0.9340	0.4801
8285	0.6183	0.9561	0.8671	0.9290	0.4762
8290	0.6168	0.9556	0.8671	0.9320	0.4763
8295	0.6154	0.9561	0.8672	0.9360	0.4776

Continued on next page

Table B.2 (Continued)

Wavelength	Transmission (%)				
(Å)	QE	Filter	Optics	Atmosphere	Total
8300	0.6139	0.9562	0.8672	0.9370	0.4770
8305	0.6125	0.9567	0.8672	0.9380	0.4767
8310	0.6110	0.9570	0.8672	0.9410	0.4772
8315	0.6096	0.9560	0.8673	0.9390	0.4746
8320	0.6081	0.9560	0.8673	0.9400	0.4739
8325	0.6067	0.9565	0.8673	0.9400	0.4731
8330	0.6052	0.9563	0.8674	0.9420	0.4729
8335	0.6038	0.9560	0.8674	0.9450	0.4732
8340	0.6023	0.9556	0.8675	0.9450	0.4718
8345	0.6009	0.9556	0.8675	0.9470	0.4717
8350	0.5994	0.9559	0.8676	0.9470	0.4708
8355	0.5979	0.9574	0.8676	0.9480	0.4708
8360	0.5965	0.9564	0.8677	0.9480	0.4693
8365	0.5950	0.9571	0.8677	0.9480	0.4684
8370	0.5935	0.9566	0.8678	0.9490	0.4676
8375	0.5921	0.9541	0.8678	0.9500	0.4657
8380	0.5906	0.9536	0.8679	0.9500	0.4644
8385	0.5891	0.9538	0.8680	0.9500	0.4633
8390	0.5876	0.9532	0.8680	0.9510	0.4623
8395	0.5862	0.9527	0.8681	0.9510	0.4611
8400	0.5847	0.9509	0.8682	0.9510	0.4591
8405	0.5832	0.9482	0.8683	0.9510	0.4566
8410	0.5817	0.9474	0.8683	0.9510	0.4551
8415	0.5803	0.9456	0.8684	0.9510	0.4532
8420	0.5788	0.9441	0.8685	0.9510	0.4513
8425	0.5773	0.9421	0.8686	0.9510	0.4493
8430	0.5758	0.9402	0.8687	0.9520	0.4477
8435	0.5743	0.9381	0.8688	0.9520	0.4456
8440	0.5728	0.9361	0.8689	0.9520	0.4435
8445	0.5714	0.9317	0.8690	0.9520	0.4404
8450	0.5699	0.9277	0.8691	0.9520	0.4374
8455	0.5684	0.9245	0.8693	0.9520	0.4349
8460	0.5669	0.9212	0.8694	0.9530	0.4327
8465	0.5654	0.9183	0.8695	0.9530	0.4302
8470	0.5639	0.9153	0.8696	0.9530	0.4277
8475	0.5624	0.9126	0.8698	0.9530	0.4254
8480	0.5610	0.9083	0.8699	0.9530	0.4224
8485	0.5595	0.9030	0.8700	0.9530	0.4189
8490	0.5580	0.8986	0.8702	0.9530	0.4158
8495	0.5565	0.8944	0.8703	0.9530	0.4128
8500	0.5550	0.8905	0.8705	0.9530	0.4100
8505	0.5535	0.8873	0.8707	0.9530	0.4075
8510	0.5520	0.8849	0.8708	0.9530	0.4054
8515	0.5505	0.8815	0.8710	0.9530	0.4028
8520	0.5490	0.8770	0.8712	0.9530	0.3997
8525	0.5476	0.8754	0.8714	0.9530	0.3981
8530	0.5461	0.8747	0.8715	0.9530	0.3967
8535	0.5446	0.8742	0.8717	0.9530	0.3955
8540	0.5431	0.8725	0.8719	0.9530	0.3937
8545	0.5416	0.8709	0.8721	0.9530	0.3920
8550	0.5401	0.8684	0.8723	0.9530	0.3899
8555	0.5386	0.8676	0.8725	0.9530	0.3885
8560	0.5371	0.8676	0.8728	0.9540	0.3880
8565	0.5356	0.8689	0.8730	0.9540	0.3876

Continued on next page

Table B.2 (Continued)

Wavelength	Transmission (%)				
(Å)	QE	Filter	Optics	Atmosphere	Total
8570	0.5341	0.8714	0.8732	0.9540	0.3877
8575	0.5326	0.8742	0.8734	0.9540	0.3879
8580	0.5312	0.8760	0.8736	0.9540	0.3878
8585	0.5297	0.8787	0.8739	0.9540	0.3880
8590	0.5282	0.8813	0.8741	0.9540	0.3882
8595	0.5267	0.8857	0.8743	0.9540	0.3891
8600	0.5252	0.8921	0.8746	0.9540	0.3909
8605	0.5237	0.8974	0.8748	0.9540	0.3922
8610	0.5222	0.9028	0.8751	0.9550	0.3940
8615	0.5207	0.9095	0.8753	0.9550	0.3959
8620	0.5192	0.9150	0.8756	0.9550	0.3973
8625	0.5177	0.9216	0.8758	0.9550	0.3991
8630	0.5162	0.9266	0.8761	0.9550	0.4002
8635	0.5147	0.9295	0.8764	0.9550	0.4004
8640	0.5132	0.9313	0.8766	0.9550	0.4001
8645	0.5118	0.9331	0.8769	0.9550	0.3999
8650	0.5103	0.9317	0.8772	0.9550	0.3983
8655	0.5088	0.9277	0.8775	0.9550	0.3956
8660	0.5073	0.9216	0.8777	0.9550	0.3919
8665	0.5058	0.9093	0.8780	0.9550	0.3856
8670	0.5043	0.8929	0.8783	0.9560	0.3781
8675	0.5028	0.8738	0.8786	0.9560	0.3690
8680	0.5013	0.8494	0.8789	0.9560	0.3578
8685	0.4998	0.8195	0.8792	0.9560	0.3443
8690	0.4983	0.7867	0.8795	0.9560	0.3296
8695	0.4968	0.7505	0.8798	0.9560	0.3136
8700	0.4953	0.7096	0.8801	0.9560	0.2957
8705	0.4938	0.6668	0.8804	0.9560	0.2771
8710	0.4923	0.6231	0.8807	0.9560	0.2583
8715	0.4908	0.5799	0.8810	0.9560	0.2397
8720	0.4893	0.5348	0.8813	0.9560	0.2205
8725	0.4878	0.4909	0.8816	0.9560	0.2018
8730	0.4863	0.4477	0.8819	0.9560	0.1836
8735	0.4848	0.4076	0.8822	0.9560	0.1667
8740	0.4833	0.3676	0.8825	0.9570	0.1500
8745	0.4818	0.3319	0.8828	0.9570	0.1351
8750	0.4803	0.2992	0.8831	0.9570	0.1214
8755	0.4788	0.2687	0.8834	0.9570	0.1088
8760	0.4773	0.2409	0.8838	0.9570	0.0973
8765	0.4758	0.2159	0.8841	0.9570	0.0869
8770	0.4743	0.1937	0.8844	0.9570	0.0778
8775	0.4728	0.1728	0.8847	0.9570	0.0692
8780	0.4713	0.1551	0.8850	0.9570	0.0619
8785	0.4698	0.1383	0.8854	0.9570	0.0551
8790	0.4683	0.1243	0.8857	0.9570	0.0493
8795	0.4668	0.1118	0.8860	0.9570	0.0443
8800	0.4653	0.1002	0.8863	0.9570	0.0395
8805	0.4638	0.0903	0.8867	0.9570	0.0355
8810	0.4623	0.0819	0.8870	0.9570	0.0321
8815	0.4608	0.0747	0.8873	0.9570	0.0292
8820	0.4593	0.0678	0.8876	0.9570	0.0265
8825	0.4578	0.0607	0.8880	0.9570	0.0236
8830	0.4563	0.0549	0.8883	0.9570	0.0213
8835	0.4548	0.0502	0.8886	0.9570	0.0194

Continued on next page

Table B.2 (Continued)

Wavelength	Transmission (%)				
(Å)	QE	Filter	Optics	Atmosphere	Total
8840	0.4533	0.0457	0.8889	0.9570	0.0176
8845	0.4518	0.0423	0.8893	0.9570	0.0163
8850	0.4503	0.0386	0.8896	0.9580	0.0148
8855	0.4488	0.0356	0.8899	0.9570	0.0136
8860	0.4473	0.0328	0.8903	0.9570	0.0125
8865	0.4458	0.0306	0.8906	0.9570	0.0116
8870	0.4443	0.0281	0.8909	0.9570	0.0106
8875	0.4428	0.0261	0.8912	0.9570	0.0099
8880	0.4413	0.0243	0.8916	0.9580	0.0092
8885	0.4398	0.0223	0.8919	0.9580	0.0084
8890	0.4382	0.0207	0.8922	0.9570	0.0077
8895	0.4367	0.0194	0.8925	0.9580	0.0072
8900	0.4352	0.0180	0.8928	0.9580	0.0067
8905	0.4337	0.0173	0.8932	0.9580	0.0064
8910	0.4322	0.0161	0.8935	0.9580	0.0060
8915	0.4307	0.0148	0.8938	0.9580	0.0055
8920	0.4292	0.0138	0.8941	0.9570	0.0051
8925	0.4277	0.0133	0.8944	0.9560	0.0049
8930	0.4262	0.0124	0.8948	0.9550	0.0045
8935	0.4247	0.0117	0.8951	0.9550	0.0042
8940	0.4232	0.0113	0.8954	0.9530	0.0041
8945	0.4216	0.0103	0.8957	0.9530	0.0037
8950	0.4201	0.0100	0.8960	0.9480	0.0036
8955	0.4186	0.0103	0.8963	0.9460	0.0037
8960	0.4171	0.0102	0.8966	0.9380	0.0036
8965	0.4156	0.0096	0.8969	0.9320	0.0033
8970	0.4141	0.0091	0.8972	0.9330	0.0032
8975	0.4126	0.0088	0.8975	0.9280	0.0030
8980	0.4111	0.0083	0.8978	0.9320	0.0029
8985	0.4095	0.0082	0.8981	0.9120	0.0028
8990	0.4080	0.0081	0.8984	0.9160	0.0027
8995	0.4065	0.0077	0.8987	0.9120	0.0026
9000	0.4050	0.0074	0.8990	0.9080	0.0024
9005	0.4035	0.0069	0.8993	0.9250	0.0023
9010	0.4020	0.0067	0.8996	0.9160	0.0022
9015	0.4005	0.0063	0.8999	0.9250	0.0021
9020	0.3989	0.0068	0.9001	0.9180	0.0022
9025	0.3974	0.0065	0.9004	0.9220	0.0021
9030	0.3959	0.0070	0.9007	0.9330	0.0023
9035	0.3944	0.0066	0.9010	0.9360	0.0022
9040	0.3929	0.0058	0.9012	0.9500	0.0020
9045	0.3913	0.0058	0.9015	0.9520	0.0019
9050	0.3898	0.0058	0.9018	0.9490	0.0019
9055	0.3883	0.0058	0.9020	0.9470	0.0019
9060	0.3868	0.0053	0.9023	0.9460	0.0017
9065	0.3853	0.0053	0.9026	0.9310	0.0017
9070	0.3838	0.0051	0.9028	0.9310	0.0016
9075	0.3822	0.0046	0.9031	0.9220	0.0015
9080	0.3807	0.0048	0.9033	0.9140	0.0015
9085	0.3792	0.0045	0.9036	0.9230	0.0014
9090	0.3777	0.0049	0.9039	0.9260	0.0015
9095	0.3762	0.0045	0.9041	0.9270	0.0014
9100	0.3746	0.0045	0.9043	0.9270	0.0014
9105	0.3731	0.0050	0.9046	0.9300	0.0016

Continued on next page

Table B.2 (Continued)

Wavelength	Transmission (%)				
(Å)	QE	Filter	Optics	Atmosphere	Total
9110	0.3716	0.0052	0.9048	0.9340	0.0016
9115	0.3701	0.0051	0.9051	0.9340	0.0016
9120	0.3686	0.0045	0.9053	0.9370	0.0014
9125	0.3670	0.0047	0.9056	0.9300	0.0015
9130	0.3655	0.0055	0.9058	0.9150	0.0017
9135	0.3640	0.0051	0.9060	0.9260	0.0016
9140	0.3625	0.0050	0.9063	0.9250	0.0015
9145	0.3610	0.0041	0.9065	0.9310	0.0012
9150	0.3595	0.0040	0.9067	0.9270	0.0012
9155	0.3579	0.0041	0.9070	0.9290	0.0012
9160	0.3564	0.0047	0.9072	0.9290	0.0014
9165	0.3549	0.0042	0.9074	0.9280	0.0013
9170	0.3534	0.0040	0.9076	0.9330	0.0012
9175	0.3519	0.0047	0.9079	0.9340	0.0014
9180	0.3503	0.0048	0.9081	0.9290	0.0014
9185	0.3488	0.0044	0.9083	0.9320	0.0013
9190	0.3473	0.0041	0.9085	0.9400	0.0012
9195	0.3458	0.0039	0.9087	0.9450	0.0012
9200	0.3443	0.0030	0.9089	0.9500	0.0009
9205	0.3428	0.0028	0.9092	0.9490	0.0008
9210	0.3413	0.0036	0.9094	0.9500	0.0011
9215	0.3397	0.0043	0.9096	0.9500	0.0013
9220	0.3382	0.0041	0.9098	0.9490	0.0012
9225	0.3367	0.0038	0.9100	0.9490	0.0011
9230	0.3352	0.0043	0.9102	0.9500	0.0012
9235	0.3337	0.0043	0.9104	0.9500	0.0012
9240	0.3322	0.0040	0.9106	0.9480	0.0011
9245	0.3307	0.0042	0.9108	0.9460	0.0012
9250	0.3292	0.0049	0.9110	0.9480	0.0014
9255	0.3277	0.0042	0.9112	0.9470	0.0012
9260	0.3262	0.0044	0.9114	0.9500	0.0012
9265	0.3246	0.0045	0.9116	0.9520	0.0013
9270	0.3231	0.0041	0.9118	0.9500	0.0011
9275	0.3216	0.0036	0.9120	0.9420	0.0010
9280	0.3201	0.0035	0.9122	0.9350	0.0010
9285	0.3186	0.0043	0.9124	0.9300	0.0012
9290	0.3171	0.0036	0.9126	0.9210	0.0010
9295	0.3156	0.0034	0.9128	0.9150	0.0009
9300	0.3141	0.0040	0.9130	0.9060	0.0010
9305	0.3126	0.0037	0.9132	0.8870	0.0009
9310	0.3111	0.0025	0.9133	0.8530	0.0006
9315	0.3096	0.0025	0.9135	0.8480	0.0006
9320	0.3081	0.0028	0.9137	0.8070	0.0006
9325	0.3066	0.0050	0.9139	0.8220	0.0012
9330	0.3051	0.0047	0.9141	0.7930	0.0010
9335	0.3036	0.0055	0.9143	0.7810	0.0012
9340	0.3021	0.0055	0.9145	0.7660	0.0012
9345	0.3006	0.0047	0.9146	0.7720	0.0010
9350	0.2992	0.0039	0.9148	0.7510	0.0008
9355	0.2977	0.0040	0.9150	0.7550	0.0008
9360	0.2962	0.0036	0.9152	0.8070	0.0008
9365	0.2947	0.0038	0.9154	0.7570	0.0008
9370	0.2932	0.0053	0.9155	0.7780	0.0011
9375	0.2917	0.0048	0.9157	0.7820	0.0010

Continued on next page

Table B.2 (Continued)

Wavelength	Transmission (%)				
(Å)	QE	Filter	Optics	Atmosphere	Total
9380	0.2902	0.0039	0.9159	0.7790	0.0008
9385	0.2887	0.0059	0.9161	0.8180	0.0013
9390	0.2873	0.0066	0.9162	0.8460	0.0015
9395	0.2858	0.0080	0.9164	0.8780	0.0018
9400	0.2843	0.0071	0.9166	0.8900	0.0016
9405	0.2828	0.0065	0.9168	0.8930	0.0015
9410	0.2813	0.0053	0.9169	0.8850	0.0012
9415	0.2799	0.0064	0.9171	0.8850	0.0015
9420	0.2784	0.0119	0.9173	0.8520	0.0026
9425	0.2769	0.0101	0.9175	0.8490	0.0022
9430	0.2754	0.0068	0.9176	0.8340	0.0014
9435	0.2740	0.0052	0.9178	0.7920	0.0010
9440	0.2725	0.0072	0.9180	0.7910	0.0014
9445	0.2710	0.0112	0.9181	0.8480	0.0024
9450	0.2696	0.0126	0.9183	0.8130	0.0025
9455	0.2681	0.0108	0.9185	0.8180	0.0022
9460	0.2666	0.0093	0.9187	0.8490	0.0019
9465	0.2652	0.0085	0.9188	0.8410	0.0017
9470	0.2637	0.0095	0.9190	0.8440	0.0019
9475	0.2623	0.0114	0.9192	0.8390	0.0023
9480	0.2608	0.0089	0.9193	0.8530	0.0018
9485	0.2594	0.0064	0.9195	0.8690	0.0013
9490	0.2579	0.0054	0.9197	0.8430	0.0011
9495	0.2564	0.0046	0.9198	0.8210	0.0009
9500	0.2550	0.0047	0.9200	0.8520	0.0009
9505	0.2536	0.0047	0.9202	0.8540	0.0009
9510	0.2521	0.0047	0.9203	0.8640	0.0009
9515	0.2507	0.0047	0.9205	0.8560	0.0009
9520	0.2492	0.0047	0.9207	0.8640	0.0009
9525	0.2478	0.0047	0.9208	0.8540	0.0009
9530	0.2463	0.0047	0.9210	0.8450	0.0009
9535	0.2449	0.0047	0.9212	0.8690	0.0009
9540	0.2435	0.0047	0.9213	0.8760	0.0009
9545	0.2420	0.0047	0.9215	0.8820	0.0009
9550	0.2406	0.0047	0.9217	0.8650	0.0009
9555	0.2392	0.0047	0.9218	0.8680	0.0009
9560	0.2377	0.0047	0.9220	0.8710	0.0009
9565	0.2363	0.0047	0.9222	0.8700	0.0009
9570	0.2349	0.0047	0.9223	0.8880	0.0009
9575	0.2334	0.0047	0.9225	0.8800	0.0009
9580	0.2320	0.0047	0.9227	0.8930	0.0009
9585	0.2306	0.0047	0.9228	0.8840	0.0009
9590	0.2292	0.0047	0.9230	0.8790	0.0009
9595	0.2278	0.0047	0.9232	0.8860	0.0009
9600	0.2263	0.0047	0.9233	0.8820	0.0009
9605	0.2249	0.0047	0.9235	0.8970	0.0009
9610	0.2235	0.0047	0.9237	0.9090	0.0009
9615	0.2221	0.0047	0.9238	0.9020	0.0009
9620	0.2207	0.0047	0.9240	0.9020	0.0009
9625	0.2193	0.0047	0.9242	0.9140	0.0009
9630	0.2178	0.0047	0.9243	0.9040	0.0009
9635	0.2164	0.0047	0.9245	0.9090	0.0009
9640	0.2150	0.0047	0.9247	0.9100	0.0009
9645	0.2136	0.0047	0.9248	0.9170	0.0009

Continued on next page

Table B.2 (Continued)

Wavelength	Transmission (%)				
(Å)	QE	Filter	Optics	Atmosphere	Total
9650	0.2122	0.0047	0.9250	0.9130	0.0008
9655	0.2108	0.0047	0.9252	0.9160	0.0008
9660	0.2094	0.0047	0.9253	0.9220	0.0008
9665	0.2080	0.0047	0.9255	0.9240	0.0008
9670	0.2066	0.0047	0.9257	0.9300	0.0008
9675	0.2052	0.0047	0.9258	0.9260	0.0008
9680	0.2038	0.0047	0.9260	0.9430	0.0008
9685	0.2024	0.0047	0.9262	0.9480	0.0008
9690	0.2010	0.0047	0.9263	0.9500	0.0008
9695	0.1996	0.0047	0.9265	0.9460	0.0008
9700	0.1982	0.0047	0.9267	0.9510	0.0008
9705	0.1968	0.0047	0.9268	0.9520	0.0008
9710	0.1954	0.0047	0.9270	0.9480	0.0008
9715	0.1940	0.0047	0.9272	0.9460	0.0008
9720	0.1926	0.0047	0.9273	0.9490	0.0008
9725	0.1912	0.0047	0.9275	0.9490	0.0008
9730	0.1898	0.0047	0.9276	0.9410	0.0008
9735	0.1884	0.0047	0.9278	0.9400	0.0008
9740	0.1870	0.0047	0.9280	0.9420	0.0008
9745	0.1856	0.0047	0.9281	0.9340	0.0008
9750	0.1842	0.0047	0.9283	0.9310	0.0007
9755	0.1829	0.0047	0.9285	0.9330	0.0007
9760	0.1815	0.0047	0.9286	0.9380	0.0007
9765	0.1801	0.0047	0.9288	0.9440	0.0007
9770	0.1787	0.0047	0.9290	0.9450	0.0007
9775	0.1773	0.0047	0.9291	0.9460	0.0007
9780	0.1759	0.0047	0.9293	0.9500	0.0007
9785	0.1745	0.0047	0.9295	0.9450	0.0007
9790	0.1731	0.0047	0.9296	0.9460	0.0007
9795	0.1717	0.0047	0.9298	0.9440	0.0007
9800	0.1704	0.0047	0.9300	0.9490	0.0007
9805	0.1690	0.0047	0.9301	0.9500	0.0007
9810	0.1676	0.0047	0.9303	0.9560	0.0007
9815	0.1662	0.0047	0.9304	0.9570	0.0007
9820	0.1648	0.0047	0.9306	0.9590	0.0007
9825	0.1634	0.0047	0.9308	0.9580	0.0007
9830	0.1621	0.0047	0.9309	0.9590	0.0007
9835	0.1607	0.0047	0.9311	0.9590	0.0007
9840	0.1593	0.0047	0.9313	0.9590	0.0007
9845	0.1579	0.0047	0.9314	0.9610	0.0007
9850	0.1565	0.0047	0.9316	0.9620	0.0007
9855	0.1551	0.0047	0.9318	0.9630	0.0007
9860	0.1538	0.0047	0.9319	0.9640	0.0006
9865	0.1524	0.0047	0.9321	0.9640	0.0006
9870	0.1510	0.0047	0.9322	0.9650	0.0006
9875	0.1496	0.0047	0.9324	0.9650	0.0006
9880	0.1482	0.0047	0.9326	0.9650	0.0006
9885	0.1468	0.0047	0.9327	0.9650	0.0006
9890	0.1455	0.0047	0.9329	0.9660	0.0006
9895	0.1441	0.0047	0.9331	0.9660	0.0006
9900	0.1427	0.0047	0.9332	0.9660	0.0006
9905	0.1413	0.0047	0.9334	0.9660	0.0006
9910	0.1399	0.0047	0.9336	0.9660	0.0006
9915	0.1385	0.0047	0.9337	0.9660	0.0006

Continued on next page

Table B.2 (Continued)

Wavelength	Transmission (%)				
(Å)	QE	Filter	Optics	Atmosphere	Total
9920	0.1372	0.0047	0.9339	0.9660	0.0006
9925	0.1358	0.0047	0.9340	0.9660	0.0006
9930	0.1344	0.0047	0.9342	0.9660	0.0006
9935	0.1330	0.0047	0.9344	0.9660	0.0006
9940	0.1316	0.0047	0.9345	0.9660	0.0006
9945	0.1302	0.0047	0.9347	0.9670	0.0006
9950	0.1289	0.0047	0.9349	0.9670	0.0005
9955	0.1275	0.0047	0.9350	0.9670	0.0005
9960	0.1261	0.0047	0.9352	0.9670	0.0005
9965	0.1247	0.0047	0.9354	0.9670	0.0005
9970	0.1233	0.0047	0.9355	0.9670	0.0005
9975	0.1219	0.0047	0.9357	0.9670	0.0005
9980	0.1205	0.0047	0.9358	0.9670	0.0005
9985	0.1192	0.0047	0.9360	0.9670	0.0005
9990	0.1178	0.0047	0.9362	0.9670	0.0005
9995	0.1164	0.0047	0.9363	0.9670	0.0005
10000	0.1150	0.0047	0.9365	0.9670	0.0005
10005	0.1136	0.0047	0.9365	0.9670	0.0005
10010	0.1122	0.0047	0.9365	0.9670	0.0005
10015	0.1108	0.0047	0.9365	0.9670	0.0005
10020	0.1094	0.0047	0.9365	0.9670	0.0005
10025	0.1081	0.0047	0.9365	0.9670	0.0005
10030	0.1067	0.0047	0.9365	0.9670	0.0005
10035	0.1053	0.0047	0.9365	0.9670	0.0004
10040	0.1039	0.0047	0.9365	0.9680	0.0004
10045	0.1025	0.0047	0.9365	0.9670	0.0004
10050	0.1011	0.0047	0.9365	0.9670	0.0004
10055	0.0997	0.0047	0.9365	0.9680	0.0004
10060	0.0983	0.0047	0.9365	0.9680	0.0004
10065	0.0969	0.0047	0.9365	0.9680	0.0004
10070	0.0955	0.0047	0.9365	0.9680	0.0004
10075	0.0941	0.0047	0.9365	0.9680	0.0004
10080	0.0927	0.0047	0.9365	0.9680	0.0004
10085	0.0913	0.0047	0.9365	0.9670	0.0004
10090	0.0899	0.0047	0.9365	0.9670	0.0004
10095	0.0885	0.0047	0.9365	0.9670	0.0004
10100	0.0871	0.0047	0.9365	0.9670	0.0004
10105	0.0857	0.0047	0.9365	0.9680	0.0004
10110	0.0843	0.0047	0.9365	0.9680	0.0004
10115	0.0829	0.0047	0.9365	0.9680	0.0004
10120	0.0815	0.0047	0.9365	0.9680	0.0003
10125	0.0801	0.0047	0.9365	0.9680	0.0003
10130	0.0787	0.0047	0.9365	0.9680	0.0003
10135	0.0773	0.0047	0.9365	0.9680	0.0003
10140	0.0759	0.0047	0.9365	0.9680	0.0003
10145	0.0745	0.0047	0.9365	0.9680	0.0003
10150	0.0731	0.0047	0.9365	0.9680	0.0003
10155	0.0717	0.0047	0.9365	0.9680	0.0003
10160	0.0703	0.0047	0.9365	0.9680	0.0003
10165	0.0689	0.0047	0.9365	0.9680	0.0003
10170	0.0675	0.0047	0.9365	0.9680	0.0003
10175	0.0661	0.0047	0.9365	0.9680	0.0003
10180	0.0647	0.0047	0.9365	0.9680	0.0003
10185	0.0633	0.0047	0.9365	0.9680	0.0003

Continued on next page

Table B.2 (Continued)

Wavelength	Transmission (%)				
(Å)	QE	Filter	Optics	Atmosphere	Total
10190	0.0619	0.0047	0.9365	0.9680	0.0003
10195	0.0605	0.0047	0.9365	0.9680	0.0003
10200	0.0591	0.0047	0.9365	0.9680	0.0003
10205	0.0577	0.0047	0.9365	0.9680	0.0002
10210	0.0563	0.0047	0.9365	0.9690	0.0002
10215	0.0549	0.0047	0.9365	0.9690	0.0002
10220	0.0535	0.0047	0.9365	0.9690	0.0002
10225	0.0521	0.0047	0.9365	0.9690	0.0002
10230	0.0507	0.0047	0.9365	0.9680	0.0002
10235	0.0493	0.0047	0.9365	0.9680	0.0002
10240	0.0479	0.0047	0.9365	0.9680	0.0002
10245	0.0465	0.0047	0.9365	0.9690	0.0002
10250	0.0451	0.0047	0.9365	0.9690	0.0002
10255	0.0437	0.0047	0.9365	0.9690	0.0002
10260	0.0423	0.0047	0.9365	0.9690	0.0002
10265	0.0408	0.0047	0.9365	0.9690	0.0002
10270	0.0394	0.0047	0.9365	0.9690	0.0002
10275	0.0380	0.0047	0.9365	0.9690	0.0002
10280	0.0366	0.0047	0.9365	0.9690	0.0002
10285	0.0352	0.0047	0.9365	0.9690	0.0002
10290	0.0338	0.0047	0.9365	0.9690	0.0001
10295	0.0324	0.0047	0.9365	0.9690	0.0001
10300	0.0310	0.0047	0.9365	0.9690	0.0001
10305	0.0296	0.0047	0.9365	0.9690	0.0001
10310	0.0282	0.0047	0.9365	0.9690	0.0001
10315	0.0268	0.0047	0.9365	0.9690	0.0001
10320	0.0254	0.0047	0.9365	0.9690	0.0001
10325	0.0240	0.0047	0.9365	0.9690	0.0001
10330	0.0225	0.0047	0.9365	0.9690	0.0001
10335	0.0211	0.0047	0.9365	0.9690	0.0001
10340	0.0197	0.0047	0.9365	0.9690	0.0001
10345	0.0183	0.0047	0.9365	0.9690	0.0001
10350	0.0169	0.0047	0.9365	0.9690	0.0001
10355	0.0155	0.0047	0.9365	0.9690	0.0001
10360	0.0141	0.0047	0.9365	0.9690	0.0001
10365	0.0127	0.0047	0.9365	0.9690	0.0001
10370	0.0113	0.0047	0.9365	0.9690	0.0000
10375	0.0099	0.0047	0.9365	0.9690	0.0000
10380	0.0085	0.0047	0.9365	0.9690	0.0000
10385	0.0070	0.0047	0.9365	0.9690	0.0000
10390	0.0056	0.0047	0.9365	0.9690	0.0000
10395	0.0042	0.0047	0.9365	0.9690	0.0000
10400	0.0028	0.0047	0.9365	0.9690	0.0000
10405	0.0014	0.0047	0.9365	0.9690	0.0000
10410	0.0000	0.0047	0.9365	0.9690	0.0000
10415	0.0000	0.0047	0.9365	0.9690	0.0000
10420	0.0000	0.0047	0.9365	0.9690	0.0000
10425	0.0000	0.0047	0.9365	0.9690	0.0000

C

Photometric Measurements of SN Ia from the ESSENCE Survey

Table C.1: Photometry of ESSENCE Objects

MJD	Passband	$Flux_{25}$	σ_{Flux}
	b010		
52547.1193	R	-2.0606	1.6575
52547.1280	I	0.3818	2.1101
52551.1772	R	-0.1298	2.0014
52555.1026	R	0.5541	1.2363
52555.1232	R	-0.2734	0.8583
52555.1439	I	0.1713	0.6664
52559.1135	R	-1.5034	1.3487
52561.1428	R	-1.1724	0.7813
52583.1746	R	5.9774	0.4556
52583.1792	I	7.8838	1.1964
52589.1466	R	7.4677	0.4611
52589.1513	I	8.4811	0.6642
52593.1571	R	7.1580	1.2075
52593.1617	I	6.3800	1.8248
52593.1687	I	10.3092	1.7043
52606.1733	R	5.2145	0.3885
52606.1780	I	7.1359	0.6489
52614.1812	R	3.9863	0.5962
52614.1851	I	4.7361	1.1831
52618.1252	R	1.6945	0.5583
52618.1298	I	4.8864	1.0209
52622.1163	R	3.3260	0.8215
52622.1211	I	2.5561	1.6038
52624.1339	R	1.5746	1.8741
52624.1385	I	3.4408	1.6203
52637.1412	R	0.6358	0.2819
52637.1459	I	3.1081	1.3777
52637.1511	I	3.3009	0.9829
52642.1342	R	0.6535	0.4069
	b013		
52547.1280	I	0.4951	2.0613
52549.1231	I	-2.8718	2.9160
52555.1026	R	-0.5586	1.1360
	Continued		

Table C.1 (Continued)

MJD	Passband	$Flux_{25}$	σ_{Flux}
52555.1232	R	-0.7951	0.7965
52555.1439	I	-0.2669	0.8409
52559.1135	R	0.1025	1.0670
52561.1428	R	-0.5095	0.8376
52583.1746	R	12.9288	0.5017
52583.1792	I	16.5309	1.1604
52589.1466	R	13.9040	0.3446
52589.1513	I	16.5426	0.6101
52593.1571	R	13.6587	0.9811
52593.1617	I	16.7791	1.8025
52593.1687	I	17.0856	1.7327
52606.1733	R	6.9794	0.3460
52606.1780	I	11.1176	0.5252
52614.1812	R	4.0879	0.4384
52614.1851	I	8.7039	1.0127
52618.1252	R	3.0214	0.6029
52618.1298	I	8.8794	1.0113
52622.1163	R	2.1714	0.7859
52622.1211	I	5.3350	1.5360
52624.1339	R	2.6927	1.1386
52624.1385	I	6.2534	1.5138
52624.1455	I	5.1759	1.4569
52637.1412	R	1.0919	0.3401
52637.1459	I	3.4528	1.2514
52637.1511	I	4.0482	0.9594
52642.1342	R	1.2124	0.3035
52642.1389	I	2.7049	0.8014
	b016		
52526.0758	I	1.7669	2.8629
52526.1050	I	0.3990	3.2989
52545.8215	I	-4.3922	5.0243
52546.9976	I	0.4068	3.3267
52551.0049	I	-3.3140	3.3635
52553.9654	I	-0.5470	1.5123
52579.0170	R	10.0441	1.5510
	Continued		

Table C.1 (Continued)

MJD	Passband	$Flux_{25}$	σ_{Flux}
52579.0247	I	19.5971	1.5549
52587.0194	R	15.2353	0.8525
52587.0262	I	20.2111	1.1339
52591.0291	R	14.4885	1.5456
52591.0359	I	16.2645	1.7432
52608.0359	R	5.4057	1.4866
52608.0424	I	9.0221	1.7633
52610.0242	R	6.0415	1.6320
52610.0309	I	12.5408	2.2718
52618.0336	R	2.6989	1.8520
52618.0367	I	7.6002	1.8902
52624.0367	R	2.9354	1.4820
52624.0396	I	9.3462	1.7919
52637.0396	R	2.7224	0.7846
52637.0442	I	4.9936	1.2292
52642.0556	R	2.6502	1.3256
b017			
52526.0758	I	0.1600	2.7652
52526.1050	I	1.5436	2.8231
52545.8215	I	-1.7022	4.7314
52546.9976	I	2.2600	3.2457
52551.0049	I	-3.2203	3.3769
52553.9654	I	0.1135	1.2665
52579.0170	R	5.8146	1.6057
52579.0247	I	7.0799	1.6524
52587.0194	R	24.4458	0.9512
52587.0262	I	30.2998	1.1453
52591.0291	R	30.8111	1.5601
52591.0359	I	36.7279	1.7779
52608.0359	R	25.6091	1.5209
52608.0424	I	27.1968	1.7929
52610.0242	R	22.8125	1.5365
52610.0309	I	22.8489	2.1168
52618.0336	R	14.7309	1.9600
52618.0367	I	22.6951	1.9138
Continued			

Table C.1 (Continued)

MJD	Passband	$Flux_{25}$	σ_{Flux}
52624.0367	R	12.5325	1.5905
52624.0396	I	19.4135	1.7969
52637.0396	R	5.5618	0.6963
52637.0442	I	11.3781	1.0692
52642.0556	R	7.4081	1.3185
b020			
52559.1541	R	-0.1813	0.9798
52561.3023	R	-0.2445	0.5643
52579.1365	R	1.0162	0.4379
52579.1538	I	1.1790	0.6691
52585.1454	R	4.7137	0.4249
52587.1390	R	7.1057	0.4810
52587.1568	I	8.4914	0.4913
52591.1444	R	9.7271	0.5027
52610.1363	R	12.3206	0.5005
52610.1537	I	17.2728	1.6593
52622.0905	R	5.6878	1.2243
b022			
52553.1394	I	-1.2536	1.7570
52559.1393	R	-0.0835	1.2676
52561.2836	R	-0.9675	0.8263
52579.1309	R	2.0209	0.4692
52579.1413	I	2.3511	0.6882
52585.1408	R	6.3811	0.4203
52587.1342	R	7.9088	0.4320
52587.1440	I	8.2832	0.7297
52591.1397	R	9.3720	0.5137
52591.1491	I	7.1039	0.8689
52591.1555	I	8.1777	0.8422
52610.1316	R	5.7180	0.5611
52610.1409	I	7.8353	1.1001
52622.0567	R	2.7171	1.0289
52622.0617	I	2.5983	1.1832
52622.0687	I	4.4969	1.1912
c015			
Continued			

Table C.1 (Continued)

MJD	Passband	$Flux_{25}$	σ_{Flux}
52547.1193	R	2.2149	1.7236
52547.1280	I	0.1594	2.2077
52549.1231	I	1.9166	2.7680
52555.1026	R	0.6062	1.2299
52555.1232	R	-0.9627	0.7661
52555.1439	I	-0.9574	0.7677
52559.1135	R	0.2459	1.3568
52561.1428	R	0.1829	0.7453
52583.1746	R	0.6180	0.4752
52583.1792	I	-0.4301	1.0667
52589.1466	R	-0.2142	0.4166
52593.1571	R	0.3563	1.0721
52606.1733	R	3.8458	0.3100
52606.1780	I	5.0258	0.6113
52614.1812	R	7.6555	0.5292
52614.1851	I	8.1656	1.1645
52618.1252	R	8.1129	0.6206
52618.1298	I	10.4719	1.0118
52622.1163	R	6.0748	0.8722
52622.1211	I	10.4165	0.9639
52624.1339	R	5.3816	1.3368
52637.1412	R	4.4804	0.3029
52637.1459	I	3.6671	1.2816
52637.1511	I	6.5076	1.0443
52642.1342	R	3.1631	0.3708
52642.1389	I	6.0245	0.7776
	do33		
52931.0123	R	7.5805	0.5406
52931.0278	I	10.3641	0.7139
52934.0040	R	7.8571	0.5362
52934.0187	I	9.7346	0.7020
52940.0266	R	6.7547	0.4952
52940.0454	I	9.2966	0.6447
52944.0067	R	3.8508	1.2190
52958.0241	R	4.0123	0.6442

Continued

Table C.1 (Continued)

MJD	Passband	$Flux_{25}$	σ_{Flux}
52958.0402	I	7.0976	1.2400
52962.0245	R	4.0136	0.7952
52962.0435	I	4.9858	2.4088
52966.0344	R	3.9763	0.6547
52966.0492	I	5.2173	1.3717
52970.0719	R	1.9606	0.6115
52970.0900	I	5.5786	1.0475
52972.0414	R	1.9194	0.6191
52972.0603	I	3.7092	0.9490
52976.0334	R	1.1084	0.8530
52976.0551	I	3.0530	1.1089
52986.0296	R	1.2035	0.9715
52986.0474	I	2.6325	1.0376
52990.0353	R	1.2424	0.6521
52990.0426	I	2.9219	1.0162
52994.0398	R	0.8164	0.5813
52994.0498	I	2.1900	0.9405
	do58		
52932.0954	R	4.6031	0.4459
52932.0994	I	7.6687	0.8793
52934.0444	R	6.2484	0.6382
52934.0624	I	8.0265	0.8644
52940.0578	R	5.8447	0.4962
52940.0746	I	9.6648	0.7855
52944.0363	R	5.8998	0.6686
52944.0469	I	6.2622	1.8660
52958.0792	I	8.1992	1.4980
52962.0836	R	2.8766	0.8904
52962.0882	I	6.0275	1.5980
52966.0748	R	0.7734	0.6809
52966.0902	I	4.4059	1.0218
52972.0800	R	0.8501	0.5528
52972.0990	I	3.9119	1.0059
52974.0299	R	1.9802	0.5780
52974.0486	I	3.9288	0.8239

Continued

Table C.1 (Continued)

MJD	Passband	$Flux_{25}$	σ_{Flux}
52986.0713	R	1.3522	0.3901
52986.0855	I	4.0423	0.6739
52990.0546	R	0.2823	0.4817
52990.0686	I	1.7260	0.9850
52994.0565	R	1.1832	0.4189
52994.0711	I	2.5107	0.7829
52996.0724	R	1.2891	0.3907
52996.0917	I	2.4103	0.8508
52998.0635	R	0.7694	0.4393
52998.0909	I	1.2018	1.1898
53000.0702	R	0.9477	0.4586
53000.0869	I	1.1640	0.6628
53002.0446	R	1.5683	0.5406
53002.0687	I	3.4667	1.1594
	do83		
52910.1838	R	-0.2217	0.6429
52931.1509	R	47.3370	0.3680
52931.1720	I	53.0459	0.5855
52934.1387	R	52.4798	0.6150
52934.1648	I	57.7544	1.0392
52940.1642	R	52.6077	0.4868
52940.1858	I	61.1221	0.7866
52944.1272	R	46.9150	0.7234
52944.1483	I	50.6055	1.1934
52958.1546	R	31.3892	0.7582
52958.1768	I	41.5246	0.9610
52962.1627	R	24.5177	0.5800
52962.1841	I	35.4632	0.9724
52966.1698	R	21.6584	0.5484
52966.1925	I	33.8568	0.8986
52972.1730	R	15.7780	0.4360
52974.1152	R	13.1086	0.4540
52974.1362	I	26.6193	0.7072
52976.1244	R	11.2088	0.5435
52976.1497	I	22.2389	0.8347
	Continued		

Table C.1 (Continued)

MJD	Passband	$Flux_{25}$	σ_{Flux}
52986.1605	R	8.6672	0.5446
52986.1824	I	18.4518	0.8444
52990.1418	R	7.8810	0.5233
52990.1628	I	16.4409	0.8059
52994.1375	R	6.6606	0.4696
	do84		
52910.1838	R	-1.0959	0.7379
52931.1509	R	4.9784	0.3337
52931.1720	I	7.5048	0.6285
52934.1387	R	6.7458	0.5944
52934.1648	I	9.4956	0.9747
52940.1642	R	5.8622	0.4881
52940.1858	I	7.8629	0.7340
52944.1272	R	4.9298	0.7345
52944.1483	I	2.5780	1.3221
52958.1546	R	3.5181	0.7616
52958.1768	I	3.7620	0.8506
52962.1627	R	1.6230	0.5319
52962.1841	I	2.8421	1.0330
52966.1698	R	1.6498	0.4782
52966.1925	I	2.0499	0.8973
52972.1730	R	1.3649	0.4104
52974.1152	R	1.3493	0.5014
52974.1362	I	0.4141	0.7422
52976.1244	R	0.0630	0.5412
52976.1497	I	1.0276	0.9057
52986.1605	R	1.0203	0.5566
52986.1824	I	0.2587	0.8881
52990.1418	R	0.7448	0.4921
52990.1628	I	1.1919	0.7928
52994.1375	R	0.1007	0.4623
	do85		
52910.0392	R	2.4938	1.1952
52932.0126	R	12.1193	0.5095
52932.0339	I	11.3630	0.7416
	Continued		

Table C.1 (Continued)

MJD	Passband	$Flux_{25}$	σ_{Flux}
52936.0189	R	16.5981	0.6865
52936.0420	I	16.7434	1.9960
52940.0190	R	15.4816	0.5721
52940.0337	I	20.4516	0.9144
52944.0028	R	13.6914	1.0144
52960.0403	R	9.1488	1.0517
52960.0660	I	16.7395	1.5482
52964.0359	R	7.9646	0.4640
52964.0714	I	13.4758	0.9783
52966.1262	R	6.8634	0.6357
52966.1474	I	11.8204	1.2007
52970.0438	R	5.2091	0.6069
52972.0378	R	3.9172	0.5711
52972.0543	I	9.6325	1.0219
52976.0282	R	4.9853	0.8634
52976.0491	I	7.5605	1.3620
52988.0517	R	1.9285	0.5528
52988.0727	I	5.6507	1.1051
	d086		
52910.0392	R	-0.3615	1.0444
52910.0711	I	-1.7941	1.9813
52932.0126	R	12.0865	0.5140
52932.0339	I	17.7546	0.7369
52936.0189	R	26.2784	0.6918
52936.0420	I	35.4645	1.5885
52940.0190	R	40.0762	0.5709
52940.0337	I	49.8649	0.8623
52944.0028	R	48.0072	1.0703
52960.0403	R	37.1221	0.9952
52960.0660	I	34.7286	1.4262
52964.0359	R	30.8231	0.4912
52964.0714	I	31.1704	0.9924
52966.1262	R	27.8959	0.5954
52966.1474	I	28.6349	1.2433
52970.0438	R	24.8077	0.6138
	Continued		

Table C.1 (Continued)

MJD	Passband	$Flux_{25}$	σ_{Flux}
52970.0656	I	28.3289	0.8880
52972.0378	R	21.9532	0.5571
52972.0543	I	30.5459	1.0004
52976.0282	R	20.1733	0.8803
52976.0491	I	25.7210	1.3270
52988.0517	R	10.9773	0.5851
52988.0727	I	16.3711	0.9448
	d089		
52910.1932	R	2.9534	0.6558
52931.1474	R	16.8884	0.4373
52931.1661	I	19.3883	0.8453
52934.1528	I	19.9711	1.0446
52934.1720	R	15.6268	0.5526
52940.1567	R	13.3133	0.4962
52940.1740	I	17.7047	1.0636
52944.1366	I	14.2992	1.4306
52958.1471	R	4.3915	0.5940
52958.1641	I	10.6428	1.4865
52962.1556	R	3.9559	0.6323
52962.1724	I	9.1551	1.1188
52966.1625	R	3.2466	0.5013
52966.1798	I	7.5993	1.0431
52976.1563	R	2.8662	0.9947
52976.1609	I	3.4018	1.1375
52986.1534	R	0.8083	0.5251
52986.1702	I	4.0216	0.9739
52990.1348	R	1.0887	0.4636
52990.1512	I	3.0318	0.9325
52994.1304	R	0.6991	0.5082
52994.1471	I	3.9407	0.9315
52996.1628	R	0.8416	0.4773
52996.1907	I	2.0768	0.8943
52998.1496	R	0.4477	0.7994
52998.1648	I	2.1227	1.2158
	d093		
	Continued		

Table C.1 (Continued)

MJD	Passband	$Flux_{25}$	σ_{Flux}
52931.1885	R	5.3963	0.3800
52931.2096	I	9.0810	0.7914
52936.1483	R	11.1498	0.6129
52942.1521	R	20.6986	0.6136
52942.1753	I	24.4399	0.8523
52944.1163	R	21.1411	0.6828
52944.1307	I	23.9530	1.2317
52960.1619	R	20.3894	0.8199
52960.1847	I	21.0937	1.7839
52964.1659	R	16.2161	0.6832
52964.1872	I	19.5539	1.0432
52968.1602	R	15.1448	0.8405
52968.1818	I	16.0419	0.8902
52970.1639	R	11.7760	0.5064
52970.1743	R	11.3195	0.4410
52970.1778	I	16.1654	0.7863
52972.1657	R	10.4167	0.5151
52972.1824	I	13.8184	0.8786
52974.1083	R	9.4312	0.5041
52974.1246	I	13.4837	0.7702
52976.1150	R	8.4137	0.5721
52976.1357	I	10.9790	1.0194
52988.1652	R	5.7987	0.6157
52988.1865	I	11.5512	0.9721
52992.1721	R	4.5541	0.4698
52992.1900	I	10.1354	0.8848
52996.1591	R	4.4518	0.4434
52996.1784	I	6.5411	0.8045
52998.1460	R	3.3315	0.5825
53002.1275	R	2.5781	0.7555
53002.1440	I	6.2960	1.1031
53004.1584	R	3.3575	0.7793
53004.1740	I	5.0925	1.5846
d097			
52931.1885	R	12.6064	0.3593
52931.2096	I	16.9281	0.6781
52936.1483	R	16.4588	0.5826
52942.1521	R	15.5094	0.5360
52942.1753	I	18.7097	0.7080
52944.1163	R	14.0865	0.6298
52944.1307	I	18.8320	1.0685
52960.1619	R	13.3733	0.8492
52960.1847	I	11.9978	1.6031
52964.1659	R	4.9193	0.6756
52964.1872	I	9.2626	0.9474
52968.1602	R	5.9310	0.8002
52968.1818	I	8.6014	0.7724
52970.1639	R	4.1086	0.4471
52970.1743	R	4.7446	0.3899
52970.1778	I	8.8127	0.6690
52972.1657	R	3.7397	0.4552
52972.1824	I	7.1383	0.7774
52974.1083	R	3.0461	0.4850
52974.1246	I	6.7084	0.6887
52976.1150	R	3.4118	0.5583
52976.1357	I	6.4180	0.8890
52988.1652	R	2.4916	0.5886
52988.1865	I	6.6720	0.7920
52992.1721	R	0.9245	0.4737
52992.1900	I	3.4803	0.8199
52996.1591	R	0.7297	0.4407
52996.1784	I	3.8535	0.6437
52998.1460	R	0.4526	0.5422
53002.1275	R	0.5018	0.7338
53002.1440	I	2.6241	0.8978
53004.1584	R	1.5021	0.7341
53004.1740	I	1.2607	1.3089
d099			
52932.1094	R	47.2433	0.5535
52932.1294	I	46.7328	1.0069

Continued

Continued

Table C.1 (Continued)

MJD	Passband	$Flux_{25}$	σ_{Flux}
52936.0947	R	8.3006	1.2966
52936.1133	I	35.5492	1.7943
52942.0985	R	30.1501	0.5881
52944.0657	R	24.6261	0.9648
52944.0927	I	28.8644	1.1884
52960.1166	R	15.7281	0.7016
52960.1332	I	22.2834	1.3336
52964.1207	R	12.0527	0.6410
52964.1372	I	16.5415	1.4928
52968.0659	R	11.5113	1.0581
52968.0905	I	15.0865	0.9997
52970.1194	R	8.6473	0.4771
52970.1364	I	10.8528	1.0318
52972.1143	R	7.4825	0.6426
52972.1445	I	13.7399	1.2005
52974.0707	R	7.6667	0.5295
52974.0873	I	11.6862	0.7380
52976.0728	R	7.3088	0.6149
52976.0926	I	9.3247	1.0093
52988.1204	R	6.6080	0.5026
52988.1373	I	7.5803	1.1009
52992.1478	R	5.7408	0.6011
52996.1176	R	5.4602	0.4652
52996.1344	I	7.4034	0.8868
53002.0869	R	4.6949	0.6827
53002.0941	I	4.5990	0.9552
53004.1169	R	5.0936	0.7033
53004.1335	I	2.3201	2.0741
d100			
52931.0164	R	157.7932	0.9361
52931.0336	I	200.5808	1.5863
52934.0077	R	136.5623	1.0587
52934.0246	I	169.9290	1.3091
52940.0301	R	114.0419	0.9443
52940.0513	I	156.0720	1.2860
52944.0104	R	92.9022	1.9101
52958.0295	R	64.7769	1.2656
52958.0461	I	97.8922	2.0726
52962.0296	R	54.2509	1.1961
52962.0494	I	78.4806	4.3643
52966.0380	R	51.1161	1.0925
52966.0552	I	75.0509	1.6093
52970.0759	R	45.6803	0.8869
52970.0825	R	46.6109	0.8223
52970.0959	I	63.8601	1.3594
52972.0450	R	45.5536	0.8781
52972.0662	I	60.4846	1.3912
52976.0382	R	38.7119	1.1406
52976.0610	I	49.5945	1.7718
52986.0331	R	33.4885	1.0503
52986.0533	I	44.2714	1.3890
52990.0388	R	31.5776	0.9323
52990.0484	I	37.4130	1.4935
d117			
52910.1730	R	-0.5588	0.6735
52931.1398	R	0.8391	0.4317
52931.1544	I	0.8260	0.8335
52934.1353	R	2.6388	0.5528
52934.1588	I	3.2175	0.8741
52940.1604	R	10.3743	0.4442
52940.1798	I	12.4557	0.8284
52944.1237	R	13.3326	1.1845
52944.1424	I	17.8554	1.4336
52958.1510	R	14.3582	0.7694
52958.1707	I	17.7153	1.0207
52962.1591	R	10.8121	0.6174
52962.1782	I	13.2077	1.0558
52966.1662	R	8.4646	0.4989
52966.1862	I	12.9278	1.1227
52972.1693	R	5.1864	0.4988

Continued

Table C.1 (Continued)

MJD	Passband	$Flux_{25}$	σ_{Flux}
52974.1118	R	4.1607	0.4644
52974.1304	I	9.1858	0.7556
52976.1198	R	3.9657	0.5828
52976.1415	I	7.2127	0.9940
52986.1570	R	1.4928	0.5820
52986.1763	I	7.0088	0.9592
52990.1383	R	2.4392	0.4797
52990.1570	I	3.3622	0.9646
52994.1340	R	3.2100	0.5107
	d149		
52910.1501	R	-1.3231	0.7155
52932.1164	R	0.6219	0.4544
52932.1414	I	-0.5610	0.7071
52936.1032	R	2.8362	1.1347
52936.1257	I	3.9264	1.4111
52942.1062	R	8.5804	0.5578
52942.1275	I	12.2395	0.8220
52944.0692	R	9.1641	1.0677
52944.0985	I	14.7380	1.4341
52960.1239	R	19.8274	0.7321
52964.1279	R	19.2126	0.5592
52964.1490	I	24.6726	0.8447
52968.0806	R	15.2108	0.6233
52968.1025	I	19.8872	0.7937
52970.1270	R	14.6276	0.4112
52970.1485	I	18.1101	0.7520
52972.1316	R	13.5149	0.6006
52972.1503	I	16.9914	1.0731
52974.0741	R	11.8614	0.4901
52974.0931	I	15.5431	0.6487
52976.0775	R	10.3213	0.5995
52976.0985	I	14.5371	0.9169
52988.1280	R	6.7183	0.7399
52988.1489	I	10.9196	0.9866
52996.1214	R	3.8678	0.5086
52996.1403	I	10.0360	0.9480
52998.1078	R	2.8667	0.5382
52998.1307	I	7.7899	1.0124
53000.1082	R	2.6321	0.3769
53000.1224	I	7.5463	0.6416
53004.1203	R	1.4857	1.2749
53004.1395	I	4.7946	1.5558
	e020		
52931.0123	R	-1.1620	2.0342
52931.0278	I	1.0590	1.1523
52934.0040	R	-1.4899	2.2956
52934.0187	I	0.7982	1.1584
52940.0266	R	-1.1498	2.0523
52940.0454	I	-1.3564	1.1362
52944.0067	R	-2.7389	3.4633
52958.0241	R	31.1799	2.3668
52958.0402	I	29.2754	1.7994
52962.0245	R	29.5242	2.9209
52962.0435	I	56.6210	2.9546
52966.0344	R	36.5883	2.4429
52966.0492	I	64.6596	2.0199
52970.0719	R	48.1332	2.2793
52970.0900	I	64.4939	1.5566
52972.0414	R	49.4650	2.2287
52972.0603	I	62.8951	1.4428
52976.0334	R	39.7391	2.9272
52976.0551	I	48.3276	1.5886
52986.0296	R	39.6046	2.9874
52986.0474	I	36.7624	1.5023
52990.0353	R	40.3301	2.3461
52990.0426	I	35.6871	1.4738
52994.0398	R	39.0940	2.2086
52994.0498	I	35.2092	1.4402
	e108		
52910.1730	R	-0.5397	0.5699

Continued

Table C.1 (Continued)

MJD	Passband	$Flux_{25}$	σ_{Flux}
52931.1398	R	0.1895	0.3811
52931.1544	I	-1.0632	0.6359
52934.1353	R	0.3841	0.4869
52934.1588	I	1.6686	1.0085
52940.1604	R	0.2404	0.4397
52940.1798	I	0.4342	0.8165
52944.1237	R	0.0804	1.0254
52944.1424	I	2.6535	1.3375
52958.1510	R	1.2176	0.6820
52958.1707	I	0.8849	0.9770
52962.1591	R	4.8064	0.5316
52962.1782	I	5.4566	1.0306
52966.1662	R	8.9035	0.6016
52966.1862	I	9.1241	0.9756
52972.1693	R	13.1881	0.5236
52974.1118	R	13.9162	0.4622
52974.1304	I	15.7166	0.7527
52976.1198	R	14.0379	0.5166
52976.1415	I	15.5627	0.9864
52986.1570	R	14.4558	0.5407
52986.1763	I	16.3445	0.9013
52990.1383	R	13.9249	0.4742
52990.1570	I	17.3307	0.9269
52994.1340	R	12.0979	0.4645
e132			
52932.1057	R	1.3992	0.5173
52932.1236	I	-0.2057	0.8669
52936.1073	I	-1.8737	2.1666
52942.0936	R	0.3885	0.5850
52942.1097	I	1.8610	0.9309
52944.0621	R	-0.3507	1.3471
52944.0869	I	-0.4692	1.2016
52960.1131	R	9.2034	0.8753
52960.1274	I	14.9501	1.7869
52964.1172	R	21.3537	0.7187
Continued			

Table C.1 (Continued)

MJD	Passband	$Flux_{25}$	σ_{Flux}
52964.1314	I	27.8086	1.1116
52968.0622	R	27.2529	0.9321
52968.0843	I	28.4992	1.3016
52970.1158	R	30.4145	0.5401
52970.1305	I	35.9471	1.0447
52970.1842	R	30.0710	0.6055
52972.1108	R	32.7989	0.6761
52972.1387	I	39.0905	1.3076
52974.0672	R	31.3215	0.6258
52974.0814	I	40.0063	0.8197
52976.0678	R	31.0577	0.7211
52976.0868	I	37.1402	1.0644
52988.1169	R	20.3577	0.5489
52988.1315	I	23.4670	1.3158
52992.1430	R	18.4719	0.6449
52996.1139	R	15.1444	0.5245
52996.1285	I	22.2730	1.2187
52998.1039	R	14.0204	0.6908
52998.1249	I	21.3107	1.2850
53000.1047	R	12.1855	0.5273
53000.1166	I	22.0638	0.8802
53004.1134	R	8.7221	1.3135
53004.1276	I	16.6580	1.8356
e136			
52932.1057	R	-0.0782	0.4400
52932.1236	I	-0.6757	0.6907
52936.0900	R	-2.7928	2.7942
52936.1073	I	-1.0991	2.0526
52942.0936	R	-1.0793	0.5197
52942.1097	I	0.2312	0.7173
52944.0621	R	0.9102	1.2856
52944.0869	I	-1.4128	1.0941
52960.1131	R	9.1965	0.7582
52960.1274	I	9.8410	1.6662
52964.1172	R	12.5301	0.5474
Continued			

Table C.1 (Continued)

MJD	Passband	$Flux_{25}$	σ_{Flux}
52964.1314	I	15.7213	1.1628
52968.0622	R	12.7190	0.8263
52968.0843	I	13.8373	0.9266
52970.1158	R	12.8345	0.4581
52970.1305	I	16.6825	0.8090
52970.1842	R	11.9312	0.4661
52972.1108	R	11.3655	0.5381
52972.1387	I	17.2430	1.2910
52974.0672	R	11.2592	0.4870
52974.0814	I	15.6734	0.6328
52976.0678	R	10.5392	0.5818
52976.0868	I	15.3923	0.9068
52988.1169	R	5.4474	0.4691
52988.1315	I	7.9687	0.9840
52992.1430	R	3.1637	0.5709
52996.1139	R	3.6710	0.4171
52996.1285	I	6.1345	0.8553
52998.1039	R	2.2410	0.5465
52998.1249	I	7.6560	1.1245
53000.1047	R	3.0965	0.3951
53000.1166	I	7.0968	0.6603
53004.1134	R	0.8111	1.2179
53004.1276	I	7.7861	1.6946
e138			
52931.1780	R	0.0698	0.3239
52931.1920	I	1.8747	0.6135
52936.1321	R	-0.6284	1.2287
52936.1522	I	2.6181	1.8669
52936.1792	I	0.3859	1.3960
52942.1415	R	3.5792	0.4710
52942.1575	I	4.2236	0.7713
52960.1509	R	0.5453	0.5236
52964.1551	R	4.7891	0.4871
52964.1697	I	8.2080	0.9430
52968.1477	R	4.7846	0.7385
Continued			

Table C.1 (Continued)

MJD	Passband	$Flux_{25}$	σ_{Flux}
52968.1639	I	16.5626	3.6320
52972.1620	R	4.3589	0.7054
52972.1766	I	7.1676	0.8551
52974.1047	R	3.9915	0.4489
52974.1188	I	6.5368	0.6900
52976.1103	R	2.6747	0.5437
52976.1292	I	4.6471	1.0152
52988.1547	R	1.3552	0.5843
52988.1687	I	4.0336	1.3036
52992.1530	R	1.4130	0.4137
52992.1777	I	2.7068	0.8376
52996.1555	R	1.2564	0.4226
52996.1724	I	2.1769	0.6475
53002.1239	R	0.3995	0.5956
53004.1548	R	0.5327	0.5053
53004.1680	I	2.5997	1.3339
e140			
52931.1885	R	0.2007	0.2602
52931.2096	I	1.1650	0.7944
52936.1483	R	0.6949	0.6111
52942.1521	R	0.5800	0.5736
52942.1753	I	0.9328	0.7543
52944.1163	R	1.0819	0.6698
52944.1307	I	0.2704	1.1929
52960.1619	R	1.3976	0.8107
52960.1847	I	7.0030	1.6676
52964.1659	R	7.4896	0.7535
52964.1872	I	9.6380	0.9154
52968.1602	R	6.8551	0.9130
52968.1818	I	10.6627	0.8864
52970.1639	R	8.1898	0.5161
52970.1743	R	8.3760	0.4585
52970.1778	I	10.1252	0.7508
52972.1657	R	7.3673	0.4518
52972.1824	I	9.3812	0.8474
Continued			

Table C.1 (Continued)

MJD	Passband	$Flux_{25}$	σ_{Flux}
52974.1083	R	7.6150	0.4866
52974.1246	I	10.4287	0.7743
52976.1150	R	7.4680	0.5686
52976.1357	I	7.9400	1.0612
52988.1652	R	5.1396	0.6405
52988.1865	I	6.2292	1.0449
52992.1721	R	3.2474	0.5489
52992.1900	I	5.8529	0.9453
52996.1591	R	2.5227	0.4840
52996.1784	I	4.9873	0.8004
52998.1460	R	1.7718	0.5515
53002.1275	R	2.2736	0.7806
53002.1440	I	4.2721	1.1480
53004.1584	R	2.2343	0.7799
53004.1740	I	0.2456	1.4900
e147			
52931.1885	R	-0.0046	0.2996
52931.2096	I	0.3048	0.5849
52936.1483	R	0.3661	0.6089
52942.1521	R	2.0420	0.4798
52942.1753	I	1.8792	0.7057
52944.1163	R	2.3709	0.6424
52944.1307	I	3.1808	1.0254
52960.1619	R	2.4668	0.7691
52960.1847	I	9.8188	1.8000
52964.1659	R	8.0670	0.7414
52964.1872	I	9.7713	0.8582
52968.1602	R	7.7451	0.9451
52968.1818	I	8.3518	0.7968
52970.1639	R	6.7714	0.4563
52970.1743	R	6.5424	0.4194
52970.1778	I	8.6642	0.6961
52972.1657	R	6.0880	0.4909
52972.1824	I	9.2989	0.8245
52974.1083	R	5.8861	0.4589

Continued

Table C.1 (Continued)

MJD	Passband	$Flux_{25}$	σ_{Flux}
52974.1246	I	8.1274	0.6742
52976.1150	R	5.3790	0.5462
52976.1357	I	8.1671	0.9991
52988.1652	R	2.8450	0.5974
52988.1865	I	3.8061	0.8969
52992.1721	R	2.1502	0.4945
52992.1900	I	3.1182	0.8242
52996.1591	R	1.7414	0.4586
52996.1784	I	2.4364	0.7002
52998.1460	R	1.4548	0.5899
53002.1275	R	1.1465	0.7237
53002.1440	I	1.2447	0.9702
53004.1584	R	1.1928	0.7851
53004.1740	I	0.2953	1.3715
e148			
52931.1885	R	-0.2020	0.3347
52931.2096	I	0.7534	0.6551
52936.1483	R	-0.9707	0.5826
52942.1521	R	0.0842	0.5204
52942.1753	I	-1.2291	0.6582
52944.1163	R	0.1190	0.5579
52944.1307	I	0.7801	1.0795
52960.1619	R	-0.0863	0.6990
52960.1847	I	3.3348	1.5604
52964.1659	R	7.4387	0.6411
52964.1872	I	9.3293	0.8240
52968.1602	R	8.0836	0.7268
52968.1818	I	10.8009	0.7667
52970.1639	R	11.7845	0.4281
52970.1743	R	12.4689	0.3679
52970.1778	I	13.6034	0.6442
52972.1657	R	12.6650	0.3929
52972.1824	I	12.6436	0.7673
52974.1083	R	12.5538	0.4339
52974.1246	I	15.6147	0.6941

Continued

Table C.1 (Continued)

MJD	Passband	$Flux_{25}$	σ_{Flux}
52976.1150	R	12.6954	0.5054
52976.1357	I	13.5441	0.9841
52988.1652	R	11.2710	0.5696
52988.1865	I	13.4591	0.8553
52992.1721	R	8.5115	0.4771
52992.1900	I	12.8026	0.8475
52996.1591	R	6.8930	0.4151
52996.1784	I	10.9182	0.6880
52998.1460	R	5.1975	0.5362
53002.1275	R	3.9073	0.7042
53002.1440	I	6.3605	1.0227
53004.1584	R	3.3448	0.7039
53004.1740	I	8.1390	1.2853
e149			
52931.1885	R	0.7438	0.3318
52931.2096	I	2.6415	0.6708
52936.1483	R	3.0293	0.5280
52942.1521	R	8.2990	0.5298
52942.1753	I	9.0409	0.7233
52944.1163	R	9.0324	0.6109
52944.1307	I	8.8835	1.1022
52960.1619	R	8.7847	0.7747
52960.1847	I	11.4893	1.5913
52964.1659	R	7.4875	0.6233
52964.1872	I	9.9590	0.8944
52968.1602	R	7.6791	0.7547
52968.1818	I	9.0770	0.7991
52970.1639	R	5.0201	0.4006
52970.1743	R	5.4025	0.3488
52970.1778	I	6.9288	0.6285
52972.1657	R	4.9310	0.4302
52972.1824	I	7.1375	0.7710
52974.1083	R	4.4013	0.4567
52974.1246	I	4.7742	0.6931
52976.1150	R	3.6146	0.5188
52976.1357	I	6.2046	0.9199
52988.1652	R	2.4384	0.5616
52988.1865	I	3.4759	0.8937
52992.1721	R	1.7103	0.4728
52992.1900	I	2.9349	0.7941
52996.1591	R	1.0230	0.4188
52996.1784	I	1.9334	0.6999
52998.1460	R	0.8220	0.5016
53002.1275	R	1.6676	0.7050
53002.1440	I	1.4321	0.9700
53004.1584	R	1.3824	0.7646
53004.1740	I	0.6154	1.3347
e531			
52932.1057	R	-0.4078	0.4248
52932.1236	I	0.4032	0.8642
52936.1073	I	-0.1062	1.9760
52942.0936	R	0.9945	0.5345
52942.1097	I	1.6137	0.8753
52944.0621	R	2.5922	1.2859
52944.0869	I	5.3506	1.1879
52960.1131	R	4.4247	0.7536
52960.1274	I	8.4497	1.6431
52964.1172	R	4.0998	0.5449
52964.1314	I	7.5650	1.0473
52968.0622	R	3.1949	0.7561
52968.0843	I	6.0597	1.1545
52970.1158	R	4.4171	0.4409
52970.1305	I	6.4629	0.9899
52970.1842	R	3.5647	0.4387
52972.1108	R	3.0655	0.5585
52972.1387	I	8.8708	1.2570
52974.0672	R	2.9556	0.5043
52974.0814	I	6.1892	0.6662
52976.0678	R	2.8943	0.5830
52976.0868	I	6.1122	0.9542

Continued

Continued

Table C.1 (Continued)

MJD	Passband	$Flux_{25}$	σ_{Flux}
52988.1169	R	1.6980	0.4292
52988.1315	I	2.8592	1.1374
52992.1430	R	0.7285	0.5200
52996.1139	R	1.6560	0.3677
52996.1285	I	2.2950	0.9458
52998.1039	R	1.2814	0.5114
52998.1249	I	3.8394	1.1700
53000.1047	R	1.3792	0.3992
53000.1166	I	2.3531	0.6812
53004.1134	R	1.2940	1.1149
53004.1276	I	1.8533	1.7763
	f011		
52910.1550	R	1.0604	0.6841
52931.1050	R	-0.1823	0.4227
52931.1219	I	1.4297	0.6676
52934.0910	R	0.7457	0.5252
52934.1079	I	0.2896	0.8498
52940.1121	R	-0.5685	0.4114
52940.1340	I	1.3539	0.6968
52944.0727	R	-0.6958	1.1197
52944.1044	I	1.5901	1.0999
52958.1078	R	0.7487	0.5206
52958.1247	I	0.8860	1.1003
52962.1165	R	-0.5687	0.5776
52962.1344	I	-0.7306	1.1953
52968.1124	R	2.6047	0.4497
52968.1297	I	2.6664	1.0701
52986.1145	R	9.8160	0.4137
52986.1313	I	8.9506	0.8558
52990.0967	R	8.3790	0.5020
52990.1138	I	10.9196	0.6619
52994.1008	R	7.3984	0.4832
52994.1179	I	8.5122	0.7747
52996.1250	R	6.3519	0.4049
52996.1461	I	9.5664	0.8427

Continued

Table C.1 (Continued)

MJD	Passband	$Flux_{25}$	σ_{Flux}
52998.1214	R	6.5939	0.4230
52998.1366	I	6.7345	1.0149
53000.1129	R	4.9360	0.3712
53000.1294	I	8.0104	0.6948
53004.1239	R	5.3019	1.1627
53004.1453	I	6.7164	1.4348
	f041		
52932.0954	R	-0.0404	0.4131
52932.0994	I	-1.1336	0.8829
52934.0444	R	-0.2873	0.7290
52934.0624	I	1.2239	0.9705
52940.0578	R	-0.6569	0.5673
52940.0746	I	-0.2407	0.7493
52944.0363	R	-0.2636	0.7811
52944.0469	I	-2.8289	2.0142
52958.0792	I	-3.3071	1.6309
52962.0836	R	0.8911	0.9807
52962.0882	I	-1.4672	1.8043
52966.0748	R	2.0591	0.6448
52966.0902	I	-0.6510	1.1556
52972.0800	R	5.1599	0.5510
52972.0990	I	4.2107	1.0691
52974.0299	R	7.3026	0.6831
52974.0486	I	5.8942	0.8928
52986.0713	R	9.2232	0.4284
52986.0855	I	9.8099	0.8288
52990.0546	R	8.8325	0.6054
52990.0686	I	11.3666	1.2197
52994.0565	R	9.1081	0.4269
52994.0711	I	11.4711	0.8775
52996.0724	R	8.4148	0.4291
52996.0917	I	9.3623	0.8512
52998.0635	R	8.4804	0.5058
52998.0909	I	9.7468	1.2366
53000.0702	R	7.7674	0.4831

Continued

Table C.1 (Continued)

MJD	Passband	$Flux_{25}$	σ_{Flux}
53000.0869	I	8.5675	0.7875
53002.0446	R	7.6426	0.6715
53002.0687	I	8.2214	1.2059
f096			
52932.0088	R	9.2118	13.6690
52932.0280	I	0.9222	0.7665
52936.0140	R	-27.7769	16.6024
52936.0359	I	4.6158	2.3410
52942.0136	R	8.9723	12.8676
52942.0334	I	-0.3521	0.7787
52960.0590	I	-0.5782	1.3418
52964.0302	R	4.9210	12.8659
52964.0655	I	0.5157	1.1909
52966.1225	R	4.2513	14.0001
52966.1416	I	0.3273	1.0951
52970.0401	R	2.7449	14.2979
52970.0598	I	3.0632	1.0613
52988.0482	R	17.0226	13.7303
52988.0669	I	13.3027	0.9606
52996.0481	R	21.6403	14.2413
52996.0580	I	14.3535	0.9041
52998.0428	R	1.3546	17.9649
52998.0527	I	16.1035	1.5496
53000.0419	R	19.2492	15.1322
53000.0593	I	16.0653	1.0397
53004.0596	R	-26.3683	31.6203
53004.0798	I	11.5359	1.9948
f123			
52932.1057	R	-0.0151	0.4608
52932.1236	I	0.3238	0.8422
52936.1073	I	-1.9521	2.1085
52942.0936	R	-0.9339	0.5592
52942.1097	I	-0.0643	0.9402
52944.0621	R	-3.2137	1.3049
52944.0869	I	-0.8475	1.1847

Continued

Table C.1 (Continued)

MJD	Passband	$Flux_{25}$	σ_{Flux}
52960.1131	R	-0.5331	0.7543
52960.1274	I	-4.0845	1.6683
52964.1172	R	-0.8220	0.6663
52964.1314	I	0.7771	1.2006
52968.0622	R	1.2480	0.8966
52968.0843	I	0.4309	1.2741
52970.1158	R	1.6509	0.4629
52970.1305	I	0.2463	1.0227
52970.1842	R	1.7661	0.4776
52972.1108	R	2.7729	0.6171
52972.1387	I	1.8036	1.4672
52974.0672	R	3.3483	0.5725
52974.0814	I	4.3234	0.8073
52976.0678	R	3.1419	0.6379
52976.0868	I	1.3086	1.0428
52988.1169	R	6.5549	0.5038
52988.1315	I	7.5971	1.0889
52992.1430	R	5.3813	0.5669
52996.1139	R	6.2039	0.4821
52996.1285	I	8.5745	1.0921
52998.1039	R	4.8697	0.6172
52998.1249	I	8.7166	1.2392
53000.1047	R	4.3005	0.4430
53000.1166	I	7.1544	0.7037
53004.1134	R	1.1126	1.2242
53004.1276	I	4.0618	1.9066
f216			
52931.1780	R	-0.2378	0.3222
52931.1920	I	-0.2390	0.6427
52936.1321	R	-1.5754	1.3837
52936.1522	I	0.1699	2.1335
52936.1792	I	-2.6189	1.6235
52942.1415	R	-0.3765	0.5533
52942.1575	I	0.4489	0.8845
52964.1551	R	0.0572	0.6072

Continued

Table C.1 (Continued)

MJD	Passband	$Flux_{25}$	σ_{Flux}
52964.1697	I	0.5006	1.1644
52968.1477	R	0.4415	1.1495
52968.1639	I	-1.4218	3.7655
52972.1620	R	3.1088	0.7251
52972.1766	I	2.0184	0.8507
52974.1047	R	3.3658	0.4726
52974.1188	I	2.8487	0.7181
52976.1103	R	3.3535	0.5642
52976.1292	I	3.8381	0.9407
52988.1547	R	5.0887	0.6009
52988.1687	I	6.5711	1.3826
52992.1530	R	4.5427	0.5194
52992.1777	I	5.7697	1.0129
52996.1555	R	2.7947	0.4332
52996.1724	I	6.0611	0.7283
53002.1239	R	2.3980	0.6484
53004.1548	R	-0.0647	0.9576
53004.1680	I	-0.3506	1.3616
	f231		
52910.0830	I	0.7212	1.7154
52932.0014	R	-0.0484	0.5719
52932.0163	I	-0.5055	0.7973
52936.0041	R	0.3044	0.8395
52936.0235	I	-2.9099	2.2987
52942.0091	R	0.2620	0.4989
52942.0274	I	-0.2171	0.7646
52960.0262	R	0.5166	3.7026
52960.0450	I	0.4725	1.3157
52964.0206	R	1.1901	0.4886
52964.0408	I	1.0481	0.9869
52964.0535	I	1.3339	0.7480
52966.1145	R	1.1722	0.6070
52966.1299	I	0.8118	1.1072
52970.0320	R	3.3721	0.4682
52970.0476	I	4.4757	0.9302

Continued

Table C.1 (Continued)

MJD	Passband	$Flux_{25}$	σ_{Flux}
52970.1081	I	3.8121	0.9837
52972.0248	R	4.6961	0.6341
52972.0485	I	6.5056	0.8185
52976.0235	R	5.5342	1.0103
52976.0429	I	7.4334	1.3561
52988.0413	R	7.6154	0.5327
52988.0552	I	8.9335	0.9396
52994.0361	R	7.0661	0.8059
52994.0437	I	9.8820	0.8872
52996.0443	R	6.3282	0.5847
52996.0521	I	8.2676	0.8597
52998.0389	R	6.9380	1.0478
52998.0466	I	7.9576	1.3247
53000.0384	R	6.0246	0.8192
53000.0534	I	8.5024	0.9475
53004.0740	I	11.5106	2.0708
	f235		
52932.0507	R	1.3879	0.4148
52932.0823	I	0.0326	0.7526
52936.0600	R	1.5016	1.2937
52936.0834	I	3.1228	3.3359
52942.0653	R	-0.2281	0.5692
52942.0873	I	-0.0970	0.9498
52944.0325	R	0.3600	1.0793
52944.0401	I	1.4790	1.4048
52944.0584	R	1.5888	1.3361
52960.0859	R	0.2127	1.1580
52960.1071	I	-2.2084	1.4173
52964.0887	R	0.2657	0.5369
52964.1109	I	1.1312	0.8991
52968.0335	R	1.0965	0.3863
52968.0559	I	2.1789	1.0585
52972.0763	R	3.8655	0.5105
52972.0930	I	3.8604	0.9963
52974.0264	R	5.0902	0.6997

Continued

Table C.1 (Continued)

MJD	Passband	$Flux_{25}$	σ_{Flux}
52974.0428	I	4.5408	0.8302
52988.0896	R	15.7956	0.5423
52988.1110	I	18.4515	0.8412
52992.1221	R	20.7900	0.7501
52996.0685	R	15.6536	0.4559
52996.0858	I	18.7742	0.7917
52998.0596	R	13.4925	0.6412
52998.0722	I	17.2856	0.9539
53002.0410	R	11.8565	0.8414
53002.0619	I	15.5737	1.2616
f244			
52910.1769	R	0.2391	0.6848
52931.1433	R	-0.5996	0.3857
52931.1602	I	0.5202	0.7597
52934.1261	R	0.4080	0.5424
52934.1460	I	1.7736	1.2061
52940.1518	R	-0.4099	0.4545
52940.1680	I	-0.1249	0.7795
52958.1432	R	0.2273	0.7382
52958.1581	I	0.0243	1.4826
52962.1521	R	-1.0124	0.6069
52962.1663	I	0.9350	1.0048
52966.1570	R	0.7487	0.5232
52966.1738	I	3.5454	1.0116
52986.1497	R	7.1828	0.5130
52986.1640	I	10.5118	0.9630
52990.1312	R	8.3173	0.4887
52990.1453	I	8.1629	1.0008
52994.1411	I	10.2513	0.9151
52996.1519	R	5.8947	0.4533
52996.1663	I	7.2357	0.8281
52998.1425	R	5.2883	0.6515
52998.1531	I	7.3649	1.0688
53002.1203	R	4.7460	0.6643
53002.1312	I	5.9588	1.2910

Continued

Table C.1 (Continued)

MJD	Passband	$Flux_{25}$	σ_{Flux}
53004.1512	R	3.6604	1.1854
53004.1619	I	4.2304	1.4073
f301			
52910.1932	R	-0.3172	0.6484
52931.1474	R	-0.2900	0.3738
52931.1661	I	1.7146	0.7916
52934.1528	I	1.9655	1.0674
52934.1720	R	-0.6466	0.5133
52940.1567	R	-0.9662	0.4786
52940.1740	I	0.5389	0.8895
52944.1200	R	-0.8760	1.7706
52944.1366	I	0.2233	1.3717
52958.1471	R	-0.4612	0.5760
52958.1641	I	0.3907	1.0663
52962.1556	R	-0.8604	0.5498
52962.1724	I	1.5624	1.0313
52966.1625	R	-0.1547	0.5217
52966.1798	I	-2.0842	0.9209
52976.1563	R	-0.3315	1.1516
52976.1609	I	-0.7976	0.9674
52986.1534	R	3.5423	0.5082
52986.1702	I	3.7188	0.9195
52990.1348	R	5.2888	0.4248
52990.1512	I	8.5951	1.0007
52994.1304	R	5.5765	0.4470
52994.1471	I	6.7634	0.8890
52996.1628	R	5.0601	0.4268
52996.1907	I	7.1748	0.7197
52998.1496	R	5.1855	0.6942
52998.1648	I	7.9701	1.0946
f308			
52910.1932	R	-0.9140	0.6447
52931.1474	R	-0.4705	0.3169
52931.1661	I	0.1174	0.5876
52934.1528	I	-0.9292	1.0925

Continued

Table C.1 (Continued)

MJD	Passband	$Flux_{25}$	σ_{Flux}
52934.1720	R	-0.3019	0.5286
52940.1567	R	-0.0053	0.3864
52940.1740	I	-0.0218	0.8764
52944.1200	R	1.8807	2.0902
52944.1366	I	-1.3818	1.1956
52958.1471	R	-0.0302	0.6038
52958.1641	I	-0.1282	1.1163
52962.1556	R	-0.2057	0.5293
52962.1724	I	-1.3451	0.8521
52966.1625	R	-0.6617	0.5008
52966.1798	I	-0.4617	0.9845
52976.1563	R	2.4297	1.2518
52976.1609	I	0.8114	0.9448
52986.1534	R	7.4706	0.5268
52986.1702	I	9.7425	0.8432
52990.1348	R	8.5958	0.4397
52990.1512	I	9.6180	0.8679
52994.1304	R	10.0713	0.4862
52994.1471	I	10.2264	0.8594
52996.1628	R	10.7879	0.4562
52996.1907	I	11.6723	0.6951
52998.1496	R	9.1958	0.7665
52998.1648	I	10.4158	1.1462
g001			
53266.1104	I	1.1542	1.7829
53268.0270	R	0.8594	1.1550
53268.0305	I	4.1950	1.5377
53285.0220	I	36.6360	2.0823
53287.0046	R	35.4378	1.0850
53287.0196	I	39.4144	1.6179
53291.0054	R	29.1216	1.0162
53291.0203	I	36.1950	1.4615
53295.0048	R	29.4174	0.8271
53295.0195	I	31.1001	1.0560
53299.0157	R	22.8617	0.8134

Continued

Table C.1 (Continued)

MJD	Passband	$Flux_{25}$	σ_{Flux}
53299.0297	I	24.9241	1.0524
53301.0021	R	8.7023	2.6227
53301.0237	I	19.5533	2.9371
53321.0139	R	6.7663	0.7259
53321.0297	I	13.4297	1.1452
53325.0202	R	5.0997	0.7294
53325.0345	I	13.0913	1.0859
53344.0373	R	3.8531	0.7634
53344.0595	I	3.9177	1.1756
53266.0961	R	1.2763	1.3058
g005			
53266.0997	R	-0.8145	0.9046
53266.1163	I	0.0207	1.2692
53268.0365	R	-0.2747	0.7287
53268.0400	I	0.3558	1.1671
53285.0278	I	37.9282	1.6553
53287.0081	R	36.6947	0.6054
53291.0096	R	46.5061	1.0182
53291.0261	I	49.0543	1.1751
53295.0084	R	46.7224	0.6550
53295.0253	I	53.9885	0.8418
53299.0192	R	46.7467	0.6878
53299.0356	I	53.7068	0.7740
53301.0056	R	41.6226	2.6600
53301.0295	I	47.3784	3.1707
53321.0184	R	20.7198	0.7263
53321.0362	I	28.9989	0.8709
53325.0237	R	19.5324	0.5275
53325.0404	I	30.9481	0.7844
53331.0967	I	21.5573	3.4499
53344.0422	R	9.5193	0.5530
53344.0653	I	14.6530	0.8573
53348.0383	R	5.9711	1.0591
53348.0463	R	7.7567	0.5248
53348.0538	I	12.2577	0.8071

Continued

Table C.1 (Continued)

MJD	Passband	$Flux_{25}$	σ_{Flux}
53352.0294	R	6.9954	0.7288
53352.0341	I	10.0519	0.9448
53356.0462	R	6.4752	0.8287
53356.0568	I	10.4344	0.9605
53360.0389	R	7.7206	1.0555
53360.0462	I	9.6552	1.3928
g050			
53266.1399	R	0.0898	0.5763
53266.1494	I	-0.0155	1.1446
53268.0740	R	0.5846	0.7413
53268.0775	I	-1.0193	0.9996
53283.0417	R	2.5319	0.8202
53283.0906	I	2.5122	1.2350
53287.1684	R	4.6104	1.5048
53289.0112	R	5.1791	0.6187
53289.0281	I	6.2767	1.2022
53293.0152	I	7.8510	2.0793
53297.0022	R	9.2816	0.6367
53297.0349	I	10.4300	1.0096
53301.0128	R	9.3703	3.4214
53301.0423	I	5.5597	2.9897
53315.0274	R	5.8916	0.4885
53315.0451	I	9.3665	0.8513
53323.0321	R	4.0093	0.3984
53323.0606	I	5.2348	0.8157
53331.0369	R	1.0918	1.4564
53331.0548	I	4.9679	2.4034
53331.0586	I	1.8372	2.9283
53342.0587	I	2.2472	0.8623
g052			
53350.0305	R	1.4796	0.6674
53350.0376	I	3.8841	1.0247
53268.0058	R	-0.6786	0.9195
53268.0146	I	-0.0529	1.3946
53283.0452	R	4.1797	0.6680
Continued			

Table C.1 (Continued)

MJD	Passband	$Flux_{25}$	σ_{Flux}
53283.0971	I	3.9671	1.0814
53287.1721	R	10.5565	2.0386
53289.0150	R	12.7825	0.5755
53293.0212	I	15.3049	1.7963
53297.0221	R	15.4892	0.5316
53297.0408	I	19.1924	0.9304
53301.0483	I	20.0019	2.3536
53315.0314	R	6.9697	0.4218
53315.0509	I	10.7327	0.8133
53323.0358	R	4.6221	0.3976
53323.0664	I	8.8970	0.8811
53331.0407	R	6.3022	2.3976
53331.0623	I	13.1009	3.9903
53331.0658	I	1.8584	4.4575
53342.0646	I	4.0208	0.8442
53346.0452	R	0.6601	1.3134
g053			
53350.0305	R	0.2963	0.6645
53350.0376	I	1.2411	1.0222
53268.0058	R	2.1507	0.9334
53268.0146	I	1.7482	1.3817
53283.0452	R	8.0452	0.7286
53283.0971	I	8.1084	1.0542
53287.1721	R	9.2981	2.0836
53289.0150	R	7.3036	0.6094
53293.0212	I	8.1828	1.7818
53297.0221	R	5.3509	0.5444
53297.0408	I	7.5689	0.9390
53301.0483	I	3.9397	2.3516
53315.0314	R	1.2663	0.3892
53315.0509	I	4.8640	0.8093
53323.0358	R	1.1315	0.3930
53323.0664	I	3.4656	0.8868
53331.0407	R	8.1953	2.4318
53331.0623	I	-1.5816	3.9963
Continued			

Table C.1 (Continued)

MJD	Passband	$Flux_{25}$	σ_{Flux}
53331.0658	I	6.1786	4.5627
53342.0646	I	0.9360	0.8424
53346.0452	R	-1.1975	1.3482
g055			
53268.1072	R	1.5387	0.8059
53268.1484	I	3.2759	1.2309
53283.1311	R	7.2076	1.0985
53283.1629	I	13.1553	1.4923
53289.0561	R	10.6675	0.8744
53289.0726	I	16.0265	1.1157
53293.0558	I	20.3584	1.5308
53297.0640	R	9.2344	0.6100
53297.0809	I	14.5207	1.0401
53301.0728	R	5.1396	1.0644
53301.0973	I	12.0698	1.0404
53315.0736	R	4.1882	0.5751
53315.0906	I	9.0881	0.7981
53323.0829	R	3.1429	0.4295
53323.1006	I	6.8372	0.7393
53329.0363	R	1.3028	0.6699
53329.0533	I	6.5315	0.8747
53342.0814	R	1.0485	0.4003
53342.0984	I	4.8762	0.8642
53346.0734	R	1.2031	0.5050
53346.0919	I	3.0535	1.0079
53350.0550	R	-0.4808	1.0616
53350.0724	I	1.9919	1.1976
53358.0431	R	0.0473	0.7345
53358.0720	I	3.4706	0.9269
53360.0755	R	1.3929	1.2766
53360.1073	I	1.8570	2.0071
53385.0554	R	0.8139	0.8106
53385.0589	I	1.1336	1.1789
g097			
53350.0376	I	9.8833	1.0895

Continued

Table C.1 (Continued)

MJD	Passband	$Flux_{25}$	σ_{Flux}
53268.0058	R	-0.2132	1.0101
53268.0146	I	0.8636	1.4370
53283.0452	R	5.0683	0.8800
53283.0971	I	6.9414	1.2604
53287.1721	R	8.5835	2.3041
53289.0150	R	12.5234	0.7152
53289.0345	I	17.5055	1.1874
53293.0212	I	23.2028	2.0319
53297.0221	R	20.1971	0.6347
53297.0408	I	23.6986	1.1082
53301.0483	I	20.5808	2.1181
53315.0314	R	13.8825	0.5022
53315.0509	I	20.4629	0.8641
53323.0358	R	9.1876	0.5116
53323.0664	I	16.8032	1.0306
53331.0407	R	1.4924	2.7579
53342.0646	I	10.7028	1.2115
53350.0305	R	3.9588	0.7695
g120			
53268.0884	R	-1.5803	0.9782
53268.1189	I	-0.1988	1.2244
53287.0463	R	8.1737	0.9336
53287.0615	I	10.0933	2.0201
53291.0444	R	12.3220	1.2048
53295.0434	R	12.8198	0.5881
53295.0637	I	13.0746	1.0494
53299.0538	R	12.8810	0.5887
53299.0714	I	14.6595	0.8161
53301.0605	R	11.2502	1.1518
53301.0797	I	16.8979	1.2307
53321.0552	R	5.1260	0.5147
53321.0708	I	9.0959	1.1919
53325.0585	R	3.7443	0.4874
53325.0727	I	7.6057	0.8459
53331.1162	R	4.0930	1.5837

Continued

Table C.1 (Continued)

MJD	Passband	$Flux_{25}$	σ_{Flux}
53331.1330	I	8.8885	1.8817
53344.0837	R	1.1360	0.4854
53344.1000	I	3.6712	0.9554
53348.0662	R	0.3064	0.4439
53348.0805	I	3.2693	0.8594
53352.0405	R	0.5858	0.4689
53352.0514	I	3.2473	0.7048
53356.0749	R	0.2830	0.5480
53356.0862	I	3.0260	0.8178
53358.0324	R	1.3210	0.8399
53358.0539	I	3.4094	0.9687
53360.0604	R	1.3064	1.3247
53360.0793	I	3.4456	2.0384
53379.0519	R	0.6789	0.4896
53379.0555	I	1.9882	0.9427
53387.0429	I	-0.0467	2.6803
g133			
53266.1749	I	19.6231	1.6703
53287.1168	I	19.0307	2.1394
53295.0980	R	9.4734	0.6047
53295.1192	I	13.8656	0.7491
53299.1057	R	8.1256	0.4650
53299.1267	I	11.8068	0.6746
53321.1075	R	3.1393	0.4010
53321.1303	I	4.1214	1.0758
53325.1071	R	2.2354	0.3867
53325.1298	I	4.3384	0.8143
53331.1608	R	1.3713	1.1020
53331.1704	I	5.7406	1.3266
53344.1387	R	1.6570	0.5220
53344.1613	I	5.1525	0.9760
53348.1149	R	1.3329	0.3289
53348.1371	I	2.5345	0.8845
53352.0764	R	1.2935	0.3398
53352.0917	I	2.5688	0.6899

Continued

Table C.1 (Continued)

MJD	Passband	$Flux_{25}$	σ_{Flux}
53354.0815	R	1.4878	0.3664
53354.1055	I	3.7896	0.7031
53358.0967	R	1.1667	0.5203
53358.1174	I	2.4938	0.7111
53360.1214	R	0.7574	0.9758
53360.1372	I	0.6906	1.4028
53379.0668	R	0.9269	0.4433
53379.0825	I	2.2925	1.0587
53385.0686	R	1.4233	0.5143
53385.0849	I	2.2703	0.9108
g142			
53266.0997	R	-0.0719	0.8147
53266.1163	I	-0.3266	1.3039
53268.0365	R	-0.8188	0.6982
53268.0400	I	0.6548	1.2234
53285.0278	I	6.9740	1.5727
53287.0081	R	4.9705	0.6155
53287.0254	I	9.0050	2.3176
53291.0096	R	6.2172	0.9088
53291.0261	I	9.3549	1.1406
53295.0084	R	8.8001	0.5965
53295.0253	I	11.7811	0.8182
53299.0192	R	8.6711	0.6482
53299.0356	I	10.6781	0.7367
53301.0056	R	7.9099	2.4305
53301.0295	I	11.2933	3.1685
53321.0184	R	2.7172	0.6713
53321.0362	I	4.9521	0.8344
53325.0237	R	1.5120	0.4877
53325.0404	I	4.5900	0.7654
53331.0967	I	1.1548	3.2948
53344.0422	R	1.5637	0.6315
53344.0653	I	0.6097	0.8480
53348.0383	R	-1.3947	1.0534
53348.0463	R	1.3583	0.4965

Continued

Table C.1 (Continued)

MJD	Passband	$Flux_{25}$	σ_{Flux}
53348.0538	I	2.0695	0.7567
53352.0294	R	0.7765	0.7073
53352.0341	I	3.2546	0.9260
53356.0462	R	1.3276	0.8318
53356.0568	I	1.9475	0.8958
53360.0389	R	0.0584	0.9895
53360.0462	I	1.4270	1.2633
	g160		
53268.2081	R	5.4618	0.4465
53283.2499	R	12.1003	0.7607
53289.1373	R	11.4040	0.6812
53289.1566	I	14.9673	1.1403
53293.1469	I	13.0629	1.8564
53297.1441	R	9.2377	0.5209
53297.1635	I	12.7401	0.7799
53301.1210	R	7.5351	0.7323
53301.1517	I	10.1446	0.7945
53315.1542	R	3.4325	0.3962
53315.1728	I	5.4740	0.8355
53323.1667	R	2.6651	0.3450
53329.1354	R	2.7879	0.7025
53329.1556	I	5.0550	0.8061
53342.1631	R	1.7879	0.5324
53342.1820	I	4.2020	0.8823
53346.1695	R	0.6751	0.4852
53346.1897	I	2.1280	1.0339
53350.1527	R	0.7078	0.3217
53350.1720	I	1.7253	0.6995
53354.1453	R	0.8780	0.3990
53354.1666	I	1.4646	0.7981
53377.0938	R	0.6546	0.4678
53377.1071	I	0.2635	0.7416
53381.0792	R	1.4056	0.4011
53381.0922	I	1.3957	0.7620
53385.1062	R	1.4816	0.5385

Continued

Table C.1 (Continued)

MJD	Passband	$Flux_{25}$	σ_{Flux}
53385.1191	I	0.1012	1.0675
53389.0891	R	-0.1242	1.4785
53389.1022	I	-0.6706	2.2957
	g225		
53266.1069	R	0.1543	0.8722
53266.1280	I	-0.7298	1.3677
53268.0553	R	-0.7285	0.7330
53268.0587	I	-0.2573	1.1998
53285.0185	R	0.9264	1.0216
53287.0161	R	1.6406	0.7310
53287.0378	I	2.5103	1.2825
53291.0168	R	1.9000	0.8024
53291.0378	I	4.5304	1.2484
53295.0160	R	3.9872	0.5227
53295.0371	I	2.9767	0.7801
53299.0262	R	4.1385	0.5597
53299.0475	I	6.3440	0.6654
53301.0092	R	3.4375	2.8211
53301.0364	I	8.7102	2.1704
53321.0262	R	5.0951	0.5696
53321.0488	I	7.1770	0.7424
53325.0308	R	5.8423	0.4314
53325.0520	I	5.5420	0.7416
53331.0862	R	8.5424	2.8003
53331.1084	I	10.5268	3.1088
53331.1119	I	8.8787	4.0063
53344.0549	R	4.4068	0.4389
53344.0771	I	5.0938	0.8287
53356.0533	R	4.3313	0.6977
53356.0684	I	4.5453	1.0180
	g230		
53268.1000	R	1.9373	1.1541
53268.1366	I	2.3704	1.2816
53287.0790	I	1.5827	1.9379
53291.0560	R	-0.1430	1.1749

Continued

Table C.1 (Continued)

MJD	Passband	$Flux_{25}$	σ_{Flux}
53295.0602	R	4.3502	0.6235
53295.0812	I	4.3786	0.9790
53299.0649	R	6.2548	0.6459
53299.0888	I	5.3743	0.7927
53301.0856	I	9.4689	1.1797
53321.0663	R	6.0488	1.6642
53321.0900	I	11.4847	1.2648
53325.0691	R	7.0854	0.5201
53325.0903	I	10.4879	0.9816
53331.1294	R	7.9887	2.4608
53331.1490	I	1.7258	2.5582
53331.1527	I	-4.8465	2.8463
53344.0965	R	3.1587	0.5608
53344.1204	I	8.0311	1.0301
53348.0769	R	2.5582	0.5481
53348.0982	I	6.4651	0.9132
53352.0478	R	1.5351	0.4341
53352.0632	I	3.8685	0.7822
53354.0430	R	0.6037	0.5203
53354.0597	I	1.2017	0.8199
53356.0824	R	0.4307	0.5255
53356.0981	I	2.8334	0.8549
53358.0361	R	-1.1755	0.8325
53358.0598	I	1.3849	0.9659
53360.0682	R	1.7380	1.3852
53360.0951	I	2.5472	1.7087
53377.0512	I	1.8069	0.9021
53377.0570	R	1.0991	0.4963
53381.0378	I	2.0126	1.2179
53381.0436	R	0.4071	0.6249
	g240		
53266.0961	R	-0.6772	0.9837
53266.1104	I	-0.7518	1.1106
53268.0270	R	-0.5221	0.8287
53268.0305	I	1.2296	1.0842

Continued

Table C.1 (Continued)

MJD	Passband	$Flux_{25}$	σ_{Flux}
53285.0220	I	0.3207	1.6331
53287.0046	R	2.4373	0.7567
53287.0196	I	3.6210	1.4568
53291.0054	R	4.6605	0.7123
53291.0203	I	5.2953	1.2225
53295.0048	R	5.7069	0.5799
53295.0195	I	6.4451	0.7571
53299.0157	R	7.9343	0.6489
53299.0297	I	9.1495	0.7414
53301.0021	R	8.0124	2.5606
53301.0237	I	6.8650	2.8213
53321.0139	R	4.2069	0.5269
53321.0297	I	7.4547	0.9330
53325.0202	R	3.4324	0.5129
53325.0345	I	7.0789	0.6427
53331.0753	R	2.6189	2.3601
53331.0897	I	3.0879	3.8304
53331.0932	I	3.7984	3.7015
53344.0373	R	1.6513	0.5079
53344.0595	I	1.8219	0.8690
	h283		
53268.1824	R	-0.5441	0.6869
53283.2039	R	1.0777	0.7630
53283.2362	I	1.2118	1.3635
53289.1028	R	0.3095	0.7447
53289.1240	I	-0.8172	1.2241
53293.0885	R	1.5444	0.6503
53293.1113	I	-0.5778	1.6379
53297.1099	R	-0.3035	0.6060
53297.1311	I	0.7102	0.8949
53315.1192	R	7.6866	0.4776
53315.1414	I	8.0059	0.8837
53321.1762	R	9.1996	1.6565
53323.1315	R	8.1483	0.4609
53323.1531	I	9.4988	0.6879

Continued

Table C.1 (Continued)

MJD	Passband	$Flux_{25}$	σ_{Flux}
53327.1796	R	7.4472	0.7436
53329.0817	R	5.5135	0.6323
53329.1029	I	9.3754	0.7600
53342.1285	R	3.9278	0.4061
53342.1499	I	6.4166	0.8612
53346.1210	R	1.8447	0.4692
53346.1475	I	5.1073	1.2438
53350.1016	R	2.8398	0.4923
53350.1393	I	3.8084	0.7455
53354.0957	R	0.9085	0.3805
53354.1288	I	3.7776	0.7761
53356.1112	R	-0.0594	0.4200
53356.1265	I	2.3962	0.7861
53377.0689	R	0.8759	0.4073
53377.0845	I	1.1147	0.8420
53381.0546	R	-0.3658	0.4342
53381.0698	I	1.5815	0.7334
53385.0756	R	0.3329	0.5559
53385.0966	I	0.5362	1.1310
53389.0623	R	2.6268	2.0690
53389.0778	I	3.4708	2.6491
	h300		
53268.2081	R	0.2945	0.3598
53283.2499	R	0.2725	0.7894
53289.1373	R	1.5902	0.6339
53289.1566	I	1.8529	1.1470
53293.1469	I	3.6345	1.7730
53297.1441	R	5.0868	0.5101
53297.1635	I	7.1930	0.7509
53301.1210	R	6.1311	0.7915
53301.1517	I	8.1838	0.7792
53315.1542	R	6.2772	0.4043
53315.1728	I	7.5914	0.8411
53323.1667	R	5.3060	0.3390
53329.1354	R	2.5006	0.7322

Continued

Table C.1 (Continued)

MJD	Passband	$Flux_{25}$	σ_{Flux}
53329.1556	I	6.5836	0.7973
53342.1631	R	1.2351	0.4585
53342.1820	I	4.0748	0.7952
53346.1695	R	1.6793	0.5453
53346.1897	I	3.1943	1.0530
53350.1527	R	0.8914	0.3238
53350.1720	I	1.9713	0.6857
53354.1453	R	1.5679	0.3912
53354.1666	I	1.1924	0.7762
53377.0938	R	-0.0425	0.4616
53377.1071	I	1.2232	0.8352
53381.0792	R	0.9378	0.4364
53381.0922	I	0.3349	0.7995
53385.1062	R	0.1491	0.5331
53385.1191	I	0.5927	1.1138
53389.0891	R	0.9411	1.6153
53389.1022	I	0.6774	2.4960
	h311		
53266.1033	R	0.0288	0.7246
53266.1222	I	-0.2629	1.5368
53268.0458	R	-0.4577	0.6788
53268.0493	I	-1.2203	1.1651
53285.0150	R	0.6989	1.0195
53285.0336	I	2.8563	3.7584
53287.0126	R	0.4880	0.8021
53287.0320	I	0.4244	1.4011
53291.0131	R	1.9720	0.9162
53291.0320	I	2.9078	1.3209
53295.0119	R	1.8295	0.5710
53295.0312	I	3.7378	0.8152
53299.0227	R	3.3418	0.5652
53299.0417	I	5.4304	0.6983
53321.0220	R	5.1433	0.5857
53321.0422	I	6.6827	0.7281
53325.0273	R	3.4453	0.4169

Continued

Table C.1 (Continued)

MJD	Passband	$Flux_{25}$	σ_{Flux}
53325.0462	I	6.7793	0.7314
53331.1048	I	8.9787	2.5599
53344.0480	R	2.1729	0.4428
53344.0711	I	1.7848	0.8788
53348.0502	R	1.9737	0.4348
53348.0597	I	2.6565	0.8245
53354.0294	R	0.1721	0.8943
53354.0331	I	4.0451	1.1418
53356.0498	R	-0.0295	0.6777
53356.0626	I	1.9363	0.9568
53360.0427	R	-0.0783	0.9127
53360.0541	I	2.2790	1.3626
	h319		
53266.1604	R	0.3302	0.7578
53266.1815	I	-0.9066	1.4626
53283.1929	R	-0.3685	0.8862
53283.2074	I	0.0412	1.5748
53289.0904	R	0.8468	0.8528
53289.1066	I	0.5806	1.0810
53293.0738	R	0.7673	0.8079
53293.0936	I	-1.2486	0.8852
53297.0987	R	-0.6814	0.6441
53297.1135	I	0.1801	0.9466
53315.1085	R	0.1221	0.5032
53315.1230	I	0.6644	0.8609
53323.1206	R	6.3174	0.6571
53323.1352	I	8.2214	0.8808
53327.1697	R	9.4501	0.9635
53329.0712	R	10.1989	0.6157
53329.0852	I	10.6459	0.7943
53342.1162	R	11.5961	0.4451
53342.1323	I	14.9199	0.8504
53346.1100	R	11.0857	0.4683
53346.1248	I	12.3290	0.9121
53350.0903	R	8.2203	0.4586

Continued

Table C.1 (Continued)

MJD	Passband	$Flux_{25}$	σ_{Flux}
53350.1064	I	9.3898	0.7884
53354.0850	R	8.2811	0.3921
53354.1113	I	9.4528	0.6914
53383.0516	R	1.4258	0.4188
53383.0613	I	4.9663	0.7405
53387.0531	R	1.4243	1.5418
53387.0632	I	4.5327	1.7034
	h323		
53268.2009	R	0.6218	0.4277
53283.2463	R	-1.2561	0.8709
53283.2635	I	-1.6155	1.2404
53289.1337	R	0.2434	0.6543
53289.1508	I	0.3949	1.1983
53297.1404	R	0.4597	0.5124
53297.1576	I	0.6358	0.8128
53315.1507	R	3.9667	0.4388
53315.1670	I	4.7446	0.8267
53323.1632	R	6.7211	0.3285
53323.1827	I	8.3889	0.7432
53329.1318	R	6.0019	0.7172
53329.1496	I	7.4887	0.8553
53342.1593	R	4.9577	0.5025
53342.1761	I	7.7713	0.7417
53346.1657	R	2.9716	0.5652
53346.1828	I	6.8886	1.0511
53350.1490	R	3.0976	0.3828
53350.1660	I	11.1568	0.7580
53356.1545	R	1.3609	0.4199
53356.1816	I	3.8408	0.7980
53358.1369	R	1.4598	0.5556
53358.1559	I	4.1367	0.8612
53360.1438	R	0.2291	1.0928
53360.1588	I	5.0358	1.7162
53379.0988	R	1.0436	0.5830
53379.1201	I	4.5767	1.1727

Continued

Table C.1 (Continued)

MJD	Passband	$Flux_{25}$	σ_{Flux}
53383.0779	R	-0.0450	0.4389
53383.0995	I	1.4268	0.7033
53387.0807	R	-0.3228	1.0316
53387.1019	I	-0.1682	1.5750
h359			
53266.1713	R	0.6280	0.8085
53266.1993	I	-1.1952	1.2028
53283.2005	R	-1.1082	0.5405
53283.2301	I	1.2499	1.0748
53289.0992	R	0.9985	0.7776
53289.1182	I	0.2694	1.0127
53293.0809	R	0.4225	0.6331
53293.1053	I	0.1009	1.2282
53297.1063	R	-0.0691	0.6259
53297.1251	I	-1.0750	1.0808
53315.1157	R	0.1062	0.4802
53315.1350	I	0.6414	0.7869
53323.1280	R	1.2142	0.4271
53323.1472	I	1.8556	0.7215
53329.0782	R	5.3387	0.5624
53329.0970	I	7.8181	0.7574
53342.1249	R	13.9693	0.4241
53342.1440	I	17.6629	0.6622
53346.1173	R	14.3868	0.5354
53346.1414	I	19.2256	1.1115
53350.0981	R	11.9567	0.4777
53350.1334	I	15.3660	0.7373
53354.0922	R	11.0778	0.3791
53354.1229	I	14.6024	0.7455
53358.1002	R	9.2462	0.5121
53358.1240	I	11.6399	0.7001
53377.0653	R	3.7505	0.3556
53377.0786	I	8.1654	0.7232
53381.0511	R	2.6241	0.3735
53381.0639	I	6.6635	0.6615

Continued

Table C.1 (Continued)

MJD	Passband	$Flux_{25}$	σ_{Flux}
53385.0721	R	2.2038	0.5250
53385.0907	I	4.8218	1.0004
53389.0571	R	1.0824	1.7560
53389.0720	I	1.6866	2.7303
h363			
53268.1824	R	1.6577	0.7132
53283.2039	R	0.3643	0.8091
53283.2362	I	4.5295	1.5515
53289.1028	R	-0.6962	0.6239
53289.1240	I	-0.2885	1.2189
53293.0885	R	0.8975	0.5817
53293.1113	I	1.6093	1.7968
53297.1099	R	0.2478	0.6107
53297.1311	I	-1.2798	0.9910
53315.1192	R	0.0448	0.4993
53315.1414	I	-0.7790	0.8686
53321.1762	R	1.3384	1.5043
53323.1315	R	2.9805	0.5173
53323.1531	I	4.3837	0.7829
53327.1796	R	10.0131	0.6899
53329.0817	R	14.8043	0.6223
53329.1029	I	22.0353	0.8484
53342.1285	R	28.0622	0.5271
53342.1499	I	35.8648	0.8883
53346.1210	R	25.4216	0.5622
53346.1475	I	30.5299	1.1829
53350.1016	R	20.2837	0.5598
53350.1393	I	25.4530	0.8034
53354.0957	R	17.7874	0.4345
53354.1288	I	22.3069	0.9398
53356.1112	R	14.8466	0.4695
53356.1265	I	18.6771	0.8388
53377.0689	R	5.9197	0.4524
53377.0845	I	11.5091	0.9740
53381.0546	R	6.4241	0.4794

Continued

Table C.1 (Continued)

MJD	Passband	$Flux_{25}$	σ_{Flux}
53381.0698	I	7.3385	0.8067
53385.0756	R	4.4917	0.5919
53385.0966	I	6.7834	1.2911
53389.0623	R	4.9993	2.0827
53389.0778	I	3.0161	2.7648
h364			
53268.2116	R	0.2482	0.3909
53283.2537	R	0.1526	0.5798
53289.1408	R	-0.4333	0.6307
53289.1625	I	-0.0330	0.9356
53293.1529	I	-1.3986	1.4252
53295.1696	R	-0.2469	0.3588
53297.1482	R	-0.2663	0.5025
53297.1693	I	0.2247	0.7116
53301.1245	R	-1.4357	0.7588
53301.1339	I	0.7237	0.9072
53315.1577	R	3.4372	0.4512
53315.1787	I	2.8281	0.7837
53323.1718	R	17.6851	0.4188
53329.1402	R	24.9036	0.6588
53329.1614	I	25.7810	0.8009
53342.1666	R	23.5357	0.4685
53342.1879	I	29.4935	1.2392
53346.1730	R	20.5056	0.5246
53346.1957	I	22.5029	1.0860
53350.1562	R	17.0835	0.3754
53350.1783	I	20.9220	0.7408
53358.1404	R	9.2727	0.5677
53358.1619	I	17.4290	0.8539
53360.1473	R	7.2885	1.0711
53360.1648	I	12.4878	1.6178
53377.0974	R	3.5515	0.4895
53377.1129	I	9.6900	0.9348
53381.0827	R	3.6788	0.4184
53381.0980	I	9.6148	0.8544

Continued

Table C.1 (Continued)

MJD	Passband	$Flux_{25}$	σ_{Flux}
53385.1097	R	3.2478	0.6322
53385.1249	I	5.9884	1.1994
53389.0928	R	2.7393	1.7811
53389.1081	I	6.4137	2.4773
k396			
53266.0997	R	0.6700	0.8263
53266.1163	I	-0.5624	1.1870
53268.0365	R	-0.2260	0.6658
53268.0400	I	-4.3754	1.2001
53285.0278	I	-0.1003	1.4162
53287.0081	R	0.2017	0.6275
53291.0096	R	0.5988	0.9749
53291.0261	I	-4.4327	1.1098
53295.0084	R	-0.1441	0.5333
53295.0253	I	-2.2557	0.7837
53299.0192	R	0.7633	0.6185
53299.0356	I	-2.3005	0.7381
53301.0056	R	1.4283	2.4300
53301.0295	I	-2.8725	2.7706
53321.0184	R	0.2814	0.6981
53321.0362	I	-3.2498	0.8255
53325.0237	R	0.4820	0.4530
53325.0404	I	-0.0820	0.6595
53331.0967	I	-0.3847	3.0839
53344.0422	R	7.0569	0.6015
53344.0653	I	7.9192	0.8711
53348.0383	R	18.6495	1.0226
53348.0463	R	15.5427	0.4784
53348.0538	I	17.9600	0.7421
53352.0294	R	22.7127	0.6428
53352.0341	I	24.1379	0.9227
53356.0462	R	26.6823	0.8613
53356.0568	I	30.8130	0.9708
53360.0389	R	29.2248	0.9782
53360.0462	I	33.6666	1.3245

Continued

Table C.1 (Continued)

MJD	Passband	$Flux_{25}$	σ_{Flux}
	k411		
53266.1033	R	0.1979	0.7357
53266.1222	I	0.0524	1.3098
53268.0458	R	-0.4447	0.6388
53268.0493	I	-0.3160	1.1195
53285.0150	R	-1.0064	0.9144
53285.0336	I	-1.5193	3.8149
53287.0126	R	-0.6278	0.7147
53287.0320	I	1.5123	1.4586
53291.0131	R	-0.4435	0.8470
53291.0320	I	0.5288	1.1643
53295.0119	R	0.1430	0.5626
53295.0312	I	-0.4944	0.7584
53299.0227	R	0.1284	0.5658
53299.0417	I	-1.7952	0.6744
53321.0220	R	2.0792	0.5324
53321.0422	I	1.3909	0.7340
53325.0273	R	4.8265	0.4217
53325.0462	I	5.3429	0.7229
53331.1048	I	7.9527	2.6561
53344.0480	R	9.8201	0.4990
53344.0711	I	12.4570	0.9067
53348.0502	R	10.1738	0.4022
53348.0597	I	11.7490	0.8381
53354.0294	R	8.5491	0.9350
53354.0331	I	9.6617	1.0879
53356.0498	R	8.3083	0.6944
53356.0626	I	9.8621	0.9304
53360.0427	R	5.8863	0.9752
53360.0541	I	5.2810	1.3429
	k425		
53268.1072	R	0.0295	0.8369
53268.1484	I	-0.2541	1.2485
53283.1311	R	-0.8155	0.7463
53283.1629	I	1.0642	1.6317

Continued

Table C.1 (Continued)

MJD	Passband	$Flux_{25}$	σ_{Flux}
53289.0561	R	0.1495	0.7649
53289.0726	I	-1.3600	1.2534
53293.0558	I	1.0896	1.5447
53297.0640	R	-0.5213	0.6169
53297.0809	I	-1.1819	0.9458
53301.0728	R	0.0853	1.0940
53301.0973	I	-1.5192	1.0855
53315.0736	R	0.7777	0.4935
53315.0906	I	0.2078	0.8522
53323.0829	R	10.4720	0.4776
53323.1006	I	11.7886	0.6497
53329.0363	R	17.8309	0.6550
53329.0533	I	24.4610	0.8922
53342.0814	R	24.3617	0.5825
53342.0984	I	30.7810	0.9637
53346.0734	R	20.9663	0.5432
53346.0919	I	25.4658	1.0226
53350.0550	R	17.5239	1.0838
53350.0724	I	21.2505	1.1890
53358.0431	R	10.4273	0.7200
53358.0720	I	16.3450	0.9159
53360.0755	R	10.4645	1.2572
53360.1073	I	14.2514	2.4626
53385.0554	R	1.9244	0.7849
53385.0589	I	4.6613	1.1514
	k429		
53268.1901	R	0.7785	0.4971
53283.2422	R	-0.5947	0.8415
53283.2573	I	-1.4669	1.6150
53289.1299	R	0.8113	0.7868
53289.1443	I	0.0877	0.9827
53293.1171	R	-0.3420	0.5387
53297.1369	R	0.1885	0.4884
53297.1517	I	1.3441	0.7512
53315.1472	R	-0.1195	0.4504

Continued

Table C.1 (Continued)

MJD	Passband	$Flux_{25}$	σ_{Flux}
53315.1612	I	0.1333	0.8504
53323.1593	R	0.5772	0.3289
53323.1757	I	0.4022	0.5768
53327.1831	R	0.0782	0.5781
53329.1281	R	0.5628	0.5696
53329.1437	I	-0.9556	0.8394
53342.1558	R	50.8432	0.5272
53342.1702	I	59.3147	0.8938
53346.1581	R	71.8268	0.5657
53346.1767	I	71.5491	0.9537
53350.1452	R	79.3126	0.4277
53350.1598	I	76.1887	0.7162
53356.1472	R	75.0646	0.5053
53356.1699	I	74.8973	0.8868
53379.0883	R	31.4314	0.5174
53379.1024	I	38.7936	1.2332
53383.0671	R	27.6697	0.4344
53383.0816	I	38.9405	0.8449
53387.0700	R	23.2500	0.8683
53387.0843	I	31.6609	1.4703
	k430		
53268.0884	R	0.7778	0.9479
53268.1189	I	1.8895	1.1118
53287.0463	R	-0.6303	0.9262
53287.0615	I	-0.8281	1.9528
53291.0444	R	-1.2684	1.1324
53295.0434	R	0.0680	0.6520
53295.0637	I	-1.7004	1.0086
53299.0538	R	0.0950	0.5894
53299.0714	I	1.4351	0.7080
53301.0605	R	0.2323	1.1880
53301.0797	I	1.1614	1.1057
53321.0552	R	-0.6877	0.4866
53321.0708	I	0.5281	1.2525
53325.0585	R	0.5959	0.4688

Continued

Table C.1 (Continued)

MJD	Passband	$Flux_{25}$	σ_{Flux}
53325.0727	I	0.4345	0.7298
53331.1162	R	1.9850	1.7187
53331.1330	I	2.5577	1.8689
53344.0837	R	5.3480	0.4069
53344.1000	I	5.2188	0.9210
53348.0662	R	5.0859	0.4349
53348.0805	I	6.8908	0.9363
53352.0405	R	5.3862	0.4539
53352.0514	I	7.2098	0.6033
53356.0749	R	4.0050	0.5244
53356.0862	I	6.3342	0.7263
53358.0324	R	3.2456	0.8814
53358.0539	I	6.8620	1.0373
53360.0604	R	3.4328	1.6327
53360.0793	I	3.1755	2.1120
53379.0519	R	1.0857	0.4820
53379.0555	I	1.9744	0.8414
53387.0393	R	1.3959	2.5392
53387.0429	I	0.5553	3.0172
	k432		
53266.0997	R	-0.5339	0.8921
53266.1163	I	-0.0517	1.1981
53268.0365	R	-0.9045	0.7280
53268.0400	I	-0.8142	1.1018
53285.0278	I	-2.8361	1.6686
53287.0081	R	0.4165	0.5893
53287.0254	I	-1.8834	2.1334
53291.0096	R	-1.8463	0.8045
53291.0261	I	-0.3987	0.9701
53295.0084	R	-0.3760	0.6021
53295.0253	I	-1.4134	0.7773
53299.0192	R	-0.7292	0.6354
53299.0356	I	-1.1671	0.7333
53301.0295	I	0.6158	2.6600
53321.0184	R	1.9930	0.6532

Continued

Table C.1 (Continued)

MJD	Passband	$Flux_{25}$	σ_{Flux}
53321.0362	I	3.6695	0.8320
53325.0237	R	4.2243	0.4887
53325.0404	I	4.0875	0.6355
53331.0967	I	2.7169	3.3353
53344.0422	R	3.8472	0.5463
53344.0653	I	6.0853	0.7548
53348.0383	R	2.1288	1.0194
53348.0463	R	3.1060	0.4523
53348.0538	I	5.0390	0.7190
53352.0294	R	2.9016	0.6533
53352.0341	I	4.6854	0.8493
53356.0462	R	1.7335	0.8764
53356.0568	I	1.3311	0.8739
53360.0389	R	0.4415	0.9306
53360.0462	I	4.3554	1.3474
	k441		
53268.1973	R	-0.0916	0.4715
53287.1338	R	-0.0689	0.6876
53291.1564	I	0.7199	1.2132
53295.1360	R	0.7549	0.4688
53295.1585	I	-0.4784	0.6775
53299.1434	R	0.2091	0.4482
53299.1650	I	0.9138	0.7274
53321.1475	R	0.1053	0.6059
53321.1700	I	-2.5320	5.3660
53325.1470	R	-0.0759	0.5414
53325.1685	I	-0.6184	0.7461
53331.1799	R	0.0420	0.6244
53331.1893	I	1.5584	1.3521
53344.1801	R	4.4169	0.5378
53348.1539	R	5.6906	0.4413
53348.1752	I	7.7794	0.9973
53352.1049	R	5.6973	0.3818
53352.1204	I	9.8491	0.9928
53354.1418	R	5.5601	0.3642

Continued

Table C.1 (Continued)

MJD	Passband	$Flux_{25}$	σ_{Flux}
53354.1608	I	8.6796	0.8358
53356.1510	R	5.5852	0.3933
53356.1758	I	7.3660	0.8254
53358.1333	R	5.8146	0.4504
53358.1500	I	7.3057	0.6618
53360.1545	R	5.1555	0.5748
53360.1774	I	7.7474	1.3967
53377.0903	R	2.7928	0.6044
53377.1012	I	4.0882	0.9980
53381.0756	R	2.3520	0.4420
53381.0862	I	3.7318	0.7468
53385.1027	R	1.6952	0.4292
53385.1132	I	1.8498	1.0454
53389.0838	R	1.1801	0.6425
53389.0964	I	-2.4081	2.6016
	k448		
53268.1035	R	0.4350	0.7806
53268.1425	I	-0.2399	1.3301
53283.1271	R	-1.2415	0.9805
53283.1531	I	0.8691	1.5747
53289.0523	R	-1.6245	1.0420
53289.0668	I	0.3461	1.2694
53293.0499	I	0.8065	1.5709
53295.1650	R	0.3328	0.4706
53297.0600	R	-0.2433	0.6987
53297.0747	I	1.4446	1.0501
53301.0692	R	0.0594	1.0913
53301.0915	I	-0.0899	1.1936
53315.0700	R	0.6754	0.5892
53315.0845	I	0.6322	0.9611
53321.1802	R	-1.1379	0.7711
53323.0792	R	0.3911	0.6317
53323.0947	I	0.3823	0.9245
53329.0325	R	1.0855	0.6945
53329.0472	I	0.4860	0.8570

Continued

Table C.1 (Continued)

MJD	Passband	$Flux_{25}$	σ_{Flux}
53342.0776	R	2.0765	0.4504
53342.0924	I	3.5894	0.8219
53346.0856	I	5.2587	0.9451
53350.0505	R	4.7336	0.8892
53350.0665	I	8.3400	1.3836
53354.0465	R	7.2546	0.4721
53354.0657	I	10.4259	0.7413
53358.0396	R	6.6792	0.8009
53358.0660	I	6.8197	0.9965
53360.0719	R	7.2612	1.4005
53360.1011	I	9.9818	1.7839
53383.0372	R	2.2031	0.8490
53383.0406	I	4.9296	1.0426
53389.0397	R	1.9262	2.2757
53389.0460	I	5.5784	3.2289
k467			
53268.1866	R	-0.7432	0.5454
53287.1303	R	-0.4294	1.1641
53287.1497	I	2.3445	2.3236
53291.1505	I	-0.6544	1.3866
53295.1325	R	0.9095	0.4303
53295.1525	I	-0.4350	0.8276
53299.1399	R	0.5528	0.4563
53299.1592	I	-0.3149	0.7218
53301.1093	R	0.1055	0.7848
53301.1280	I	-0.2770	1.0776
53321.1439	R	0.5614	1.5289
53321.1641	I	1.0814	0.7176
53325.1434	R	3.9080	0.4318
53325.1625	I	5.3338	0.9182
53331.1763	R	5.9312	0.9291
53331.1834	I	8.6074	1.7055
53344.1766	R	6.6562	0.4438
53348.1503	R	6.5809	0.4071
53348.1691	I	8.1389	1.0372
Continued			

Table C.1 (Continued)

MJD	Passband	$Flux_{25}$	σ_{Flux}
53352.1014	R	5.4171	0.3493
53352.1145	I	6.2679	1.0395
53354.1382	R	4.8177	0.3901
53354.1546	I	6.1497	0.8160
53356.1437	R	4.5632	0.4617
53356.1640	I	5.7374	0.7449
53358.1298	R	4.3659	0.4913
53358.1439	I	5.4970	0.6825
53360.1509	R	0.7085	1.1058
53360.1706	I	5.8765	1.7099
53379.0953	R	0.6827	0.4170
53379.1141	I	3.2185	1.2298
53383.0742	R	0.7770	0.3922
53383.0932	I	2.3410	0.7665
53387.0770	R	1.4690	0.9886
53387.0959	I	2.3755	1.5513
k485			
53266.1749	I	1.3876	1.6188
53287.1168	I	0.3160	2.0223
53295.0980	R	0.7571	0.5982
53295.1192	I	-1.0707	0.6656
53299.1057	R	-0.9443	0.4588
53299.1267	I	0.5696	0.7246
53321.1075	R	0.3274	0.3554
53321.1303	I	0.3464	1.1130
53325.1071	R	0.2301	0.4145
53325.1298	I	-0.5407	0.8111
53331.1608	R	-0.8792	1.0647
53331.1704	I	-0.5579	1.3694
53344.1387	R	5.5467	0.4983
53344.1613	I	7.0586	0.9744
53348.1149	R	5.6419	0.4144
53348.1371	I	8.9734	0.9780
53352.0764	R	6.1081	0.3628
53352.0917	I	9.7670	0.7226
Continued			

Table C.1 (Continued)

MJD	Passband	$Flux_{25}$	σ_{Flux}
53354.0815	R	5.2979	0.4309
53354.1055	I	9.0662	0.7562
53358.0967	R	4.2530	0.5195
53358.1174	I	8.9210	0.7537
53360.1214	R	1.6493	1.0898
53360.1372	I	9.6285	1.3718
53379.0668	R	1.9067	0.4830
53379.0825	I	5.8980	0.9776
53385.0686	R	0.7238	0.5014
53385.0849	I	2.4127	0.9818
	k490		
53268.1866	R	0.3179	0.5481
53287.1303	R	2.0349	1.1376
53291.1505	I	0.1987	1.4364
53295.1325	R	0.2007	0.4051
53295.1525	I	-0.3578	0.7187
53299.1399	R	0.8767	0.4171
53299.1592	I	-0.6222	0.6708
53301.1093	R	0.5998	0.8519
53301.1280	I	-0.3015	1.3145
53321.1439	R	0.3983	1.5668
53321.1641	I	0.6174	0.6463
53325.1434	R	1.1191	0.4176
53325.1625	I	-0.6434	0.9418
53331.1763	R	0.5858	0.8142
53331.1834	I	1.2227	1.5714
53344.1766	R	4.4827	0.3790
53348.1503	R	3.0871	0.4479
53348.1691	I	7.1767	0.9491
53352.1014	R	3.3173	0.3280
53352.1145	I	5.3928	0.9528
53354.1382	R	3.9620	0.3815
53354.1546	I	5.3007	0.6891
53356.1437	R	3.4438	0.4307
53356.1640	I	6.3762	0.6782

Continued

Table C.1 (Continued)

MJD	Passband	$Flux_{25}$	σ_{Flux}
53358.1298	R	2.3347	0.5026
53358.1439	I	6.1333	0.6224
53360.1509	R	3.6604	1.1041
53360.1706	I	5.3994	1.6311
53379.0953	R	0.1989	0.5446
53379.1141	I	4.1578	1.2006
53383.0742	R	0.4654	0.4430
53383.0932	I	2.2041	0.6666
53387.0770	R	1.7238	0.9769
53387.0959	I	0.9799	1.1829
	m001		
53639.0808	R	27.5868	0.8193
53639.0948	I	32.1592	0.9270
53649.0801	R	20.3803	0.7250
53649.1012	I	22.8113	1.4372
53652.0493	R	11.7245	0.6327
53652.0659	I	13.9736	0.8458
53654.0476	R	15.5497	0.7484
53654.0685	I	17.5607	0.9770
53682.0670	R	3.6403	0.4514
53682.0959	I	4.0836	0.6810
53696.0741	R	2.4375	0.4083
53696.0881	I	5.0391	0.6885
53702.0986	R	2.1648	0.4416
53702.1127	I	4.0788	0.8612
	m022		
53639.0080	R	12.3879	0.7725
53639.0570	I	17.1301	0.8015
53640.9973	R	11.5503	1.0061
53641.0261	I	16.9207	1.6193
53643.0698	I	13.6829	1.7879
53649.0333	R	9.6326	0.5796
53649.0500	I	15.9507	1.1363
53652.0124	R	9.7729	0.7776
53652.0396	I	13.2609	1.2889

Continued

Table C.1 (Continued)

MJD	Passband	$Flux_{25}$	σ_{Flux}
53654.0191	R	10.0732	0.6674
53654.0262	I	14.8688	1.1949
53682.0344	R	6.9269	0.8073
53682.0488	I	4.0111	0.8464
53698.0203	R	5.3410	1.2381
53698.0343	I	5.7953	1.2753
53700.0965	R	3.9153	0.4538
53704.0357	R	4.0602	0.4113
53704.0549	I	3.4813	0.8395
53706.0312	R	3.0909	0.4560
53706.0469	I	4.4213	0.8401
53708.0435	R	5.1051	0.4234
53708.0647	I	2.5467	0.9907
53712.0580	R	2.6014	1.1324
53712.0738	I	6.3438	1.8293
53728.0429	R	2.2244	1.6978
53731.0560	R	2.7488	0.6482
53738.0432	R	2.1442	0.7307
53738.0470	I	0.7523	2.1345
	m026		
53698.0518	I	2.2144	1.1651
53700.1039	R	0.8459	0.4510
53704.0462	R	-0.0488	0.3371
53704.0723	I	0.8629	0.9235
53706.0382	R	-0.6045	0.3807
53706.0588	I	-0.9483	0.8248
53708.0365	R	-0.4281	0.4694
53708.0531	I	-0.4534	0.8217
53712.0500	R	-0.3980	1.2481
53712.0617	I	-2.4689	2.2152
53735.0522	R	0.6480	0.6743
53741.0483	R	-0.5284	1.2635
53639.0534	R	5.2846	0.4937
53639.0744	I	8.2137	0.7354
53641.0083	R	5.5367	1.0400
	Continued		

Table C.1 (Continued)

MJD	Passband	$Flux_{25}$	σ_{Flux}
53641.0436	I	8.2072	1.4561
53648.9990	R	2.7520	0.7571
53649.0178	I	2.8759	1.4242
53654.0138	R	2.1804	0.5996
53682.0453	R	0.9158	0.7970
53698.0308	R	-0.3004	0.7485
	m027		
53639.0948	I	19.9391	0.9012
53649.0801	R	14.1379	0.8008
53649.1012	I	18.9094	1.4035
53652.0493	R	11.9296	1.1246
53652.0659	I	17.5301	1.5237
53654.0476	R	10.6172	0.8329
53654.0685	I	14.3967	0.9386
53682.0670	R	4.0463	0.8810
53682.0959	I	8.4129	1.6250
53696.0741	R	2.2182	0.4110
53696.0881	I	3.1795	0.6175
53702.0986	R	1.9059	0.4594
53702.1127	I	3.6822	0.7805
	m032		
53638.9971	R	72.2914	0.8317
53639.0208	I	66.7245	1.0363
53641.0153	R	68.6840	0.9773
53641.0598	I	59.4507	1.6222
53643.0512	I	50.5872	1.7442
53649.0026	R	48.2322	0.8499
53649.0238	I	40.6885	1.2126
53651.9999	R	41.8589	0.9429
53652.0222	I	40.0879	1.2334
53682.0607	I	19.1731	1.5513
53696.0398	R	9.9734	0.4537
53696.0561	I	11.2652	0.8201
53700.0857	R	9.2153	0.5396
53702.0367	I	10.5355	0.7809
	Continued		

Table C.1 (Continued)

MJD	Passband	$Flux_{25}$	σ_{Flux}
53702.0578	R	8.5113	0.4699
53706.0420	R	7.9697	0.4707
53706.0646	I	9.1988	0.8199
53708.0277	R	7.3830	0.8438
53708.0330	R	7.5874	0.8986
53708.0473	I	8.5383	0.7963
53712.0541	R	7.8225	1.0931
53712.0679	I	6.4482	2.0168
53735.0561	R	4.4592	0.8442
53741.0518	R	3.9939	1.3843
m034			
53639.1560	R	6.4038	0.5680
53639.1950	I	10.7550	0.8727
53643.1524	R	4.5944	1.0627
53643.1663	I	7.4377	1.6721
53649.1524	R	2.9803	1.4544
53652.1329	R	3.4929	0.5209
53652.1493	I	5.8383	0.7924
53654.1580	R	3.3816	0.5200
53654.1801	I	6.6526	0.8070
53682.1369	R	0.6862	0.8185
53682.1662	I	0.3803	1.6010
53696.1593	R	0.4735	0.3675
53696.1737	I	2.3345	0.7710
53700.2523	R	0.2880	0.4201
53702.1795	R	0.3553	0.3480
53702.1936	I	0.4381	0.6583
53706.1472	R	0.0598	0.3281
53706.1612	I	1.1565	0.7015
53708.1562	R	0.6719	0.4102
53708.1701	I	-0.1087	0.7809
53712.1615	R	0.3921	0.4604
53712.1768	I	-0.5374	0.8473
53714.0758	R	-0.6756	0.9123
53714.0864	I	0.3781	1.1875

Continued

Table C.1 (Continued)

MJD	Passband	$Flux_{25}$	σ_{Flux}
53735.0873	R	0.9910	0.3902
53738.0910	R	0.3872	0.3656
m039			
53639.1560	R	22.9915	0.7000
53639.1950	I	31.0196	1.0530
53643.1524	R	17.4320	1.1080
53643.1663	I	22.8509	1.9164
53649.1524	R	10.4513	1.6126
53652.1329	R	12.4546	0.6652
53652.1493	I	16.8656	0.9817
53654.1580	R	11.4354	0.6770
53654.1801	I	17.7396	0.9628
53682.1369	R	3.2290	0.8886
53682.1662	I	3.6635	1.7860
53696.1593	R	3.0771	0.4344
53696.1737	I	3.7667	0.9246
53700.2523	R	2.6221	0.4974
53702.1795	R	1.3804	0.4454
53702.1936	I	3.6644	0.8653
53706.1472	R	2.0930	0.4428
53706.1612	I	3.8496	0.7481
53708.1562	R	1.9035	0.4746
53708.1701	I	2.9240	1.0464
53712.1615	R	2.1694	0.6274
53712.1768	I	4.0240	0.8696
53714.0758	R	1.5835	1.0340
53714.0864	I	5.1339	1.3703
53735.0873	R	1.1341	0.4307
53738.0910	R	1.5424	0.4674
m040			
53639.1560	R	4.9016	0.5172
53639.1950	I	6.5351	0.9959
53643.1524	R	3.0561	1.0054
53643.1663	I	5.9603	1.6913
53649.1524	R	1.3060	1.3503

Continued

Table C.1 (Continued)

MJD	Passband	$Flux_{25}$	σ_{Flux}
53652.1329	R	0.9709	0.5295
53652.1493	I	3.0130	0.7880
53654.1580	R	1.2737	0.5382
53654.1801	I	3.1002	0.8412
53682.1369	R	0.9908	0.7994
53682.1662	I	1.2159	1.7483
53696.1593	R	0.0959	0.3198
53696.1737	I	-1.0868	0.8066
53700.2523	R	-0.3025	0.3711
53702.1795	R	1.2878	0.3309
53702.1936	I	0.8608	0.6798
53706.1472	R	0.5254	0.3187
53706.1612	I	0.1904	0.6122
53708.1562	R	0.6277	0.3676
53708.1701	I	-0.3119	0.8420
53712.1615	R	0.2720	0.4969
53712.1768	I	0.9457	0.7312
53714.0758	R	1.1696	0.9035
53714.0864	I	0.8728	1.1100
53735.0873	R	-0.1609	0.3118
53738.0910	R	0.6490	0.3132
m043			
53639.0080	R	15.0446	0.7569
53639.0570	I	9.2246	0.9932
53640.9973	R	10.7005	0.5852
53641.0261	I	21.8934	0.8764
53643.0698	I	16.2890	0.8767
53649.0333	R	12.0957	0.5900
53649.0500	I	20.8945	1.4647
53652.0124	R	8.4184	0.3845
53652.0396	I	17.4752	1.0624
53654.0191	R	10.3646	0.6542
53654.0262	I	12.9021	0.8186
53682.0344	R	4.3187	0.4922
53682.0488	I	12.9779	1.0646

Continued

Table C.1 (Continued)

MJD	Passband	$Flux_{25}$	σ_{Flux}
53698.0203	R	2.2807	1.1604
53698.0343	I	5.4723	0.8270
53700.0965	R	3.9469	0.5480
53704.0357	R	3.4177	0.4396
53704.0549	I	4.1103	1.1908
53706.0166	I	3.8634	0.8422
53706.0312	R	3.8913	0.5184
53706.0469	I	4.5134	1.2755
53712.0580	R	0.2813	1.0173
53738.0432	R	1.7743	0.7237
m057			
53641.1271	R	20.4629	0.8066
53641.1483	I	26.0083	1.1999
53649.1220	R	16.7026	0.8722
53649.1466	I	17.4966	2.0405
53652.0858	R	15.7503	0.7988
53652.1003	I	18.3511	1.1237
53654.0864	R	14.5812	0.6748
53654.1094	I	17.8641	1.0133
53682.1268	R	6.5359	1.1505
53698.1074	R	3.6790	0.7392
53698.1286	I	5.9547	1.6094
53704.1274	R	4.8824	0.3341
53704.1484	I	5.6308	0.5165
53706.1135	R	5.5305	0.3245
53706.1298	I	5.0786	0.7299
53708.1215	R	4.7514	0.3794
53708.1386	I	3.7944	0.7627
53712.1266	R	3.7116	0.4453
53712.1432	I	2.9259	0.8400
53714.0419	R	4.1426	0.7380
53714.0582	I	2.7199	0.9935
53728.1070	R	4.8372	0.6052
53728.1282	I	3.3908	0.8241
53731.1112	R	3.3902	0.4755

Continued

Table C.1 (Continued)

MJD	Passband	$Flux_{25}$	σ_{Flux}
53731.1224	I	2.2276	0.8243
53733.0695	R	2.7285	0.3511
53733.0938	I	1.7913	0.7215
53738.0840	R	2.5833	0.4605
m062			
53641.0816	R	17.4171	2.6776
53641.0981	I	23.2636	1.9709
53649.0725	R	22.7706	1.1135
53649.0895	I	26.2023	1.4469
53652.0458	R	19.8622	1.6597
53652.0601	I	25.0161	1.6617
53654.0440	R	15.5644	1.2767
53654.0627	I	20.2571	1.3703
53682.0851	R	2.9035	1.4544
53698.0615	R	0.9882	1.0686
53698.0788	I	6.3123	1.5012
53700.1533	R	2.4069	0.8629
53704.0828	R	2.0574	0.7606
53704.0992	I	5.1311	0.9114
m070			
53698.1344	R	5.7969	0.9269
53698.1507	I	9.6773	1.3742
53700.2594	R	5.0207	0.4370
53704.1543	R	4.3135	0.3237
53704.1686	I	5.5736	0.8606
53641.1545	R	50.8840	0.6707
53641.1687	I	18.5967	1.2164
53649.1559	R	38.4339	1.4300
53652.1235	I	29.0721	1.2379
53652.1400	R	30.8407	0.6162
53654.1389	R	27.2527	0.6166
53654.1685	I	28.4223	1.1179
53682.1521	R	6.7767	0.9141
m075			
53639.0491	R	43.3241	0.9688

Continued

Table C.1 (Continued)

MJD	Passband	$Flux_{25}$	σ_{Flux}
53641.0048	R	47.0556	1.4263
53641.0378	I	44.2914	4.8023
53643.0266	R	40.7464	2.3672
53648.9948	R	36.0885	1.2030
53649.0120	I	50.6828	2.9169
53652.0085	R	31.3277	1.3909
53652.0338	I	43.7718	3.1448
53654.0104	R	30.8931	1.0866
53654.0378	I	41.8189	2.6392
53682.0418	R	16.3200	1.0288
53698.0273	R	15.1330	1.1744
53698.0459	I	30.2567	2.1366
53700.0975	R	14.8494	1.3592
53700.1217	R	6.2096	1.6878
53704.0202	R	10.6288	2.9796
53704.0263	I	12.7035	2.1553
53704.0427	R	9.9620	1.1731
53706.0347	R	10.2421	0.7915
53708.0400	R	13.6600	1.0267
53733.0580	R	6.5501	1.0837
53738.0504	R	3.2749	1.1026
m087			
53641.1545	R	24.9131	0.6732
53641.1687	I	31.6992	1.2309
53649.1559	R	20.3028	1.5251
53649.1807	I	23.8548	3.9971
53652.1235	I	20.4438	1.0009
53652.1400	R	17.1942	0.6020
53654.1389	R	16.1360	0.5653
53654.1685	I	21.1567	0.8270
53682.1521	R	3.3791	0.9497
53698.1344	R	0.7431	1.0588
53698.1507	I	7.7552	1.6312
53700.2594	R	2.6144	0.3786
53704.1543	R	2.0875	0.3116

Continued

Table C.1 (Continued)

MJD	Passband	$Flux_{25}$	σ_{Flux}
53704.1686	I	5.7086	0.6712
	m138		
53704.0992	I	2.9956	0.6923
53641.0816	R	5.5960	2.1525
53641.0981	I	4.0726	1.5425
53649.0725	R	8.0678	0.6903
53649.0895	I	6.7571	1.0291
53652.0458	R	8.7614	1.1390
53652.0601	I	7.7162	1.4421
53654.0440	R	8.9343	0.8074
53654.0627	I	8.6304	1.1161
53682.0851	R	2.6308	0.9864
53698.0615	R	0.9565	0.6622
53698.0788	I	1.2381	1.3092
53700.1533	R	1.4085	0.5280
53704.0828	R	1.4670	0.3804
	m158		
53696.0503	I	5.6123	0.8936
53700.0591	R	2.4144	0.5653
53700.0820	R	2.0457	0.4698
53702.0302	I	3.7590	0.8163
53702.0543	R	1.6572	0.4097
53638.9932	R	1.8226	0.8113
53639.0149	I	0.5303	1.1738
53641.0118	R	2.0459	0.8957
53641.0530	I	4.0737	1.5569
53643.0336	I	0.3451	2.1886
53649.0297	R	8.1182	0.5989
53649.0442	I	9.9809	1.1018
53651.9964	R	8.4906	0.9290
53652.0160	I	10.0357	1.0358
53654.0226	R	10.2301	0.5998
53654.0320	I	10.0753	1.0306
53682.0224	R	3.8113	0.6523
53682.0548	I	6.2627	1.1628

Continued

Table C.1 (Continued)

MJD	Passband	$Flux_{25}$	σ_{Flux}
53696.0363	R	1.7029	0.3497
	m193		
53639.1560	R	1.0615	0.5730
53639.1950	I	-1.1824	0.9610
53643.1524	R	3.4699	1.1110
53643.1663	I	3.4869	1.5646
53649.1524	R	11.0570	1.5225
53652.1329	R	16.2130	0.5734
53652.1493	I	17.8498	0.9138
53654.1580	R	19.5300	0.5893
53654.1801	I	24.1914	0.9788
53682.1369	R	18.4115	0.8728
53682.1662	I	19.4978	1.8949
53696.1593	R	8.1482	0.3745
53696.1737	I	15.3757	0.9271
53700.2523	R	6.4848	0.4776
53702.1795	R	5.9847	0.3811
53702.1936	I	11.7296	0.7454
53706.1472	R	4.7639	0.3604
53706.1612	I	10.7747	0.7025
53708.1562	R	4.7407	0.4248
53708.1701	I	10.2046	0.9884
53712.1615	R	4.0735	0.5273
53712.1768	I	8.4011	0.8306
53714.0758	R	4.1314	0.8963
53714.0864	I	6.9695	1.4102
53735.0873	R	2.4520	0.3995
53738.0910	R	2.6220	0.3857
	m226		
53639.1292	R	4.0397	0.6215
53643.1373	R	5.0195	1.0409
53652.0968	R	4.6609	0.7566
53652.1177	I	10.3025	0.8572
53654.1020	R	5.4065	0.6908
53654.1269	I	9.6901	0.8707

Continued

Table C.1 (Continued)

MJD	Passband	$Flux_{25}$	σ_{Flux}
53682.1126	R	1.1516	0.7058
53682.1310	I	0.0139	2.0754
53696.1310	R	0.5735	0.3388
53696.1534	I	2.3026	1.0504
53700.2486	R	0.7572	0.4004
53702.1525	R	1.3014	0.3420
53702.1737	I	1.8867	0.8029
53708.1290	R	0.4226	0.4493
53708.1504	I	-0.2279	0.8338
53712.1338	R	0.2715	0.4756
53712.1548	I	1.2920	1.0348
53714.0489	R	-1.1217	0.8308
53714.0699	I	1.7690	1.1627
53728.0685	R	-0.4898	0.4878
53728.0899	I	0.1549	1.0362
53731.0742	R	-0.7510	0.4797
53731.1018	I	0.7250	0.8994
53733.0810	R	-0.0929	0.4507
53733.1115	I	0.9456	0.6308
53738.0875	R	0.0926	0.4100
n246			
53652.0717	I	-1.2945	2.2175
53682.0710	R	0.9111	0.9081
53696.0776	R	4.9945	0.3526
53696.0940	I	7.8767	1.5456
53700.1642	R	7.2065	0.4976
53702.1021	R	5.9576	0.3896
53702.1185	I	9.3857	1.7411
53706.0758	R	7.8950	0.3517
53706.0924	I	10.5733	1.7625
53708.0780	R	7.1944	0.4223
53708.1001	I	10.1150	1.7143
53735.0641	R	2.4628	0.5131
53738.0579	R	1.4884	0.4539
53738.0614	I	5.7692	1.7380

Continued

Table C.1 (Continued)

MJD	Passband	$Flux_{25}$	σ_{Flux}
53639.0843	R	0.0974	0.6046
53639.1007	I	1.2687	1.9587
53643.1220	R	0.4274	0.8337
53652.0528	R	1.8040	1.2988
n256			
53639.1560	R	0.8452	0.5814
53639.1950	I	-0.6786	0.9709
53643.1524	R	0.1932	0.9880
53643.1663	I	1.7070	1.6478
53649.1524	R	-1.1035	1.3415
53652.1329	R	0.0426	0.5526
53652.1493	I	0.4557	0.8455
53654.1580	R	0.4235	0.5343
53654.1801	I	-0.0108	0.8240
53682.1369	R	4.3680	0.7879
53682.1662	I	3.0376	1.5268
53696.1593	R	8.0061	0.3365
53696.1737	I	9.2334	0.6905
53700.2523	R	7.5331	0.3976
53702.1795	R	7.1462	0.3601
53702.1936	I	8.9614	0.6638
53706.1472	R	6.4217	0.3710
53706.1612	I	8.8115	0.6817
53708.1562	R	5.9674	0.3727
53708.1701	I	6.7200	0.8828
53712.1615	R	4.1587	0.4965
53712.1768	I	7.3284	0.7366
53714.0758	R	4.5834	0.8947
53714.0864	I	9.0462	1.2818
53735.0873	R	1.7189	0.3524
53738.0910	R	1.6272	0.3538
n258			
53639.1187	R	0.6014	0.5893
53639.1327	I	-0.4199	1.0161
53643.1257	R	1.4461	1.1193

Continued

Table C.1 (Continued)

MJD	Passband	$Flux_{25}$	σ_{Flux}
53643.1407	I	2.8939	2.1431
53649.1107	R	1.0865	1.1880
53652.0893	R	1.1075	0.8728
53652.1061	I	0.1119	1.0554
53654.0939	R	1.1601	0.6659
53654.1153	I	0.2693	0.9670
53682.1020	R	2.5550	0.8715
53696.1117	R	8.9780	0.3293
53696.1345	I	8.8293	0.7086
53700.2276	R	8.3529	0.4440
53702.1419	R	8.3891	0.3430
53702.1561	I	8.9181	0.8387
53706.1170	R	10.0033	0.3506
53706.1356	I	8.3925	0.9365
53708.1254	R	5.9449	0.4152
53708.1445	I	9.0860	0.8162
53712.1303	R	4.6968	0.4570
53712.1490	I	4.8895	0.8251
53714.0454	R	3.8930	0.8022
53714.0641	I	8.4051	1.3082
53728.0570	R	1.7873	0.5105
53728.0722	I	5.5046	1.0645
53731.0633	R	1.8201	0.4739
53731.0777	I	4.3230	1.2565
53733.0730	R	1.3081	0.4082
53733.0996	I	3.4898	0.7403
53735.0839	R	1.1303	0.4043
n263			
53639.1292	R	-0.1133	0.6107
53639.1502	I	-1.0490	0.9987
53643.1373	R	-1.2447	1.0322
53652.0968	R	-0.6682	0.7877
53652.1177	I	-1.3606	0.8923
53654.1020	R	-0.2767	0.6575
53654.1269	I	0.6786	0.8769

Continued

Table C.1 (Continued)

MJD	Passband	$Flux_{25}$	σ_{Flux}
53682.1126	R	2.6651	0.7459
53682.1310	I	2.8411	2.0019
53696.1310	R	18.6063	0.3202
53696.1534	I	18.1571	0.8073
53700.2486	R	22.0583	0.4397
53702.1525	R	23.1961	0.3849
53702.1737	I	24.6081	0.7408
53708.1290	R	21.8162	0.5121
53708.1504	I	26.8673	0.8188
53712.1338	R	19.0224	0.4652
53712.1548	I	22.8961	1.1183
53714.0489	R	17.0506	0.8524
53714.0699	I	21.8152	1.1554
53728.0685	R	7.0580	0.5473
53728.0899	I	13.5032	1.0230
53731.0742	R	7.3011	0.5248
53731.1018	I	12.3512	0.9592
53733.0810	R	5.2314	0.4689
53733.1115	I	11.8493	0.8011
53738.0875	R	4.0316	0.4474
n278			
53639.0534	R	-1.0179	0.4591
53639.0744	I	0.2980	0.6771
53641.0083	R	-0.1409	1.0857
53641.0436	I	1.0408	1.5084
53648.9990	R	-0.0169	0.7520
53649.0178	I	0.2735	1.3736
53654.0138	R	0.1653	0.6453
53682.0453	R	0.7544	0.7878
53698.0308	R	25.3091	0.8736
53698.0518	I	31.2697	1.2644
53700.1039	R	26.5887	0.5902
53704.0217	R	27.6649	1.9800
53704.0278	I	32.9693	2.9309
53704.0462	R	25.3503	0.4135

Continued

Table C.1 (Continued)

MJD	Passband	$Flux_{25}$	σ_{Flux}
53704.0723	I	33.9878	0.9502
53706.0382	R	26.4220	0.4684
53706.0588	I	30.9093	0.8673
53708.0365	R	24.7193	0.6187
53708.0531	I	31.3253	1.0529
53712.0500	R	20.7478	1.1288
53712.0617	I	20.3490	2.0072
53735.0522	R	5.7258	0.7164
53741.0483	R	4.6755	1.3116
	n285		
53639.0491	R	-0.1132	0.5558
53639.0686	I	-0.3165	0.7686
53641.0048	R	-1.4002	1.0867
53641.0378	I	0.4566	1.7019
53648.9948	R	-0.7016	0.7918
53649.0120	I	1.1738	1.7938
53652.0085	R	-2.4759	0.9167
53652.0338	I	-0.7617	1.6663
53654.0104	R	-0.4196	0.6819
53654.0378	I	-0.5123	1.0914
53682.0418	R	7.9474	0.7298
53698.0273	R	6.2081	0.7643
53698.0459	I	9.5303	1.1698
53700.0975	R	7.5860	0.5534
53700.1217	R	7.1716	1.2452
53704.0202	R	4.6156	2.1136
53704.0263	I	7.5710	3.5709
53704.0427	R	5.3213	0.4495
53704.0665	I	7.5375	0.9182
53706.0347	R	4.5424	0.4056
53706.0527	I	8.3852	0.7827
53708.0400	R	4.7016	0.5693
53708.0589	I	8.6143	1.1821
53733.0580	R	1.5522	0.7853
53738.0504	R	0.8611	0.7203

Continued

Table C.1 (Continued)

MJD	Passband	$Flux_{25}$	σ_{Flux}
	n322		
53700.2558	R	3.4055	0.3949
53702.1901	R	2.4435	0.3898
53702.2119	I	4.9113	0.6577
53706.1577	R	3.2626	0.3482
53706.1789	I	5.2527	0.8630
53708.1631	R	3.6313	0.4425
53708.1817	I	3.0167	0.8109
53712.1689	R	2.0241	0.4761
53735.0951	R	0.6408	0.3346
53735.1044	I	2.0670	0.6329
53738.1032	R	0.6183	0.3314
53639.1677	R	-1.1362	0.5609
53639.1888	I	0.1978	0.8513
53652.1364	R	0.1296	0.5038
53652.1551	I	1.3869	0.7901
53654.1615	R	0.0395	0.5198
53654.1859	I	0.4966	0.7819
53682.1485	R	-2.7813	1.5865
53696.1702	R	2.4212	0.3205
	n326		
53639.0080	R	0.1688	0.6974
53639.0570	I	-0.4088	0.7572
53640.9973	R	0.4980	0.9882
53643.0698	I	0.9949	2.1678
53649.0333	R	-0.0467	0.4614
53649.0500	I	0.7542	1.0872
53652.0124	R	0.1197	0.7602
53652.0396	I	-0.0173	0.2110
53654.0191	R	-1.2550	0.6591
53654.0262	I	-0.8593	1.1566
53682.0344	R	-0.7771	0.8623
53682.0488	I	-0.1631	1.3910
53698.0203	R	5.5858	1.0916
53698.0343	I	7.4094	1.4112

Continued

Table C.1 (Continued)

MJD	Passband	$Flux_{25}$	σ_{Flux}
53700.0965	R	8.3911	0.4969
53704.0357	R	14.7541	0.4432
53704.0549	I	21.0251	0.8100
53706.0312	R	18.4573	0.5043
53706.0469	I	23.2691	0.8070
53708.0435	R	20.3516	0.4840
53708.0647	I	24.6719	1.1535
53712.0580	R	20.7976	1.0904
53712.0738	I	25.0893	1.7100
53731.0560	R	6.0654	0.6505
53738.0432	R	2.2709	0.7791
53738.0470	I	10.9321	2.1924
n400			
53702.1056	R	4.0746	0.4165
53702.1302	I	4.1213	0.7514
53706.0793	R	3.7440	0.3872
53706.0982	I	5.6984	0.6458
53708.0814	R	3.0830	0.4728
53708.1059	I	4.9100	0.7781
53712.0871	R	4.2439	0.5190
53712.1088	I	5.5613	1.0507
53652.0563	R	0.4146	0.9246
53652.0775	I	1.0656	1.1628
53682.0745	R	-1.1212	0.8300
53696.0811	R	1.3463	0.3439
53696.0999	I	1.3955	0.6671
53700.1677	R	2.6745	0.5079
n404			
53639.1633	R	-0.0015	0.4831
53639.1830	I	1.4100	0.8411
53643.1780	I	-1.7966	1.8202
53649.1595	R	-0.1603	1.1493
53649.1865	I	3.7223	3.4392
53652.1434	I	1.1109	0.9675
53654.1545	R	-0.1550	0.5488

Continued

Table C.1 (Continued)

MJD	Passband	$Flux_{25}$	σ_{Flux}
53654.1743	I	0.1827	0.7788
53682.1450	R	1.3671	1.1326
53696.1667	R	2.3035	0.3861
53696.1854	I	2.6953	0.8903
53702.1866	R	11.1300	0.3766
53702.2061	I	15.2772	0.7976
53706.1543	R	18.8622	0.3834
53706.1731	I	26.6520	0.7813
53708.1597	R	22.6906	0.4657
53708.1759	I	28.2361	0.8225
53712.1654	R	24.3997	0.5038
53712.1826	I	29.3369	1.0228
53714.0793	R	27.9544	0.9012
53714.0922	I	31.4393	1.2132
53731.1284	R	15.1717	0.4424
53735.0908	R	12.4459	0.4552
53735.0986	I	16.2907	0.6988
53738.0982	R	11.5651	0.4127
n406			
53639.1633	R	-0.5352	0.5014
53639.1830	I	0.4078	0.8587
53643.1780	I	0.8124	1.5917
53649.1595	R	-0.1217	1.1681
53649.1865	I	-4.2744	3.2701
53652.1434	I	0.1912	0.8884
53654.1545	R	0.5102	0.5504
53654.1743	I	0.8107	0.8272
53682.1450	R	1.1428	1.1024
53696.1667	R	2.3959	0.3567
53696.1854	I	2.1914	0.9270
53702.1866	R	4.2268	0.3749
53702.2061	I	5.0190	0.7877
53706.1543	R	4.7656	0.3731
53706.1731	I	4.2267	0.7881
53708.1597	R	5.2932	0.4470

Continued

Table C.1 (Continued)

MJD	Passband	$Flux_{25}$	σ_{Flux}
53708.1759	I	6.9735	0.8178
53712.1654	R	5.7285	0.4954
53712.1826	I	7.8816	1.0432
53714.0793	R	4.1874	0.8976
53714.0922	I	9.4038	1.2230
53731.1284	R	2.6314	0.3976
53735.0908	R	2.0678	0.4125
53735.0986	I	4.9450	0.6876
53738.0982	R	1.3923	0.3729
p425			
53639.0080	R	0.1533	0.7265
53639.0570	I	-1.3324	0.8061
53640.9973	R	1.0928	1.1116
53641.0261	I	0.0682	1.5080
53643.0698	I	0.9075	1.9711
53649.0333	R	0.6480	0.5373
53649.0500	I	-0.8840	1.1257
53652.0124	R	0.5318	0.7394
53652.0396	I	0.0939	1.3548
53654.0191	R	1.2876	0.6825
53654.0262	I	-0.7537	1.1872
53682.0344	R	1.5289	0.8515
53682.0488	I	2.4651	0.8607
53698.0203	R	5.8528	1.2387
53698.0343	I	8.4149	1.3650
53700.0965	R	6.3104	0.4860
53704.0357	R	5.8856	0.4216
53704.0549	I	9.4411	0.8631
53706.0312	R	5.3591	0.4806
53706.0469	I	7.5699	0.8693
53708.0435	R	5.3898	0.4093
53708.0647	I	6.0940	1.0966
53712.0580	R	2.9992	1.1406
53712.0738	I	7.3633	1.8465
53728.0429	R	3.3995	1.6965
Continued			

Table C.1 (Continued)

MJD	Passband	$Flux_{25}$	σ_{Flux}
53731.0560	R	2.0373	0.6182
53738.0432	R	1.9284	0.7232
53738.0470	I	4.3499	2.1603
p429			
53639.0491	R	-1.0667	0.5334
53639.0686	I	1.0607	0.7258
53641.0048	R	0.4854	1.1178
53641.0378	I	-0.0229	1.7619
53648.9948	R	0.7823	0.7890
53649.0120	I	0.1891	1.7012
53652.0085	R	0.1120	0.8711
53652.0338	I	0.0878	1.3193
53654.0104	R	0.5077	0.7270
53654.0378	I	-0.7166	1.0780
53682.0418	R	1.4964	0.7409
53698.0273	R	5.0348	0.7989
53698.0459	I	5.3829	1.2493
53700.0975	R	5.5082	0.5816
53700.1217	R	2.5710	1.1747
53704.0202	R	3.7896	2.0463
53704.0263	I	1.0718	3.2098
53704.0427	R	4.9440	0.4718
53704.0665	I	6.8747	0.8957
53706.0347	R	5.0155	0.4596
53706.0527	I	6.5115	0.7949
53708.0400	R	5.4063	0.5526
53708.0589	I	6.4948	1.1393
53733.0580	R	2.7670	0.8567
53738.0504	R	4.8423	0.7400
p434			
53698.0695	R	3.7759	0.7293
53698.0905	I	7.6286	1.0952
53700.1607	R	3.5966	0.5093
53704.0898	R	4.1565	0.3639
53704.1108	I	8.1645	0.7922
Continued			

Table C.1 (Continued)

MJD	Passband	$Flux_{25}$	σ_{Flux}
53708.0745	R	4.3655	0.4516
53708.0943	I	6.8293	0.8137
53712.0835	R	4.3615	0.5189
53712.1000	I	8.6856	0.8376
53641.0888	R	0.4711	1.1273
53641.1100	I	2.8952	1.3773
53654.0591	R	0.4398	0.6388
53654.0803	I	-0.9384	1.3081
53682.0922	R	-0.2852	1.2970
p444			
53641.1197	R	0.3113	0.6400
53641.1365	I	-0.1453	1.2118
53649.1072	R	-0.8297	1.0350
53682.1196	R	1.4965	0.8968
53698.1002	R	3.8787	0.6810
53698.1168	I	6.6164	1.2906
53704.1203	R	3.2477	0.3420
53704.1368	I	5.9708	0.6034
53706.1100	R	4.0748	0.3484
53706.1240	I	5.1534	0.6848
53708.1177	R	3.2754	0.3802
53708.1325	I	5.6350	0.8206
53712.1220	R	2.1524	0.4329
53712.1373	I	4.7505	0.8226
53714.0384	R	1.2983	0.7975
53714.0524	I	3.8578	0.9505
53728.0993	R	0.9150	0.5719
53728.1165	I	3.7529	0.9332
53731.1077	R	1.0202	0.4254
53731.1166	I	1.2929	0.8388
53733.0654	R	1.5308	0.3792
53733.0880	I	1.9653	0.7151
53735.0710	R	0.9548	0.4041
53738.0710	R	0.8804	0.3662
p445			

Continued

Table C.1 (Continued)

MJD	Passband	$Flux_{25}$	σ_{Flux}
53641.0923	I	-1.7250	1.6303
53649.0687	R	0.0576	0.9842
53649.0836	I	-0.5413	1.2951
53654.0511	R	0.0437	0.7057
53654.0743	I	-0.1371	0.9772
53682.0815	R	1.0900	0.8602
53698.0580	R	4.2021	0.6220
53698.0729	I	4.6330	1.2054
53700.1438	R	2.6551	0.6207
53704.0792	R	3.5995	0.3454
53704.0933	I	6.6979	0.7100
53706.0709	R	4.0995	0.4026
53706.0863	I	5.5073	0.6656
53708.0710	R	3.2090	0.4833
53708.0885	I	5.2823	0.8355
53712.0800	R	2.2964	0.4855
53712.0941	I	5.7623	0.8408
53733.0618	R	1.0180	0.4665
53738.0545	R	0.6664	0.4256
p454			
53641.1197	R	0.6972	0.7005
53641.1365	I	-0.4255	1.2741
53649.1072	R	-0.1502	0.9610
53682.1196	R	-0.1760	0.9017
53698.1002	R	4.2121	0.5965
53698.1168	I	8.3580	1.2301
53704.1203	R	4.3398	0.3212
53704.1368	I	6.2030	0.5707
53706.1100	R	5.2711	0.3958
53706.1240	I	8.1331	0.7116
53708.1177	R	4.5530	0.3831
53708.1325	I	5.9466	0.7701
53712.1220	R	4.4731	0.4477
53712.1373	I	6.4411	0.8618
53714.0384	R	2.6839	0.7300

Continued

Table C.1 (Continued)

MJD	Passband	$Flux_{25}$	σ_{Flux}
53714.0524	I	5.1261	0.9558
53728.0993	R	1.2013	0.5501
53728.1165	I	3.5631	0.8266
53731.1077	R	1.1329	0.4366
53731.1166	I	3.9075	0.8271
53733.0654	R	1.6399	0.3959
53733.0880	I	2.8692	0.6052
53735.0710	R	1.4061	0.4304
53738.0710	R	0.9756	0.4146
p455			
53641.1271	R	0.2309	0.7858
53641.1483	I	-0.3331	1.4831
53649.1220	R	1.2410	0.8010
53649.1466	I	0.6161	1.8441
53652.0858	R	-0.6390	0.8394
53652.1003	I	-0.2402	1.0861
53654.0864	R	0.9069	0.6948
53654.1094	I	0.9398	1.0200
53682.1268	R	1.5001	1.1704
53698.1074	R	0.0943	0.7406
53698.1286	I	0.9874	1.6153
53704.1274	R	3.5136	0.3409
53704.1484	I	3.4429	0.5983
53706.1135	R	6.3892	0.3696
53706.1298	I	8.0522	0.7577
53708.1215	R	9.0193	0.3659
53708.1386	I	11.7613	0.7845
53712.1266	R	19.6209	0.4739
53712.1432	I	23.2214	0.9708
53714.0419	R	21.8296	0.7360
53714.0582	I	26.5940	1.0172
53728.1070	R	27.9647	0.6718
53728.1282	I	31.2392	0.8230
53731.1112	R	24.9110	0.4213
53731.1224	I	27.8664	0.9038

Continued

Table C.1 (Continued)

MJD	Passband	$Flux_{25}$	σ_{Flux}
53733.0695	R	23.5053	0.4377
53733.0938	I	25.4982	0.6798
53738.0840	R	17.5822	0.4232
p459			
53641.1271	R	-0.6113	0.7156
53641.1483	I	-2.4906	1.2087
53649.1220	R	0.8459	0.7045
53649.1466	I	0.8468	2.0889
53652.0858	R	0.0161	0.7873
53652.1003	I	0.3268	0.9659
53654.0864	R	-0.1056	0.6710
53654.1094	I	-0.7074	0.9056
53682.1268	R	2.6397	1.1396
53698.1074	R	4.1115	0.7337
53698.1286	I	5.5514	1.6051
53704.1274	R	2.9635	0.3347
53704.1484	I	5.9454	0.5568
53706.1135	R	2.8040	0.3582
53706.1298	I	5.6588	0.5864
53708.1215	R	1.9249	0.3450
53708.1386	I	6.1108	0.7551
53712.1266	R	2.6594	0.4354
53712.1432	I	4.6104	0.8389
53714.0419	R	2.5469	0.7500
53714.0582	I	4.7671	0.9517
53728.1070	R	0.6087	0.5316
53728.1282	I	1.5091	0.6965
53731.1112	R	0.3546	0.4102
53731.1224	I	1.6841	0.8167
53733.0695	R	-0.0794	0.3632
53733.0938	I	1.5052	0.6930
53738.0840	R	0.2534	0.3991
p520			
53641.1197	R	1.0417	0.7000
53641.1365	I	-0.0893	1.2552

Continued

Table C.1 (Continued)

MJD	Passband	$Flux_{25}$	σ_{Flux}
53649.1072	R	-0.4618	1.0134
53682.1196	R	0.3233	0.8406
53698.1002	R	-0.8880	0.6983
53698.1168	I	1.2474	1.3319
53704.1203	R	0.3502	0.3485
53704.1368	I	-1.0431	0.6248
53706.1100	R	0.3033	0.3454
53706.1240	I	0.8437	0.7919
53708.1177	R	1.3467	0.3950
53708.1325	I	1.9093	0.7762
53712.1220	R	1.4039	0.4590
53712.1373	I	3.2789	0.8177
53714.0384	R	3.5072	0.7888
53714.0524	I	2.3259	0.9832
53728.0993	R	5.4160	0.5385
53728.1165	I	7.1311	0.9208
53731.1077	R	4.8749	0.4928
53731.1166	I	7.6556	0.8098
53733.0654	R	5.5069	0.3551
53733.0880	I	8.2108	0.7372
53738.0710	R	5.0556	0.3739
p524			
53639.1633	R	-0.3502	0.5302
53639.1830	I	-0.6963	0.8272
53643.1780	I	-1.5370	1.8248
53649.1595	R	-0.1735	1.0171
53649.1865	I	1.4756	3.1188
53652.1434	I	-0.8277	0.8434
53654.1545	R	0.1400	0.5238
53654.1743	I	0.6130	0.7398
53682.1450	R	-1.2058	0.9727
53696.1667	R	0.0771	0.3031
53696.1854	I	0.3048	0.7269
53702.1866	R	3.5354	0.3487
53702.2061	I	3.8768	0.6778

Continued

Table C.1 (Continued)

MJD	Passband	$Flux_{25}$	σ_{Flux}
53706.1543	R	6.9683	0.3386
53706.1731	I	6.9753	0.7377
53708.1597	R	8.0910	0.4172
53708.1759	I	9.1495	0.8045
53712.1654	R	9.8153	0.4642
53712.1826	I	10.2338	0.8555
53714.0793	R	10.1951	0.8774
53714.0922	I	11.3675	1.1247
53731.1284	R	10.7682	1.7603
53735.0908	R	8.3566	0.3791
53735.0986	I	9.7711	0.5886
53738.0982	R	6.6696	0.2860
p527			
53641.1197	R	0.2205	0.7600
53641.1365	I	-1.6963	1.2177
53649.1072	R	-0.4818	1.0598
53682.1196	R	-0.7053	0.9185
53698.1002	R	-0.5048	0.7095
53698.1168	I	1.1960	1.2265
53704.1203	R	0.1658	0.3809
53704.1368	I	-0.0014	0.5238
53706.1100	R	-0.0419	0.4129
53706.1240	I	0.9412	0.8288
53708.1177	R	0.8178	0.4651
53708.1325	I	-0.9650	0.7763
53712.1220	R	0.7603	0.5022
53712.1373	I	0.1554	0.8499
53714.0384	R	-1.1832	0.7893
53714.0524	I	1.3730	0.9124
53728.0993	R	2.9857	0.6485
53728.1165	I	4.3369	0.8825
53731.1077	R	5.8417	0.4650
53731.1166	I	7.3248	0.9025
53733.0654	R	7.9670	0.4671
53733.0880	I	11.0908	0.6978

Continued

Table C.1 (Continued)

MJD	Passband	$Flux_{25}$	σ_{Flux}
53738.0710	R	13.1121	0.4560
	p528		
53641.1197	R	-0.2892	0.5533
53641.1365	I	0.1355	1.2576
53645.1634	R	-0.5377	0.7215
53649.1072	R	1.6436	1.0411
53649.1255	I	-0.9005	5.3862
53682.1196	R	1.6099	0.8910
53698.1002	R	0.5150	0.7367
53698.1168	I	1.3348	1.2950
53704.1203	R	-0.2287	0.3872
53704.1368	I	3.2458	0.5651
53706.1100	R	0.1044	0.3605
53706.1240	I	1.9162	0.8017
53708.1177	R	0.5401	0.3708
53708.1325	I	1.8921	0.7599
53712.1220	R	1.4561	0.4121
53712.1373	I	3.8169	0.8597
53714.0384	R	1.5945	0.5783
53714.0524	I	5.3170	1.0043
53728.0993	R	2.9078	0.6980
53728.1165	I	7.3724	0.9149
53731.1077	R	3.7729	0.4861
53731.1166	I	6.4021	0.9373
53733.0654	R	3.6262	0.4113
53733.0880	I	6.7925	0.6240
53735.0710	R	3.4734	0.4107
53738.0710	R	3.2096	0.4143
	p534		
53641.1425	I	-0.0596	1.4429
53649.1179	R	-1.5606	0.8420
53682.1233	R	-1.0203	1.3587
53698.1039	R	0.1806	0.7119
53698.1226	I	-2.2661	1.4561
53704.1238	R	-0.0222	0.3525
	Continued		

Table C.1 (Continued)

MJD	Passband	$Flux_{25}$	σ_{Flux}
53704.1426	I	-0.2121	0.5230
53728.1032	R	3.9729	0.5839
53728.1223	I	3.5625	0.8159
53733.1233	R	6.8926	0.4686
53733.1268	I	7.5574	0.7279
53735.0745	R	8.0484	0.3933
53735.0780	I	7.6546	0.7757
53738.0745	R	7.4596	0.4337
53738.0780	I	10.9646	0.7176
53641.1232	R	-0.0435	0.6774
	q002		
53994.2909	R	8.4645	0.5092
53994.3204	I	9.8516	1.0253
54003.2785	R	10.5113	0.8352
54003.3065	I	17.3723	1.2594
54006.2564	R	11.1690	0.6598
54006.2599	I	19.1711	1.2911
54021.3492	R	5.5462	1.0724
54023.2741	R	4.4147	0.6374
54023.2942	I	9.6524	1.2660
54027.2992	R	1.7400	0.6702
54027.3178	I	5.1823	1.5186
54031.3137	R	1.2798	0.6221
54031.3288	I	4.6943	1.4234
54037.2864	I	3.3621	1.3666
54037.2957	R	3.1214	0.8264
54039.2793	R	0.4817	0.9159
54053.0936	R	1.6447	0.5641
54053.1136	I	1.9457	0.8508
54057.2536	I	2.4123	2.3032
54069.2261	R	-2.9330	1.3406
54084.1394	I	-10.8859	2.5275
54088.1116	R	-0.0214	0.5361
54095.1047	R	-0.7713	0.9014
54095.1071	I	-5.1300	1.4935
	Continued		

Table C.1 (Continued)

MJD	Passband	$Flux_{25}$	σ_{Flux}
54096.1102	R	-1.0479	1.3170
54098.1184	R	-4.6841	1.4438
54112.1025	R	0.1375	0.6224
54112.1062	I	-0.1992	1.4573
54114.0916	R	0.9130	0.7924
54114.0941	I	0.0870	1.9186
54115.0890	R	2.6639	0.6725
	q006		
53994.2683	R	11.1663	0.4031
53994.3086	I	13.3929	0.6466
54003.2714	R	9.4802	0.6084
54003.2959	I	13.9693	0.8297
54021.3422	R	2.3991	1.1073
54023.2669	R	2.6794	0.6524
54023.2818	I	5.6452	1.0727
54027.2922	R	1.5822	0.4515
54027.3061	I	4.2766	0.8968
54031.3067	R	1.4071	0.4987
54031.3172	I	3.9793	0.9216
54037.2804	I	4.7385	1.0865
54037.2922	R	0.6671	0.6090
54039.2723	R	0.2414	1.0237
54039.3003	I	1.1718	1.8526
54053.0864	R	1.5169	0.5371
54053.1011	I	2.3482	0.5885
54059.2366	R	2.3901	0.9780
54059.2636	I	0.8228	1.6834
54063.2496	R	-0.3055	0.4813
54063.2749	I	3.0346	1.2549
54065.2239	R	0.9720	0.5028
54065.2541	I	-0.1631	0.9532
54067.2281	R	1.8065	0.6035
54067.2480	I	-0.5368	1.1640
54069.2191	R	-1.0281	1.2370
54084.1276	I	-1.6147	2.6909

Continued

Table C.1 (Continued)

MJD	Passband	$Flux_{25}$	σ_{Flux}
54088.1256	R	0.4365	0.4603
54088.1291	I	0.7642	0.9089
54090.1038	R	0.5050	0.3408
54090.1822	I	0.2101	1.0458
54092.1088	R	0.4697	0.3477
54092.1325	I	0.2340	0.6071
54094.1078	R	-0.4409	0.4839
54094.1253	I	-0.2164	0.8376
54096.1242	R	0.6679	1.0685
54096.1463	I	0.9977	1.6872
54098.1547	I	-5.4661	2.2850
54099.0631	I	0.3218	2.3865
54111.1055	R	1.1470	0.5546
54111.1287	I	0.3208	1.0745
54113.0980	R	1.6676	0.5401
54113.1015	I	1.7241	1.0487
54114.0853	R	0.8387	0.6862
54114.0881	I	1.5474	1.2663
	q007		
53994.2718	R	23.9192	0.4082
53994.3146	I	38.7928	0.6993
54003.2749	R	28.6006	0.6604
54003.3013	I	45.2948	1.0688
54006.2763	I	43.7498	0.8070
54006.2822	R	27.8346	0.5612
54021.3457	R	15.8714	1.2385
54023.2706	R	13.6587	0.6157
54023.2879	I	32.2168	1.3958
54027.2957	R	11.3177	0.5650
54027.3120	I	26.4264	1.1467
54031.3102	R	10.5398	0.4944
54031.3230	I	24.2053	1.0089
54053.0901	R	4.4116	0.5072
54053.1078	I	8.9190	0.6326
54059.2543	I	5.1536	1.5800

Continued

Table C.1 (Continued)

MJD	Passband	$Flux_{25}$	σ_{Flux}
54063.2350	R	2.9664	0.4947
54063.2691	I	4.9736	1.3364
54065.2274	R	3.3974	0.5597
54065.2601	I	5.5059	1.0788
54067.2316	R	3.9013	0.7361
54067.2538	I	7.7090	1.2451
54069.2226	R	-0.1963	1.1475
54069.2472	I	3.9631	1.4343
54082.1125	R	3.0429	0.6350
54082.1431	I	5.5873	1.5156
54086.0956	R	2.7313	0.5059
54086.1270	I	3.9750	1.2292
54088.1151	R	3.1598	0.4457
54090.0847	R	2.2326	0.3815
54090.1073	I	3.2855	0.6309
54092.1127	R	2.3571	0.4053
54092.1383	I	4.6094	0.7166
54094.1113	R	1.4130	0.4800
54094.1311	I	4.6019	1.0232
54095.0989	R	3.1728	0.9109
54095.1013	I	2.8511	1.2104
54096.1207	R	1.5890	1.2868
54098.1289	R	0.6473	1.5017
54099.0666	R	1.5303	1.9183
54099.0689	I	1.5864	2.7094
54111.1021	R	1.8753	0.5272
54111.1229	I	3.5520	0.9039
54113.0886	R	2.2356	0.6255
54113.0921	I	0.6115	1.0125
	q008		
53994.3532	R	13.3679	0.5386
53994.3913	I	15.0359	1.0003
54003.3419	R	28.0426	0.6878
54003.3667	I	35.6589	1.4042
54006.2657	R	29.5896	0.5389
54006.2692	I	37.6500	0.9308
54021.3564	R	20.5365	1.4152
54023.3149	R	18.0862	1.0313
54023.3299	I	20.0502	1.2368
54027.3334	I	22.0305	1.2295
54027.3566	R	12.9159	0.7113
54031.3678	R	12.3151	0.9308
54037.3196	I	17.3507	1.2669
54037.3375	R	8.5847	0.8152
54039.3418	R	6.8101	0.8270
54053.1401	R	3.4749	0.4321
54053.1542	I	8.6249	0.6687
54055.3092	R	4.3042	1.0711
54057.2655	R	3.9820	1.1878
54057.2795	I	6.1392	1.7631
54059.2965	R	4.4788	0.9344
54059.3147	I	4.6445	2.3770
54063.2979	R	3.4687	0.6948
54063.3073	I	8.8132	1.0965
54065.2898	R	2.5784	0.6925
54065.3017	I	6.5480	1.2521
54067.2846	R	3.8665	0.6872
54067.3095	I	3.2287	1.9153
54069.2721	R	2.9275	0.6943
54069.3003	I	4.7498	1.3783
54084.1452	R	0.9068	1.2617
54084.1592	I	6.0626	2.1988
54086.1507	R	2.2304	0.7653
54088.1527	R	1.8754	0.4427
54088.1724	I	4.6022	0.9777
54090.1358	R	2.1259	0.3807
54090.1486	I	4.0556	0.7436
54092.1576	R	1.6709	0.3948
54092.1777	I	3.6966	0.7927
54094.1682	R	1.7792	0.5171

Continued

Table C.1 (Continued)

Continued

Table C.1 (Continued)

MJD	Passband	$Flux_{25}$	σ_{Flux}
54094.1885	I	2.7772	0.9577
54095.1382	R	1.4027	0.8258
54095.1406	I	5.3375	1.4204
54096.1811	R	-0.2698	1.0932
54098.1886	R	4.9648	2.6290
54111.1548	R	-1.0382	0.7153
54112.1654	I	0.8315	1.6600
54113.1343	R	1.5617	0.5374
54114.1413	R	0.9290	0.9356
54114.1437	I	2.3943	1.7342
	q014		
53994.3713	R	10.4753	0.5218
53994.4029	I	14.6825	1.5273
54003.3489	R	22.3575	0.7582
54003.3771	I	29.3692	1.6104
54006.3556	R	24.9179	0.5035
54006.3752	I	29.8186	0.8370
54023.3259	R	16.8779	0.7508
54023.3478	I	23.7575	1.3628
54027.3508	I	19.1738	1.4399
54027.3671	R	13.6659	0.9307
54031.3346	R	12.1947	0.6591
54031.3451	I	18.6767	1.5939
54037.3136	I	17.9157	1.2009
54037.3421	R	8.8710	0.8550
54039.3166	R	10.1246	1.0238
54039.3581	I	15.6146	2.1559
54053.1507	R	5.2172	0.4125
54053.1717	I	8.5059	1.0482
54055.3022	R	3.9363	0.9721
54057.2760	R	3.4799	0.9730
54063.3132	R	3.4570	0.6381
54063.3262	I	7.9881	2.1437
54069.2826	R	1.8635	0.6405
54084.1557	R	1.2610	1.4797

Continued

Table C.1 (Continued)

MJD	Passband	$Flux_{25}$	σ_{Flux}
54084.1766	I	3.1763	2.0428
54086.1542	R	0.7226	0.7360
54088.1631	R	2.9044	0.5160
54088.1666	I	4.4156	1.0719
54095.1619	R	1.2664	0.7260
54095.1642	I	3.1419	1.3084
54098.1851	R	-0.9003	2.1596
54099.1437	R	2.5302	2.5164
54099.1463	I	2.9635	3.4047
	q022		
53992.2895	R	27.2143	1.2846
53994.2090	R	28.6563	0.5957
53994.2406	I	35.4157	0.7739
54003.2164	R	21.9081	0.8722
54003.2490	I	27.3092	1.4469
54023.2342	R	9.7325	0.6073
54023.2560	I	17.2835	1.0269
54027.2545	R	8.1355	0.6812
54027.2754	I	16.1161	1.1101
54031.2446	R	7.3067	0.5848
54031.2760	I	13.8644	1.1427
54037.2298	R	4.3540	0.5784
54037.2506	I	9.5897	1.3047
54039.2213	R	4.2313	0.9607
54053.0464	R	3.7239	0.4765
54053.0687	I	5.3120	0.7054
54059.1957	R	3.4610	0.6835
54059.2120	I	5.0760	2.7849
54082.0806	R	2.7926	0.6339
54082.0846	I	1.8736	1.2251
54086.0638	R	1.4756	0.4984
54086.0673	I	3.6096	0.9298
54096.0561	R	3.4419	1.4717
54099.0513	R	-1.2900	1.8565
54099.0536	I	-2.7395	2.3872

Continued

Table C.1 (Continued)

MJD	Passband	$Flux_{25}$	σ_{Flux}
54112.0616	R	0.7271	0.9036
54112.0652	I	3.4915	1.8554
q048			
54021.2305	R	9.7217	0.8475
54021.2475	I	12.6803	1.6168
54025.2260	R	11.0708	0.6230
54025.2506	I	13.4109	1.2851
54029.2397	R	9.2111	0.5646
54029.2560	I	13.3180	0.9039
54031.2551	R	7.6774	0.5642
54031.2938	I	12.5522	1.0441
54033.2198	R	9.5421	1.9427
54037.2368	R	4.9217	0.6788
54037.2622	I	10.7844	1.4164
54039.2285	R	3.9626	1.1540
54039.2578	I	7.1626	1.8880
54051.0442	R	1.8070	0.6471
54051.0650	I	6.2283	1.0136
54055.1999	R	1.3218	0.8286
54055.2181	I	4.9150	1.7464
54069.1979	R	2.1393	1.6356
54084.0635	R	1.6594	0.7559
54084.0806	I	2.1014	2.0943
54088.0686	R	0.7714	0.4973
54088.0912	I	1.1677	0.9883
54095.0881	R	-0.3572	0.9960
54095.0904	I	3.6478	1.4327
54096.0646	R	-3.0873	1.5743
54098.0911	R	1.0169	1.9309
54112.0851	R	-0.0647	0.8135
54112.0921	I	2.4871	1.2266
54114.0651	R	-0.0512	0.7642
54114.0676	I	3.2180	1.3643
q049			
53992.3476	R	0.5049	1.0345
Continued			

Table C.1 (Continued)

MJD	Passband	$Flux_{25}$	σ_{Flux}
53994.3842	R	0.8142	0.5023
54003.3597	R	8.5856	0.6950
54003.3937	I	6.9061	1.3796
54006.3917	R	8.8968	0.6654
54021.3110	R	11.9709	1.1794
54021.3298	I	17.1469	1.2191
54023.3789	R	9.1994	1.2161
54025.3258	R	10.4417	1.7171
54029.3463	I	14.1142	0.8016
54029.3654	R	10.2710	0.6434
54031.3416	R	9.5471	0.6064
54031.3567	I	12.0484	1.2100
54033.3380	R	6.5307	1.2009
54037.3316	I	7.5206	1.2642
54037.3492	R	5.2822	0.7106
54039.3239	R	5.2413	1.0030
54039.3640	I	10.2073	2.3057
54051.1523	R	2.7109	0.4739
54051.1716	I	8.8490	1.2088
54055.2716	R	1.3304	0.9667
54055.2929	I	5.7707	1.7955
54059.2895	R	1.4627	0.6273
54059.3053	I	6.5283	1.7809
54063.3168	R	1.4569	0.5917
54063.3203	I	2.7584	1.2520
54069.2933	R	0.6885	0.7253
54082.1563	R	1.4425	0.5929
54082.1693	I	2.0002	1.1844
54086.1432	R	0.0180	0.5731
54086.1637	I	2.8337	1.9345
54096.1706	R	-0.1044	1.0195
54098.1781	R	1.3486	2.0110
54099.1196	R	0.7077	2.0035
54099.1219	I	-0.9618	2.8979
54114.1531	R	-0.2530	0.8840
Continued			

Table C.1 (Continued)

MJD	Passband	$Flux_{25}$	σ_{Flux}
54114.1555	I	3.8147	1.8110
	q054		
53992.3476	R	-0.4170	1.0456
53994.3842	R	0.1007	0.5373
54003.3597	R	1.8039	0.7448
54003.3937	I	0.2401	1.4193
54006.3917	R	3.0228	0.6615
54021.3110	R	24.6992	1.3474
54021.3298	I	30.1074	1.5941
54023.3789	R	24.8295	1.2261
54025.3258	R	21.2015	1.7756
54029.3463	I	30.0062	0.8272
54029.3654	R	23.9349	0.6421
54031.3416	R	23.4975	0.6133
54031.3567	I	28.1785	1.2728
54033.3380	R	20.9318	1.4140
54037.3316	I	22.4615	1.2668
54037.3492	R	18.4433	0.7152
54039.3239	R	20.9746	1.0951
54039.3640	I	24.0094	2.5140
54051.1523	R	9.0700	0.5380
54051.1716	I	15.3718	1.3203
54055.2716	R	8.7499	0.8998
54055.2929	I	10.5886	1.9003
54059.2895	R	5.9773	0.8247
54059.3053	I	11.7855	1.7772
54063.3168	R	4.3789	0.5900
54063.3203	I	14.5538	1.2796
54069.2933	R	3.5168	0.7613
54082.1563	R	2.8386	0.6234
54082.1693	I	7.6762	1.2491
54086.1432	R	2.1126	0.6317
54086.1637	I	6.6759	1.7365
54096.1706	R	1.6757	0.9939
54098.1781	R	3.5201	2.0240

Continued

Table C.1 (Continued)

MJD	Passband	$Flux_{25}$	σ_{Flux}
54099.1196	R	-0.5280	1.8524
54099.1219	I	0.5558	2.9758
54114.1531	R	1.6970	0.8846
54114.1555	I	3.5507	1.7156
	q061		
53994.2053	R	-0.1825	0.5407
53994.2347	I	0.6745	0.8471
54003.2062	R	-0.6379	0.5630
54003.2437	I	-1.4289	1.3720
54023.2301	R	9.7917	0.7069
54023.2502	I	13.8971	0.9703
54025.2407	R	9.0101	0.5314
54027.2478	R	9.5620	0.5313
54027.2696	I	16.3964	1.2257
54031.2516	R	9.3694	0.6086
54031.2880	I	14.2276	1.0713
54037.2260	R	8.5053	0.5487
54037.2448	I	12.6807	1.4079
54039.2177	R	6.3364	0.9169
54039.2401	I	12.9475	1.3621
54053.0428	R	2.7634	0.5147
54053.0629	I	7.5948	0.6727
54059.1922	R	1.9155	0.6851
54059.2074	I	6.8990	1.6114
54063.1937	R	1.8991	0.4687
54063.2122	I	7.7785	1.0121
54065.2037	R	1.3689	0.5649
54065.2077	I	6.8225	1.1035
54067.2026	R	1.1186	0.9208
54067.2061	I	4.4205	1.7566
54082.0771	R	1.2907	0.5600
54082.0901	I	4.2248	1.2561
54086.0603	R	1.3222	0.4937
54086.0731	I	3.5107	0.9876
54090.0542	R	0.3655	0.3606

Continued

Table C.1 (Continued)

MJD	Passband	$Flux_{25}$	σ_{Flux}
54090.0651	I	2.6087	0.6766
54092.0568	R	-0.2047	0.3804
54094.0580	R	0.5355	0.5741
54099.0478	I	3.1426	2.5561
54112.0713	R	1.1008	0.8995
54112.0756	I	0.9472	1.3452
q067			
53994.3567	R	0.1365	0.5123
53994.3971	I	0.6186	1.1363
54003.3455	R	-0.2102	0.7123
54003.3719	I	-0.4555	1.6236
54006.3807	R	0.3500	0.5107
54021.3643	R	35.3960	1.2813
54023.3222	R	44.8607	0.8682
54023.3418	I	49.7573	1.3923
54027.3450	I	68.5877	1.4045
54027.3636	R	65.5731	0.8766
54031.3643	R	74.0055	0.8816
54039.3201	R	82.6250	1.1320
54039.3523	I	83.3625	2.1554
54053.1472	R	52.0811	0.4243
54053.1659	I	55.0301	0.8516
54055.2987	R	48.4053	1.1972
54057.2725	R	43.6428	1.1521
54057.2912	I	51.9931	1.9586
54069.2791	R	26.3828	0.7404
54084.1522	R	12.7776	1.3043
54084.1708	I	18.3783	2.5514
54088.1596	R	14.4839	0.6369
54092.1611	R	11.9071	0.4053
54092.1655	I	17.6880	0.8045
54094.1732	R	11.4400	0.5301
54094.1767	I	13.9233	0.8723
54095.1558	R	11.2077	0.8836
54095.1581	I	14.2485	1.5786
Continued			

Table C.1 (Continued)

MJD	Passband	$Flux_{25}$	σ_{Flux}
54096.1741	R	11.5744	1.2192
54098.1816	R	12.8899	2.4440
54099.1376	R	10.9460	2.4669
54099.1400	I	14.1968	3.0672
54111.1590	R	7.1478	0.7547
54111.1634	I	12.6303	1.3070
54113.1382	R	7.5074	0.5402
54113.1417	I	9.7430	1.0646
q069			
53992.2895	R	-0.7569	0.9998
53994.2090	R	-0.4911	0.5127
53994.2406	I	0.6181	0.6906
54003.2490	I	-1.5617	1.4089
54023.2342	R	24.4394	0.6469
54023.2560	I	31.6373	0.8791
54027.2545	R	17.9434	0.6689
54027.2754	I	24.6911	1.0805
54031.2446	R	13.2645	0.6606
54031.2760	I	24.2027	1.1166
54037.2298	R	9.1258	0.5559
54037.2506	I	16.1211	1.2013
54039.2213	R	7.7386	0.9641
54053.0464	R	5.4220	0.4391
54053.0687	I	7.6716	0.7155
54059.1957	R	4.0133	0.6264
54059.2120	I	4.6030	2.4814
54069.1909	R	1.0026	1.7008
54082.0806	R	2.7888	0.5919
54082.0846	I	2.8524	1.0657
54086.0638	R	3.0134	0.5039
54086.0673	I	5.9408	0.8766
54096.0561	R	3.4480	1.1064
54112.0616	R	2.1716	0.7972
54112.0652	I	0.9974	1.6687
q075			
Continued			

Table C.1 (Continued)

MJD	Passband	$Flux_{25}$	σ_{Flux}
53994.3567	R	2.0714	0.4258
53994.3971	I	2.9591	0.9847
54003.3455	R	7.9850	0.6775
54003.3719	I	8.5700	1.5501
54006.3807	R	10.6087	0.4414
54021.3643	R	18.8995	1.3523
54023.3222	R	17.5194	0.6890
54023.3418	I	21.1655	1.2846
54027.3450	I	18.2034	1.2938
54027.3636	R	16.4448	0.7653
54031.3643	R	12.1983	0.7505
54039.3201	R	8.9109	0.8926
54039.3523	I	12.1020	1.8838
54053.1472	R	3.8568	0.3395
54053.1659	I	8.9337	0.7425
54057.2912	I	7.7742	2.0129
54069.2791	R	2.1243	0.6583
54084.1522	R	3.5497	1.0896
54084.1708	I	4.9875	2.7472
54088.1596	R	-0.1169	0.5247
54092.1611	R	0.7710	0.3313
54092.1655	I	2.9460	0.7222
54094.1732	R	0.9182	0.5116
54094.1767	I	3.4520	0.8281
54095.1558	R	1.8370	0.7407
54095.1581	I	4.7547	1.4855
54096.1741	R	1.0374	1.0340
54099.1400	I	2.7035	3.8166
54113.1382	R	1.1430	0.4712
54113.1417	I	2.6644	0.9108
	q102		
53994.2053	R	0.6945	0.4357
53994.2347	I	-0.2852	0.7837
54003.2062	R	-0.8154	0.5233
54003.2437	I	-1.9426	1.4132

Continued

Table C.1 (Continued)

MJD	Passband	$Flux_{25}$	σ_{Flux}
54023.2301	R	11.7134	0.6289
54023.2502	I	13.5182	0.9533
54025.2407	R	14.2848	0.5315
54027.2478	R	13.9823	0.5975
54027.2696	I	17.0116	1.2824
54031.2516	R	15.3171	0.6171
54031.2880	I	19.1183	1.0180
54037.2260	R	13.3363	0.5987
54037.2448	I	17.8501	1.3422
54039.2177	R	11.6930	1.0275
54039.2401	I	17.6976	1.3859
54053.0428	R	6.1635	0.4566
54053.0629	I	9.7856	0.6177
54059.1922	R	3.8925	0.6451
54059.2074	I	7.7693	1.4960
54063.1937	R	4.2546	0.4821
54063.2122	I	7.7263	0.9058
54065.2037	R	2.2725	0.5842
54065.2077	I	8.6470	1.0546
54067.2026	R	3.0626	1.0603
54067.2061	I	7.5895	2.0033
54069.1874	R	2.9031	1.9027
54082.0771	R	2.0627	0.6100
54082.0901	I	2.9850	1.2165
54086.0603	R	0.8053	0.5328
54086.0731	I	2.5893	1.0848
54090.0542	R	1.4803	0.3530
54090.0651	I	4.1210	0.6363
54092.0568	R	1.3863	0.3603
54094.0580	R	0.5940	0.5710
54096.0691	R	0.4196	1.7266
54099.0453	R	-1.7049	1.8599
54099.0478	I	3.1907	2.4892
54112.0713	R	0.3309	0.9835
54112.0756	I	3.8036	1.2822

Continued

Table C.1 (Continued)

MJD	Passband	$Flux_{25}$	σ_{Flux}
q106			
53994.3713	R	0.7081	0.1918
53994.4029	I	0.9789	0.8624
54003.3489	R	0.7079	0.6730
54003.3771	I	-1.6882	1.4427
54006.3556	R	0.3512	0.4391
54006.3752	I	0.6433	0.8248
54023.3259	R	7.4938	0.6577
54023.3478	I	7.1908	1.2869
54027.3508	I	10.7123	1.2599
54027.3671	R	10.4907	0.7741
54031.3346	R	11.8771	0.5890
54031.3451	I	12.5212	1.2862
54037.3136	I	12.2400	1.2311
54037.3421	R	12.9511	0.8044
54039.3166	R	14.7126	0.8396
54039.3581	I	18.6808	1.7551
54053.1507	R	7.4652	0.3777
54053.1717	I	11.6878	0.8752
54055.3022	R	5.6972	1.0104
54057.2760	R	5.7604	0.9276
54063.3132	R	4.1999	0.6124
54063.3262	I	8.0325	1.7215
54069.2826	R	2.6823	0.6330
54084.1557	R	2.3343	1.3980
54084.1766	I	2.1914	2.0422
54086.1542	R	2.8108	0.7053
54088.1631	R	1.9231	0.5097
54088.1666	I	2.0023	0.9062
54095.1619	R	0.0598	0.6469
54095.1642	I	0.3161	1.2057
54098.1851	R	3.0736	2.2600
54099.1437	R	3.0505	1.9869
54099.1463	I	-0.6459	2.7504
q107			

Continued

Table C.1 (Continued)

MJD	Passband	$Flux_{25}$	σ_{Flux}
53994.2683	R	0.0442	0.3492
53994.3086	I	0.9348	0.6627
54003.2714	R	-0.5139	0.6596
54003.2959	I	0.1858	0.7825
54021.3422	R	3.1074	1.2565
54023.2669	R	4.6628	0.7612
54023.2818	I	7.4977	1.1227
54027.2922	R	5.8838	0.4854
54027.3061	I	6.7927	1.0256
54031.3067	R	6.5581	0.5122
54031.3172	I	7.6221	1.0354
54037.2804	I	9.9339	1.1850
54037.2922	R	5.6476	0.6495
54039.2723	R	7.7829	0.9940
54039.3003	I	6.5750	1.9460
54053.0864	R	2.6559	0.5121
54053.1011	I	5.7488	0.6955
54059.2366	R	2.8693	0.9869
54059.2636	I	3.3704	1.6608
54063.2496	R	1.8221	0.5034
54063.2749	I	1.0851	1.4705
54065.2239	R	0.9521	0.4946
54065.2541	I	3.7980	1.0967
54067.2281	R	1.4596	0.6115
54067.2480	I	3.9886	1.1743
54069.2191	R	1.5542	1.1843
54084.1276	I	2.8924	2.8652
54088.1256	R	0.5713	0.4799
54088.1291	I	1.1071	0.8620
54090.1038	R	0.3316	0.3293
54090.1822	I	1.5901	1.1483
54092.1088	R	0.2137	0.3313
54092.1325	I	0.6880	0.6547
54094.1078	R	0.4250	0.4758
54094.1253	I	2.3006	1.0098

Continued

Table C.1 (Continued)

MJD	Passband	$Flux_{25}$	σ_{Flux}
54096.1242	R	-0.2636	1.0776
54096.1463	I	2.9473	1.9430
54098.1326	R	1.8728	1.4435
54098.1547	I	-4.6573	2.6893
54099.0631	I	1.1654	2.4736
54111.1055	R	-0.1814	0.5552
54111.1287	I	1.7874	1.1349
54113.0980	R	0.0955	0.5089
54113.1015	I	0.6451	0.9459
54114.0853	R	-0.2340	0.7048
54114.0881	I	-0.3013	1.2633
q108			
53994.2909	R	0.3008	0.3721
53994.3204	I	0.8316	0.6806
54003.2785	R	2.9390	0.6462
54003.3065	I	2.6300	0.9139
54006.2564	R	3.3396	0.4567
54006.2599	I	6.2670	0.8282
54021.3492	R	4.1928	0.9492
54023.2741	R	4.0697	0.5972
54023.2942	I	6.7598	1.0251
54027.2992	R	4.6344	0.5192
54027.3178	I	7.0210	1.1345
54031.3137	R	2.9048	0.4672
54031.3288	I	6.2274	1.0497
54037.2864	I	4.1378	1.1183
54037.2957	R	1.8649	0.7063
54039.2793	R	1.7788	0.9859
54053.0936	R	0.6515	0.4137
54053.1136	I	1.3417	0.5724
54057.2536	I	1.6167	1.9988
54069.2261	R	0.0720	1.2562
54084.1134	R	1.6814	1.5954
54084.1394	I	0.4868	2.0745
54088.1116	R	0.1944	0.4726

Continued

Table C.1 (Continued)

MJD	Passband	$Flux_{25}$	σ_{Flux}
54095.1047	R	0.8634	0.7740
54095.1071	I	-1.6113	1.1826
54096.1102	R	-1.3708	1.1792
54098.1184	R	-1.3251	1.4165
54112.1025	R	-0.5232	0.6333
54112.1062	I	-0.0911	1.3768
54114.0916	R	-0.3733	0.6105
54114.0941	I	-0.6140	1.4916
q112			
53992.3002	R	-0.3528	1.0465
53994.2196	R	0.4923	0.5085
53994.2581	I	-0.0581	0.7257
54003.2272	R	0.9276	0.6577
54003.2659	I	1.0403	0.8812
54021.2382	R	6.5466	0.9277
54021.2591	I	7.8440	1.8714
54025.2330	R	7.0121	0.6113
54025.2623	I	9.8278	2.1754
54029.2467	R	6.6222	0.6472
54029.2677	I	9.4539	0.9846
54031.2309	R	7.9726	0.5263
54031.2644	I	7.2704	1.0415
54033.2276	R	7.5186	1.0291
54037.2410	R	6.2928	0.7756
54037.2682	I	8.3469	1.2760
54039.2320	R	5.5529	1.1654
54039.2517	I	9.1030	1.7703
54051.0555	R	3.2705	0.6067
54051.0767	I	9.8132	1.2080
54055.1929	R	4.1867	0.8355
54055.2088	I	6.8218	2.1600
54069.2049	R	-0.0038	1.8385
54084.0713	R	5.0806	1.1205
54084.0922	I	4.1601	1.9069
54088.0757	R	0.1890	0.5105

Continued

Table C.1 (Continued)

MJD	Passband	$Flux_{25}$	σ_{Flux}
54088.0792	I	2.4418	1.0851
54090.0615	R	0.8551	0.3479
54094.0652	R	0.9882	0.4788
54094.0922	I	0.9779	1.1540
54096.0526	R	0.3334	1.0121
54096.0819	I	-0.4122	1.5710
54098.0581	I	4.6523	1.7188
54098.0642	R	-1.8440	1.6379
54099.0395	R	2.0365	1.8428
54099.0418	I	2.2795	2.4329
54111.0506	R	0.7227	0.6433
54111.0853	I	2.1412	1.2926
54113.0453	R	0.2546	0.6930
54113.0488	I	1.4773	1.1714
	q114		
53992.2930	R	0.2285	1.2622
53994.2126	R	1.5316	0.4949
53994.2465	I	-0.1561	0.7028
54003.2200	R	-0.8682	0.7464
54003.2546	I	0.5176	1.5953
54006.2473	R	-0.5293	0.4505
54006.2508	I	-0.7076	0.8075
54021.2260	R	1.9272	0.7691
54021.2417	I	0.2544	1.4942
54025.2216	R	1.5434	0.8181
54025.2447	I	3.6502	0.8824
54029.2328	R	5.7572	0.5787
54029.2502	I	7.7210	1.0427
54031.2409	R	6.4181	0.5153
54031.2702	I	7.7595	1.1060
54033.2158	R	4.4956	1.6740
54033.2418	I	3.5543	1.8887
54037.2333	R	6.3353	0.5647
54037.2564	I	8.7006	1.2587
54039.2248	R	6.6897	0.8642

Continued

Table C.1 (Continued)

MJD	Passband	$Flux_{25}$	σ_{Flux}
54039.2459	I	10.1387	1.3664
54051.0400	R	3.6109	0.6250
54051.0591	I	7.6435	1.1640
54055.1888	R	3.6730	0.7173
54055.2041	I	5.0943	1.6051
54069.1944	R	2.1007	1.7499
54084.0600	R	0.6447	1.1144
54084.0748	I	2.5005	1.5720
54088.0645	R	0.0348	0.4016
54088.0854	I	2.3985	0.8587
54090.0577	R	0.9591	0.3240
54094.0617	R	-0.3594	0.5111
54094.0862	I	0.5484	0.9971
54095.0822	R	-0.5508	0.8054
54095.0846	I	-0.1898	1.4704
54096.0491	R	-0.2321	0.7733
54096.0761	I	-2.7610	1.9374
54098.0391	I	3.9665	2.0505
54098.0449	R	0.7692	1.5047
54112.0580	R	-1.2762	0.8958
54114.0587	R	-0.0181	0.6882
54114.0615	I	1.6024	1.3678
	q125		
54003.2200	R	15.8218	0.8525
54006.2473	R	15.2743	0.5027
54006.2508	I	22.4564	0.8369
54021.2260	R	7.6057	0.8813
54021.2417	I	11.4993	1.6057
54025.2447	I	9.6026	0.3333
54029.2328	R	4.4392	0.1740
54029.2502	I	8.4202	0.5485
54031.2409	R	5.2250	0.5509
54031.2702	I	9.0208	1.0865
54033.2158	R	3.1517	1.6094
54033.2418	I	8.4952	1.7938

Continued

Table C.1 (Continued)

MJD	Passband	$Flux_{25}$	σ_{Flux}
54037.2333	R	3.5184	0.6090
54037.2564	I	10.0732	1.4812
54039.2248	R	3.2902	0.9095
54039.2459	I	8.7755	1.3813
54051.0400	R	1.7281	0.7731
54051.0591	I	5.4009	1.1345
54055.1888	R	0.2761	0.7307
54055.2041	I	0.5858	1.6548
54069.1944	R	3.5502	1.6727
54084.0600	R	-1.0047	1.1793
54084.0748	I	2.1357	1.6134
54088.0645	R	0.7235	0.5252
54088.0854	I	2.4047	1.1353
54090.0577	R	0.6091	0.4176
54094.0617	R	1.0793	0.5242
54094.0862	I	1.6298	1.0402
54095.0822	R	1.4464	0.8663
54095.0846	I	4.0197	1.3692
54096.0491	R	1.6649	0.7987
54096.0761	I	5.7272	1.8603
54098.0391	I	6.7603	2.2270
54098.0449	R	3.8764	2.0334
54112.0580	R	-0.1897	1.0777
54114.0587	R	-0.6636	0.7230
54114.0615	I	2.1538	1.2409
r185			
53994.2161	R	-1.4163	0.6717
53994.2523	I	-0.9891	0.8537
54003.2237	R	1.4624	0.9465
54003.2607	I	-1.5689	1.3753
54021.2340	R	0.0648	1.0532
54021.2533	I	0.0909	1.7036
54025.2295	R	-0.4423	0.9682
54029.2432	R	-0.1812	0.9257
54029.2618	I	0.3372	1.0760
Continued			

Table C.1 (Continued)

MJD	Passband	$Flux_{25}$	σ_{Flux}
54033.2236	R	-0.1724	2.0994
54039.2133	R	7.9704	1.0553
54051.0518	R	39.9070	1.0247
54051.0709	I	50.8599	1.3132
54055.1964	R	43.1284	1.1416
54055.2134	I	49.0935	2.2326
54059.1992	R	37.1658	0.9036
54059.2155	I	40.2796	2.8393
54063.1972	R	26.6497	0.6232
54063.2180	I	33.1220	1.1461
54065.1965	R	24.9239	0.7936
54065.2127	I	31.2727	1.2868
54067.1956	R	69.4285	1.3149
54067.2119	I	33.2935	1.8706
54069.2014	R	16.9563	2.0575
54084.0670	R	4.7607	1.0603
54084.0864	I	9.9577	1.9292
54088.0722	R	6.4431	0.7699
54088.0973	I	6.7289	1.3635
54092.0491	R	4.1847	0.4956
54094.0509	R	5.3816	0.7365
54094.0803	I	9.5261	1.1001
54096.0608	R	5.7156	1.4213
54098.0716	R	5.2292	2.0254
54098.0751	I	10.2598	2.5018
54111.0543	R	3.3702	0.7246
54111.0920	I	6.4008	1.3820
54113.0546	R	2.3901	0.6918
54113.0582	I	3.6081	1.1638
r186			
53992.3185	R	-0.4999	1.3253
53994.2981	R	-0.7250	0.3718
53994.3321	I	0.1202	0.9171
54003.2854	R	-0.4425	0.6855
54003.3260	I	-0.0795	1.1463
Continued			

Table C.1 (Continued)

MJD	Passband	$Flux_{25}$	σ_{Flux}
54021.2653	R	-1.1192	1.0427
54021.2794	I	-2.2412	1.7656
54023.3546	R	0.8911	0.8254
54025.2683	R	2.4323	0.4977
54025.2864	I	-0.6537	1.6161
54029.2858	R	12.1830	0.6135
54029.3004	I	12.4045	0.9725
54033.2770	R	23.0700	1.7118
54033.2928	I	22.1855	3.1576
54039.2828	R	35.8871	0.9510
54051.0923	R	38.6373	0.7098
54051.1073	I	47.7580	1.2083
54055.2266	R	35.9443	0.8146
54055.2429	I	45.5855	1.6829
54059.2261	R	29.0808	0.7924
54065.2344	R	21.1057	0.5663
54065.2725	I	27.5592	1.3751
54067.2392	R	18.2557	0.5711
54067.2656	I	27.4878	1.3312
54069.2331	R	14.6278	1.0927
54069.2530	I	22.3468	1.7337
54084.1024	R	5.8315	1.3966
54084.1400	I	17.2449	2.4640
54088.1043	R	6.8519	0.4599
54088.1349	I	15.5736	0.9508
54090.1000	R	7.3334	0.3562
54090.1882	I	16.1215	1.0958
54096.1137	R	5.2673	0.9774
54098.1219	R	3.0559	1.4184
54099.0904	I	6.0283	2.6711
54112.1121	R	3.6042	0.6457
54112.1157	I	6.7679	0.9890
54114.1079	R	2.4451	0.8005
54114.1102	I	6.4302	1.6046
54115.1019	R	4.5328	1.1367

Continued

Table C.1 (Continued)

MJD	Passband	$Flux_{25}$	σ_{Flux}
	r190		
54006.3176	R	-0.0675	0.4696
54006.3343	I	-0.6102	0.8770
54021.2689	R	-1.2385	1.0895
54021.2852	I	1.8475	1.8147
54023.3582	R	0.4955	0.9377
54025.2721	R	-0.7948	0.6340
54025.2922	I	2.8098	1.9682
54029.2893	R	-0.6100	0.5805
54029.3160	I	-0.4376	1.0002
54033.2816	R	-1.5317	1.4838
54039.2898	R	0.0053	0.9261
54051.0962	R	11.2622	0.6881
54051.1132	I	12.1860	1.3601
54055.2336	R	15.6502	0.8462
54055.2547	I	17.1709	1.6829
54059.2401	R	18.1342	0.8306
54059.2740	I	22.1064	2.1457
54063.2533	R	17.6630	0.5272
54063.2574	I	23.4338	1.2161
54065.2424	R	18.6567	0.5059
54065.2773	I	23.7129	1.3737
54067.2445	R	18.5585	0.6501
54067.2714	I	22.8493	1.3727
54069.2367	R	15.5503	1.2351
54069.2589	I	20.6111	1.5033
54082.1195	R	9.9195	0.7752
54086.1026	R	8.9095	0.5106
54090.0925	R	7.2887	0.4135
54092.1197	R	6.1306	0.4808
54094.1183	R	6.0851	0.5108
54095.1106	R	3.9641	0.7852
54096.1312	R	4.9727	0.9716
54098.1361	R	3.3340	1.6621
54111.1130	R	2.3762	0.5810

Continued

Table C.1 (Continued)

MJD	Passband	$Flux_{25}$	σ_{Flux}
54111.1414	I	6.5925	1.5451
54113.1213	R	2.1630	0.6117
r193			
53994.3532	R	-0.7353	0.4596
53994.3913	I	0.2569	0.8748
54003.3419	R	-0.5232	0.5777
54003.3667	I	-1.9932	1.2939
54006.2657	R	0.0586	0.4178
54006.2692	I	1.2513	0.8117
54021.3564	R	-1.3485	1.1661
54023.3149	R	-1.2283	0.9976
54023.3299	I	-0.3114	1.1985
54027.3334	I	1.5024	1.1691
54027.3566	R	0.9456	0.6369
54031.3678	R	2.6785	0.8643
54037.3196	I	4.8786	1.1005
54037.3375	R	4.4897	0.6908
54039.3418	R	6.0010	0.7492
54053.1401	R	8.5342	0.3619
54053.1542	I	8.5888	0.6380
54055.3092	R	8.7364	0.9763
54057.2655	R	7.1307	1.0510
54057.2795	I	10.7401	1.5235
54059.2965	R	8.4269	0.7749
54059.3147	I	3.5153	2.2355
54063.2979	R	6.2516	0.6490
54063.3073	I	8.4157	1.0548
54065.2898	R	6.4632	0.5639
54065.3017	I	7.8633	1.1156
54067.2846	R	4.7182	0.6819
54067.3095	I	7.5599	1.7768
54069.2721	R	4.8017	0.6418
54069.3003	I	6.6256	1.3490
54084.1452	R	1.2843	1.1876
54084.1592	I	4.6764	2.0187
Continued			

Table C.1 (Continued)

MJD	Passband	$Flux_{25}$	σ_{Flux}
54086.1507	R	0.9971	0.7202
54088.1527	R	0.8453	0.4273
54088.1724	I	4.0120	0.9620
54090.1358	R	2.1169	0.3454
54090.1486	I	3.1399	0.7365
54092.1576	R	1.4368	0.3590
54092.1777	I	2.8751	0.7044
54094.1682	R	0.6006	0.4610
54094.1885	I	2.7185	0.8460
54095.1382	R	0.8228	0.6930
54095.1406	I	1.4375	1.2806
54096.1811	R	-0.3105	1.0564
54111.1548	R	0.3683	0.6289
54112.1654	I	0.2355	1.5799
54113.1343	R	0.5299	0.4419
54114.1413	R	1.1259	0.7975
54114.1437	I	3.8699	1.4874
r195			
53994.2683	R	-0.8311	0.3686
53994.3086	I	-0.1443	0.6751
54003.2714	R	0.5336	0.6924
54003.2959	I	0.3270	0.8872
54021.3422	R	-0.9319	1.0675
54023.2669	R	-0.2998	0.7114
54023.2818	I	-0.6060	1.1947
54027.2922	R	-0.4132	0.4929
54027.3061	I	1.8721	0.9837
54031.3067	R	0.6717	0.5567
54031.3172	I	1.1770	0.9955
54037.2804	I	4.0498	1.1890
54037.2922	R	4.2501	0.7009
54039.2723	R	4.3030	1.0511
54039.3003	I	5.2110	1.9765
54053.0864	R	7.6810	0.5103
54053.1011	I	10.4670	0.6301
Continued			

Table C.1 (Continued)

MJD	Passband	$Flux_{25}$	σ_{Flux}
54059.2366	R	6.0793	0.9098
54059.2636	I	8.3681	1.5909
54063.2496	R	5.7694	0.5124
54063.2749	I	7.1699	1.4254
54065.2239	R	5.4447	0.4654
54065.2541	I	9.7916	1.0581
54067.2281	R	5.4193	0.6200
54067.2480	I	5.1297	1.1766
54069.2191	R	3.9486	1.1655
54084.1276	I	5.9753	2.6753
54088.1256	R	1.2509	0.4931
54088.1291	I	4.1915	0.8899
54090.1038	R	0.9466	0.3687
54090.1822	I	4.5500	1.2505
54092.1088	R	1.0016	0.3621
54092.1325	I	2.3978	0.6477
54094.1078	R	1.0774	0.5056
54094.1253	I	4.2729	0.9579
54096.1242	R	-0.4604	1.0135
54096.1463	I	-0.2712	1.9398
54098.1326	R	1.4085	1.4591
54098.1547	I	2.0409	2.1611
54099.0631	I	6.5140	2.2065
54111.1055	R	0.3902	0.5744
54111.1287	I	1.6134	1.0561
54113.0980	R	0.9147	0.5610
54113.1015	I	2.4878	1.0497
54114.0853	R	0.4287	0.7481
54114.0881	I	-1.0213	1.2819
	r199		
54006.3516	R	0.0792	0.4867
54006.3640	I	0.2618	0.8377
54021.3604	R	1.0541	1.1106
54023.3186	R	1.1848	0.6596
54023.3360	I	2.7764	1.1735

Continued

Table C.1 (Continued)

MJD	Passband	$Flux_{25}$	σ_{Flux}
54027.3392	I	5.8736	1.1467
54027.3601	R	4.6135	0.6562
54039.3380	R	11.1384	0.7425
54053.1436	R	9.3072	0.3274
54053.1600	I	13.2083	0.6694
54055.3057	R	6.3564	0.9941
54057.2853	I	14.0262	1.8594
54059.2930	R	6.3788	0.7640
54059.3100	I	10.5793	1.8679
54061.2945	R	5.3581	0.9614
54063.2945	R	4.5772	0.5189
54063.3014	I	8.1367	1.1452
54065.2934	R	4.2601	0.5871
54065.2969	I	6.8597	1.3039
54067.2881	R	5.3860	0.6187
54067.2916	I	8.7949	1.1944
54069.2756	R	2.7118	0.6784
54069.3061	I	7.0979	1.3559
54084.1487	R	1.1879	1.1287
54084.1650	I	4.9850	2.7751
54088.1561	R	1.3592	0.5193
54088.1784	I	4.4300	0.8055
54090.1393	R	1.2933	0.3243
54090.1545	I	2.9596	0.8198
54092.1541	R	0.7569	0.3338
54092.1836	I	4.1393	0.6910
54094.1647	R	1.1773	0.4264
54094.1949	I	3.4353	0.8222
54095.1441	R	1.7674	0.6602
54095.1464	I	3.7122	1.2387
54096.1856	R	-0.5757	1.1740
54111.1513	R	0.0112	0.5303
54112.1596	I	2.9286	1.3496
54113.1308	R	0.0705	0.4165
54114.1472	R	-0.3453	0.7590

Continued

Table C.1 (Continued)

MJD	Passband	$Flux_{25}$	σ_{Flux}
54114.1496	I	1.5041	1.7407
r200			
53994.1983	R	0.1130	0.6105
53994.2231	I	0.4710	0.7281
54003.1964	R	-0.4920	0.5318
54003.2329	I	-0.2953	1.3538
54023.2226	R	-0.8114	0.7486
54023.2379	I	0.9949	0.8113
54025.2365	R	0.8967	0.6038
54027.2403	R	0.3073	0.5669
54027.2580	I	-0.7441	0.9526
54031.2481	R	0.7537	0.5589
54031.2818	I	-1.4477	1.1244
54039.2042	R	1.4176	0.9845
54053.0355	R	8.8744	0.5062
54053.0513	I	14.9377	0.7627
54059.1885	R	16.0329	0.6858
54059.2027	I	23.6540	1.3967
54065.2002	R	17.8826	0.5438
54065.2189	I	27.4973	1.4441
54067.1991	R	18.8996	1.0469
54067.2221	I	29.1842	1.6000
54069.1804	R	18.7761	1.6033
54082.0699	R	12.5162	0.5937
r206			
53994.2053	R	0.2874	0.5305
53994.2347	I	-0.0879	0.9224
54003.2062	R	-0.2599	0.5476
54003.2437	I	-0.9020	1.4535
54023.2301	R	0.4067	0.6376
54023.2502	I	0.6947	0.9251
54025.2407	R	-0.3947	0.5182
54027.2478	R	0.9236	0.5607
54027.2696	I	0.6248	1.1954
54031.2516	R	0.8910	0.5251
Continued			

Table C.1 (Continued)

MJD	Passband	$Flux_{25}$	σ_{Flux}
54031.2880	I	0.4042	1.0398
54037.2260	R	2.1316	0.5835
54037.2448	I	2.4913	1.2490
54039.2177	R	2.9611	0.9361
54039.2401	I	2.4099	1.2818
54053.0428	R	7.2840	0.4796
54053.0629	I	8.6511	0.6468
54059.1922	R	6.1323	0.6735
54059.2074	I	8.2333	1.4607
54063.1937	R	5.9890	0.4725
54063.2122	I	8.7664	0.9566
54065.2037	R	5.9074	0.5707
54065.2077	I	7.7062	1.0516
54067.2026	R	3.5205	0.9873
54067.2061	I	6.2572	1.7135
54082.0771	R	1.4029	0.4965
54082.0901	I	4.7546	1.1866
54086.0603	R	1.1881	0.4488
54086.0731	I	1.7694	1.0254
54090.0542	R	1.1526	0.3537
54090.0651	I	3.3442	0.6493
54092.0568	R	0.0614	0.3804
54094.0580	R	1.5713	0.6128
54112.0713	R	1.4444	1.0048
54112.0756	I	-1.2126	1.3867
r207			
53994.2718	R	-0.5897	0.3348
53994.3146	I	0.6687	0.6874
54003.2749	R	-0.2633	0.4745
54003.3013	I	-0.5910	0.9370
54006.2763	I	1.1869	0.6871
54006.2822	R	0.5183	0.5245
54021.3457	R	0.3815	1.3190
54023.2706	R	-0.4446	0.5008
54023.2879	I	1.7812	1.2202
Continued			

Table C.1 (Continued)

MJD	Passband	$Flux_{25}$	σ_{Flux}
54027.2957	R	2.1117	0.4709
54027.3120	I	2.6026	1.0314
54031.3102	R	5.6716	0.4657
54031.3230	I	5.3522	1.0653
54039.2758	R	7.3789	1.2510
54053.0901	R	7.3292	0.4798
54053.1078	I	10.9465	0.6241
54059.2543	I	6.5638	1.5040
54063.2350	R	4.5323	0.4242
54063.2691	I	6.5021	1.3068
54065.2274	R	5.2021	0.4656
54065.2601	I	7.1761	1.0231
54067.2316	R	3.4509	0.5499
54067.2538	I	6.5576	1.2159
54069.2226	R	1.4899	1.1144
54069.2472	I	5.3422	1.4588
54082.1125	R	-0.1689	0.4740
54082.1431	I	3.8205	1.4936
54086.0956	R	0.7294	0.3863
54086.1270	I	2.4496	1.3450
54088.1151	R	1.4987	0.4062
54090.0847	R	1.1661	0.7358
54090.1073	I	2.3386	0.6095
54092.1127	R	0.8411	0.3665
54092.1383	I	2.8684	0.6833
54094.1113	R	0.9898	0.4394
54094.1311	I	2.6749	1.0314
54095.0989	R	1.2451	0.7980
54095.1013	I	0.4097	1.1943
54096.1207	R	-0.9427	1.1921
54098.1289	R	1.7400	1.3085
54099.0689	I	2.1716	2.6134
54111.1021	R	0.5198	0.4716
54111.1229	I	3.2101	0.9081
54113.0886	R	-0.2575	0.4742
54113.0921	I	1.9497	0.9903
		r209	
53994.2718	R	-0.9594	0.3852
53994.3146	I	-0.2408	0.6781
54003.2749	R	-0.0393	0.4171
54003.3013	I	0.3601	0.9803
54006.2763	I	-0.7048	0.7330
54006.2822	R	-0.3444	0.5600
54021.3457	R	1.1959	1.4551
54023.2706	R	0.0167	0.4165
54023.2879	I	1.1224	1.2384
54027.2957	R	-0.3032	0.5195
54027.3120	I	1.4676	1.0735
54031.3102	R	1.0685	0.4788
54031.3230	I	1.5383	1.0276
54039.2758	R	7.6908	1.2162
54053.0901	R	14.8673	0.5113
54053.1078	I	17.8347	0.6065
54059.2543	I	17.0227	1.4439
54063.2350	R	10.9189	0.4705
54063.2691	I	17.2788	1.3957
54065.2274	R	9.1589	0.5178
54065.2601	I	12.4942	1.1709
54067.2316	R	8.8014	0.6270
54067.2538	I	11.1276	1.3552
54069.2226	R	7.2423	1.2284
54069.2472	I	12.4367	1.6053
54082.1125	R	2.8582	0.5993
54082.1431	I	8.1237	1.4153
54086.0956	R	2.0280	0.4934
54086.1270	I	5.1425	1.2406
54088.1151	R	1.8687	0.4254
54090.0847	R	2.6885	0.3864
54090.1073	I	5.3647	0.5916
54092.1127	R	2.3109	0.3764

Continued

Table C.1 (Continued)

MJD	Passband	$Flux_{25}$	σ_{Flux}
54092.1383	I	5.7634	0.6291
54094.1113	R	1.8264	0.4857
54094.1311	I	4.4475	0.8774
54095.0989	R	1.0991	0.7999
54095.1013	I	3.6348	1.1565
54096.1207	R	1.0691	1.1854
54098.1289	R	0.6927	1.3672
54099.0689	I	7.7265	2.3706
54111.1021	R	0.9665	0.5156
54111.1229	I	3.4568	1.0089
54113.0886	R	0.8761	0.6786
54113.0921	I	2.5175	1.1760
r212			
53994.2683	R	0.5749	0.3921
53994.3086	I	-0.0623	0.7105
54003.2714	R	-0.9341	0.6662
54003.2959	I	-0.2078	0.7982
54021.3422	R	0.6093	1.1124
54023.2669	R	0.6548	0.6109
54023.2818	I	0.1087	1.1467
54027.2922	R	-0.0238	0.4876
54027.3061	I	0.6997	0.9204
54031.3067	R	0.2970	0.5055
54031.3172	I	0.7560	1.0341
54037.2804	I	0.9677	1.1725
54037.2922	R	1.6224	0.6172
54039.2723	R	2.8367	0.9288
54039.3003	I	0.9960	1.8224
54053.0864	R	5.1217	0.5414
54053.1011	I	7.6663	0.6400
54059.2366	R	6.7815	1.0297
54059.2636	I	10.4466	1.6446
54063.2496	R	4.8599	0.5009
54063.2749	I	5.5599	1.3048
54065.2239	R	4.0274	0.5779
Continued			

Table C.1 (Continued)

MJD	Passband	$Flux_{25}$	σ_{Flux}
54065.2541	I	6.2150	1.0433
54067.2281	R	3.3832	0.6501
54067.2480	I	4.6301	1.1937
54069.2191	R	2.9693	1.2019
54084.1063	R	1.3826	1.8669
54084.1276	I	0.5525	2.5929
54088.1256	R	-0.1549	0.5337
54088.1291	I	2.2339	0.9274
54090.1038	R	0.6777	0.3462
54090.1822	I	-1.0174	1.3230
54092.1088	R	0.7162	0.3639
54092.1325	I	1.7856	0.6438
54094.1078	R	0.6810	0.5334
54094.1253	I	0.4643	0.9284
54096.1242	R	0.6212	1.0596
54096.1463	I	-2.0332	2.0208
54098.1326	R	2.7711	1.3244
54099.0608	R	-1.5043	1.9314
54099.0631	I	2.2208	2.3352
54111.1055	R	0.2529	0.7244
54111.1287	I	1.0649	1.2573
54113.0980	R	-0.2727	0.5642
54113.1015	I	1.1204	1.1982
54114.0853	R	0.5491	0.7100
54114.0881	I	1.5219	1.4076
r213			
53992.3150	R	-1.1759	1.2848
53994.2946	R	-0.4972	0.4068
53994.3263	I	-0.2743	0.9804
54003.2819	R	-1.2218	0.6402
54003.3205	I	-2.5929	1.1541
54006.3130	R	-1.2565	0.5077
54006.3291	I	-0.9446	0.9850
54021.3528	R	-1.7831	1.2516
54023.2781	R	-1.3290	0.6303
Continued			

Table C.1 (Continued)

MJD	Passband	$Flux_{25}$	σ_{Flux}
54023.3001	I	-1.6513	1.2537
54025.2827	R	-2.8468	0.7213
54027.3027	R	-0.8225	0.5764
54027.3236	I	-1.6563	1.3757
54039.2863	R	-0.7473	1.0140
54053.0972	R	13.0408	0.4370
54053.1196	I	15.7815	0.6604
54057.2382	R	16.5275	1.3118
54059.2331	R	19.2093	0.9556
54059.2694	I	22.9404	1.8859
54063.2462	R	20.7392	0.5580
54063.2807	I	25.3810	1.4657
54065.2309	R	21.5866	0.5862
54065.2678	I	25.1205	1.4026
54067.2351	R	20.2249	0.6956
54067.2598	I	28.2923	1.2597
54069.2296	R	15.1318	1.2136
54069.2649	I	28.2253	1.7459
54082.1159	R	10.7746	0.6579
54082.1376	I	14.9092	1.3531
54086.0991	R	8.6382	0.5328
54086.1212	I	13.9611	1.0701
54088.1221	R	6.8366	0.4852
54090.0885	R	7.4820	0.4410
54090.1252	I	13.5064	0.8069
54092.1162	R	6.7265	0.4255
54092.1441	I	13.4718	0.7642
54094.1148	R	6.0977	0.5268
54094.1369	I	12.9039	0.8910
54096.1277	R	6.3347	1.2837
54096.1405	I	11.7541	2.0541
54098.1396	R	2.4582	1.4832
54098.1431	I	8.8173	2.4426
54111.1092	R	1.7942	0.6483
54111.1350	I	8.4977	1.2614

Continued

Table C.1 (Continued)

MJD	Passband	$Flux_{25}$	σ_{Flux}
54113.1116	R	1.2395	0.5885
54113.1151	I	4.8677	0.9369
54114.0979	R	0.1093	1.1729
54114.1002	I	5.3217	1.6902
	r225		
53992.3259	R	1.2505	1.2152
53994.3050	R	-0.6404	0.3727
53994.3441	I	-0.3328	1.0594
54003.2925	R	0.1124	0.5587
54003.3365	I	-0.0567	1.4098
54006.3250	R	0.5878	0.4528
54006.3458	I	-0.0081	0.7893
54021.2759	R	1.0958	1.1275
54023.3667	R	-0.7733	1.1177
54025.2791	R	-0.9461	0.7011
54029.2969	R	0.6186	0.5612
54029.3286	I	0.8530	1.0901
54033.3110	I	8.3262	3.2849
54039.2968	R	3.3016	0.9741
54051.1035	R	5.7974	0.5642
54051.1249	I	7.8867	1.1245
54055.2231	R	5.2333	0.8103
54055.2371	I	10.0802	1.5382
54059.2191	R	4.6408	0.7760
54059.2447	R	5.6716	0.8157
54059.2496	I	9.6600	1.4643
54063.2315	R	4.4634	0.4594
54063.2632	I	8.5985	1.2892
54065.2459	R	4.1565	0.5214
54065.2494	I	9.6477	1.1678
54069.2437	R	4.4166	1.1583
54082.1230	R	1.7224	0.6512
54082.1265	I	2.3728	1.0275
54086.1061	R	1.1513	0.4418
54086.1096	I	4.4620	0.9168

Continued

Table C.1 (Continued)

MJD	Passband	$Flux_{25}$	σ_{Flux}
54088.1186	R	0.4265	0.4157
54090.0965	R	1.5560	0.4167
54090.1133	I	2.5863	0.6760
54092.1232	R	0.8348	0.3861
54092.1267	I	1.9072	0.6936
54094.1218	R	1.9003	0.4739
54094.1490	I	2.4000	0.7200
54095.1164	R	-0.8543	0.7427
54095.1187	I	1.3134	1.2682
54096.1067	R	0.0931	1.2063
54096.1347	I	1.4167	1.6036
54098.1137	R	1.5071	1.5824
54098.1489	I	-2.4690	2.3415
54111.0980	R	-1.0875	0.5159
54111.1171	I	1.7252	0.7670
54114.0759	R	1.3257	0.4883
54114.0794	I	1.5759	0.9765
r230			
54006.3516	R	0.2279	0.4705
54006.3640	I	1.2944	0.7925
54021.3604	R	-0.4284	1.0701
54023.3186	R	-0.1324	0.6806
54023.3360	I	0.6790	1.0774
54027.3392	I	1.3254	1.1582
54027.3601	R	-0.7651	0.6490
54039.3380	R	0.1040	0.7640
54053.1436	R	2.4520	0.3636
54053.1600	I	4.3952	0.6591
54055.3057	R	5.6204	1.0292
54057.2853	I	16.9571	1.8324
54059.2930	R	16.9800	0.8302
54059.3100	I	21.9113	1.5438
54061.2945	R	21.9418	0.9653
54063.2945	R	27.0482	0.5792
54063.3014	I	29.7073	1.1842

Continued

Table C.1 (Continued)

MJD	Passband	$Flux_{25}$	σ_{Flux}
54065.2934	R	29.5492	0.6419
54065.2969	I	33.2711	1.3084
54067.2881	R	34.0426	0.6558
54067.2916	I	40.4794	1.2453
54069.2756	R	35.1202	0.7392
54069.3061	I	39.9617	1.3211
54084.1487	R	25.0951	1.1650
54084.1650	I	26.9503	2.7095
54088.1561	R	21.0423	0.5837
54088.1784	I	25.0883	0.8540
54090.1393	R	20.4961	0.3745
54090.1545	I	21.4026	0.7948
54092.1541	R	18.0048	0.3777
54092.1836	I	22.1188	0.7363
54094.1949	I	21.1857	0.8159
54095.1441	R	15.9609	0.7172
54095.1464	I	16.9924	1.2680
54096.1856	R	15.1794	1.1743
54111.1513	R	7.7124	0.6119
54112.1596	I	13.2728	1.4427
54113.1308	R	6.4936	0.4495
54114.1472	R	5.8762	0.8480
54114.1496	I	9.3921	1.8117
r311			
53994.2161	R	0.1296	0.4749
53994.2523	I	1.1459	0.5714
54003.2237	R	-0.2234	0.6735
54003.2607	I	-0.2329	1.0172
54021.2340	R	0.5377	0.9555
54021.2533	I	0.6846	1.6409
54025.2295	R	0.3110	0.7452
54029.2432	R	-0.3885	0.7380
54029.2618	I	-0.3812	0.8689
54033.2236	R	-1.9778	1.7792
54039.2133	R	2.1914	0.9194

Continued

Table C.1 (Continued)

MJD	Passband	$Flux_{25}$	σ_{Flux}
54051.0518	R	3.2645	0.6585
54051.0709	I	6.4484	1.3110
54055.1964	R	2.2161	0.8157
54055.2134	I	4.1935	2.0144
54059.1992	R	3.2814	0.7300
54059.2155	I	6.3683	2.3187
54063.1972	R	3.1966	0.4729
54063.2180	I	8.3937	0.9639
54065.1965	R	2.3725	0.5805
54065.2127	I	6.6848	1.0692
54067.1956	R	1.4745	0.9874
54067.2119	I	3.3752	1.6563
54069.2014	R	2.4812	1.5157
54069.2085	I	5.3885	2.1213
54084.0670	R	1.6225	0.9356
54084.0864	I	0.2158	1.6452
54088.0722	R	1.0444	0.5101
54088.0973	I	2.6282	1.0844
54092.0491	R	1.0783	0.3662
54094.0509	R	-0.2851	0.6289
54094.0803	I	1.6075	0.8931
54096.0608	R	-0.7409	1.0882
54098.0716	R	0.9838	1.7179
54098.0751	I	4.0482	2.1700
54099.0334	R	-1.5949	2.0866
54111.0543	R	0.5336	0.6071
54111.0920	I	1.0091	1.4076
54113.0546	R	0.2674	0.5401
54113.0582	I	0.4219	0.9466
r317			
53994.1983	R	0.7561	0.6562
53994.2231	I	-0.5432	0.6298
54003.1964	R	-0.3559	0.4745
54003.2329	I	1.2836	1.2905
54023.2226	R	0.4838	0.7338
54023.2379	I	-0.0480	0.7925
54025.2365	R	0.9051	0.5446
54027.2403	R	0.1818	0.5727
54027.2580	I	0.9855	0.9478
54031.2481	R	0.6038	0.5800
54031.2818	I	-1.0609	1.0177
54039.2042	R	0.2909	1.0777
54053.0355	R	3.8294	0.5050
54053.0513	I	4.9678	0.7206
54059.1885	R	3.9607	0.6702
54059.2027	I	3.3644	1.3260
54065.2002	R	4.3920	0.5171
54065.2189	I	6.8380	1.2524
54067.1991	R	3.6155	1.0674
54067.2221	I	9.1571	1.4701
54069.1804	R	3.5705	1.5415
54082.0699	R	2.6658	0.6293
54082.1012	I	5.3434	1.1672
54086.0533	R	1.6046	0.5331
54086.0847	I	4.9931	1.1197
54092.0455	R	1.0895	0.3888
54094.0474	R	1.5514	0.6256
54094.0687	I	2.4199	0.7753
54095.0757	R	0.3795	1.0338
54095.0787	I	1.3404	1.3668
54096.0726	R	1.7494	1.1577
54111.0676	R	0.5538	0.6491
54111.0714	I	2.9560	1.0489
54113.0649	R	-0.2666	0.4883
54113.0684	I	1.2963	0.9834
54114.0462	R	-0.2961	0.7517
54114.0485	I	2.0496	1.1859
r318			
53994.2718	R	0.1910	0.3806
53994.3146	I	0.6300	0.6803

Continued

Continued

Table C.1 (Continued)

MJD	Passband	$Flux_{25}$	σ_{Flux}
54003.2749	R	-2.0210	0.5840
54003.3013	I	-1.0320	0.9908
54006.2763	I	-0.7797	0.7158
54006.2822	R	-0.3128	0.5240
54021.3457	R	0.2982	1.3233
54023.2706	R	-1.0604	0.5201
54023.2879	I	1.4966	1.3066
54027.2957	R	0.0682	0.5159
54027.3120	I	-0.7124	0.9336
54031.3102	R	0.6698	0.4764
54031.3230	I	0.7245	1.0202
54039.2758	R	0.0100	1.2405
54053.0901	R	0.6805	0.4406
54053.1078	I	0.1971	0.6328
54059.2543	I	8.2707	1.5267
54063.2350	R	20.9074	0.4549
54063.2691	I	22.2893	1.4140
54065.2274	R	30.1657	0.5026
54065.2601	I	33.8308	1.1037
54067.2316	R	38.5123	0.6586
54067.2538	I	42.1429	1.2100
54069.2226	R	44.7392	1.0796
54069.2472	I	48.7203	1.4672
54082.1125	R	77.1276	0.7307
54082.1431	I	80.4492	1.6192
54086.0956	R	77.5942	0.5462
54086.1270	I	80.1727	1.3557
54088.1151	R	76.1893	0.5319
54090.0847	R	73.4805	0.4268
54090.1073	I	78.0088	0.6734
54092.1127	R	70.6002	0.4154
54092.1383	I	77.8118	0.6936
54094.1113	R	67.0729	0.5476
54094.1311	I	76.6345	1.0124
54095.0989	R	62.0539	0.8498

Continued

Table C.1 (Continued)

MJD	Passband	$Flux_{25}$	σ_{Flux}
54095.1013	I	69.8425	1.1689
54096.1207	R	68.1151	1.3918
54098.1289	R	56.6629	1.3648
54099.0689	I	63.2552	2.5765
54111.1021	R	42.2464	0.5599
54111.1229	I	59.4189	0.9862
54113.0886	R	39.4428	0.7956
54113.0921	I	57.2161	1.0568
	r322		
53992.3259	R	-0.0531	1.1915
53994.3050	R	-0.6162	0.3646
53994.3441	I	0.3664	1.1440
54003.2925	R	0.1311	0.6045
54003.3365	I	0.3087	1.3351
54006.3250	R	-0.0611	0.4925
54006.3458	I	2.6397	0.8655
54021.2759	R	-0.0674	1.0437
54023.3667	R	-1.4103	1.0778
54025.2791	R	-0.7440	0.6149
54029.2969	R	0.3477	0.5718
54029.3286	I	-0.6371	1.1156
54033.3110	I	-1.4748	3.3200
54039.2968	R	-0.6055	1.0623
54051.1035	R	0.1809	0.5794
54051.1249	I	0.4701	1.1785
54055.2231	R	1.9271	0.7397
54055.2371	I	2.2715	1.5317
54059.2191	R	3.3696	0.8430
54059.2447	R	3.8884	0.8389
54059.2496	I	4.4981	1.5719
54063.2315	R	5.9423	0.4459
54063.2632	I	5.7487	1.2357
54065.2459	R	7.1043	0.5410
54065.2494	I	6.8670	1.1785
54069.2437	R	8.8355	1.1239

Continued

Table C.1 (Continued)

MJD	Passband	$Flux_{25}$	σ_{Flux}
54082.1230	R	10.9426	0.6538
54082.1265	I	12.6070	1.0044
54086.1061	R	9.7675	0.4391
54086.1096	I	10.6192	0.9945
54088.1186	R	9.9529	0.4692
54090.0965	R	7.8840	0.4190
54090.1133	I	11.3339	0.6183
54092.1232	R	6.8957	0.3690
54092.1267	I	9.5869	0.6830
54094.1218	R	6.4693	0.4412
54094.1490	I	9.5001	0.7366
54095.1164	R	6.2694	0.8181
54095.1187	I	8.0407	1.2645
54096.1067	R	6.5050	1.1424
54096.1347	I	5.6220	1.6646
54098.1137	R	5.1658	1.4369
54098.1489	I	9.9593	2.2545
54111.0980	R	2.1371	0.5217
54111.1171	I	4.5113	0.8101
54114.0759	R	1.9479	0.4562
54114.0794	I	5.6995	1.0360
s340			
53994.2018	R	-0.1386	0.5250
53994.2289	I	1.2779	0.7055
54003.1999	R	0.1653	0.4671
54003.2384	I	0.7969	1.2514
54023.2263	R	-1.0800	0.8376
54023.2442	I	-0.8098	1.0174
54027.2440	R	-0.6941	0.5975
54027.2638	I	-0.2681	0.9322
54031.2268	R	-0.6260	0.5106
54031.2586	I	-2.4009	1.0715
54039.2098	R	-1.3138	0.8561
54053.0393	R	3.6948	0.4442
54053.0571	I	4.5353	0.6176
Continued			

Table C.1 (Continued)

MJD	Passband	$Flux_{25}$	σ_{Flux}
54069.1839	R	9.7054	1.6546
54082.0736	R	7.0223	0.5747
54082.0956	I	10.4576	1.2483
54086.0568	R	5.8609	0.4694
54086.0789	I	7.8573	1.3225
54090.0505	R	5.1306	0.3790
54090.0710	I	7.9092	0.7072
54092.0526	R	4.2658	0.3664
54094.0545	R	4.0733	0.5680
54094.0745	I	7.3669	0.9455
54095.0692	R	5.4404	0.8905
54095.0715	I	7.0115	1.2125
54096.0879	I	5.4874	1.9229
54096.0937	R	0.7812	1.9106
54098.0484	R	5.1004	1.7733
54098.0523	I	3.6027	2.1137
54109.0530	R	4.2642	2.2030
54109.0691	R	4.6241	1.8505
54111.0791	I	4.6179	1.2347
54112.0454	R	5.0270	1.7556
54112.0477	R	1.4609	0.9608
54112.0514	I	6.1598	1.7363
54114.0525	R	1.8038	0.6691
54114.0550	I	1.9909	1.1314
s346			
53992.3002	R	-1.3770	1.4081
54003.2272	R	-1.1865	0.8036
54003.2659	I	-0.1556	0.9787
54021.2382	R	0.3623	1.2363
54021.2591	I	-2.9726	2.1085
54025.2330	R	0.7746	0.4862
54025.2623	I	-3.0921	1.9680
54029.2467	R	0.7672	0.5304
54029.2677	I	0.5529	0.5597
54031.2309	R	-0.1585	0.7162
Continued			

Table C.1 (Continued)

MJD	Passband	$Flux_{25}$	σ_{Flux}
54031.2644	I	0.7236	0.9958
54033.2276	R	-2.2755	1.2244
54037.2410	R	-0.8778	0.9296
54037.2682	I	1.4994	1.3074
54039.2320	R	-0.2781	1.4388
54039.2517	I	-1.1607	1.6463
54051.0555	R	-1.9502	0.7806
54051.0767	I	2.0065	1.3665
54055.1929	R	2.0843	1.0539
54055.2088	I	2.0970	2.1730
54069.2049	R	16.5249	2.0321
54084.0713	R	18.6607	1.3135
54084.0922	I	20.9085	1.7907
54088.0757	R	16.8110	0.7787
54088.0792	I	21.7657	1.2124
54090.0615	R	15.6600	0.5938
54094.0652	R	11.5352	0.7127
54094.0922	I	14.5490	1.4025
54096.0526	R	10.5742	1.1855
54096.0819	I	13.8379	1.6178
54098.0581	I	7.3040	1.8129
54099.0418	I	6.4944	2.3678
54111.0506	R	5.4274	0.8593
54111.0853	I	9.9125	1.3295
54113.0453	R	4.6005	0.9119
54113.0488	I	10.1881	1.2612
s347			
54096.0761	I	29.4501	2.0626
54098.0391	I	25.2748	1.9475
54098.0449	R	24.4969	0.8598
54112.0580	R	23.6962	1.2895
54114.0587	R	23.8391	0.9543
54114.0615	I	20.9255	1.3577
53992.2930	R	0.3017	0.4589
53994.2126	R	0.4169	0.6916
Continued			

Table C.1 (Continued)

MJD	Passband	$Flux_{25}$	σ_{Flux}
53994.2465	I	-0.0686	0.7571
54003.2200	R	-0.2448	0.6041
54003.2546	I	0.2518	1.6898
54006.2473	R	-0.6500	0.6208
54006.2508	I	1.3554	0.7028
54021.2260	R	0.3286	0.5365
54021.2417	I	0.5317	1.5962
54025.2216	R	-0.0253	0.8636
54025.2447	I	-0.6511	0.8454
54029.2328	R	-0.4704	0.8281
54029.2502	I	-2.4083	1.0279
54031.2409	R	0.6782	0.6335
54031.2702	I	1.3087	1.1451
54033.2158	R	0.8968	0.5681
54033.2418	I	0.0361	2.0658
54037.2333	R	0.3158	0.8639
54037.2564	I	-0.7724	1.6316
54039.2248	R	-0.1935	0.7012
54039.2459	I	0.0390	1.3664
54051.0400	R	0.0073	0.8100
54051.0591	I	-0.3646	1.1540
54055.1888	R	0.2525	0.6606
54055.2041	I	1.9883	1.5831
54069.1944	R	0.2620	0.7595
54084.0600	R	5.4566	1.2969
54084.0748	I	13.8413	1.5838
54088.0645	R	12.7420	0.7599
54088.0854	I	21.0671	1.1349
54090.0577	R	17.5387	0.4833
54094.0617	R	20.5820	0.3890
54094.0862	I	30.4801	0.9703
54095.0822	R	24.8923	0.5466
54095.0846	I	28.3566	1.6300
54096.0491	R	24.5566	0.8601
s349			
Continued			

Table C.1 (Continued)

MJD	Passband	$Flux_{25}$	σ_{Flux}
53992.2930	R	-0.0788	1.2391
53994.2126	R	0.0612	0.6417
53994.2465	I	1.2974	0.8430
54003.2200	R	-1.6467	0.9257
54003.2546	I	2.0456	1.7000
54006.2473	R	-0.2980	0.5441
54006.2508	I	1.0746	0.9477
54021.2260	R	0.4135	0.9758
54021.2417	I	1.0289	1.6490
54025.2216	R	-1.0708	1.0567
54025.2447	I	1.3950	0.9179
54029.2328	R	1.4021	0.7040
54029.2502	I	0.1924	1.1787
54031.2409	R	0.1054	0.6453
54031.2702	I	-0.3645	1.0685
54033.2158	R	-2.3138	1.7719
54033.2418	I	-3.6569	2.0207
54037.2333	R	-0.1111	0.6790
54037.2564	I	0.3917	1.4671
54039.2248	R	-1.2416	0.9925
54039.2459	I	1.0195	1.6160
54051.0400	R	-0.3005	0.4819
54051.0591	I	-0.7509	1.2724
54055.1888	R	-0.1719	0.8152
54055.2041	I	-0.1242	1.5978
54069.1944	R	2.0332	1.9796
54084.0600	R	23.4410	1.3021
54084.0748	I	31.2300	1.8330
54088.0645	R	25.7879	0.5480
54088.0854	I	31.0226	1.0354
54090.0577	R	22.7614	0.4394
54094.0617	R	20.7223	0.6165
54094.0862	I	25.1721	1.0027
54095.0822	R	19.9431	0.9887
54095.0846	I	18.2027	1.6996
54096.0491	R	18.3156	0.9012
54096.0761	I	23.9099	2.1162
54098.0391	I	13.5218	2.4054
54098.0449	R	16.5637	1.6961
54112.0580	R	10.2054	0.9003
54114.0587	R	6.1766	0.7937
54114.0615	I	13.8915	1.5620
		s350	
53994.2718	R	-0.1517	0.2864
53994.3146	I	0.3969	0.4321
54003.2749	R	0.4586	0.6514
54003.3013	I	-0.4483	0.9179
54006.2763	I	-0.4171	0.7484
54006.2822	R	-0.1658	0.5416
54021.3457	R	-0.2113	1.2634
54023.2706	R	-0.5219	0.5000
54023.2879	I	-1.9397	1.2733
54027.2957	R	0.1098	0.4610
54027.3120	I	0.7439	0.9662
54031.3102	R	0.4093	0.4819
54031.3230	I	0.1245	1.0652
54039.2758	R	-0.8018	1.2746
54053.0901	R	-0.3135	0.4189
54053.1078	I	0.0989	0.6414
54059.2543	I	-2.1157	1.5459
54063.2350	R	-0.0533	0.4225
54063.2691	I	-0.9987	1.3128
54065.2274	R	-0.0168	0.4687
54065.2601	I	-1.6122	1.0713
54067.2316	R	0.7034	0.5873
54067.2538	I	-1.7735	1.2561
54069.2226	R	-0.4771	1.0082
54069.2472	I	-0.8771	1.4746
54082.1125	R	1.9242	0.6397
54082.1431	I	8.0030	1.4128

Continued

Continued

Table C.1 (Continued)

MJD	Passband	$Flux_{25}$	σ_{Flux}
54086.0956	R	4.9155	0.4297
54086.1270	I	5.2100	1.2859
54088.1151	R	4.3767	0.3975
54090.0847	R	4.7425	0.3629
54090.1073	I	6.3624	0.5739
54092.1127	R	5.1944	0.3687
54092.1383	I	7.3451	0.6628
54094.1113	R	4.7276	0.4758
54094.1311	I	8.3137	0.9359
54095.0989	R	5.3728	0.8008
54095.1013	I	7.1069	1.0673
54096.1207	R	6.9760	1.2621
54098.1289	R	4.2239	1.6067
54099.0666	R	3.8671	1.9080
54099.0689	I	4.7482	2.6759
54111.1021	R	2.6190	0.4768
54111.1229	I	4.0709	0.8827
54113.0886	R	2.8179	0.6920
54113.0921	I	3.2711	0.9640
s351			
53992.3150	R	-0.9656	1.2020
53994.2946	R	-0.1325	0.2230
53994.3263	I	0.2584	0.3246
54003.2819	R	-0.8633	0.6056
54003.3205	I	-2.3667	1.1692
54006.3130	R	-0.6543	0.5337
54006.3291	I	-0.8573	0.8628
54021.3528	R	-0.4662	1.0071
54023.2781	R	0.0416	0.5276
54023.3001	I	0.8850	1.1709
54025.2827	R	0.0026	0.4742
54027.3027	R	-0.0045	0.4837
54027.3236	I	0.1531	1.0313
54039.2863	R	-0.7709	0.7988
54053.0972	R	-0.3516	0.4188

Continued

Table C.1 (Continued)

MJD	Passband	$Flux_{25}$	σ_{Flux}
54053.1196	I	0.2165	0.5616
54057.2382	R	0.6010	1.1153
54059.2331	R	0.7110	1.0122
54059.2694	I	-2.1542	1.8170
54063.2462	R	-0.7769	0.4394
54063.2807	I	-0.6438	1.1380
54065.2309	R	-0.1795	0.5383
54065.2678	I	0.5891	1.1148
54067.2351	R	1.0077	0.6189
54067.2598	I	1.7505	1.1398
54069.2296	R	0.7588	0.9454
54069.2649	I	3.0460	1.3988
54082.1159	R	3.4196	0.5739
54082.1376	I	6.3161	1.0690
54086.0991	R	2.6258	0.4520
54086.1212	I	4.1570	0.9549
54088.1221	R	2.6634	0.5154
54090.0885	R	2.5211	0.3701
54090.1252	I	4.5330	0.6907
54092.1162	R	3.1853	0.3614
54092.1441	I	5.8119	0.6649
54094.1148	R	2.2950	0.4567
54094.1369	I	3.8500	0.8313
54096.1277	R	2.9295	1.3078
54096.1405	I	3.9893	1.8423
54098.1396	R	1.5051	1.2512
54098.1431	I	2.3050	2.4426
54099.0748	I	4.3059	2.1528
54111.1092	R	0.6399	0.5847
54111.1350	I	2.7628	1.1891
54113.1116	R	1.1364	0.5458
54113.1151	I	1.4178	0.9060
54114.0979	R	1.4948	1.0290
54114.1002	I	1.4564	1.3794
s353			

Continued

Table C.1 (Continued)

MJD	Passband	$Flux_{25}$	σ_{Flux}
53994.3763	R	-0.3855	0.5339
54003.3524	R	-2.6376	0.7225
54003.3824	I	-1.8598	1.4422
54006.3841	R	-0.0416	0.4591
54021.3180	I	-1.2765	1.5300
54023.3709	R	-0.9120	1.0514
54025.3182	R	0.6250	0.9109
54029.3347	I	0.1747	0.9349
54029.3583	R	0.2662	0.5281
54039.3310	R	1.5504	0.9145
54051.1441	R	-0.2826	0.4816
54051.1597	I	-0.2299	1.1191
54055.2606	R	-0.0295	0.8427
54055.2754	I	0.0271	1.8433
54065.3080	R	0.1428	0.6211
54065.3218	I	3.6829	1.5984
54067.2772	R	0.7244	0.6892
54067.2974	I	3.3044	1.3504
54069.2861	R	1.9525	0.7678
54082.1487	R	4.7622	0.7876
54082.1805	I	7.8686	1.0920
54086.1354	R	4.3503	0.5483
54086.1771	I	14.0734	1.3727
54088.1847	R	3.9577	0.4718
54088.1882	I	7.4625	1.0071
54090.1316	R	4.4607	0.3715
54090.1428	I	6.5312	0.6805
54092.1503	R	3.6574	0.3579
54092.1718	I	6.3906	0.6925
54094.1612	R	3.3126	0.5004
54094.1826	I	6.4792	0.8652
54095.1677	R	2.5882	0.5988
54095.1701	I	3.2594	1.3273
54098.1606	I	9.0885	3.2713
54098.1664	R	0.3870	1.5319
54099.1526	I	11.3859	3.2431
54109.1355	R	-0.6147	1.2482
54114.1265	R	1.5992	0.5950
54114.1306	I	3.6060	1.1022

Continued

Table C.1 (Continued)

MJD	Passband	$Flux_{25}$	σ_{Flux}
	s354		
53992.3259	R	-1.9849	1.2821
53994.3050	R	0.3138	0.3420
53994.3441	I	-0.2546	0.8229
54003.2925	R	0.1613	0.5409
54003.3365	I	-1.7390	1.1009
54006.3250	R	-0.0279	0.4932
54006.3458	I	0.7177	0.7955
54021.2759	R	-0.8746	0.8623
54021.2976	I	0.8446	1.9392
54023.3667	R	-0.4530	1.1057
54025.2791	R	-0.0714	0.5980
54029.2969	R	-0.1505	0.5139
54029.3286	I	-0.6434	1.0098
54033.3110	I	3.8473	2.6723
54039.2968	R	-0.3801	1.0332
54051.1035	R	0.1586	0.6051
54051.1249	I	0.2637	1.0444
54055.2231	R	-0.2305	0.7053
54055.2371	I	-1.7766	1.5854
54059.2191	R	0.7347	0.7925
54059.2447	R	-0.7608	0.7309
54059.2496	I	-1.1143	1.4626
54063.2315	R	1.0357	0.4244
54063.2632	I	1.1446	1.1287
54065.2459	R	3.3101	0.4878
54065.2494	I	2.4327	1.0405
54069.2437	R	2.7689	1.0075
54082.1230	R	4.6735	0.6191
54082.1265	I	4.2105	0.9655
54086.1061	R	6.5356	0.4311

Continued

Table C.1 (Continued)

MJD	Passband	$Flux_{25}$	σ_{Flux}
54086.1096	I	7.2651	0.9337
54088.1186	R	6.4432	0.5055
54090.0965	R	5.7124	0.3872
54090.1133	I	6.9350	0.6104
54092.1232	R	5.9117	0.3439
54092.1267	I	7.7329	0.6467
54094.1218	R	5.4427	0.4644
54094.1490	I	5.7865	0.7095
54095.1164	R	6.0548	0.7537
54095.1187	I	7.7074	1.1616
54096.1067	R	7.0347	1.0693
54096.1347	I	7.1755	1.6240
54098.1489	I	2.6325	2.7648
54111.0980	R	3.0159	0.4592
54111.1171	I	6.2545	0.7480
54114.0759	R	2.2517	0.4132
54114.0794	I	4.4221	1.0009
s355			
53992.3259	R	-0.8355	1.2699
53994.3050	R	0.1402	0.3454
53994.3441	I	0.5759	1.0018
54003.2925	R	-0.0979	0.6071
54003.3365	I	0.6198	1.2540
54006.3250	R	0.1125	0.4710
54006.3458	I	-0.2866	0.7823
54021.2759	R	-0.2707	0.9908
54021.2976	I	-2.7657	2.0298
54023.3667	R	0.5656	1.0048
54025.2791	R	0.6555	0.6264
54025.3049	I	-1.9228	4.8019
54029.2969	R	-0.1133	0.5345
54029.3286	I	-0.1009	1.0737
54033.3110	I	6.1455	2.9037
54039.2968	R	-0.6054	1.0299
54051.1035	R	0.6612	0.5648

Continued

Table C.1 (Continued)

MJD	Passband	$Flux_{25}$	σ_{Flux}
54051.1249	I	0.7918	0.9166
54055.2231	R	1.8545	0.8103
54055.2371	I	0.4593	1.4748
54059.2191	R	0.9110	0.8640
54059.2447	R	0.0440	0.7770
54059.2496	I	0.4640	1.3870
54063.2315	R	0.5392	0.4308
54063.2632	I	-0.8863	1.1082
54065.2459	R	-0.6715	0.4805
54065.2494	I	1.4580	1.0031
54069.2437	R	0.3938	1.0088
54082.1230	R	4.7331	0.5760
54082.1265	I	6.4417	1.0076
54086.1061	R	4.6032	0.4232
54086.1096	I	6.0850	0.8892
54088.1186	R	5.3018	0.4585
54090.0965	R	4.0817	0.3762
54090.1133	I	6.3527	0.6130
54092.1232	R	4.7679	0.3320
54092.1267	I	6.1173	0.5755
54094.1218	R	4.7392	0.4262
54094.1490	I	5.9490	0.6519
54095.1164	R	3.1953	0.7150
54095.1187	I	6.0812	1.1811
54096.1067	R	2.9784	1.0844
54096.1347	I	8.2783	1.5927
54098.1489	I	9.2450	2.7190
54111.0980	R	0.9912	0.4313
54111.1171	I	5.1545	0.6920
54114.0759	R	0.7010	0.4480
54114.0794	I	4.0233	0.9498
s370			
53994.3567	R	0.7273	1.3192
53994.3971	I	0.5616	1.0574
54003.3455	R	-0.5528	0.6617

Continued

Table C.1 (Continued)

MJD	Passband	$Flux_{25}$	σ_{Flux}
54003.3719	I	-0.9297	1.6976
54006.3807	R	1.5143	2.1883
54021.3643	R	-0.8738	1.2743
54023.3222	R	1.7498	0.7726
54027.3636	R	0.4697	0.7965
54031.3643	R	0.2195	0.8038
54039.3201	R	2.1366	0.9562
54057.2725	R	1.1841	1.1093
54057.2912	I	0.1701	2.0093
54069.2791	R	-0.1110	0.6633
54084.1522	R	9.6925	1.1771
54084.1708	I	5.6872	2.1459
54088.1596	R	11.5820	0.5494
54092.1611	R	13.6420	0.3980
54092.1655	I	15.2380	0.8960
54094.1732	R	14.5148	0.4842
54094.1767	I	15.1739	0.8623
54095.1558	R	13.1332	0.7861
54095.1581	I	15.7084	1.1281
54096.1741	R	15.6696	0.9768
54098.1816	R	12.6070	2.2535
54099.1376	R	11.2242	2.6799
54099.1400	I	15.8023	1.8664
54111.1590	R	9.3580	0.6535
54111.1634	I	13.1133	1.3948
54113.1382	R	8.0621	0.5318
54113.1417	I	13.2942	1.0849
	s372		
53994.2718	R	1.1412	0.3985
53994.3146	I	0.2703	0.6514
54003.2749	R	-0.1259	0.5763
54003.3013	I	-0.5737	1.0258
54006.2763	I	-0.7816	0.7545
54006.2822	R	0.0939	0.4819
54021.3457	R	0.5851	1.3656

Continued

Table C.1 (Continued)

MJD	Passband	$Flux_{25}$	σ_{Flux}
54023.2706	R	-0.5942	0.5417
54023.2879	I	-1.9535	1.4246
54027.2957	R	0.6669	0.5583
54027.3120	I	-2.3670	1.1728
54031.3102	R	-0.4831	0.4865
54031.3230	I	-1.0272	1.1351
54039.2758	R	-0.5427	1.3020
54053.0901	R	0.2030	0.4457
54053.1078	I	-0.6796	0.6120
54059.2543	I	-2.9129	1.5309
54063.2350	R	-0.4510	0.4559
54063.2691	I	0.3571	1.5156
54065.2274	R	-0.0844	0.5022
54065.2601	I	-2.0583	1.2132
54067.2316	R	0.7719	0.6078
54067.2538	I	0.7641	1.2157
54069.2226	R	-0.0809	1.1704
54069.2472	I	-1.4252	1.6467
54082.1125	R	4.2669	0.6357
54082.1431	I	4.0137	1.6081
54086.0956	R	4.9684	0.4904
54086.1270	I	5.4750	1.2935
54088.1151	R	4.1271	0.4621
54090.0847	R	5.3701	0.3957
54090.1073	I	5.9940	0.6564
54092.1127	R	4.3092	0.4003
54092.1383	I	5.7928	0.6584
54094.1113	R	3.7961	0.4969
54094.1311	I	5.9114	0.9174
54095.0989	R	1.9843	0.7910
54095.1013	I	1.5895	1.2770
54096.1207	R	3.3525	1.2003
54098.1289	R	-0.0024	1.3477
54099.0666	R	0.9906	1.8366
54099.0689	I	2.0599	2.8545

Continued

Table C.1 (Continued)

MJD	Passband	$Flux_{25}$	σ_{Flux}
54111.1021	R	1.9758	0.5134
54111.1229	I	4.4182	0.9824
54113.0886	R	2.0136	0.7528
54113.0921	I	0.9876	1.2105
	s373		
53992.3150	R	-0.1919	1.1501
53994.2946	R	-0.1827	0.3716
53994.3263	I	-1.2752	0.7835
54003.2819	R	-0.1252	0.5856
54003.3205	I	0.1972	1.0638
54006.3130	R	0.0019	0.4496
54006.3291	I	-0.7520	0.8362
54021.3528	R	0.8873	1.0877
54023.2781	R	0.6254	0.6006
54023.3001	I	-0.7960	1.2299
54025.2827	R	0.0826	0.6499
54027.3027	R	0.3548	0.4891
54027.3236	I	0.7356	1.1324
54039.2863	R	-1.4848	0.8760
54053.0972	R	0.7307	0.3835
54053.1196	I	0.4627	0.5238
54057.2382	R	-0.3314	1.1540
54059.2331	R	-0.8888	0.9735
54059.2694	I	-0.3141	1.7551
54063.2462	R	-0.4012	0.4794
54063.2807	I	-2.7466	1.1566
54065.2309	R	0.0725	0.5452
54065.2678	I	0.9473	1.2017
54067.2351	R	-0.0072	0.6661
54067.2598	I	1.1225	1.2433
54069.2296	R	1.0703	1.2239
54069.2649	I	0.7709	1.3566
54082.1159	R	4.1954	0.5873
54082.1376	I	3.6548	1.1837
54086.0991	R	5.5939	0.4526

Continued

Table C.1 (Continued)

MJD	Passband	$Flux_{25}$	σ_{Flux}
54086.1212	I	4.9848	1.0357
54088.1221	R	4.5935	0.4390
54090.0885	R	5.1793	0.3544
54090.1252	I	5.8501	0.6561
54092.1162	R	4.5867	0.3833
54092.1441	I	6.3200	0.6517
54094.1369	I	4.4925	0.8363
54096.1277	R	4.5704	1.1396
54096.1405	I	5.7405	1.9153
54098.1396	R	4.0592	1.7647
54098.1431	I	3.0975	2.7788
54099.0725	R	3.7225	1.8066
54099.0748	I	0.9139	2.3572
54111.1092	R	1.7973	0.5381
54111.1350	I	3.4710	1.0746
54113.1116	R	1.4279	0.5369
54113.1151	I	4.2956	0.8224
54114.0979	R	1.0617	1.0187
54114.1002	I	3.7808	1.5415
	s374		
53994.3532	R	0.0621	0.4606
53994.3913	I	-1.0968	0.8248
54003.3419	R	0.4300	0.5989
54003.3667	I	0.3938	1.1999
54006.2657	R	-0.2640	0.4172
54006.2692	I	1.0462	0.7521
54021.3564	R	-1.1191	1.2452
54023.3149	R	0.3721	0.8900
54023.3299	I	0.1163	1.2290
54027.3334	I	0.2587	1.0369
54027.3566	R	0.2461	0.6548
54031.3678	R	-0.5449	0.8046
54037.3196	I	-1.1365	1.1253
54037.3375	R	-0.4783	0.7738
54039.3418	R	0.5712	0.7860

Continued

Table C.1 (Continued)

MJD	Passband	$Flux_{25}$	σ_{Flux}
54053.1401	R	-0.1692	0.3234
54053.1542	I	-0.2342	0.6037
54055.3092	R	0.3154	0.9191
54057.2655	R	1.6462	1.0389
54057.2795	I	-0.7047	1.8027
54059.2965	R	-0.1002	0.7448
54059.3147	I	-0.6537	2.1867
54063.2979	R	0.0529	0.5683
54063.3073	I	-0.2414	1.0052
54065.2898	R	-0.7324	0.5888
54065.3017	I	1.0739	1.1205
54067.2846	R	1.0935	0.6241
54067.3095	I	-0.9008	1.6679
54069.2721	R	-0.1521	0.5417
54069.3003	I	0.5775	1.2001
54084.1452	R	3.2435	1.1457
54084.1592	I	1.7345	2.0333
54086.1507	R	3.3723	0.7001
54088.1527	R	3.5342	0.3880
54088.1724	I	6.1739	0.9639
54090.1358	R	2.9332	0.3070
54090.1486	I	5.5145	0.7303
54092.1576	R	3.7250	0.3394
54092.1777	I	6.2162	0.6791
54094.1682	R	3.1497	0.4756
54094.1885	I	5.4951	0.8726
54095.1382	R	3.6282	0.7682
54095.1406	I	3.4792	1.2655
54096.1811	R	2.6985	0.9882
54098.1886	R	-0.8000	2.2647
54111.1548	R	1.1067	0.5937
54112.1654	I	7.5485	1.6769
54113.1343	R	1.5698	0.4376
54114.1413	R	0.7391	0.8384
54114.1437	I	2.9320	1.4568

Continued

Table C.1 (Continued)

MJD	Passband	$Flux_{25}$	σ_{Flux}
	s375		
53994.2683	R	-0.2607	0.3782
53994.3086	I	-0.4064	0.6350
54003.2714	R	0.5908	0.5786
54003.2959	I	-0.1201	0.8406
54021.3422	R	-1.9286	1.1046
54023.2669	R	-0.3570	0.7436
54023.2818	I	-1.0646	1.0865
54027.2922	R	-0.1155	0.4713
54027.3061	I	0.3285	1.0035
54031.3067	R	-0.3592	0.5614
54031.3172	I	0.9861	1.0181
54037.2804	I	-1.3842	1.1577
54037.2922	R	-0.2066	0.6551
54039.2723	R	0.6495	1.0438
54039.3003	I	1.2865	1.9338
54053.0864	R	-0.5912	0.5168
54053.1011	I	-0.2069	0.6145
54059.2366	R	-0.8608	0.9012
54059.2636	I	-1.0302	1.5764
54063.2496	R	-0.7290	0.4735
54063.2749	I	-1.3949	1.3298
54065.2239	R	-0.3905	0.4901
54065.2541	I	0.9528	1.0242
54067.2281	R	-0.9820	0.5716
54067.2480	I	0.0823	1.1330
54069.2191	R	-2.3052	1.1245
54084.1063	R	3.9255	1.7407
54084.1276	I	6.5243	2.6452
54088.1256	R	6.5455	0.4834
54088.1291	I	9.4823	0.7891
54090.1038	R	7.8739	0.3487
54090.1822	I	7.3384	1.2286
54092.1088	R	8.7200	0.3553
54092.1325	I	9.6692	0.6222

Continued

Table C.1 (Continued)

MJD	Passband	$Flux_{25}$	σ_{Flux}
54094.1078	R	10.1782	0.4899
54094.1253	I	11.6708	0.8895
54096.1242	R	10.6142	1.0338
54096.1463	I	11.8189	1.8558
54098.1326	R	10.3644	1.3182
54099.0608	R	10.2160	1.7661
54099.0631	I	9.2255	2.2463
54111.1055	R	9.3943	0.7107
54111.1287	I	13.2112	1.1694
54113.0980	R	8.3114	0.5853
54113.1015	I	12.2338	1.1992
54114.0853	R	8.3565	0.7422
54114.0881	I	13.2613	1.3721
s377			
53992.2930	R	0.5099	1.0762
53994.2126	R	-0.2808	0.5228
53994.2465	I	1.3536	0.6405
54003.2200	R	-1.1962	0.8026
54003.2546	I	-1.2466	1.5131
54006.2473	R	-0.2813	0.4551
54006.2508	I	0.3602	0.9272
54021.2260	R	-1.0221	0.8693
54021.2417	I	-0.3766	1.4256
54025.2216	R	-1.3231	0.8706
54025.2447	I	-1.4633	0.8952
54029.2328	R	-0.2605	0.6706
54029.2502	I	-0.5224	1.0972
54031.2409	R	-0.8034	0.5124
54031.2702	I	1.1066	1.1313
54033.2158	R	0.3209	1.6329
54033.2418	I	1.1678	1.8597
54037.2333	R	-0.5003	0.6522
54037.2564	I	-3.6481	1.3729
54039.2248	R	-0.9514	0.8419
54039.2459	I	-3.6305	1.3596

Continued

Table C.1 (Continued)

MJD	Passband	$Flux_{25}$	σ_{Flux}
54051.0400	R	-0.4367	0.6820
54051.0591	I	0.5728	1.1635
54055.1888	R	-1.0284	0.7501
54055.2041	I	-0.1760	1.6498
54069.1944	R	9.9991	1.7658
54084.0600	R	16.2108	1.0835
54084.0748	I	24.8378	1.5589
54088.0645	R	17.6132	0.5057
54088.0854	I	24.0532	1.0631
54090.0577	R	17.5054	0.3796
54094.0617	R	15.2174	0.5644
54094.0862	I	24.5512	1.1190
54095.0822	R	14.0124	0.8516
54095.0846	I	19.3172	1.4572
54096.0491	R	15.1291	0.7805
54096.0761	I	22.9314	1.9526
54098.0391	I	20.7248	2.0770
54098.0449	R	12.1336	1.5382
54112.0580	R	5.4139	0.9225
54114.0587	R	4.2953	0.7143
54114.0615	I	14.7831	1.4274
s379			
53994.2018	R	-0.5782	0.6140
53994.2289	I	0.9248	1.0715
54003.1999	R	1.0147	0.5358
54003.2384	I	-0.3034	1.7612
54023.2263	R	0.4554	0.9208
54023.2442	I	-1.0524	1.3627
54027.2440	R	-1.2679	0.8466
54027.2638	I	0.1400	1.3118
54031.2268	R	0.2890	0.6400
54031.2586	I	0.4012	1.3287
54039.2098	R	-1.6301	0.9781
54053.0393	R	-1.1798	0.5045
54053.0571	I	1.2771	0.9837

Continued

Table C.1 (Continued)

MJD	Passband	$Flux_{25}$	σ_{Flux}
54069.1839	R	-3.7535	1.6388
54082.0736	R	0.6512	0.6020
54082.0956	I	-2.2888	1.5973
54086.0568	R	8.5698	0.5285
54086.0789	I	9.2862	1.7109
54090.0505	R	24.6728	0.4370
54090.0710	I	30.8262	1.1114
54092.0526	R	34.1277	0.4568
54094.0545	R	44.8771	0.6968
54094.0745	I	52.9633	1.4043
54095.0692	R	44.4813	1.0587
54095.0715	I	52.0046	1.7373
54096.0879	I	55.1138	2.7331
54096.0937	R	52.3917	2.2640
54098.0484	R	54.5623	1.9649
54098.0523	I	51.5678	2.7455
54109.0530	R	52.2364	2.6586
54109.0691	R	67.2557	2.1707
54111.0791	I	56.8841	1.8591
54112.0454	R	51.9101	2.3248
54112.0477	R	52.4008	1.1739
54112.0514	I	50.3819	2.2672
54114.0525	R	46.9692	0.7711
54114.0550	I	41.4376	1.6763
s380			
54006.3176	R	0.1447	0.4841
54006.3343	I	0.9101	0.8265
54021.2689	R	-0.8506	1.0306
54021.2852	I	-1.1210	1.5203
54023.3582	R	-0.0179	0.8731
54025.2721	R	0.5322	0.6706
54025.2922	I	1.8884	1.6597
54029.2893	R	0.4745	0.6166
54029.3160	I	-0.9478	0.9396
54033.2816	R	0.9518	1.3051
Continued			

Table C.1 (Continued)

MJD	Passband	$Flux_{25}$	σ_{Flux}
54039.2898	R	2.0589	0.9684
54051.0962	R	0.9732	0.6073
54051.1132	I	-0.2144	0.9920
54055.2336	R	0.6840	0.8880
54055.2547	I	0.1237	1.6328
54059.2401	R	-0.3343	0.7878
54059.2740	I	1.5480	1.7822
54063.2533	R	0.6372	0.5124
54063.2574	I	0.2740	1.0054
54065.2424	R	-0.8958	0.4438
54065.2773	I	-2.4682	1.2058
54067.2445	R	0.2914	0.6992
54067.2714	I	-1.6222	1.1899
54069.2367	R	1.2835	1.0753
54069.2589	I	-0.7608	1.3396
54082.1195	R	1.7056	0.6603
54082.1320	I	4.1939	1.2467
54086.1026	R	2.2945	0.4281
54086.1154	I	1.7525	0.8746
54090.0925	R	3.4934	0.3752
54090.1193	I	6.3104	0.6734
54092.1197	R	4.1701	0.3701
54094.1183	R	4.2413	0.4897
54094.1432	I	6.7016	0.6925
54095.1106	R	4.7457	0.7228
54095.1129	I	6.7072	1.1865
54096.1312	R	3.3686	0.9589
54098.1361	R	3.5188	1.5003
54099.0815	R	5.1392	2.0923
54099.0838	I	7.9793	2.4672
54111.1130	R	3.1453	0.4916
54111.1414	I	7.2939	1.1380
54113.1213	R	2.4887	0.4872
54113.1248	I	5.7211	0.9315
x017			
Continued			

Table C.1 (Continued)

MJD	Passband	$Flux_{25}$	σ_{Flux}
54351.2807	R	-0.8092	0.5461
54354.2929	R	0.0894	0.5910
54357.2790	I	0.1528	0.8166
54377.2155	R	15.1760	0.7834
54377.2473	I	21.4907	0.8975
54379.2209	R	13.6696	0.8063
54379.2544	I	20.5815	1.5904
54381.2046	R	14.6781	0.5129
54381.2381	I	19.7462	0.7858
54383.2411	R	14.0778	0.6632
54389.2246	R	12.0228	0.9948
54393.2437	R	9.9556	0.7754
54407.2046	R	4.3915	0.8418
54409.2404	R	2.6284	0.4918
54411.2079	R	3.7409	0.4756
54421.0222	R	1.7581	0.6202
54423.1249	R	0.9232	0.6910
54435.1562	R	0.5822	0.6919
54437.1415	R	0.4912	0.6790
54437.1602	I	2.0816	1.2181
54439.0851	R	0.6987	0.4468
54441.0296	R	1.2608	0.7496
54441.0516	I	3.6412	0.8015
54443.0490	R	-0.8783	0.8225
54443.0772	I	1.1554	1.6389
54445.0443	R	0.6817	0.5224
54445.0690	I	3.1562	0.8242
54447.0466	R	-0.0462	0.4469
54447.0717	I	3.0333	0.9545
54449.0489	R	-0.4971	0.5902
54449.0743	I	5.7218	1.1031
54464.0458	R	1.4008	0.5534
54464.0566	I	3.0080	0.8699
54467.0703	R	-0.0235	0.4702
54467.0868	I	2.1340	0.9424

Continued

Table C.1 (Continued)

MJD	Passband	$Flux_{25}$	σ_{Flux}
54469.0582	R	0.0684	0.4740
54472.0605	R	-0.9639	0.7173
54472.0825	I	2.2159	1.0366
54474.0536	R	-0.4219	0.7224
	x020		
54351.3084	R	1.1837	0.5202
54354.3153	R	0.1502	0.6480
54357.3527	R	1.5674	0.8513
54360.3555	I	2.9794	1.3152
54363.3616	R	4.0890	0.5105
54377.2681	R	4.2186	0.4851
54377.2896	I	6.6702	0.9917
54379.2835	R	2.9876	0.7069
54381.2504	R	3.3439	0.3954
54381.2777	I	4.6522	0.9070
54383.3196	R	2.9842	0.3613
54393.2886	R	1.6807	0.5246
54407.2437	R	0.6729	0.7442
54407.2587	I	0.8564	1.6988
54409.2900	R	1.0765	0.4749
54411.2689	R	0.6414	0.4698
54411.2878	I	2.2343	0.9609
54415.1234	R	1.1088	0.4890
54417.0638	R	0.2824	0.3853
54417.0949	I	-0.0753	0.8276
54421.0941	R	1.1488	0.4609
54423.2532	R	0.5968	0.7009
54437.1719	R	0.0774	0.6346
54437.1859	I	0.6954	1.2969
54441.0760	R	0.3522	0.3914
54441.0938	I	-0.8646	0.9129
	x025		
54472.0570	R	0.8150	0.5890
54472.0766	I	0.8084	0.9979
54474.0501	R	-0.5870	0.6397

Continued

Table C.1 (Continued)

MJD	Passband	$Flux_{25}$	σ_{Flux}
54351.2738	R	15.7253	0.4088
54354.2860	R	17.9513	0.4963
54357.2637	I	21.2725	1.0844
54363.2768	I	25.3880	1.4585
54377.2080	R	9.2238	0.6061
54377.2355	I	12.6887	0.8807
54379.2174	R	7.2739	0.9449
54379.2485	I	12.8122	1.5702
54381.1970	R	5.8426	0.4768
54381.2254	I	13.3161	0.7908
54383.2374	R	6.5458	0.5436
54389.2210	R	3.9948	1.0138
54389.2282	I	8.0974	2.0932
54393.2332	R	3.6524	0.6301
54393.2375	I	9.0153	0.9371
54407.1976	R	2.1091	0.5480
54407.2124	I	4.6496	1.7439
54409.2369	R	1.3431	0.4799
54411.1979	R	1.2290	0.3782
54411.2164	I	4.9770	0.6331
54423.1034	R	2.2097	0.8082
54437.1289	R	1.7790	0.7486
54437.1486	I	1.4709	1.3286
54441.0256	R	0.1396	0.8033
54441.0458	I	3.1082	0.6150
54443.0447	R	1.0967	0.7192
54443.0714	I	3.9775	1.2067
54445.0407	R	0.8996	0.5003
54445.0631	I	2.1242	0.8531
54447.0432	R	1.2200	0.3647
54447.0658	I	1.9060	0.6617
54449.0454	R	1.3506	0.5232
54449.0685	I	3.4956	0.7171
54451.0869	R	1.1217	0.9045
54451.0904	I	1.9201	1.4236

Continued

Table C.1 (Continued)

MJD	Passband	$Flux_{25}$	σ_{Flux}
54453.0673	R	-0.4882	2.1250
54464.0419	R	0.7624	0.6065
54464.0618	I	1.4337	0.6307
54467.0633	R	0.5468	0.4813
54467.0816	I	0.7792	0.8519
54469.0538	R	0.8530	0.4968
	x028		
54467.0868	I	0.7414	0.9721
54469.0582	R	0.2419	0.4280
54472.0605	R	1.0094	0.6895
54472.0825	I	0.8522	1.0050
54474.0536	R	0.8230	0.6778
54351.2807	R	1.3657	0.5168
54354.2929	R	3.5059	0.5042
54357.2790	I	5.7622	0.8731
54377.2155	R	6.4748	0.5930
54377.2473	I	7.7096	0.8892
54379.2209	R	6.2779	0.7920
54379.2544	I	10.3372	1.3273
54381.2046	R	5.6831	0.5637
54381.2381	I	8.6546	0.7250
54383.2411	R	5.6852	0.6304
54389.2246	R	4.4002	0.9274
54393.2437	R	3.6719	0.7527
54407.2046	R	1.7160	0.6952
54409.2404	R	0.9162	0.4439
54411.2079	R	1.0639	0.3823
54421.0222	R	-0.3383	0.6408
54423.1249	R	1.3525	0.6688
54435.1562	R	0.8711	0.8173
54437.1415	R	0.3861	0.6008
54437.1602	I	1.1655	1.2879
54439.0851	R	1.4793	0.3983
54441.0296	R	0.9852	0.6862
54441.0516	I	1.0347	0.7437

Continued

Table C.1 (Continued)

MJD	Passband	$Flux_{25}$	σ_{Flux}
54443.0490	R	0.0538	0.7710
54443.0772	I	-0.1551	1.3569
54445.0443	R	0.0352	0.4406
54445.0690	I	0.1824	0.9547
54447.0466	R	0.5687	0.3983
54449.0489	R	0.1790	0.5386
54449.0743	I	1.0425	1.0970
54464.0458	R	1.3147	0.5499
54464.0566	I	2.8277	0.8167
54467.0703	R	0.4534	0.4590
x033			
54407.2366	R	9.0621	0.9650
54409.2135	I	12.7592	0.8533
54415.0327	R	9.4828	0.6721
54415.0466	I	10.7336	0.9197
54417.0349	R	4.9771	0.4188
54417.0519	I	10.0923	0.8520
54419.0331	R	5.0909	0.4476
54419.0371	I	9.5637	0.7589
54421.0260	R	3.4409	0.5748
54421.0674	I	10.6075	0.9768
54423.1294	R	3.7079	0.6662
54423.2267	I	10.1580	1.4640
54435.1148	R	2.2938	0.8164
54435.1291	I	6.8862	1.5164
54439.0337	R	2.5375	1.1614
54439.0495	I	4.1937	0.7901
54451.0407	R	1.6648	1.0213
54451.0517	I	3.1163	1.4942
54351.2877	R	0.5938	0.5055
54354.3004	R	0.6706	0.5657
54357.2914	I	-1.3454	0.9707
54379.2247	I	14.9785	1.1187
54381.2171	R	14.7846	0.4408
54383.2045	R	16.2084	0.5924

Continued

Table C.1 (Continued)

MJD	Passband	$Flux_{25}$	σ_{Flux}
54383.2448	I	18.3499	1.1142
54389.2013	R	18.9911	0.7757
x034			
54351.3264	R	-0.0401	0.5723
54351.4022	I	-0.4114	1.1729
54354.3388	R	0.2112	0.5528
54360.3145	R	3.1205	0.8264
54363.3271	I	7.8773	1.1360
54363.3768	R	6.3308	0.6693
54375.3008	R	9.1917	1.1271
54375.3172	I	8.9562	1.6239
54379.2670	R	8.0153	0.8625
54379.3008	I	9.7457	1.5365
54381.2664	R	6.3667	0.6282
54381.3029	I	9.6161	0.9223
54383.2796	R	5.1572	0.4493
54383.2973	I	9.7300	0.6654
54385.3147	I	9.1714	1.5490
54387.2624	R	5.4239	0.7909
54387.2914	I	7.1499	2.0396
54389.2815	I	6.5851	1.8201
54391.3226	R	4.0795	1.1293
54393.2784	R	2.9910	0.4823
54393.2819	I	5.6265	0.9070
54409.2550	R	0.5627	0.6683
54409.2801	I	1.8003	0.7138
54413.1065	I	7.9807	1.9618
54415.0884	R	-0.4606	0.5491
54415.1100	I	3.3562	0.8622
54417.0853	R	-0.1323	0.4186
54417.1265	I	2.3884	0.6649
54419.0853	R	0.0647	0.3957
54419.1232	I	2.5245	0.6371
54421.0771	R	0.0555	0.5673
54421.1212	I	3.5991	0.8477

Continued

Table C.1 (Continued)

MJD	Passband	$Flux_{25}$	σ_{Flux}
54423.2425	R	0.5366	0.7264
54423.2788	I	1.6541	1.0451
54435.1736	R	-0.4635	0.7472
54435.1904	I	-1.2287	1.3894
54439.0926	R	0.3597	0.3312
54439.1093	I	0.2330	0.7195
54441.1811	R	-0.4597	0.5071
54453.1564	R	2.5829	1.6888
54453.1599	I	1.7721	2.2154
54467.1181	R	0.9275	0.5207
54472.1027	R	-0.3258	0.4693
x038			
54351.3338	R	-0.7807	0.8083
54354.3478	R	0.8722	0.6288
54354.3979	I	0.0844	0.9464
54360.3218	R	0.9436	0.9459
54363.3401	I	1.2121	0.9387
54363.3803	R	0.8009	0.6182
54375.3079	R	6.6293	1.2185
54379.2793	R	8.3353	0.9759
54379.3164	I	14.1580	1.7430
54381.2740	R	9.4319	0.6055
54383.2873	R	7.7035	0.7324
54383.3093	I	10.5384	0.9219
54387.2696	R	7.4837	0.7849
54387.3102	I	14.5967	2.5936
54389.2756	I	10.9235	2.4695
54391.3188	R	5.5666	1.1127
54393.2622	R	8.8994	0.8154
54407.2890	R	4.6964	1.0075
54409.2439	R	4.3605	0.5776
54409.2627	I	8.3393	0.8059
54415.0765	R	4.4982	0.5921
54415.0920	I	8.3992	0.9457
54417.0817	R	2.3047	0.4465

Continued

Table C.1 (Continued)

MJD	Passband	$Flux_{25}$	σ_{Flux}
54417.1193	I	6.7024	0.6935
54419.0655	R	2.2131	0.4001
54419.0898	I	7.0084	0.6607
54421.0850	R	3.1866	0.6055
54423.2497	R	2.1227	0.7282
54435.1808	R	1.4877	0.8941
54435.2034	I	4.5896	1.6338
54439.0999	R	1.1579	0.4154
54439.1213	I	4.1459	0.6543
54441.1848	R	1.9704	0.7118
54451.1068	R	1.2784	0.7936
54451.1103	I	4.0721	1.2160
54453.0891	R	1.6639	1.3531
54453.1054	I	1.7817	2.2078
x039			
54383.3510	I	19.1014	0.7751
54385.3596	I	14.8767	1.4079
54387.3172	R	8.2433	1.3980
54387.3467	I	14.7738	1.2083
54389.3007	R	6.2685	0.9432
54393.3055	R	4.6567	0.6028
54409.3036	R	2.3137	0.6995
54409.3245	I	3.3458	0.9780
54413.1502	R	1.4946	0.7075
54415.1310	R	1.4164	0.4388
54415.1506	I	5.8838	0.8214
54419.1507	R	1.0261	0.3825
54419.1736	I	3.4839	0.7628
54421.1270	R	1.3017	0.4660
54423.2846	R	0.4276	0.6352
54435.2168	R	1.7924	0.7731
54435.2326	I	3.7827	1.6003
54439.1346	R	0.5887	0.3697
54439.1491	I	2.6908	0.7392
54441.1621	R	1.0889	0.6759

Continued

Table C.1 (Continued)

MJD	Passband	$Flux_{25}$	σ_{Flux}
54443.1136	R	1.1228	0.6019
54443.1282	I	4.5781	1.2044
54445.1098	R	0.2160	0.4229
54445.1320	I	2.0519	0.8074
54447.1844	R	1.0873	0.4357
54449.1839	R	1.0513	0.4938
54453.1848	R	-0.8490	1.2378
54464.1561	R	0.8034	0.5328
54464.1599	I	3.0236	0.8881
54469.1223	R	0.1164	0.3971
54469.1293	I	2.5934	0.7547
54351.3521	R	1.1260	0.8291
54354.3729	R	-0.1311	0.5447
54354.4039	I	0.2928	1.0019
54360.3409	R	6.9474	0.5741
54375.3513	I	19.4825	1.9929
54379.3293	R	11.6545	1.0000
54381.3157	R	10.7357	0.8500
54381.3440	I	19.5563	0.9764
54383.3355	R	9.9292	0.6160
x055			
54351.3487	R	2.8562	0.6070
54354.3693	R	3.4774	0.6227
54357.3460	I	13.1792	1.4238
54360.3374	R	19.5481	0.6444
54363.4021	I	32.2879	1.2423
54377.3389	R	34.6078	0.7817
54381.3818	R	28.9789	0.6618
54381.3856	I	42.5739	1.7437
54383.3749	R	25.7004	0.9221
54385.3378	R	24.8301	0.7796
54385.3654	I	34.6945	1.9963
54387.3210	R	19.7643	1.3231
54387.3534	I	32.8229	0.8777
54389.3090	R	19.7514	1.0321
Continued			

Table C.1 (Continued)

MJD	Passband	$Flux_{25}$	σ_{Flux}
54389.3593	I	30.8486	2.3686
54393.3133	R	16.0717	0.5189
54407.3041	R	9.6269	0.8837
54407.3250	I	14.7336	2.0626
54409.3489	R	6.0007	0.6771
54411.3131	R	5.8515	0.4968
54411.3353	I	8.9263	0.9850
54417.1574	I	8.5096	0.5634
54417.1740	R	5.0453	0.3627
54419.1697	R	4.7947	0.3921
54421.1530	R	3.5952	0.4191
54423.3093	R	6.3092	1.0446
54435.2565	R	3.8705	1.1632
54437.2326	R	2.3765	0.6967
54437.2536	I	9.3253	2.0284
54439.1731	R	3.2541	0.5244
54441.1528	R	3.1557	0.4939
54441.1563	I	3.3871	0.9573
54443.1516	R	1.8921	0.6475
54443.1591	I	4.1882	1.3821
54445.1617	R	3.5654	0.6279
54445.1704	I	3.3460	1.5516
x066			
54351.3191	R	29.0270	0.6216
54351.3897	I	31.5900	1.1962
54354.3260	R	27.8965	0.6454
54360.3070	R	27.9456	0.9230
54363.3696	R	25.1272	0.6114
54377.3072	I	17.8695	1.1578
54381.2619	R	9.3074	0.4301
54381.2971	I	16.8348	1.0463
54383.3304	R	9.6309	0.5311
54387.2589	R	7.4792	0.6048
54387.2850	I	11.9465	2.8211
54393.2927	R	5.1534	0.5155
Continued			

Table C.1 (Continued)

MJD	Passband	$Flux_{25}$	σ_{Flux}
54407.2552	R	3.1042	0.7089
54409.2865	R	3.3254	0.4663
54409.2937	I	7.8421	1.0113
54411.2724	R	2.7873	0.5197
54411.2937	I	7.2821	0.8687
54413.1338	R	2.5029	0.6784
54417.0745	R	3.0857	0.4194
54417.1127	I	5.3246	0.6462
54419.0809	R	2.5828	0.4066
54419.1173	I	6.4804	0.6194
54421.1153	I	4.7564	0.9216
54423.2636	R	2.1543	0.6997
54423.2730	I	5.9725	1.1380
54437.1824	R	1.8191	0.6368
54437.2067	I	4.1095	1.2736
54439.1311	R	1.9473	0.4196
54441.0866	R	2.1266	0.4612
54441.1171	I	3.1878	0.9894
54445.1861	R	1.2082	0.8615
54447.1552	R	1.6568	0.4746
54447.1590	I	3.1184	0.9904
54449.1406	R	1.4014	0.5294
54449.1441	I	3.5820	1.0115
54451.1447	R	2.0544	0.9848
54453.1468	R	2.5787	1.5104
54453.1503	I	1.4371	1.9515
54464.0994	R	1.4621	0.4208
54464.1029	I	1.9919	0.7469
54467.1110	R	1.3898	0.5868
54469.1093	R	1.4260	0.3529
54469.1165	I	2.9988	0.6657
54472.0955	R	1.3536	0.4649
	x071		
54417.0853	R	4.7179	0.4652
54417.1265	I	7.3435	0.7131

Continued

Table C.1 (Continued)

MJD	Passband	$Flux_{25}$	σ_{Flux}
54419.0853	R	3.6928	0.4080
54419.1232	I	6.8828	0.7133
54421.0771	R	5.0444	0.5655
54421.1212	I	6.8586	0.9333
54423.2425	R	2.8066	0.7426
54423.2788	I	7.3237	1.1935
54435.1736	R	2.3725	0.6886
54435.1904	I	4.6018	1.6493
54439.0926	R	1.3911	0.4095
54439.1093	I	3.0321	0.7324
54441.1811	R	1.9835	0.6215
54453.1564	R	0.1479	1.5773
54453.1599	I	-0.3719	2.1792
54467.1181	R	1.9100	0.6624
54472.1027	R	0.1582	0.5539
54351.3264	R	-0.6591	0.6878
54354.3388	R	0.0684	0.5011
54363.3271	I	-0.8626	1.3063
54363.3768	R	-1.1661	0.6450
54379.2670	R	5.3878	0.7224
54379.3008	I	6.2321	1.5598
54381.2664	R	6.9152	0.5612
54381.3029	I	7.3902	1.1237
54383.2796	R	8.1359	0.5064
54383.2973	I	8.2963	0.7546
54387.2624	R	8.7486	0.8300
54387.2914	I	6.5979	2.1049
54389.2815	I	11.0234	1.7627
54391.3226	R	12.2041	1.1898
54393.2784	R	12.7697	0.5603
54393.2819	I	13.3009	0.8492
54409.2550	R	8.6832	0.7209
54409.2801	I	9.4751	0.7690
54415.0884	R	4.7654	0.6272
54415.1100	I	8.9805	0.8465

Continued

Table C.1 (Continued)

MJD	Passband	$Flux_{25}$	σ_{Flux}
	x077		
54351.3620	R	0.8191	0.4891
54354.3803	R	0.2646	0.4938
54357.3161	I	0.6241	1.0643
54360.3483	R	-0.2554	0.4924
54375.3639	I	5.3331	1.8160
54381.3282	R	8.9619	0.5935
54381.3566	I	11.3841	0.9610
54383.3433	R	10.1815	0.4317
54383.3629	I	10.8560	1.0144
54385.3496	R	10.3231	0.7779
54387.3387	R	11.4200	0.5532
54387.3781	I	12.3810	1.0924
54389.3125	R	8.8811	1.0037
54389.3235	I	11.0362	2.1467
54391.2625	R	11.3207	0.6264
54391.3634	R	10.6155	0.5329
54393.3172	R	10.1984	0.4829
54393.3530	I	11.8694	1.0026
54407.3311	R	6.7334	1.0272
54409.3144	R	5.2291	0.5104
54409.3430	I	8.9623	1.0100
54411.3505	R	5.6935	0.7293
54413.1613	R	2.9195	0.7565
54415.1470	R	3.6929	0.4443
54417.1810	R	3.0102	0.3790
54419.1445	I	6.3518	0.6548
54419.1586	R	3.0336	0.3561
54421.1349	R	3.1915	0.4935
54421.1565	I	4.8875	0.5952
54423.2916	R	1.8653	0.5866
54423.3290	I	8.0842	1.4383
54435.2245	R	1.1455	0.7923
54435.2448	I	3.3770	1.5974
54439.1421	R	0.8576	0.4049
54439.1610	I	3.2940	0.8932
54441.1696	R	1.6582	0.5446
54443.1719	R	1.3228	0.5432
54445.1286	R	1.4657	0.4304
54445.1555	I	2.6658	1.2722
54447.1751	R	0.7848	0.3976
54447.1786	I	1.6017	0.8956
54449.1653	R	0.7837	0.4290
54449.1740	I	3.2790	0.8133
54451.1759	R	0.2198	0.9257
54453.1753	R	0.7149	1.2005
54453.1788	I	6.8756	3.7863
54464.1661	R	1.3938	0.5364
54464.1695	I	2.3251	0.8420
54469.1258	R	0.3995	0.3706
54469.1351	I	2.7912	0.7075
54472.1873	R	0.0149	0.6715
54474.2000	R	0.1115	1.1346
	x080		
54351.2953	R	0.7897	0.6116
54354.3076	R	-0.1708	0.7492
54357.3033	I	0.0787	1.0796
54360.2884	R	1.5007	1.7787
54379.2101	R	9.2391	1.1734
54379.2366	I	11.4445	1.4164
54383.2299	R	10.1338	0.5658
54383.2572	I	14.1441	0.9842
54389.2124	R	10.8045	0.8959
54393.2258	R	9.4183	0.6115
54407.2401	R	4.2842	0.8739
54409.2053	R	4.0042	0.5346
54409.2251	I	7.3120	1.0231
54415.0396	R	2.9633	0.6436
54415.0591	I	6.0137	1.5816
54419.0209	R	1.4108	0.5701

Continued

Continued

Table C.1 (Continued)

MJD	Passband	$Flux_{25}$	σ_{Flux}
54421.0335	R	1.7038	0.6210
54423.1683	R	1.1109	0.8443
54435.1219	R	2.1449	0.8205
54435.1410	I	3.6290	1.4338
54439.0417	R	1.9800	0.7499
54439.0626	I	2.6446	0.8682
54441.0388	R	1.4492	0.4692
54441.0641	I	4.3373	0.8767
54443.0360	R	0.7463	0.7229
54443.0592	I	2.5423	1.1269
54445.0514	I	3.1283	0.8766
54447.0360	R	1.1362	0.5052
54447.0542	I	2.8594	0.7193
54449.0379	R	0.7551	0.6372
54449.0558	I	2.2089	0.8832
54451.0669	R	1.5481	1.0690
54451.0704	I	1.5104	1.4266
54464.0531	R	-1.3659	0.5215
54464.0739	I	0.7084	0.9564
54467.0781	R	0.8910	0.4315
54467.0973	I	0.3434	1.1827
54469.0657	R	0.9225	0.4530
54472.0693	R	0.8629	0.6190
54474.0680	R	1.5176	0.8716
54474.0809	I	3.2762	1.5963
	x085		
54439.1456	R	0.6955	0.3940
54439.1670	I	2.5653	0.8426
54441.1733	R	0.9229	0.4333
54443.1172	R	0.2712	0.5030
54443.1340	I	0.3191	1.1782
54445.1180	R	-0.1662	0.4074
54445.1379	I	1.1168	0.7618
54351.3655	R	-0.1923	0.5603
54354.3838	R	-0.2175	0.4332

Continued

Table C.1 (Continued)

MJD	Passband	$Flux_{25}$	σ_{Flux}
54357.3224	I	1.0691	0.9467
54360.3519	R	-0.3800	0.6014
54375.3706	I	4.4056	1.9828
54381.3327	R	4.6516	0.4521
54381.3625	I	5.9157	1.0088
54383.3474	R	5.2842	0.4988
54383.3688	I	7.0434	1.5289
54385.3531	R	5.3706	0.6493
54387.3421	R	5.1706	0.6946
54387.3839	I	6.9543	2.1038
54389.2875	R	7.5443	1.0036
54391.2587	R	3.3677	1.8436
54391.3306	R	7.3761	0.9678
54391.3596	R	6.8732	1.0218
54391.3711	R	6.3451	0.5281
54393.2969	R	6.7297	0.4710
54393.3594	I	6.8184	0.9597
54409.3109	R	2.4046	0.5779
54409.3372	I	5.0038	1.0119
54411.3469	R	2.1969	0.5616
54415.1388	R	2.2117	0.4480
54421.1384	R	1.1339	0.4573
54423.2951	R	0.8555	0.6256
54435.2283	R	-0.8360	0.7100
54435.2506	I	-0.0319	1.4300
	x089		
54441.0831	R	0.4648	0.4787
54441.1113	I	2.3294	1.0390
54445.1826	R	0.2016	1.0852
54447.1251	R	0.7208	0.4407
54447.1286	I	2.3811	0.9328
54449.1122	R	0.8904	0.4707
54449.1157	I	0.3337	0.9591
54451.1033	R	0.0731	0.9596
54453.0786	R	0.2785	1.3413

Continued

Table C.1 (Continued)

MJD	Passband	$Flux_{25}$	σ_{Flux}
54453.0821	I	-0.9231	1.8206
54464.0901	R	-0.2050	0.4553
54464.0936	I	1.6862	0.8444
54467.1074	R	0.2858	0.5467
54467.1304	I	-0.7081	0.8577
54469.1059	R	-0.2996	0.4024
54472.0920	R	0.3201	0.4704
54472.1441	I	1.0672	1.0886
54474.1201	R	-0.4954	0.6876
54351.3155	R	-0.5804	0.8818
54351.3819	I	-1.8011	1.2069
54354.3224	R	0.6304	0.6312
54357.3600	R	-0.9073	0.7819
54360.3034	R	-0.7310	0.8752
54363.3207	I	0.8423	1.4582
54363.3661	R	0.6945	0.6869
54377.2751	R	4.1163	0.7379
54377.3013	I	5.1522	1.0153
54379.2911	R	3.2377	0.9216
54381.2580	R	4.1461	0.5297
54381.2911	I	7.0324	1.0186
54383.3268	R	4.0866	0.6059
54385.3275	I	8.3202	1.3764
54387.2548	R	3.8749	0.6339
54387.2790	I	7.1668	1.3649
54391.2864	R	5.2535	2.1811
54391.3149	R	4.3385	1.2410
54393.2583	R	5.9630	0.7628
54407.2517	R	3.4140	0.7751
54407.2703	I	6.3247	1.9037
54411.2607	R	2.1447	0.4743
54411.2759	I	3.7437	0.9747
54415.1275	R	1.7269	0.4697
54417.0710	R	1.3847	0.4701
54417.1068	I	3.4112	0.7123

Continued

Table C.1 (Continued)

MJD	Passband	$Flux_{25}$	σ_{Flux}
54419.0690	R	1.2000	0.4065
54419.0993	I	2.2260	0.5606
54421.1011	R	1.2463	0.4942
54423.2602	R	0.3276	0.5663
54437.1789	R	-0.2430	0.6628
54437.2009	I	0.8618	1.2209
	x093		
54439.1456	R	-0.2333	0.3571
54439.1670	I	0.3871	0.9085
54441.1733	R	0.8799	0.4750
54443.1172	R	-0.2288	0.4651
54443.1340	I	-0.5876	1.3255
54445.1180	R	0.7344	0.3929
54445.1379	I	-0.9043	0.7543
54351.3655	R	0.2369	0.5820
54354.3838	R	0.3032	0.5237
54357.3224	I	0.5782	1.0646
54360.3519	R	0.7236	0.6434
54375.3706	I	1.9772	2.0747
54381.3327	R	3.9925	0.4597
54381.3625	I	6.1600	0.8834
54383.3474	R	3.8730	0.4460
54383.3688	I	4.0059	1.3390
54385.3531	R	4.1580	0.7692
54387.3421	R	2.5791	0.6443
54387.3839	I	3.7562	1.8678
54389.2875	R	4.0423	0.9535
54391.2587	R	4.4967	1.6717
54391.3306	R	4.8892	1.0044
54391.3596	R	3.2134	0.9808
54391.3711	R	4.4524	0.5207
54393.2969	R	3.4989	0.5016
54393.3594	I	6.2694	1.0520
54409.3109	R	1.2710	0.5272
54409.3372	I	0.0257	1.0229

Continued

Table C.1 (Continued)

MJD	Passband	$Flux_{25}$	σ_{Flux}
54411.3469	R	0.0677	0.5527
54415.1388	R	0.6996	0.4859
54421.1384	R	0.5905	0.4306
54423.2951	R	-0.3194	0.5767
54435.2283	R	0.5441	0.7810
54435.2506	I	-0.4464	1.5559
	x103		
54443.0656	I	10.6291	1.1442
54445.0366	R	4.7093	0.5555
54445.0573	I	8.9502	0.9146
54447.0397	R	4.6305	0.5462
54447.0600	I	8.6836	0.6837
54449.0417	R	3.5497	0.4075
54449.0627	I	7.3245	0.8260
54451.0765	R	2.7936	0.5009
54451.0811	I	4.0608	1.5005
54467.0746	R	2.9161	0.9188
54467.0921	I	5.9194	0.9508
54469.0621	R	2.9269	0.4184
54472.0657	R	2.2208	0.4263
54474.0570	R	2.5381	0.5317
54474.0751	I	3.0731	1.4639
54351.2842	R	0.3245	0.6029
54354.2966	R	0.1318	0.4275
54357.2853	I	1.2073	0.7192
54363.3020	I	0.1570	1.9534
54377.2191	R	0.6901	0.6033
54381.2134	R	4.8362	0.5889
54389.2088	R	10.3321	0.4755
54391.2209	R	21.3427	0.8840
54393.2198	R	24.2306	0.9608
54407.2084	R	24.1342	0.7566
54407.2307	I	25.1285	1.8369
54419.0591	I	14.6492	0.7135
54421.0517	R	18.7662	0.7508

Continued

Table C.1 (Continued)

MJD	Passband	$Flux_{25}$	σ_{Flux}
54423.1992	R	11.1910	0.5808
54437.1451	R	8.1629	0.8661
54437.1660	I	12.7735	1.4685
54441.0345	R	4.6094	0.6127
54441.0576	I	9.6189	0.6681
54443.0405	R	4.0351	0.4723
	x107		
54351.3521	R	-0.0904	0.5907
54354.3729	R	0.4923	0.5092
54354.4039	I	0.3041	1.0548
54360.3409	R	-0.8537	0.5699
54375.3513	I	0.0022	1.8179
54379.3293	R	-0.3379	0.8445
54381.3157	R	-1.1436	0.7965
54381.3440	I	1.3543	0.9164
54383.3355	R	0.3111	0.5231
54383.3510	I	1.0479	0.7597
54385.3572	I	7.6916	4.7714
54385.3596	I	6.9991	1.5834
54387.3172	R	8.5107	1.3014
54387.3467	I	13.6508	1.0977
54389.3007	R	23.0616	0.9393
54393.3055	R	61.3770	0.5991
54409.3036	R	122.4964	0.6703
54409.3245	I	104.5219	1.1706
54413.1502	R	109.7876	0.9457
54415.1310	R	99.8762	0.6268
54415.1506	I	85.0472	1.0682
54419.1507	R	81.7217	0.4959
54419.1736	I	66.2979	0.8337
54421.1270	R	74.3809	0.6763
54423.2846	R	67.4615	0.6747
54435.2168	R	48.1496	0.8405
54435.2326	I	58.6381	1.5633
54439.1346	R	44.3748	0.4469

Continued

Table C.1 (Continued)

MJD	Passband	$Flux_{25}$	σ_{Flux}
54439.1491	I	58.4686	0.7233
54441.1621	R	40.9818	0.6527
54443.1136	R	38.4205	0.6589
54443.1282	I	53.5149	1.3133
54445.1098	R	34.7140	0.4942
54445.1320	I	49.5596	1.0164
54447.1844	R	31.2376	0.4891
54449.1839	R	28.7222	0.5878
54453.1848	R	22.4633	1.4800
54464.1561	R	16.6551	0.6579
54464.1599	I	21.0702	0.8436
54469.1223	R	15.6739	0.4439
54469.1293	I	19.5977	0.7680
	y125		
54351.3338	R	-0.1270	0.6558
54354.3478	R	-0.0740	0.5087
54354.3979	I	-0.6962	0.9126
54360.3218	R	-0.5508	0.9415
54363.3401	I	1.1419	1.0795
54363.3803	R	0.3355	0.6276
54375.3079	R	-0.6356	1.2072
54379.2793	R	-0.5324	0.7744
54379.3164	I	2.3931	1.6178
54381.2740	R	-0.0988	0.5436
54383.2873	R	-0.1362	0.5568
54383.3093	I	-0.3703	0.7078
54387.2696	R	-0.4472	0.6369
54387.3102	I	-5.3023	2.4204
54389.2756	I	2.8990	1.9679
54391.3188	R	2.4188	0.9553
54393.2622	R	3.4463	0.6136
54407.2890	R	26.4578	1.0011
54409.2439	R	27.5633	0.4397
54409.2627	I	32.7925	0.7758
54415.0765	R	27.9885	0.7235
54415.0920	I	35.9144	0.9337
54417.0817	R	26.4955	0.4213
54417.1193	I	32.7395	0.6845
54419.0655	R	26.3598	0.4630
54419.0898	I	33.8385	0.6652
54421.0850	R	24.5422	0.6100
54423.2497	R	21.7448	0.7583
54435.1808	R	12.4434	0.8440
54435.2034	I	17.3765	1.6789
54439.0999	R	11.4665	0.3810
54439.1213	I	14.1542	0.7312
54441.1848	R	9.6537	0.6777
54451.1068	R	6.2910	0.7961
54451.1103	I	13.0699	1.1966
54453.0891	R	6.4106	1.4109
	y127		
54351.3585	R	1.1034	0.6529
54354.3767	R	1.2548	0.5225
54354.4120	I	-1.3473	1.9667
54360.3448	R	0.0641	0.7632
54375.3580	I	-1.0065	1.9207
54381.3245	R	0.7368	0.7094
54381.3506	I	-1.5273	0.8536
54383.3397	R	0.7706	0.4435
54383.3569	I	1.6600	0.7743
54385.3419	R	0.4369	0.7562
54387.3254	R	2.4712	0.6367
54387.3723	I	1.7573	0.9306
54391.3672	R	5.5433	0.5839
54393.3012	R	7.6128	0.4963
54409.3074	R	11.1700	0.5066
54409.3305	I	11.4739	1.1573
54411.3421	R	8.8914	0.6206
54413.1269	I	13.2518	1.9539
54413.1542	R	10.0868	0.8596

Continued

Table C.1 (Continued)

MJD	Passband	$Flux_{25}$	σ_{Flux}
54415.1352	R	8.8674	0.5579
54415.1567	I	11.0791	0.9411
54417.1775	R	9.2459	0.4313
54419.1543	R	7.9890	0.4083
54421.1314	R	7.1350	0.4893
54421.1626	I	8.5309	0.8793
54423.2881	R	3.5173	0.9103
54435.2210	R	2.1029	0.8555
54435.2388	I	3.4624	1.5313
54439.1385	R	2.2605	0.4001
54439.1552	I	5.4696	0.9403
54441.1660	R	3.2895	0.4976
54449.1804	R	1.4115	0.4807
54451.1857	R	1.5461	0.7380
	y134		
54351.2877	R	0.5452	0.8263
54354.3004	R	0.0561	0.6712
54357.2914	I	1.9031	1.0549
54379.2247	I	1.1766	1.2055
54381.2171	R	0.8310	0.5942
54383.2045	R	0.1743	0.6199
54383.2448	I	0.0504	1.2954
54389.2013	R	-0.1022	0.6215
54407.2366	R	2.1350	0.9304
54409.2135	I	27.0282	0.9408
54415.0327	R	22.8692	1.0456
54415.0466	I	27.2823	1.1661
54417.0349	R	24.8645	0.8353
54417.0519	I	27.4389	1.0843
54419.0331	R	21.8908	0.5868
54419.0371	I	27.7856	0.8893
54421.0260	R	20.7923	0.5786
54421.0674	I	25.9734	1.2420
54423.1294	R	20.4366	0.7699
54423.2267	I	20.9065	1.8378

Continued

Table C.1 (Continued)

MJD	Passband	$Flux_{25}$	σ_{Flux}
54435.1148	R	19.2896	0.8320
54435.1291	I	15.2360	1.9389
54439.0337	R	7.9706	0.9472
54439.0495	I	15.2616	0.8274
54451.0407	R	6.3807	1.4129
54451.0517	I	5.7284	1.7764
	y136		
54351.3620	R	1.3520	0.5802
54354.3803	R	0.5624	0.4685
54357.3161	I	0.5612	0.9953
54360.3483	R	1.3267	0.6048
54375.3639	I	-0.6996	1.8552
54381.3282	R	0.7759	0.5894
54381.3566	I	0.7886	1.0067
54383.3433	R	-0.6726	0.4318
54383.3629	I	-1.7276	1.1788
54385.3496	R	0.6492	0.7898
54387.3387	R	-0.8014	0.5974
54387.3781	I	-2.2930	1.1995
54389.3125	R	0.5244	0.9613
54391.2625	R	1.1702	0.6539
54391.3634	R	0.4796	0.5372
54393.3172	R	1.4985	0.4802
54393.3530	I	2.8055	0.8857
54407.3311	R	5.9666	1.2740
54409.3144	R	5.6483	0.5850
54409.3430	I	8.8594	1.0666
54411.3505	R	6.7242	0.7472
54413.1613	R	5.3742	0.6793
54415.1470	R	4.7142	0.4875
54417.1810	R	4.8163	0.3985
54419.1445	I	7.0641	0.6486
54419.1586	R	4.4772	0.3856
54421.1349	R	4.2763	0.4726
54421.1565	I	13.1261	0.6557

Continued

Table C.1 (Continued)

MJD	Passband	$Flux_{25}$	σ_{Flux}
54423.2916	R	4.9777	0.6727
54423.3290	I	5.3730	1.7089
54435.2245	R	1.0684	0.9031
54435.2448	I	4.3080	1.7085
54439.1421	R	2.8515	0.3972
54439.1610	I	3.9234	0.7724
54441.1696	R	1.4605	0.4754
54443.1719	R	1.4489	0.5750
54445.1286	R	2.4194	0.3834
54445.1555	I	1.8714	1.3503
54447.1751	R	1.6409	0.4207
54447.1786	I	3.2714	1.0546
54449.1653	R	1.3823	0.4917
54449.1740	I	4.0369	0.8511
54451.1759	R	2.3735	0.9595
54453.1753	R	1.4081	1.4058
54453.1788	I	0.7433	2.7771
54464.1661	R	1.2304	0.5892
54464.1695	I	1.5502	0.9313
54469.1258	R	0.5093	0.3541
54469.1351	I	1.6402	0.7076
54472.1873	R	0.6120	0.6683
54474.2000	R	0.3813	1.2400
	y137		
54351.2953	R	0.2851	0.5994
54354.3076	R	1.0727	0.5560
54357.3033	I	1.2725	1.0383
54360.2884	R	0.7376	1.7325
54379.2101	R	1.7061	1.0051
54379.2366	I	-0.5071	1.2118
54383.2299	R	-0.8300	0.5586
54383.2572	I	1.3462	0.8557
54389.2124	R	-0.2851	0.8439
54393.2258	R	0.9780	0.5506
54407.2401	R	12.0907	0.8773

Continued

Table C.1 (Continued)

MJD	Passband	$Flux_{25}$	σ_{Flux}
54409.2053	R	13.8623	0.4732
54409.2251	I	15.3562	0.9372
54415.0396	R	18.8836	0.5969
54415.0591	I	22.8784	1.3283
54419.0209	R	21.8977	0.5285
54421.0335	R	20.7810	0.5412
54423.1683	R	19.3568	0.8375
54435.1219	R	12.3022	0.8224
54435.1410	I	18.1287	1.4909
54439.0417	R	11.2394	0.7395
54439.0626	I	15.0571	0.7820
54441.0388	R	10.5203	0.4798
54441.0641	I	14.7715	0.7908
54443.0360	R	8.6623	0.7040
54443.0592	I	14.0794	0.9776
54445.0514	I	12.7505	0.7599
54447.0360	R	7.2372	0.4714
54447.0542	I	13.0114	0.6872
54449.0379	R	6.0260	0.5643
54449.0558	I	11.9467	0.7978
54451.0669	R	5.4766	0.9951
54451.0704	I	12.2081	1.4342
54464.0531	R	3.0589	0.4668
54464.0739	I	7.7676	0.8187
54467.0781	R	2.5497	0.4413
54467.0973	I	8.0445	1.0877
54469.0657	R	2.5980	0.3980
54472.0693	R	2.7817	0.6069
54474.0680	R	2.4802	0.8320
54474.0809	I	4.7744	1.4596
	y142		
54447.1786	I	5.6358	0.9071
54449.1653	R	2.4753	0.4638
54449.1740	I	7.2160	0.7914
54451.1759	R	3.3768	1.0604

Continued

Table C.1 (Continued)

MJD	Passband	$Flux_{25}$	σ_{Flux}
54453.1753	R	3.7290	1.1130
54453.1788	I	0.8740	2.7686
54464.1661	R	0.6216	0.5613
54464.1695	I	3.0423	0.8179
54469.1258	R	1.1713	0.3767
54469.1351	I	3.4506	0.7271
54472.1873	R	1.1933	0.7125
54474.2000	R	0.7286	1.1651
54351.3620	R	0.2816	0.5690
54354.3803	R	-1.4117	0.4590
54354.4178	I	-0.2850	3.6224
54357.3161	I	0.5034	1.2111
54360.3483	R	0.5029	0.6021
54375.3639	I	0.5638	1.9009
54381.3282	R	0.0783	0.5990
54381.3566	I	1.1337	0.8782
54383.3433	R	0.1894	0.4280
54383.3629	I	-0.7311	1.0410
54385.3496	R	-0.8934	0.8109
54387.3387	R	-1.0422	0.5430
54387.3781	I	0.4976	1.1722
54389.3125	R	0.6007	0.9587
54389.3235	I	-0.3422	2.0936
54391.2625	R	-0.0429	0.5878
54391.3634	R	0.2676	0.5081
54393.3172	R	0.6732	0.4497
54393.3530	I	-1.2695	1.0014
54407.3311	R	4.6969	1.2524
54409.3144	R	5.7028	0.5582
54409.3430	I	7.9064	0.9899
54411.3505	R	7.9534	0.6870
54413.1613	R	8.6466	0.7049
54415.1470	R	8.6319	0.4512
54417.1810	R	9.6039	0.3692
54419.1445	I	11.8598	0.6197

Continued

Table C.1 (Continued)

MJD	Passband	$Flux_{25}$	σ_{Flux}
54419.1586	R	9.3981	0.3690
54421.1349	R	9.5024	0.4872
54421.1565	I	13.0159	0.5571
54423.2916	R	10.1368	0.7567
54423.3290	I	10.3542	1.5741
54435.2245	R	6.3114	0.7571
54435.2448	I	11.4211	1.5621
54439.1421	R	6.2161	0.3713
54439.1610	I	6.8840	0.8745
54441.1696	R	4.7020	0.4806
54443.1719	R	4.8708	0.6028
54445.1286	R	2.8826	0.4834
54445.1555	I	8.9950	1.3168
54447.1751	R	3.5967	0.4146
	y143		
54351.3119	R	-1.0812	0.5649
54351.3749	I	-0.5070	1.1692
54354.3188	R	0.5421	0.6555
54360.3616	I	1.8292	1.6824
54377.2716	R	0.0214	0.5232
54377.2955	I	-0.2097	0.9855
54379.2873	R	0.7160	0.9609
54379.3224	I	-0.8448	1.7876
54381.2542	R	1.2163	0.4564
54381.2851	I	-1.9968	1.2707
54383.3233	R	0.4648	0.4594
54387.2732	I	1.3954	1.3139
54391.2393	R	3.0283	1.4169
54393.2664	R	7.5788	0.5822
54407.2482	R	12.9618	0.6794
54407.2645	I	14.7952	1.5903
54411.2654	R	11.5640	0.4570
54411.2818	I	13.4281	0.8007
54415.1162	R	10.3883	0.4857
54417.0673	R	8.8974	0.4210

Continued

Table C.1 (Continued)

MJD	Passband	$Flux_{25}$	σ_{Flux}
54417.1010	I	11.5595	0.7507
54419.0732	R	8.8932	0.4406
54419.1054	I	11.6965	0.6330
54421.0976	R	8.1335	0.5087
54421.1081	I	11.1935	0.8365
54423.2567	R	6.9081	0.6983
54423.2671	I	11.6843	1.1949
54435.2095	R	1.2548	0.9200
54437.1754	R	1.8122	0.8032
54437.1949	I	7.6113	1.2992
54439.1275	R	2.2268	0.4396
54441.0795	R	2.8798	0.4909
54441.1054	I	6.2433	0.9081
54443.0908	R	2.3187	0.7837
54443.1075	I	5.9895	1.0737
54445.0878	R	2.8729	0.5110
54445.1040	I	5.2586	0.9520
54447.1151	R	1.2514	0.4751
54449.1024	R	1.6088	0.4648
54449.1061	I	5.9432	0.7264
54451.1161	R	0.6997	0.8133
54451.1196	I	4.5355	1.2386
54453.1113	R	0.9129	1.5612
54453.1150	I	0.1074	3.3456
54464.0805	R	-0.0503	0.4470
54464.0842	I	3.3031	0.8252
54467.1038	R	0.7559	0.4905
54467.1251	I	2.9856	0.8941
54469.1023	R	0.7322	0.3647
54472.0885	R	0.1895	0.5086
54472.1218	I	1.6415	0.8743
54474.1164	R	0.4805	0.5183
	y145		
54351.2773	R	-0.2640	0.4154
54354.2895	R	0.0902	0.5307

Continued

Table C.1 (Continued)

MJD	Passband	$Flux_{25}$	σ_{Flux}
54357.2699	I	-0.3904	1.0084
54360.2687	R	0.0136	1.1760
54363.2826	I	3.3023	3.0796
54377.2119	R	-0.2732	0.5333
54381.2009	R	-0.0776	0.5357
54389.2050	R	-0.2692	0.7192
54407.2011	R	7.7164	0.6410
54411.2030	R	9.8514	0.3955
54411.2228	I	11.7606	0.7878
54417.0313	R	9.9882	0.5476
54417.0420	I	10.5011	0.8410
54419.0288	R	11.6559	0.4846
54419.0530	I	12.9758	0.7013
54421.0473	R	10.8723	0.5339
54423.2032	R	11.9844	0.9859
54423.2148	I	11.7001	2.2524
54435.1526	R	7.6629	0.8422
54437.1380	R	7.4858	0.5933
54437.1544	I	7.7795	1.3354
54439.0748	R	6.5345	0.4947
54441.0423	R	5.4669	0.5169
54441.0699	I	8.8467	0.7818
54451.0576	R	2.7985	1.1242
54453.0400	R	3.3306	2.4230
	y151		
54351.3191	R	-0.6218	0.6059
54351.3897	I	-0.2332	1.1680
54354.3260	R	0.4147	0.6521
54360.3070	R	-1.1138	0.9256
54363.3696	R	-0.2215	0.6733
54377.3072	I	-0.8518	0.9891
54381.2619	R	0.2079	0.4958
54381.2971	I	-0.1983	1.0730
54383.3304	R	-0.9313	0.6188
54387.2589	R	1.0594	0.6071

Continued

Table C.1 (Continued)

MJD	Passband	$Flux_{25}$	σ_{Flux}
54387.2850	I	-5.5818	2.7420
54393.2927	R	-1.0493	0.5803
54407.2552	R	1.2281	0.7752
54409.2865	R	2.3842	0.4384
54409.2937	I	2.6816	1.0060
54411.2724	R	3.5497	0.5258
54411.2937	I	4.8579	0.8781
54413.1338	R	3.2816	0.7680
54417.0745	R	5.1508	0.4292
54417.1127	I	6.1930	0.7174
54419.0809	R	6.6216	0.4553
54419.1173	I	7.3201	0.6585
54421.1153	I	9.3268	0.7713
54423.2636	R	7.4398	0.6752
54423.2730	I	9.5224	1.2883
54437.1824	R	6.5908	0.6965
54437.2067	I	9.5487	1.2004
54439.1311	R	5.9893	0.4252
54441.0866	R	5.7113	0.4704
54441.1171	I	7.5900	0.9896
54445.1861	R	3.5463	0.9308
54447.1552	R	4.1888	0.4770
54447.1590	I	6.8005	1.0324
54449.1406	R	2.9401	0.5179
54449.1441	I	7.3905	1.0977
54451.1447	R	1.4895	1.0469
54453.1468	R	0.9798	1.5837
54453.1503	I	0.4558	2.1765
54464.0994	R	1.7554	0.3984
54464.1029	I	3.3818	0.8189
54467.1110	R	1.0873	0.6258
54469.1093	R	0.4681	0.3967
54469.1165	I	2.5091	0.7735
54472.0955	R	0.7604	0.4514
y154			
Continued			

Table C.1 (Continued)

MJD	Passband	$Flux_{25}$	σ_{Flux}
54351.3264	R	-0.7600	0.6589
54354.3388	R	-0.2860	0.5059
54360.3145	R	0.9258	0.8024
54363.3271	I	-0.0865	1.0056
54363.3768	R	0.2112	0.6483
54375.3008	R	0.4739	1.0436
54375.3172	I	-1.7373	1.7267
54379.2670	R	0.3659	0.7850
54379.3008	I	-1.1198	1.5272
54381.2664	R	-0.0733	0.5283
54381.3029	I	0.7930	0.9134
54383.2796	R	-0.1140	0.4486
54383.2973	I	0.4336	0.6408
54385.3147	I	-1.7630	1.6085
54387.2624	R	-1.0990	0.7777
54387.2914	I	-0.2857	1.9296
54389.2815	I	1.2462	1.6301
54391.3226	R	-1.3995	1.2003
54393.2784	R	0.5715	0.5068
54393.2819	I	0.8457	0.8844
54409.2550	R	6.3789	0.6606
54409.2801	I	5.7034	0.7779
54415.0884	R	7.6666	0.6050
54415.1100	I	8.7281	0.9672
54417.0853	R	7.3457	0.4361
54417.1265	I	8.9375	0.6412
54419.0853	R	6.7391	0.4216
54419.1232	I	7.5981	0.5846
54421.0771	R	6.9049	0.6050
54421.1212	I	8.4800	0.8531
54423.2425	R	6.7700	0.8202
54423.2788	I	8.3284	1.1720
54435.1736	R	3.6424	0.7909
54435.1904	I	5.8953	1.4042
54439.0926	R	2.9965	0.3424
Continued			

Table C.1 (Continued)

MJD	Passband	$Flux_{25}$	σ_{Flux}
54439.1093	I	4.7525	0.7008
54441.1811	R	2.6794	0.5860
54453.1564	R	0.9694	1.5714
54453.1599	I	2.2356	1.8156
54467.1181	R	1.1823	0.5319
54472.1027	R	0.6762	0.5095
y158			
54351.3227	R	-0.3155	0.4275
54351.3962	I	0.9503	1.1121
54354.3297	R	-0.1561	0.4958
54360.3109	R	-0.0235	0.9971
54363.3731	R	0.6633	0.5845
54375.3114	I	-0.0203	1.5896
54377.2825	R	0.8604	0.4573
54377.3159	I	-0.7835	1.2782
54379.2635	R	0.2485	0.6772
54379.2950	I	0.4941	1.1076
54383.2696	R	-0.0436	0.4759
54383.2911	I	-0.2361	0.8696
54393.2703	R	0.7690	0.5103
54409.2515	R	5.7886	0.4931
54409.2743	I	7.0348	0.7933
54415.0843	R	8.7524	0.6013
54417.0780	R	9.3968	0.3937
54417.1323	I	11.3254	0.7006
54419.0770	R	10.5506	0.4006
54419.1112	I	11.8746	0.6074
54421.0734	R	11.8587	0.5146
54421.1686	I	13.2348	0.5961
54423.2388	R	11.8451	0.8456
54435.1598	R	8.9901	0.6046
54435.1843	I	11.1225	1.3352
54439.0889	R	6.9656	0.4263
54439.1034	I	8.3848	0.7422
54441.1775	R	7.0687	0.6382

Continued

Table C.1 (Continued)

MJD	Passband	$Flux_{25}$	σ_{Flux}
54443.0834	R	5.6306	0.6416
54443.1758	I	6.1244	1.2525
54445.0808	R	5.1699	0.4088
54445.0914	I	8.5434	0.6646
54447.1352	R	4.0347	0.4252
54447.1390	I	7.9895	0.9094
54449.1215	R	3.5839	0.4786
54449.1252	I	5.8478	0.9927
54451.1258	R	2.7602	0.7669
54451.1293	I	3.2911	1.2735
54453.1270	R	2.9568	1.2562
54453.1307	I	6.7001	1.7058
54467.1145	R	1.5675	0.5091
54472.0991	R	1.7317	0.4549
y163			
54351.3155	R	0.0000	0.5458
54351.3819	I	2.2659	1.2877
54354.3224	R	-0.3624	0.4731
54357.3600	R	-0.8840	0.7285
54360.3034	R	0.4734	1.0385
54363.3207	I	0.6734	1.7867
54363.3661	R	-0.7899	0.5255
54377.2751	R	0.5940	0.6245
54377.3013	I	1.3538	1.0025
54379.2911	R	-1.6871	0.8318
54381.2580	R	0.0297	0.4309
54381.2911	I	0.4094	1.0584
54383.3268	R	-0.3019	0.4258
54385.3275	I	-2.3788	1.3162
54387.2548	R	0.5421	0.5615
54387.2790	I	-0.0678	1.2846
54391.2864	R	-1.1688	1.7965
54391.3149	R	1.0553	1.1269
54393.2583	R	-0.0484	0.6303
54407.2517	R	0.8949	0.6741

Continued

Table C.1 (Continued)

MJD	Passband	$Flux_{25}$	σ_{Flux}
54407.2703	I	-0.2665	1.8840
54411.2607	R	2.8867	0.4502
54411.2759	I	3.4366	0.8974
54415.1275	R	3.8824	0.4489
54417.0710	R	3.5430	0.4053
54417.1068	I	6.2922	0.7061
54419.0690	R	4.3698	0.4084
54419.0993	I	5.9668	0.7043
54421.1011	R	3.0035	0.5295
54423.2602	R	3.3199	0.5997
54437.1789	R	2.3456	0.7799
54437.2009	I	2.6121	1.2762
54441.0831	R	1.0107	0.4271
54441.1113	I	4.9615	0.8718
54445.1826	R	1.8465	0.9753
54447.1251	R	0.7504	0.4518
54447.1286	I	2.8502	0.9441
54449.1122	R	0.7911	0.4758
54449.1157	I	3.9286	0.9258
54451.1033	R	0.4393	0.9896
54453.0786	R	-5.4689	1.2501
54464.0901	R	0.5848	0.3612
54464.0936	I	0.7882	0.7300
54467.1074	R	0.2048	0.4327
54467.1304	I	2.8698	0.8250
54469.1059	R	-0.3575	0.3808
54472.0920	R	-0.0021	0.4638
54472.1441	I	0.1362	1.1230
54474.1201	R	-0.1643	0.6348
	y175		
54351.3373	R	0.1770	0.6235
54354.3523	R	0.3531	0.5544
54357.3282	I	-0.4169	1.3943
54360.3254	R	0.8461	0.8530
54363.3460	I	0.4024	1.1670

Continued

Table C.1 (Continued)

MJD	Passband	$Flux_{25}$	σ_{Flux}
54363.3839	R	1.4967	0.6035
54377.3282	R	0.6293	0.7081
54381.3367	R	0.1609	0.5326
54381.3685	I	0.3855	1.1012
54383.3785	R	1.4595	0.6773
54389.3530	I	-0.4041	2.1565
54393.3256	R	-0.3775	0.6231
54407.2925	R	0.0686	1.0418
54407.3076	I	0.4835	1.5261
54409.3001	R	3.1935	0.5907
54409.3187	I	2.1941	0.9979
54411.3021	R	2.2912	0.5184
54411.3168	I	4.1003	1.0307
54415.1747	R	4.3505	0.5922
54417.1384	I	9.9342	0.6939
54417.1632	R	8.9490	0.3993
54419.1294	I	11.1697	0.6822
54419.1623	R	9.7051	0.4968
54421.1425	R	11.6596	0.5339
54421.1745	I	14.3052	0.8190
54423.2986	R	13.1822	0.7481
54437.2127	R	5.7818	0.5979
54437.2361	I	13.8291	1.5197
54439.1802	R	8.1997	0.6970
54441.1234	R	4.6820	0.5945
54441.1273	I	10.4395	0.8766
54443.1245	R	5.5458	0.7489
54443.1456	I	9.8524	1.3077
54445.1250	R	4.3708	0.5966
54445.1495	I	9.9251	1.1130
54447.1658	R	4.5724	0.5231
54447.1693	I	7.5140	0.9250
54449.1502	R	3.5042	0.5931
54449.1548	R	4.5198	0.9465
54449.1587	I	9.3716	0.9245

Continued

Table C.1 (Continued)

MJD	Passband	$Flux_{25}$	σ_{Flux}
54451.1666	R	1.6096	1.0018
54451.1701	I	5.7016	1.5564
54453.1660	R	2.2400	1.4473
54453.1695	I	7.3642	1.8224
54467.1915	R	1.2115	0.6193
54472.1835	R	1.8882	0.7208
	y177		
54351.3373	R	-0.2821	0.5175
54354.3523	R	-0.2634	0.6870
54357.3282	I	1.5422	1.5913
54360.3254	R	0.7409	0.9581
54363.3460	I	-1.4577	1.1246
54363.3839	R	-0.7997	0.5919
54377.3282	R	-0.5574	0.6433
54381.3367	R	-0.0383	0.4323
54381.3685	I	0.7077	1.0196
54383.3785	R	0.0721	1.0294
54389.3530	I	-1.8414	2.2610
54393.3256	R	0.5775	0.5129
54407.2925	R	-0.2879	1.0626
54407.3076	I	-0.1037	1.5652
54409.3001	R	-0.3964	0.4836
54409.3187	I	0.8404	0.9377
54411.3021	R	-0.2656	0.4377
54411.3168	I	0.3961	0.8398
54415.1747	R	2.2773	0.5867
54417.1384	I	4.1447	0.6306
54417.1632	R	3.0941	0.3259
54419.1294	I	7.2391	0.6065
54419.1623	R	5.6264	0.3742
54421.1425	R	9.2939	0.4464
54421.1745	I	11.7253	0.6472
54423.2986	R	13.0493	0.6592
54437.2127	R	30.4342	0.6929
54437.2361	I	38.3957	1.5069
	Continued		

Table C.1 (Continued)

MJD	Passband	$Flux_{25}$	σ_{Flux}
54439.1802	R	31.8834	0.6139
54441.1234	R	32.0635	0.5714
54441.1273	I	39.3786	1.1004
54443.1245	R	31.0868	0.6366
54443.1456	I	39.9101	1.3016
54445.1250	R	29.4114	0.5584
54445.1495	I	36.8502	0.9703
54447.1658	R	26.2771	0.4836
54447.1693	I	33.7745	0.8591
54449.1548	R	26.3676	0.6234
54449.1587	I	33.4068	0.8297
54451.1666	R	22.7828	1.0314
54451.1701	I	28.8475	1.5482
54453.1660	R	22.1680	1.3147
54453.1695	I	29.1629	4.1104
54467.1915	R	11.3691	0.4611
54472.1835	R	8.7626	0.6313
	z180		
54351.2953	R	0.7738	0.6548
54354.3076	R	-0.2261	0.5628
54357.3033	I	0.5968	1.1259
54360.2884	R	-2.5964	1.7965
54379.2101	R	-0.3720	0.9561
54379.2366	I	-0.9349	1.1758
54383.2299	R	0.0798	0.4886
54383.2572	I	0.8629	0.8678
54389.2124	R	0.4742	0.7787
54393.2258	R	-0.3949	0.5262
54407.2401	R	0.1749	0.8406
54409.2053	R	0.0126	0.4163
54409.2251	I	0.2341	0.9128
54415.0396	R	0.0817	0.5225
54415.0591	I	-0.6530	1.4510
54419.0209	R	0.8004	0.4845
54421.0335	R	1.6575	0.5340
	Continued		

Table C.1 (Continued)

MJD	Passband	$Flux_{25}$	σ_{Flux}
54423.1683	R	2.0244	0.7818
54435.1219	R	15.1689	0.7395
54435.1410	I	16.5446	1.5353
54439.0417	R	16.4348	0.7223
54439.0626	I	19.8749	0.8872
54441.0388	R	18.0406	0.4287
54441.0641	I	20.3693	0.7971
54443.0360	R	15.4835	0.7310
54443.0592	I	19.9325	1.2159
54445.0514	I	21.9972	0.8122
54447.0360	R	15.9047	0.4615
54447.0542	I	20.0436	0.7324
54449.0379	R	16.1105	0.6708
54449.0558	I	20.4347	0.8041
54451.0669	R	14.7624	1.0322
54451.0704	I	18.0526	1.3544
54464.0531	R	7.8076	0.4835
54464.0739	I	11.3643	0.8863
54467.0781	R	5.4584	0.3979
54467.0973	I	11.1753	1.1487
54469.0657	R	5.0781	0.3753
54472.0693	R	5.1863	0.5315
54474.0680	R	3.9340	0.8485
54474.0809	I	10.1572	1.4577
z181			
54351.3302	R	-0.4133	0.5130
54351.4080	I	-0.8733	1.1344
54354.3440	R	-0.5900	0.5251
54360.3181	R	-0.0528	0.8768
54363.3331	I	0.8669	0.9691
54375.3044	R	-1.0838	1.2210
54377.2861	R	0.3444	0.5574
54377.3217	I	-0.7905	1.3108
54379.2711	R	-0.3903	0.7600
54379.3073	I	1.2575	1.6856

Continued

Table C.1 (Continued)

MJD	Passband	$Flux_{25}$	σ_{Flux}
54381.2700	R	-0.6308	0.5373
54381.3089	I	1.3937	0.9719
54383.2835	R	0.0619	0.4552
54383.3031	I	0.6003	0.6400
54387.2659	R	-0.7042	0.7076
54387.3040	I	1.0228	1.4948
54393.2746	R	0.6945	0.4801
54409.2474	R	0.8471	0.5483
54409.2685	I	-0.6013	0.7670
54415.0807	R	0.2018	0.5149
54415.0982	I	1.5004	0.9649
54421.0815	R	1.9298	0.4518
54423.2462	R	2.3739	0.7136
54435.1772	R	6.1077	0.7691
54435.1974	I	7.8462	1.3651
54439.0963	R	6.5060	0.3695
54439.1154	I	7.7373	0.7262
54441.0901	R	6.1569	0.4718
54441.0996	I	9.4924	0.9154
54443.0872	R	6.9216	0.6604
54443.1015	I	-0.1947	1.8709
54443.1818	I	10.0751	1.5445
54445.0843	R	4.9632	0.3985
54445.0976	I	7.1408	0.7711
54447.1451	R	4.9099	0.5262
54447.1488	I	8.1115	1.0260
54449.1311	R	4.9210	0.5779
54449.1346	I	7.3119	1.0555
54451.1354	R	4.3691	0.7919
54451.1389	I	5.9107	1.4319
54453.1372	R	2.6351	1.2413
54453.1407	I	3.9508	1.6793
54464.1087	R	1.6812	0.4221
54467.1217	R	1.3857	0.3914
54467.1356	I	4.7908	0.9570

Continued

Table C.1 (Continued)

MJD	Passband	$Flux_{25}$	σ_{Flux}
54469.1129	R	1.6106	0.3782
	z183		
54351.2738	R	-0.1558	0.4232
54354.2860	R	-0.3881	0.4801
54357.2637	I	-0.4627	0.8131
54363.2768	I	-2.3180	1.5096
54377.2080	R	-0.2639	0.5326
54377.2355	I	0.8456	1.0182
54379.2174	R	0.2543	0.8284
54379.2485	I	0.0685	1.6679
54381.1970	R	0.6987	0.5305
54381.2254	I	0.0387	0.7677
54383.2374	R	-0.5599	0.6367
54389.2210	R	0.2145	1.0060
54393.2332	R	-0.6461	0.6636
54393.2375	I	0.2346	1.0381
54407.1976	R	-0.0113	0.6251
54409.2369	R	0.5429	0.4967
54411.1979	R	0.8595	0.4301
54411.2164	I	1.4301	0.9232
54421.0187	R	12.2479	0.6621
54423.1034	R	15.1935	0.8220
54437.1289	R	37.1997	0.6891
54437.1486	I	39.1028	1.4253
54441.0256	R	34.5042	0.8996
54441.0458	I	43.3840	0.7865
54443.0447	R	37.3118	0.7377
54443.0714	I	43.4283	1.5659
54445.0407	R	35.1923	0.7025
54445.0631	I	41.2619	0.8141
54447.0432	R	33.1223	0.4378
54447.0658	I	39.7396	0.8234
54449.0454	R	32.5332	0.6546
54449.0685	I	37.1319	0.9094
54451.0869	R	26.7109	0.9545

Continued

Table C.1 (Continued)

MJD	Passband	$Flux_{25}$	σ_{Flux}
54451.0904	I	30.9885	1.5437
54464.0419	R	14.6496	0.6568
54464.0618	I	23.9242	0.8166
54467.0633	R	12.6404	0.5700
54467.0816	I	20.4752	0.9311
54469.0538	R	12.7716	0.4524
54472.0570	R	9.8104	0.6440
54472.0766	I	18.3112	1.0846
54474.0501	R	8.7846	0.7265
	z185		
54351.2807	R	-0.0478	0.4330
54354.2929	R	0.5178	0.4743
54357.2790	I	-0.4935	0.7969
54377.2155	R	-0.1749	0.6748
54377.2473	I	0.5818	0.8464
54379.2209	R	-0.7531	0.7068
54379.2544	I	-1.1035	1.5297
54381.2046	R	-0.2708	0.4857
54381.2381	I	-0.5446	0.7612
54383.2411	R	0.0966	0.6109
54389.2246	R	0.8639	0.9805
54393.2437	R	0.8415	0.7315
54407.2046	R	0.5959	0.7460
54409.2404	R	1.4070	0.5049
54411.2079	R	1.0567	0.4502
54421.0222	R	11.2414	0.6965
54423.1249	R	11.1373	0.7478
54435.1562	R	14.9071	0.7722
54437.1415	R	15.0575	0.6571
54437.1602	I	14.9717	1.2831
54439.0851	R	12.9090	0.4677
54441.0296	R	11.4975	0.7614
54441.0516	I	14.7835	0.7105
54443.0490	R	12.6044	0.8592
54443.0772	I	15.0846	1.4071

Continued

Table C.1 (Continued)

MJD	Passband	$Flux_{25}$	σ_{Flux}
54445.0443	R	11.4452	0.4891
54445.0690	I	14.0333	0.7808
54447.0466	R	9.1967	0.4418
54447.0717	I	12.5879	0.9740
54449.0489	R	7.1693	0.6290
54464.0458	R	2.6723	0.5306
54464.0566	I	6.1686	0.7946
54467.0703	R	2.6780	0.4742
54467.0868	I	6.9147	0.8918
54469.0582	R	2.0136	0.4762
54472.0605	R	1.7688	0.7106
54472.0825	I	4.9449	0.9843
54474.0536	R	1.8189	0.7037
z187			
54407.2307	I	1.2729	1.6927
54411.2123	R	-0.3013	0.7205
54419.0591	I	0.6499	0.6537
54421.0517	R	-0.4591	0.4443
54423.1992	R	3.7025	0.5441
54437.1451	R	10.9129	0.9536
54437.1660	I	35.5652	1.5933
54441.0345	R	30.0168	0.7253
54441.0576	I	35.2502	0.6890
54443.0405	R	30.2890	0.5466
54443.0656	I	36.0132	1.2794
54445.0366	R	28.1078	0.7064
54445.0573	I	34.7863	1.0273
54447.0397	R	25.6255	0.6349
54447.0600	I	31.0314	0.7664
54449.0417	R	25.8356	0.4781
54449.0627	I	28.6017	0.8565
54451.0765	R	24.1814	0.5938
54451.0811	I	25.4901	1.6314
54464.0493	R	19.7959	0.9415
54464.0681	I	16.2820	0.8479

Continued

Table C.1 (Continued)

MJD	Passband	$Flux_{25}$	σ_{Flux}
54467.0746	R	10.3901	0.5744
54467.0921	I	13.4859	1.0535
54469.0621	R	8.8635	0.5297
54472.0657	R	8.0708	0.4764
54474.0570	R	5.9216	0.5668
54474.0751	I	13.4333	1.4445
54351.2842	R	-0.4552	0.6180
54354.2966	R	-0.7226	0.4709
54357.2853	I	-1.1864	0.7025
54363.3020	I	-1.6464	1.7976
54377.2191	R	-0.7450	0.5655
54381.2134	R	-0.9484	0.5612
54389.2088	R	-0.3071	0.5119
54391.2209	R	0.6161	0.8416
54393.2198	R	0.2838	0.9928
54407.2084	R	-0.5037	0.7614
z200			
54351.2738	R	-0.3107	0.3792
54354.2860	R	-0.0588	0.5066
54357.2637	I	0.2616	0.9825
54363.2768	I	-2.4459	1.4161
54377.2080	R	-1.6508	0.5622
54377.2355	I	0.4808	1.0957
54379.2174	R	-1.4989	0.8243
54379.2485	I	-0.5169	1.4807
54381.1970	R	1.0373	0.5953
54381.2254	I	-1.1856	0.8566
54383.2374	R	-1.2402	0.6030
54389.2210	R	0.8271	1.0446
54393.2332	R	-0.5577	0.6605
54393.2375	I	1.5158	1.0550
54407.1976	R	-0.1719	0.6089
54407.2124	I	0.0858	1.7999
54409.2369	R	-0.2574	0.5143
54411.1979	R	0.1683	0.4417

Continued

Table C.1 (Continued)

MJD	Passband	$Flux_{25}$	σ_{Flux}
54411.2164	I	0.2506	0.7790
54421.0187	R	1.7726	0.7543
54423.1034	R	-1.4189	0.8160
54437.1289	R	3.1625	0.6721
54437.1486	I	3.5708	1.2017
54441.0256	R	7.3642	0.8692
54441.0458	I	6.5507	0.7335
54443.0447	R	7.5400	0.8621
54443.0714	I	8.2989	1.3581
54445.0407	R	8.4226	0.6180
54445.0631	I	10.5747	0.7800
54447.0432	R	8.9832	0.4444
54447.0658	I	9.7648	0.7267
54449.0454	R	9.6401	0.5593
54449.0685	I	12.8153	0.7788
54451.0869	R	10.9192	0.8724
54451.0904	I	15.2099	1.3332
54453.0673	R	9.7120	2.1843
54464.0419	R	7.9541	0.6736
54464.0618	I	11.2804	0.8196
54467.0633	R	5.9747	0.4939
54467.0816	I	9.5553	0.8754
54469.0538	R	6.1680	0.4740
54472.0570	R	5.7102	0.6042
54472.0766	I	6.2296	1.0547
54474.0501	R	4.0186	0.6313
z202			
54423.2602	R	0.9639	0.8700
54437.1789	R	22.1786	0.8183
54437.2009	I	24.9774	1.4589
54441.0831	R	42.8984	0.7857
54441.1113	I	51.2668	1.1041
54445.1826	R	56.0064	1.1826
54447.1251	R	57.5735	0.6729
54447.1286	I	58.7801	1.1639
Continued			

Table C.1 (Continued)

MJD	Passband	$Flux_{25}$	σ_{Flux}
54449.1122	R	61.7452	0.7511
54449.1157	I	67.5644	1.2393
54451.1033	R	60.1865	1.1100
54453.0786	R	48.8958	1.9550
54453.0821	I	43.6697	3.1742
54464.0901	R	43.7145	0.6385
54464.0936	I	45.7261	1.2182
54467.1074	R	37.4949	0.7011
54467.1304	I	38.8754	1.0787
54469.1059	R	31.5901	0.5797
54472.0920	R	27.0611	0.6959
54472.1441	I	32.7154	1.4780
54474.1201	R	23.7085	0.8152
54351.3155	R	1.4524	0.9076
54351.3819	I	-0.4662	1.7968
54354.3224	R	-0.0439	0.8466
54357.3600	R	-0.8810	0.9682
54360.3034	R	-1.1998	1.1582
54363.3207	I	1.8005	1.8265
54363.3661	R	0.0384	0.8158
54377.2751	R	1.3932	0.8809
54377.3013	I	0.4224	1.3581
54379.2911	R	-1.0517	0.9852
54381.2580	R	0.2162	0.6906
54381.2911	I	1.3080	1.2836
54383.3268	R	0.8251	0.6636
54385.3275	I	0.0698	1.6445
54387.2548	R	-2.8708	0.7930
54387.2790	I	-7.8976	1.7551
54391.2864	R	-4.0877	2.4641
54391.3149	R	-3.6474	1.4208
54393.2583	R	0.6926	0.8054
54407.2517	R	0.4557	1.0142
54407.2703	I	0.4194	1.9494
54411.2607	R	1.1202	0.6616
Continued			

Table C.1 (Continued)

MJD	Passband	$Flux_{25}$	σ_{Flux}
54411.2759	I	1.7145	1.0982
54415.1275	R	-0.0641	0.6318
54417.0710	R	-0.4849	0.6106
54417.1068	I	-0.0547	1.0082
54419.0690	R	-0.8683	0.6132
54419.0993	I	-0.0608	0.9783
54421.1011	R	-0.3839	0.7209
	z203		
54464.0842	I	7.8753	0.8558
54467.1038	R	5.2951	0.4235
54467.1251	I	7.7385	0.9169
54469.1023	R	4.7300	0.3436
54472.0885	R	3.1208	0.4416
54472.1218	I	4.2686	0.9306
54474.1164	R	4.0427	0.5503
54351.3119	R	-0.0860	0.6800
54351.3749	I	0.7320	1.0224
54354.3188	R	-0.4250	0.6536
54360.3616	I	-0.9047	1.6406
54377.2716	R	-0.0818	0.5160
54377.2955	I	-1.2587	0.9807
54379.2873	R	-0.6589	1.0100
54379.3224	I	0.4037	2.0287
54381.2542	R	-0.1076	0.4358
54381.2851	I	-0.8320	1.2358
54383.3233	R	-0.3226	0.4963
54387.2732	I	-0.1887	1.4054
54391.2393	R	2.5495	1.7017
54393.2664	R	-0.8517	0.6921
54407.2482	R	0.1441	0.6729
54407.2645	I	-2.6808	1.4708
54411.2654	R	-0.3726	0.4682
54411.2818	I	-0.8394	0.7669
54415.1162	R	-0.3965	0.4633
54417.0673	R	-0.4214	0.4191

Continued

Table C.1 (Continued)

MJD	Passband	$Flux_{25}$	σ_{Flux}
54417.1010	I	-0.1206	0.7568
54419.0732	R	0.4175	0.4089
54419.1054	I	-0.4612	0.6456
54421.0976	R	-0.2333	0.4941
54421.1081	I	-0.2660	0.8034
54423.2567	R	-0.4687	0.5917
54423.2671	I	-0.5517	1.2706
54435.2095	R	2.5113	0.8570
54437.1754	R	2.9622	0.7872
54437.1949	I	0.7227	1.2637
54439.1275	R	3.7961	0.4154
54441.0795	R	4.2792	0.5288
54441.1054	I	4.0740	0.8671
54443.0908	R	5.9407	0.8047
54443.1075	I	5.6474	1.0732
54445.0878	R	5.6886	0.4250
54445.1040	I	6.8296	0.9189
54447.1151	R	5.9767	0.4198
54449.1024	R	7.3875	0.5390
54449.1061	I	8.6999	0.7667
54451.1161	R	6.6769	0.8390
54451.1196	I	8.2480	1.2829
54453.1113	R	3.9420	1.3516
54453.1150	I	9.1110	2.0240
54464.0805	R	5.4227	0.5584
	z204		
54449.1839	R	6.9171	0.4543
54453.1848	R	3.6783	1.3173
54464.1561	R	4.6557	0.5329
54464.1599	I	8.2658	0.7837
54469.1223	R	3.9974	0.3962
54469.1293	I	6.8644	0.7142
54474.1928	R	2.5807	1.5864
54351.3521	R	-0.1932	0.5772
54354.3729	R	0.4018	0.5704

Continued

Table C.1 (Continued)

MJD	Passband	$Flux_{25}$	σ_{Flux}
54354.4039	I	-0.5095	1.0579
54360.3409	R	-0.4962	0.6345
54375.3513	I	1.9572	1.9130
54379.3293	R	-1.4731	0.9463
54381.3157	R	-1.5504	0.7531
54381.3440	I	0.6900	0.8912
54383.3355	R	-0.5144	0.5095
54383.3510	I	0.6927	0.6828
54385.3340	R	-0.0811	0.9326
54385.3596	I	-0.6277	1.5096
54387.3172	R	-2.2563	1.1805
54387.3467	I	-2.1170	1.0232
54389.3007	R	-2.0738	0.9190
54389.3404	I	-2.2311	2.6169
54393.3055	R	0.1420	0.5251
54409.3036	R	-0.7911	0.5830
54409.3245	I	-0.5603	1.1360
54413.1502	R	-0.6788	0.7328
54415.1310	R	-0.7663	0.5243
54415.1506	I	-0.3850	0.9595
54419.1507	R	0.0764	0.3841
54419.1736	I	1.8120	0.7084
54421.1270	R	-1.3311	0.5579
54423.2846	R	-0.5915	0.6659
54435.2168	R	3.0186	0.9052
54435.2326	I	1.4383	1.3911
54439.1346	R	4.1956	0.3479
54439.1491	I	3.7913	0.6853
54441.1621	R	4.2714	0.6185
54443.1136	R	6.3984	0.6388
54443.1282	I	6.4455	1.1478
54445.1098	R	6.2650	0.4314
54445.1320	I	7.7948	0.8846
54447.1844	R	6.7152	0.4521
z205			
Continued			

Table C.1 (Continued)

MJD	Passband	$Flux_{25}$	σ_{Flux}
54351.3620	R	-0.1696	0.5990
54354.3803	R	-0.3081	0.4911
54357.3161	I	-0.3604	0.8755
54360.3483	R	-0.7309	0.5600
54375.3639	I	0.7309	1.8020
54381.3282	R	-1.1742	0.6086
54381.3566	I	0.9084	0.9018
54383.3433	R	0.0299	0.4569
54383.3629	I	0.5400	1.0311
54385.3496	R	-0.4544	0.8466
54387.3387	R	0.7152	0.5569
54387.3781	I	-1.3868	1.1142
54389.3125	R	-1.4020	0.9966
54389.3235	I	-2.4979	1.9989
54391.2625	R	-0.3994	0.5807
54391.3634	R	-1.3688	0.5120
54393.3172	R	-0.1492	0.4747
54393.3530	I	0.2868	0.9938
54407.3311	R	-0.4830	1.0990
54409.3144	R	0.1333	0.5086
54409.3430	I	1.5425	0.9731
54411.3505	R	0.1056	0.6939
54413.1613	R	-1.4175	0.6893
54415.1470	R	0.8087	0.4109
54417.1810	R	-0.4553	0.3636
54419.1445	I	0.2659	0.6340
54419.1586	R	-0.1798	0.3602
54421.1349	R	0.2299	0.4887
54421.1565	I	0.7967	0.6249
54423.2916	R	-0.7777	0.6477
54423.3290	I	-1.8125	1.5568
54435.2245	R	3.3927	0.7563
54435.2448	I	5.0304	1.6709
54439.1421	R	7.9527	0.3910
54439.1610	I	8.9833	0.7693
Continued			

Table C.1 (Continued)

MJD	Passband	$Flux_{25}$	σ_{Flux}
54441.1696	R	10.0278	0.5177
54443.1719	R	11.5985	0.5831
54445.1286	R	13.9201	0.4089
54445.1555	I	15.6790	1.2621
54447.1751	R	14.0488	0.4120
54447.1786	I	16.8452	0.9401
54449.1653	R	16.0738	0.5017
54449.1740	I	20.7700	0.8612
54451.1759	R	16.9033	1.0099
54453.1753	R	15.3659	1.1746
54453.1788	I	24.9572	3.6710
54464.1661	R	14.2556	0.5794
54464.1695	I	20.6364	0.8008
54469.1258	R	10.8964	0.3694
54469.1351	I	16.0586	0.6922
54472.1873	R	7.9382	0.6665
54474.2000	R	4.9880	1.2648
	z208		
54351.2738	R	-0.1266	0.4200
54354.2860	R	-0.5089	0.4481
54357.2637	I	0.7121	0.9321
54363.2768	I	0.1692	1.4275
54377.2080	R	-0.3411	0.5345
54377.2355	I	-1.9337	0.8717
54379.2174	R	0.9594	0.9222
54379.2485	I	-1.7181	1.6118
54381.1970	R	-0.2449	0.4632
54381.2254	I	-0.2823	0.6579
54383.2374	R	-0.4208	0.6439
54389.2210	R	0.3627	1.0125
54393.2332	R	-1.1214	0.6007
54393.2375	I	0.1992	1.0090
54407.1976	R	-0.0909	0.7077
54407.2124	I	0.6968	1.8761
54409.2369	R	-0.2870	0.4908
	Continued		

Table C.1 (Continued)

MJD	Passband	$Flux_{25}$	σ_{Flux}
54411.1979	R	1.1692	0.3561
54411.2164	I	-1.1998	0.6782
54421.0187	R	-0.6862	0.6159
54423.1034	R	-0.8238	0.7655
54437.1289	R	2.0735	0.5710
54437.1486	I	0.9832	1.2140
54441.0256	R	4.8457	0.8347
54441.0458	I	5.7696	0.6350
54443.0447	R	6.9943	0.7706
54443.0714	I	7.4975	1.1957
54445.0407	R	7.1239	0.5792
54445.0631	I	8.7396	0.7681
54447.0432	R	8.5804	0.4346
54447.0658	I	10.4068	0.7699
54449.0454	R	9.1269	0.6066
54449.0685	I	10.1355	0.8018
54451.0869	R	8.9172	0.9082
54451.0904	I	12.5860	1.3622
54453.0673	R	8.5650	2.1046
54464.0419	R	8.5497	0.5949
54464.0618	I	10.0439	0.5801
54467.0633	R	8.4206	0.4546
54467.0816	I	8.7894	0.8043
54469.0538	R	7.7214	0.4634
54472.0570	R	5.6117	0.5461
54472.0766	I	8.1252	1.0057
54474.0501	R	6.7115	0.6439

Note: These tables only contain measurements from the year in which each event was discovered. The machine readable tables that will be made available together with Narayan et al. [91, in prep.] contain measurements of the baseline flux at the location of each object for at least one, and typically 3 additional observing seasons. The 20 objects listed in Table 4.1 for which light curves have not been presented here are discussed in §5.

Table C.2: *MLCS2k2* light curve fit parameters for ESSENCE SN Ia and "Ia?" objects

ID	μ [1]	σ_μ	$T^B_{\max}$	$\sigma_{T_{\max}}$	$\Phi_{\rm First}$ [2]	$\Phi_{\rm Last}$	Δ	σ_Δ	A_V [3]	σ_{A_V}	Q[4]
b010	43.082	0.180	52592.10	1.41	-5.626	13.912	-0.221	0.170	0.113	0.099	T
b013	42.104	0.251	52586.95	1.57	-2.646	21.850	-0.057	0.179	0.223	0.198	T
b016	41.691	0.338	52583.47	1.73	-3.361	30.618	-0.188	0.188	0.437	0.293	T
b017	41.060	0.212	52594.12	0.74	-5.632	38.048	-0.128	0.124	0.189	0.198	T
b020	41.942	0.384	52600.27	0.71	-10.604	6.934	-0.047	0.311	0.275	0.240	F
b022	42.879	0.225	52595.26	1.21	-6.619	9.742	-0.065	0.221	0.091	0.095	T
c015	42.518	0.315	52617.92	0.64	-8.658	17.846	-0.141	0.178	0.359	0.264	T
d058	43.073	0.222	52941.66	1.61	-6.037	28.048	-0.401	0.101	0.205	0.163	F
d083	40.856	0.106	52936.54	0.84	-4.045	43.207	-0.281	0.061	0.085	0.082	T
d084	42.849	0.387	52936.02	1.95	-3.202	5.324	-0.015	0.351	0.272	0.233	F
d085	41.971	0.224	52941.59	0.85	-6.815	33.086	-0.171	0.131	0.207	0.169	T
d086	40.249	0.289	52945.39	0.35	-11.111	35.450	-0.217	0.078	0.536	0.306	T
d089	42.009	0.204	52929.41	2.15	1.221	25.822	-0.108	0.148	0.184	0.162	T
d093	41.779	0.135	52947.25	0.54	-11.786	40.272	-0.265	0.079	0.095	0.100	T
d097	42.226	0.143	52938.25	0.90	-4.923	40.397	-0.227	0.082	0.113	0.109	T
d099	40.515	0.230	52921.56	1.62	8.715	68.225	-0.192	0.083	0.245	0.196	F
d100	38.247	0.318	52922.91	2.02	6.997	57.974	-0.306	0.058	1.115	0.335	F
d117	41.570	0.252	52948.84	0.48	-6.691	34.923	0.231	0.190	0.240	0.191	T
d149	41.498	0.255	52954.66	0.37	-9.377	33.951	-0.100	0.091	0.306	0.214	T
e108	42.370	0.140	52979.48	0.59	-11.768	9.954	-0.338	0.111	0.097	0.102	T
e132	40.765	0.265	52972.60	0.38	-10.034	25.347	-0.139	0.105	0.513	0.275	T
e136	41.796	0.264	52968.10	0.84	-5.867	23.526	0.209	0.173	0.324	0.251	T
e138	43.214	0.184	52956.30	1.10	-8.790	11.059	-0.262	0.160	0.122	0.099	T
e140	43.017	0.153	52969.00	1.81	-3.009	16.924	-0.187	0.150	0.104	0.088	T
e147	43.127	0.169	52965.73	1.86	-3.382	6.338	-0.114	0.182	0.066	0.060	F
e148	42.359	0.186	52976.14	0.60	-8.394	19.642	-0.166	0.144	0.154	0.135	T
e149	42.578	0.208	52951.74	0.71	-10.460	16.359	0.023	0.177	0.103	0.110	T
f011	42.713	0.215	52985.33	1.07	-11.207	9.637	0.079	0.204	0.121	0.115	T
f041	42.910	0.128	52986.30	0.86	-9.130	10.118	-0.289	0.123	0.077	0.077	T
f096	42.031	0.355	52993.31	1.87	-3.724	7.648	0.100	0.351	0.202	0.221	F
f123	42.950	0.316	52987.52	1.07	-8.813	8.258	-0.116	0.253	0.229	0.201	F
f216	43.371	0.271	52985.39	1.46	-7.069	6.758	-0.049	0.266	0.144	0.113	F
f231	43.093	0.141	52985.81	0.84	-9.738	11.275	-0.297	0.134	0.099	0.082	T
f235	41.913	0.212	52989.61	0.70	-12.372	8.789	0.099	0.220	0.135	0.107	F
f244	42.820	0.242	52984.70	2.66	0.941	11.285	-0.076	0.250	0.164	0.137	T
f301	42.864	0.390	52994.27	2.07	-5.364	2.570	0.018	0.359	0.331	0.238	F
f308	42.475	0.274	52993.72	1.14	-5.455	3.199	0.046	0.300	0.145	0.144	F
g005	40.455	0.240	53293.78	0.58	-7.185	54.406	-0.289	0.057	0.414	0.247	T
g050	42.849	0.211	53301.51	1.07	-7.785	13.430	-0.066	0.193	0.101	0.088	T

Continued on next page

Table C.2 (Continued)

ID	μ	σ_μ	$T^B_{\max}$	$\sigma_{T_{\max}}$	Φ_{First}	Φ_{Last}	Δ	σ_Δ	A_V	σ_{A_V}	Q
g052	41.682	0.240	53297.05	0.71	-10.122	18.795	0.320	0.194	0.169	0.171	T
g055	41.127	0.327	53289.89	1.23	-5.213	40.287	-0.142	0.138	1.278	0.310	T
g097	41.698	0.275	53298.87	0.57	-11.781	38.102	-0.386	0.075	0.292	0.253	T
g120	42.273	0.228	53298.01	1.21	-7.280	17.970	-0.046	0.180	0.204	0.156	T
g133	41.890	0.221	53272.79	1.58	-4.659	57.264	-0.230	0.144	0.180	0.156	T
g142	42.164	0.376	53296.82	1.24	-6.991	20.097	0.350	0.335	0.273	0.247	T
g160	42.492	0.183	53283.51	0.96	-10.155	30.288	-0.281	0.090	0.159	0.140	T
g225	43.327	0.115	53310.91	1.12	-10.068	28.588	-0.685	0.070	0.069	0.071	F
g240	43.126	0.170	53305.94	1.26	-8.841	11.306	-0.202	0.162	0.066	0.055	T
h283	42.915	0.209	53320.54	1.56	-3.626	19.799	-0.210	0.156	0.171	0.148	T
h300	43.171	0.149	53309.29	1.16	-7.334	19.862	-0.289	0.125	0.085	0.067	T
h311	43.498	0.141	53312.45	1.47	-7.628	7.158	-0.261	0.142	0.049	0.043	F
h319	42.609	0.165	53336.17	0.72	-8.755	31.473	-0.294	0.111	0.126	0.121	T
h323	43.092	0.181	53329.20	0.98	-8.792	13.120	-0.337	0.121	0.170	0.125	T
h359	41.980	0.270	53341.80	0.51	-9.439	29.126	-0.152	0.099	0.305	0.236	T
h363	40.212	0.309	53338.54	0.29	-12.724	38.444	0.149	0.117	0.923	0.315	T
h364	41.471	0.134	53333.58	0.48	-13.706	38.341	-0.053	0.102	0.083	0.085	T
k396	41.200	0.304	53358.22	0.92	-11.153	1.439	-0.032	0.398	0.157	0.152	F
k411	42.724	0.150	53340.64	0.82	-9.976	12.398	-0.257	0.133	0.099	0.092	T
k425	41.207	0.254	53335.19	0.43	-9.535	19.618	-0.087	0.177	0.310	0.236	T
k429	40.038	0.145	53350.08	0.45	-6.765	31.570	-0.135	0.090	0.153	0.140	T
k430	43.223	0.258	53348.34	2.37	-2.699	6.166	-0.061	0.269	0.170	0.127	F
k432	43.682	0.161	53335.68	1.74	-6.246	9.587	-0.237	0.163	0.065	0.055	F
k441	43.347	0.145	53354.55	1.63	-6.204	15.876	-0.273	0.137	0.089	0.066	T
k448	42.492	0.426	53355.36	1.84	-6.583	3.364	0.144	0.410	0.291	0.274	F
k467	43.201	0.154	53338.63	0.93	-8.394	12.142	-0.224	0.143	0.085	0.075	T
k485	42.292	0.398	53350.14	1.48	-4.219	20.355	-0.145	0.318	0.778	0.295	T
k490	43.675	0.148	53345.15	3.02	-0.569	7.570	-0.286	0.149	0.072	0.055	F
m001	41.058	0.180	53633.42	1.74	4.395	48.690	0.220	0.154	0.121	0.098	F
m022	41.474	0.358	53639.73	2.20	-0.586	55.088	-0.729	0.063	0.967	0.378	F
m026	43.240	0.216	53634.40	3.41	2.809	4.012	-0.150	0.209	0.098	0.074	F
m027	41.625	0.288	53639.87	1.52	-0.601	43.614	-0.078	0.187	0.363	0.276	T
m032	40.121	0.153	53632.12	2.05	5.953	89.121	-0.197	0.080	0.101	0.109	F
m034	42.670	0.268	53627.22	3.01	7.664	17.313	-0.116	0.213	0.140	0.148	F
m039	40.728	0.382	53626.03	2.29	10.521	64.211	0.163	0.256	0.262	0.282	F
m040	43.023	0.412	53642.75	3.16	-2.431	-2.404	0.074	0.343	0.232	0.203	F
m043	41.203	0.292	53640.46	1.11	-1.147	51.835	-0.604	0.058	1.206	0.294	F
m057	41.316	0.255	53631.49	2.35	8.158	90.255	-0.574	0.073	0.252	0.256	F
m062	41.489	0.265	53644.74	1.63	-2.786	45.173	0.021	0.269	0.191	0.171	T
m070	41.084	0.088	53641.82	1.06	-0.551	51.440	-0.246	0.087	0.046	0.041	F
m075	39.472	0.448	53640.71	1.15	-1.513	83.949	-0.663	0.048	1.516	0.497	F
m087	41.178	0.285	53636.35	2.23	3.734	52.696	-0.126	0.144	0.327	0.261	T
m138	42.932	0.228	53656.48	2.70	-4.663	-1.521	-0.043	0.229	0.084	0.084	F
m158	42.735	0.244	53656.72	1.77	-5.265	26.919	-0.243	0.167	0.159	0.151	T
m193	41.289	0.224	53663.09	0.58	-10.477	56.394	-0.075	0.143	0.132	0.104	T
m226	43.238	0.193	53651.66	2.18	-7.478	1.475	-0.213	0.205	0.099	0.080	F
n246	43.136	0.160	53708.26	1.79	-7.139	-0.091	-0.201	0.175	0.074	0.056	F
n256	43.154	0.140	53696.67	1.37	-8.911	10.678	-0.209	0.153	0.076	0.069	T
n258	42.847	0.226	53698.79	1.74	-1.761	19.279	0.018	0.241	0.098	0.103	T
n263	41.497	0.176	53703.71	0.71	-5.540	25.130	0.156	0.146	0.121	0.123	T
n278	41.165	0.207	53700.58	1.01	-1.955	26.436	0.087	0.201	0.190	0.155	T
n285	42.736	0.267	53688.64	1.80	-4.309	12.685	-0.118	0.226	0.149	0.157	T
n322	44.018	0.144	53709.35	2.49	-7.445	-0.669	-0.282	0.139	0.047	0.042	F
n326	40.624	0.279	53709.77	0.59	-9.296	16.839	0.899	0.236	0.203	0.187	T
n346	41.647	0.384	53683.16	1.74	-0.890	19.671	0.368	0.339	0.378	0.307	T

Continued on next page

Table C.2 (Continued)

ID	μ	σ_μ	$T^B_{\max}$	$\sigma_{T_{\max}}$	Φ_{First}	Φ_{Last}	Δ	σ_Δ	A_V	σ_{A_V}	Q
n400	43.221	0.407	53707.40	1.95	-5.082	3.304	0.109	0.373	0.257	0.254	F
n404	41.138	0.262	53713.62	0.42	-13.584	19.047	-0.124	0.154	0.405	0.258	T
p425	42.752	0.352	53696.76	2.76	0.874	7.754	0.027	0.337	0.263	0.232	F
p429	43.369	0.171	53710.18	2.10	-7.850	18.004	-0.478	0.098	0.114	0.110	F
p434	41.687	0.420	53704.07	1.43	-4.482	6.002	0.406	0.482	1.088	0.414	F
p444	43.613	0.200	53697.91	3.05	0.117	8.713	-0.162	0.211	0.115	0.089	F
p445	43.886	0.127	53702.17	3.30	-2.278	5.489	-0.318	0.120	0.043	0.031	F
p454	43.539	0.156	53703.60	2.41	-3.251	6.183	-0.211	0.169	0.078	0.059	F
p455	41.302	0.224	53721.63	0.44	-13.496	12.685	-0.193	0.197	0.208	0.175	T
p459	43.593	0.204	53692.29	3.40	3.415	12.787	-0.245	0.163	0.082	0.059	T
p524	42.642	0.165	53719.41	0.65	-11.397	12.370	-0.265	0.135	0.104	0.101	T
p528	43.661	0.117	53722.87	1.48	-10.514	8.529	-0.328	0.118	0.052	0.036	F
p534	42.926	0.211	53742.71	1.90	-9.012	-2.859	-0.105	0.227	0.104	0.085	F
q002	41.212	0.359	54002.83	0.75	-6.340	15.192	0.594	0.279	0.549	0.369	T
q006	41.846	0.358	53995.49	1.45	-0.944	21.547	0.376	0.384	0.198	0.205	F
q007	39.254	0.259	54000.19	0.77	-4.873	75.741	-0.133	0.082	1.990	0.266	T
q008	40.877	0.277	54005.99	0.38	-9.044	65.389	-0.046	0.083	0.446	0.265	T
q014	41.074	0.287	54006.35	0.49	-9.440	64.470	-0.318	0.064	0.581	0.290	T
q022	40.645	0.333	53991.76	2.01	0.429	55.001	-0.098	0.107	0.646	0.347	T
q048	42.017	0.338	54022.19	1.88	-0.669	20.049	0.325	0.327	0.270	0.242	T
q049	42.170	0.267	54015.38	0.77	-8.466	25.204	-0.188	0.145	0.256	0.220	T
q054	41.428	0.201	54024.27	1.18	-2.231	43.631	-0.165	0.098	0.225	0.171	T
q061	41.232	0.321	54026.58	1.19	-2.574	29.716	-0.129	0.168	1.249	0.283	T
q067	39.987	0.204	54033.25	0.33	-10.045	67.535	-0.256	0.060	0.221	0.205	T
q069	40.077	0.353	54005.53	1.74	14.027	63.815	0.610	0.250	0.174	0.199	F
q075	42.031	0.169	54017.44	0.63	-9.869	25.019	-0.175	0.119	0.112	0.116	T
q102	42.167	0.225	54030.72	0.92	-5.219	41.356	-0.192	0.121	0.209	0.182	T
q106	42.325	0.204	54036.39	0.72	-8.860	18.250	-0.067	0.168	0.131	0.130	T
q107	43.184	0.198	54034.39	1.46	-6.733	11.326	-0.116	0.198	0.102	0.075	T
q108	43.396	0.216	54016.42	1.38	-6.262	9.187	-0.188	0.208	0.113	0.107	T
q112	43.167	0.132	54032.05	1.65	-6.602	14.140	-0.324	0.122	0.093	0.075	T
q114	43.245	0.163	54037.82	1.86	-5.093	10.293	-0.209	0.172	0.080	0.061	T
q125	41.575	0.322	54000.53	2.55	1.992	28.698	0.014	0.173	0.384	0.262	T
r185	40.022	0.209	54052.35	0.51	-11.145	35.392	0.621	0.130	0.243	0.190	F
r186	40.906	0.194	54044.24	0.37	-11.389	51.696	-0.098	0.083	0.154	0.156	T
r190	41.790	0.209	54062.16	0.57	-8.168	25.068	-0.226	0.088	0.251	0.182	T
r193	43.137	0.116	54051.77	1.13	-8.946	23.787	-0.344	0.094	0.068	0.067	T
r195	42.836	0.244	54051.08	1.46	-8.942	10.472	-0.207	0.194	0.204	0.167	T
r196	41.755	0.416	54046.31	1.30	-7.167	36.366	-0.401	0.100	1.406	0.423	F
r199	42.165	0.348	54041.45	0.78	-10.005	35.984	-0.132	0.151	0.335	0.284	T
r200	40.678	0.313	54064.06	0.60	-8.613	14.070	-0.239	0.178	1.174	0.309	T
r206	43.132	0.178	54055.41	2.20	-1.471	21.524	-0.166	0.182	0.110	0.091	T
r207	42.759	0.216	54044.16	0.98	-8.239	14.801	-0.184	0.168	0.172	0.133	T
r209	42.142	0.200	54051.26	1.10	-8.290	29.672	-0.063	0.120	0.191	0.158	T
r212	43.298	0.209	54054.71	2.48	-0.980	7.573	-0.124	0.220	0.103	0.076	F
r213	41.460	0.277	54062.91	0.45	-7.394	37.834	-0.086	0.094	0.354	0.244	T
r225	41.862	0.413	54054.51	1.45	-2.405	7.592	0.579	0.438	0.583	0.351	F
r230	40.960	0.200	54070.37	0.31	-13.670	34.747	-0.176	0.079	0.288	0.194	T
r311	43.693	0.167	54057.31	3.66	3.270	4.391	-0.306	0.133	0.048	0.034	F
r317	43.619	0.153	54064.67	2.14	-6.703	1.469	-0.256	0.158	0.065	0.049	F
r318	40.117	0.178	54078.63	0.25	-15.872	28.222	-0.455	0.053	0.239	0.174	F
r322	42.621	0.178	54077.17	0.68	-9.209	24.376	-0.141	0.146	0.111	0.108	T
s340	42.706	0.224	54069.31	0.79	-10.629	16.825	-0.259	0.144	0.176	0.145	T
s346	41.455	0.237	54076.32	1.25	-5.599	28.924	-0.009	0.157	0.199	0.185	T
s347	41.502	0.228	54098.22	0.59	-10.772	12.067	-0.471	0.083	0.272	0.210	F

Continued on next page

Table C.2 (Continued)

ID	μ	σ_μ	$T^B_{\max}$	$\sigma_{T_{\max}}$	Φ_{First}	Φ_{Last}	Δ	σ_Δ	A_V	σ_{A_V}	Q
s349	40.801	0.278	54082.46	1.66	1.314	26.006	0.125	0.175	0.422	0.289	T
s350	43.500	0.148	54091.06	2.28	-5.303	11.914	-0.252	0.150	0.087	0.064	T
s351	43.860	0.170	54080.11	3.32	1.163	8.106	-0.275	0.152	0.068	0.052	F
s353	42.760	0.285	54068.94	2.98	8.359	15.976	-0.131	0.219	0.144	0.144	F
s354	43.298	0.136	54081.85	1.40	-10.649	20.672	-0.415	0.081	0.103	0.097	F
s355	43.588	0.145	54090.11	2.05	-4.785	12.577	-0.254	0.147	0.080	0.062	T
s370	42.380	0.176	54095.61	1.03	-7.957	12.175	-0.221	0.162	0.115	0.115	T
s372	43.689	0.153	54088.34	2.83	-3.646	3.395	-0.214	0.167	0.066	0.054	F
s373	43.589	0.165	54090.14	2.42	-4.862	13.914	-0.168	0.174	0.071	0.062	T
s374	43.910	0.134	54090.61	3.39	-1.398	2.037	-0.265	0.149	0.054	0.045	F
s375	42.609	0.208	54101.27	0.73	-8.442	8.232	-0.264	0.170	0.138	0.137	F
s377	41.434	0.330	54082.37	1.22	-9.418	22.653	-0.189	0.139	0.504	0.308	T
s379	40.394	0.194	54102.08	0.36	-13.444	10.044	-0.435	0.090	0.265	0.201	F
s380	43.411	0.240	54099.42	1.29	-8.141	8.376	-0.144	0.241	0.148	0.107	F
x016	42.189	0.399	54370.25	0.88	-7.399	12.649	0.296	0.365	0.332	0.336	T
x017	41.829	0.311	54374.82	2.54	1.682	52.180	-0.279	0.116	0.426	0.288	T
x020	43.578	0.207	54370.41	2.25	-4.272	7.824	-0.145	0.208	0.096	0.075	F
x025	41.588	0.284	54357.28	1.51	-4.435	61.817	0.031	0.201	0.256	0.245	T
x028	43.033	0.194	54369.71	1.05	-9.637	8.456	-0.187	0.192	0.112	0.096	F
x033	41.925	0.230	54388.66	0.99	-6.714	35.866	-0.077	0.160	0.125	0.127	T
x034	42.507	0.302	54372.23	1.13	-5.814	13.751	0.193	0.259	0.204	0.177	T
x038	42.607	0.289	54383.77	2.17	-5.579	36.515	-0.455	0.085	0.336	0.234	F
x039	42.656	0.117	54376.29	1.37	-9.007	21.942	-0.284	0.105	0.046	0.042	T
x055	40.887	0.188	54371.71	0.37	-12.846	54.432	0.105	0.112	0.163	0.134	T
x066	41.329	0.184	54354.28	1.26	-2.225	51.916	-0.090	0.101	0.157	0.136	T
x071	42.636	0.169	54393.83	0.67	-9.796	19.802	-0.196	0.132	0.107	0.104	T
x077	42.659	0.180	54388.69	1.14	-4.845	22.788	-0.261	0.102	0.160	0.132	T
x080	42.006	0.440	54384.94	1.54	-4.178	17.699	0.132	0.343	0.315	0.276	T
x085	43.257	0.186	54392.38	1.50	-6.756	0.600	-0.133	0.207	0.091	0.075	F
x089	42.998	0.411	54387.22	1.89	-6.629	4.026	-0.117	0.308	0.352	0.269	F
x093	43.161	0.425	54385.69	2.25	-2.905	5.111	-0.006	0.353	0.306	0.248	F
x107	39.579	0.148	54404.07	0.30	-14.616	56.773	-0.232	0.061	0.155	0.142	T
y125	41.318	0.175	54412.02	0.62	-14.306	29.819	-0.124	0.103	0.175	0.150	T
y127	42.765	0.137	54405.28	0.88	-8.964	23.123	-0.304	0.091	0.090	0.089	T
y134	41.649	0.141	54412.48	1.28	-2.480	20.175	-0.296	0.116	0.119	0.115	T
y136	42.422	0.288	54411.89	1.72	-1.695	21.866	-0.425	0.096	0.719	0.241	F
y137	41.804	0.181	54418.70	0.64	-8.343	36.654	-0.188	0.097	0.153	0.139	T
y142	42.728	0.185	54421.15	0.90	-7.482	17.714	-0.173	0.133	0.134	0.123	T
y143	42.544	0.164	54404.78	1.05	-7.873	30.295	-0.296	0.080	0.143	0.130	T
y145	42.754	0.137	54418.78	1.02	-7.460	14.363	-0.303	0.109	0.090	0.089	T
y151	42.992	0.184	54427.39	0.77	-11.427	13.735	-0.226	0.147	0.152	0.114	T
y154	43.202	0.154	54419.41	1.41	-6.141	11.909	-0.067	0.154	0.061	0.046	T
y155	41.642	0.087	54436.58	0.71	-11.832	7.948	-0.361	0.087	0.035	0.028	F
y158	42.588	0.191	54422.53	0.68	-8.936	17.897	-0.201	0.128	0.179	0.141	T
y163	43.662	0.196	54421.29	2.33	-6.154	12.159	-0.255	0.182	0.134	0.107	T
y175	41.655	0.268	54425.80	0.53	-11.680	16.528	0.548	0.197	0.221	0.226	T
y177	41.024	0.263	54436.17	0.29	-14.572	27.576	-0.311	0.074	0.383	0.245	T
z180	42.002	0.207	54441.79	1.04	-4.577	22.144	-0.138	0.131	0.211	0.174	T
z181	43.246	0.173	54438.53	2.30	-2.072	17.656	-0.206	0.184	0.117	0.092	T
z183	41.083	0.118	54436.07	0.46	-11.691	29.514	-0.210	0.072	0.105	0.098	T
z185	42.107	0.174	54430.83	0.79	-6.969	29.321	0.027	0.130	0.104	0.115	T
z187	41.138	0.203	54441.72	0.56	-14.291	24.965	0.035	0.105	0.218	0.188	F
z200	42.427	0.271	54452.44	0.66	-7.845	14.853	-0.033	0.225	0.217	0.187	T
z202	40.360	0.188	54448.76	0.38	-9.484	20.771	-0.130	0.120	0.219	0.187	T
z203	42.479	0.324	54451.19	0.64	-9.647	18.344	-0.214	0.176	0.426	0.337	T

Continued on next page

Table C.2 (Continued)

ID	μ	σ_μ	$T^B_{\max}$	$\sigma_{T_{\max}}$	Φ_{First}	Φ_{Last}	Δ	σ_Δ	A_V	σ_{A_V}	Q
z204	43.125	0.194	54452.72	0.86	-8.386	10.128	-0.132	0.191	0.103	0.085	T
z205	41.843	0.291	54452.83	0.55	-9.736	13.767	-0.229	0.164	0.299	0.249	T
z208	42.807	0.156	54454.79	0.68	-8.995	12.590	-0.264	0.132	0.109	0.102	T

[1] *MLCS2k2* reports distance moduli with a $H_o = 65$ km s^{-1} Mpc^{-1}.

[2] $\Phi_{\text{First|Last}}$ is the rest-frame phase of the first and last observation respectively and is dependent on *B*-band time of maximum, T^B_{max}.

[3] We use the Galactic reddening law of O'Donnell [95], with R_V fixed to 3.1 to model the extinction in the host-galaxy of the supernova.

[4] Flag describing if the object passes (T) or fails (F) the light curve quality cuts described in WV07.

Table C.3: *SALT2* light curve fit parameters for ESSENCE SN Ia and "Ia?" objects

ID	m_B [5]	σ_{m_B}	m_V	σ_{m_V}	$T^B_{\max}$ [6]	$\sigma_{T_{\max}}$	x_1	σ_{x_1}	c [7]	σ_c	$Cov(c, x_1)$ [8]	Q[9]
b010	23.4583	0.0666	23.5138	0.0937	52593.2578	0.8841	0.9105	0.7618	-0.0781	0.1012	0.0248	T
b013	22.6982	0.0441	22.6821	0.0343	52588.2349	0.6787	-0.1382	0.4106	-0.0069	0.0553	-0.0015	T
b016	22.5752	0.1009	22.4429	0.0410	52584.7886	1.4696	0.4887	0.8185	0.1069	0.0889	0.0066	T
b017	21.4923	0.0797	21.4956	0.0352	52595.4475	0.2830	-0.2884	0.3204	-0.0260	0.0609	0.0035	T
b020	22.7302	0.0822	22.6162	0.0900	52601.8351	0.9118	0.8373	0.9984	0.0886	0.0887	-0.0035	F
b022	23.1333	0.0626	23.4180	0.0843	52596.2911	0.6042	-1.1228	0.5926	-0.3011	0.0913	0.0060	F
c015	23.2594	0.0872	23.1716	0.0469	52619.0456	0.5744	0.4944	0.5771	0.0630	0.0865	0.0125	T
d033	23.4614	0.0637	23.3019	0.0826	52936.7009	1.9256	3.3665	0.9741	0.1311	0.0958	-0.0139	F
d058	23.6319	0.0678	23.2789	0.1034	52941.9994	1.0806	1.2436	0.7267	0.3238	0.1057	-0.0035	F
d083	21.0610	0.0479	21.1507	0.0225	52938.2117	0.4522	1.2102	0.1921	-0.1119	0.0449	-0.0009	F
d084	23.6840	0.0580	23.5824	0.0863	52936.2854	1.1608	-0.8144	0.8059	0.0777	0.0989	-0.0119	T
d085	22.4700	0.0528	22.4655	0.0452	52942.7811	0.3767	0.8873	0.3907	-0.0192	0.0619	-0.0038	T
d086	20.9939	0.0743	20.9406	0.0257	52947.0097	0.1326	0.0660	0.1678	0.0294	0.0575	0.0003	T
d089	22.4754	0.0474	22.5214	0.0372	52929.4122	0.6286	0.4573	0.3600	-0.0684	0.0574	-0.0027	T
d093	21.9899	0.0540	22.0881	0.0307	52949.4497	0.2449	1.1777	0.2756	-0.1201	0.0506	0.0017	T
d097	22.5686	0.0449	22.6021	0.0363	52939.6901	0.4616	1.1890	0.3218	-0.0567	0.0546	-0.0025	T
d099	20.9724	0.0986	21.0124	0.0606	52918.3226	0.6958	2.0693	0.5334	-0.0639	0.0817	-0.0178	F
d100	20.0110	0.1119	19.8475	0.0424	52929.2329	0.9004	2.1698	0.3017	0.1361	0.0869	-0.0066	F
d117	22.3145	0.0862	22.3156	0.0388	52949.1832	0.2747	-1.7648	0.3176	-0.0225	0.0711	0.0049	T
d149	22.1197	0.0523	22.0998	0.0307	52955.8454	0.2586	0.0015	0.2362	-0.0033	0.0478	-0.0007	T
e020	21.7497	0.2797	21.0455	0.0744	52974.3431	0.8528	3.8656	1.0929	0.6702	0.2220	0.0927	F
e108	22.7046	0.0571	22.7138	0.0504	52982.0137	0.7895	2.8731	0.9164	-0.0343	0.0672	0.0176	F
e132	21.6510	0.0584	21.5453	0.0201	52973.6715	0.1880	0.0844	0.1908	0.0810	0.0482	0.0017	T
e136	22.7645	0.0494	22.6838	0.0261	52967.9480	0.5024	-0.7407	0.3937	0.0571	0.0514	-0.0007	T
e138	24.0052	0.0848	23.5880	0.1539	52958.8777	0.9445	3.7621	1.0456	0.3851	0.1367	-0.0316	F
e140	23.3562	0.0371	23.3736	0.0748	52972.6678	0.6435	-0.5625	0.4455	-0.0395	0.0767	0.0014	T
e147	23.4887	0.0432	23.5845	0.0835	52964.0667	0.6514	0.8702	0.4969	-0.1176	0.0790	0.0038	T
e148	22.7213	0.0417	22.7610	0.0327	52977.7135	0.2648	0.2216	0.2999	-0.0621	0.0490	-0.0002	F
e149	22.9999	0.0611	23.1688	0.0562	52952.4141	0.3075	-0.2293	0.3723	-0.1884	0.0710	0.0072	T
f011	23.1913	0.0508	23.3118	0.0617	52985.3738	0.6284	-0.7538	0.4554	-0.1406	0.0737	0.0067	T
f041	23.2151	0.0547	23.3547	0.0733	52989.6182	1.1049	2.5583	0.9827	-0.1617	0.0759	0.0120	F
f096	22.4723	0.7368	22.7005	0.0751	52993.6277	1.6711	-0.1097	2.4140	-0.2466	0.6468	0.2074	F
f123	23.6000	0.0677	23.5107	0.0941	52988.7551	0.8700	-0.4000	0.7952	0.0652	0.1026	0.0085	T

Continued on next page

Table C.3 (Continued)

ID	m_B	σ_{m_B}	m_V	σ_{m_V}	$T^B_{\max}$	$\sigma_{T_{\max}}$	x_1	σ_{x_1}	c	σ_c	$Cov(c, x_1)$	Q
f216	23.6903	0.1012	23.9354	0.1618	52984.1900	0.7385	-3.2609	0.8793	-0.2608	0.1657	0.0344	F
f231	23.5144	0.0789	23.4800	0.1066	52990.3566	1.6953	3.7531	1.8284	0.0078	0.1093	0.0752	F
f235	22.4115	0.0458	22.5296	0.0349	52989.9928	0.4777	-0.3129	0.4195	-0.1385	0.0549	0.0004	F
f244	23.3649	0.0592	23.3709	0.0783	52986.1800	0.9165	-0.3328	0.7171	-0.0285	0.0896	0.0081	T
f301	23.8662	0.0705	23.5720	0.1076	53003.2781	1.2802	5.0000	1.6537	0.2625	0.1239	0.0000	F
f308	22.9912	0.0604	23.0399	0.0445	52996.3113	2.1191	1.4827	1.8214	-0.0719	0.0721	0.0117	F
g001	21.5380	0.0641	21.5587	0.0276	53286.0117	0.5405	-0.7699	0.2664	-0.0426	0.0523	0.0004	F
g005	21.2137	0.0719	21.0864	0.0244	53295.0501	0.3713	1.3354	0.2449	0.1011	0.0585	-0.0009	T
g050	23.2239	0.0702	23.4278	0.1084	53302.2280	0.5811	-0.2400	0.5682	-0.2226	0.1069	0.0153	T
g052	22.4627	0.0631	22.4921	0.0403	53297.1287	0.4029	-1.1883	0.3363	-0.0507	0.0704	-0.0003	T
g053	23.4662	0.0648	23.6604	0.1395	53287.0857	1.1470	-0.0611	0.6761	-0.2132	0.1209	0.0080	T
g055	23.2292	0.1051	22.7479	0.0403	53289.7042	0.9378	0.2126	0.5193	0.4517	0.0832	0.0030	F
g097	22.3097	0.0847	22.1334	0.0428	53300.8226	0.4055	1.6368	0.4938	0.1491	0.0700	0.0085	T
g120	22.8643	0.0446	22.8299	0.0533	53298.9711	0.6943	0.3097	0.4151	0.0106	0.0685	-0.0004	T
g133	21.7833	0.2214	22.2327	0.0877	53272.8899	0.9993	-0.4481	0.8376	-0.4625	0.1532	0.0928	F
g142	23.2658	0.0817	23.1028	0.0492	53296.3777	0.7751	-1.3548	0.6054	0.1387	0.0898	-0.0040	T
g160	22.9379	0.0570	22.9323	0.0657	53285.1450	0.6304	1.6888	0.4974	-0.0188	0.0767	0.0018	T
g225	23.8654	0.0637	23.8810	0.1301	53334.2791	2.2526	5.0000	1.1594	-0.0422	0.1318	0.0000	F
g230	22.8274	0.1199	22.9291	0.0878	53310.6496	0.4415	-0.2586	0.5898	-0.1225	0.0990	0.0022	F
g240	23.3988	0.0952	23.5517	0.1200	53307.0413	0.6828	0.1855	0.8960	-0.1731	0.1016	0.0341	T
h283	23.3473	0.0514	23.3307	0.0628	53321.2118	0.9090	-0.5594	0.5436	-0.0062	0.0795	-0.0018	T
h300	23.5692	0.0792	23.6237	0.1248	53310.9055	0.7499	1.7150	0.8095	-0.0777	0.0984	0.0069	T
h311	23.8232	0.0950	23.9011	0.1650	53315.3237	1.0857	2.6953	1.0677	-0.1015	0.1243	0.0205	F
h319	22.9405	0.0503	23.0163	0.0509	53337.7782	0.4908	1.2528	0.5071	-0.0983	0.0629	0.0038	T
h323	23.4921	0.0594	23.3174	0.0873	53329.8365	0.6337	0.6074	0.5493	0.1485	0.0930	0.0094	F
h359	22.6038	0.0520	22.5678	0.0275	53342.9415	0.3482	0.2210	0.2660	0.0123	0.0514	-0.0009	T
h363	21.8893	0.0760	21.6406	0.0257	53339.2308	0.1866	-0.7550	0.1842	0.2226	0.0613	-0.0006	T
h364	21.7670	0.0491	21.8908	0.0259	53334.0477	0.1977	0.2617	0.2306	-0.1446	0.0468	0.0010	T
k396	21.7503	0.0946	21.7029	0.0391	53361.2948	1.0275	1.9752	0.8884	0.0221	0.0834	0.0429	F
k411	23.0522	0.0511	23.1933	0.0760	53342.7973	0.7353	1.5361	0.7139	-0.1625	0.0797	0.0045	T
k425	21.9104	0.0622	21.8304	0.0256	53336.3330	0.2477	-0.2448	0.2967	0.0560	0.0514	0.0020	T
k429	20.4364	0.0839	20.4809	0.0269	53351.0711	0.1812	0.3730	0.1418	-0.0669	0.0633	-0.0004	T
k430	23.7691	0.0555	23.6982	0.0985	53347.5867	1.2664	-0.6160	0.9686	0.0473	0.1047	0.0014	T
k432	23.8125	0.1445	24.0866	0.1583	53335.6225	0.9447	-1.5615	1.3778	-0.2905	0.1630	0.1419	F
k441	23.6810	0.0454	23.6852	0.1004	53355.8840	1.0612	1.0498	0.6641	-0.0278	0.0849	0.0076	T

Continued on next page

Table C.3 (Continued)

ID	m_B	σ_{m_B}	m_V	σ_{m_V}	$T^B_{\max}$	$\sigma_{T_{\max}}$	x_1	σ_{x_1}	c	σ_c	$Cov(c, x_1)$	Q
k448	23.4709	0.0879	23.2815	0.0589	53357.0838	1.5019	-0.3872	1.1569	0.1639	0.1002	-0.0058	T
k467	23.5194	0.0729	23.7493	0.1072	53340.9072	0.7840	0.6415	0.6746	-0.2487	0.0934	0.0124	T
k485	23.7586	0.0685	23.3314	0.0490	53350.0235	0.8867	-1.4635	0.9912	0.3995	0.0831	-0.0091	F
k490	23.9589	0.0676	23.8262	0.1333	53349.2034	1.4763	0.0667	1.0362	0.1075	0.1082	0.0221	T
m001	21.7235	0.0953	21.7998	0.0438	53637.6811	0.9515	-2.1337	0.4151	-0.0961	0.0747	-0.0031	F
m022	22.8951	0.1052	22.5488	0.0396	53641.3330	1.2189	0.9313	0.6791	0.3174	0.0827	0.0040	F
m026	22.3500	0.4535	23.1400	0.2375	53616.0645	3.2559	-1.6072	1.4118	-0.7934	0.3960	0.4653	F
m027	22.5307	0.1123	22.3609	0.0460	53641.3247	1.3194	0.2608	0.8020	0.1439	0.0829	-0.0070	F
m032	20.5396	0.1368	20.5039	0.0754	53632.4770	2.4228	1.2530	0.9453	0.0111	0.1052	0.0243	F
m034	23.2896	0.1959	23.0804	0.1311	53627.4271	4.8914	1.5744	1.5743	0.1816	0.1644	0.0460	F
m039	21.9462	0.1211	21.7622	0.0889	53631.8543	2.1447	-1.1710	0.8505	0.1592	0.0754	0.0171	F
m040	22.1793	0.7274	23.1579	0.2103	53621.6532	2.7408	-3.5000	0.7281	-0.9763	0.5939	0.3171	F
m043	23.1040	0.1207	22.5762	0.0455	53639.2515	1.4737	5.0000	0.7916	0.4937	0.1035	0.0000	F
m057	22.4255	0.1850	22.0259	0.0622	53639.6535	1.1983	1.8654	1.0813	0.3693	0.1470	0.0519	F
m062	22.0414	0.0928	22.0845	0.0449	53644.8605	1.0827	-1.3465	1.0464	-0.0641	0.0769	0.0150	T
m070	19.5829	0.1687	20.4357	0.0811	53622.0860	1.7494	0.8312	0.4625	-0.8547	0.1009	0.0053	F
m075	26.2051	0.0505	22.3018	0.0502	53640.3370	1.0284	1.8606	0.5860	4.0000	1.6263	0.0000	F
m087	21.9348	0.0714	21.8453	0.0368	53639.1987	1.4325	-0.3253	0.8816	0.0654	0.0591	0.0050	F
m138	23.3608	0.1017	23.6810	0.1609	53658.3095	1.5835	1.5827	1.1046	-0.3375	0.1286	0.0054	F
m158	23.0549	0.0782	23.1014	0.0795	53659.6888	0.6083	0.9868	0.6352	-0.0693	0.0905	0.0008	T
m193	21.5612	0.0833	21.6825	0.0549	53664.1930	0.1994	-0.3418	0.2990	-0.1417	0.0570	0.0024	T
m226	23.6021	0.0708	23.2621	0.1581	53651.3938	2.0210	0.6357	1.0882	0.3115	0.1544	0.0377	F
n246	23.3812	0.0748	23.3462	0.1746	53709.8276	0.9684	0.4924	0.6411	0.0110	0.1179	0.0113	T
n256	23.4379	0.0438	23.5728	0.0813	53697.9705	0.9806	0.8878	0.6175	-0.1558	0.0789	0.0092	T
n258	23.2428	0.0393	23.4242	0.0639	53699.3885	0.6790	-0.9953	0.5138	-0.2000	0.0719	-0.0018	F
n263	22.0192	0.0425	22.1161	0.0238	53703.6252	0.2486	-0.6489	0.2685	-0.1174	0.0452	-0.0005	T
n278	21.7854	0.0506	21.8036	0.0220	53701.5420	0.5195	-1.0085	0.5638	-0.0399	0.0475	0.0034	T
n285	23.2297	0.0972	23.1655	0.0961	53689.6364	1.2069	0.2228	1.1534	0.0400	0.1161	0.0674	T
n322	24.3561	0.0919	24.4587	0.2019	53707.8798	1.4726	0.1779	1.0967	-0.1237	0.1342	0.0518	T
n326	22.0658	0.1151	22.0876	0.0435	53709.2121	0.4490	-3.7617	0.5910	-0.0413	0.0948	0.0161	F
n400	24.0897	0.1003	23.9321	0.0920	53707.0709	1.7317	-4.1715	5.1853	0.1357	0.1393	0.0160	F
n404	21.8702	0.0802	21.7000	0.0258	53714.0553	0.2202	-0.1815	0.2845	0.1448	0.0627	0.0067	T
n406	23.8601	0.0705	24.0906	0.1329	53715.0012	0.7150	0.1731	0.5746	-0.2489	0.0859	0.0103	T
p425	23.6726	0.0776	23.5157	0.0756	53700.3857	1.5386	1.4599	1.4828	0.1302	0.0998	0.0239	T
p429	23.9145	0.0604	23.7990	0.1366	53713.6481	1.7484	5.0000	0.9107	0.0863	0.1382	0.0000	F

Continued on next page

Table C.3 (Continued)

ID	m_B	σ_{m_B}	m_V	σ_{m_V}	$T^B_{\max}$	$\sigma_{T_{\max}}$	x_1	σ_{x_1}	c	σ_c	$Cov(c, x_1)$	Q
p434	24.3087	0.2358	23.5397	0.0892	53710.4678	4.3975	4.9364	9.3685	0.7339	0.2248	0.4241	F
p444	24.0781	0.0784	23.9370	0.1270	53699.1613	2.1878	0.9862	1.0074	0.1151	0.1204	0.0204	T
p445	24.2080	0.0729	24.3789	0.1568	53705.4561	2.2305	0.5518	1.6851	-0.1909	0.1060	0.0777	T
p454	23.8985	0.0487	23.8752	0.1094	53706.3840	1.5493	0.5749	0.8033	-0.0005	0.0923	0.0092	T
p455	21.6367	0.0534	21.7212	0.0252	53721.6950	0.1964	-0.7354	0.2612	-0.1052	0.0454	0.0018	T
p459	23.9485	0.1308	23.7126	0.1643	53696.8230	3.2608	-0.8275	1.0894	0.2101	0.1439	0.0307	T
p524	23.0226	0.0783	23.0937	0.0757	53721.0248	0.4854	1.8509	0.7723	-0.0942	0.0752	0.0148	T
p527	22.5446	0.0839	22.3348	0.1173	53747.3342	2.3997	0.3779	1.7257	0.1832	0.0998	-0.0266	F
p528	24.0024	0.0821	23.7831	0.1830	53734.2394	2.0274	4.2584	2.0348	0.1892	0.1422	0.1392	F
p534	23.3210	0.1333	23.4629	0.2933	53742.3189	7.0535	-0.8193	3.4511	-0.1615	0.1749	0.5612	F
q002	22.8550	0.1007	22.6752	0.0487	54001.9704	0.6189	-2.6505	0.5734	0.1563	0.0982	0.0027	T
q006	22.8905	0.1105	22.7712	0.0432	53996.3154	1.0510	-2.1751	0.5566	0.0963	0.0925	0.0054	T
q007	22.2260	0.0812	21.5884	0.0262	54000.7846	0.3328	0.2380	0.2772	0.6067	0.0634	0.0020	F
q008	21.7498	0.0559	21.6706	0.0225	54006.8207	0.2427	-0.2647	0.1775	0.0552	0.0491	0.0003	T
q014	21.9967	0.0719	21.8155	0.0279	54008.3365	0.3058	0.9766	0.2655	0.1545	0.0601	0.0028	T
q022	21.8703	0.0806	21.6339	0.0289	53992.4503	1.0168	0.3006	0.3211	0.2095	0.0661	-0.0013	T
q048	23.0639	0.0729	22.9408	0.0529	54023.6837	1.2934	-2.2007	0.9229	0.1000	0.0834	-0.0102	T
q049	22.7786	0.0759	22.7394	0.0592	54016.4163	0.4863	0.8448	0.5649	0.0150	0.0747	0.0049	T
q054	21.9276	0.0523	21.9448	0.0253	54025.3712	0.4783	0.6215	0.2964	-0.0403	0.0500	0.0000	T
q061	23.2000	0.0767	22.7918	0.0303	54027.3989	0.9402	-0.0799	0.5965	0.3796	0.0692	0.0037	F
q067	20.3989	0.0929	20.3907	0.0277	54034.7868	0.1961	0.8291	0.2075	-0.0155	0.0740	0.0013	T
q069	22.0914	0.1004	21.8677	0.0477	54018.4893	0.7645	-2.1882	0.3435	0.1992	0.0777	0.0008	F
q075	22.3419	0.0534	22.4547	0.0496	54018.8690	0.4026	0.6685	0.4024	-0.1341	0.0673	0.0011	T
q102	22.6528	0.0432	22.6330	0.0377	54031.4251	0.4495	0.3796	0.3896	-0.0038	0.0551	-0.0019	T
q106	22.7735	0.0482	22.8680	0.0566	54037.0120	0.4339	0.2544	0.3763	-0.1158	0.0701	0.0015	T
q107	23.6076	0.0633	23.6306	0.1206	54035.2369	0.8985	0.3444	0.6625	-0.0458	0.1037	0.0097	T
q108	23.7523	0.0967	23.6387	0.1510	54017.0607	0.8552	-0.8286	0.8402	0.0895	0.1431	0.0239	T
q112	23.5556	0.0780	23.4724	0.1251	54034.8121	1.6635	3.6606	1.2495	0.0558	0.1118	0.0448	F
q114	23.5407	0.0686	23.6445	0.1346	54039.8512	0.9367	-0.8345	0.7933	-0.1241	0.1061	0.0171	T
q125	22.4435	0.0775	22.4027	0.0402	54001.4395	1.6448	-0.3898	0.4623	0.0175	0.0625	-0.0040	T
r186	21.3735	0.0490	21.3828	0.0237	54045.4268	0.1922	0.4117	0.1644	-0.0323	0.0460	-0.0005	T
r190	22.3083	0.0514	22.2945	0.0294	54063.3751	0.3907	1.1219	0.2884	-0.0103	0.0567	0.0008	T
r193	23.3562	0.0472	23.6080	0.0939	54052.6620	0.6757	1.0114	0.4539	-0.2704	0.0858	0.0036	F
r195	23.3975	0.0615	23.2803	0.0771	54052.7438	0.6851	0.3250	0.5450	0.0921	0.0907	0.0049	T
r199	22.9096	0.0657	22.8114	0.0568	54042.5490	0.4736	0.1856	0.3997	0.0735	0.0717	-0.0014	T

Continued on next page

Table C.3 (Continued)

ID	m_B	σ_{m_B}	m_V	σ_{m_V}	$T^B_{\max}$	$\sigma_{T_{\max}}$	x_1	σ_{x_1}	c	σ_c	$Cov(c, x_1)$	Q
r200	22.5015	0.0877	22.0856	0.0307	54066.4317	0.5870	1.3868	0.5602	0.3859	0.0798	0.0210	F
r206	23.4720	0.0515	23.5624	0.1021	54055.0639	0.8126	-0.4959	0.4651	-0.1112	0.1015	0.0058	T
r207	23.2020	0.0696	23.1964	0.0814	54045.7051	0.5134	-0.1189	0.4520	-0.0173	0.0933	0.0104	T
r209	22.6669	0.0504	22.6848	0.0377	54052.0218	0.5171	-0.3448	0.2762	-0.0402	0.0584	0.0001	T
r212	23.7139	0.0651	23.8608	0.1366	54055.3079	1.0731	-1.3401	0.5881	-0.1660	0.1241	0.0105	T
r213	22.1991	0.0509	22.1173	0.0230	54063.5615	0.2399	-0.0183	0.2188	0.0575	0.0478	0.0006	T
r225	23.7168	0.0913	23.3714	0.0751	54052.8641	1.6453	-0.6543	0.7490	0.3180	0.1156	-0.0358	F
r230	21.4134	0.0556	21.4469	0.0210	54071.4034	0.1394	0.0256	0.1645	-0.0558	0.0462	0.0012	T
r311	24.0307	0.0969	23.8825	0.2108	54058.7940	2.3796	0.8043	1.3055	0.1222	0.1493	0.0328	T
r317	23.9761	0.1507	23.6856	0.0748	54061.7527	1.2865	0.4075	1.1008	0.2628	0.1418	0.0139	F
r318	20.7156	0.1004	20.5668	0.0343	54082.7021	0.4279	3.7147	0.5835	0.1202	0.0867	0.0059	F
r322	22.9680	0.0518	23.0576	0.0524	54077.7130	0.3442	0.3277	0.4020	-0.1111	0.0641	0.0060	T
s340	23.2475	0.1171	23.1487	0.0945	54071.0726	0.6515	1.7077	0.8404	0.0728	0.1070	0.0407	T
s346	22.0831	0.0945	22.1017	0.0530	54077.7498	0.8850	0.4304	0.5864	-0.0415	0.0707	0.0051	F
s347	21.9412	0.0745	21.8413	0.0355	54101.7341	0.4543	1.9025	0.5544	0.0737	0.0660	0.0114	F
s349	21.9374	0.0860	21.7752	0.0302	54085.4942	0.6436	-1.4941	0.6750	0.1379	0.0737	0.0105	T
s350	23.8269	0.0525	23.8425	0.1088	54095.0873	1.0240	-0.4534	0.8585	-0.0378	0.0945	0.0242	T
s351	24.2855	0.0801	24.1537	0.1674	54088.6564	1.6628	0.2173	1.4625	0.1065	0.1310	0.0363	T
s353	23.8244	0.0821	23.4622	0.0996	54083.4828	1.2715	-1.3897	0.9058	0.3352	0.1233	0.0463	F
s354	23.6884	0.0433	23.7003	0.0767	54091.4525	1.1957	1.0084	0.7540	-0.0353	0.0828	0.0009	T
s355	23.9028	0.0490	23.9202	0.1033	54089.8178	1.1111	-0.3781	0.8920	-0.0396	0.0928	0.0203	T
s370	22.6954	0.0451	22.7677	0.0417	54096.8170	0.5367	0.7838	0.4880	-0.0945	0.0590	0.0021	T
s372	24.0335	0.0686	24.2893	0.1424	54089.8789	1.2827	-1.3515	1.1317	-0.2727	0.1054	0.0283	F
s373	23.9640	0.0506	24.1761	0.1167	54090.4976	1.1778	-0.1033	0.8617	-0.2308	0.1020	0.0171	T
s374	24.1435	0.0676	24.0899	0.1608	54094.4964	1.6398	0.3000	1.2940	0.0295	0.1187	0.0603	T
s375	23.0683	0.0712	23.0140	0.0796	54103.4443	1.0471	1.9149	1.1050	0.0288	0.0728	0.0116	T
s377	22.4095	0.0529	22.2456	0.0359	54083.5998	1.0858	1.3617	0.6105	0.1371	0.0574	-0.0052	T
s379	20.7474	0.0863	20.7618	0.0286	54102.6432	0.1802	0.2934	0.2928	-0.0372	0.0646	0.0075	T
s380	23.8648	0.0752	23.5938	0.1271	54099.9126	0.9675	-0.5541	0.9387	0.2444	0.1219	0.0329	T
x017	22.6885	0.0510	22.4829	0.0374	54379.5261	1.2391	-0.4830	0.5868	0.1798	0.0681	-0.0120	F
x020	23.9894	0.1303	24.1161	0.2289	54373.0684	1.4222	-0.5980	1.3055	-0.1467	0.1754	0.0890	T
x025	22.2673	0.0822	22.2316	0.0345	54357.8319	0.6157	-0.6693	0.4700	0.0128	0.0727	0.0165	T
x028	23.4907	0.0799	23.4519	0.1104	54372.4066	1.0017	1.6558	0.9596	0.0139	0.1238	0.0519	T
x033	22.3561	0.0551	22.4182	0.0477	54389.4339	0.4386	0.5885	0.4297	-0.0843	0.0606	-0.0036	T
x034	23.3350	0.0705	23.1830	0.0685	54373.2170	0.5694	-1.7059	0.4758	0.1280	0.0907	0.0060	T

Continued on next page

Table C.3 (Continued)

ID	m_B	σ_{m_B}	m_V	σ_{m_V}	$T^B_{\max}$	$\sigma_{T_{\max}}$	x_1	σ_{x_1}	c	σ_c	$Cov(c, x_1)$	Q
x038	23.3872	0.0658	22.9736	0.0847	54386.8216	0.8979	3.6348	0.8110	0.3817	0.0942	-0.0063	F
x039	22.8000	0.0458	22.9287	0.0991	54377.2993	0.6764	-0.7227	0.4299	-0.1486	0.0866	0.0138	T
x055	21.4731	0.0497	21.4423	0.0314	54371.7267	0.2240	-1.0790	0.1778	0.0083	0.0531	-0.0027	F
x066	21.7553	0.0530	21.8051	0.0274	54354.9573	0.6157	0.0524	0.3102	-0.0718	0.0576	-0.0027	T
x071	22.9287	0.0514	23.0307	0.0493	54394.9566	0.3462	0.4667	0.3329	-0.1234	0.0650	0.0028	T
x077	23.0453	0.0380	23.0271	0.0588	54390.2104	0.5707	0.8043	0.3618	-0.0056	0.0662	-0.0031	T
x080	22.9853	0.0742	22.8054	0.0549	54385.9402	1.0200	-0.1654	0.6365	0.1543	0.0931	-0.0146	T
x085	23.6371	0.0608	23.7956	0.1542	54391.8397	0.7719	-0.5811	0.5386	-0.1779	0.1205	0.0037	T
x089	23.9825	0.0885	23.6363	0.1118	54388.3302	1.2429	1.0622	1.0014	0.3173	0.1224	-0.0117	F
x093	24.0569	0.0682	23.8930	0.1565	54386.3484	1.1756	-3.1692	1.1104	0.1411	0.1687	-0.0512	F
x107	19.9776	0.1103	20.0055	0.0335	54404.9748	0.2586	1.3476	0.1648	-0.0513	0.0863	-0.0050	T
y125	21.8048	0.0486	21.7984	0.0215	54412.3552	0.4591	0.9537	0.2956	-0.0173	0.0455	0.0002	T
y127	22.9975	0.0502	23.1558	0.0749	54406.4834	0.4584	0.5374	0.4629	-0.1786	0.0801	0.0047	T
y134	22.0532	0.0588	22.0157	0.0241	54418.7132	0.4025	-1.2900	0.5225	0.0151	0.0544	0.0060	F
y136	23.7734	0.0531	23.2402	0.0720	54413.2097	0.7646	1.8555	0.6512	0.5017	0.0869	-0.0067	F
y137	22.1794	0.0444	22.1948	0.0286	54420.0259	0.2651	0.7089	0.2288	-0.0386	0.0501	-0.0018	T
y142	23.1411	0.0372	23.0899	0.0634	54422.5750	0.4331	0.6207	0.3211	0.0269	0.0689	0.0023	T
y143	22.8987	0.0480	22.9255	0.0437	54406.4119	0.5055	0.6174	0.3462	-0.0496	0.0566	0.0013	T
y145	23.0351	0.0423	23.0817	0.0682	54420.7813	0.5852	1.7521	0.4795	-0.0700	0.0738	0.0037	T
y151	23.3770	0.0599	23.3508	0.0805	54428.4959	0.4368	0.2279	0.4901	0.0027	0.0843	0.0089	T
y154	23.5828	0.0402	23.8149	0.0861	54418.9368	0.9335	0.3117	0.5900	-0.2507	0.0783	0.0061	F
y158	23.0390	0.0428	23.0350	0.0419	54423.9295	0.3869	0.7066	0.3417	-0.0195	0.0568	0.0025	T
y163	24.0333	0.0673	23.7489	0.1486	54421.9164	0.9259	-1.2513	0.7018	0.2583	0.1334	0.0031	F
y175	22.8360	0.0601	22.6964	0.0459	54425.8623	0.2861	-1.9635	0.3382	0.1161	0.0685	-0.0007	T
y177	21.6761	0.0493	21.6179	0.0223	54437.7168	0.2485	1.1990	0.2590	0.0333	0.0456	0.0003	T
z180	22.5201	0.0375	22.5149	0.0276	54442.8254	0.3996	0.4254	0.2769	-0.0181	0.0469	0.0006	T
z181	23.6384	0.0449	23.6948	0.0923	54439.2132	0.8229	-0.1018	0.5110	-0.0782	0.0908	0.0117	T
z183	21.4047	0.0502	21.4208	0.0207	54437.4468	0.2451	0.9457	0.1815	-0.0395	0.0438	0.0001	T
z185	22.5041	0.0477	22.6490	0.0408	54431.6451	0.3612	-0.0396	0.3277	-0.1650	0.0566	-0.0013	T
z187	21.7861	0.0520	21.7779	0.0205	54444.4417	0.3247	-1.5587	0.3057	-0.0136	0.0464	0.0017	F
z200	23.0644	0.0512	23.0241	0.0454	54453.2799	0.3546	-0.0769	0.4278	0.0168	0.0606	0.0013	T
z202	20.7892	0.0644	20.8219	0.0211	54449.9709	0.1539	0.0645	0.1891	-0.0551	0.0520	0.0021	F
z203	23.4393	0.1337	23.2272	0.0496	54452.9035	0.6130	2.0928	0.8403	0.1840	0.1075	0.0427	F
z204	23.5196	0.0648	23.5714	0.1171	54453.3551	0.7247	0.2490	0.7035	-0.0740	0.0939	-0.0006	T
z205	22.5140	0.0439	22.4191	0.0344	54453.8289	0.2631	0.7741	0.3069	0.0697	0.0513	-0.0007	T

Continued on next page

Table C.3 (Continued)

ID	m_B	σ_{m_B}	m_V	σ_{m_V}	$T^B_{\max}$	$\sigma_{T_{\max}}$	x_1	σ_{x_1}	c	σ_c	$Cov(c, x_1)$	Q
z208	23.1779	0.0733	23.2067	0.0664	54457.1693	0.8213	1.9027	1.0265	-0.0527	0.0708	0.0222	T

[5] *SALT2* does not directly report distance estimates. The distance modulus is determined using a global fit for all SN Ia together with other cosmological parameters.

[6] While the *SALT2* shape estimates are strongly affected by measurements pre-maximum, it uses significanly more low S/N measurements on the decline, as well as measurements for faint and/or high-z objects. Conseqeuntly the cut on number of measurements post-maximum has very little impact. We instead require a total of 8 observations be used in the fit, to ensure that the measured parameters are reliable.

[7] We use the updated *SALT2* color law described in Guy et al. [47]. This differs signiciantly from the CCM89 law in the NUV.

[8] Covariances between all the fit parameters are calculated and Cov(m_B,x_1), Cov(m_B,c), and Cov(x_1,c) are propagated to simple_cosfitter. These values will be included in the machine readable tables provided with Narayan et al. [91, in prep.].

[9] Flag describing if the object passes (T) or fails (F) the light curve quality cuts for *SALT* described in WV07 and the shape and color cuts described in Conley et al. [23].

References

[1] K. N. Abazajian, J. K. Adelman-McCarthy, M. A. Agüeros, S. S. Allam, C. Allende Prieto, D. An, K. S. J. Anderson, S. F. Anderson, J. Annis, N. A. Bahcall, and et al. The Seventh Data Release of the Sloan Digital Sky Survey. *ApJS*, 182:543, June 2009. doi: 10.1088/0067-0049/182/2/543.

[2] A. Albrecht, G. Bernstein, R. Cahn, W. L. Freedman, J. Hewitt, W. Hu, J. Huth, M. Kamionkowski, E. W. Kolb, L. Knox, J. C. Mather, S. Staggs, and N. B. Suntzeff. Report of the Dark Energy Task Force. *ArXiv Astrophysics e-prints*, September 2006.

[3] J. Allington-Smith, M. Breare, R. Ellis, D. Gellatly, K. Glazebrook, P. Jorden, J. Maclean, P. Oates, G. Shaw, N. Tanvir, K. Taylor, P. Taylor, J. Webster, and S. Worswick. A low-dispersion survey spectrograph (LDSS-2) for the William Herschel Telescope. *PASP*, 106:983–991, September 1994. doi: 10.1086/133471.

[4] L. Anderson, E. Aubourg, S. Bailey, D. Bizyaev, M. Blanton, A. S. Bolton, J. Brinkmann, J. R. Brownstein, A. Burden, A. J. Cuesta, L. A. N. da Costa, K. S. Dawson, R. de Putter, D. J. Eisenstein, J. E. Gunn, H. Guo, J.-C. Hamilton, P. Harding, S. Ho, K. Honscheid, E. Kazin, D. Kirkby, J.-P. Kneib, A. Labatie, C. Loomis, R. H. Lupton, E. Malanushenko, V. Malanushenko, R. Mandelbaum, M. Manera, C. Maraston, C. K. McBride, K. T. Mehta, O. Mena, F. Montesano, D. Muna, R. C. Nichol, S. E. Nuza, M. D. Olmstead, D. Oravetz, N. Padmanabhan, N. Palanque-Delabrouille, K. Pan, J. Parejko, I. Pâris, W. J. Percival, P. Petitjean, F. Prada, B. Reid, N. A. Roe, A. J. Ross, N. P. Ross, L. Samushia, A. G. Sánchez, D. J. Schlegel, D. P. Schneider, C. G. Scóccola, H.-J. Seo, E. S. Sheldon, A. Simmons, R. A. Skibba, M. A. Strauss, M. E. C. Swanson, D. Thomas, J. L. Tinker, R. Tojeiro, M. V. Magaña, L. Verde, C. Wagner, D. A. Wake, B. A. Weaver, D. H. Weinberg, M. White, X. Xu, C. Yèche, I. Zehavi, and G.-B. Zhao. The clustering of galaxies in the SDSS-III Baryon Oscillation Spectroscopic Survey: baryon acoustic oscillations in the Data Release 9 spectroscopic galaxy sample. *MNRAS*, 427:3435–3467, December 2012. doi: 10.1111/j.1365-2966.2012.22066.x.

[5] I. Appenzeller, K. Fricke, W. Furtig, W. Gassler, R. Hafner, R. Harkl, H.-J. Hess,

W. Hummel, P. Jurgens, R.-P. Kudritzki, K.-H. Mantel, W. Meisl, B. Muschielok, H. Nicklas, G. Rupprecht, W. Seifert, O. Stahl, T. Szeifert, and K. Tarantik. Successful commissioning of FORS1 - the First Optical Instrument on the VLT. *The ESO Messenger*, 94:1–6, 1998.

[6] P. Astier, J. Guy, N. Regnault, R. Pain, E. Aubourg, D. Balam, S. Basa, R. G. Carlberg, S. Fabbro, D. Fouchez, I. M. Hook, D. A. Howell, H. Lafoux, J. D. Neill, N. Palanque-Delabrouille, K. Perrett, C. J. Pritchet, J. Rich, M. Sullivan, R. Taillet, G. Aldering, P. Antilogus, V. Arsenijevic, C. Balland, S. Baumont, J. Bronder, H. Courtois, R. S. Ellis, M. Filiol, A. C. Gonçalves, A. Goobar, D. Guide, D. Hardin, V. Lusset, C. Lidman, R. McMahon, M. Mouchet, A. Mourao, S. Perlmutter, P. Ripoche, C. Tao, and N. Walton. The Supernova Legacy Survey: measurement of Ω_M, Ω_Λ and w from the first year data set. *A&A*, 447:31–48, February 2006. doi: 10.1051/0004-6361:20054185.

[7] R. L. Barone-Nugent, C. Lidman, J. S. B. Wyithe, J. Mould, D. A. Howell, I. M. Hook, M. Sullivan, P. E. Nugent, I. Arcavi, S. B. Cenko, J. Cooke, A. Gal-Yam, E. Y. Hsiao, M. M. Kasliwal, K. Maguire, E. Ofek, D. Poznanski, and D. Xu. Near-infrared observations of Type Ia supernovae: the best known standard candle for cosmology. *MNRAS*, 425:1007–1012, September 2012. doi: 10.1111/j.1365-2966.2012.21412.x.

[8] B. J. Barris, J. L. Tonry, M. C. Novicki, and W. M. Wood-Vasey. The NN2 Flux Difference Method for Constructing Variable Object Light Curves. *AJ*, 130: 2272–2277, November 2005. doi: 10.1086/491583.

[9] E. Bertin, Y. Mellier, M. Radovich, G. Missonnier, P. Didelon, and B. Morin. The TERAPIX Pipeline. In D. A. Bohlender, D. Durand, and T. H. Handley, editors, *Astronomical Data Analysis Software and Systems XI*, volume 281 of *Astronomical Society of the Pacific Conference Series*, page 228, 2002.

[10] M. S. Bessell. UBVRI passbands. *PASP*, 102:1181–1199, October 1990. doi: 10.1086/132749.

[11] M. Betoule, J. Marriner, N. Regnault, J.-C. Cuillandre, P. Astier, J. Guy, C. Balland, P. El Hage, D. Hardin, R. Kessler, L. Le Guillou, J. Mosher, R. Pain, P.-F. Rocci, M. Sako, and K. Schahmaneche. Improved Photometric Calibration of the SNLS and the SDSS Supernova Surveys. *ArXiv e-prints*, December 2012.

[12] S. Blondin and J. L. Tonry. Determining the Type, Redshift, and Age of a Supernova Spectrum. *ApJ*, 666:1024–1047, September 2007. doi: 10.1086/520494.

[13] S. Blondin, J. R. Walsh, B. Leibundgut, and G. Sainton. Extracting clean supernova spectra. Towards a quantitative analysis of high-redshift Type Ia supernova spectra. *A&A*, 431:757–771, February 2005.

[14] S. Blondin, L. Dessart, B. Leibundgut, D. Branch, P. Höflich, J. L. Tonry, T. Matheson, R. J. Foley, R. Chornock, A. V. Filippenko, J. Sollerman, J. Spyromilio, R. P. Kirshner, W. M. Wood-Vasey, A. Clocchiatti, C. Aguilera, B. Barris, A. C. Becker, P. Challis, R. Covarrubias, T. M. Davis, P. Garnavich, M. Hicken, S. Jha, K. Krisciunas, W. Li, A. Miceli, G. Miknaitis, G. Pignata, J. L. Prieto, A. Rest, A. G. Riess, M. E. Salvo, B. P. Schmidt, R. C. Smith, C. W. Stubbs, and N. B. Suntzeff. Using Line Profiles to Test the Fraternity of Type Ia Supernovae at High and Low Redshifts. *AJ*, 131:1648–1666, March 2006. doi: 10.1086/498724.

[15] S. Blondin, K. S. Mandel, and R. P. Kirshner. Do spectra improve distance measurements of Type Ia supernovae? *A&A*, 526:A81, February 2011. doi: 10.1051/0004-6361/201015792.

[16] D. Branch and J. B. Doggett. The subluminous Type I supernova 1957a in NGC 2841. *AJ*, 90:2218–2220, November 1985. doi: 10.1086/113924.

[17] T. J. Bronder, I. M. Hook, P. Astier, D. Balam, C. Balland, S. Basa, R. G. Carlberg, A. Conley, D. Fouchez, J. Guy, D. A. Howell, J. D. Neill, R. Pain, K. Perrett, C. J. Pritchet, N. Regnault, M. Sullivan, S. Baumont, S. Fabbro, M. Filliol, S. Perlmutter, and P. Ripoche. SNLS spectroscopy: testing for evolution in type Ia supernovae. *A&A*, 477:717–734, January 2008. doi: 10.1051/0004-6361:20077655.

[18] J. A. Cardelli, G. C. Clayton, and J. S. Mathis. The relationship between infrared, optical, and ultraviolet extinction. *ApJ*, 345:245–256, October 1989. doi: 10.1086/167900.

[19] S. A. Colgate. Supernovae as a standard candle for cosmology. *ApJ*, 232: 404–408, September 1979. doi: 10.1086/157300.

[20] E. D. Commins. Observational selection, host galaxy dust, and Type Ia supernovae. *New Astronomy Review*, 48:567–573, May 2004. doi: 10.1016/j.newar.2003.12.035.

[21] A. Conley, R. G. Carlberg, J. Guy, D. A. Howell, S. Jha, A. G. Riess, and M. Sullivan. Is There Evidence for a Hubble Bubble? The Nature of Type Ia Supernova Colors and Dust in External Galaxies. *ApJ*, 664:L13–L16, July 2007. doi: 10.1086/520625.

[22] A. Conley, M. Sullivan, E. Y. Hsiao, J. Guy, P. Astier, D. Balam, C. Balland, S. Basa, R. G. Carlberg, D. Fouchez, D. Hardin, D. A. Howell, I. M. Hook, R. Pain, K. Perrett, C. J. Pritchet, and N. Regnault. SiFTO: An Empirical Method for Fitting SN Ia Light Curves. *ApJ*, 681:482–498, July 2008. doi: 10.1086/588518.

[23] A. Conley, J. Guy, M. Sullivan, N. Regnault, P. Astier, C. Balland, S. Basa, R. G. Carlberg, D. Fouchez, D. Hardin, I. M. Hook, D. A. Howell, R. Pain, N. Palanque-Delabrouille, K. M. Perrett, C. J. Pritchet, J. Rich, V. Ruhlmann-Kleider, D. Balam, S. Baumont, R. S. Ellis, S. Fabbro, H. K. Fakhouri, N. Fourmanoit, S. González-Gaitán, M. L. Graham, M. J. Hudson, E. Hsiao, T. Kronborg, C. Lidman, A. M. Mourao, J. D. Neill, S. Perlmutter, P. Ripoche, N. Suzuki, and E. S. Walker. Supernova Constraints and Systematic Uncertainties from the First Three Years of the Supernova Legacy Survey. *ApJS*, 192:1, January 2011. doi: 10.1088/0067-0049/192/1/1.

[24] C. Contreras, M. Hamuy, M. M. Phillips, G. Folatelli, N. B. Suntzeff, S. E. Persson, M. Stritzinger, L. Boldt, S. González, W. Krzeminski, N. Morrell, M. Roth, F. Salgado, M. José Maureira, C. R. Burns, W. L. Freedman, B. F. Madore, D. Murphy, P. Wyatt, W. Li, and A. V. Filippenko. The Carnegie Supernova Project: First Photometry Data Release of Low-Redshift Type Ia Supernovae. *AJ*, 139:519–539, February 2010. doi: 10.1088/0004-6256/139/2/519.

[25] A. Cooray and R. R. Caldwell. Large-scale bulk motions complicate the Hubble diagram. *Phys. Rev. D*, 73(10):103002, May 2006. doi: 10.1103/PhysRevD.73.103002.

[26] T. M. Davis, E. Mörtsell, J. Sollerman, A. C. Becker, S. Blondin, P. Challis, A. Clocchiatti, A. V. Filippenko, R. J. Foley, P. M. Garnavich, S. Jha, K. Krisciunas, R. P. Kirshner, B. Leibundgut, W. Li, T. Matheson, G. Miknaitis, G. Pignata, A. Rest, A. G. Riess, B. P. Schmidt, R. C. Smith, J. Spyromilio, C. W. Stubbs, N. B. Suntzeff, J. L. Tonry, W. M. Wood-Vasey, and A. Zenteno. Scrutinizing Exotic Cosmological Models Using ESSENCE Supernova Data Combined with Other Cosmological Probes. *ApJ*, 666:716–725, September 2007. doi: 10.1086/519988.

[27] A. Dressler. *A User's Manual for IMACS*, 2004. URL http://www.ociw.edu/lco/magellan/instruments/IMACS/observing_with_IMACS_2.html.

[28] D. J. Eisenstein, I. Zehavi, D. W. Hogg, R. Scoccimarro, M. R. Blanton, R. C. Nichol, R. Scranton, H.-J. Seo, M. Tegmark, Z. Zheng, S. F. Anderson, J. Annis,

N. Bahcall, J. Brinkmann, S. Burles, F. J. Castander, A. Connolly, I. Csabai, M. Doi, M. Fukugita, J. A. Frieman, K. Glazebrook, J. E. Gunn, J. S. Hendry, G. Hennessy, Z. Ivezić, S. Kent, G. R. Knapp, H. Lin, Y.-S. Loh, R. H. Lupton, B. Margon, T. A. McKay, A. Meiksin, J. A. Munn, A. Pope, M. W. Richmond, D. Schlegel, D. P. Schneider, K. Shimasaku, C. Stoughton, M. A. Strauss, M. SubbaRao, A. S. Szalay, I. Szapudi, D. L. Tucker, B. Yanny, and D. G. York. Detection of the Baryon Acoustic Peak in the Large-Scale Correlation Function of SDSS Luminous Red Galaxies. *ApJ*, 633:560–574, November 2005. doi: 10.1086/466512.

[29] S. M. Faber, A. C. Phillips, R. I. Kibrick, B. Alcott, S. L. Allen, J. Burrous, T. Cantrall, D. Clarke, A. L. Coil, D. J. Cowley, M. Davis, W. T. S. Deich, K. Dietsch, D. K. Gilmore, C. A. Harper, D. F. Hilyard, J. P. Lewis, M. McVeigh, J. Newman, J. Osborne, R. Schiavon, R. J. Stover, D. Tucker, V. Wallace, M. Wei, G. Wirth, and C. A. Wright. The DEIMOS spectrograph for the Keck II Telescope: integration and testing. In M. et al. Iye, editor, *Instrument Design and Performance for Optical/Infrared Ground-based Telescopes. Edited by Iye, Masanori; Moorwood, Alan F. M. Proceedings of the SPIE, Volume 4841, pp. 1657-1669 (2003).*, pages 1657–1669, March 2003.

[30] D. Fabricant, P. Cheimets, N. Caldwell, and J. Geary. The FAST Spectrograph for the Tillinghast Telescope. *PASP*, 110:79–85, January 1998.

[31] J. D. Fernie. On the variability of VEGA. *PASP*, 93:333–337, June 1981. doi: 10.1086/130834.

[32] A. V. Filippenko. Optical Spectra of Supernovae. *ARA&A*, 35:309–355, 1997.

[33] A. V. Filippenko, M. W. Richmond, D. Branch, M. Gaskell, W. Herbst, C. H. Ford, R. R. Treffers, T. Matheson, L. C. Ho, A. Dey, W. L. W. Sargent, T. A. Small, and W. J. M. van Breugel. The subluminous, spectroscopically peculiar type IA supernova 1991bg in the elliptical galaxy NGC 4374. *AJ*, 104: 1543–1556, October 1992. doi: 10.1086/116339.

[34] A. V. Filippenko, M. W. Richmond, T. Matheson, J. C. Shields, E. M. Burbidge, R. D. Cohen, M. Dickinson, M. A. Malkan, B. Nelson, J. Pietz, D. Schlegel, P. Schmeer, H. Spinrad, C. C. Steidel, H. D. Tran, and W. Wren. The peculiar Type IA SN 1991T - Detonation of a white dwarf? *ApJ*, 384:L15–L18, January 1992. doi: 10.1086/186252.

[35] G. Folatelli, M. M. Phillips, C. R. Burns, C. Contreras, M. Hamuy, W. L. Freedman, S. E. Persson, M. Stritzinger, N. B. Suntzeff, K. Krisciunas, L. Boldt, S. González, W. Krzeminski, N. Morrell, M. Roth, F. Salgado, B. F. Madore,

D. Murphy, P. Wyatt, W. Li, A. V. Filippenko, and N. Miller. The Carnegie Supernova Project: Analysis of the First Sample of Low-Redshift Type-Ia Supernovae. *AJ*, 139:120–144, January 2010. doi: 10.1088/0004-6256/139/1/120.

[36] R. J. Foley. *Type Ia supernova evolution and dark energy*. PhD thesis, University of California, Berkeley, 2008.

[37] R. J. Foley and D. Kasen. Measuring Ejecta Velocity Improves Type Ia Supernova Distances. *ApJ*, 729:55, March 2011. doi: 10.1088/0004-637X/729/1/55.

[38] R. J. Foley, T. Matheson, S. Blondin, R. Chornock, J. M. Silverman, P. Challis, A. Clocchiatti, A. V. Filippenko, R. P. Kirshner, B. Leibundgut, J. Sollerman, J. Spyromilio, J. L. Tonry, T. M. Davis, P. M. Garnavich, S. W. Jha, K. Krisciunas, W. Li, G. Pignata, A. Rest, A. G. Riess, B. P. Schmidt, R. C. Smith, C. W. Stubbs, B. E. Tucker, and W. M. Wood-Vasey. Spectroscopy of High-Redshift Supernovae from the Essence Project: The First Four Years. *AJ*, 137: 3731–3742, April 2009. doi: 10.1088/0004-6256/137/4/3731.

[39] R. J. Foley, A. V. Filippenko, R. Kessler, B. Bassett, J. A. Frieman, P. M. Garnavich, S. W. Jha, K. Konishi, H. Lampeitl, A. G. Riess, M. Sako, D. P. Schneider, J. Sollerman, and M. Smith. A Mismatch in the Ultraviolet Spectra between Low-redshift and Intermediate-redshift Type Ia Supernovae as a Possible Systematic Uncertainty for Supernova Cosmology. *AJ*, 143:113, May 2012. doi: 10.1088/0004-6256/143/5/113.

[40] W. L. Freedman, C. R. Burns, M. M. Phillips, P. Wyatt, S. E. Persson, B. F. Madore, C. Contreras, G. Folatelli, E. S. Gonzalez, M. Hamuy, E. Hsiao, D. D. Kelson, N. Morrell, D. C. Murphy, M. Roth, M. Stritzinger, L. Sturch, N. B. Suntzeff, P. Astier, C. Balland, B. Bassett, L. Boldt, R. G. Carlberg, A. J. Conley, J. A. Frieman, P. M. Garnavich, J. Guy, D. Hardin, D. A. Howell, R. Kessler, H. Lampeitl, J. Marriner, R. Pain, K. Perrett, N. Regnault, A. G. Riess, M. Sako, D. P. Schneider, M. Sullivan, and M. Wood-Vasey. The Carnegie Supernova Project: First Near-Infrared Hubble Diagram to z ˜ 0.7. *ApJ*, 704:1036–1058, October 2009. doi: 10.1088/0004-637X/704/2/1036.

[41] M. Fukugita, T. Ichikawa, J. E. Gunn, M. Doi, K. Shimasaku, and D. P. Schneider. The Sloan Digital Sky Survey Photometric System. *AJ*, 111:1748, April 1996. doi: 10.1086/117915.

[42] M. Ganeshalingam, W. Li, A. V. Filippenko, C. Anderson, G. Foster, E. L. Gates, C. V. Griffith, B. J. Grigsby, N. Joubert, J. Leja, T. B. Lowe, B. Macomber,

T. Pritchard, P. Thrasher, and D. Winslow. Results of the Lick Observatory Supernova Search Follow-up Photometry Program: BVRI Light Curves of 165 Type Ia Supernovae. *ApJS*, 190:418–448, October 2010. doi: 10.1088/0067-0049/190/2/418.

[43] A. Garg, C. W. Stubbs, P. Challis, W. M. Wood-Vasey, S. Blondin, M. E. Huber, K. Cook, S. Nikolaev, A. Rest, R. C. Smith, K. Olsen, N. B. Suntzeff, C. Aguilera, J. L. Prieto, A. Becker, A. Miceli, G. Miknaitis, A. Clocchiatti, D. Minniti, L. Morelli, and D. L. Welch. Light Curves of Type Ia Supernovae from Near the Time of Explosion. *AJ*, 133:403–419, February 2007. doi: 10.1086/510118.

[44] K. Glazebrook and J. Bland-Hawthorn. Microslit Nod-Shuffle Spectroscopy: A Technique for Achieving Very High Densities of Spectra. *PASP*, 113:197–214, February 2001. doi: 10.1086/318625.

[45] G. Goldhaber, D. E. Groom, A. Kim, G. Aldering, P. Astier, A. Conley, S. E. Deustua, R. Ellis, S. Fabbro, A. S. Fruchter, A. Goobar, I. Hook, M. Irwin, M. Kim, R. A. Knop, C. Lidman, R. McMahon, P. E. Nugent, R. Pain, N. Panagia, C. R. Pennypacker, S. Perlmutter, P. Ruiz-Lapuente, B. Schaefer, N. A. Walton, and T. York. Timescale Stretch Parameterization of Type Ia Supernova B-Band Light Curves. *ApJ*, 558:359–368, September 2001. doi: 10.1086/322460.

[46] J. Guy, P. Astier, S. Baumont, D. Hardin, R. Pain, N. Regnault, S. Basa, R. G. Carlberg, A. Conley, S. Fabbro, D. Fouchez, I. M. Hook, D. A. Howell, K. Perrett, C. J. Pritchet, J. Rich, M. Sullivan, P. Antilogus, E. Aubourg, G. Bazin, J. Bronder, M. Filiol, N. Palanque-Delabrouille, P. Ripoche, and V. Ruhlmann-Kleider. SALT2: using distant supernovae to improve the use of Type Ia supernovae as distance indicators. *ArXiv Astrophysics e-prints*, January 2007.

[47] J. Guy, M. Sullivan, A. Conley, N. Regnault, P. Astier, C. Balland, S. Basa, R. G. Carlberg, D. Fouchez, D. Hardin, I. M. Hook, D. A. Howell, R. Pain, N. Palanque-Delabrouille, K. M. Perrett, C. J. Pritchet, J. Rich, V. Ruhlmann-Kleider, D. Balam, S. Baumont, R. S. Ellis, S. Fabbro, H. K. Fakhouri, N. Fourmanoit, S. González-Gaitán, M. L. Graham, E. Hsiao, T. Kronborg, C. Lidman, A. M. Mourao, S. Perlmutter, P. Ripoche, N. Suzuki, and E. S. Walker. The Supernova Legacy Survey 3-year sample: Type Ia supernovae photometric distances and cosmological constraints. *A&A*, 523:A7, November 2010. doi: 10.1051/0004-6361/201014468.

[48] M. Hamuy, J. Maza, M. M. Phillips, N. B. Suntzeff, M. Wischnjewsky, R. C. Smith, R. Antezana, L. A. Wells, L. E. Gonzalez, P. Gigoux, M. Navarrete,

F. Barrientos, R. Lamontagne, M. della Valle, J. E. Elias, A. C. Phillips, S. C. Odewahn, J. A. Baldwin, A. R. Walker, T. Williams, C. R. Sturch, F. K. Baganoff, B. C. Chaboyer, R. A. Schommer, H. Tirado, M. Hernandez, P. Ugarte, P. Guhathakurta, S. B. Howell, P. Szkody, P. C. Schmidtke, and J. Roth. The 1990 Calan/Tololo Supernova Search. *AJ*, 106:2392–2407, December 1993. doi: 10.1086/116811.

[49] M. Hamuy, M. M. Phillips, L. A. Wells, and J. Maza. K Corrections for type IA supernovae. *PASP*, 105:787–793, July 1993.

[50] M. Hamuy, M. M. Phillips, N. B. Suntzeff, R. A. Schommer, J. Maza, and R. Aviles. The Absolute Luminosities of the Calan/Tololo Type IA Supernovae. *AJ*, 112:2391, December 1996. URL http://adsabs.harvard.edu/cgi-bin/nph-bib_query?bibcode=1996AJ....112.2391H&db_key=AST.

[51] K. Hatano, D. Branch, and J. Deaton. Extinction and Radial Distribution of Supernova Properties in Their Parent Galaxies. *ApJ*, 502:177, July 1998. doi: 10.1086/305903.

[52] P. H. Hauschildt, E. Baron, and F. Allard. Parallel Implementation of the PHOENIX Generalized Stellar Atmosphere Program. *ApJ*, 483:390, July 1997. doi: 10.1086/304233.

[53] M. Hicken, P. Challis, S. Jha, R. P. Kirshner, T. Matheson, M. Modjaz, A. Rest, W. Michael Wood-Vasey, G. Bakos, E. J. Barton, P. Berlind, A. Bragg, C. Briceño, W. R. Brown, N. Caldwell, M. Calkins, R. Cho, L. Ciupik, M. Contreras, K.-C. Dendy, A. Dosaj, N. Durham, K. Eriksen, G. Esquerdo, M. Everett, E. Falco, J. Fernandez, A. Gaba, P. Garnavich, G. Graves, P. Green, T. Groner, C. Hergenrother, M. J. Holman, V. Hradecky, J. Huchra, B. Hutchison, D. Jerius, A. Jordan, R. Kilgard, M. Krauss, K. Luhman, L. Macri, D. Marrone, J. McDowell, D. McIntosh, B. McNamara, T. Megeath, B. Mochejska, D. Munoz, J. Muzerolle, O. Naranjo, G. Narayan, M. Pahre, W. Peters, D. Peterson, K. Rines, B. Ripman, A. Roussanova, R. Schild, A. Sicilia-Aguilar, J. Sokoloski, K. Smalley, A. Smith, T. Spahr, K. Z. Stanek, P. Barmby, S. Blondin, C. W. Stubbs, A. Szentgyorgyi, M. A. P. Torres, A. Vaz, A. Vikhlinin, Z. Wang, M. Westover, D. Woods, and P. Zhao. CfA3: 185 Type Ia Supernova Light Curves from the CfA. *ApJ*, 700:331–357, July 2009. doi: 10.1088/0004-637X/700/1/331.

[54] M. Hicken, W. M. Wood-Vasey, S. Blondin, P. Challis, S. Jha, P. L. Kelly, A. Rest, and R. P. Kirshner. Improved Dark Energy Constraints from ˜100 New CfA

Supernova Type Ia Light Curves. *ApJ*, 700:1097–1140, August 2009. doi: 10.1088/0004-637X/700/2/1097.

[55] M. Hicken, P. Challis, R. P. Kirshner, A. Rest, C. E. Cramer, W. M. Wood-Vasey, G. Bakos, P. Berlind, W. R. Brown, N. Caldwell, M. Calkins, T. Currie, K. de Kleer, G. Esquerdo, M. Everett, E. Falco, J. Fernandez, A. S. Friedman, T. Groner, J. Hartman, M. J. Holman, R. Hutchins, S. Keys, D. Kipping, D. Latham, G. H. Marion, G. Narayan, M. Pahre, A. Pal, W. Peters, G. Perumpilly, B. Ripman, B. Sipocz, A. Szentgyorgyi, S. Tang, M. A. P. Torres, A. Vaz, S. Wolk, and A. Zezas. CfA4: Light Curves for 94 Type Ia Supernovae. *ApJS*, 200:12, June 2012. doi: 10.1088/0067-0049/200/2/12.

[56] J. A. Holtzman, J. Marriner, R. Kessler, M. Sako, B. Dilday, J. A. Frieman, D. P. Schneider, B. Bassett, A. Becker, D. Cinabro, F. DeJongh, D. L. Depoy, M. Doi, P. M. Garnavich, C. J. Hogan, S. Jha, K. Konishi, H. Lampeitl, J. L. Marshall, D. McGinnis, G. Miknaitis, R. C. Nichol, J. L. Prieto, A. G. Riess, M. W. Richmond, R. Romani, M. Smith, N. Takanashi, K. Tokita, K. van der Heyden, N. Yasuda, and C. Zheng. The Sloan Digital Sky Survey-II: Photometry and Supernova IA Light Curves from the 2005 Data. *AJ*, 136:2306–2320, December 2008. doi: 10.1088/0004-6256/136/6/2306.

[57] I. Hook, J. R. Allington-Smith, S. M. Beard, D. Crampton, R. L. Davies, C. G. Dickson, A. W. Ebbers, J. M. Fletcher, I. Jorgensen, I. Jean, S. Juneau, R. G. Murowinski, R. Nolan, K. Laidlaw, B. Leckie, G. E. Marshall, T. Purkins, I. M. Richardson, S. C. Roberts, D. A. Simons, M. J. Smith, J. R. Stilburn, K. Szeto, C. Tierney, R. J. Wolff, and R. Wooff. Gemini-north multiobject spectrograph integration, test, and commissioning. In *Instrument Design and Performance for Optical/Infrared Ground-based Telescopes. Edited by Iye, Masanori; Moorwood, Alan F. M. Proceedings of the SPIE, Volume 4841, pp. 1645-1656 (2003).*, pages 1645–1656, March 2003.

[58] K. Horne. An optimal extraction algorithm for CCD spectroscopy. *PASP*, 98: 609–617, June 1986. doi: 10.1086/131801.

[59] D. A. Howell, M. Sullivan, K. Perrett, T. J. Bronder, I. M. Hook, P. Astier, E. Aubourg, D. Balam, S. Basa, R. G. Carlberg, S. Fabbro, D. Fouchez, J. Guy, H. Lafoux, J. D. Neill, R. Pain, N. Palanque-Delabrouille, C. J. Pritchet, N. Regnault, J. Rich, R. Taillet, R. Knop, R. G. McMahon, S. Perlmutter, and N. A. Walton. Gemini Spectroscopy of Supernovae from the Supernova Legacy Survey: Improving High-Redshift Supernova Selection and Classification. *ApJ*, 634:1190–1201, December 2005. doi: 10.1086/497119.

[60] E. P. Hubble. The law of red shifts (George Darwin Lecture). *MNRAS*, 113:658, 1953.

[61] L. Hui and P. B. Greene. Correlated fluctuations in luminosity distance and the importance of peculiar motion in supernova surveys. *Phys. Rev. D*, 73(12): 123526, June 2006. doi: 10.1103/PhysRevD.73.123526.

[62] Ž. Ivezić, J. A. Smith, G. Miknaitis, H. Lin, D. Tucker, R. H. Lupton, J. E. Gunn, G. R. Knapp, M. A. Strauss, B. Sesar, M. Doi, M. Tanaka, M. Fukugita, J. Holtzman, S. Kent, B. Yanny, D. Schlegel, D. Finkbeiner, N. Padmanabhan, C. M. Rockosi, M. Jurić, N. Bond, B. Lee, C. Stoughton, S. Jester, H. Harris, P. Harding, H. Morrison, J. Brinkmann, D. P. Schneider, and D. York. Sloan Digital Sky Survey Standard Star Catalog for Stripe 82: The Dawn of Industrial 1% Optical Photometry. *AJ*, 134:973–998, September 2007. doi: 10.1086/519976.

[63] S. Jha, R. P. Kirshner, P. Challis, P. M. Garnavich, T. Matheson, A. M. Soderberg, G. J. M. Graves, M. Hicken, J. F. Alves, H. G. Arce, Z. Balog, P. Barmby, E. J. Barton, P. Berlind, A. E. Bragg, C. Briceño, W. R. Brown, J. H. Buckley, N. Caldwell, M. L. Calkins, B. J. Carter, K. D. Concannon, R. H. Donnelly, K. A. Eriksen, D. G. Fabricant, E. E. Falco, F. Fiore, M. R. Garcia, M. Gómez, N. A. Grogin, T. Groner, P. J. Groot, K. E. Haisch, Jr., L. Hartmann, C. W. Hergenrother, M. J. Holman, J. P. Huchra, R. Jayawardhana, D. Jerius, S. J. Kannappan, D.-W. Kim, J. T. Kleyna, C. S. Kochanek, D. M. Koranyi, M. Krockenberger, C. J. Lada, K. L. Luhman, J. X. Luu, L. M. Macri, J. A. Mader, A. Mahdavi, M. Marengo, B. G. Marsden, B. A. McLeod, B. R. McNamara, S. T. Megeath, D. Moraru, A. E. Mossman, A. A. Muench, J. A. Muñoz, J. Muzerolle, O. Naranjo, K. Nelson-Patel, M. A. Pahre, B. M. Patten, J. Peters, W. Peters, J. C. Raymond, K. Rines, R. E. Schild, G. J. Sobczak, T. B. Spahr, J. R. Stauffer, R. P. Stefanik, A. H. Szentgyorgyi, E. V. Tollestrup, P. Väisänen, A. Vikhlinin, Z. Wang, S. P. Willner, S. J. Wolk, J. M. Zajac, P. Zhao, and K. Z. Stanek. UBVRI Light Curves of 44 Type Ia Supernovae. *AJ*, 131: 527–554, January 2006. doi: 10.1086/497989.

[64] S. Jha, A. G. Riess, and R. P. Kirshner. Improved Distances to Type Ia Supernovae with Multicolor Light-Curve Shapes: MLCS2k2. *ApJ*, 659: 122–148, April 2007. doi: 10.1086/512054.

[65] H. L. Johnson and W. W. Morgan. Fundamental stellar photometry for standards of spectral type on the revised system of the Yerkes spectral atlas. *ApJ*, 117:313, May 1953. doi: 10.1086/145697.

[66] B. C. Kelly. Some Aspects of Measurement Error in Linear Regression of Astronomical Data. *ApJ*, 665:1489–1506, August 2007. doi: 10.1086/519947.

[67] P. L. Kelly, M. Hicken, D. L. Burke, K. S. Mandel, and R. P. Kirshner. Hubble Residuals of Nearby Type Ia Supernovae are Correlated with Host Galaxy Masses. *ApJ*, 715:743–756, June 2010. doi: 10.1088/0004-637X/715/2/743.

[68] R. Kessler, A. C. Becker, D. Cinabro, J. Vanderplas, J. A. Frieman, J. Marriner, T. M. Davis, B. Dilday, J. Holtzman, S. W. Jha, H. Lampeitl, M. Sako, M. Smith, C. Zheng, R. C. Nichol, B. Bassett, R. Bender, D. L. Depoy, M. Doi, E. Elson, A. V. Filippenko, R. J. Foley, P. M. Garnavich, U. Hopp, Y. Ihara, W. Ketzeback, W. Kollatschny, K. Konishi, J. L. Marshall, R. J. McMillan, G. Miknaitis, T. Morokuma, E. Mörtsell, K. Pan, J. L. Prieto, M. W. Richmond, A. G. Riess, R. Romani, D. P. Schneider, J. Sollerman, N. Takanashi, K. Tokita, K. van der Heyden, J. C. Wheeler, N. Yasuda, and D. York. First-Year Sloan Digital Sky Survey-II Supernova Results: Hubble Diagram and Cosmological Parameters. *ApJS*, 185:32–84, November 2009. doi: 10.1088/0067-0049/185/1/32.

[69] R. Kessler, J. P. Bernstein, D. Cinabro, B. Dilday, J. A. Frieman, S. Jha, S. Kuhlmann, G. Miknaitis, M. Sako, M. Taylor, and J. Vanderplas. SNANA: A Public Software Package for Supernova Analysis. *PASP*, 121:1028–1035, September 2009. doi: 10.1086/605984.

[70] A. Kim, A. Goobar, and S. Perlmutter. A Generalized K Correction for Type IA Supernovae: Comparing R-band Photometry beyond z=0.2 with B, V, and R-band Nearby Photometry. *PASP*, 108:190, February 1996.

[71] C. T. Kowal. Absolute magnitudes of supernovae. *AJ*, 73:1021–1024, December 1968.

[72] K. Krisciunas, N. C. Hastings, K. Loomis, R. McMillan, A. Rest, A. G. Riess, and C. Stubbs. Uniformity of (V-Near-Infrared) Color Evolution of Type Ia Supernovae and Implications for Host Galaxy Extinction Determination. *ApJ*, 539:658–674, August 2000. doi: 10.1086/309263.

[73] K. Krisciunas, M. M. Phillips, and N. B. Suntzeff. Hubble Diagrams of Type Ia Supernovae in the Near-Infrared. *ApJ*, 602:L81–L84, February 2004. doi: 10.1086/382731.

[74] K. Krisciunas, D. Bastola, J. Espinoza, D. Gonzalez, L. Gonzalez, S. Gonzalez, M. Hamuy, E. Y. Hsiao, N. Morrell, M. M. Phillips, and N. B. Suntzeff. Fixing the U-band Photometry of Type Ia Supernovae. *AJ*, 145:11, January 2013. doi: 10.1088/0004-6256/145/1/11.

[75] H. Lampeitl, M. Smith, R. C. Nichol, B. Bassett, D. Cinabro, B. Dilday, R. J. Foley, J. A. Frieman, P. M. Garnavich, A. Goobar, M. Im, S. W. Jha, J. Marriner, R. Miquel, J. Nordin, L. Östman, A. G. Riess, M. Sako, D. P. Schneider,

J. Sollerman, and M. Stritzinger. The Effect of Host Galaxies on Type Ia Supernovae in the SDSS-II Supernova Survey. *ApJ*, 722:566–576, October 2010. doi: 10.1088/0004-637X/722/1/566.

[76] A. U. Landolt. UBVRI photometric standard stars around the celestial equator. *AJ*, 88:439–460, March 1983. doi: 10.1086/113329.

[77] A. U. Landolt. UBVRI photometric standard stars in the magnitude range 11.5-16.0 around the celestial equator. *AJ*, 104:340–371, July 1992. doi: 10.1086/116242.

[78] A. U. Landolt and A. K. Uomoto. Optical Multicolor Photometry of Spectrophotometric Standard Stars. *AJ*, 133:768–790, March 2007. doi: 10.1086/510485.

[79] B. Leibundgut. Supernova studies. II - The effect of redshift on supernovae IA light curves. *A&A*, 229:1–6, March 1990.

[80] B. Leibundgut, R. P. Kirshner, M. M. Phillips, L. A. Wells, N. B. Suntzeff, M. Hamuy, R. A. Schommer, A. R. Walker, L. Gonzalez, P. Ugarte, R. E. Williams, G. Williger, M. Gomez, R. Marzke, B. P. Schmidt, B. Whitney, N. Coldwell, J. Peters, F. H. Chaffee, C. B. Foltz, D. Rehner, L. Siciliano, T. G. Barnes, K.-P. Cheng, P. M. N. Hintzen, Y.-C. Kim, J. Maza, J. W. Parker, A. C. Porter, P. C. Schmidtke, and G. Sonneborn. SN 1991bg - A type IA supernova with a difference. *AJ*, 105:301–313, January 1993. doi: 10.1086/116427.

[81] P. Lira. Master's thesis, University of Chile, 1995.

[82] K. Maguire, M. Sullivan, R. S. Ellis, P. E. Nugent, D. A. Howell, A. Gal-Yam, J. Cooke, P. Mazzali, Y.-C. Pan, B. Dilday, R. C. Thomas, I. Arcavi, S. Ben-Ami, D. Bersier, F. B. Bianco, B. J. Fulton, I. Hook, A. Horesh, E. Hsiao, P. A. James, P. Podsiadlowski, E. S. Walker, O. Yaron, M. M. Kasliwal, R. R. Laher, N. M. Law, E. O. Ofek, D. Poznanski, and J. Surace. Hubble Space Telescope studies of low-redshift Type Ia supernovae: evolution with redshift and ultraviolet spectral trends. *MNRAS*, 426:2359–2379, November 2012. doi: 10.1111/j.1365-2966.2012.21909.x.

[83] K. S. Mandel, W. M. Wood-Vasey, A. S. Friedman, and R. P. Kirshner. Type Ia Supernova Light-Curve Inference: Hierarchical Bayesian Analysis in the Near-Infrared. *ApJ*, 704:629–651, October 2009. doi: 10.1088/0004-637X/704/1/629.

[84] K. S. Mandel, G. Narayan, and R. P. Kirshner. Type Ia Supernova Light Curve Inference: Hierarchical Models in the Optical and Near-infrared. *Astrophys. J.*, 731:120, April 2011. doi: 10.1088/0004-637X/731/2/120.

[85] T. Matheson, S. Blondin, R. J. Foley, R. Chornock, A. V. Filippenko, B. Leibundgut, R. C. Smith, J. Sollerman, J. Spyromilio, R. P. Kirshner, A. Clocchiatti, C. Aguilera, B. Barris, A. C. Becker, P. Challis, R. Covarrubias, P. Garnavich, M. Hicken, S. Jha, K. Krisciunas, W. Li, A. Miceli, G. Miknaitis, J. L. Prieto, A. Rest, A. G. Riess, M. E. Salvo, B. P. Schmidt, C. W. Stubbs, N. B. Suntzeff, and J. L. Tonry. Spectroscopy of High-Redshift Supernovae from the ESSENCE Project: The First 2 Years. *AJ*, 129:2352–2375, May 2005.

[86] T. Matheson et al. 2013.

[87] G. Miknaitis, G. Pignata, A. Rest, W. M. Wood-Vasey, S. Blondin, P. Challis, R. C. Smith, C. W. Stubbs, N. B. Suntzeff, R. J. Foley, T. Matheson, J. L. Tonry, C. Aguilera, J. W. Blackman, A. C. Becker, A. Clocchiatti, R. Covarrubias, T. M. Davis, A. V. Filippenko, A. Garg, P. M. Garnavich, M. Hicken, S. Jha, K. Krisciunas, R. P. Kirshner, B. Leibundgut, W. Li, A. Miceli, G. Narayan, J. L. Prieto, A. G. Riess, M. E. Salvo, B. P. Schmidt, J. Sollerman, J. Spyromilio, and A. Zenteno. The ESSENCE Supernova Survey: Survey Optimization, Observations, and Supernova Photometry. *ApJ*, 666:674–693, September 2007. doi: 10.1086/519986.

[88] R. Minkowski. Spectra of Supernovae. *PASP*, 53:224, August 1941. URL http://adsabs.harvard.edu/cgi-bin/nph-bib_query?bibcode=1941PASP...53..224M&db_key=AST.

[89] J. Mosher, M. Sako, L. Corlies, G. Folatelli, J. Frieman, J. Holtzman, S. W. Jha, R. Kessler, J. Marriner, M. M. Phillips, M. Stritzinger, N. Morrell, and D. P. Schneider. A Precision Photometric Comparison between SDSS-II and CSP Type Ia Supernova Data. *AJ*, 144:17, July 2012. doi: 10.1088/0004-6256/144/1/17.

[90] G. Narayan and K. Mandel. 2013.

[91] G. Narayan et al. 2013.

[92] J. D. Neill, M. J. Hudson, and A. Conley. The Peculiar Velocities of Local Type Ia Supernovae and Their Impact on Cosmology. *ApJ*, 661:L123–L126, June 2007. doi: 10.1086/518808.

[93] J. Nordin, L. Östman, A. Goobar, C. Balland, H. Lampeitl, R. C. Nichol, M. Sako, D. P. Schneider, M. Smith, J. Sollerman, and J. C. Wheeler. Evidence for a Correlation Between the Si II λ4000 Width and Type Ia Supernova Color. *ApJ*, 734:42, June 2011. doi: 10.1088/0004-637X/734/1/42.

[94] P. Nugent, A. Kim, and S. Perlmutter. K-Corrections and Extinction Corrections for Type Ia Supernovae. *PASP*, 114:803–819, August 2002.

[95] J. E. O'Donnell. *R_nu*-dependent optical and near-ultraviolet extinction. *ApJ*, 422:158–163, February 1994.

[96] E. O. Ofek, R. Laher, N. Law, J. Surace, D. Levitan, B. Sesar, A. Horesh, D. Poznanski, J. C. van Eyken, S. R. Kulkarni, P. Nugent, J. Zolkower, R. Walters, M. Sullivan, M. Agüeros, L. Bildsten, J. Bloom, S. B. Cenko, A. Gal-Yam, C. Grillmair, G. Helou, M. M. Kasliwal, and R. Quimby. The Palomar Transient Factory Photometric Calibration. *PASP*, 124:62–73, January 2012. doi: 10.1086/664065.

[97] J. B. Oke and R. E. Schild. The Absolute Spectral Energy Distribution of Alpha Lyrae. *ApJ*, 161:1015, September 1970. doi: 10.1086/150603.

[98] J. B. Oke, J. G. Cohen, M. Carr, J. Cromer, A. Dingizian, F. H. Harris, S. Labrecque, R. Lucinio, W. Schaal, H. Epps, and J. Miller. The Keck Low-Resolution Imaging Spectrometer. *PASP*, 107:375, April 1995.

[99] N. Padmanabhan, D. J. Schlegel, D. P. Finkbeiner, J. C. Barentine, M. R. Blanton, H. J. Brewington, J. E. Gunn, M. Harvanek, D. W. Hogg, Ž. Ivezić, D. Johnston, S. M. Kent, S. J. Kleinman, G. R. Knapp, J. Krzesinski, D. Long, E. H. Neilsen, Jr., A. Nitta, C. Loomis, R. H. Lupton, S. Roweis, S. A. Snedden, M. A. Strauss, and D. L. Tucker. An Improved Photometric Calibration of the Sloan Digital Sky Survey Imaging Data. *ApJ*, 674:1217–1233, February 2008. doi: 10.1086/524677.

[100] S. Perlmutter, S. Gabi, G. Goldhaber, A. Goobar, D. E. Groom, I. M. Hook, A. G. Kim, M. Y. Kim, J. C. Lee, R. Pain, C. R. Pennypacker, I. A. Small, R. S. Ellis, R. G. McMahon, B. J. Boyle, P. S. Bunclark, D. Carter, M. J. Irwin, K. Glazebrook, H. J. M. Newberg, A. V. Filippenko, T. Matheson, M. Dopita, W. J. Couch, and The Supernova Cosmology Project. Measurements of the Cosmological Parameters Omega and Lambda from the First Seven Supernovae at Z >= 0.35. *ApJ*, 483:565, July 1997. doi: 10.1086/304265.

[101] S. Perlmutter, G. Aldering, G. Goldhaber, R. A. Knop, P. Nugent, P. G. Castro, S. Deustua, S. Fabbro, A. Goobar, D. E. Groom, I. M. Hook, A. G. Kim, M. Y. Kim, J. C. Lee, N. J. Nunes, R. Pain, C. R. Pennypacker, R. Quimby, C. Lidman, R. S. Ellis, M. Irwin, R. G. McMahon, P. Ruiz-Lapuente, N. Walton, B. Schaefer, B. J. Boyle, A. V. Filippenko, T. Matheson, A. S. Fruchter, N. Panagia, H. J. M. Newberg, W. J. Couch, and The Supernova Cosmology Project. Measurements of Omega and Lambda from 42 High-Redshift Supernovae. *ApJ*, 517:565–586, June 1999. doi: 10.1086/307221.

[102] D. M. Peterson, C. A. Hummel, T. A. Pauls, J. T. Armstrong, J. A. Benson, G. C. Gilbreath, R. B. Hindsley, D. J. Hutter, K. J. Johnston, D. Mozurkewich, and

H. R. Schmitt. Vega is a rapidly rotating star. *Nature*, 440:896–899, April 2006. doi: 10.1038/nature04661.

[103] M. M. Phillips. The absolute magnitudes of Type Ia supernovae. *ApJ*, 413: L105–L108, August 1993. doi: 10.1086/186970.

[104] M. M. Phillips, L. A. Wells, N. B. Suntzeff, M. Hamuy, B. Leibundgut, R. P. Kirshner, and C. B. Foltz. SN 1991T - Further evidence of the heterogeneous nature of type IA supernovae. *AJ*, 103:1632–1637, May 1992. doi: 10.1086/116177.

[105] M. M. Phillips, P. Lira, N. B. Suntzeff, R. A. Schommer, M. Hamuy, and J. Maza. The Reddening-Free Decline Rate Versus Luminosity Relationship for Type Ia Supernovae. *AJ*, 118:1766–1776, October 1999. doi: 10.1086/301032.

[106] Planck collaboration, P. A. R. Ade, N. Aghanim, C. Armitage-Caplan, M. Arnaud, M. Ashdown, F. Atrio-Barandela, J. Aumont, C. Baccigalupi, A. J. Banday, and et al. Planck 2013 results. XV. CMB power spectra and likelihood. *ArXiv e-prints*, March 2013.

[107] Planck Collaboration, P. A. R. Ade, N. Aghanim, C. Armitage-Caplan, M. Arnaud, M. Ashdown, F. Atrio-Barandela, J. Aumont, C. Baccigalupi, A. J. Banday, and et al. Planck 2013 results. XVI. Cosmological parameters. *ArXiv e-prints*, March 2013.

[108] J. L. Prieto, A. Rest, and N. B. Suntzeff. A New Method to Calibrate the Magnitudes of Type Ia Supernovae at Maximum Light. *ApJ*, 647:501–512, August 2006. doi: 10.1086/504307.

[109] I. P. Pskovskii. Light curves, color curves, and expansion velocity of type I supernovae as functions of the rate of brightness decline. *Soviet Ast.*, 21: 675–682, December 1977.

[110] I. Ramírez, C. Allende Prieto, S. Redfield, and D. L. Lambert. Fundamental parameters and abundances of metal-poor stars: the SDSS standard BD +17 4708. *A&A*, 459:613–625, November 2006. doi: 10.1051/0004-6361:20065647.

[111] N. Regnault, A. Conley, J. Guy, M. Sullivan, J.-C. Cuillandre, P. Astier, C. Balland, S. Basa, R. G. Carlberg, D. Fouchez, D. Hardin, I. M. Hook, D. A. Howell, R. Pain, K. Perrett, and C. J. Pritchet. Photometric calibration of the Supernova Legacy Survey fields. *A&A*, 506:999–1042, November 2009. doi: 10.1051/0004-6361/200912446.

[112] A. Rest, C. Stubbs, A. C. Becker, G. A. Miknaitis, A. Miceli, R. Covarrubias, S. L. Hawley, R. C. Smith, N. B. Suntzeff, K. Olsen, J. L. Prieto, R. Hiriart, D. L. Welch, K. H. Cook, S. Nikolaev, M. Huber, G. Prochtor, A. Clocchiatti, D. Minniti, A. Garg, P. Challis, S. C. Keller, and B. P. Schmidt. Testing LMC Microlensing Scenarios: The Discrimination Power of the SuperMACHO Microlensing Survey. *ApJ*, 634:1103–1115, December 2005. doi: 10.1086/497060.

[113] A. Rest et al. 2013.

[114] M. Riello and F. Patat. Extinction correction for Type Ia supernova rates - I. The model. *MNRAS*, 362:671–680, September 2005. doi: 10.1111/j.1365-2966.2005.09348.x.

[115] A. G. Riess, W. H. Press, and R. P. Kirshner. A Precise Distance Indicator: Type Ia Supernova Multicolor Light-Curve Shapes. *ApJ*, 473:88, December 1996. doi: 10.1086/178129.

[116] A. G. Riess, A. V. Filippenko, P. Challis, A. Clocchiatti, A. Diercks, P. M. Garnavich, R. L. Gilliland, C. J. Hogan, S. Jha, R. P. Kirshner, B. Leibundgut, M. M. Phillips, D. Reiss, B. P. Schmidt, R. A. Schommer, R. C. Smith, J. Spyromilio, C. Stubbs, N. B. Suntzeff, and J. Tonry. Observational Evidence from Supernovae for an Accelerating Universe and a Cosmological Constant. *AJ*, 116:1009–1038, September 1998. doi: 10.1086/300499.

[117] A. G. Riess, R. P. Kirshner, B. P. Schmidt, S. Jha, P. Challis, P. M. Garnavich, A. A. Esin, C. Carpenter, R. Grashius, R. E. Schild, P. L. Berlind, J. P. Huchra, C. F. Prosser, E. E. Falco, P. J. Benson, C. Briceño, W. R. Brown, N. Caldwell, I. P. dell'Antonio, A. V. Filippenko, A. A. Goodman, N. A. Grogin, T. Groner, J. P. Hughes, P. J. Green, R. A. Jansen, J. T. Kleyna, J. X. Luu, L. M. Macri, B. A. McLeod, K. K. McLeod, B. R. McNamara, B. McLean, A. A. E. Milone, J. J. Mohr, D. Moraru, C. Peng, J. Peters, A. H. Prestwich, K. Z. Stanek, A. Szentgyorgyi, and P. Zhao. BVRI Light Curves for 22 Type IA Supernovae. *AJ*, 117:707–724, February 1999. doi: 10.1086/300738.

[118] A. G. Riess, L. Strolger, J. Tonry, S. Casertano, H. C. Ferguson, B. Mobasher, P. Challis, A. V. Filippenko, S. Jha, W. Li, R. Chornock, R. P. Kirshner, B. Leibundgut, M. Dickinson, M. Livio, M. Giavalisco, C. C. Steidel, N. Benitez, and Z. Tsvetanov. Type Ia Supernova Discoveries at z>1 From the Hubble Space Telescope: Evidence for Past Deceleration and Constraints on Dark Energy Evolution. *ArXiv Astrophysics e-prints*, (0402512), February 2004.

[119] A. G. Riess, L.-G. Strolger, S. Casertano, H. C. Ferguson, B. Mobasher, B. Gold, P. J. Challis, A. V. Filippenko, S. Jha, W. Li, J. Tonry, R. Foley, R. P. Kirshner,

M. Dickinson, E. MacDonald, D. Eisenstein, M. Livio, J. Younger, C. Xu, T. Dahlen, and D. Stern. New Hubble Space Telescope Discoveries of Type Ia Supernovae at z > 1: Narrowing Constraints on the Early Behavior of Dark Energy. *ArXiv Astrophysics e-prints*, November 2006.

[120] B. W. Rust. *Use of supernovae light curves for testing the expansion hypothesis and other cosmological relations*. PhD thesis, University of Texas, December 1974.

[121] A. Sandage. The Ability of the 200-INCH Telescope to Discriminate Between Selected World Models. *ApJ*, 133:355, March 1961. doi: 10.1086/147041.

[122] P. L. Schechter, M. Mateo, and A. Saha. DOPHOT, a CCD photometry program: Description and tests. *PASP*, 105:1342–1353, November 1993.

[123] E. F. Schlafly, D. P. Finkbeiner, M. Jurić, E. A. Magnier, W. S. Burgett, K. C. Chambers, T. Grav, K. W. Hodapp, N. Kaiser, R.-P. Kudritzki, N. F. Martin, J. S. Morgan, P. A. Price, H.-W. Rix, C. W. Stubbs, J. L. Tonry, and R. J. Wainscoat. Photometric Calibration of the First 1.5 Years of the Pan-STARRS1 Survey. *ApJ*, 756:158, September 2012. doi: 10.1088/0004-637X/756/2/158.

[124] D. J. Schlegel, D. P. Finkbeiner, and M. Davis. Maps of Dust Infrared Emission for Use in Estimation of Reddening and Cosmic Microwave Background Radiation Foregrounds. *ApJ*, 500:525, June 1998. URL http://adsabs.harvard.edu/cgi-bin/nph-bib_query?bibcode=1998ApJ...500..525S&db_key=AST.

[125] B. P. Schmidt, N. B. Suntzeff, M. M. Phillips, R. A. Schommer, A. Clocchiatti, R. P. Kirshner, P. Garnavich, P. Challis, B. Leibundgut, J. Spyromilio, A. G. Riess, A. V. Filippenko, M. Hamuy, R. C. Smith, C. Hogan, C. Stubbs, A. Diercks, D. Reiss, R. Gilliland, J. Tonry, J. Maza, A. Dressler, J. Walsh, and R. Ciardullo. The High-Z Supernova Search: Measuring Cosmic Deceleration and Global Curvature of the Universe Using Type IA Supernovae. *ApJ*, 507: 46–63, November 1998. doi: 10.1086/306308.

[126] G. D. Schmidt, R. J. Weymann, and C. B. Foltz. A moderate-resolution, high-throughput CCD channel for the Multiple Mirror Telescope spectrograph. *PASP*, 101:713–724, August 1989.

[127] D. Scolnic et al. 2013.

[128] A. I. Sheinis, M. Bolte, H. W. Epps, R. I. Kibrick, J. S. Miller, M. V. Radovan, B. C. Bigelow, and B. M. Sutin. ESI, a New Keck Observatory Echellette Spectrograph and Imager. *PASP*, 114:851–865, August 2002.

[129] J. M. Silverman, M. Ganeshalingam, W. Li, and A. V. Filippenko. Berkeley Supernova Ia Program - III. Spectra near maximum brightness improve the accuracy of derived distances to Type Ia supernovae. *MNRAS*, 425:1889–1916, September 2012. doi: 10.1111/j.1365-2966.2012.21526.x.

[130] R. Sordo, A. Vallenari, R. Tantalo, F. Allard, R. Blomme, J.-C. Bouret, I. Brott, Y. Fremat, C. Martayan, Y. Damerdji, B. Edvardsson, E. Josselin, B. Plez, O. Kochukhov, M. Kontizas, U. Munari, T. Saguner, J. Zorec, A. Schweitzer, and P. Tsalmantza. Synthetic stellar and SSP libraries as templates for Gaia simulations. *Ap&SS*, 328:331–335, July 2010. doi: 10.1007/s10509-010-0272-7.

[131] P. B. Stetson. Homogeneous Photometry for Star Clusters and Resolved Galaxies. II. Photometric Standard Stars. *PASP*, 112:925–931, July 2000. doi: 10.1086/316595.

[132] P. B. Stetson. Homogeneous Photometry. IV. On the Standard Sequence in the Globular Cluster NGC 2419. *PASP*, 117:563–588, June 2005. doi: 10.1086/430281.

[133] M. Stritzinger, N. B. Suntzeff, M. Hamuy, P. Challis, R. Demarco, L. Germany, and A. M. Soderberg. An Atlas of Spectrophotometric Landolt Standard Stars. *PASP*, 117:810–822, August 2005. doi: 10.1086/431468.

[134] C. W. Stubbs and J. L. Tonry. Toward 1% Photometry: End-to-End Calibration of Astronomical Telescopes and Detectors. *ApJ*, 646:1436–1444, August 2006. doi: 10.1086/505138.

[135] C. W. Stubbs, S. K. Slater, Y. J. Brown, D. Sherman, R. C. Smith, J. L. Tonry, N. B. Suntzeff, A. Saha, J. Masiero, and S. Rodney. Preliminary Results from Detector-Based Throughput Calibration of the CTIO Mosaic Imager and Blanco Telescope Using a Tunable Laser. In C. Sterken, editor, *The Future of Photometric, Spectrophotometric and Polarimetric Standardization*, volume 364 of *Astronomical Society of the Pacific Conference Series*, page 373, April 2007.

[136] C. W. Stubbs, P. Doherty, C. Cramer, G. Narayan, Y. J. Brown, K. R. Lykke, J. T. Woodward, and J. L. Tonry. Precise Throughput Determination of the PanSTARRS Telescope and the Gigapixel Imager Using a Calibrated Silicon Photodiode and a Tunable Laser: Initial Results. *ApJS*, 191:376–388, December 2010. doi: 10.1088/0067-0049/191/2/376.

[137] M. Sullivan, A. Conley, D. A. Howell, J. D. Neill, P. Astier, C. Balland, S. Basa, R. G. Carlberg, D. Fouchez, J. Guy, D. Hardin, I. M. Hook, R. Pain, N. Palanque-Delabrouille, K. M. Perrett, C. J. Pritchet, N. Regnault, J. Rich, V. Ruhlmann-Kleider, S. Baumont, E. Hsiao, T. Kronborg, C. Lidman,

S. Perlmutter, and E. S. Walker. The dependence of Type Ia Supernovae luminosities on their host galaxies. *MNRAS*, 406:782–802, August 2010. doi: 10.1111/j.1365-2966.2010.16731.x.

[138] B. J. Taylor. Transformation equations and other aids for VRI photometry. *ApJS*, 60:577–599, February 1986. doi: 10.1086/191098.

[139] J. Tonry and M. Davis. A survey of galaxy redshifts. I - Data reduction techniques. *AJ*, 84:1511–1525, October 1979.

[140] J. L. Tonry, C. W. Stubbs, K. R. Lykke, P. Doherty, I. S. Shivvers, W. S. Burgett, K. C. Chambers, K. W. Hodapp, N. Kaiser, R.-P. Kudritzki, E. A. Magnier, J. S. Morgan, P. A. Price, and R. J. Wainscoat. The Pan-STARRS1 Photometric System. *ApJ*, 750:99, May 2012. doi: 10.1088/0004-637X/750/2/99.

[141] D. L. Tucker, J. T. Annis, H. Lin, S. Kent, C. Stoughton, J. Peoples, S. S. Allam, J. J. Mohr, W. A. Barkhouse, C. Ngeow, T. Alam, C. Beldica, D. Cai, G. Daues, R. Plante, C. Miller, C. Smith, and N. B. Suntzeff. The Photometric Calibration of the Dark Energy Survey. In C. Sterken, editor, *The Future of Photometric, Spectrophotometric and Polarimetric Standardization*, volume 364 of *Astronomical Society of the Pacific Conference Series*, page 187, April 2007.

[142] B. E. Tucker et al. 2013.

[143] A. Uomoto and R. P. Kirshner. Peculiar Type I supernovas. *A&A*, 149:L7–L9, August 1985.

[144] R. V. Wagoner. Determining qo from Supernovae. *ApJ*, 214:L5+, May 1977.

[145] E. S. Walker, I. M. Hook, M. Sullivan, D. A. Howell, P. Astier, C. Balland, S. Basa, T. J. Bronder, R. Carlberg, A. Conley, D. Fouchez, J. Guy, D. Hardin, R. Pain, K. Perrett, C. Pritchet, N. Regnault, J. Rich, G. Aldering, H. K. Fakhouri, T. Kronborg, N. Palanque-Delabrouille, S. Perlmutter, V. Ruhlmann-Kleider, and T. Zhang. Supernova Legacy Survey: using spectral signatures to improve Type Ia supernovae as distance indicators. *MNRAS*, 410: 1262–1282, January 2011. doi: 10.1111/j.1365-2966.2010.17519.x.

[146] X. Wang, A. V. Filippenko, M. Ganeshalingam, W. Li, J. M. Silverman, L. Wang, R. Chornock, R. J. Foley, E. L. Gates, B. Macomber, F. J. D. Serduke, T. N. Steele, and D. S. Wong. Improved Distances to Type Ia Supernovae with Two Spectroscopic Subclasses. *ApJ*, 699:L139–L143, July 2009. doi: 10.1088/0004-637X/699/2/L139.

[147] J. C. Wheeler and R. Levreault. The peculiar Type I supernova in NGC 991. *ApJ*, 294:L17–L20, July 1985. doi: 10.1086/184500.

[148] D. M. Wittman, J. A. Tyson, G. M. Bernstein, R. W. Lee, I. P. dell'Antonio, P. Fischer, D. R. Smith, and M. M. Blouke. Big Throughput Camera: the first year. In S. D'Odorico, editor, *Society of Photo-Optical Instrumentation Engineers (SPIE) Conference Series*, volume 3355 of *Society of Photo-Optical Instrumentation Engineers (SPIE) Conference Series*, pages 626–634, July 1998.

[149] W. M. Wood-Vasey, G. Miknaitis, C. W. Stubbs, S. Jha, A. G. Riess, P. M. Garnavich, R. P. Kirshner, C. Aguilera, A. C. Becker, J. W. Blackman, S. Blondin, P. Challis, A. Clocchiatti, A. Conley, R. Covarrubias, T. M. Davis, A. V. Filippenko, R. J. Foley, A. Garg, M. Hicken, K. Krisciunas, B. Leibundgut, W. Li, T. Matheson, A. Miceli, G. Narayan, G. Pignata, J. L. Prieto, A. Rest, M. E. Salvo, B. P. Schmidt, R. C. Smith, J. Sollerman, J. Spyromilio, J. L. Tonry, N. B. Suntzeff, and A. Zenteno. Observational Constraints on the Nature of Dark Energy: First Cosmological Results from the ESSENCE Supernova Survey. *ApJ*, 666:694–715, September 2007. doi: 10.1086/518642.

[150] W. M. Wood-Vasey, A. S. Friedman, J. S. Bloom, M. Hicken, M. Modjaz, R. P. Kirshner, D. L. Starr, C. H. Blake, E. E. Falco, A. H. Szentgyorgyi, P. Challis, S. Blondin, K. S. Mandel, and A. Rest. Type Ia Supernovae Are Good Standard Candles in the Near Infrared: Evidence from PAIRITEL. *ApJ*, 689:377–390, December 2008. doi: 10.1086/592374.

[151] N. Zacharias, S. E. Urban, M. I. Zacharias, G. L. Wycoff, D. M. Hall, D. G. Monet, and T. J. Rafferty. The Second US Naval Observatory CCD Astrograph Catalog (UCAC2). *AJ*, 127:3043–3059, May 2004. doi: 10.1086/386353.

[152] I. Zehavi, A. G. Riess, R. P. Kirshner, and A. Dekel. A Local Hubble Bubble from Type IA Supernovae? *ApJ*, 503:483, August 1998. doi: 10.1086/306015.

Colophon

This thesis was typeset using LaTeX, originally developed by Leslie Lamport and based on Donald Knuth's TeX. The body text is set in 11 point Arno Pro, designed by Robert Slimbach in the style of book types from the Aldine Press in Venice, and issued by Adobe in 2007. A template, which can be used to format a PhD thesis with this look and feel, has been released under the permissive MIT (X11) license, and can be found online at github.com/suchow/ or from the author at suchow@post.harvard.edu.